Talanta

The International Journal of Pure and Applied Analytical Chemistry

Publication information: *Talanta* (ISSN 0039-9140). For 2008, volumes 74–76 are scheduled for publication. Subscription prices are available upon request from the Publisher or from the Regional Sales Office nearest you or from this journal's website (http://www.elsevier.com/locate/talanta). Further information is available on this journal and other Elsevier products through Elsevier's website: (http://www.elsevier.com). Subscriptions are accepted on a prepaid basis only and are entered on a calendar year basis. Issues are sent by standard mail (surface within Europe, air delivery outside Europe). Priority rates are available upon request. Claims for missing issues should be made within six months of the date of dispatch.

Orders, claims, and journal enquiries: please contact the Customer Service Department at the Regional Sales Office nearest you:
Orlando: Elsevier, Customer Service Department, 6277 Sea Harbor Drive, Orlando, FL 32887-480 USA; phone: (+1) (877) 8397126 [toll free number for US customers], or (+1) (407) 3454020 [customers outside US]; fax: (+1) (407) 3631354; e-mail: usjcs@elsevier.com
Amsterdam: Elsevier, Customer Service Department, PO Box 211, 1000 AE Amsterdam, The Netherlands; phone: (+31) (20) 4853757; fax: (+31) (20) 4853432; e-mail: nlinfo-f@elsevier.com
Tokyo: Elsevier, Customer Service Department, 4F Higashi-Azabu, 1-Chome Bldg, 1-9-15 Higashi-Azabu, Minato-ku, Tokyo 106-0044, Japan; phone: (+81) (3) 5561 5037; fax: (+81) (3) 5561 5047; e-mail: jp.info@elsevier.com
Singapore: Elsevier, Customer Service Department, 3 Killiney Road, #08-01 Winsland House I, Singapore 239519; phone: (+65) 63490222; fax: (+65) 67331510; e-mail: asiainfo@elsevier.com

USA mailing notice: *Talanta* (ISSN 0039-9140) is published monthly by Elsevier B.V. (P.O. Box 211, 1000 AE Amsterdam, The Netherlands). Annual subscription price in the USA US$ 4,085 (valid in North, Central and South America), including air speed delivery. Application to mail at periodical postage rate is paid at Rathway, NJ and additional mailing offices.
USA POSTMASTER: Send address changes to *Talanta*, Publications Expediting Inc., 200 Meacham Avenue, Elmont, NY 11003.
AIRFREIGHT AND MAILING in the USA by Publications Expediting Inc., 200 Meacham Avenue, Elmont, NY 11003.

Talanta 76 (2008) 353–359

Contents lists available at ScienceDirect

Talanta

journal homepage: www.elsevier.com/locate/talanta

A high precision, fast response, and low power consumption in situ optical fiber chemical pCO_2 sensor

Zhongming Lu [a], Minhan Dai [a,*], Kunming Xu [a], Jinshun Chen [a], Yinhao Liao [b]

[a] State Key Laboratory of Marine Environmental Science, Xiamen University, Xiamen, China
[b] College of Computer and Information Engineering, Xiamen University, Xiamen, China

ARTICLE INFO

Article history:
Received 30 September 2007
Received in revised form 6 March 2008
Accepted 9 March 2008
Available online 15 March 2008

Keywords:
Carbon dioxide
In situ chemical sensor
Optical fiber

ABSTRACT

A sensor system suitable for monitoring changes in partial pressure of carbon dioxide (pCO_2) in surface seawater or in the atmosphere has been developed. Surface seawater samples are pumped into a PVC tube enclosing an inner Teflon AF tube, which served as a long pathlength gas-permeable liquid-core waveguide for spectrophotometry. The Teflon cell contains a pH-sensitive indicator-buffer solution consisting of bromothymol blue (BTB) and sodium carbonate. Carbon dioxide in the sample diffuses into the indicator-buffer solution to reach equilibrium, resulting in pH changes, which are detected by changes in the absorbance of BTB at wavelengths of 620 and 434 nm. The pCO_2 in the sample is then derived from the pH change. The sensor has a response time of 2 min at the 95% equilibrium value and a measurement precision of 0.26–0.37% in the range 200–800 μatm pCO_2. This chemical sensor takes advantage of a combination of long pathlength, multiple wavelength detection, indicator solution renewal, and in situ automatic control technology, and has the feature of low power consumption (the average being ~4 W with a peak of ~8 W).

1. Introduction

Developing in situ chemical sensors has been recently a fast growing field along with the increasing need for monitoring environmental and climate changes [1,2]. pCO_2 in seawater is one of the most important parameters affecting global carbon cycle and climate, monitoring the variability of oceanic CO_2 over varying temporal and spatial scales has become one of the central tasks in numerous climate and/or ocean related programs. Surface seawater pCO_2 measurements are typically carried out shipboard by pumping seawater through the so-called shower head water–air equilibrator into a non-dispersive infrared (NDIR) pCO_2 measurement system [3]. Such a system is however difficult to deploy unattended for time-series observations due to its complexity in sampling configuration, calibration and data reduction towards an in situ pCO_2 value. A high precision, fast response, and low power consumption pCO_2 sensor, which suits in situ sampling platforms such as buoys or moorings for long time automatic deployment, is increasingly in demand for ocean carbon studies.

Over the past two decades, researchers have made great progress in developing a variety of pCO_2 sensors. Lefévre et al. [4] and Merlivat and Brault [5] devised pCO_2 sensors based on a colorimetric method. Through two calibration experiments, made over a fugacity of CO_2 (fCO_2) range from 340 to 590 μatm, the system could measure pCO_2 lasting for 3 or 4 days with a variation of ±1 μatm. The sensor was accurate within 3 ± 6 μatm of shipboard fCO_2 data for periods up to 50 days. Although the sensor measured three different wavelengths, only one of them indicated fCO_2 variations, the other two were used for correction of baseline shifts and as an indication of dye solution degradation. The sensor used two CO_2-permeable silicone membranes to separate seawater from a color indicator, a thymol blue solution diluted in artificial seawater. Since the dye solution could not be renewed, photodegradation was observed during extended time measurements.

Tabacco et al. [6] developed a pCO_2 sensor using a pH-sensitive fluorescent dye as an indicator of pCO_2 with a gas-permeable PTEE membrane for low-level pCO_2 measurements in seawater. The indicator solution was immobilized by the PTEE membrane at the end of an optical fiber. The system was highly automated and was deployed in the Atlantic Ocean on a buoy for about 50 days of observations. The sensitivity (±1 ppm between 200 and 1000 ppm pCO_2) was quite good. However, as with those built by Merlivat and Brault [5], the sensor was designed with embedded indicator solution. Since the solution cannot be renewed, a potential problem is degradation of this solution with time, which hampers its long-term deployment. Additionally, most sensors with embedded

* Corresponding author. Tel.: +86 592 2182132; fax: +86 592 2180655.
E-mail address: mdai@xmu.edu.cn (M. Dai).

0039-9140/$ – see front matter © 2008 Elsevier B.V. All rights reserved.
doi:10.1016/j.talanta.2008.03.005

Table 1
Comparison of main features of different chemical CO_2 sensors

Authors	Reagent renewable	Long path-length waveguide	Multi-wavelength detection	Unattended run in situ
Tabacco et al. [6]			√	√
Lefévre et al. [4]			√	√
Merlivat and Brault [5]			√	√
DeGrandpre et al. [7]	√		√	√
Dasgupta et al. [10]	√	√		
Wang et al. [12]	√	√		
Wang et al. [14]	√	√	√	
Nakano et al. [15]	√	√	√	
This work	√	√	√	√

Long path-length waveguide means whether the sensor used a long tube made of gas-permeable materials (such as Teflon AF 2400) to serve both as a semi-permeable membrane and an absorption cell.

indicator solutions have a relatively short light path, and this would limit their detection sensitivity as compared to sensors with long light paths.

DeGrandpre et al. [7] designed a calibration-free optical chemical pCO_2 sensor. It was an indicator-based pCO_2 sensor that has an excellent sensor-to-sensor reproducibility and measurement stability. This sensor used tubular silicone rubber as the gas-permeable membrane, and BTB (bromothymol blue) as an acid–base indicator. The system achieved an optimal sensitivity of ±1 ppm and a 95% response time of 5 min [8]. To minimize signal drifting, three techniques were adopted: frequent renewal of indicator reagent, periodic measurement of solution blanks, and the use of absorbance ratios. During a mooring deployment for 90 days, the instrument showed good stability in its early stages of development [8,9].

The application of a new fluoropolymer by DuPont (Teflon AF 2400) showed significant advantage over other membranes in terms of response time and sensitivity. Dasgupta et al. [10] conducted a preliminary experiment to test a Teflon AF 2400 based sensor. The results show that the response time is as short as ~2 min. In addition, because amorphous fluoropolymer such as Teflon AF 2400 tubing has a low refractive index, it can serve as both a CO_2-permeable membrane equilibrator and a long pathlength liquid-core waveguide spectrophotometric cell, this enables the system to achieve a better precision with relative low indicator concentration, it also makes it easier to couple the spectrophotometric cell with common optical fiber [11]. Wang et al. [12] report the first long pathlength fiber optic-based sensor to measure pCO_2 in natural waters and atmosphere. The sensor was based on a liquid-core waveguide made of Teflon AF 2400. This sensor achieved a precision of ±3 μatm in the pCO_2 range of 200–500 μatm, and a response time (99%) of 2 min for low-level pCO_2 (<1000 μatm) measurements. It should be noted that their sensor was initially based on single wavelength spectrophotometric detection, which they later replaced with a multiple wavelength technique for underway pCO_2 measurements [13]. The final results of their Teflon AF pCO_2 sensor during the underway monitoring agree well with the "showerhead equilibrator plus infrared analyzer". Recently, Wang et al. [14] developed a multi-parameter flow-through underway CO_2 system which contains a pCO_2 sensor similar to their previous work. With modifications, especially on automatic controlling, it achieves a good performance of 0.9 μatm for field precision and 1.0 ± 2.5 μatm for field agreement with established standard methods.

The in situ pCO_2 profiler developed by Nakano et al. [15] is also a pH reagent based optical fiber chemical sensor. They used a 1600 mm long Teflon AF tube to serve as the gas-permeable membrane and, for every single measurement the equilibrated indicator solution was pumped into a glass flow cell for determination. The precision of this sensor is within 2.5%. The unique character of this sensor is its ability to resist water pressure to 3000 m depth.

Despite this progress, there has not been a single report concerning the development of an unattended in situ pCO_2 sensor based on long pathlength liquid-core waveguide. Here we report our new in situ pCO_2 sensor based on such long pathlength liquid-core waveguide spectrophotometric measurement. Compared to our earlier version of the sensor [16], which was based on single wavelength measurements, major modifications were made to the sensor design, as well as the detection and controlling systems. The current sensor used a waveguide made of Teflon AF 2400 to serve both as a semipermeable membrane and an absorption cell, and also used multi-wavelength spectrophotometry to detect the changes of light signals. The liquid-core waveguide consumed little indicator solution, which made it feasible to furnish the sensor with renewable indicator solution. While maintaining high sensitivity, this long pathlength liquid-core waveguide method used a relatively lower indicator concentration to avoid buffer effects, so that the sensor rapidly responded to environmental pCO_2 change. The sensor achieved a response time of less than 2 min and an optimal precision of <1 μatm. With low power consumption design, the sensor is particularly suitable for buoy or mooring based long-term time series monitoring of pCO_2 in air or water. A comparison of our sensor with other reported pCO_2 sensors can be found in Table 1.

2. Principle

The theoretical principle of CO_2 measurement is generally based on spectrophotometric pH measurements [17,18]. More specifically, it relies on determination of the absorbance of acid and base forms of the indicator solution equilibrating with seawater or atmosphere samples. The theoretical considerations have been elucidated by many researchers [4,5,7–9,12,13], and so here we introduce it only briefly. The hydrolization and ionization processes in the indicator-buffer solution, which consisted of sodium carbonate and BTB, can be expressed by the following equations:

$$CO_2(g) = CO_2(aq) \qquad K_h = [CO_2*]/pCO_2$$

$$CO_2(aq) + H_2O = H^+ + HCO_3^- \qquad K_1 = [H^+][HCO_3^-]/[CO_2*]$$

$$HCO_3^- = H^+ + CO_3^{2-} \qquad K_2 = [H^+][CO_3^{2-}]/[HCO_3^-]$$

$$HIn = H^+ + In^- \qquad K_a = [H^+][In^-]/[HIn]$$

where K_h is Henry's law constant, K_1 and K_2 are the carbonic acid dissociation constants, HIn refers to BTB reagent and K_a is the indicator dissociation constant. As a water or air sample is pumped into the sensor for measurements, CO_2 in the sample will penetrate the semi-permeable membrane (the wall of the Teflon AF tube) and dissolve into the indicator-buffer solution. When CO_2 in the indicator-buffer solution reaches equilibration with the outer

samples, the following equation can be derived from the above hydrolization and ionization equations:

$$[H^+]^3 + ([Na^+] - K_a c_{HIn}/(K_a + [H^+]))[H^+]^2 - (K_1 K_h pCO_2 + K_w)[H^+] - 2K_1 K_2 K_h pCO_2 = 0 \quad (1)$$

where $[H^+]$ is the hydrogen ion concentration, $[Na^+]$ is the concentration of sodium ion introduced by Na_2CO_3, K_w is the water dissociation constant, c_{HIn} is the concentration of indicator. From Eq. (1), we can theoretically calculate pCO_2 of the indicator-buffer solution through its pH value, since the other parameters are known.

The pH value of the indicator-buffer solution can be obtained by spectrophotometric measurements:

$$R_{CO_2} = -\log\left(\frac{A_R - \varepsilon_{620(HIn)}/\varepsilon_{434(HIn)}}{\varepsilon_{620(In)}/\varepsilon_{434(HIn)} - A_R \times \varepsilon_{434(In)}/\varepsilon_{434(HIn)}}\right) = pK_a - pH \quad (2)$$

where R_{CO_2} is the instrumental response of CO_2, A_R is the absorbance ratio of the indicator at 434 nm and 620 nm, ε represents the molar absorptivities, and the subscripts 434 and 620 represent the wavelength of the acid and base absorbance peaks of the indicator, respectively. A_R was obtained from light intensity signals passing through the sample so that R_{CO_2} and pH can be calculated. Combining Eqs. (1) and (2), a relationship can be established between the sensor's optical signal and the pCO_2 value in seawater or the atmosphere.

3. Experimental

3.1. Gas sensing device

The gas sensing device is the core part of the sensor, acting as reaction cell and optic fiber simultaneously. The basic construction of the gas sensing device is shown schematically in Fig. 1(A). A 12 cm length of Teflon AF 2400 tubing with an inner diameter of 0.61 mm and an outer diameter of 0.81 mm was purchased from Biogeneral Inc. (San Diego, CA). It was used as a long path length liquid-core waveguide spectrophotometric cell. A solenoid actuated pump (110TP12-40, Bio-Chem Valve Inc. NJ) was used for injecting indicator solution into the liquid-core cell. Teflon AF polymers are distinct from other fluoropolymers as a result of their high gas permeability and the lowest index of refraction of any known polymer. When filled with aqueous solution, a tube made of this material behaves as a liquid-core optical fiber, which makes it practicable for light signals to get through the long-path length optical cells without significant loss.

Surrounding the liquid-core waveguide, a PVC tube of 10 mm i.d. served as the sampling tube. To measure seawater pCO_2, a micropump (DC335C motor and GA-T23.PFSC pump, Micropump Inc. WA) was used to pump seawater from outside the sensor into the PVC tube; to measure atmospheric pCO_2, a micro air pump (PBW6003, Ruiyi Inc. Chengdu, China) was used to suck air into the tube. Carbon dioxide within the sample penetrated through the Teflon to react with the indicator solution, resulting in a pH change for spectrophotometry.

3.2. Indicator-buffer solution preparation

Wang et al. [13] and DeGrandpre [9] evaluated two types of indicators: PhR (phenol red) and BTB and found that BTB exhibited higher sensitivity than did PhR. We also used similar experiments to compare these two indicators and obtained the same result, and so we used BTB as the colorimetric acid–base indicator in this study.

All chemicals were analytical reagents or their equivalent. The indicator-buffer solution was prepared as follows: Na_2CO_3 was dried for 8 h in an 110 °C oven and kept in a desiccator before use. All solutions were prepared using ultrapure water (Milli-Q water). Generally we used 0.05 mM BTB and 1 mM Na_2CO_3 as stock solution, and prepared indicator-buffer solution from the stock solution just before the sensor's deployment. The indicator-buffer solution was bubbled with pure nitrogen gas to purge dissolved CO_2, and then kept in sealed aluminum laminate bags (Pollution Measurement, Oak Park, IL) before being placed into the sensor.

The concentration of indicator-buffer solution is crucial to the sensor's response sensitivity and precision. On one hand, a high indicator concentration for heavy light absorption is beneficial to the sensor's sensitivity according to the principle of spectrophotometric analysis. On the other hand, high indicator concentration may decrease the sensor's sensitivity ($\Delta R_{CO_2}/\Delta pCO_2$) due to the buffer effect of the indicator dissociation [13]. Thus, increasing the optical pathlength while decreasing the indicator concentration is the best solution if the light intensity would not be attenuated along the path. Because of the short optical pathlength, DeGrandpre [9] used 50 μM BTB for the sensor. With a 21 cm optical pathlength for their underway system, Wang et al. [13] used 5 μM BTB and suggested that 50 μM Na_2CO_3 was optimal for oceanic pCO_2 measurements. In this study, by theoretical calculation and experimental tests, we used an indicator-buffer solution consisting

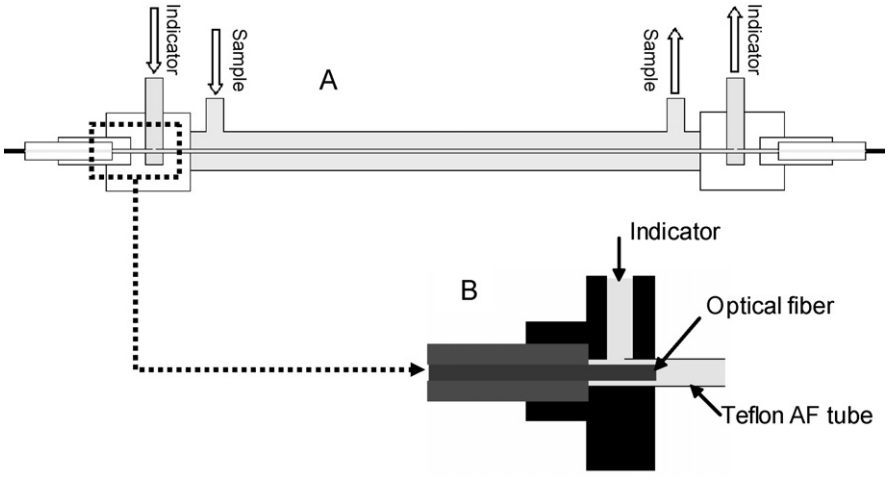

Fig. 1. Sketch of gas sensing device (A) and the coupling of optical fiber, indicator/blank solution intake (or outlet) and Teflon AF tube (B).

of 2.5 μM BTB and 50 μM Na_2CO_3. More details on optimizing indicator-buffer solutions can be found elsewhere [12,16].

3.3. Light source and detection

An LED light source (Huibo Inc., Xiamen, China) with three emission wavelengths of 434 nm, 620 nm, and 740 nm was adopted for multiple wavelength spectrophotometric detection. The specified half-width of the three LEDs was 79 nm, 13 nm, and 21 nm, respectively. Three filters (Xingchang Inc., Shanghai, China) with a central wavelength of 433.6 nm, 621.5 nm, and 739.2 nm and half-width of 21.3 nm, 8.7 nm, and 8.7 nm, respectively, were placed in front of the corresponding LED to further narrow the spectral bands. The three LEDs emitted light alternately and periodically. A convex lens was placed in front of each filter to focus the light into an optical fiber. The optical fiber led the light from the three LEDs into the waveguide, and another optical fiber led the light signal out of the waveguide to a photodiode detector. At the junctions, the optical fibers were inserted into the Teflon AF tube to reduce light signal losses (Fig. 1(B)).

The three light signals were attenuated to various extents as they passed through the liquid-core waveguide cell and were then received by the detector. The sensor used a photodiode as detector (Model S1226-44BQ Hamamatsu Corp., Hamamatsu, Japan), which had a photosensitive surface area of 13 mm^2 and noise equivalent power of 3.6×10^{-15} $W/Hz^{1/2}$. The light detected was converted into valid data through a carefully designed circuit and stored in a memory chip. This circuit (which we have patented) could self-adjust the detection range to obtain better precision.

Determination of the optimum length of the liquid-core waveguide involved a compromise between several factors. Longer optical path length certainly can gain higher sensitivity with a relatively lower indicator concentration, but the light signal will be attenuated quickly. Although this attenuation can be compensated by enhancing the power of the light source, it increases power consumption, which runs against our objective of strict power saving for mooring-based autonomous sensors. Furthermore, a longer liquid-core waveguide is more susceptible to bubble formation or impurity adsorption. Based upon many experiments and adjustments, we first determined 12 cm as the optical pathlength liquid-core waveguide and provided proper indicator concentrations, and then tuned optimal power for the light source and set the optimal light signal detection circuit accordingly.

3.4. System configuration and operation

The sensor configuration is shown schematically in Fig. 2. Light from the modulated light source is coupled into to the liquid-core waveguide via an optical fiber, and the light signals out of the liquid-core waveguide are introduced by another optical fiber into the photodiode detector. Volt signals of the detector are transformed into digital signals by a control circuit, and are then saved in a data logger. The automatic controller and data logger were all made in-house. A set of current data was transmitted to the central controller of the mooring through an RS-232 port and then to the land-based station at the request of the controller on the mooring. This data transmission strategy was adopted for our pCO_2 sensors mounted on a buoy in the Taiwan Strait for three months, with good performance.

The indicator-buffer solution was pumped into the liquid-core waveguide by a solenoid operated Teflon micro pump that delivers 20 μL per pulse, three pulses per second, lasting 10 s for one time, i.e., a total of 0.6 ml indicator-buffer solution was used for one solution renewal. The inlet and outlet of the indicator-buffer solution were sealed off from the sampling tube with glue and

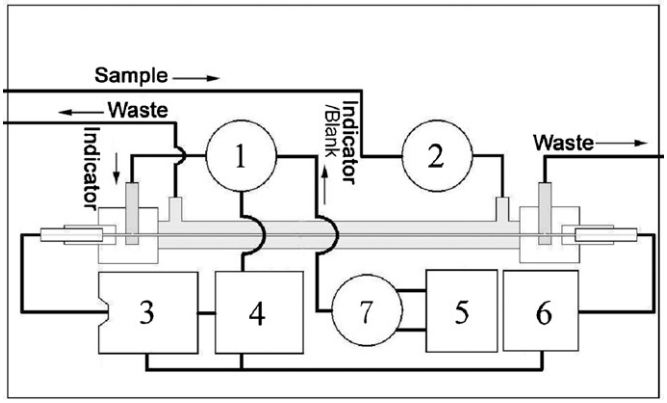

Fig. 2. The structure of pCO_2 sensor system. 1: Indicator/blank solution pump, 2: water/air pump, 3: detector, 4: automatic controller, 5: indicator/blank solution reservoir, 6: light source, 7: three way pinch valve.

O-rings. Before every renewal of indicator-buffer solution, blank solution (pure water and detergent) was pumped into the liquid-core waveguide to obtain the sensor's blank constants. The blank solution shared the same pump with the indicator-buffer solution, and a three-way pinch valve was used to separate these two solutions. Indicator-buffer solution and blank solution (enough for three months use) were stored in two aluminum laminate gas impermeable bags respectively, and wastes were collected in another bag.

The light source and detector started up and measured once every 3 min, while the sampling pump was kept running except when the light source and detector were turned on (lasting for 9 s) for measurements. Electrical and mechanical operation of the whole system was controlled by a homemade 8-bit controller.

The instrument was housed in an anodized aluminum pressure vessel (PREVCO subsea housings, PREVCO LLC) that is capable of withstanding pressures of at least 1608 psig (test pressure: 1769 psig). A homemade stainless steel housing was available for alternative usage. The system was powered by external power supplies, such as a solar battery on the mooring, and had a built-in 10 Ah battery for emergency use. The whole system's average power consumption was less than 4 W at 12 V DC with a peak power consumption of 8 W, which only lasted for 9 s while renewing the reagent. The instrument gross weight was approximately 40 kg in the air and 10 kg in water. PVC and nylon housings were also used for the pCO_2 sensors deployed in the air or surface water (<5 m). Thus, these sensors were much lighter in weight.

4. Results and discussion

4.1. Response time

Teflon AF 2400 is highly permeable to a number of trace gases including CO_2. Compared to common poly tetrafluoroethylene (PTFE)-type Teflon, the new amorphous fluoropolymer is three orders of magnitude more permeable to many gases. Therefore, the sensor with a liquid-core waveguide made of this material has a very short response time (Fig. 3). In this study, our sensor can reach 95% of full equilibrium within 2 min, and no difference in response time was found for gas-phase and water-phase samples based on laboratory tests [12]. Using Teflon tubing with thinner wall thickness would obtain even faster responses.

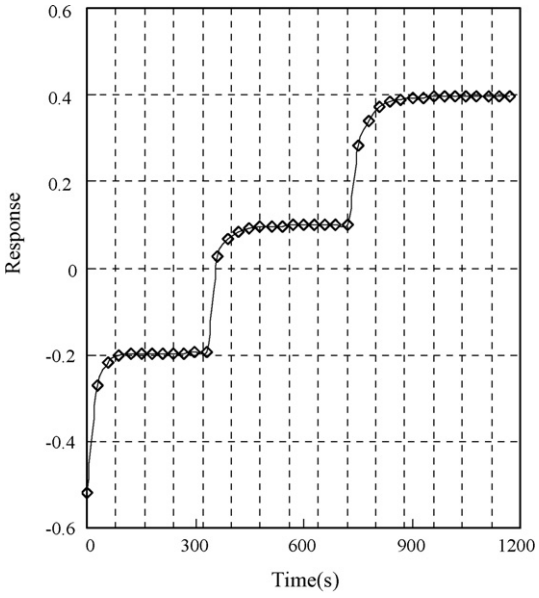

Fig. 3. Sensor's response to 200, 400, 800 ppm standard CO_2 gases. The sensor had [BTB] = 2.5 μM and [Na_2CO_3] = 50 μM.

4.2. Temperature dependency

According to the principle of this kind of chemical sensor, almost all parameters affecting the sensor's responses, such as carbonic acid dissociation constants, indicator dissociation constants, and Henry's law constant, are temperature-dependent. It is therefore important to accurately quantify the temperature dependency of the sensor's response. The temperature dependency experiment was conducted in a temperature control water bath with a precision of 0.1 °C, and the sensor's responses to various CO_2 concentrations (209 ppm, 599 ppm, and 801 ppm) were tested within the temperature range 25–37 °C. The results of the sensor's temperature dependency experiments are shown in Fig. 4.

All the instrumental responses and temperature showed good linear relationships. Linear curve fitting gave slopes of −0.0095, −0.0094 and −0.0093 (R_{CO_2} unit °C^{-1}) at CO_2 concentrations of 209, 599, and 801 ppm, respectively (Fig. 4A–C). Theoretical calculation at a CO_2 concentration of 400 μatm gives a slope value of −0.0064 (Fig. 4D). The experimental slopes are a little higher than those of DeGrandpre [7] (−0.0071 and −0.0076 R_{CO_2} unit °C^{-1} at 325 and 506 μatm for theoretical slopes, −0.0058 and −0.0064 R_{CO_2} unit °C^{-1} at 325 and 506 μatm for experimental slopes, respectively) due to different design parameters. The difference between experimental and theoretical slopes can be attributed to the deviation of thermodynamic constants from their real values. However the experimental slopes agree well with each other so that they are trustworthy for normalizing pCO_2 to any temperature. Based on the linear temperature effect, we incorporated a temperature probe into the sensor and adjusted the sensor responses properly through software application to account for temperature fluctuations in the field.

4.3. Sensitivity and precision

The sensor's response (R_{CO_2}) showed a logarithmic fit with pCO_2 (Fig. 5). For a given sensor system, if the detector response remains linear within the normal pCO_2 range, the sensor's sensitivity would alter with the variation of pCO_2. As shown in Fig. 5, the sensitivity ($\Delta R_{CO_2}/\Delta$ppm) of a given pCO_2 equalled the slope of the tangent at this point on the curve, which decreased with increasing pCO_2. So the sensor's sensitivity decreased with increasing of pCO_2. According to the fitting curve of the measured data, the sensor's sensitivities at pCO_2 of 200 μatm, 400 μatm, and 800 μatm were 0.0022 R_{CO_2}/μatm, 0.0011 R_{CO_2}/μatm, and 0.0005 R_{CO_2}/μatm, respectively.

Theoretical response (R_{CO_2}) curves based on Eqs. (1) and (2) are also shown in Fig. 5. Using the functions of Millero [19] K_1, K_2, K_h were calculated. Under the condition of [BTB] = 2.5 μmol L^{-1} and [Na_2CO_3] = 50 μmol L^{-1}, the curve for the theoretical data was $y = 0.4276 \ln(x) - 2.7456$ while that for the measured data was $y = 0.4339 \ln(x) - 2.5036$. The discrepancy between theoretical and measured curves was probably due to uncertainties in the ther-

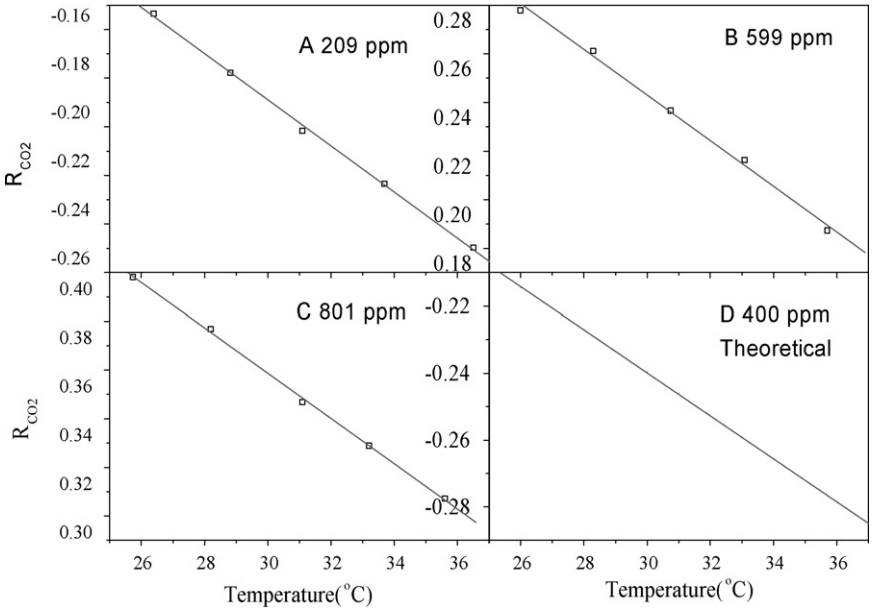

Fig. 4. Measured temperature response of sensor at CO_2 concentrations of 209 ppm (A), 599 ppm (B) and 801 ppm (C) along with theoretical calculated temperature response at 400 μatm CO_2 (D).

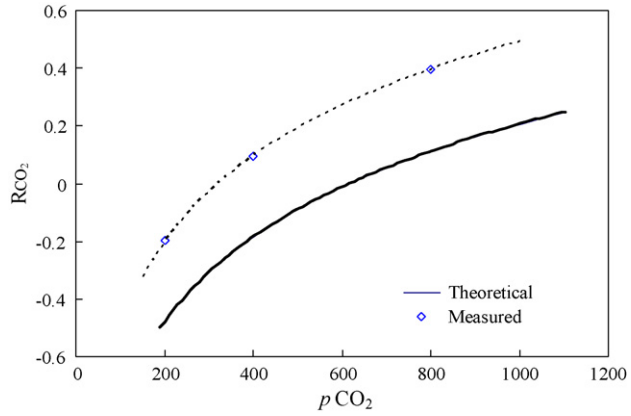

Fig. 5. Theoretical and measured responses of the sensor at various CO_2 concentrations.

modynamic constants, the light source, detector and light path, etc.

In this study, precision of the sensor was determined by repeated measurements of known concentration of CO_2 gases [20], and the RSD (relative standard deviation) of the replicated analyses was calculated from 12 measurements over a 1 h interval. The RSD is 0.37%, 0.31%, 0.33% and 0.26% at the standard gases concentration of 401 ppm, 601 ppm, 805 ppm and 1030 ppm, respectively under the indicator-buffer condition of [BTB] = 2.5 μmol L^{-1} and [Na_2CO_3] = 50 μmol L^{-1}). Obviously, the precision of the sensor for all CO_2 concentrations was below 0.4%.

4.4. Long-term stability

Long-term stability is particularly important for an in situ autonomous sensor. We evaluated the sensor's long-term stability in the laboratory by repeatedly checking a set of CO_2 gases of known concentration against the analysis sensor's response drift over time. After the sensor had been calibrated, three CO_2 gases (203 ppm, 399 ppm, 801 ppm) were checked at random times. Room temperature was also recorded simultaneously using a mercury thermometer with a precision of 0.1 °C, and the sensor's responses were normalized to the temperature at which the sensor had been calibrated. The experiment was conducted from April 12 to May 8, 2005. Variations in the sensor's response to the three CO_2 gas standards are shown in Fig. 6, the S.D. (standard deviation) of the responses is 2.7 ppm, 5.2 ppm and 13.6 ppm at the CO_2 gas concentration of 203 ppm, 399 ppm and 801 ppm, respectively (under the indicator-buffer condition of [BTB] = 2.5 μmol L^{-1} and [Na_2CO_3] = 50 μmol L^{-1}). This demonstrates that the sensor's long-term stability was ~1–2% during a month-long experiment.

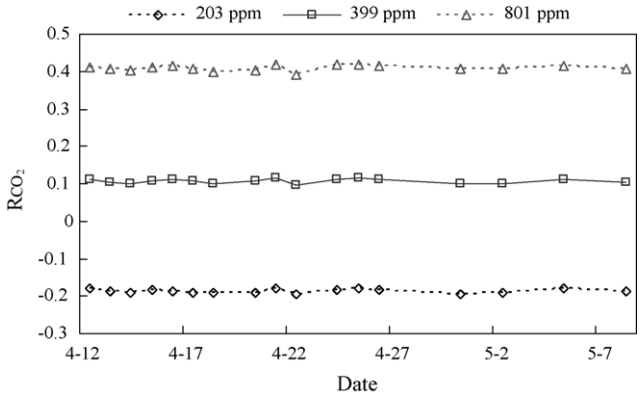

Fig. 6. Sensor's long-term stability in measuring three CO_2 concentrations for 26 days in 2005. The sensor had [BTB] = 2.5 μmol L^{-1} and [Na_2CO_3] = 50 μmol L^{-1}.

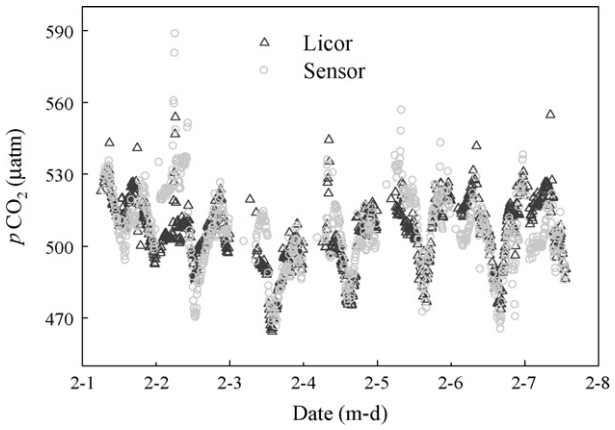

Fig. 7. Comparison between our sensor and the air–water equilibrator-NDIR (Licor) system for time-series measurements of seawater pCO_2 in Xiamen Bay in 2007. The sensor had [BTB] = 2.5 μmol L^{-1} and [Na_2CO_3] = 50 μmol L^{-1}.

4.5. Field experiments

To evaluate the sensor's performance for in situ measurements, field experiments comparing the sensor with an air–water equilibrator-NDIR (non-dispersive infrared) pCO_2 measurement system were conducted at a wharf in Xiamen Bay. The sensor was deployed in seawater at a depth of about 1 m to measure seawater pCO_2. Meanwhile seawater samples were pumped into the air–water equilibrator from where the sensor was deployed, and the equilibrated gas in the equilibrator was then pumped into a NDIR CO_2 analyzer (Licor 7000) for determination [21]. Both instruments simultaneously measured seawater pCO_2. The field experiment lasted for 7 days and the data are shown in Fig. 7. The sensor results differed overall from the equilibrator-NDIR based measurements by a mean of only 0.4 ± 11.7 μatm (S.D., n = 802), demonstrating an excellent agreement between the two systems. Random deviations were however observable, but it is difficult to determine whether these resulted from our measuring system (such as light path, light source, detector, and controlling circuit) or from expected environmental factors (such as bubble formation, particle adsorption, drastic vibrations, and instant power failure, etc). However, the sensor can overcome these problems by periodical renewal of the Indicator-buffer solution and by automatically resetting itself to the initial working conditions after the unexpected error, and so diminish the abnormal data to a minimum.

In another field experiment, we deployed the sensor on a mooring in Shenhu Bay (which is 100 km from Xiamen) in June 2005. During the period of deployment, a set of data (data measured by all sensors mounted on the mooring) were recorded every 3 h and transmitted to a land-based station via satellite. In this experiment, we had no other methods to measure the pCO_2 simultaneously for comparison, but from Fig. 8 we can see that the surface seawater pCO_2 exhibited a good inverse correlation with tides. This is reasonable because of the higher pCO_2 in near-shore water and the lower pCO_2 in offshore water. However, we must point out that this sensor exhibited a substantial decline of signals in all three wavelengths (data not shown) after about 7–30 days of deployment, the reasons of which are complex but may be related to the stability of the light sources, membrane permeability deterioration as well as chemical and biological fouling.

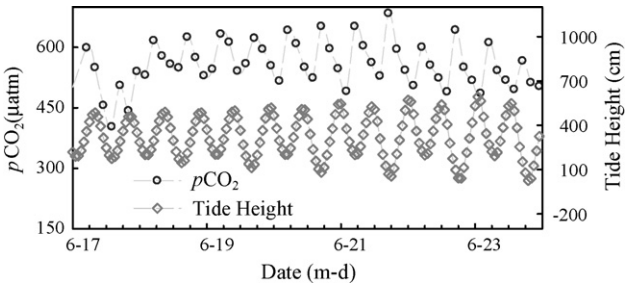

Fig. 8. Diurnal variations of surface seawater pCO_2 and tide height at a station in Shenhu Bay in 2005 (*note*: tide height data is from the nearby Xiamen Bay).

5. Summary and future improvement

An in situ autonomous fiber optical chemical pCO_2 sensor was developed based on the modern technologies for long path length liquid-core waveguide and multiple wavelength detection, and for spectrophotometry. The indicator-buffer solution, which was composed of 2.5 μM BTB and 50 μM Na_2CO_3, was periodically renewed during the sensor deployment for long-term unattended pCO_2 measurements. This sensor was shown to have fast responses (about 2 min for a 95% response), high precision (an optimal precision of 1 μatm and <1% within the normal pCO_2 range), and excellent long-term stability (drift about 1–2% in about one month). In a field test, it was demonstrated that the sensor produced time-series seawater pCO_2 data consistent with those produced by the equilibrator-NDIR pCO_2 measurement system.

We must point out that this research is still in progress. Among others, an outstanding problem to be resolved is how to reduce chemical, physical and biological fouling to the sensor during in situ deployment. In several field experiments at Xiamen Bay, the Taiwan Strait, and Xisha Island of China, we observed significant reduction of the signals of all three wavelengths with time, which may be at least related to these fouling processes.

Acknowledgments

This study was financially supported by the 863 (Hi-tech research and development program of China) program under contract no. 2002AA635140. George T.F. Wong is appreciated for his comments on the early version of this paper and John Hodgkiss is thanked for his assistance with English. Dr. Jianhua Wang and two anonymous reviewers provided valuable comments which strengthened the manuscript.

References

[1] K.S. Johnson, J.A. Needoba, S.C. Riser, W.J. Showers, Chem. Rev. 107 (2007) 623.
[2] C.M. McGraw, S.E. Stitzel, J. Cleary, C. Slater, D. Diamond, Talanta 71 (2007) 1180.
[3] R.A. Feely, R. Wanninkhof, H.B. Milburn, C.E. Cosca, M. Stapp, P.P. Murphy, Anal. Chim. Acta. 377 (1998) 185.
[4] N. Lefévre, J.P. Ciabrini, G. Michard, B. Brient, M. Duchaffaut, L. Merlivat, Mar. Chem. (1993) 189.
[5] L. Merlivat, P. Brault, Sea Technol. (1995) 23.
[6] M.B. Tabacco, M. Uttamial, M. McAllister, D.R. Walt, Anal. Chem. 71 (1999) 1483.
[7] M.D. DeGrandpre, M.M. Baehr, T.R. Hammar, Anal. Chem. 71 (1999) 1152.
[8] M.D. DeGrandpre, T.R. Hammar, S.P. Smith, F.L. Sayles, Limnol. Oceanogr. 40 (1995) 969.
[9] M.D. DeGrandpre, Anal. Chem. 65 (1993) 331.
[10] P.K. Dasgupta, Z. Genfa, S.K. Poruthoor, S. Caldwell, S. Dong, S.Y. Liu, Anal. Chem. 70 (1998) 4661.
[11] L.Q. Guo, Q.Y. Ni, J.Q. Li, L. Zhang, X.C. Lin, Z.H. Xie, G. Chen, Talanta 74 (2008) 1032.
[12] Z.H. Wang, Y.H. Wang, W.J. Cai, S.Y. Liu, Talanta 57 (2002) 69.
[13] Z.A. Wang, W.J. Cai, Y.C. Wang, B.L. Upchurch, Mar. Chem. 84 (2003) 73.
[14] Z.H.A. Wang, X.W. Liu, R.H. Byrne, R. Wanninkhof, R.E. Bernstein, E.A. Kaltenbacher, J. Patten, Anal. Chim. Acta. 596 (2007) 23.
[15] Y. Nakano, H. Kimoto, S. Watanabe, K. Harada, Y.W. Watanabe, J. Oceanogr. 62 (2006) 71.
[16] Z. Lu, M. Dai, K. Xu, J. Chen, High Technol. Lett. (2003) 38, in Chinese.
[17] G.L. Robert-Baldo, M.J. Morris, R.M. Byrne, Anal. Chem. 57 (1985) 2564–2567.
[18] R.H. Byrne, J.A. Breland, Deep-Sea Res. 36 (1989) 803.
[19] F.J. Millero, Chemical Oceanography, CRC Press, 1996.
[20] K. Friis, A. Körtzinger, D.W.R. Wallace, Limnol. Oceanogr. 2 (2004) 126–136.
[21] W. Zhai, M. Dai, W.-J. Cai, Y. Wang, Z. Wang, Mar. Chem. 93 (2005) 21–32.

Talanta 76 (2008) 360–364

Contents lists available at ScienceDirect

Talanta

journal homepage: www.elsevier.com/locate/talanta

The detection of *Mycobacterium tuberculosis* in sputum sample based on a wireless magnetoelastic-sensing device

Pengfei Pang [a], Qingyun Cai [a,*], Shouzhuo Yao [a], Craig A. Grimes [b]

[a] *State Key Laboratory of Chemo/Biosensing and Chemometrics, Department of Chemistry and Chemical Engineering, Hunan University, Changsha 410082, PR China*
[b] *Department of Electrical Engineering and Department of Materials Science and Engineering, Pennsylvania State University, University Park, PA 16802, USA*

ARTICLE INFO

Article history:
Received 2 January 2008
Received in revised form 7 March 2008
Accepted 9 March 2008
Available online 20 March 2008

Keywords:
Magnetoelastic sensor
Mycobacterium tuberculosis (*M. TB*)
Sputum
Drug-resistance

ABSTRACT

This paper presents a real-time detection of *Mycobacterium tuberculosis* (*M. TB*) using a wireless magnetoelastic sensor. The sensor is fabricated by coating a magnetoelastic ribbon (Metglas 2826MB™) with a polyurethane protecting film. *M. TB* consumes the nutrients of a liquid culture medium in growing and reproducing process, which results in properties changes (viscosity, density, elasticity, ion concentration, etc.) of the culture medium, and consequently changes in the resonance frequency of the magnetoelastic sensor. Using the described technique *M. TB* is quantified and sensor response is proportional to logarithmic values of the *M. TB* concentration from 10^4 to 10^9 cells ml^{-1}, with a detection limit of 10^4 cells ml^{-1} at a noise level of ~10 Hz. The sensor can be used effectively for monitoring the bacterial growth and good results were obtained when used in sputum sample. The drug-resistance of isoniazid (INH) and rifampin (RFP) on *M. TB* growth in culture medium was evaluated based on this proposed method. The wireless nature of the presented device facilitates the aseptic operations.

1. Introduction

Tuberculosis (TB) is the world's second commonest cause of morbidity and mortality from infectious disease, after HIV/AIDS, and killing nearly 2 million people each year [1]. Furthermore, the global tuberculosis caseload appears to be growing slowly over past decade, and the most common clinical manifestation of tuberculosis is pulmonary disease. Therefore, rapid and accurate diagnosis of tuberculosis is very important for early and successful treatment.

Tuberculosis is difficult to control due to the time consumed for microbiological diagnosis [2,3]. Over the past decades, there are number of rapid molecular methods [4] that have been developed for the diagnosis of tuberculosis. The molecular diagnostic tests are focused on (i) detection of nucleic acids both DNA and RNA [5], which are specific to *Mycobacterium tuberculosis*, by amplification techniques such as polymerase chain reaction (PCR) [6] and (ii) detection of mutations in the genes which are associated with resistance to anti-tuberculosis drugs by sequencing [7] or nucleic acid hybridization [8]. PCR assays can be used directly on clinical specimens and are most reliable in smear-positive respiratory samples from patients with previously untreated tuberculosis. Widespread implementation of nucleic acid amplification assays has been limited by high cost and potential for poor performance under field conditions. Even if other methods are done, however, sputum smear (which provides a gauge of infectiousness) and culture (which is necessary for drug-susceptibility testing) are still the major backbone for laboratory diagnosis of tuberculosis. The definitive diagnosis of tuberculosis infection remains based on conventional sputum smear and culture for *Mycobacterium tuberculosis* in developing countries.

In recent years, magnetoelastic sensor technique [9] has attracted more attention due to its low cost and wireless excitation and detection. The magnetoelastic-sensing platform is based on amorphous, magnetostrictive alloy ribbons and has been used to determine different physical and chemical parameters including pressure [10], temperature [11], flow velocity [12], elasticity [13], liquid viscosity and density [14–16], and mass loading [17–19]. The phage- or antibody-based magnetoelastic sensors have been used for the detection of microorganism [20,21] or bacterial spores [22].

When a magnetoelastic sensor is immersed in a liquid, the shear wave that is created in the liquid due to the sensor vibration acts as a damping force to the oscillation of the sensor. The sensor resonant frequency shift upon immersion in liquid is given by [14,15]

$$\Delta f = -\frac{\sqrt{\pi f_0}}{2\pi\rho_s d}(\eta\rho_l)^{1/2}$$

* Corresponding author at: State Key Laboratory of Chemo/Biosensing and Chemometrics, Department of Chemistry and Chemical Engineering, B-107 Chemistry Department Building, Hunan University, Changsha 410082, PR China.
E-mail address: qycai0001@hnu.cn (Q. Cai).

0039-9140/$ – see front matter © 2008 Elsevier B.V. All rights reserved.
doi:10.1016/j.talanta.2008.03.008

where f_0 is the resonant frequency of the sensor in air, ρ_s and d are the density and thickness of the sensor, η and ρ_l are the density and viscosity of the liquid, respectively. The frequency shift is proportional to the square root of the liquid viscosity and density product. The response of the magnetoelastic sensor to liquid viscosity and density allows the device to function as a sensor to in situ, remote query monitoring liquid properties changes [23].

In this work, a magnetoelastic sensor is used for the direct (no immobilization with antibody or phage), real-time quantification of *M. TB* with a liquid medium. As bacteria consume the nutrients and produce the small molecular within a liquid medium its growth alters the liquid viscosity and density that, in turn, changes the resonant characteristics of the sensor. Owing to the need of an aseptic environment for microbial analysis, the remote query (wireless and passive) operating characteristics of the magnetoelastic sensors are of great utility.

2. Experimental

2.1. Materials

Sensors with the size of 20 mm × 6 mm × 28 μm were cut from a 6-mm wide 28-μm-thick ribbon of Metglas alloy 2826MB^{TM} ($Fe_{40}Ni_{38}Mo_4B_{18}$) purchased from Honeywell Corporation (Morristown, NJ, USA) at a material cost of approximately US$ 300 kg^{-1}. The resonant frequency of sensor in air is approximate 100 kHz. Bayhydrol 110, an anionic dispersion of an aliphatic polyester urethane resin in water/*N*-methyl-2-pyrrolidone solution (50%, w/v) was purchased from Bayer Corporation (Pittsburgh, PA, USA). Rifampicin (RFP) and isoniazid (INH) drug power for drug-resistance testing were purchased from Jiehui Biology Co. Ltd. (Changsha, China). All reagents and apparatus involved were sterilized at 121° for 20 min. All operations were done in a laminar flow cabinet. Double-distilled water was used throughout the experiment.○

2.2. Strain and culture medium

The attenuated *Mycobacterium tuberculosis H37Ra* (ATCC 25177) strain was obtained from Medical School of Central South University (Hunan, China).

The stock medium was the Sauton liquid medium prepared by adding 8.0 g sodium glutamate, 2.0 g citric acid, 60 ml glycerol, 0.5 g dipotassium hydrogen phosphate, 0.5 g magnesium sulfate, and 0.05 g ferric ammonium citrate in 1000 ml water and adjusting pH to 7.2 with ammonia liquid. *M. TB* was inoculated on Löwenstein–Jensen (L–J) solid culture for 6–8 weeks, and then inoculated into sterilized Sauton medium for 4 weeks at 37 °C. The stock suspension was then stored in a refrigerator at 4 °C. The concentration of stock suspension was about 2×10^{10} cfu ml^{-1} by conventional plate counting method. The suspension was serially diluted with water to prepare bacterial concentrations ranging from 10^4 to 10^9 cfu ml^{-1}.

The testing culture medium was Middlebrook 7H9 broth prepared by adding 0.5 g ammonium sulfate, 0.5 g sodium glutamate, 0.1 g sodium citrate, 1.0 mg pyridoxine, 0.5 mg biotin, 2.5 g disodium hydrogen phosphate, 1.0 g potassium dihydrogen phosphate, 0.04 g ferric ammonium citrate, 0.05 g magnesium sulfate, 0.5 mg calcium chloride, 1.0 mg zinc sulfate, 1.0 mg copper sulfate, and 2 ml glycerol in 1000 ml water. After sterilization, the Middlebrook 7H9 broth was aseptically supplemented with bovine serum albumin (BSA-V) 50 g l^{-1}, glucose 20 g l^{-1} and catalase 0.03 g l^{-1}.

2.3. Sensor platform and set-up

The sensor in size of 20 mm × 6 mm × 28 μm was ultrasonically cleaned in H_2O and acetone for 15 min, respectively, to remove any debris and organic film on sensor surface, and then dried in a stream of nitrogen. To protect the iron-rich magnetoelastic sensors from corrosion, 10 μl Bayhydrol 110 was applied to the cleaned sensors by coating. The polyurethane-coated sensors were dried in air and then heated at 140 °C for 2 h to form a robust membrane of about 1 μm-thick assuming the membrane density of 1 g cm^{-3}. And the corresponding frequency shift was about 1 kHz before and after coating. The sensors were vertically and freely placed in 2 ml vials which stood in coils connected to a magnetoelastic sensor reader. The resonant frequency was monitored by the magnetoelastic sensor reader, using a frequency counting technique of the pulse-wise excited sensor [24,25], the details and schematic illustrations of which can be found in our previous reports [18]. The difference of set-up in this work is that four coils (channels) were connected to the magnetoelastic sensor reader, which can be monitoring four sensor frequency shifts, simultaneously, and facilitate the monitoring of sensor frequency shifts resulted from the bacterial growth at different initial bacterial concentrations.

3. Results and discussion

3.1. The effect of concentration of culture medium (CM)

In this work the non-functionalized magnetoelastic sensor is responding to liquid properties changes due to the nutrient consumption by *M. TB*. The proliferation of *M. TB* decomposes the macromolecules into small molecules, such as ammonia, carbon dioxide, organic acid, etc., resulting in changes in medium properties. The properties of CM are determined by its composition and concentration.

Sensor response sensitivity was affected by the concentration of culture medium (CM). Standard 7H9 CM, diluted two times (0.5-time), and enriched two times (2-time) CM concentrations, were selected to investigate the sensor response sensitivity at same *M. TB* concentration, 1×10^6 cfu ml^{-1}, as shown in Fig. 1. It can be found from Fig. 1 that the sensor showed a better response at standard CM concentration than other two conditions. In 0.5-time CM, the

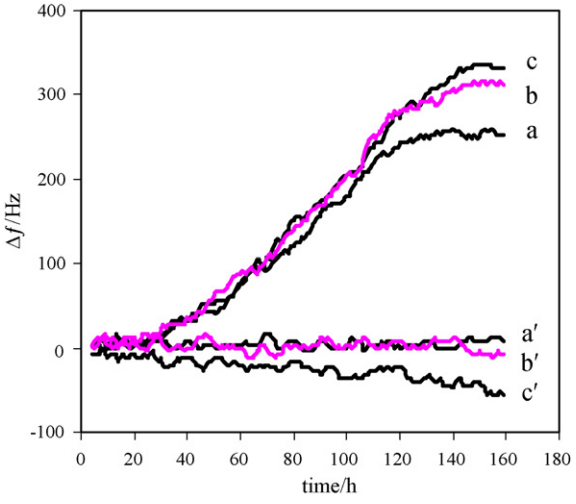

Fig. 1. The effect of CM concentrations on sensor frequency shifts: (a) 0.5-time CM, (b) standard CM and (c) 2-time CM concentrations. (a′)–(c′) are corresponding control curves. *M. TB* concentration, 1×10^6 cfu ml^{-1}.

sensor response was decreased ~16% since the nutrition is too poor to supply the *M. TB* normal growth. Although the sensor response was increased ~10% in 2-time CM, the control curve was not stable and the decreasing resulted from non-specific adsorption. So the concentration of standard 7H9 CM was selected for testing in this experiment.

3.2. Typical frequency response for M. TB

The typical frequency response curves of magnetoelastic sensors to *M. TB* at initial concentrations of 1×10^4, 1×10^6, and 1×10^9 cfu ml^{-1} are shown in Fig. 2, the sample without adding *M. TB* is used as a control. The response curves reflected the course of bacterial growth demonstrating three distinct stages: (i) vivification stage, where the *M. TB* initiated their physiological activity corresponding to a stable resonant frequency changes; (ii) active stage, *M. TB* reproduced exponentially corresponding a significant increase in resonant frequency; (iii) a stable or steady-state stage, where *M. TB* growth was restrained and was balanced by their dying.

The frequency shift caused by *M. TB* was positive and the response speed was slow compared to other microorganism [23]. The proliferation of *M. TB* during the active stage corresponds to nutrient consumption and the resultant production of small molecules, with the corresponding properties changes in culture medium such as viscosity, density, ion concentration, and elasticity. A change in medium conductivity was not observed during the culture course monitored using a pair of Pt electrodes, indicating that the culture medium produced negligible changes in the impedance of the culture medium. The viscosity change of the culture medium resulted from the incubation of *M. TB* was measured with a capillary viscometer which was calibrated using water–glycerin mixtures. A 160-h incubation of 1×10^7 cfu ml^{-1} *M. TB* the medium viscosity was decreased from 1.084 to 1.080 that was equivalent to a decrease in glycerin concentration from 2.26% to 1.42%, a 37% change in culture medium composition. Such a change, however, produced only ~80 Hz frequency shifts based on our measurements with glycerin–water solution. Owing to the absolute viscosity of the culture medium was close to the value of water, even medium composition changed significantly, the viscosity change was small. Therefore the viscosity change is not enough to result in the frequency increasing due to (i) the changes in density and elasticity can also contribute to the sensor response besides viscosity effect, and (ii) the interfacial viscosity properties can be significantly higher than that of the bulk solution as bacterial proliferation [14,26–28]. In the case of water, the interfacial viscosity can be a factor of 5.4 greater than that of the bulk liquid viscosity [26,27]. The slow response of sensor was ascribed to *M. TB* long generation time (14–16 h).

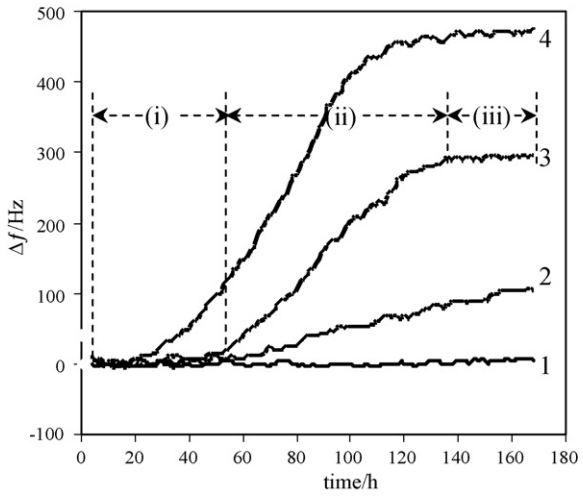

Fig. 2. Typical sensor response curves for (1) control, (2) 1×10^4 cfu ml^{-1}, (3) 1×10^6 cfu ml^{-1} and (4) 1×10^9 cfu ml^{-1} *M. TB*. The bacterial growth experiences three stages: (i) vivification, (ii) active and (iii) stable stages.

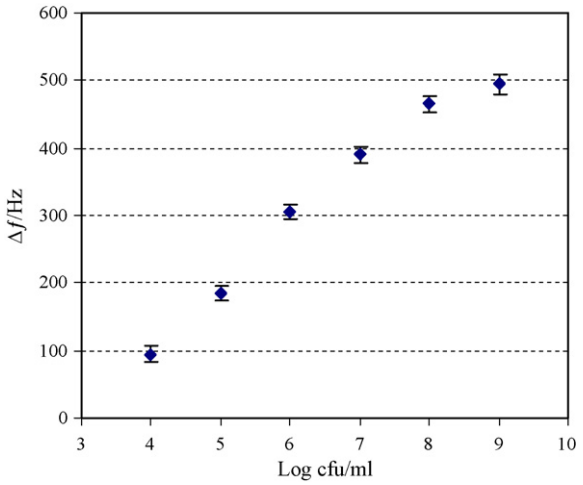

Fig. 3. Calibration curve of sensor frequency shifts plotted to logarithm values of *M. TB* concentration in the range of 10^4 to 10^9 cfu ml^{-1}.

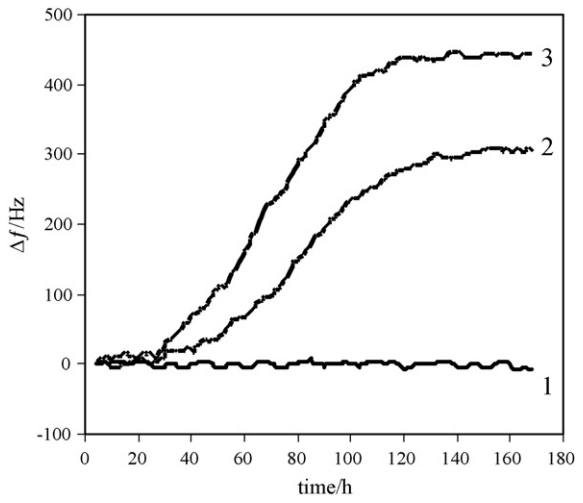

Fig. 4. The frequency response of a sensor in sputum sample in which different concentrations of *M. TB* was added: (1) control, (2) 1×10^6 cfu ml^{-1} and (3) 1×10^8 cfu ml^{-1}.

Table 1
The inhibition effects of INH and RFP on *M. TB* of 1×10^8 cfu ml^{-1}, shown in Fig. 5

Drug	C_{drug} (μg ml^{-1})	Δf (Hz)	RR (%)[a]	IE (%)[b]
Control	0	465 ± 20[c]	–	–
	0.2	380 ± 18	84 ± 4	18 ± 4
INH	2	200 ± 15	44 ± 3	57 ± 3
	20	0	0	100
	0.5	320 ± 16	71 ± 3	31 ± 3
RFP	5	140 ± 14	31 ± 3	70 ± 3
	50	0	0	100
INH + RFP	1 + 1	160 ± 15	36 ± 3	66 ± 3
	5 + 5	20 ± 10	4 ± 2	96 ± 2

[a] RR, relative response, $\Delta f_{drug}/\Delta f_0 \times 100\%$.
[b] IE, inhibition effects, defined as $(\Delta f_0 - \Delta f_{drug})/\Delta f_0 \times 100\%$.
[c] Mean ± S.D. ($n = 4$).

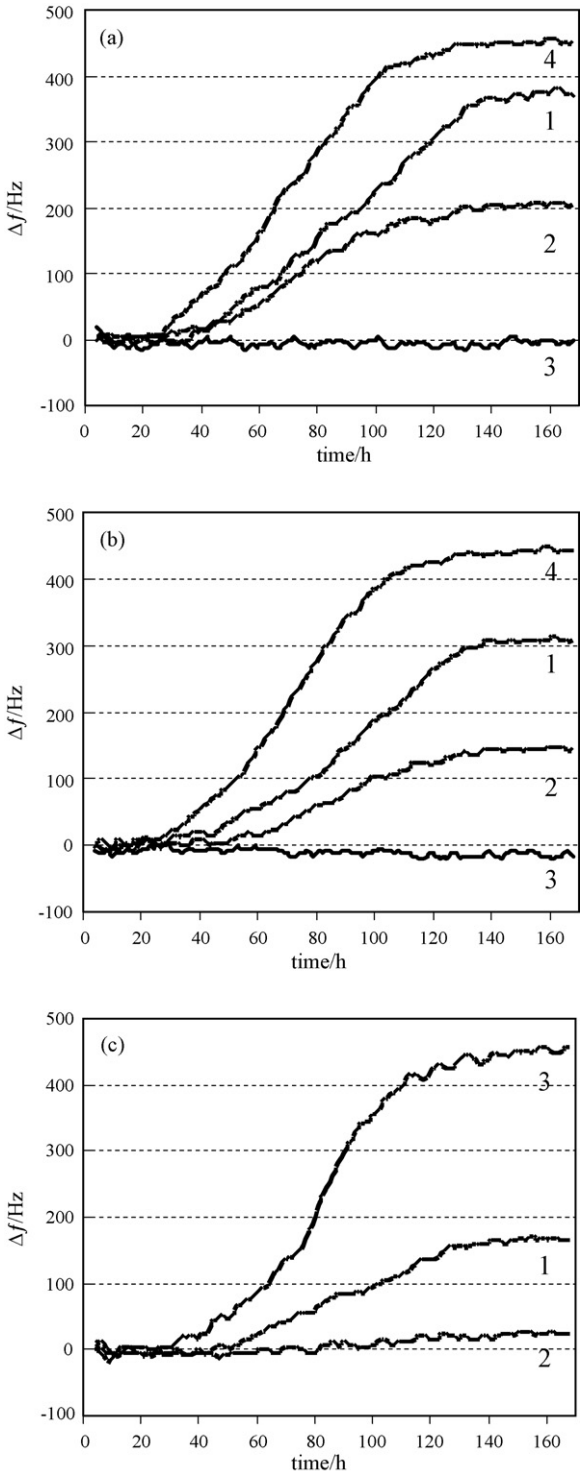

Fig. 5. Inhibition effects of drugs on *M. TB* of 1×10^8 cfu ml^{-1}: (a) (1) 0.2 μg ml^{-1}, (2) 2 μg ml^{-1}, (3) 20 μg ml^{-1} INH, and (4) control; (b) (1) 0.5 μg ml^{-1}, (2) 5 μg ml^{-1}, (3) 50 μg ml^{-1} RFP, and (4) control; (c) (1) 1 μg ml^{-1} INH + 1 μg ml^{-1} RFP, (2) 5 μg ml^{-1} INH + 5 μg ml^{-1} RFP, and (3) control.

As shown in Fig. 2, the sensor frequency shifts (Δf) between stages (iii) and (i) were increased with the increasing of the initial concentration of *M. TB* and showed a linear relationship with logarithm of the bacterial concentration in the range of 1×10^4 to 1×10^9 cfu ml^{-1} as shown in Fig. 3, with a detection limit of 1×10^4 cfu ml^{-1} at the noise of ~10 Hz. The sensor response repeatability was measured by running four parallel sensors at same bacterial concentration, with the R.S.D. < 10%. The *M. TB* can be identified and quantitative from its characteristic growth curve since different microorganism showed different response profiles to their culture medium [29,30].

3.3. Determination of M. TB in sputum sample

This method was used to determine *M. TB* concentration in sputum sample. The collected sample was transferred to the vial, treated with two times volume of NaOH (2%, w/v), stirred homogeneously, waited for 10 min, centrifuged, discarded the upper solution. The sediment was washed with sterilized PBS solution (pH 6.8) two times, centrifuged and discarded the upper solution. The treated sputum sample was dissolved in 7H9 culture medium and then spiked with different concentration of *M. TB* for testing.

Fig. 4 shows the sensors frequency shifts for different concentration of added *M. TB* in sputum sample, 1×10^6, 1×10^8 cfu ml^{-1}, and without *M. TB* used as a control, respectively. It can be seen from Figs. 2 and 4 that there were no obvious differences in the response curve between culture medium and sputum sample adding same amount *M. TB* concentration. The magnitude of sensor frequency shift (Δf) was almost same as well. Therefore, this proposed technique can potential use for other bacterial cultures if a suitable culture medium was selected, without complicated sensor fabrication and sample treatment.

3.4. Evaluation of the drug-resistance

Correct and rapid detection of drug-resistance facilitates the appropriate and timely delivery of anti-tuberculosis therapy and reduction of overall treatment cost. Rifampicin (RFP) and isoniazid (INH) were selected for assessing bacterial growth and antimicrobial susceptibility based on this culture methods. The cytotoxicity of RFP and INH to *M. TB* was evaluated by adding different concentrations of drugs to the culture medium containing 1×10^8 cfu ml^{-1} M. TB. Fig. 5 illustrates the sensor frequency shifts curves during incubating 1×10^8 cfu ml^{-1} *M. TB* in culture medium with different concentrations of (a) INH, (b) RFP, (c) INH-RFP, and without adding drugs used as a control for 7 days.

The *M. TB* growth characteristics in the presence of INH and RFP are similar to that of without drugs. Table 1 shows the inhibition effects of drugs on *M. TB* growth. The sensor frequency shifts (Δf) were decreased with increasing drugs concentrations since bacteria activity was inhibited. Sensor responses (Δf) decreased to 84% and 44% with adding 0.2 and 2 μg ml^{-1} INH, and to 71% and 31% with 0.5 and 5 μg ml^{-1} RFP, respectively. When INH and RFP concentrations were reached to 20 and 50 μg ml^{-1}, respectively, bacteria growth activity was inhibited completely (100%). For INH-RFP, Δf deceased to 36% by adding both 1 μg ml^{-1}, and bacteria growth activity was almost inhibited completely (96%) by adding only both 5 μg ml^{-1}, indicating that the inhibition effects of multi-drug (INH-RFP) is better than the same amount of INH or RFP, individually. These data demonstrate that the proposed method is an effective method for drug-resistance testing of *M. TB* for use in clinical microbiology/reference laboratory settings.

4. Conclusions

A remote query (wireless, passive) magnetoelastic sensor has been described for the real-time monitoring *M. TB* growth, with an initial detection limit of 1×10^4 cfu ml^{-1}. The drug-resistance of INH and RFP to *M. TB* was evaluated based on proposed technique. Our results indicated that the presented method can be readily, and cost effectively, used for detection of bacteria and evaluating of the

drug-resistance. Due to its low unit cost and remote query nature, the magnetoelastic sensor is potentially useful for the monitoring the environmental and food quality.

Acknowledgements

We are grateful for the financial support from the National Science Foundation of China under the grant 20475016 and 20775024, the Specialized Research Fund for the Doctoral Program of Higher Education under grant 20050532024. Craig A. Grimes gratefully acknowledges partial support of this work by the National Institutes of Health under grant no. 5 R21 EB006397-02.

References

[1] T.R. Frieden, T.R. Sterling, S.S. Munsiff, C.J. Watt, C. Dye, Lancet 362 (2003) 887.
[2] S.N. Cho, P.J. Brennan, Tuberculosis 87 (2007) S14.
[3] S.A. Watterson, F.A. Drobniewski, J. Clin. Pathol. 53 (2000) 727.
[4] J.F. Huggett, T.D. McHugh, A. Zumla, Int. J. Biochem. Cell B 35 (2003) 1407.
[5] N.W. Schluger, R. Condos, S. Lewis, W.N. Rom, Lancet 344 (1994) 232.
[6] L.E. Newport, O. Billington, W.J. Olver, S.H. Gillespie, J. Microbiol. Method 30 (1997) 251.
[7] X. Tang, S.L. Morris, J.J. Langone, L.E. Bockstahler, J. Microbiol. Method 63 (2005) 318.
[8] T.C. Victor, A.M. Jordaan, A. van Rie, G.D. van der Spuy, M. Richardson, P.D. van Helden, R. Warren, Tuber. Lung Dis. 79 (1999) 343.
[9] C.A. Grimes, C.S. Mungle, K.F. Zeng, M.K. Jain, W.R. Dreschel, M. Paulose, K.G. Ong, Sensors 2 (2002) 294.
[10] C.A. Grimes, D. Kouzoudis, Sensors Actuators A 84 (2000) 205.
[11] M.K. Jain, S. Schmidt, K.G. Ong, C. Mungle, C.A. Grimes, Smart Mater. Struct. 9 (2000) 502.
[12] D. Kouzoudis, C.A. Grimes, J. Appl. Phys. 87 (2000) 6301.
[13] S. Schmidt, C.A. Grimes, Sensors Actuators A 94 (2001) 189.
[14] P.G. Stoyanov, C.A. Grimes, Sensors Actuators A 80 (2000) 8.
[15] C.A. Grimes, K.G. Ong, K. Loiselle, P.G. Stoyanov, D. Kouzoudis, Y. Liu, C. Tong, F. Tefiku, Smart Mater. Struct. 8 (1999) 639.
[16] C.A. Grimes, D. Kouzoudis, C. Mungle, Rev. Sci. Instrum. 71 (2000) 3822.
[17] C.M. Ruan, K.F. Zeng, O.K. Varghese, C.A. Grimes, Anal. Chem. 75 (2003) 6494.
[18] Q.Y. Cai, K.F. Zeng, C.M. Ruan, T.A. Desai, C.A. Grimes, Anal. Chem. 76 (2004) 4038.
[19] R. Zhang, M.I. Tejedor-Tejedor, C.A. Grimes, M.A. Anderson, Anal. Chem. 79 (2007) 7078.
[20] R. Guntupalli, J. Hu, R.S. Lakshmanan, T.S. Huang, J.M. Barbaree, B.A. Chin, Biosens. Bioelectron. 22 (2007) 1474.
[21] R.S. Lakshmanan, R. Guntupalli, J. Hu, D.J. Kim, V.A. Petrenko, J.M. Barbaree, B.A. Chin, J. Microbiol. Method 71 (2007) 55.
[22] J.H. Wan, M.L. Johnson, R. Guntupalli, V.A. Petrenko, B.A. Chin, Sensors Actuators B 127 (2007) 559.
[23] P.F. Pang, S.J. Huang, Q.Y. Cai, S.Z. Yao, K.F. Zeng, C.A. Grimes, Biosens. Bioelectron. 23 (2007) 295.
[24] K.F. Zeng, K.G. Ong, C.M. Mungle, C.A. Grimes, Rev. Sci. Instrum. 73 (2002) 4375.
[25] K.F. Zeng, M. Paulose, K.G. Ong, C.A. Grimes, Sensors Actuators A 121 (2005) 66.
[26] K.H. Adlfinger, G. Pechel, Deut. Bunsenges. Phys. Chem. II 74 (1970) 347.
[27] K.H. Adlfinger, G. Pechel, Deut. Bunsenges. Phys. Chem. III 74 (1970) 351.
[28] M.K. Jain, C.A. Grimes, Sensors Actuators A 100 (2002) 63.
[29] K.G. Ong, J. Wang, R.S. Singh, L.G. Bachas, C.A. Grimes, Biosens. Bioelectron. 16 (2001) 305.
[30] F.J. He, J.W. Zhao, L.D. Zhang, X.L. Su, Talanta 59 (2003) 935.

Talanta 76 (2008) 314–319

Contents lists available at ScienceDirect

Talanta

journal homepage: www.elsevier.com/locate/talanta

A new evanescent wave ammonia sensor based on polyaniline composite

A. Airoudj[a,b], D. Debarnot[a,*], B. Bêche[c], F. Poncin-Epaillard[a]

[a] Laboratoire Polymères, Colloïdes, Interfaces, UMR 6120, Université du Maine, Avenue Olivier Messiaen, 72085 Le Mans, France
[b] Laboratoire d'Acoustique de l'Université du Maine, UMR-CNRS 6613, Avenue Olivier Messiaen, 72085 Le Mans, France
[c] Laboratoire PALMS-GMCM, UMR-CNRS 6627-6626, Institut de Physique de Rennes, 35042 Rennes, France

ARTICLE INFO

Article history:
Received 18 December 2007
Received in revised form 19 February 2008
Accepted 26 February 2008
Available online 18 March 2008

Keywords:
Ammonia detection
Polymer sensitive layer
Planar waveguide sensor
Light power variations

ABSTRACT

A single-mode TE_0–TM_0 optical planar waveguide ammonia sensor based on polyaniline/polymethyl methacrylate (PANI/PMMA) composite is designed and developed. The sensing properties of the photonic sensor to ammonia at room temperature are studied. A significant change is observed in the guided light output power of the sensor after it is exposed to ammonia gas. The metrological parameters (sensitivity, response time and recovery time) of the sensor are strongly influenced by the interaction length (length of sensing region). Compared with the conventional optical ammonia sensor based on absorption spectroscopy, the integrated optical sensor is more sensitive to ammonia.

1. Introduction

It is well known that ammonia, used in the production of explosives, fertilizers, and as an industrial coolant, is very dangerous for human health even at very low concentration [1]. Thus, it is necessary to detect such substance with sensitive and selective devices. Moreover, these devices must be simple, small, with the possibility of mass production leading then to low cost.

In recent years, a lot of attention has been focused on the use of conducting polymers as sensing layers for gas sensors, because of their easy fabrication, low cost, large variety in structure, and particularly, their sensitivity at room temperature, their selectivity and the versatility of their chemical and physical interactions with the detected species [2–4]. The gas adsorption onto this kind of layer leads to changes in the work function, the conductivity or the optical absorption coefficient. Polyaniline (PANI) is one of the most promising conducting polymers because of its good combination of easy synthesis through chemical or electrochemical methods, low cost, easy conductivity control and selectivity to ammonia [5–9]. The most important characteristic that makes PANI so interesting as sensitive layer is the variation of its electrical and optical properties when it is protonated/deprotonated by some chemical agents. In particular, the interaction between the conductive form of PANI, the emeraldine salt (ES), and the ammonia gas results in a decrease of the polaron density inside the band gap of the polymer. However, in order to improve mechanical properties and chemical stability of the sensitive layer, PANI/polymer composites have been elaborated [10–12]. PANI composite can be prepared by chemical or electrochemical polymerization of aniline in a solution of the polymeric matrix. Moreover, PANI can also be mixed with other polymers in the melt state. Different polymers can be used, such as polymethyl methacrylate (PMMA) [10,11,13], polyvinyl chloride [11], polystyrene [14], and epoxy resin [15] for different applications. However, for ammonia detection application, to our knowledge, only one study presents conventional optical sensors based on PANI/PMMA composite coatings using a null optical-transmittance bridge [13]. These gas sensors show low sensitivity due to low interaction length between sensitive material and light.

Since 1990, the use of the optical methods for gas detection has become more popular [16]. Their main advantages, compared to electrical methods, are their insensitivity to electro-magnetic interferences, fast response time, use in dangerous environment. Recently, several new approaches have been reported for the optical chemical sensor elaboration [17]. For example, one of such approaches is based on the guided waves or modes in optical waveguides, in particular of the orthogonally polarized TE_0 and TM_0 modes in planar waveguides. The principle of the planar waveguide sensor or integrated optical sensor is based on the optical intensity modulation induced within the single-mode waveguide. One of the ways to induce optical intensity modulation consists to change the refractive index of the cladding material. The field of guided mode penetrates as an evanescent wave on a small distance d_p into the cladding layer, which in sensor application, is the sensitive material covering the waveguide core. More precisely, the evanescent field

* Corresponding author. Tel.: +33 2 43 83 39 82; fax: +33 2 43 83 35 58.
E-mail address: Dominique.Debarnot@univ-lemans.fr (D. Debarnot).

0039-9140/$ – see front matter © 2008 Elsevier B.V. All rights reserved.
doi:10.1016/j.talanta.2008.02.045

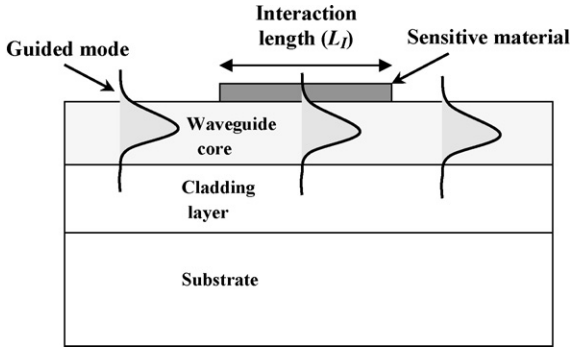

Fig. 1. Schematic illustration of the planar waveguide sensor.

decreases proportionally to $\exp(-x/d_p)$ where x is the distance from the core–cladding interface and d_p is the penetration depth defined as [17,18]:

$$d_p = \left(\frac{\lambda}{2\pi}\right)[n_{eff}^2 - n_c^2]^{1/2} \quad (1)$$

where n_{eff} is the effective refractive index of the guided mode, n_c is the refractive index of the cladding layer and λ is the wavelength.

The structure of the planar optical waveguide sensor is shown in Fig. 1. On a small section of the planar waveguide core, known as interaction length (L_I), the sensitive material was deposited. The basic planar waveguide sensor effect is caused by interaction of the evanescent wave of the guided mode with the sensitive material. The evanescent wave changes the refractive index distribution near the waveguide surface. Thus modification in the effective refractive index of the guided mode is induced. Moreover, the refractive index of the sensitive material is modified when the material is exposed to different vapors or gases, leading then to alteration of the transmitted light intensity.

In the present work, we designed and developed a new evanescent planar waveguide sensor for ammonia detection. The sensor is based on polyaniline/polymethyl methacrylate (PMMA) sensitive material deposited on a small section of single-mode planar glycidyl ether of bisphenol A waveguide. The glycidyl ether of bisphenol A (epoxy-based) polymer, which common name is SU-8, widely used as negative photoresist, has also been studied for micro-electro-optical-mechanical system (MEOMS) applications [19–22]. It is thermally stable and shows a good control of its thickness [21]. Due to its excellent optical transparency in the optical telecommunication wavelengths and its easy processing, SU-8 is a good candidate for the simple fabrication of optical waveguides [20,23,24]. The sensing properties of the integrated optical sensor to ammonia gas were investigated at room temperature. In order to compare the sensing properties of this new sensor to those of the conventional optical sensor, optical absorption method is used to study absorbance variations to ammonia of PANI/PMMA coatings.

2. Experimental

2.1. Elaboration of planar optical waveguides on SU-8 polymer

To obtain single-mode TE_0–TM_0 planar waveguides on SU-8 polymer (SU-8 as core, silicon dioxide layer as lower cladding layer and air as superstrate) with a good confinement of both optical modes, all optogeometric parameters of planar waveguides have to be defined. To this end, a numerical method based on semi-vectorial finite difference (SVFD) simulation is used [25]. The single-mode planar waveguide structure is realized on a (1 0 0) silicon substrate. At first, the lower cladding, the SiO_2 layer, is obtained by thermal oxidation of the silicon wafer yielding a thickness of 1.2 μm with an index value $n_{SiO_2} = 1.45$ at 980 nm. Then, the guiding layer of SU-8 polymer (MicroChem, USA) with $n_{SU-8} = 1.56$ at 980 nm, is deposited by spin coating yielding a thickness of 1 μm. After deposition, the SU-8 was dried according to different steps of temperature [20]. In such planar structures, the index of the superstrate above the SU-8 planar waveguide is the unity (air).

In order to illustrate the optical propagation of single-mode TE_0–TM_0 into the SU-8 planar waveguides, a specific microoptical bench was designed and allowed to realize effective injection (Fig. 2). This micro-optical injection bench consists of a laser source operating at 980 nm, fitted with an enhanced control in temperature (Opton Laser International) and associated with objectives and polarizers (Newport Inc.). Hence, the excitation of the fundamental mode of the structure is allowed, as the light is focused onto the cleaved input face of the planar waveguide. The extremity of this optical bench is fitted with a highly sensitive powermeter (Ophir Optronics Inc.—photodiode allowing a power range until 3 W with supplied filter, resolution 1 nW, response time 0.2 s, automatic background subtraction) and a video system with CCD camera to visualize and quantify the set up output signal (Jai Inc.—625 lines, 25 frames/s, resolution 752 × 582 pixels, sensitivity 0.02 Lux).

As an example, the photograph in Fig. 2 represents the single-mode TE_0 optical distribution, visualized by the video system, for a specific Si/SiO_2/SU-8 planar waveguide at wavelength $\lambda = 980$ nm.

2.2. Deposition of pure PANI-sensitive layers

PANI films were deposited following the method described in Refs. [26,27] with a slight modification. 1 mL of aniline monomer (99.8%, Aldrich) was added drop wise into 100 mL of 1 M hydrochloric acid (HCl, Aldrich) aqueous solution under stirring at room temperature. Then, SU-8 waveguide was immersed in the monomer solution. After the yellow drops of aniline dissolved completely in the acidic solution, 5 mL of 0.1 M ammonium persulfate ($(NH_4)_2S_2O_8$, Aldrich) aqueous solution was added into the monomer solution to initiate the polymerization of the aniline monomer. Polymerization begins immediately with an evident color change after 3–5 min, indicating polymer formation. The thickness of the green film deposited on the waveguide depends on the polymerization time and varies between 50 and 130 nm.

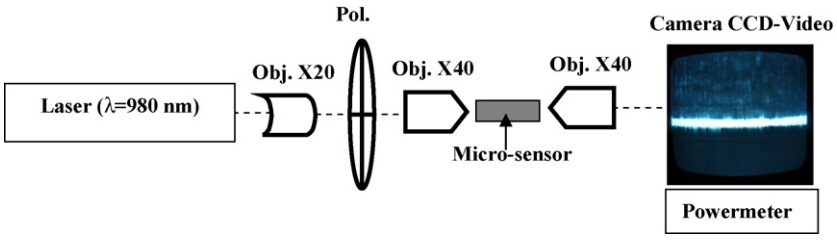

Fig. 2. Schematic diagram of the optical injection set-up for measuring the optical response of the sensor.

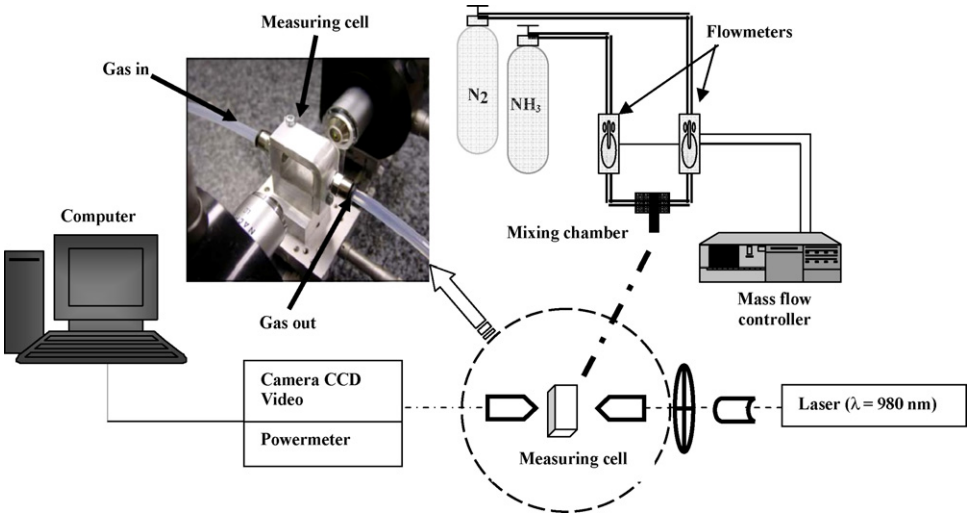

Fig. 3. Schematic diagram of the micro-optical bench set-up for the characterization of the gas photonic sensor and photograph of the measuring cell between two 40× microscope objectives.

The PANI-coated SU-8 substrate was then thoroughly washed with 0.1 M HCl aqueous solution, and immersed into another aniline solution (1 mL aniline dissolved in 100 mL of 1 M HCl) for 30 min. This step is necessary to completely convert the polypernigraniline form into the polyemeraldine salt (conducting form) [28]. Finally, the thin film was dried under airflow at room temperature.

2.3. Deposition of PANI/PMMA composite sensitive layers

The conducting PANI/PMMA composites were deposited on the surface of the SU-8 waveguide by the following method. PMMA (Aldrich) was first weighed and dissolved in chloroform (Aldrich). The aniline monomer was then added to the PMMA solution to get mixture of aniline and polymer; the concentration of aniline (in weight percent) was defined as the ratio of the weight of aniline to the total weight of aniline and matrix polymer in the solution. The resulting solution was spin-coated onto SU-8 planar waveguide to form Ani/PMMA film. In order to obtain the conducting PANI/PMMA composite, the sample was introduced into a chamber saturated with an oxidizing atmosphere consisting of 0.1 M $(NH_4)_2S_2O_8$ and 2 M HCl (2:1 in v/v). The polymerization of the aniline in the PMMA matrix can be observed by the color change of the film from transparent to light green. The polymerization time depends on the concentration of aniline in the PMMA matrix.

In order to compare the photonic sensor with the conventional optical sensor, the PANI composite was also deposited by spin-coating onto clean glass substrates. The thickness of PANI/PMMA composite films is about 1.5 μm for conventional sensor and 0.5 μm for photonic sensor.

2.4. Ammonia sensing system of the integrated optical sensor

The validation of our new ammonia photonic sensor is achieved by the characterization of the device, after having cleaved both input and output faces of the waveguide. To this end, the optical bench presented in Fig. 2, was used to measure the optical intensity of the photonic sensor exposed to ammonia gas. Fig. 3 shows the sensing system for the characterization of the gas sensor. A sealed measuring chamber was customized and associated to the optical bench. This cell is equipped with two optical glass windows (transparent and plane) allowing the light injection into the cleaved input face of the planar waveguide without perturbation. The optical bench and measuring cell are linked to the gas dilution system with mass flowmeters and a computer for data collection and analysis.

Nitrogen gas (99.99%, Air Liquide) was used as dilution gas. The concentration and flow of the ammonia gas and nitrogen gas were precisely controlled by two flowmeters, which were plugged in a mass flow controller (MFC). The concentration of NH_3 gas in the atmosphere of the measuring chamber was varied by mixing different flows of NH_3 gas and 500 sccm of N_2 gas. The concentration of NH_3 (ppm) was defined as the ratio of the flow rate of NH_3 gas to the total flow rate of NH_3 and N_2 gases. In this work, the ammonia concentration was varied between 92 ppm and 4618 ppm. The ammonia concentrations lower than 92 ppm were not measured due to experimental set-up limitation. After inserting the sensor inside the measuring chamber, a certain amount of dried ammonia gas, diluted in nitrogen gas, was introduced into the measuring chamber. The interaction between NH_3 gas and the PANI/PMMA film leads to output power variation. When the output power variation tends to a constant value depending on time, the NH_3 gas introduction was turned off and stream of pure N_2 gas was passed through the sensor to purge completely the NH_3 molecules in the measuring chamber and to regenerate the polyaniline sensor.

As an illustration, the zoom in Fig. 3 represents a relevant part of the optical bench showing the measuring cell between two 40× microscope objectives. During all the sensing experiments, the 980 nm laser was used as the incident beam. All experiments were performed at room temperature.

The sensitivity (S) was calculated as $(P - P_0)/P_0$ ratio, where P_0 is the initial transmitted light power of the sensor before ammonia exposition and P the transmitted light power when exposed to ammonia gas.

Finally, SU-8 waveguide (without sensitive layer) was placed in the measuring chamber. The injection of NH_3 into the chamber did not lead to any change of the transmitted light power, indicating that there is no interaction between the NH_3 gas and the SU-8 polymer.

2.5. Ammonia sensing system of the conventional optical sensor

The experimental set-up for the optical ammonia gas sensing system consists of a Carry 100 spectrophotometer in which the sealed measuring chamber has been inserted, a gas dilution system with mass flowmeters and a computer for data collection and analysis. The light source was a LS-1 tungsten halogen one powered

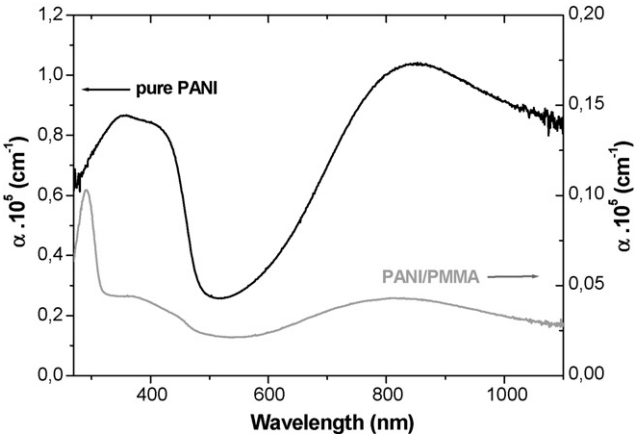

Fig. 4. Absorption coefficient curves of pure PANI and PANI/PMMA composite (10 wt.% of aniline) in the whole wavelength range (270–1100 nm).

with a 12 V dc. The monochromator allows selecting the working wavelength. The photodetector was used for signal detection. The spectrometer system was connected at a Compaq Progsignia 320 desktop computer. Windows-based Carry software was used for data acquisition and analysis. At the beginning of the experiment, the zero point of spectrometer was carried out without the PANI sensor.

For this sensor, the sensitivity (S) was calculated as $(A - A_0)/A_0$ ratio, where A_0 is the initial optical absorbance of the sensor before ammonia exposition and A the optical absorbance of the sensor when exposed to the ammonia gas. The wavelength of the light source used in the experiment was fixed at 632 nm.

3. Results and discussion

3.1. Preliminary study on the sensitive layer

In a first time, we wanted to design a photonic sensor based on pure PANI as sensitive material. To this end, we have deposited a pure PANI film by chemical way (Cf. Section 2) on a small section of the SU-8 waveguide. Different interaction lengths (0.5–5 mm) and PANI thicknesses (50–130 nm) have been tested. Then, the optical injection was realized into the Si/SiO_2/SU-8/pure PANI structure. No optical signal was detected at the exit of the sensor, whatever interaction lengths and PANI thicknesses are. It means that the propagation conditions in this structure are not favorable for light propagation.

In order to explain these results, we have determined the absorption coefficient of chemical PANI layer which has been found equal to about $10^5\ cm^{-1}$ at $\lambda = 980$ nm. This high absorption coefficient explains the absence of transmitted light at the exit of the structure; all the guided light being completely absorbed by the PANI layer. According to these results, it is thus necessary to revise the optical quality of the sensitive material deposited onto the SU-8 waveguide. The optical quality of the sensitive material can be improved by the dispersion of PANI into transparent polymer matrix. According to literature [10,13], PMMA appears to be the appropriate matrix since the addition of little amount of PANI into the PMMA matrix leads to a composite material sensitive to ammonia with good chemical stability. The absorption coefficient of the PANI/PMMA composite depends on the aniline concentration into the polymeric solution and on the wavelength. Fig. 4 shows the optical absorption coefficient (α) of the pure PANI and PANI/PMMA composite (10 wt.% of aniline) as a function of the wavelength. The PANI/PMMA spectrum shows four absorption bands: one at around 290 nm corresponding to C=O groups of the PMMA matrix, one at 350 nm associated to π–π^* transition of the PANI conjugated ring system and the two bands at ~420 nm and between 820 and 900 nm are assigned to PANI polaron transition [13,29]. The three last bands well confirm the presence of PANI under its conducting form (ES) in the composite [13,30]. The absorption coefficient of the PANI/PMMA composite is lower than that of pure PANI. At $\lambda = 980$ nm, the PANI/PMMA absorption coefficient is about $3 \times 10^3\ cm^{-1}$. After optical injection into the Si/SiO_2/SU-8/(PANI/PMMA) structure, the guided wave propagates effectively in the waveguide through the PANI/PMMA layer. So, PANI/PMMA layer presents suitable optical properties as sensitive layer of waveguide sensor.

3.2. Sensing properties of PANI/PMMA-based evanescent wave sensor

Fig. 5 shows the variation of the transmitted light power versus NH_3 concentration at $\lambda = 980$ nm for Si/SiO_2/SU-8/(PANI/PMMA) sensor. This figure shows that the transmitted light power increases after ammonia exposition. The variation of the output power after NH_3 introduction in the measuring cell can be attributed to the interaction between the NH_3 molecules and the reactive sites of PANI. When the ammonia injection is on, the charge carrier (polaron) distribution and the surface conductivity of the sensitive layer are modified and consequently, the complex refractive index of the sensitive layer is modified. The complex refractive index n ($n = n_r + in_i$) consists of a real part n_r and an imaginary part n_i. The real part n_r influences the light propagation constant through the waveguide and the imaginary part n_i is related to the light absorption. The principle of our planar optical waveguide sensor is mainly based on the change of the complex refractive index. The change of the complex refractive index of the sensitive layer (cladding layer) modifies the propagation conditions of the guiding structure which leads in this case to an increase in the total transmitted intensity of the SU-8 waveguide. When the equilibrium between the adsorbed ammonia at the PANI/PMMA surface and gas phase is obtained, no more variation of the refractive index is observed and then the output power is stabilized (tends to a constant value with time). Finally, when the injection of ammonia is turned off, the regeneration of the sensor starts. Then, the ammonia molecule desorption begins to restore the equilibrium of the concentrations and as a result, the output power of the sensor decreases. Indeed, the regeneration of

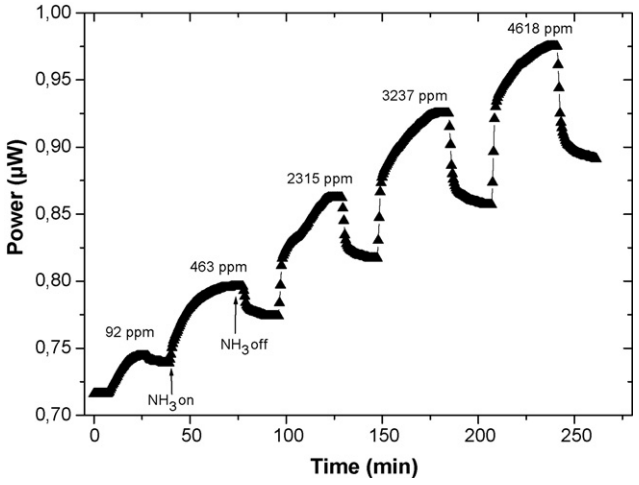

Fig. 5. Transmitted light power variations of Si/SiO_2/SU-8/(PANI/PMMA) sensor exposed to different NH_3 concentrations (PANI/PMMA film thickness: 500 nm, interaction length: 5 mm).

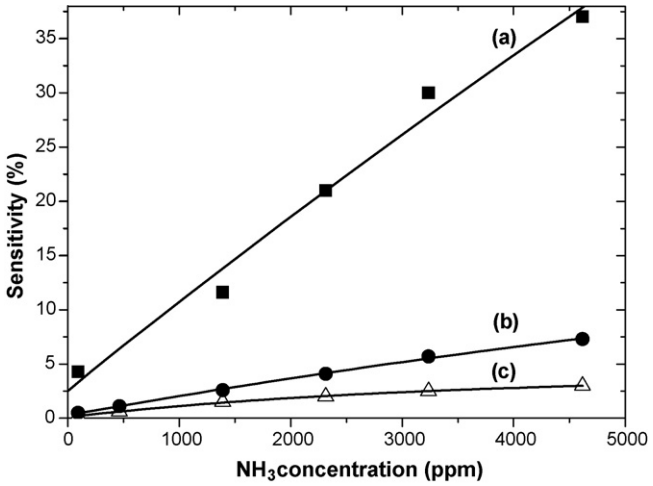

Fig. 6. Sensor sensitivity as a function of ammonia concentration: (a) planar waveguide sensor with $L_I = 5$ mm, (b) planar waveguide sensor with $L_I = 2$ mm, (c) conventional optical sensor.

the sensitive layer increases the charge carrier concentration, thus increasing absorption at $\lambda = 980$ nm.

In order to compare with conventional optical sensor, Fig. 6 presents the evolution of the sensitivity with ammonia concentration for the planar waveguide sensor and the conventional optical sensor. It appears that the conventional optical sensor is less sensitive to ammonia compared with the waveguide sensor. Indeed, the sensitivity at 4618 ppm of NH_3 is about 3% for the conventional sensor and 37% for the waveguide sensor ($L_I = 5$ mm). The higher sensitivity of the evanescent waveguide sensor can be due to the high interaction length between the evanescent wave and the sensitive material. Indeed, the interaction length for the waveguide sensor corresponds to the length of the sensitive layer deposited onto the waveguide surface (5 mm) whereas for the conventional optical sensor, it corresponds to the sensitive layer thickness (1.5 μm).

It is also noticed from Fig. 6 that the sensitivity of the sensors increases with the increase of ammonia concentration. One can rather note a nonlinear variation of the optical response of the sensors according to the NH_3 concentration. The non-linear sensing response to the detected gas is a well-known phenomenon in gas detection [31]. The non-linear behavior of the sensor response with ammonia concentration was also observed for several polyaniline ammonia sensors [13,32]. This behavior can be explained by the diffusion phenomenon of gas in the material. Then, the relationship between output power of the integrated sensor and ammonia concentration (N) can be expressed by the following equation [32]:

$$P = P_0 \exp[(\alpha N)^{\gamma}] \quad (2)$$

where P is the transmitted light power at ammonia concentration equals to N, P_0 is the initial transmitted light power at $N = 0$ ppm, α and γ are constants.

3.3. Response time and recovery time

The response time and recovery time of the planar waveguide sensor can be investigated from Fig. 5. As shown in this figure, the NH_3 desorption corresponding to the regeneration of the sensor is slowly reversible. Thus the NH_3 molecules are slowly desorbed from the PANI/PMMA sensitive layer. For example, after exposition to 4618 ppm of NH_3, the output power decreases of only 33% after 15 min of regeneration. In addition, the recovery time seems to increase with the increase of ammonia concentration. Based on the definition of response time determined as the time interval between 10% and 90% of the stationary value [33], the response time of the photonic sensor to ammonia is about 6 min at 4618 ppm. The low absorption and desorption processes of ammonia molecules could be due to the evanescent sensing mechanism. When the ammonia gas is introduced in the measuring cell, the ammonia molecules diffuse into the inner sensing layer where the evanescent field can interact with the polarons. Thus, this type of sensors usually has relatively longer response and recovery times. Similar results concerning response and recovery times were also reported for optical sensors based on the evanescent field sensing method [28,34–37]. However, the improvement of these metrological parameters can be obtained through optimization of the thickness of sensitive film. When the sensitive material thickness is close to the penetration depth d_p of the evanescent wave expressed in Eq. (1), the variation of the polaron density, due to the interaction between ammonia molecules and polaron lattice, immediately occurs at the surface where the evanescent wave of the guided mode interacts with the polarons. Thus the sensor has the optimized response and recovery times. However, if the cladding thickness decreases further, the sensor sensitivity will decrease due to the low interaction of evanescent field with the polarons of the sensitive material. In addition, the gas absorption and desorption processes can be accelerated by increasing the temperature [9,38]. On the other hand, PANI can be fully regenerated by exposition to the doping agents such as hydrochloric acid at room temperature [32].

Fig. 7 presents the optical absorbance variation of the PANI/PMMA-based conventional optical sensor exposed to different NH_3 concentrations. The comparison with the waveguide sensor shows that desorption of the NH_3 molecules is faster for the conventional optical sensor whatever the ammonia concentration is. Indeed, the recovery time of the conventional sensor after exposition to 4618 ppm of NH_3 is equal to 9 min. Moreover, the recovery time of the conventional sensor depends also on the ammonia concentration: it increases with the ammonia concentration. Concerning the response time, it is lower for the conventional sensor, with a value of about 1.5 min at 4618 ppm of ammonia. The faster response and recovery times for the conventional sensor could be due to the sensing mechanism. Indeed, the interaction between ammonia molecules and polarons immediately occurs at the sensitive layer surface where the polarons absorb the light in direct contact with the PANI/PMMA surface.

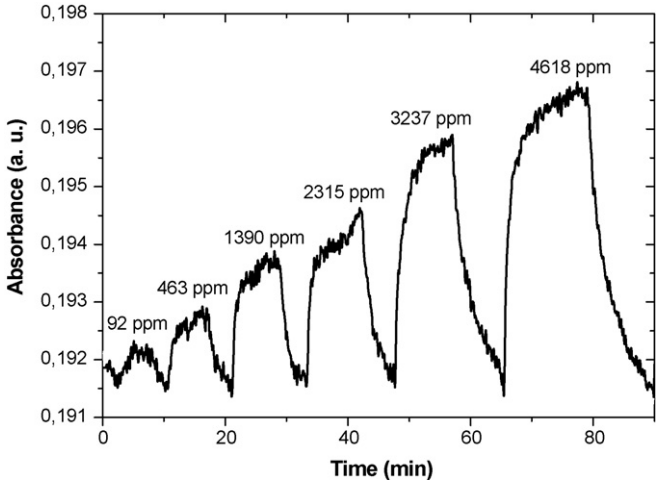

Fig. 7. Optical absorbance variations of PANI/PMMA composite coating exposed to different NH_3 concentrations. (aniline concentration: 10 wt.%, film thickness: 1.5 μm).

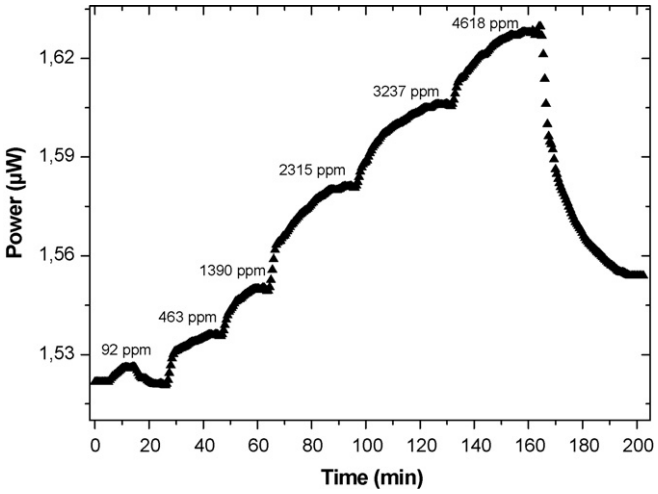

Fig. 8. Transmitted light power variations of $Si/SiO_2/SU-8/(PANI/PMMA)$ sensor exposed to different NH_3 concentrations. (PANI/PMMA film thickness: 500 nm, interaction length: 2 mm).

3.4. Influence of the interaction length

In order to study the effect of the interaction length (L_I) between the sensitive layer of the waveguide sensor and the evanescent field of the guided mode on the metrological parameters (sensitivity, response time, recovery time), two interaction lengths have been studied: 5 mm (Fig. 5) and 2 mm (Fig. 8). First of all, the initial output power of the sensor with $L_I = 2$ mm is higher than that of the sensor with $L_I = 5$ mm. Therefore, the decrease in the interaction length decreases the absorption of the evanescent field by the PANI/PMMA sensitive layer. Moreover, the desorption of NH_3 molecules is faster for the sensor with $L_I = 2$ mm. For example, after exposition to 4618 ppm of NH_3, the output power decreases of about 64% after 15 min of regeneration (33% for $L_I = 5$ mm). The same observations can be done for the response time which is about 4 min at 4618 ppm of ammonia, for the sensor with $L_I = 2$ mm (6 min for $L_I = 5$ mm). These results show that the decrease in the interaction length seems to improve the response and recovery times.

As shown in Fig. 6, the interaction length significantly affects the sensitivity of this type of sensor. Indeed, the increase in the interaction length considerably increases the sensitivity of the sensor. As an example, the sensitivity at 4618 ppm of NH_3 is about 37% for $L_I = 5$ mm and 8% for $L_I = 2$ mm. This phenomenon is due to the higher concentration of NH_3 adsorption sites (polarons) when the interaction length increases.

4. Conclusion

We have designed and developed a new evanescent wave ammonia sensor based on polyaniline/polymethyl methacrylate (PANI/PMMA) composite. For this type of sensor, it was found that the sensitive material must be transparent (low absorption coefficient). The sensing properties of the integrated optical sensor to ammonia at room temperature were investigated. The variation of the complex refractive index of the PANI/PMMA composite, due to the interaction between the ammonia molecules and the polaron lattice of the polyaniline, influences the total transmitted intensity of the SU-8 waveguide. The metrological parameters of the sensor depend on the interaction length between sensitive layer and evanescent field of the guided mode. Moreover, these experimental results have demonstrated that the evanescent wave sensor is more sensitive compared to the conventional optical sensor based on the optical absorption spectroscopy method. Besides, results have demonstrated that the use of the polyaniline composite as sensitive material presents a potential innovation to elaborate integrated optical sensor (IOS) for ammonia detection at ambient temperature. Such IOS could be fully implemented with polymer material resulting in a small, low cost, and practical device.

Acknowledgement

The authors want to thank CER Micro-Cap-Ouest for financial support.

References

[1] C. Malins, A. Doyle, B.D. MacCrainth, F. Kvasnik, M. Landl, P. Simon, L. Kalvoda, R. Lukas, K. Pufler, I. Babusik, J. Environ. Monitor. 1 (5) (1999) 417–422.
[2] H. Liu, J. Kameoka, D.A. Czaplewski, H.G. Craighead, Nano Lett. 4 (2004) 671–675.
[3] K. Xu, L. Zhu, A. Zhang, G. Jiang, H. Tang, J. Electroanal. Chem. 608 (2007) 141–147.
[4] K. Xu, L. Zhu, J. Li, H. Tang, Electrochim. Acta 52 (2006) 723–727.
[5] Y. Cao, P. Smith, A.J. Heeger, Synth. Met. 48 (1992) 91–97.
[6] A.A. Pud, Synth. Met. 66 (1994) 1–18.
[7] D. Nicolas-Debarnot, F. Poncin-Epaillard, Anal. Chim. Acta 475 (2003) 1–15.
[8] V.V. Chabukswar, S. Pethkar, A.A. Athawale, Sens. Actuators B 77 (2001) 657–663.
[9] A.L. Kukla, Y.M. Shirshov, S.A. Piletsky, Sens. Actuators B 37 (1996) 135–140.
[10] J.L. Cadenas, H. Hu, Sol. Energy Mater. Sol. Cells 55 (1998) 105–112.
[11] M. Wan, M. Li, J. Li, Z. Liu, Thin Solid Films 259 (1995) 188–193.
[12] T. Thanpitcha, A. Sirivat, A.M. Jamieson, R. Rujiravanit, Carbohydr. Polym. 64 (2006) 560–568.
[13] M.E. Nicho, M. Trejo, A. Garcia-Valenzuela, J.M. Saniger, J. Palacios, H. Hu, Sens. Actuators B 76 (2001) 18–24.
[14] M. Matsuguchi, A. Okamoto, Y. Sakai, Sens. Actuators B 94 (2003) 46–52.
[15] X. Yang, T. Zhaoa, Y. Yu, Y. Wei, Synth. Met. 142 (2004) 57–61.
[16] M. Ando, T. Kobayashi, M. Haruta, Sens. Actuators B 24–25 (1995) 851–853.
[17] W. Lukosz, Sens. Actuators B 29 (1995) 37–50.
[18] K. Li, J. Meichsner, J. Phys. D: Appl. Phys. 34 (2001) 1318–1325.
[19] N. Pelletier, B. Bêche, E. Gaviot, L. Camberlein, N. Grossard, F. Polet, J. Zyss, IEEE Sens. J. 6 (2006) 565–570.
[20] B. Bêche, N. Pelletier, E. Gaviot, J. Zyss, Opt. Commun. 230 (2004) 91–94.
[21] J.S. Kim, J.W. Kang, J.J. Kim, Jpn. J. Appl. Phys. 42 (2003) 1277–1279.
[22] J. Zhang, K.L. Tan, H.Q. Gong, Polym. Test. 20 (2001) 693–701.
[23] B. Bêche, P. Papet, D. Debarnot, E. Gaviot, J. Zyss, F. Poncin-Epaillard, Opt. Commun. 246 (1–3) (2005) 25–28.
[24] N. Pelletier, B. Bêche, N. Tahani, J. Zyss, L. Camberlein, E. Gaviot, Sens. Actuators A 135 (2007) 179–184.
[25] B. Bêche, J.F. Jouin, N. Grossard, E. Gaviot, E. Toussaere, J. Zyss, Sens. Actuators A 114-1 (2004) 59–64.
[26] W. Zheng, Y. Min, A.G. MacDiarmid, M. Angelopoulos, Y.-H. Liao, A.J. Epstein, Synth. Met. 84 (1997) 63–64.
[27] I. Sapurina, A. Riede, J. Stejskal, Synth. Met. 123 (2001) 503–507.
[28] J. Yuan, M.A. El-Sherif, A.G. MacDiarmid, W.E. Jones Jr., SPIE Proc. vol. 4205 (2001) 170–179.
[29] P.L.B. Araujo, E.S. Araujo, R.F.S. Santos, A.P.L. Pacheco, Microelectron. J. 36 (2005) 1055–1057.
[30] S.K. Dhawan, D. Kumar, M.K. Ram, S. Chandra, D.C. Trivedi, Sens. Actuators B 40 (1997) 99–103.
[31] M.J. Madou, S.R. Morrison, Chemical Sensing with Solid State Devices, Academic Press, Boston, 1989.
[32] Z. Jin, Y. Su, Y. Duan, Sens. Actuators B 72 (2001) 75–79.
[33] A. D'Amico, C. Di Natale, A. Taroni, Proceedings of the First European School on Sensors (ESS'94), Castro Marina, Lee, Italy, September 12–17, 1994, pp. 3–13.
[34] E. Scorsone, S. Christie, K.C. Persaud, P. Simon, F. Kvasnik, Sens. Actuators B 90 (1–3) (2003) 37–45.
[35] P.S. Kumar, P.G. Vallabhan, V.P.N. Nampoori, P. Radhakrishnan, Proceeding of the Society of Photo-Optical Instrumentation Engineers (SPIE), Parts 1 and 2, vol. 5280, 2004, pp. 617–621.
[36] E. Scorsone, S. Christie, K. Persaud, P. Simon, F. Kvasnik, Proceeding of The Society of Photo-Optical Instrumentation Engineers (SPIE), Parts 1 and 2, vol. 4829, 2003, pp. 978–979.
[37] S. Christie, E. Scorsone, K. Persaud, F. Kvasnik, Sens. Actuators B 90 (1–3) (2003) 163–169.
[38] W. Cao, Y. Duan, Sens. Actuators B 110 (2005) 252–259.

Talanta 76 (2008) 389–394

Contents lists available at ScienceDirect

Talanta

journal homepage: www.elsevier.com/locate/talanta

Liquid chromatography coupled to tandem mass spectrometry for the analysis of acrylamide in typical Spanish products☆

E. Bermudo, E. Moyano, L. Puignou*, M.T. Galceran

Departament de Química Analítica, Universitat de Barcelona, Martí i Franquès 1-11, 08028 Barcelona, Spain

ARTICLE INFO

Article history:
Received 21 November 2007
Received in revised form 3 March 2008
Accepted 12 March 2008
Available online 21 March 2008

Keywords:
Acrylamide
Food
Valine
LC–MS/MS
TOF

ABSTRACT

This paper describes the use of liquid chromatography coupled to tandem mass spectrometry for the determination of acrylamide in several typical foods produced and consumed in Spain. Christmas sweets, olives, traditionally made potato crisps, pastry products, sweet fritters ("*churros*") and one of Spain's most famous dishes, Spanish omelette, were selected. Using the mass spectra information provided by an ion trap analyzer in combination with the accurate mass measurements from time-of-flight (TOF) spectrometry a co-extractive interference present in some potato products was identified as valine. A porous graphitic carbon column, which enabled the co-extractive and acrylamide to be separated, and ion trap or triple quadrupole analyzers, depending on the acrylamide concentration, were used to determine this genotoxic compound in foodstuffs. The highest values were found in potato products, sweet fritters, Christmas sweets and pastry products, with values ranging between 70 and 2000 μg/g. Spanish omelette presented relatively low levels, similar to those obtained for dried fruits.

1. Introduction

Acrylamide (AA), the monomer from which polyacrylamides are synthesized, is a known neurotoxic compound [1]. Moreover, it has been classified as "probably carcinogenic to humans" by the International Agency for Research on Cancer (IARC) on the basis of sufficient evidence for carcinogenicity in experimental animals and mechanistic considerations [2]. This compound has been found in various heat-processed starch-rich foodstuffs at levels as high as milligrams per kilogram [3–7]. Due to the potential genotoxicity of acrylamide a joint effort has been undertaken by national food authorities and the food industry in order to gain a better understanding of the mechanisms of acrylamide formation; the Maillard reaction of asparagine with reducing sugars is considered the most probable mechanism [8–12], although other routes may also be possible [13,14].

Several analytical methods have been developed in recent years to determine acrylamide in different food products [15–18]. Currently, the two main approaches used are gas chromatography with mass spectrometric detection (LC–MS) and high-performance liquid chromatography coupled to tandem mass spectrometry (LC–MS/MS), using labelled acrylamide as internal standard.

Most of the papers dealing with LC–MS use bromination as the derivatisation procedure to reduce acrylamide polarity [15–18], although direct GC analysis with polar columns such as Carbowax and positive chemical ionisation (PCI) has also been proposed [19–21]. The use of LC–MS/MS-based methods offers the advantage of being able to analyze acrylamide without derivatisation, thus simplifying both the sample treatment and mass spectrometric detection procedures and shortening analysis time. The ionisation source commonly used in LC–MS is electrospray (ESI) [15–18], while a triple quadrupole (QqQ) is mainly employed as mass analyzer; however, several authors have recently shown the applicability of ion trap analyzers [20,22,23].

Through the application of these analytical methods and in order to evaluate exposure and/or risk assessment, extensive amounts of data on AA levels in food have been collected. To date, several thousand data have been obtained and these have been incorporated into databases such as that of the Institute for Reference Materials and Measurements (IRMM) of the European Commission [24] and the FDA [25].

In the Spanish diet, processed carbohydrate-rich foods such as potatoes, crisp bread, pastry products and other sweets are commonly present. These foodstuffs are prepared in multiple ways (such as frying and baking), under conditions that favour acrylamide formation. There are published reports of the AA levels

☆ This publication reflects the authors' views and not necessarily those of the EC. The information in this document is provided as is and no guarantee or warranty is given that the information is fit for any particular purpose. The user thereof uses the information at its sole risk and liability.

* Corresponding author. Fax: +34 93 402 12 33.
E-mail address: lluis.puignou@ub.edu (L. Puignou).

0039-9140/$ – see front matter © 2008 Elsevier B.V. All rights reserved.
doi:10.1016/j.talanta.2008.03.011

found in some of these products consumed in Spain [26,27]. In this paper, in order to complete the survey of AA levels in typical Spanish products, a number of new Spanish foodstuffs that include typical breakfast products such as sweet fritters (*churros*), several Christmas sweets such as "turrones", "polvorones" and rolled wafers, or dishes such as Spanish omelette were analyzed for the first time. For this purpose, a previously published LC–MS/MS method [26] was used. Finally, both ion trap and time-of-flight mass analyzers were combined in order to characterize unequivocally an interfering co-extractive that was particularly present in potato-derived products.

2. Materials and methods

2.1. Reagents and consumables

Acrylamide (>99%), L-asparagine (>99.5%), L-valine (>99.5%), zinc acetate dihydrate and potassium hexacyanoferrate were provided by Fluka (Buchs SG, Switzerland). 2,3,3-D_3-acrylamide (D_3-AA) (98%) was purchased from Cambridge Isotope Laboratories (Andover, MA, USA) and β-alaninamide hydrochloride from TCI Europe (Belgium). Methanol, acetonitrile (analytical grade), dimethylamine (DMA), diethylamine (TEA) and triethylamine (TEA) were provided by Merck (Darmstadt, Germany). Stock solutions of acrylamide (1 mg/mL) and [D_3]-acrylamide (1 mg/mL) were prepared in Milli-Q water and stored at 4 °C for a maximum of 4 weeks. Carrez I solution was prepared by dissolving 10.6 g of potassium hexacyanoferrate in 100 mL of water, and Carrez II solution by dissolving 24 g of zinc acetate in 100 mL of water.

The solid phase extraction (SPE) cartridges Strata-X-C (200 mg, 6 mL) and ENV+ (200 mg, 3 mL) were obtained from Phenomenex (Torrance, USA) and IST (Hengoed, Mid-Glamorgan, UK), respectively. Nylon and nitrocellulose syringe filters of 0.45 μm were purchased from Teknokroma (Barcelona, Spain). Water purified with an Elix/Milli-Q water purification system (Millipore, Bedford, MA, USA) was used.

2.2. LC–MS instrumentation and working conditions

The chromatographic separation of acrylamide was carried out in a porous graphitic carbon column (Hypercarb, 3 μm, 100 mm × 2.1 mm) (Thermo Electron, San Jose, CA, USA). Isocratic elution with a mixture of methanol:water (5:95) at a flow rate of 0.2 mL/min was applied. The sample volume injected was 10 μL.

For quantitative purposes, an ion trap (LCQ, Thermo Finnigan, San Jose, CA, USA) coupled to an Alliance 2690 liquid chromatograph (Waters, Milford, MA, USA) or a triple quadrupole (API 3000, Applied Biosystems, Foster City, CA, USA) coupled to an Agilent 1100 LC liquid chromatography system (Agilent Technologies, USA), both with an APCI source, were used depending on the AA concentration. The LCQ working conditions for monitoring positive ions were: discharge current, 5 μA; sheath gas, 50 a.u.; auxiliary gas, 10 a.u.; heat capillary temperature, 150 °C; vaporizer temperature, 250 °C; capillary voltage, 11 V; and tube lens offset, 11 V. Data acquisition was performed in product ion scan. MS/MS parameters were: normalized collision energy, 33%; isolation width *m*/*z* 1.5; activation time 30 ms; activation *Q*, 0.45. Chromatograms were acquired in the centroid mode using an injection RF value of 0.35, a maximum injection time of 50 ms and 6 microscans for each data point.

The optimal ionization source working parameters for the API 3000 instrument were: nebulizer gas, 10 a.u.; curtain gas, 12 a.u.; vaporizer temperature, 250 °C; nebulizer current, 3 μA; declustering potential, 30 V. The data acquisition was performed using selected reaction monitoring (SRM), using the protonated molecular ion $[M+H]^+$ as precursor ion; the collision cell offset voltage applied was 25 V and the collision gas pressure 4 a.u.

For both instruments, *m*/*z* 55, corresponding to the loss of NH_3 from the protonated acrylamide (*m*/*z* 72), and *m*/*z* 54, assigned as $[C_3H_2NH_2]^+$, were used respectively for quantitative and confirmative purposes. The same fragmentation pattern shifted in mass according to D_3 was employed for D_3-AA, the internal standard used for isotopic dilution quantification.

For those studies that required high resolution and mass accuracy measurement a time-of-flight (API-TOF, Applied Biosystems, Foster City, CA, USA) equipped with an APCI source coupled to a Jasco PU-2089 LC liquid chromatography system (Jasco, Tokyo, Japan) was used. In order to increase mass accuracy the API-TOF instrument was calibrated every day by using a mixture of DMA (*m*/*z*: 46.0656), DEA (*m*/*z*: 74.0969), TEA (*m*/*z*: 102.1282), AA (*m*/*z*: 72.0449) and D_3-AA (*m*/*z*: 75.0634) in methanol–water (50:50) at a concentration level of 10 mg/L. The optimal ionization source working parameters were: nebulizer gas, 6 L/min; curtain gas, 2 L/min; vaporizer temperature, 250 °C; nebulizer current, 5 μA. Continuum mode TOF mass spectra were recorded using single MS mode from *m*/*z* 35 to 100 with a duty cycle of 1.0 s. D_3-AA (internal standard reference mass) was used for lock mass correction. An *m*/*z* width of ±0.05 was selected for mass chromatograms to improve selectivity and to decrease chemical noise.

2.3. Sample preparation and quantitative analysis

Several food samples comprising traditionally made potato crisps, typical pastry products such as crispy sweet bread (*coca de vidre*), puff pastry, oil-based sweet bread (*torta de aceite*), Christmas sweets such as "turrones", "polvorones" and rolled wafers, the breakfast product sweet fritters (*churros*), some dried fruits, olives and one of Spain's most popular dishes, the Spanish omelette, were analyzed. Sub-samples of 2 g, previously ground and homogenized, were weighed into 15 mL centrifuge tubes and 93 μL of D_3-AA (10 mg/L) and 10 mL water were added. Each tube was shaken for 1 h and then centrifuged at 4000 rpm for 30 min. The clear supernatant was transferred into a centrifuge tube and treated with Carrez I and II solutions (500 μL of each) to precipitate the co-extractives. Following centrifugation at 4000 rpm for 3 min, an aliquot of the aqueous solution was filtered and 3 mL was loaded onto a Strata-X-C SPE cartridge. The column was then eluted with 3 mL of water and the eluent was loaded onto a ENV+ SPE cartridge and eluted with 1 mL of MeOH:H_2O (60:40). Finally, the extract was evaporated to 400 μL under a stream of nitrogen filtered through a 0.45 μm nylon filter and transferred into amber glass vials for LC–MS analysis.

Isotope dilution employing D_3-AA as the labelled compound was used to quantify the acrylamide in food products.

3. Results and discussion

In a first step a previously developed LC–MS/MS method [26] that employs a C_{18} reversed phase column was used for the analysis of AA in several Spanish food products. However, in some potato samples an intense peak appeared near acrylamide, making it difficult to quantify this compound, especially at low concentrations. As an example, Fig. 1A shows the chromatogram corresponding to a potato crisp sample where the intensity of the interfering peak is particularly important. Tandem mass spectrometry could not solve this problem because both acrylamide and the interfering compound have the same precursor and product ions (Fig. 1C). In order to identify the interfering peak, different strategies based on the use of the ion trap and time-of-flight instruments were performed.

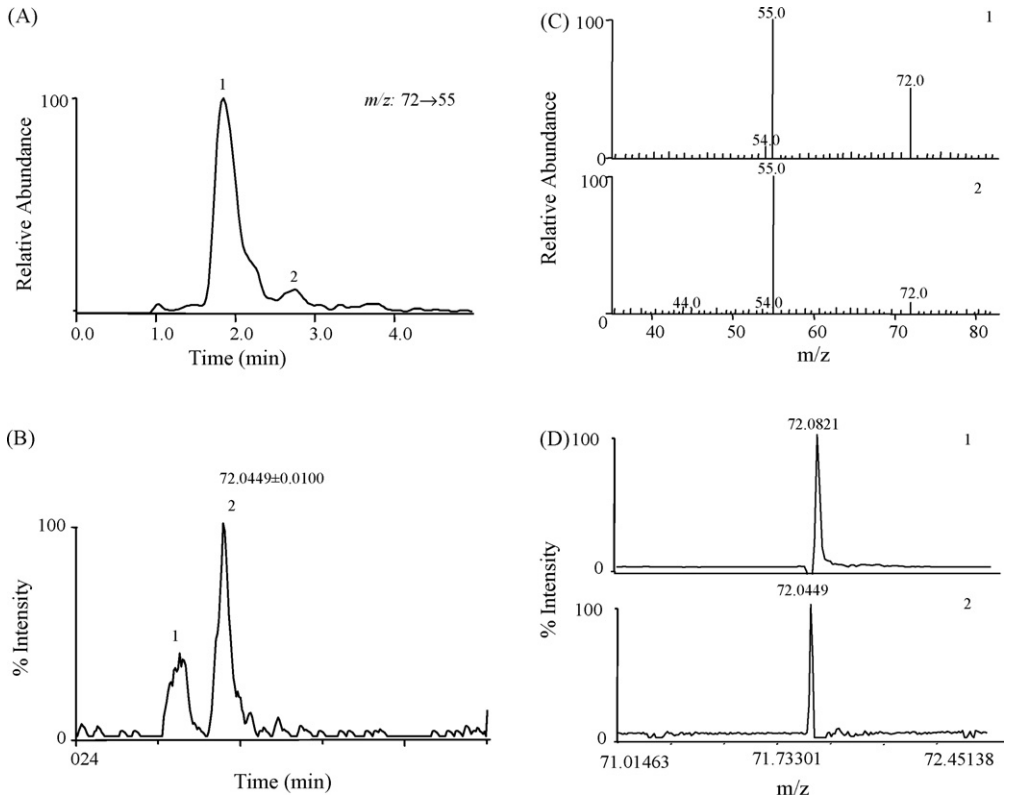

Fig. 1. LC–APCI–MS chromatograms and spectra of a potato crisp sample obtained using: (A) linear trap, product ion scan; (B) time-of-flight, MS acquisition mode; (C) linear trap, product ion spectra; (D) time-of-flight, spectra. (1) Interfering peak and (2) acrylamide.

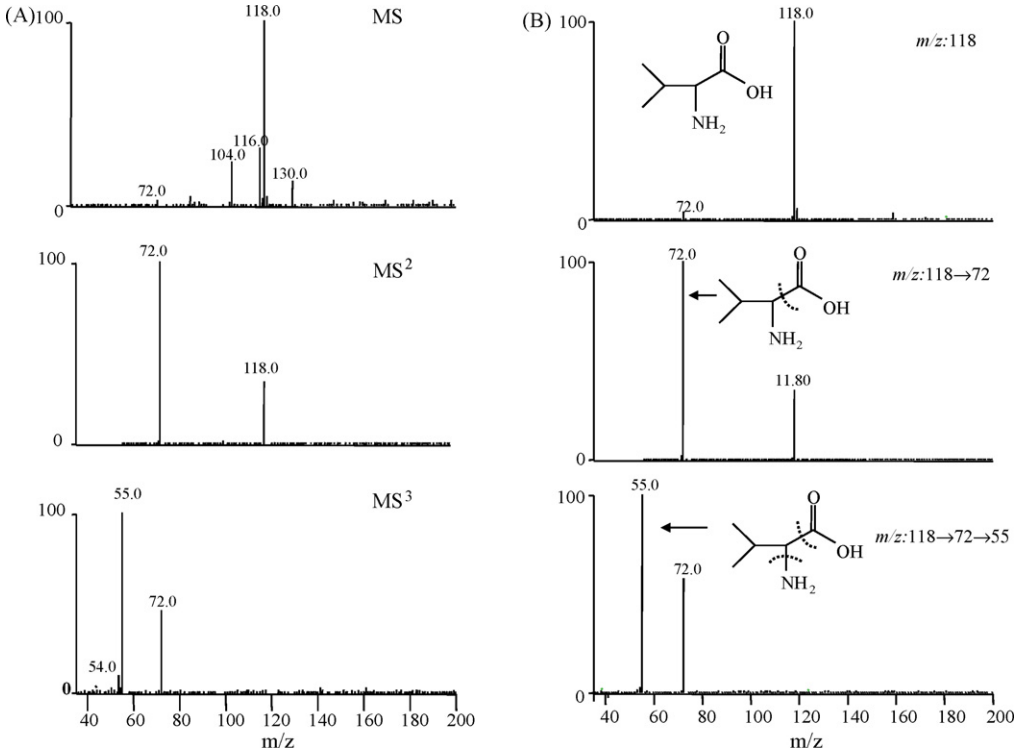

Fig. 2. MS, MS^2 (m/z: 118) and MS^3 (m/z: 72) spectra obtained in an ion trap instrument under acrylamide conditions of: (A) interfering peak of potato crisp sample and (B) valine pure standard.

Firstly, with the aim of characterising this unknown compound, full scan mass spectrum (m/z 50–300) was obtained using the ion trap instrument. As can be seen in Fig. 2A the base peak corresponded to m/z 118, although a small peak at m/z 72 also appeared in the spectrum. This small m/z 72 peak could be due to in-source fragmentation from some of the ions appearing at higher m/z values.

Nevertheless, only the MS/MS spectrum of ion m/z 118 gave a fragment at m/z 72. Finally, the MS^3 spectrum of this last ion showed a product ion at m/z 55. The ions at m/z 72 and m/z 55 corresponded to the acrylamide precursor and product ions, respectively. This could indicate that the ion at m/z 118 corresponded to the interference. Although, initially, several acrylamide precursors such as asparagine or 3-aminopropionamide were considered as the source of the potential interference, these were discarded because of their different precursor and product ions, m/z 133 and 87 for asparagine and m/z 89 and 72 for 3-aminopropionamide. Other amino acids, such as valine, that are present in potato samples were thus considered. MS, MS/MS and MS^3 spectra of the pure valine standard were obtained and compared with those of the interference. As can be seen in Fig. 2, the ions and the relative abundances of the fragments for both the interference and the valine standard are in agreement, thus identifying valine as the unknown compound. In spite of the low in-source fragmentation of the m/z 118 ion under acrylamide fragmentation conditions, a high signal corresponding to valine is obtained in potato crisp samples. This is due to the high concentration of this compound (near 1%) in this type of food.

In addition, to confirm unambiguously the identity of this unknown compound a time-of-flight mass analyzer was used. In this case, the spectrum of the interfering peak between m/z 50 and 200 was obtained, showing an ion at m/z 118.0849 as base peak and a small peak corresponding to m/z 72.0821, with associated errors lower than 0.2 and 0.8 mDa, respectively. These values indicated that valine was the potential interfering compound. In conclusion, valine was unequivocally identified as the interfering compound, with more than four identification points fulfilling the requirements of EU regulations [28] aimed to evaluate the presence of certain substances and residues in live animals and animal products (Council Directive 96/23/EC) [29]. This confirms the information provided by Senyuva et al. [30], who tentatively identified this compound in certain foodstuffs using retention time and single MS spectra (two identification points).

The problem of valine interference in the analysis of acrylamide in potato samples was partially solved by using the TOF analyzer with a narrow m/z window. As an example, Fig. 1B shows the LC–APCI–MS (TOF) chromatogram obtained using a window width of ±0.01 Da, while Fig. 1D shows the spectra obtained for both chromatographic peaks. Although a small peak due to the interference also appeared in the API-TOF chromatogram (Fig. 1B), this instrument provided enough resolution to reduce the intensity of the interfering peak, thus enabling quantification of acrylamide. However, relatively high detection limits were obtained (30 ng/g) when API-TOF was used, and so, in order to have a method for analysing AA at low concentration levels and which was free of interferences, we improved the separation between the co-extractive and AA. This was done by using a porous graphitic carbon column recommended by several authors [6,7,23,27,31–34] for the analysis of AA in food samples. Different mobile phases and temperatures were assayed in order to obtain a good separation and, as a compromise, a mobile phase of MeOH:H_2O (5:95) at a flow rate of 0.2 mL/min and at room temperature was selected. To check performance of this method, quality parameters such as limit of detection, limit of quantification, run-to-run precision and linearity range were established.

Limit of detection (LOD) and limit of quantification (LOQ) were determined as the amount of analyte that produced a signal-to-noise ratio of 3:1 and 10:1, respectively. These values were calculated analyzing three replicates of a blank sample (bread crumb) spiked with acrylamide at low levels. Limits of detection and limits of quantification were determined for both the ion trap and triple quadrupole instruments, the results being 15 and 45 ng/g for ion trap, and 2 and 6 ng/g for triple quadrupole, respectively. This produced a fivefold improvement over the results obtained previously with a C_{18} reversed phase column [26].

To determine precision, six replicates of a blank sample (bread crumb) spiked at both low (~LOQ) and medium (300 ng/g) concentration levels were analyzed obtaining RSD values lower than 15 and 13% for ion trap and triple quadrupole instruments, respec-

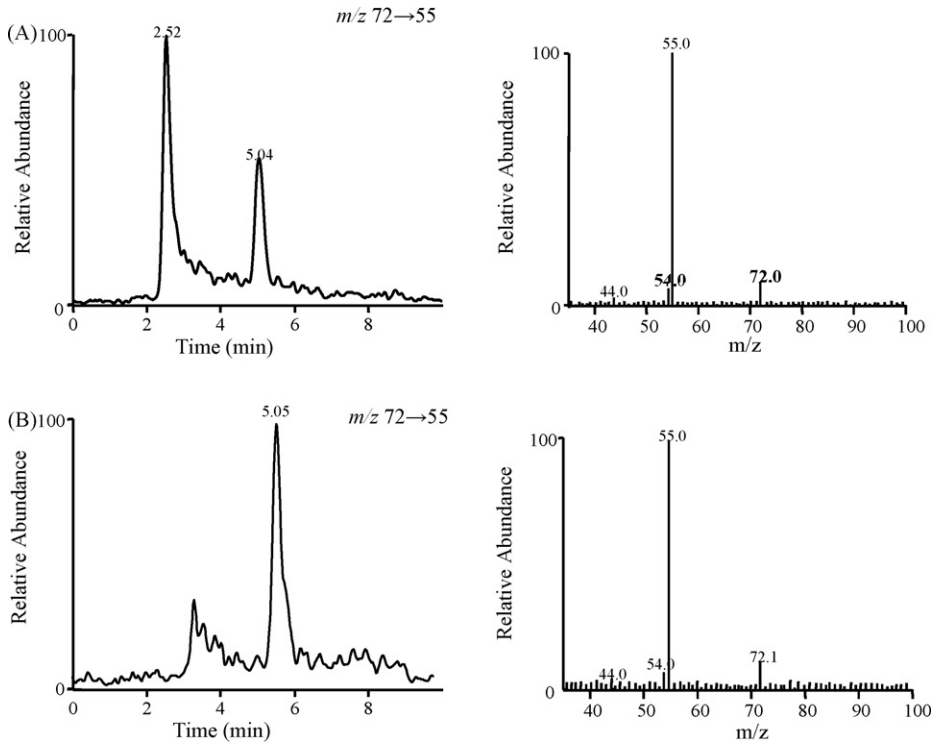

Fig. 3. Chromatograms of acrylamide in two food samples obtained using an ion trap in product ion scan. (A) Potato crisps and (B) black olives. Chromatographic conditions included in Section 2.

Table 1
Food analysis using an ion trap and a triple quadrupole mass analyzer ($n = 3$)

Sample	Product type	Concentration (μg/kg)	
		Average ($n = 3$)	R.S.D. (%)
Artisan potato crisps 1	Potato crisps	799	8
Artisan potato crisps 2	Potato crisps	2055	2
Artisan potato crisps 3	Potato crisps	264	4
Spanish omelette	Egg-based product	135	5
Rolled wafers	Christmas sweet	529	7
Chocolate rolled wafers	Christmas sweet	299	9
Chocolate Turrón	Christmas sweet	100	4
Turrón Jijona	Christmas sweet	124	12
Turrón Alicante	Christmas sweet	162	14
Turrón Guirlache	Christmas sweet	140	1
Yoke Turrón	Christmas sweet	74	3
Polvorones	Christmas sweet	81	7
Sweet fritters 1	Breakfast product	134	4
Sweet fritters 2	Breakfast product	151	2
Sweet fritters 3	Breakfast product	430	12
Sweet fritters 4	Breakfast product	328	7
Oil-based sweet bread	Pastry products	113	2
Puff pastry	Pastry products	40	12
Crispy sweet bread	Pastry product	248	1
Caramelized almonds	Dried fruits	51	2
Cashews	Dried fruits	36	4
Toasted chickpeas	Dried fruits	35	5
Fried broad beans	Dried fruits	58	13
Canned black olives 1	Olives	316	4
Canned black olives 2	Olives	177	4
Bottled black olives 1	Olives	127	2
Bottled black olives 2	Olives	124	4
Bulk black olives	Olives	N.D.	–
Canned green olives 1	Olives	N.D.	–
Canned green olives 2 (“*manzanilla*”)	Olives	93	6
Bottled green olives 1 (“*gordal*”)	Olives	N.D.	–
Bottled green olives 2 (“*arbequinas*”)	Olives	64	5
Bottled green olives 3 (“*gazpacha*”)	Olives	44	10

N.D.: non-detected.

tively. Good linearity (r^2 0.999) was obtained in the concentration range of the samples analyzed (from 6 ng/g to 4 μg/kg for the triple quadrupole). In addition, and as can be seen in Fig. 3, an important improvement in terms of separation was observed when Hypercarb was used, especially in potato crisp samples (Fig. 3A). Moreover, there was also a decrease in ion suppression, which improved the signal-to-noise ratio. Therefore, this column was selected for the analyses of several typical foodstuffs produced and consumed in Spain. Table 1 shows the concentration and standard deviation values obtained for each sample.

Potato crisps prepared by traditional methods presented values between 300 and 2000 ng/g, the highest values corresponding to the most cooked products. These values are similar to those found in the EU database [24], where the minimum and maximum levels range between 5 and 4653 ng/g. The Spanish omelette, the traditional recipe for which is based on eggs, potato and onion fried with olive oil, presented values of 135 ng/g. This result was relatively low in comparison with the potato products analyzed [24,25].

For Christmas sweets such as “turrones” or “polvorones”, both of which are based on toasted almonds cooked with sugar and other ingredients such as eggs, potato or chocolate, concentrations between 80 and 150 ng/g were obtained. These low levels, taking into account the presence of considerable precursor concentrations, are probably due to the moderate cooking temperature used in the production of these foods. For rolled wafers, another typical Christmas sweet, higher levels were obtained (300–530 ng/g), most likely as a result of the more drastic cooking conditions. Caramelized almonds prepared with heated sugar and other dried fruits showed low values between 35 and 59 ng/g.

The level of acrylamide detected in foods such as sweet fritters, a typical Spanish food based on wheat flour pastry that is deep fried in olive oil, ranged from 134 to 430 ng/g. For typical pastry products such as puff pastry, oil-based sweet bread and crispy sweet bread, concentrations in the range 40–300 ng/g were observed, the highest level corresponding to crispy sweet bread, probably due to the important degree of browning involved.

Olives are a Mediterranean product that can be consumed either as olive oil or directly after a previous treatment. Different analyses performed by the FDA showed that black olives presented relatively high contents of acrylamide [25]. For this reason, and taking into account the high consumption of this product in Spain, some olive samples were analyzed. Levels of acrylamide in different olive varieties such as “*manzanilla*”, “*gordal*”, “*arbequinas*” or “*gazpacha*” were determined, as shown in Table 1. Black olives presented the highest levels (between 316 and 124 ng/g), although the values were generally lower than those given in the FDA data base [25]. Moreover, it should be pointed out that acrylamide was not found in bulk black olives, and this could be due to the different industrial treatment of bulk and canned products. In addition, the level of maturation seems to bear some relationship to acrylamide content, since green olives always showed lower amounts of AA than did black ones.

4. Conclusions

In this paper, several typical foods produced and consumed in Spain were analyzed using LC–MS/MS in order to determine acrylamide levels. The use of accurate mass measurements on a time-of-flight instrument and the multistep mass spectra obtained in an ion trap (MS^2, MS^3) unambiguously showed that an interfer-

ing co-extracted compound present in some potato products was valine. Acrylamide concentrations in the different foodstuffs analyzed ranged between 35 and 2000 ng/g, with RSD values lower than 12%. The lowest values were obtained for green olives and dried fruits, whereas traditionally made potato crisps presented the highest values (264–2000 ng/g). In comparison with other potato-containing products, levels for Spanish omelette were relatively low (135 ng/g) showing that it can be considered as a healthier product as regards its acrylamide content.

Acknowledgements

This work has been supported by the European Commission, Priority 5 on Food Quality and Safety (Contract no. FOOD-CT-2003-506820 Specific Targeted Project), 'Heat-generated food toxicants—identification, characterisation and risk minimisation'. The authors also wish to thank the *Serveis Científico-Tècnics* of the UB for their technical support. Finally, we are grateful to Anna Martínez for her help with the analysis of some food samples.

References

[1] P.M. LeQuesne, Specific environmental neurotoxins, in: P.S. Spencer, H.H Schaumburg, Williams, Wilkins (Eds.), Experimental and Clinical Neurotoxicology, 1st ed., Baltimore, MD, 1980, pp. 309–325.
[2] International Agency for Research on Cancer (IARC), Monographs on the Evaluation of Carcinogen Risk to Humans, vol. 60, Lyon, France, 1994, pp. 389–433.
[3] E. Tareke, P. Rydberg, P. Karlssson, S. Eriksson, M. Törnqvist, Chem. Res. Toxicol. 13 (2000) 517.
[4] E. Tareke, P. Rydberg, P. Karlsson, S. Eriksson, M. Törnqvist, J. Agric. Food Chem. 50 (2002) 4998.
[5] SNFA, Press release from Livsmedelsverket. Swedish National Food Administration, Uppsala, 2002, www.slv.se.
[6] J. Rosén, K.E. Hellenäs, Analyst 127 (2002) 880.
[7] A. Becalski, B.P.-Y. Lau, D. Lewis, S.W. Seaman, J. Agric. Food Chem. 51 (2003) 802.
[8] V.A. Yaylayan, R.H. Stadler, J. AOAC Int. 88 (2005) 262.
[9] T.M. Amrein, S. Bachmann, A. Noti, M. Biedermann, M. Ferraz Barbosa, S. Biedermann-Brem, K. Grob, A. Keiser, P. Realini, F. Escher, R. Amadó, J. Agric. Food Chem. 51 (2003) 5556.
[10] D.A. Vattem, K. Shetty, Innovative Food Sci. Emerg. Technol. 4 (2003) 331.
[11] V.A. Yaylayan, A. Wnorowski, C. Perez Locas, J. Agric. Food Chem. 51 (2003) 1753.
[12] D.S. Mottram, B.L. Wedzicha, A.T. Dodson, Nature 419 (2002) 448.
[13] A. Yasuhara, Y. Tanaka, M. Hengel, T. Shibamoto, J. Agric. Food Chem. 51 (2003) 3999.
[14] C. Gertz, S. Klostermann, Eur. J. Lipid Sci. Technol. 104 (2002) 762.
[15] L. Castle, S. Eriksson, J. AOAC Int. 88 (2005) 274.
[16] R. Weisshaar, Eur. J. Lipid Sci. Technol. 106 (2004) 786.
[17] T. Wenzl, M.B. De la Calle, E. Anklam, Food Addit. Contam. 20 (2003) 885.
[18] Y. Zhang, G. Zhang, Y. Zhang, J. Chromatogr. A 1075 (2005) 1.
[19] M. Biedermann, S. Biedermann-Brem, A. Noti, K. Grob, P. Egli, H. Mändli, Mittr. Lebensm. Hyg. 93 (2002) 638.
[20] M. Jezussek, P. Schieberle, J. Agric. Food Chem. 51 (2003) 7866.
[21] L. Dunovská, T. Cajka, J. Hajslová, K. Holadová, Anal. Chim. Acta 578 (2006) 234.
[22] K. Tsutsumiuchi, M. Hibino, M. Kambe, K. Oishi, M. Okada, J. Miwa, H. Taniguchi, Shokuhin Eiseigaku Zasshi 45 (2004) 95.
[23] A. Claus, G.H. Weisz, D.R. Kammerer, R. Carle, A. Schieber, Mol. Nutr. Res. 49 (2005) 918.
[24] http://www.irmm.jrc.be/html/activities/acrylamide/database.htm, last revision: June, 2006.
[25] http://www.cfsan.fda.gov/~dms/acrydata.html, last revision: October, 2006.
[26] E. Bermudo, E. Moyano, L. Puignou, M.T. Galceran, Anal. Chim. Acta 559 (2006) 207.
[27] V. Yusà, G. Quintás, O. Pardo, P. Martí, A. Pastor, Food Addit. Contam. 23 (2006) 237.
[28] Implementing Council Directive 96/23/EC/02. Off. J. Eur. Commun. L 221/8 (August 17) (2002).
[29] Implementing Council Directive 96/23/EC. Off. J. Eur. Commun. L 125 (May 23) (1996).
[30] H.Z. Senyuva, V. Gökmen, Food Chem. 97 (2006) 539.
[31] P.C. Aguas, M.J. Fitzhenry, G. Giannikopoulos, P. Varelis, Anal. Bioanal. Chem. 385 (2006) 1526.
[32] T. Wenzl, L. Karasek, J. Rosén, K.E. Hellenäs, C. Crews, L. Castle, E. Anklam, J. Chromatogr. A 1132 (2006) 211.
[33] N.J. Nielsen, K. Granby, R.V. Hedegaard, L.H. Skibsted, Anal. Chim. Acta 557 (2006) 211.
[34] P. Föhgelberg, J. Rosén, K.E. Hellenäs, L. Abramsson-Zetterberg, Food Chem. Toxicol. 43 (2005) 951.

Talanta 76 (2008) 288–294

Contents lists available at ScienceDirect

Talanta

journal homepage: www.elsevier.com/locate/talanta

Electrochemical behavior of colchicine using graphite-based screen-printed electrodes

E. Bodoki[a,*], Serena Laschi[b], Ilaria Palchetti[b], R. Săndulescu[a], M. Mascini[b]

[a] *Faculty of Pharmacy, "Iuliu Haţieganu" University of Medicine and Pharmacy, Emil Isac Street 13, RO-400023 Cluj-Napoca, Romania*
[b] *Chemistry Department, University of Florence, 3, Via della Lastruccia, 50019 Sesto Fiorentino, FI, Italy*

ARTICLE INFO

Article history:
Received 14 November 2007
Received in revised form 19 February 2008
Accepted 26 February 2008
Available online 14 March 2008

Keywords:
Colchicine
Screen-printed electrodes
Differential pulse voltammetry
Method validation

ABSTRACT

Miniaturized electrochemical graphite based sensor for the analysis of colchicine, along with its detailed construction was described.

The electrochemical behavior of colchicine, both by cyclic and differential pulse voltammetry was investigated, showing an irreversible reduction and oxidation mechanism. The effect of several different electrochemical mediators was studied in order to decrease the oxidation potential of colchicine, but none of them showed a favorable electron transfer between the alkaloid and the electrode's surface. The influences of different biomolecules (calf thymus DNA, bovine serum albumin and β-tubulin) over colchicine's electrochemical behavior were also presented.

For quantitative determinations the anodic differential pulse voltammetric method in H_3PO_4/$HClO_4$ 0.01 M (pH 2.05) was selected, evaluating one of the oxidation peaks of colchicine at +970 mV versus Ag pseudo-reference. The electrochemical scanning parameters were optimized by an experimental design using response surface modelling. The method was validated according to ICH guidelines in the concentration range 85–1200 ng mL^{-1} (R^2 = 0.9966, n = 7) colchicine in terms of linearity, accuracy, limits of detection (LOD) (41 ng mL^{-1}), limits of quantification (LOQ) and fidelity and it was successfully applied to the determination of colchicine in tablets, without the interference of the excipients.

The studied method showed the same sensitivity as the more complex HPLC procedure and micellar electrokinetic chromatography with spectrophotometric detection.

1. Introduction

In the last few years, interest has been increasing in the application of simple, sensitive, rapid, inexpensive and disposable electrochemical sensors in fields such as clinical, environmental and pharmaceutical analysis. The most common sensors are mass-produced by the thick-film technology, which comprises layers of special inks deposited sequentially in a film of controlled pattern and thickness onto an insulating support. Single-use sensors present several advantages, apart from their low cost and simple use, such as the avoidance of sample cross-contamination and loss of response due to electrode fouling.

Moreover, electroanalytical methods are well known for their high sensitivity, thus gaining an increasing attention in the analysis of pharmaceutical drugs. These methods do not require tedious pretreatment and involve limited pre-separation, and consequently reduce the cost and time of analysis.

The aim of the study was to characterize the electrochemical behavior of colchicine by linear sweep and cyclic voltammetry on disposable graphite-based screen-printed electrodes (SPEs), followed by the optimization and validation of a differential pulse voltammetric analysis for its quantification from pharmaceutical products.

Colchicine is a protoalkaloid (Fig. 1), used as a specific anti-inflammatory agent in acute attacks of gout by inhibiting the migration of leucocytes to inflammatory areas, thus interrupting the inflammatory response that sustains the acute attack.

Many studies have dealt with the development of analytical methods for the determination of colchicine, based on TLC-

* Corresponding author. Tel.: +40 264 593118; fax: +40 264 597257.
E-mail address: bodokie@umfcluj.ro (E. Bodoki).

0039-9140/$ – see front matter © 2008 Elsevier B.V. All rights reserved.
doi:10.1016/j.talanta.2008.02.048

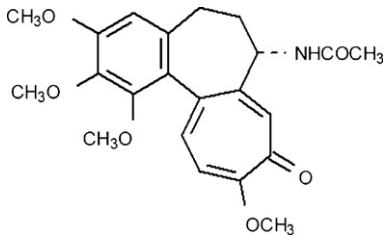

Fig. 1. Colchicine, *N*-((7*S*)-5,6,7,9-tetrahydro-1,2,3,10-tetramethoxy-9-oxobenzo-(*a*)heptalen-7-yl)-acetamide.

densitometry [1,2], high performance liquid chromatography using UV [1–6] or MS detection [7–9].

Comparatively, only a few papers have been dealing with the electrochemical behavior and dosage of colchicine [10–14], but none of them using disposable, highly sensitive screen-printed electrodes.

2. Experimental

2.1. Chemicals and standards

Analytical grade colchicine for biochemistry was purchased from Merck, Germany. The stock solutions were freshly prepared each day and they were stored in the dark, where they showed to be stable at least ten hours. Working standards of colchicine were prepared either individually or by adding appropriate amounts of stock solution directly into the working electrolyte from the voltammetric cell.

Aqueous solutions of supporting electrolytes were prepared by dissolving the appropriate amounts in ultrapure water.

The pharmaceutical samples were tablets with 1 mg declared amount of colchicine and were purchased from Biofarm S.A., Bucharest, Romania. Aside of the active compound the manufacturer declares the use of the following excipients in the formulation of tablets: starch, lactose, silicium dioxide, methylcellulose and magnesium stearate.

Perchloric acid, Suprapure grade hydrochloric acid, phosphoric acid, mercury(II) nitrate, sodium acetate trihydrate, K_2HPO_4, KH_2PO_4, potassium chloride, iron(III) chloride were of analytical grade and were purchased from Merck, Germany. $K_4Fe(CN)_6$ – Carlo Erba; ferrocenecarboxylic acid, ferroceneacetic acid – Aldrich-Chem, Milan; bismuth(III) nitrate was obtained from Fluka, Switzerland. Single-walled carbon nanotubes – Aldrich, short multi-walled nanotubes – Rosseter, multi-walled carbon nanotubes – Nanolab; dimethylformamide – Aldrich; 5% Ru/C, 5% Pd/C, 5% Pt/C catalyzers – Chimet s.p.a.

The DNA biosensor was obtained by the immobilization of double-stranded calf thymus DNA (type XV, Sigma, Milan, Italy) on the surface of working electrode.

For voltammetric assays carried out in the negative potential range, pure nitrogen saturated with water vapors was used for purging the supporting electrolyte.

2.2. Apparatus

All experiments of linear, cyclic and differential pulse voltammetry were performed with an μAutolabIII potentiostat (ECO Chemie, Utrecht, The Netherlands). The system was monitored with a personal computer using GPES 4.9 software (ECO Chemie, Utrecht, The Netherlands) for data acquisition and subsequent analysis.

For all the electrochemical assays, miniaturized graphite-based screen-printed electrodes were used, with a standardized 0.8 cm × 3.5 cm dimensions. Its detailed scheme and production process was presented in a previous paper [15].

The electrochemical cells were produced using polymeric commercial inks. The silver-based ink (Electrodag PF 410) and the graphite-based ink (Electrodag 423 SS) were purchased from Acheson (Milan, Italy). The insulating monocomponent ink (Vinylfast 36-100) was purchased form Argon Italiana (Milan, Italy). After the printing of each layer, a drying step was introduced, to ensure ink polymerization. Silver and graphite inks were dried 10 min at 120 °C; the insulating ink was dried 20 min at 70 °C in an air oven.

When necessary, the surface of the screen-printed graphite working electrode was modified using a solution containing the proper modifier. Bismuth- and mercury-films were deposited by a methodology published earlier by Hutton et al. [16].

The electrodes were preconditioned before use by cyclic voltammetry, scanning 5 cycles at 100 mV s^{-1} on the working potential range. This pretreatment eliminates the spurious peaks given by ink impurities, contributing also to the decrease of surface hydrophobicity. Before quantitative measurements, differential pulse voltammetric scans were carried out in the supporting electrolyte until low and stable baseline was achieved (3–4 potential sweeps).

2.3. Procedure

In a typical run, 2 mL of the supporting electrolyte (H_3PO_4/$HClO_4$ 0.01 M) was transferred into the dry voltammetric cell, adding the required stock solution of colchicine by a micropipette (Microman, Gilson, USA). Working in the negative potential range a 5 min nitrogen purging was carried out.

For quantitative anodic differential pulse voltammetry the scanning parameters were optimized by a surface response modeling experimental design, namely a scan rate of 124.5 mV s^{-1}, with a pulse amplitude of 100 mV (modulation time 0.002 s, interval time 0.1 s and step potential of 12.45 mV).

The calibration curve for standard colchicine was constructed using the standard addition method, plotting the intensity of the cathodic peak against the corresponding colchicine concentration on the range 84–1200 ng mL^{-1}.

The colchicine–DNA interaction studies were conducted using the following procedure:

(a) *Electrode pre-treatment*: applying potential of +1.6 V (vs. Ag-SPE pseudo-reference) for 120 s and +1.8 V (vs. Ag-SPE) for 60 s; electrode in 5 mL of 0.25 M acetate buffer, containing 10 mM KCl (pH 4.75), under stirred conditions.
(b) *DNA-immobilization*: electrode dipped in a solution of 50 ppm calf thymus ds-DNA in 0.25 M acetate buffer with containing 10 mM KCl, applying a potential of +0.5 V (vs. Ag-SPE) for 5 min, under stirred conditions.
(c) *Blank or sample interaction*: 10 μL of buffer or sample solution on the electrode surface for 2 min.
(d) *Measurement*: SWV scan in order to evaluate the oxidation of guanine residues on the electrode surface. The height of the guanine peak (at +0.95 V vs. Ag-SPE) was measured in 0.25 M acetate buffer, containing 10 mM KCl; SWV parameters: E_i = +0.2 V, E_f = +1.45 V, υ = 200 Hz, E_{step} = 15 mV, $E_{amplitude}$ = 40 mV.

2.4. Analysis of pharmaceutical dosage forms

The pharmaceutical samples were tablets with 1 mg declared amount of colchicine and were purchased from Biofarm S.A., Bucharest, Romania. After the determination of the average weight

of tablets, they were pulverized. An accurately weighted amount of powder, equivalent to 2 mg of colchicine was transferred in a 25 mL volumetric flask and suspended in distilled water. The mixture was sonicated for 8 min in an ultrasonic bath and then completed to the mark with water. The suspension was centrifuged for another 5 min at 5000 rpm and 2.5 mL of the clear supernatant was diluted to 10 mL with distilled water, which served as sample for the differential pulse voltammetric assay.

Adding a suitable volume (50 μL) of sample to the voltammetric cell containing 2 mL of the supporting electrolyte, the amount of colchicine was determined by the standard addition method.

3. Results and discussion

3.1. Cyclic voltammetry

The electrochemical behavior of colchicine at the screen-printed graphite electrode was studied by cyclic voltammetry. The used working electrolyte was $HClO_4/H_3PO_4$ 0.01 M (pH 2.05), previously reported by Kasim [10].

The assays showed an irreversible peak for colchicine at −1.037 V versus Ag pseudo-reference, where the resulted reduction product causes an electrode surface fouling (Fig. 2A). This phenomenon hinders the use of the same electrode in a standard addition method, causing non-linear calibration curves and lack of reproducibility by cathodic differential pulse voltammetry. The addition of 1% (v/v) of methanol improves the linearity, but greatly decreases the slope of the calibration curve.

Scanning in the positive potential range the assays revealed an irreversible two-step oxidation pattern, already reported by Bishop and Hussein [12] by anodic rotating disc voltammetry at platinum and gold electrodes. At the graphite screen-printed electrode in $HClO_4/H_3PO_4$ 0.01 M colchicine shows two well-defined oxidation peaks at +1.06 V and +1.22 V versus Ag pseudo-reference (Fig. 2B).

In the effort of finding a proper redox mediator, which would be able to achieve an energetic gain by shifting the peak potential towards 0 V and with this to increase the SPE's selectivity, the influence of several known mediators and catalyzers was empirically studied. Therefore, the surface of the screen-printed graphite working electrode was modified by Co-phtalocyanine, $Fe_3[Fe(CN)_6]$ or the influence of the mediator was studied in the bulk solution, such as $K_3[Fe(CN)_6]$, ferrocene acetic acid, ferrocene carboxylic acid, *para*-benzoquinone. Unfortunately, for the above studied compounds no interaction was observed with colchicine's electrochemical oxidation.

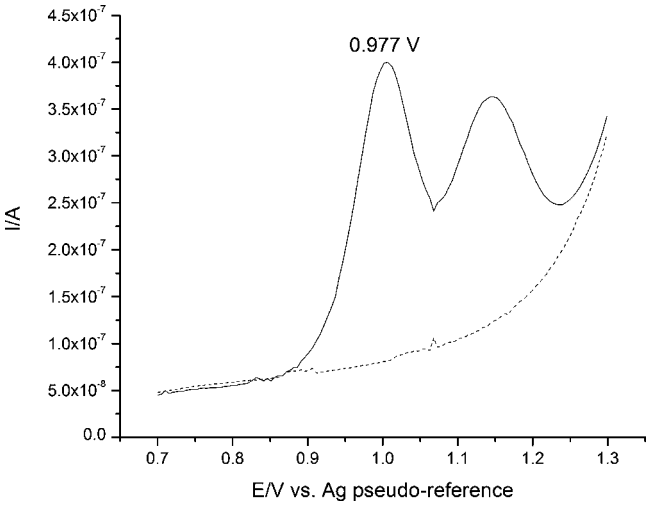

Fig. 3. Anodic differential pulse voltammograms on screen-printed graphite electrodes in $HClO_4/H_3PO_4$ 0.01 M (pH 2.05), modulation time 0.04 s, interval time 0.5 s, step potential 5.1 mV, modulation amplitude 100 mV, scan rate 10.2 mV s^{-1}: (- - -) blank; (—) colchicine (2.4 μg mL^{-1}).

Single- and multi-walled carbon nanotubes suspended in dimethylformamide or concentrated HNO_3, were deposited on the surface of the electrode, but except of an increase of the baseline current, no peak for colchicine oxidation was noticed. The immobilization of multi-walled carbon nanotubes with Nafion-film gave the same results.

The deposition of catalyzers (5% Ru/C; 5% Pd/C; 5% Pt/C suspended in dimethylformamide) brings the same increase of baseline current as the nanotubes, being impossible to observe any oxidation peak of colchicine.

3.2. Analytical application

For quantitative assays, anodic differential pulse voltammetry (DPV) was considered, using the unmodified graphite-based screen-printed electrodes. Even though its sensitivity in this case is

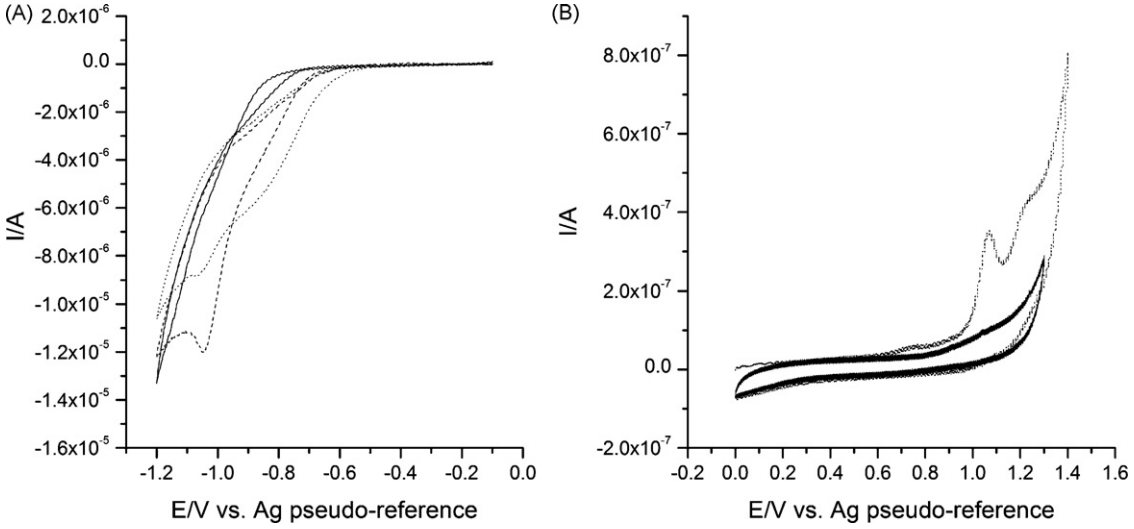

Fig. 2. (A) Cyclic voltammograms of colchicine (19.2 μg mL^{-1}) on screen-printed graphite electrodes in $HClO_4/H_3PO_4$ 0.01 M (pH 2.05), 50 mV s^{-1}: blank (—); 1st cycle (- - -); 2nd cycle after stirring, the same solution with the same electrode (···). (B) Cyclic voltammograms of colchicine (19.2 μg mL^{-1}) on screen-printed graphite electrodes in $HClO_4/H_3PO_4$ 0.01 M (pH 2.05), 75 mV s^{-1}: blank (—); 1st cycle (···).

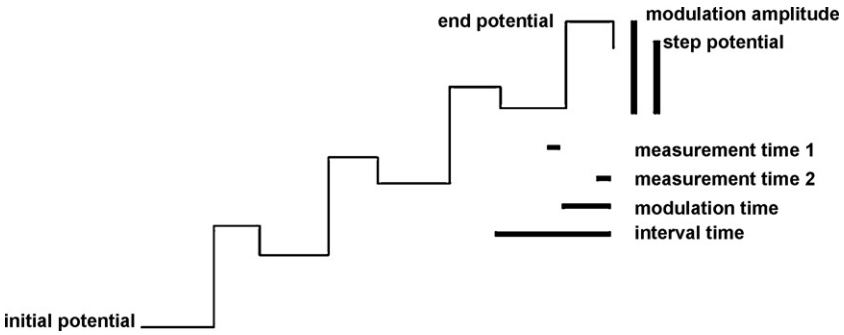

Fig. 4. The optimized scanning parameters of differential pulse voltammetric analysis.

lower, anodic DPV was preferred over cathodic one, since there is no need of oxygen removal, which considerably reduces the analysis time. Colchicine yielded two anodic peaks, from which the one from +0.977 V was chosen for analytical determination purposes (Fig. 3). Before use, the electrode was preconditioned by cyclic voltammetry, running five sweeps at 100 mV s^{-1} on the working potential range in $HClO_4/H_3PO_4$ 0.01 M (pH 2.05). Standard addition method was employed, using a new preconditioned electrode for each set of assay, showing a good linear calibration ($R^2 > 0.999$) over a wide concentration range. Using the same electrode for successive set of assays, does not affect the linear behavior of the calibration curve, but the decreasing peak currents constantly modify the slope and intercept of the calibration curves.

3.3. Method optimization

In order to obtain the highest sensitivity (highest anodic current), the anodic DPV working conditions were optimized by an experimental design using Modde 8.0 (Umetrics AB, Sweden). Response surface modeling with a circumscribed central composite design with 4 quantitative factors, 4 centerpoints and 1 response was performed, consisting of 28 experiments. The four operating DPV parameters (modulation time: m_t, interval time: i_t, step potential: i_p, modulation amplitude: m_a) are susceptible of modifying the oxidation peak's height and shape, thus being considered the quantitative factors, and colchicine's anodic peak height from +0.977 V as the response (Fig. 4).

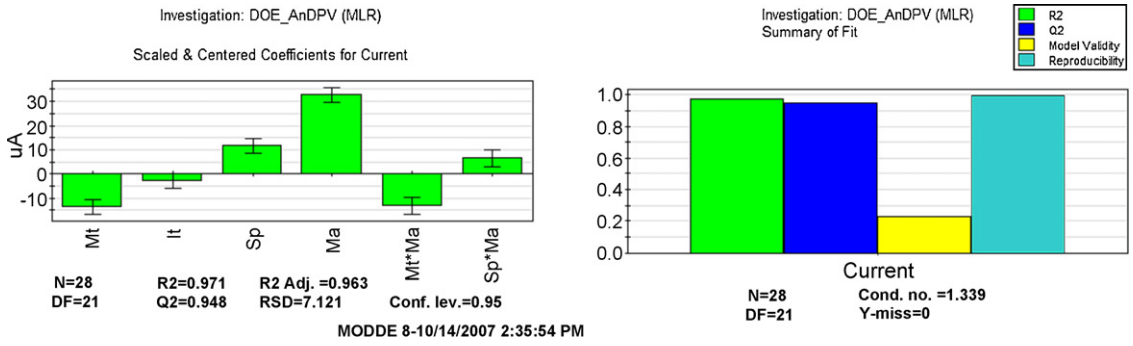

Fig. 5. Significant model terms after model pruning and summary plot for goodness of fit.

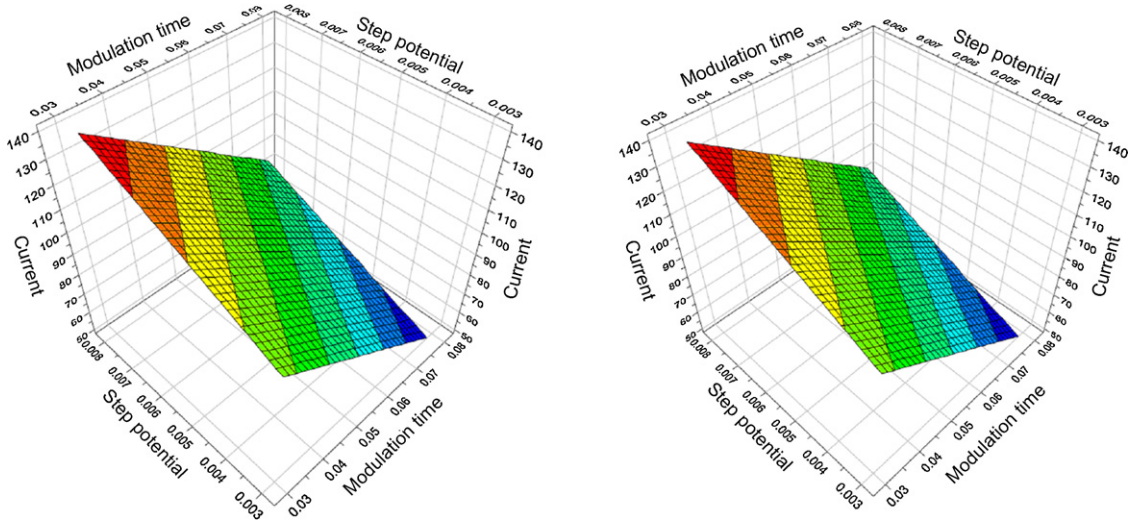

Fig. 6. Typical response surface models obtained after the model refinement.

Table 1
Initial and optimized values of the scanning parameters

Parameter	Initial	Optimized
Modulation time, m_t (s)	0.04	0.002
Interval time, i_t (s)	0.5	0.1
Step potential, s_p (V)	0.0051	0.01245
Modulation amplitude, m_a (V)	0.1	0.1
Resulting scan rate (mV s^{-1})	10.2	124.5
First oxidation peak of colchicine (A)	1.06×10^{-7}	9.39×10^{-7}
Second oxidation peak of colchicine (A)	4.06×10^{-8}	4.6×10^{-7}

The matrix contained 15 model terms (the four parameters, their interaction and a free term). The model was fitted by multiple linear regression, followed by model pruning by reducing the insignificant terms considering the goodness of fit (R^2) and the fraction of the variation of the response predicted by the model according to the cross validation (Q^2). Four linear and two interaction terms remained to best describe the model (Fig. 5). Following the response surface plots (Fig. 6) and prediction plots, the scanning parameters were optimized as presented in Table 1, gaining almost a 10-fold increase of the signal.

3.4. The study of bioselectors over the electrochemical behavior of colchicine

3.4.1. DNA biosensor

The interaction of DNA with drug molecules represents a fundamental issue in medical science and it has been the subject of several investigations. The evaluation of any interaction with DNA using biosensors helps to predict unwanted toxic side-effects and prevent DNA damage caused by therapeutic drugs.

A disposable biosensor, based on the immobilization of double-stranded calf thymus DNA was used to assess its possible interaction with colchicine. Eventually, this could have been used as a more selective way of determining the protoalkaloid from complex matrixes, without the need of separation.

The detailed protocol of production and use of the DNA biosensor was described earlier [17], where the oxidation peak of guanine was used as the transduction signal to recognize DNA interacting agents. As the result of a specific- or non-specific interaction (covalent binding, electrostatic interaction with the negatively charged nucleic acid sugar phosphate, hydrogen and/or van der Waals bonds) of the double-stranded calf thymus DNA with a genotoxic agent, a decrease of the guanine peak (measured by square-wave voltammetry) is detected. Measurement of the target analyte with the DNA modified screen-printed electrode includes four main steps: electrochemical conditioning of the electrode surface in order to oxidize the graphite impurities and to obtain a more hydrophilic surface to favor DNA immobilization, calf thymus ds-DNA immobilization, interaction with the colchicine solution and electrode surface interrogation. The experimental procedure was described in detail in Section 2.

Measuring the oxidation peak of guanine residues compared with the baseline, there is no current decrease after the exposure to colchicine of the DNA biosensor. Therefore, this assembly could not be used for the quantitative measurement of the protoalkaloid.

This may confirm a lack of DNA–colchicine interaction, a result also supported by the different antimitotic mechanism of colchicine. Colchicine specifically interacts with the tubulin dimer, arresting cell division in anaphase due to the inhibition of division spindle formation.

3.4.2. β-Tubulin

Colchicine inhibits microtubule polymerization by binding with high affinity to tubulin, one of the main constituents of the microtubules of the division spindle. Tubulin is a negatively charged protein (~120 kDa), formed by two globular polipeptidic subunits (α-tubulin and β-tubulin). Inhibitors of tubulin polymerization interacting at the colchicine binding site are potential anticancer agents, thus colchicine–tubulin interaction was very extensively studied in the last 20 years [18–22]. It has been demonstrated that the binding to the tubulin dimer (α- and β-subunits) is slow and poorly reversible due to conformational changes in the protein's structure, whereas binding to β-tubulin monomers is reversible and 3–4 times faster [21]. Therefore, the screen-printed electrodes were modified applying 5 μL of 25 ng mL^{-1} β-tubulin in 10 mM HEPES buffer on the electrode's surface, followed by drying at room temperature.

Due to the specific colchicine-β-tubulin interaction, a shift of colchicine's oxidation peak can be observed (+1.06 V vs. Ag-SPE) accompanied by a decrease of the anodic current. This decrease is not due to the electrode surface blockage by the deposited protein, since the same potential shift and current decrease was observed when β-tubulin is directly added in the voltammetric cell. Unfortunately, this specific interaction could not be exploited for analytical purposes, except maybe to increase the SPE sensor's selectivity in the analysis of complex matrices.

3.4.3. Bovine serum albumin

The literature describes also the formation of colchicine–bovine serum albumin complex, stabilized by van der Waals interactions and hydrogen bonds [23]. Therefore, this interaction's influence on the electrochemical behavior of colchicine was also investigated using bovine serum albumin (BSA) surface modified SPE's.

A similar potential shift and anodic current decrease was observed when the surface of screen-printed electrode was modified applying 7 μL of 0.025% (m/v) BSA followed by drying at room temperature or when the albumin was added to the bulk solution of the voltammetric cell. These data might be explained by the strong interaction of colchicine with the BSA resulting a less favorable conformation of the colchicine molecule for the heterogeneous electron transfer.

3.5. Method validation

The method was validated in compliance with ICH Harmonised Tripartite Guideline [24], in terms of specificity, linearity, range, accuracy, precision, detection and quantification limit.

3.5.1. Specificity

Since differential pulse voltammetry and electrochemistry in general, is considered a non-specific assay, other supporting analytical procedures should be used to demonstrate overall specificity. Because the proposed method is recommended to be used only for the quantification of the alkaloid from pharmaceutical dosage forms, a blank assay of a reconstructed tablet matrix should ascertain the lack of interference of the used excipients. Therefore, a synthetic mixture of the placebo was prepared according to the label reported by the producer and this mixture was extracted and analyzed following the protocol described at the analysis of pharmaceutical dosage forms. The obtained anodic differential pulse voltammogram presented no oxidation peak on the studied potential range, demonstrating the methods specificity towards colchicine. Since degradation product standards were unavailable, their interference was not studied.

Table 2
Linear regression data ($n = 7$)

Parameters	84–1184 μg mL^{-1} ($N = 21$)	Theoretical values	Conditions
Correlation coefficient	0.99827		
Intercept	0.017045		
Slope	0.563356		
Cochran's test			
Comparative test of the homogeneity of variances	$C_{calc.} = 0.308$	$C(0.05;7;2) = 0.68$	$C_{calc.} < C_{theor.}$
Fisher's test			
Significant slope	$F_{calc.} = 5055.08$	$F(0.05;1;19) = 4.38$	$F_{calc.} > F_{theor.}$
Fisher's test			
Validity of regression	$F_{calc.} = 1.22$	$F(0.05;3;16) = 3.24$	$F_{calc.} < F_{theor.}$
Student test			
Comparative test of intercept with 0	$t_{calc.} = -3.001$	$t_{theor.} = 2.092$	

Table 3
Statistical evaluation of method's accuracy ($N = 15$, $n = 5$)

Parameters	Calculated values	Theoretical values	Conditions
Cochran's test			
Comparative test of the homogeneity of variances	$C_{calc.} = 0.536$	$C(0.05;5;2) = 0.683$	$C_{calc.} < C_{theor.}$
Fisher's test			
Validity of average recovery	$F_{calc.} = 0.363$	$F(0.05;4;10) = 3.48$	$F_{calc.} < F_{theor.}$
Confidence limits (%)		100.43–101.89	

Specificity towards colchicine could not be demonstrated in the analysis of spiked biological samples (urine or plasma), therefore the method cannot be employed for their analysis without the use of a proper bioselector.

3.5.2. Linearity

Linearity was evaluated on seven concentration levels of colchicine by three series in 3 different days. A fresh stock solution of colchicine was prepared each day and all the assays were performed under controlled light conditions in order to prevent the photodegradation. The assays were carried out by the standard addition method, adding increasing volumes of standard stock solution of colchicine to 2 mL of $H_3PO_4/HClO_4$ 0.01 M.

The plot of peak current versus the respective concentration of colchicine was found to be linear in the concentration range (84–1184 ng mL^{-1}), the regression line being described by the following equation: $I_p(A \times 10^{-7}) = 0.017045C$ (ng mL^{-1}) + 0.563356, $R^2 = 0.9966$. Linear regression data were summarized in Table 2.

3.5.3. Accuracy

The accuracy of the method was assessed on 15 control samples over 5 levels of concentration. The statistical analysis of the data was summarized in Table 3. The statistical tests confirmed the homogeneity of variances and the validity of the obtained average recovery (Cohran and Fisher tests). The resulting average recovery of 101.16% with a confidence limit of ±0.73% proved an accurate analytical method.

3.5.4. Precision

The precision of the method was evaluated for six independently weighted samples (100% of the test concentration) analyzed by the standard addition method, and expressed in terms of variation coefficients (Table 4). The intermediate precision (inter-day precision) was assessed for 3 different days of six independent samples using different electrodes at each assay. Variation coefficients of around 10% indicate a satisfactory precision of the proposed electroanalytical method.

3.5.5. Limit of detection and limit of quantification

The limits of detection (LOD) and limits of quantification (LOQ) were calculated as ($3.3\sigma/S$) and ($10\sigma/S$), respectively, where σ is the standard deviation of the intercepts and S is the slope of the calibration curve. The calculated LOD and LOQ were found to be 40.78 ng mL^{-1} and 123.58 ng mL^{-1}, respectively.

3.6. Determination of colchicine in pharmaceutical product

In order to assess the applicability of the proposed method, the content of three samples of commercially available 1 mg colchicine tablets was determined. Furthermore, to test the reliability of this

Table 4
Intra- and inter-day precision of colchicine ($n = 6$)

Parameters	Calculated values	Theoretical values	Conditions
Cochran's test			
Comparative test of homogeneity of variances intra-group	$C_{calc.} = 0.67$	$C(0.05;3;6) = 0.677$	$C_{calc.} < C_{theor.}$
Intra-day precision (CVR) (%)		10.3	
Inter-day precision (CVR) (%)		10.5	

Table 5
Results for colchicine content of real samples

Colchicine tablets Biofarm S.A., Bucharest	Spectrophotometric assay (Romanian Pharmacopoeia Xth edition)	Anodic differential pulse voltammetry using graphite-based screen-printed electrodes
Nominal value 1 mg/tablet	1.195 mg/tablet[a]	1.176 mg/tablet[a]
Standard deviation	0.019	0.032
Confidence level of 95%	$t_{exp} = 0.923$; P(Type 1 error) = 0.408	

[a] Mean of three determinations ($N = 3$).

method, the obtained results were compared with the one obtained by the spectrophotometric determination described by the Romanian Pharmacopoeia X edition for the determination of colchicine from tablets.

3.6.1. Spectrophotometric determination

Following the described protocol in the Romanian Pharmacopoeia X edition [25] for the determination of colchicine from tablets, it was determined the content of the protoalkaloid from 1 mg colchicine tablets (Biofarm S.A., Bucharest) (Table 5).

Considering a confidence level of 95%, the obtained probability of Type 1 error showed no statistically significant difference between the obtained means, therefore the proposed anodic differential pulse voltammetric determination using graphite-based screen-printed electrodes provides the same analytical result as the spectrophotometric reference method.

4. Conclusions

The electrochemical behavior of colchicine at bare and modified graphite-based screen-printed electrode was studied and the optimal conditions were employed for the rapid quantitative determination of the active drug from tablets. The anodic differential pulse voltammetry in H_3PO_4/$HClO_4$ 0.01 M proved to be the most suitable, in terms of peak potential, current height and reproducibility, for the routine analysis of the protoalkaloid. The surface modification of working electrode with different redox mediators and biomolecules did not improve the sensitivity of the differential pulse voltammetric method.

The proposed electrochemical method provides simple, sensitive, accurate and fairly reproducible quantitative analysis of colchicine in tablets. It passed all necessary statistical tests in order to be validated as per ICH guidelines.

Real samples of tablets were determined simultaneously by spectrophotometric and differential pulse voltammetric methods and the results were correlated.

The present method was applied for the determination of colchicine in tablets without any separation, or complex sample preparation, since there was no significant interference from the excipients. Using cost effective, disposable screen-printed electrodes the developed method could be applied for quality control dissolution tests regulated by Pharmacopoeias and in vitro dissolution profile testing since cross-contamination can be easily avoided. These tests are needed in the registration requirements to establish interchangeability of multisource pharmaceutical products (generics) with the comparator product (original, patented one).

Acknowledgements

The authors are thankful for the financial support given by the Romanian National Authority for Scientific Research (research grant CEEX 6/2005) and National University Research Council of Romania (research grant CNCSIS TD 469/2006).

References

[1] T.M. Sarg, M.M. El-Domiaty, M.M. Bishr, O.M. Salama, A.R. El-Gindy, Analyst 114 (1989) 575–578.
[2] E. Bodoki, R. Oprean, L. Vlase, M. Tămaş, R. Săndulescu, Journal of Pharmaceutical and Biomedical Analysis 37 (2005) 971–977.
[3] E. Ellington, J. Bastida, F. Viladomat, C. Codina, Phytochemical Analysis 14 (2003) 164–169.
[4] R.J. Ko, W. Yen Li, R.T. Koda, Journal of Chromatography—Biomedical Applications 525 (1990) 411–418.
[5] M. Lhermitte, Journal of Chromatography—Biomedical Applications 342 (1985) 416–423.
[6] A.E. Klein, P.J. Davis, Analytical Chemistry 52 (14) (1980) 2433–2435.
[7] G. Hamscher, B. Priess, H. Nau, E. Panariti, Analytical Chemistry 77 (2005) 2421–2425.
[8] A. Tracqui, P. Kintz, B. Ludes, C. Rougé, H. Douibi, P. Mangin, Journal of Chromatography B 675 (1996) 235–242.
[9] H. Hoja, P. Marquet, B. Verneuil, H. Lotfi, J.L. Dupuy, M.F. Dreyfuss, G. Lachâtre, Analusis 24 (1996) 391–394.
[10] E.A. Kasim, Analytical Letters 35 (12) (2002) 1987–2004.
[11] J. Wang, M. Ozsoz, Talanta 37 (8) (1990) 783–787.
[12] E. Bishop, W. Hussein, Analyst 109 (1984) 623–625.
[13] H. Zhang, Bioelectrochemistry 68 (2) (2006) 197–201.
[14] E. Bodoki, R. Săndulescu, L. Roman, Central European Journal of Chemistry 5 (3) (2007) 766–778.
[15] Ilaria Palchetti, Serena Laschi, Marco Mascini, Analytica Chimica Acta 530 (2005) 61–67.
[16] E.A. Hutton, B. Ogorevc, S.B. Hočevar, F. Weldon, M.R. Smyth, J. Wang, Electrochemistry Communications 3 (2001) 707–711.
[17] Graziana Bagni, Domenico Osella, Elena Sturchio, Marco Mascini, Analytica Chimica Acta 573–574 (2006) 81–89.
[18] Bernardo Perez-Ramirez, Jose M. Andreu, Marina J. Gorbunoff, Serge N. Timasheff, Biochemistry 35 (1996) 3277–3285.
[19] Jose M. Andreu, Bernardo Perez-Ramirez, Marina J. Gorbunoff, David Ayala, Serge N. Timasheff, Biochemistry 37 (1998) 8356–8368.
[20] Milton L. Brown, Jayson M. Rieger, Timothy L. Macdonald, Bioorganic & Medicinal Chemistry 8 (2000) 1433–1441.
[21] Suroopa Banerjee, Gopal Chakrabarti, Bhabatarak Bhattacharyya, Biochemistry 36 (1997) 5600–5606.
[22] Shobha Uppuluri, Leslie Knipling, Dan L. Sackett, J. Wolff, Proceedings of the National Academy of Sciences of the United States of America, Biochemistry 90 (1993) 11598–11602.
[23] Yan-Jun Hu, Yi Liu, Li-Xia Zhang, Ru-Ming Zhao, Song-Sheng Qu, Journal of Molecular Structure 750 (1–3) (2005) 174–178.
[24] ICH Harmonised Tripartite Guideline, Validation of Analytical Procedures: Text and Methodology Q2(R1), Current Step 4 Version, November 2005, International Conference on Harmonisation of Technical Requirements for Registration of Pharmaceuticals for Human Use, http://www.ich.org/LOB/media/MEDIA417.pdf.
[25] Romanian Pharmacopoeia, Xth ed., Editura Medicală, Bucureşti, 1998.

Talanta 76 (2008) 469–474

Contents lists available at ScienceDirect

Talanta

journal homepage: www.elsevier.com/locate/talanta

A new approach to separation and pre-concentration of some trace metals with co-precipitation method using a triazole

Volkan Numan Bulut[a], Celal Duran[a], Ali Gundogdu[a], Mustafa Soylak[b,*], Nuri Yildirim[a], Latif Elci[c]

[a] Department of Chemistry, Faculty of Arts & Sciences, Karadeniz Technical University, 61080 Trabzon, Turkey
[b] Department of Chemistry, Faculty of Arts and Sciences, Erciyes University, 38039 Kayseri, Turkey
[c] Department of Chemistry, Faculty of Arts and Sciences, Pamukkale University, 20020 Denizli, Turkey

ARTICLE INFO

Article history:
Received 18 December 2007
Received in revised form 21 March 2008
Accepted 25 March 2008
Available online 8 April 2008

Keywords:
Co-precipitation
3-Benzyl-4-*p*-nitrobenzylidenamino-4,5-dihydro-1,2,4-triazole-5-on
Pre-concentration
Trace metals
Flame atomic absorption spectrometry

ABSTRACT

A new co-precipitation method was developed to separate and pre-concentrate Fe^{3+}, Cu^{2+}, Cr^{3+}, Zn^{2+}, and Pb^{2+} ions using an organic co-precipitant, 3-benzyl-4-*p*-nitrobenzylidenamino-4,5-dihydro-1,2,4-triazole-5-on (BPNBAT) without adding any carrier element, following flame atomic absorption spectrometric (FAAS) determinations. Effect of some analytical conditions, such as pH of the solution, quantity of the co-precipitant, standing time, centrifugation rate and time, sample volume, and interference of concomitant ions were investigated over the recovery yields of the metal ions. The recoveries of the analyte ions were in the range of 95–102%. The detection limits, corresponding to three times the standard deviation of the blank, were found to be in the range of 0.3–2.0 $\mu g\,L^{-1}$. The precision of the method, evaluated as the relative standard deviation (R.S.D.) obtained after analyzing a series of 10 replicates, was between 1.6% and 6.0% for the trace metal ions. The method was validated by analyzing two certified reference materials and spiked addition. The proposed procedure was applied for the trace metal ions in some environmental samples.

1. Introduction

The presence of trace metals in the environment is of major concern because of their toxicity and threat to human life and environment [1]. Hence, determination of trace metals in various samples is very important for monitoring environmental pollution. Recent rapid advances in analytical instrumentation enable the instrumental analysis of many samples. Atomic absorption spectrometry (AAS) and atomic emission spectrometry (AES) are the most widely used techniques for trace metals quantitative analysis in environmental samples [2]. Flame atomic absorption spectrometry (FAAS) has been a particularly useful tool in the determination of trace metals because of its high specificity while not being an expensive instrument. However, because of the limitations of detectability with FAAS, and, sometimes, the large amount of concomitants and dissolved solids, pre-concentration and separation is sometimes necessary for the trace metal analyses [3]. Several methods extensively used for pre-concentration and separation of trace metals include liquid–liquid extraction [4], ion exchange [5], cloud point extraction [6,7], solid phase extraction [8–11], co-precipitation [12–16], etc.

Co-precipitation is one of the important pre-concentration and separation techniques for the trace metal ions because of its some advantages including simplicity, rapidity, and ability to attain a high pre-concentration factor. The incorporation of trace impurities into a precipitate, which under the experimental conditions are usually soluble in the liquid phase, is denoted by the general term co-precipitation. This property of precipitates to carry down special impurities may be used to concentrate or enrich trace elements [17]. Inorganic and organic co-precipitants have been used successfully for separation and pre-concentration of trace metal ions at trace levels by co-precipitation procedures.

Co-precipitation is potentially important to many environmental issues, such as acid mine drainage, radionuclide immobilization in fouled waste repositories, metal contaminant transport at industrial and defense sites, metal concentrations in aquatic systems, and wastewater treatment technology. While mechanisms of co-precipitation may vary in each case and may include surface adsorption, ion exchange, surface precipitation, and occlusion [18].

The co-precipitant compound 3-benzyl-4-*p*-nitrobenzylidenamino-4,5-dihydro-1,2,4-triazole-5-on used in this study has been reported to show low growth inhibitory activity against two tumor cell lines, though total growth inhibition and lethal doses could not be determined at the concentration range used in that study [19]. The toxicity or safety information of the compound for humans is not available.

* Corresponding author. Tel.: +90 352 4374933; fax: +90 352 4374933.
E-mail address: soylak@erciyes.edu.tr (M. Soylak).

0039-9140/$ – see front matter © 2008 Elsevier B.V. All rights reserved.
doi:10.1016/j.talanta.2008.03.040

Table 1
Instrumental conditions for the measurements of the working elements by FAAS

Element	Wavelength (nm)	Slit width (nm)	amp current (mA)	Flow rate of acetylene ($L\,min^{-1}$)
Zn	213.9	0.5	7.5	1.2
Fe	248.3	0.2	11.5	0.9
Cu	324.8	0.5	3.5	1.1
Cr	357.9	0.5	9.0	4.2
Pb	217.0	0.5	6.0	1.1

In this work, a new approach to pre-concentration and separation of trace metals from aqueous solutions was presented by using an organic co-precipitant (3-benzyl-4-*p*-nitrobenzylidenamino-4,5-dihydro-1,2,4-triazole-5-on) without any carrier element.

2. Experimental

2.1. Instrumentation

A Unicam model AA-929 atomic absorption spectrometer equipped with 10.0 cm of air/acetylene-burner head (5.0 cm of N_2O/acetylene-burner head for chromium), and having a deuterium background correction was used for the determination of metal ion concentration. Single element hollow cathode lamps as radiation sources were run under the conditions suggested by the manufacturer. Detailed descriptions are depicted in Table 1.

The pH measurements were made on Hanna digital pH meter model 211 with glass electrode. MSE Mistral 2000 model centrifuge was employed for centrifugation of solutions. Milestone Ethos D closed vessel microwave system (maximum pressure 1450 psi; maximum temperature 300 °C) was operated for digestion of the solid samples.

2.2. Reagents and solutions

All chemicals used in this work were of an analytical grade of Merck (Darmstadt, Germany) or Fluka (Buchs, Switzerland), unless stated otherwise. Distilled/deionized water was used in all experiments. The single element stock solutions of the metal ions ($1000\,mg\,L^{-1}$) in 0.5 M HNO_3 obtained from Merck (Darmstadt, Germany) and Fluka (Buchs, Switzerland) were used. Metal working solutions at $mg\,L^{-1}$ level were prepared daily by diluting the stock solutions.

In this study, 3-benzyl-4-*p*-nitrobenzylidenamino-4,5-dihydro-1,2,4-triazole-5-on (BPNBAT) used as a co-precipitating agent was synthesized in the organic chemistry research laboratory (Karadeniz Technical University, Faculty of Arts and Sciences, Chemistry Department). The detailed information of its synthesis was given in the literature [20]. No safety data is available for this compound, and thus the necessary precautions were taken during its handling in the experiments.

Standard reference materials, BCR-CRM 144R sewage sludge (domestic origin) and CRM-TMDW-500 drinking water were purchased from Institute for Reference Materials and Measurements (IRMM), and high-purity standard, respectively.

The buffer solutions were used for adjusting pH values of the solutions. The buffer solution of pH 2 was prepared by mixing of appropriate volume of $1\,mol\,L^{-1}$ Na_2SO_4 and $1\,mol\,L^{-1}$ $NaHSO_4$ solutions. Acetate buffers prepared by mixing different amounts of $1\,mol\,L^{-1}$ CH_3COONa and $1\,mol\,L^{-1}$ CH_3COOH were used to maintain the pH between 4 and 6. Ammonium chloride buffer solutions ($0.1\,mol\,L^{-1}$) were prepared by adding an appropriate amount of NH_3 to NH_4Cl solutions to result in solutions of pH 8–10. pH 12 was obtained by mixing of appropriate amounts of $0.1\,mol\,L^{-1}$ NaH_2PO_4 and $0.1\,mol\,L^{-1}$ NaOH solutions.

The glassware used was soaked in 10% (v/v) nitric acid solution for 1 day before use and then cleaned repeatedly with distilled/deionized water. For storage of water samples, polypropylene and/or polyethylene bottles (5 L) were used prior to their analysis.

2.3. Sampling

Water samples were collected from a mineral water (Şana, Trabzon, Turkey), and a stream water (Yomra, Trabzon, Turkey). The water samples were acidified with HNO_3 and subsequently filtered through a nitrocellulose membrane (Millipore) of 0.45-μm pore size. The vegetable sample, kale (*Brassica oleracea* var. *acephala*), was collected from Arsin, Trabzon, Turkey. The waste tea leaf was taken from Of, Trabzon, Turkey. Kale and waste tea leaves were dried in an oven for 20 h at 80 °C and fine powdered in an agate mortar.

2.4. General procedure

2.0 mL of the co-precipitating agent solution prepared in acetonitrile (0.2%, w/v) were added into a 50-mL of aqueous solution containing 25 μg of Fe^{3+}, Cu^{2+} and Cr^{3+}, 10 μg of Zn^{2+}, and 50 μg of Pb^{2+} after its pH was adjusted to 7. After waiting for 10 min, the resulting solution was centrifuged at 3000 rpm for 15 min, and then the supernatant was removed. Finally, the precipitate collected at the bottom of the centrifuge tube was dissolved with 1.0 mL of conc. HNO_3, and analyzed by flame atomic absorption spectrometry after its final volume was made up 5.0 mL with distilled/deionized water.

2.5. Application to real samples

The solid samples were digested in a closed microwave digestion system prior to pre-concentration with the present co-precipitation method. The following was weighed into the Teflon vessels: 0.100 g of BCR-CRM 144R sewage sludge, 1.000 g of waste tea leaves and kale (*B. oleracea* var. *acephala*) leaf samples. Six milliliters HCl, 2.0 mL HNO_3 and 1.0 mL HF for BCR-CRM 144R sewage sludge, 6.0 mL HNO_3 and 2.0 mL H_2O_2 for waste tea and kale samples were added into the vessels. Then, the content of the vessel was digested by microwave irradiation at 45 bar pressure. Digestion conditions for the samples were applied according to the literature [21]. The clear solutions obtained were made up 50 mL with distilled/deionized water. A blank digest was carried out in the same way. Finally, the recommended procedure was applied to the solutions after adjusting the pH to 7 prior to flame atomic absorption spectrometric determinations.

The procedure was also applied to the water samples. 50 mL of CRM-TMDW-500 drinking water was taken for the analysis of all the studied metals. From the other real water samples, stream and mineral waters, 750 mL for the analysis of Fe and Cu, 500 mL for the analysis of Cr and Zn, and 250 mL for the analysis of Pb were taken, and the procedure was applied. The final volumes were completed to 5.0 mL, and the metal contents were determined by flame atomic absorption spectrometer.

3. Results and discussion

3.1. Effect of pH over the metal recoveries

The pH plays an important role with respect to efficiency of the co-precipitating agent (BPNBAT) over the metal uptake. In order to evaluate the effect of the pH, the pH value of the sample solu-

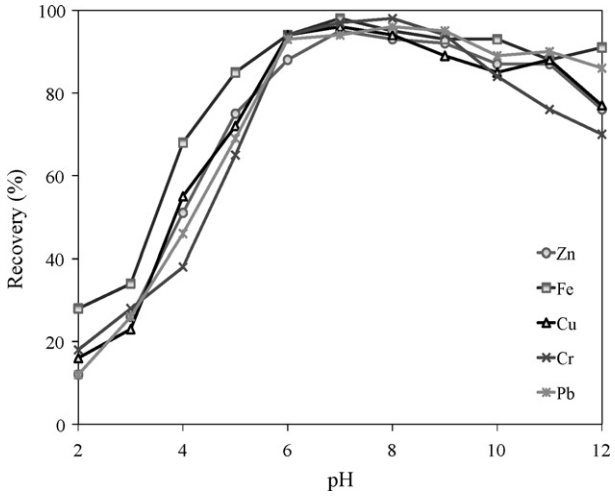

Fig. 1. Effect of pH over the recoveries of the metals ($N = 3$).

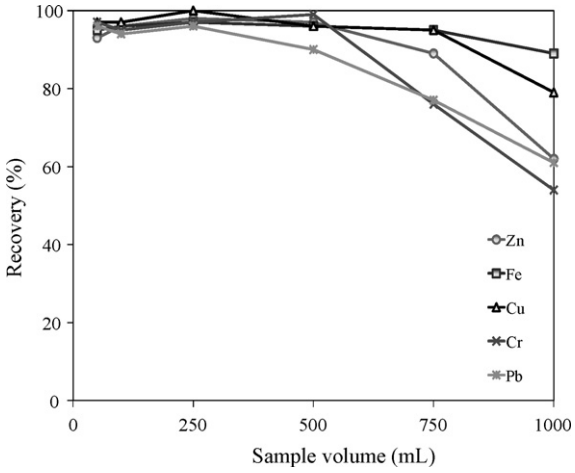

Fig. 3. Effect of sample volume over the recoveries of the metals ($N = 3$).

tions were adjusted to a range of 2–12 with related buffer solutions, and the co-precipitation procedure described above was applied to these solutions. From the data, the maximum percent recoveries were in the pH range 7–9 for Zn, 6–8 for Cu, 6–10 for Fe, and 6–9 for Cr and Pb. The results demonstrated that optimum value was in the pH 7 for all metals. The metal recoveries (%) as a function of pH are shown in Fig. 1.

3.2. Effect of the quantity of BPNBAT

The various quantities of BPNBAT, as a co-precipitating agent, over the recoveries of the studied metals were investigated from 0.0 to 10.0 mg. The recoveries of analyte ions were below 70% without adding BPNBAT under the optimum conditions. Quantitative recovery values for all the analytes were obtained after 3.0 mg of BPNBAT (Fig. 2). Thus, optimum quantity of BPNBAT was evaluated as 4.0 mg (0.2%, w/v 2.0 mL).

3.3. Effect of standing time, centrifugation time, and centrifugation rate

In order to quantitatively co-precipitate the metals with 4.0 mg of BPNBAT, effect of standing time, centrifugation time, and centrifugation rate were also examined. These factors influence the quality of the precipitate that forms in the aqueous medium. For these purposes, 2.0 mL of BPNBAT (0.2%, w/v in acetonitrile) were added into a series of solutions (50 mL) containing the metal ions after the pH was adjusted to 7. Then, the solutions were separately kept standing from 1 to 20 min. The recoveries of analytes reached quantitative values after about 8 min of standing period. As a result, the optimum standing time was determined as 10 min for all the studied metals.

After findings above, the precipitates were centrifuged in the range of 1500–3500 rpm in order to determine the optimum centrifugation rate. The highest recovery yields were obtained after 2750 rpm of centrifugation rates. Hence, the optimum centrifugation rate was specified as 3000 rpm. For optimization of centrifugation time at 3000 rpm were tried in the range of 5–25 min. After 10 min, the quantitative recoveries for all metals were obtained. Hence, the centrifugation time at 3000 rpm was optimized as 15 min.

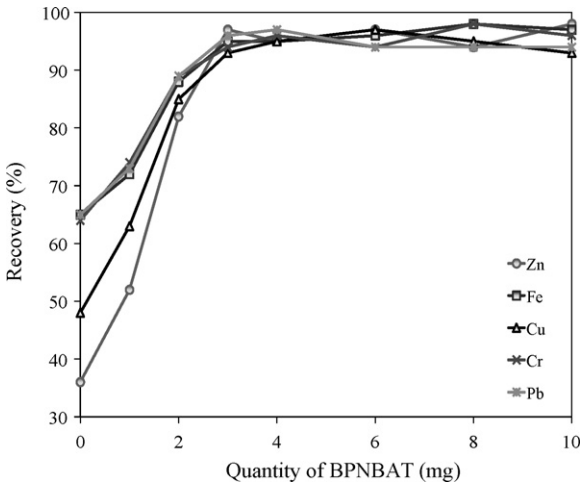

Fig. 2. Effect of quantity of BPNBAT as a co-precipitating agent ($N = 3$).

3.4. Effect of the sample volume on the metal recovery

For the analysis of real samples, the sample volume is one of the important parameters for obtaining high pre-concentration factor. In this study, hence, the effect of sample volume on the co-precipitation yields of the analytes was investigated in the sample volume range of 10–1000 mL by using the model solutions. The results show that the metal recoveries were quantitative up to 750 mL for Fe and Cu, 500 mL for Cr and Zn, and 250 mL for Pb (Fig. 3). After these results, pre-concentration factors were found to be 150 for Fe and Cu, 100 for Cr and Zn, and 50 for Pb because the final volumes were 5.0 mL.

3.5. Effect of matrix ions on the quantitative recovery

Some experiments should be carried out to examine the effects of coexisting ions on the co-precipitation because the trace metals are present together with some interfering matrix ions in real samples. In this study, the metal solutions of 0.5 $\mu g\,mL^{-1}$ of Fe^{3+}, Cu^{2+} and Cr^{3+}, 0.2 $\mu g\,mL^{-1}$ of Zn^{2+}, and 1.0 $\mu g\,mL^{-1}$ of Pb^{2+} containing the added interfering ions given in Table 2 were treated according to the recommended procedure. From the results obtained, it can be concluded that the presence of interfering cations and anions has no obvious influence on the co-precipitation of the studied metals under the optimum conditions (Table 2).

Table 2
Effect of matrix ions over the recoveries ($N = 3$; V, 0 mL)

Ions	Concentration (mg L^{-1})	Recovery (%)				
		Zn	Fe	Cu	Cr	Pb
Na^+	10.000	92 ± 4	94 ± 3	95 ± 3	94 ± 3	93 ± 4
K^+	1.000	95 ± 3	93 ± 2	96 ± 3	97 ± 4	95 ± 3
Ca^{2+}	1.000	92 ± 3	100 ± 6	100 ± 4	92 ± 4	95 ± 4
Mg^{2+}	1.000	94 ± 2	92 ± 3	94 ± 4	95 ± 2	98 ± 4
Cl^-	12.500	97 ± 4	99 ± 4	92 ± 2	99 ± 4	92 ± 1
PO_4^{3-}	1.000	91 ± 3	96 ± 2	96 ± 5	98 ± 3	95 ± 3
SO_4^{2-}	1.000	97 ± 6	94 ± 3	93 ± 5	94 ± 2	98 ± 6
NO_3^-	5.000	98 ± 2	97 ± 5	97 ± 4	93 ± 4	93 ± 4
Al^{3+}, Mo^{6+}, Ni^{2+}, Bi^{3+}, Co^{2+}, Hg^{2+}	50	102 ± 5	99 ± 5	96 ± 5	95 ± 4	97 ± 4
Mixed[a]		101 ± 4	102 ± 4	98 ± 5	98 ± 4	100 ± 3

[a] Mixed solution contains 10.000 mg L^{-1} of Na^+; 15.000 mg L^{-1} of Cl^-; 500 mg L^{-1} of Ca^{2+}; Mg^{2+} and K^+; 500 mg L^{-1} of SO_4^{2-} and PO_4^{3-}; 1.000 mg L^{-1} of NO_3^-; 10 mg L^{-1} of Al^{3+}, Mo^{6+}, Ni^{2+}, Bi^{3+}, Co^{2+} and Hg^{2+} ions.

Table 3
Statistical evaluation of the method

Statistical parameters	Zn	Fe	Cu	Cr	Pb
Sensitivity (μg L^{-1})	0.3	0.6	0.5	0.5	2.2
Detection limit, DL (μg L^{-1})	0.3	0.7	0.3	0.4	2.0
Relative standard deviation, R.S.D. (%)	4.2	5.4	2.0	1.6	6.0
Pre-concentration factors, PF	100	150	150	100	50

3.6. Analytical figure of merits

Sensitivity is defined as the concentration of a solution of an element needed to produce a signal of 0.0044 absorbance. This is equivalent to a 1% decrease in the transmitted radiation [22]. The sensitivity of the method was calculated as μg L^{-1} (ppb) for the studied metals after pre-concentration step, and the data were given in the table of statistical evaluation of the method (Table 3).

The detection limit (or limit of detection) is defined as the lowest concentration of an element in solution which can be detected with 95% certainty. It is therefore the concentration which will produce a deflection equal to twice or three times the standard deviation of a series of readings (typically 10). The detection limit is a theoretical figure and one would never attempt to measure routinely concentrations at the detection limit for real samples [22].

In the current study, the detection limit (DL) was calculated as three times the standard deviation of ten replicate measurements of blank sample with the pre-concentration step. The values obtained from blank measurements were between −0.013 and 0.019 mg L^{-1} (mean, 0.005 mg L^{-1}; s, 0.010 mg L^{-1}) for Zn, −0.062 and 0.054 mg L^{-1} (mean, 0.02 mg L^{-1}; s, 0.035 mg L^{-1}) for Fe, −0.022 and 0.028 mg L^{-1} (mean, 0.002 mg L^{-1}, s, 0.015 mg L^{-1}) for Cu, 0.004 and 0.043 mg L^{-1} (mean, 0.024 mg L^{-1}; s, 0.013 mg L^{-1}) for Cr, and 0.064 and 0.148 mg L^{-1} (mean, 0.109 mg L^{-1}; s, 0.033 mg L^{-1}) for Pb. The detection limits were calculated by dividing the instrumental detection limit by the pre-concentration factor (Table 3).

The precision of an analysis is most conveniently defined in terms of percent relative standard deviation (R.S.D.). The standard deviation (s) is relatively easily calculated following a series of discrete measurements either of absorbance or of concentration. R.S.D. is then defined as the standard deviation expressed as a percentage of the mean of the data used to calculate the standard deviation [22].

Table 4
Analysis of certified reference materials using the developed method

Element	CRM-TMDW-500[a] drinking water			BCR-CRM 144R[b] sewage sludge		
	Certified value (μg L^{-1})	Found value (μg L^{-1})	Recovery (%)	Certified value (μg g^{-1})	Found value (μg g^{-1})	Recovery,%
Fe	100.0 ± 0.5	95.1 ± 4.0	95	–[c]	152.1 ± 8.2	–
Cu	20.0 ± 0.1	18.8 ± 0.3	94	300.0 ± 12.0	283.3 ± 12.4	95
Pb	40.0 ± 0.2	39.3 ± 2.1	98	96.0 ± 1.9	91.2 ± 5.1	95
Zn	70.0 ± 0.4	66.7 ± 2.4	95	919.0 ± 18.4	938.8 ± 41.0	102

[a] Sample volume of drinking water standard was 50 mL.
[b] Quantity of sewage sludge standard was 0.1 g.
[c] Not any value reported.

Table 5
Statistical evaluation of the result obtained in the accuracy study (Table 4 using Student's t-test)

Element	CRM-TMDW-500 drinking water						BCR-CRM 144R sewage sludge					
	s	X_R	$\bar{X}$	$X_R - \bar{X}$	[a]ts/$\sqrt{N}$	Comparison	s	X_R	$\bar{X}$	$X_R - \bar{X}$	ts/$\sqrt{N}$	Comparison
Fe	4.0	100.0	95.1	4.9	9.9	4.9 < 9.9 (same)	–	–	–	–	–	–
Cu	0.3	20.0	18.8	1.2	0.8	1.2 > 0.8 (different)	12.4	300.0	283.3	16.7	30.8	16.7 < 30.8 (same)
Pb	2.1	40.0	39.3	0.7	5.2	0.7 < 5.2 (same)	5.1	96.0	91.2	4.8	12.7	4.8 < 12.7 (same)
Zn	2.4	70.0	66.7	3.3	6.0	3.3 < 6.0 (same)	41.0	919.0	938.8	19.8	101.9	19.8 < 101.9 (same)

[a] $t = 4.30$ (95% confidence intervals); N, 3; s, standard deviation; X_R, value of standard material; $\bar{X}$, mean value; –, not compared.

Table 6
Spiked recoveries of the analyte ions for water samples ($N = 3$, sample volume: 50 mL, final volume: 5.0 mL)

Element	Added (μg)	Stream water		Mineral water	
		Found (μg)	Recovery (%)	Found (μg)	Recovery (%)
Cu	0	ND	–	ND	–
	5	4.9 ± 0.2	98	5.2 ± 0.3	104
	15	15.1 ± 0.4	101	14.8 ± 0.7	99
Fe	0	ND	–	ND	–
	5	4.8 ± 0.4	96	4.7 ± 0.1	94
	15	14.9 ± 0.6	99	15.3 ± 0.4	102
Zn	0	ND	–	ND	–
	5	4.9 ± 0.3	98	4.6 ± 0.3	92
	10	9.6 ± 0.4	96	10.2 ± 0.6	102
Pb	0	ND	–	ND	–
	10	10.1 ± 0.5	101	10.2 ± 0.6	102
	20	18.6 ± 0.9	93	19.7 ± 1.1	99
Cr	0	ND	–	ND	–
	5	5.1 ± 0.3	102	5.1 ± 0.3	102
	15	14.7 ± 0.4	98	15.1 ± 0.7	101

ND: not detected.

Table 7
Spiked recoveries of the analyte ions for solid samples ($N = 3$; sample quantity, 1.000 g; final volume, 5.0 mL)

Element	Added (μg)	Waste tea leaf		Kale	
		Found (μg)	Recovery (%)	Found (μg)	Recovery (%)
Cu	0	1.30 ± 0.05	–	7.7 ± 0.3	–
	5	6.4 ± 0.3	101	13.0 ± 0.5	102
	10	10.8 ± 0.5	96	16.9 ± 0.7	95
Fe	0	42.0 ± 1.8	–	114.3 ± 5.1	–
	10	53.4 ± 2.8	103	124.7 ± 7.1	100
	20	60.8 ± 4.0	98	135.5 ± 6.0	101
Zn	0	11.5 ± 4.1	–	62.1 ± 4.5	–
	10	22.1 ± 1.0	103	71.5 ± 2.6	99
	20	31.2 ± 1.4	99	82.9 ± 3.7	101
Pb	0	2.7 ± 0.2	–	4.5 ± 1.5	–
	5	7.4 ± 0.3	96	9.1 ± 0.4	96
	10	13.1 ± 0.6	103	13.9 ± 0.6	96

The precision of the method, evaluated as the R.S.D. obtained after analyzing a series of ten replicates with the pre-concentration step, was between 1.6% and 6.0% for the five metals (Table 3).

The accuracy of a method is the closeness of the measured value to the true value for the sample. Accuracy is usually determined in one of the four ways. First, accuracy can be assessed by analyzing a sample of known concentration and comparing the measured value to the true value. Various standard reference materials are often used for this purpose. The second approach is to compare test results from the new method with results from an existing alternate method that is known to be accurate. The third approach, which is the most widely used recovery study, is performed by spiking analyte in blank matrices. The fourth approach is the technique of standard additions, which can also be used to determine recovery of spiked analyte. This approach is used if it is not possible to prepare a blank sample matrix without the presence of the analyte [23].

The accuracy of the method was verified by studying the analytical recovery and by analyzing certified reference materials (BCR-CRM 144R sewage sludge and CRM-TMDW-500 drinking water) (Table 4). In order to decide whether the difference between $\bar{X}$ and X_R is significant. As can be seen Table 5, statistical evaluation was applied to the results obtained from the accuracy study (Table 4) using Student's *t*-test [24]. The results revealed good agreement between the observed values and certified values. Analytical recovery was assessed for two concentration levels, after spiking two different solid–liquid samples. As can be seen Tables 6 and 7, good recoveries were reached for all elements.

3.7. Applications to the real samples

The method, finally, after verified by the accuracy tests, was applied to the real solid–liquid samples; the waste tea leaf, kale (*B. oleracea* var. *acephala*) leaf, stream water, and mineral water samples. After pre-concentration step with co-precipitation using BPNBAT without using an additive carrier element, the results

Table 8
Application of the presented method to real samples ($N = 3$; final volume, 5.0 mL)

Element	Stream water[a] (μg L^{-1})	Mineral water[a] (μg L^{-1})	Waste tea leaf[b] (μg g^{-1})	Kale[b] (μg g^{-1})
Fe	133 ± 7	267 ± 11	42 ± 2	114 ± 5
Cu	3.4 ± 0.2	1.8 ± 0.1	1.30 ± 0.05	7.7 ± 0.3
Pb	3.2 ± 0.2	2.2 ± 0.2	2.7 ± 0.2	4.5 ± 1.5
Zn	4.5 ± 0.1	2.7 ± 0.1	11.5 ± 4.1	62 ± 5
Cr	0.82 ± 0.04	0.95 ± 0.05	–	–

[a] Sample volume: 750 mL for analysis of Fe and Cu, 500 mL for analysis of Cr and Zn, and 250 mL for analysis of Pb.
[b] Sample quantity: 1.000 g.

Table 9
Comparison of the present system with other co-precipitation system by FAAS

Studied elements	Co-precipitating agent	PF	DL (μg L^{-1})	R.S.D. (%)	Ref.
Pb^{2+}, Cu^{2+}, Ni^{2+}, Co^{2+}, Cd^{2+}, Mn^{2+}	Dysprosium(III) hydroxide	250	14.1–25.3	<10	[13]
Cd^{2+}, Cu^{2+}, Pb^{2+}	Bi(III)4-methylpiperidinedithiocarbamate	200	0.18–0.50	<10	[14]
Fe^{3+}, Pb^{2+}, Ni^{2+}, Au^{3+}, Pd^{2+}, Cd^{2+}	Copper(II)–rubeanic acid	75	0.14–3.40	<5	[15]
Fe^{3+}, Pb^{2+}, Cr^{3+}, Mn^{2+}	Europium hydroxide	500	1.7–17.1	<10	[16]
Fe^{3+}, Pb^{2+}, Ni^{2+}, Cu^{2+}, Mn^{2+}, Co^{2+}, Cd^{2+}, Cr^{3+}	Samarium hydroxide	50	0.4–24.0	<10	[25]
Fe^{3+}, Pb^{2+}, Ni^{2+}, Cu^{2+}, Co^{2+}, Cd^{2+}	HMDTC-HMA	500	5.9–61.0	<10	[26]
Fe^{3+}, Pb^{2+}, Cu^{2+}, Mn^{2+}, Co^{2+}, Cr^{3+}	Erbium hydroxide	25	0.04–0.87	<9	[27]
Cu^{2+}, Fe^{3+}, Pb^{2+}, Cd^{2+}, Co^{2+}, Ni^{2+}	$Ce(OH)_4$	375	0.18–7.0	<9	[28]
Fe^{3+}, Pb^{2+}	Cu(II)–violuric acid	100	0.16–0.18	<7	[29]
Fe^{3+}, Pb^{2+}, Cu^{2+}, Zn^{2+}, Cr^{3+}	BPNBAT	150	0.3–2.0	<6	This work

HMDTC-HMA, hexamethylene-dithiocarbamic acid hexamethyleneammonium salt; BPNBAT, 3-benzyl-4-*p*-nitrobenzylidenamino-4,5-dihydro-1,2,4-triazole-5-on; PF, pre-concentration factor; DL, detection limit; R.S.D., relative standard deviation.

obtained from flame atomic absorption spectrometric determinations of Fe, Cu, Cr, Zn, and Pb were tabulated in Table 8.

3.8. Comparison of the method with the others

A comparison of the proposed method with other co-precipitation methods is summarized in Table 9 in terms of some optimization parameters. The parameters obtained were comparable to those presented by other methods described in the literature. The proposed co-precipitation method developed by using a new organic co-precipitating agent without any carrier element has relatively high pre-concentration factors, low RSD, and low DL when compared to other methods reported in Table 9.

4. Conclusion

This work presents an alternative procedure for the quantitative determination of trace metals at the low concentration level ($\mu g\,L^{-1}$ or $\mu g\,kg^{-1}$) in various solid–liquid samples by FAAS after the pre-concentration step with a new co-precipitation method. The results of the present investigations showed that the co-precipitation procedure using an organic co-precipitant without using an additive carrier element has a good potential for pre-concentration and separation of trace metals from various environmental solid–liquid samples. The results obtained revealed that the proposed procedure has good precision and accuracy. The system is very simple, fairly rapid, and low cost. The recovery yields obtained with model solutions in the presence of potential interfering concomitants were higher than 95%, thus confirming its independence from matrix effects. Also, that there is no contamination and interference risk for analytes from a carrier element is the one of the important advantages of the proposed system because any carrier element was not used.

Acknowledgements

Authors wish to thank Prof. H. Basri Senturk for allowing to use his laboratory facilities, and to thank Ass. Prof. Murat Kucuk for his contributions. Authors are also thankful to the Unit of the Scientific Research Projects of Karadeniz Technical University for the financial support.

References

[1] A.K. Sen Gupta, Environmental Separation of Heavy Metals Engineering Processes, CRC Press, Boca Raton, FL, USA, 2002.
[2] K. Truus, A. Viitak, M. Vaher, U. Muinasmaa, K. Paasrand, R. Tuvikene, T. Levandi, Proc. Estonian Acad. Sci.: Chem. 56 (2007) 122–133.
[3] E. Carasek, Talanta 51 (2000) 173–178.
[4] J. Wang, E.H. Hansen, Anal. Chim. Acta 456 (2002) 283–292.
[5] F.S. Rojas, C.B. Ojeda, J.M.C. Pavón, Talanta 71 (2007) 918–922.
[6] L. Tavakoli, Y. Yamini, H. Ebrahimzadeh, A. Nezhadali, S. Shariati, F. Noormohamadian, J. Hazard. Mater. 152 (2008) 737–743.
[7] K. Kiran, K.S. Kumar, B. Prasad, K. Suvardhan, L.R. Babu, K. Janardhanam, J. Hazard. Mater. 150 (2008) 582–586.
[8] V.N. Bulut, A. Gundogdu, C. Duran, H.B. Senturk, M. Soylak, L. Elci, M. Tufekci, J. Hazard. Mater. 146 (2007) 155–163.
[9] B. Puzio, B. Mikula, B. Feist, Microchim. Acta 160 (2008) 197–201.
[10] N. Rajesh, R.K. Jalan, P. Hotwany, J. Hazard. Mater. 150 (2008) 723–727.
[11] Y. Cui, X. Chang, X. Zhu, H. Luo, Z. Hu, X. Zou, Q. He, Microchem. J. 87 (2007) 20–26.
[12] M. Tuzen, K.O. Saygi, M. Soylak, Talanta 71 (2007) 424–429.
[13] D.S.K. Peker, O. Turkoglu, M. Soylak, J. Hazard. Mater. 143 (2007) 555–560.
[14] A. Efendioglu, M. Yagan, B. Batı, J. Hazard. Mater. 149 (2007) 160–165.
[15] M. Soylak, N.D. Erdogan, J. Hazard. Mater. 137 (2006) 1035–1041.
[16] M. Soylak, G. Onal, J. Hazard. Mater. 137 (2006) 1130–1134.
[17] Z.B. Alfasi, C.M. Wai, Preconcentration Techniques for Trace Elements, CRC Press, Boca Raton, 1992, pp. 33–99.
[18] C. Zhu, Geochim. Cosmochim. Acta 68 (2004) 3327–3337.
[19] A.A. Ikizler, A. Ikizler, M. Serdar, N. Yıldırım, Acta Pol. Pharm.: Drug Res. 54 (1997) 363–370.
[20] A.A. Ikizler, N. Yıldırım, H. Yuksek, Model. Meas. Control 54 (1996) 21–30.
[21] C. Duran, H.B. Senturk, A. Gundogdu, V.N. Bulut, L. Elci, M. Soylak, M. Tufekci, Y. Uygur, Chin. J. Chem. 25 (2007) 196–202.
[22] J.E. Cantle, Atomic Absorption Spectrometry Techniques and Instrumentation in Analytical Chemistry, Elsevier Scientific Publishing Company, New York, 1982.
[23] J.M. Green, A practical guide to analytical method validation, Anal. Chem. 68 (1996) 305A–309A, http://pubs.acs.org/hotartcl/ac/96/may/may.html (accessed in October 24, 2007).
[24] J.N. Miller, J.C. Miller, Statistics and Chemometrics for Analytical Chemistry, fourth ed., Pearson Education Limited, Edinburgh Gate, Harlow, England, 2000.
[25] S. Saracoglu, M. Soylak, L. Elci, Talanta 59 (2003) 287–293.
[26] L. Elci, M. Soylak, B. Ozcan, Anal. Lett. 36 (2003) 987–999.
[27] M. Soylak, S. Saracoglu, U. Divrikli, L. Elci, Talanta 66 (2005) 1098–1102.
[28] U. Divrikli, Latif Elçi, Anal. Chim. Acta 452 (2002) 231–235.
[29] S. Saracoglu, M. Soylak, D.S.K. Peker, L. Elci, W.N.L. dos Santos, V.A. Lemose, S.L.C. Ferreira, Anal. Chim. Acta 575 (2006) 133–137.

Talanta 76 (2008) 454–457

Contents lists available at ScienceDirect

Talanta

journal homepage: www.elsevier.com/locate/talanta

Amperometric detection of carbohydrates and thiols by using a glassy carbon electrode coated with Co oxide/multi-wall carbon nanotubes catalytic system

Susanna Buratti*, Barbara Brunetti, Saverio Mannino

Department of Food Science and Technology, University of Milan, Via Celoria 2, 20133 Milan, Italy

ARTICLE INFO

Article history:
Received 23 November 2007
Received in revised form 10 March 2008
Accepted 21 March 2008
Available online 28 March 2008

Keywords:
Carbohydrates
Thiols
Carbon nanotubes
Cobalt oxide
Amperometric detection

ABSTRACT

A glassy carbon electrode coated with cobalt oxide/multi-wall carbon nanotubes (MWCNT) system was used for the detection of carbohydrates and thiols. The modification of the glassy carbon electrode increased the anodic current response of these organic compounds and decreased their overvoltage. The amperometric responses were extremely stable with no loss of sensitivity over many days of storage. Such attractive performance characteristics indicate great promise for using this new catalytic system for monitoring in fast and simple way compounds of great interest for food industry, biotechnology and clinical diagnostics.

1. Introduction

Carbohydrates and thiols are of great interest in many scientific and industrial areas and also in clinical diagnostics. The electrochemical detection of these compounds is a challenge since their direct oxidation is generally hampered by poor voltammetric behaviour at glassy carbon electrode. The main problem inherent to such anodic detection is the large overvoltage encountered for oxidation at ordinary electrodes; consequently considerable effort has been devoted toward the goal of identifying new electrode materials that will reduce the overpotential for carbohydrates and thiols oxidation. Chemically modified carbon electrode containing cobalt oxide, cobalt-phthalocyanine or ruthenium dioxide have been used for amperometric measurements of sugars [1–4]; also transition metal electrodes such as copper and nickel have been employed for carbohydrates evaluation [5,6]. Electrodes modified with phthalocyanine derivatives [7–9], organic mediators [10,11] and enzyme [12], have been used for voltammetric and amperometric detection of thiols. Actually in the scientific community there is a great interest to explore application of carbon nanotubes (CNTs) because of their high electrical conductivity, high surface area and good chemical stability. Several authors have reported the excellent electrocatalytic properties of multi-wall carbon nanotubes (MWCNTs) and single-wall carbon nanotubes (SWCNTs) in the electrochemical oxidation of molecules and biomolecules such as NADH [13], dopamine and ascorbic acid [14], hydrogen peroxide [15] and also carbohydrates [16,17] and thiols [18,19]. Furthermore it has been shown that the combination of CNT with glucose oxidase [20] or copper [21], provide a mean of enhancing the detection of glucose and sugars in general.

Although some works have been published on electrosorbtion or adsorption of phthalocyanines and metallophthalocyanines on CNT [22–24] there are no works about glassy carbon electrodes modified with MWCNT and cobalt. This article reports an easy preparation method of Co oxide/multi-wall carbon nanotubes catalytic system and a fast procedure to modify glassy carbon electrode. The Co oxide/MWCNT system was prepared according to the work of Liu et al. [25]. In that work high resolution transmission electron microscopy (HRTEM) was used for investigate the microstructure of cobalt nanoparticles formed on MWCNTs surface and it has been demonstrated that cobalt nanoparticles deposited on oxidized MWCNTs gave rise to a monometallic system that exhibited high catalytic activity.

The electrocatalytic activity of the proposed electrode was evaluated towards the detection of carbohydrates and thiols in a flow injection system. In the following sections we well demonstrate that Co oxide/MWCNT catalytic system display a great promotion

* Corresponding author. Tel.: +39 02 50319217; fax: +39 02 50319061.
E-mail address: susanna.buratti@unimi.it (S. Buratti).

0039-9140/$ – see front matter © 2008 Elsevier B.V. All rights reserved.
doi:10.1016/j.talanta.2008.03.031

of the oxidation of carbohydrates and thiols and also a higher sensitivity compare to cobalt oxide and carbon nanotubes alone.

2. Experimental

2.1. Apparatus

Cyclic voltammetric studies were performed with the potentiostat CHI 1010 (CH Instruments Inc., USA). A conventional three-electrode cell was used with a saturated Ag/AgCl reference electrode, a platinum wire counter electrode, and a modified glassy carbon as working electrode. The potential scan rate was of 50 mV s^{-1}.

The amperometric measurements were performed with an EG&G Princeton Applied Research Model 400 thin layer electrochemical detector equipped with the modified glassy carbon electrode (surface area 8 mm^2), the reference (Ag/AgCl saturated) electrode and the platinum wire counter electrode. The flow injection system consisted of a carrier solution reservoir, an injection valve with a 20 μl loop, connecting tubes of PEEK (1.5 mm o.d. × 0.5 mm i.d.), an HPLC pump (Jasco 880 PU), the amperometric detector and a Philips PM 8252 recorder.

2.2. Reagents

Multi-wall carbon nanotubes with 95% purity were supplied by NanoLab Inc. (Brighton, MA). Oxidization of MWCNT was accomplished by stirring CNT in concentrate nitric acid at 70 °C for 2 h. The mixture was then separated by filtration, washed with distilled water and dried at 100 °C overnight. Cobalt(II)-chloride aqueous solution was purchased from Merck (Darmstadt, Germany), Cobalt(II) oxide was purchased from Aldrich. D-Glucose, D-galactose, lactose, sucrose, L-cystein and glutathione were obtained from Sigma (Sigma–Aldrich, Italy). Nafion solution (5 wt.% in lower aliphatic alcohols and water) was purchased from Aldrich and was diluted as required in double distilled water.

2.3. Preparation of glassy carbon electrode modified with Co oxide–MWCNT system (GC/Co oxide–MWCNT electrode)

For the preparation of Co oxide/MWCNT system, the oxidized MWCNT were impregnated with $CoCl_2$ aqueous solution, followed by drying at 100 °C for 10 h and calcination at 480 °C for 3 h. As reported in other works [26,27], the thermal decomposition of salt solution led to the formation of cobalt oxides on the surface of nanotubes. The Co oxide/MWCNT system was cast onto the glassy carbon electrode by using Nafion 1% as dispersing medium. The coating solution was prepared by dispersing 2.5 mg of Co oxide/MWCNT complex into 1 ml aqueous solution of Nafion 1%. A 20 μl aliquot of the resulting solution was placed directly onto the glassy carbon surface and left to dry at room temperature.

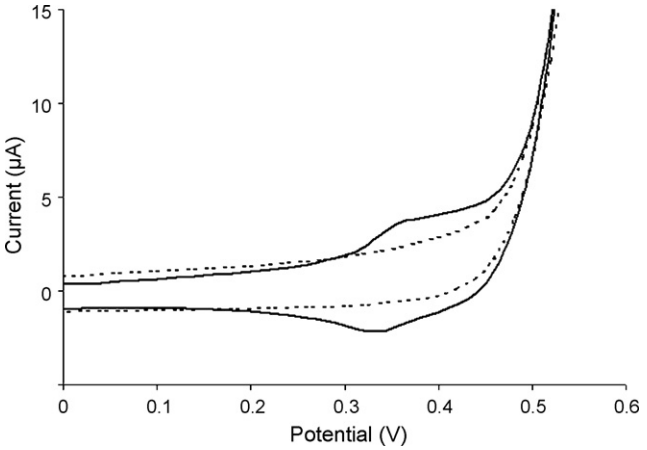

Fig. 1. Cyclic voltammograms recorded in a 0.1 M NaOH solution at a GC/Co oxide–MWCNT electrode (solid line) and a GC/MWCNT electrode (dashed line). Scan rate of 50 mV s^{-1}.

The preparation of glassy carbon/multi-wall carbon nanotube (GC/MWCNT) electrode was obtained according to the same procedure by using oxidized MWCNT. The GC/Co oxide electrode was performed by deposition on the surface of the glassy carbon of a dispersion of Co(II) oxide in Nafion 1%.

3. Results and discussion

Preliminary cyclic voltammetric experiments were performed to study the electrochemical behaviour of the glassy carbon electrode coated with cobalt oxide/multi-wall carbon nanotubes system. As previously reported [28], the electrochemical activity of Co(II)/Co(III) species depends strictly on the actual chemical and physical status of the film deposited on the electrode. In our case, as shown in Fig. 1, the voltammogram recorded in 0.1 M NaOH reveals a set of peaks at about +0.35 V in the forward and at +0.33 V in the reverse scan, respectively. These values are in agreement with previous findings about Co oxides-modified electrodes [28]. The redox couple could be attributed to the conversion between Co_3O_4/CoOOH species [28–30].

The electrocatalytic activity of GC/Co oxide–MWCNT electrode was examined by cyclic voltammetry and amperometric measurements. Fig. 2 shows two set of cyclic voltammograms at the GC/Co oxide–MWCNT electrode, in NaOH 0.1 M solutions containing increasing concentration of cystein (A) and glucose (B). The

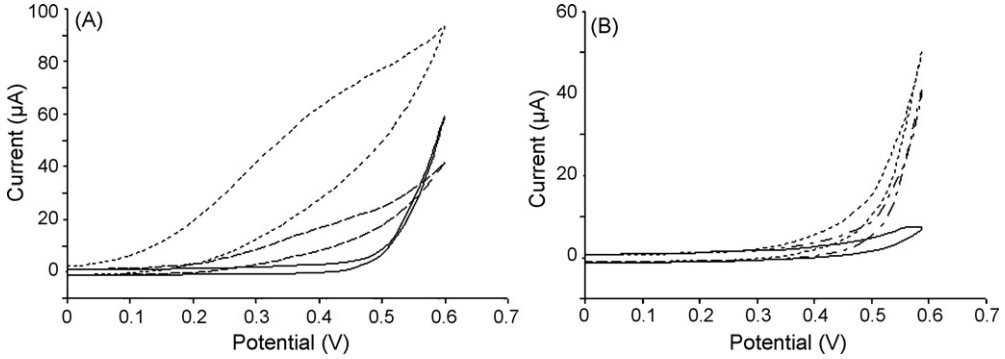

Fig. 2. Cyclic voltammograms at GC/Co oxide–MWCNT electrode in 0.1 M NaOH solution in the absence (solid lines) and presence of 5 mM (dashed lines) and 10 mM (dotted lines) cystein (A) and glucose (B). Scan rate of 50 mV s^{-1}.

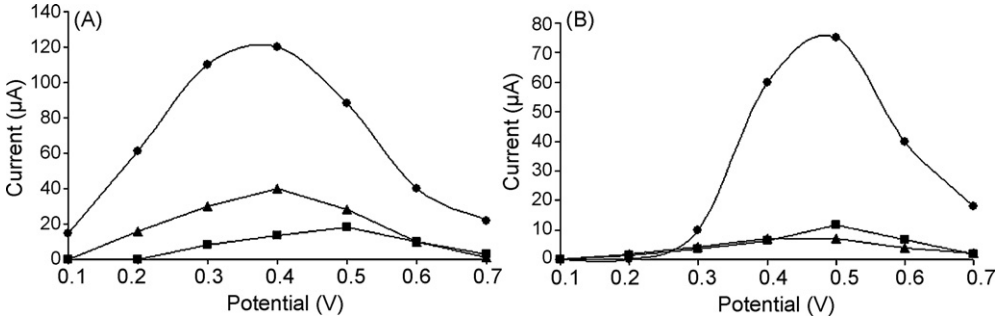

Fig. 3. Current/potential plots for 2 mM cystein (A) and glucose (B) at GC/Co oxide–MWCNT electrode (●) in comparison to GC/MWCNT (▲) and GC/Co oxide (■) electrodes. Operative conditions: carrier solution, 0.1 M NaOH; injection volume, 20 μl; reference electrode, Ag/AgCl saturated.

modified electrode exhibits significant oxidation current starting around +0.2 and +0.3 V for cystein and glucose, respectively. As can be seen, the peak of Co practically disappears in the reverse scan, as expected in the case of an electrocatalytical process confined onto the electrode surface, demonstrating the activity of the Co oxide species present onto the electrode. Such voltammetric behaviour is consistent with an electrocatalytic reaction in which cystein and glucose reduce the high valence cobalt species formed under anodic polarization and subsequently re-oxidized at the electrode surface [27,28]. In Fig. 3 are shown the current/potential plots for the oxidation of cystein (2 mM) and glucose (2 mM) (carrier solution NaOH 0.1 M) at GC/Co oxide–MWCNT electrode in comparison to GC/MWCNT electrode and GC/Co oxide electrode. The plots put in evidence that there is a significant catalytic effect induced by Co oxide–MWCNT system in term of enhancement of the anodic current in the oxidation process of both cystein and glucose. At GC/Co oxide–MWCNT electrode the maximum response for glucose oxidation was observed at a potential of +0.5 V with an enhancement of 8–10 folds in the oxidation current with respect to GC/MWCNT electrode and GC/Co oxide electrode. In the case of cystein the oxidation current at GC/Co oxide–MWCNT electrode rose rapidly up to +0.4 V, and the enhancement observed was of three and nine folds with respect to GC/MWCNT electrode and GC/Co oxide electrode. We can state that the enhanced analytical signals of GC/Co oxide–MWCNT electrode with respect to GC/MWCNT and GC/Co oxide electrodes can be attributed to a larger amount of cobalt oxide deposited on the CNT surface due to their larger surface area. This hypothesis is in agreement with other works reported in literature [31].

In order to optimize the electrocatalytic response of GC/Co oxide–MWCNT electrode towards thiols oxidation, the effect of pH on the oxidation behaviour was investigated. In Fig. 4 are reported the current/potential plots of cystein (2 mM) and glutathione (5 mM) on GC/Co(II)–MWCNT electrode in two different carrier solution: NaOH 0.1 M (pH 13) and acetate buffer 0.1 M (pH 4). In the alkaline medium the two compounds exhibit a considerable reduction in the overpotential of the oxidation process while in acid medium a considerable enhancement of the anodic current was noted only at higher positive potential. This is probably due to the deprotonation involved in the oxidation process that is facilitated at high pH values.

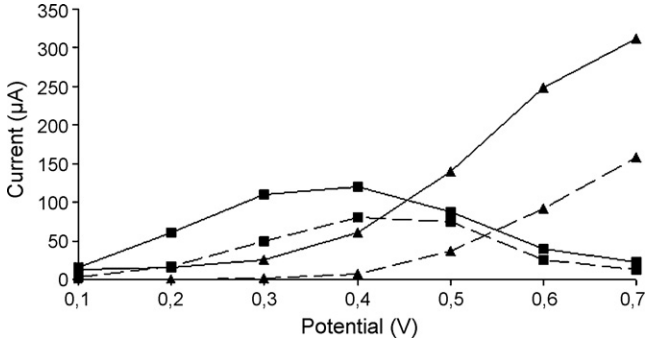

Fig. 4. Current/potential plots for 2 mM cystein (solid lines) and 5 mM glutathione (dashed lines) at GC/Co oxide–MWCNT electrode. 0.1 M NaOH pH 13 (■) and 0.1 M acetate buffer pH 4 (▲). Operative conditions as in Fig. 3.

The electrocatalytic activity of Co oxide–MWCNT system facilitated flow injection amperometric measurements of carbohydrates at +0.5 V and thiols at +0.4 V. Fig. 5 displays the flow injection amperometric responses for increasing concentration of glucose and cystein. Well-defined current signals were observed for the two compounds at all the concentration levels while in absence of thiols and carbohydrates no amperometric response was recorded. The GC/Co(II)–MWCNT electrode responded very rapidly to the concentration changes producing steady-state signals within 10–12 s. A high stable amperometric response with no loss in sensitivity or memory effect was observed for both 2 mM glucose and cystein solution over a continuous 120 min period (not shown). The reproducibility of the amperometric response evaluated as relative standard deviation (R.S.D.%) at a concentration level of 2 mM was

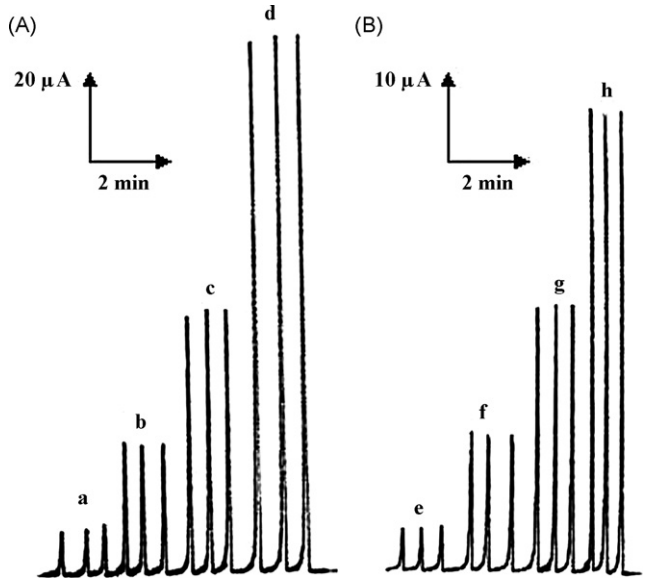

Fig. 5. Flow injection amperometric responses for increasing concentrations of cystein (A) and glucose (B) at GC/Co oxide–MWCNT electrode. Cystein concentrations: (a) 0.2 mM, (b) 0.5 mM, (c) 1 mM, (d) 2 mM; glucose concentrations: (e) 0.2 mM, (f) 0.5 mM, (g) 1 mM, (h) 2 mM. Operative conditions: working potentials: +0.4 V (vs. Ag/AgCl saturated) for cystein and +0.5 V (vs. Ag/AgCl saturated) for glucose; carrier solution, 0.1 M NaOH; injection volume, 20 μl.

Table 1
Analytical parameters for the detection of sugars and thiols

Compounds	Linear range (mM)	Regression data	Correlation coefficient	Detection limit (mM)[a]
Glucose	0.15–5	μA = 34.19 mM + 4.98	0.995	0.07
Galactose	0.15–5	μA = 43.81 mM + 10.31	0.995	0.10
Lactose	0.15–1.5	μA = 19.84 mM + 0.56	0.999	0.08
Sucrose	0.15–1.5	μA = 11.64 mM + 0.60	0.999	0.08
Cystein	0.10–5	μA = 14.49 mM + 11.14	0.995	0.05
Glutathione	0.15–1.5	μA = 3.3 mM + 0.45	0.997	0.13

[a] Signal/noise = 3.

2.8% for glucose ($n = 15$) and 3.2% for cystein ($n = 15$). Rapid amperometric responses and good linearity of the calibration plot was recorded also for other sugar and thiolic compounds. In Table 1 are summarized the principal analytical parameters of the detection of glucose, galactose, lactose, sucrose, cystein and glutathione, in terms of linear range, regression data, correlation coefficient and detection limit based on signal-to-noise ratio (S/N = 3). A high stable amperometric response was observed also using the GC/Co oxide–MWCNT electrode after leaving it at room temperature for a period of 2 weeks; the peak potential for thiols and sugars oxidation was unchanged and the current response decreased less than 5%.

4. Conclusion

Results demonstrate that the Co oxide–MWCNT system has an excellent electrocatalytic activity towards the oxidation of scarcely electroactive organic compounds such as carbohydrates and thiols. Furthermore the glassy carbon electrode modified with Co oxide–MWCNT system show striking analytical properties such as high stability, good reproducibility, low detection limit, fast response time, suggesting that it can be applied to routine analysis of sugars or thiols in biological and food matrices using a flow injection system eventually coupled with a chromatographic or electrophoretic separation system.

References

[1] L.M. Santos, R.P. Baldwin, Anal. Chem. 59 (1987) 1766.
[2] J. Wang, M.Z. Taha, Anal. Chem. 62 (1990) 1413.
[3] S. Mannino, M.S. Cosio, S. Ratti, Electroanalysis 5 (1993) 145.
[4] T.R.I. Castaldi, A. Guerrieri, I.G. Casella, E. Desimoni, Electroanalysis 7 (1995) 305.
[5] J.M. Marioli, T. Kuwana, Electroanalysis 5 (1993) 11.
[6] P. Singhai, K. Kawagoe, C. Christian, W.G. Kuhr, Anal. Chem. 69 (1997) 1662.
[7] S. Zhang, W.L. Sun, Y.T.Z. Xian, W. Zhang, L.T. Jin, K. Yamamoto, S.G. Tao, J.Y. Jin, Anal. Chim. Acta 399 (1999) 213.
[8] G.Y. Shi, J.X. Lu, F. Xu, W.L. Sun, L.T. Jin, K. Yamamoto, S.G. Tao, J.Y. Jin, Anal. Chim. Acta 391 (1999) 307.
[9] M.J. Aquirre, M. Isaacs, F. Armijo, N. Bocchi, J.H. Zagal, Electroanalysis 10 (2000) 571.
[10] N.S. Lawrence, J. Davis, L. Jiang, T.G.J. Jones, N.S. Davis, R.G. Compton, Analyst 125 (2000) 661.
[11] X. Gong, H.L. Li, J. Electrochem. Soc. 147 (2000) 238.
[12] S. Timur, D. Odaci, A. Dincer, F. Zihnioglu, A. Telefoncu, L. Gorton, Sens. Actuators B 125 (2007) 234.
[13] M. Musameh, J. Wang, A. Merkoci, Y. Lin, Electrochem. Commun. 4 (2002) 743.
[14] Z. Wang, J. Liu, Q. Liang, Y. Wang, G. Lou, Analyst 127 (2002) 653.
[15] J. Wang, M. Musameh, Y. Lin, J. Am. Chem. Soc. 125 (2003) 2408.
[16] J.S. Ye, Y. Wen, W.D. Zhang, L.M. Gan, G.Q. Xu, F.S. Sheu, Electrochem. Commun. 6 (2004) 66.
[17] R.P. Deo, J. Wang, Electrochem. Commun. 6 (2004) 284.
[18] N.S. Lawrence, J. Davis, R.G. Compton, Talanta 53 (2001) 1089.
[19] A. Salimi, R. Hallaj, Talanta 66 (2005) 967.
[20] S.H. Lim, J. Wei, J. Lin, Q. Li, J.K. You, Biosens. Bioelectron. 20 (2005) 2341.
[21] J. Wang, G. Chen, M. Wang, M.P. Chatrathi, Analyst 129 (2004) 512.
[22] X. Wang, Y. Liu, W. Qiu, D. Zhu, J. Mater. Chem. 12 (2002) 1636.
[23] J.S. Ye, Y. Wen, W.D. Zhang, H.F. Cui, G.Q. Xu, F.S. Sheu, Electroanalysis 17 (2005) 89.
[24] J.F. Silva, S. Griveau, C. Richard, J.H. Zagal, F. Bedioui, Electrochem. Commun. 9 (2007) 1629.
[25] Z.J. Liu, Z.Y. Yuan, W. Zhou, L.M. Peng, Z. Xu, Phys. Chem. Chem. Phys. 3 (2001) 2518.
[26] Z. Fan, J. Chen, K. Cui, F. Sun, Y. Xu, Y. Kuang, Electrochim. Acta 52 (2007) 2959.
[27] S. Palmas, F. Ferrara, A. Vacca, M. Mascia, A.M. Polcaro, Electrochim. Acta 53 (2007) 400.
[28] I.G. Casella, M. Gatta, J. Electroanal. Chem. 534 (2002) 31.
[29] I.G. Casella, J. Electroanal. Chem. 520 (2002) 119.
[30] C. Barbero, G.A. Planes, M.C. Miras, Electrochem. Commun. 3 (2001) 113.
[31] R.P. Deo, N.S. Lawrence, J. Wang, Analyst 129 (2004) 1076.

Talanta 76 (2008) 333–337

Contents lists available at ScienceDirect

Talanta

journal homepage: www.elsevier.com/locate/talanta

Detection of global glycosylation changes of serum proteins in type 1 diabetes using a lectin panel and multivariate data analysis

Jenny Carlsson[a,*], Camilla Gullstrand[b], Johnny Ludvigsson[b], Ingemar Lundström[c], Fredrik Winquist[c]

[a] Division of Sensor Science and Molecular Physics, Department of Physics, Chemistry and Biology (IFM), Linköping University, SE-581 83 Linköping, Sweden
[b] Division of Pediatrics and Diabetes Research Center, Department of Molecular and Clinical Medicine, Faculty of Health Sciences, Linköping University, SE-581 85 Linköping, Sweden
[c] Division of Applied Physics, Department of Physics, Chemistry and Biology (IFM), Linköping University, SE-581 83 Linköping, Sweden

ARTICLE INFO

Article history:
Received 21 November 2007
Received in revised form 27 February 2008
Accepted 29 February 2008
Available online 18 March 2008

Keywords:
Lectin panel
Glycosylation changes
Type 1 diabetes
Ellipsometry
MVDA

ABSTRACT

Global glycosylation changes of serum proteins in type 1 diabetic patients have in this paper been investigated based on the interaction of the saccharide moiety of serum proteins with different lectins. Lectins are proteins, which bind carbohydrates specifically and reversibly. Panels with lectins of various carbohydrate specificities were immobilized on gold surfaces. Sera from healthy individuals, newly diagnosed type 1 diabetes patients and type 1 diabetes patients having had the disease for 4–6 years, respectively, were applied to the lectin panel. The biorecognition was evaluated with null ellipsometry. Data obtained were related to an internal standard of lactoferrin. Multivariate data analysis (MVDA) techniques were used to analyze data.

Principal component analysis showed that the lectin panel enabled discrimination between sera from the three different above-mentioned groups. Using an artificial neuronal net (ANN), it was possible to correctly categorize unknown serum samples into one of the three groups.

1. Introduction

Most human serum proteins are glycosylated. Various diseases such as microbial infections, inflammations and autoimmune diseases, for example rheumatoid arthritis, result in glycosylation changes of serum proteins [1,2], i.e. enzyme directed glycosylation. These changes can be utilized in discriminative clinical tests and for example in cancer research much attention has been given to study glycosylation changes for possible diagnosis, measurement of effectiveness of treatment and prognosis [3].

Type 1 diabetes is characterized by beta cell destruction caused by an autoimmune process, usually resulting in total insulin deficiency. Type 1 diabetes is associated with increased non-enzymatic glycosylation, glycation, of for example hemoglobin. Less is known on enzymatic glycosylation changes of serum proteins in type 1 diabetes.

Diabetes is a group of metabolic disorders (type 1, type 2, gestational and other types) characterized by hyperglycemia, which might cause long-term effects such as damage to eyes, kidneys, nerves, heart and blood vessels. In 2007 more than 180 million people worldwide suffered from diabetes [4]. The incidence is rapidly increasing, and it is estimated that by the year 2030, this number will double. Approximately 5–10% suffer from type 1 diabetes.

Diagnosis of type 1 diabetes can be made from symptoms among which increased urine flow, increased thirst and weight loss are included. Plasma glucose levels are often measured to confirm diabetes, but diagnosis of diabetes cannot be made on hyperglycaemia alone, since this can be caused by for example infections [5].

Measuring glycation of hemoglobin or HbA1c is a test to examine overall diabetes control. The results of the HbA1c test represent average blood sugar for the previous 2–3 months. Keeping the glycated hemoglobin low has been shown to minimize long-term complications associated with diabetes [6]. HbA1c is also a good indicator for people at risk of developing type 2 diabetes [7].

The pathological process of diabetes influences a wide variety of metabolic pathways and enzymatic glycosylation of proteins is also altered in diabetes [8]. Some specific changes in single proteins have been associated with type 1 diabetes. For example abnormalities in *N*-glycolsylation in humans may be a factor in the pathogenesis of autoimmunity [9]. A causative role is suggested for O-GlcNAc modifications in the development of insulin resistance and diabetic complications [10]. Altered structure of aminooligopeptidase is common in diabetes patients [11]. Increased fucosylation of acute phase protein α_1-acid glcyoprotein (AGP) might be used as an additional marker for the development of vascular complications in type 1 diabetic patients. [12]

* Corresponding author. Tel.: +46 13 281212; fax: +46 13 288969.
E-mail address: jenca@ifm.liu.se (J. Carlsson).

0039-9140/$ – see front matter © 2008 Elsevier B.V. All rights reserved.
doi:10.1016/j.talanta.2008.02.046

There is a lack of knowledge of global enzymatic glycosylation changes of proteins in type 1 diabetes however, and this is especially true for the plasma and serum glycoproteome, where the bulk of proteins are released by a process of secretion from tissues.

In this contribution a new concept for investigating global glycosylation changes of serum proteins in type 1 diabetic patients is described. It is based on interaction studies of the saccharide moiety of serum proteins with lectins. Lectins are a class of naturally occurring proteins and glycoproteins found in all kinds of organisms, which bind carbohydrates specifically and reversibly. Lectins are selective towards one or two saccharide residues, why their ability to discriminate polysaccharide structures is limited. Lectins have been utilized for various analytical applications, such as blood typing [13], for classification of bacteria [14,15] and for monitoring induced glycosylation pattern changes of glycoproteins [16]. Also, panels of lectins with different carbohydrate specificity combined with multivariate data analysis (MVDA) open up possibilities to enhance biorecognition. Thus, lectin panels together with MVDA have for example been used to differentiate human serum samples from healthy and bacterial infected persons [17], for discrimination of meat juices and sera from various animal species [18,19] and for the identification of *Escherichia coli* subspecies [15].

Based on this, the aim of the study was to investigate if, using a seven-membered lectin panel combined with MVDA, any noticeable glycosylation differences between serum samples from healthy individuals, newly diagnosed type 1 diabetes patients (day 0) and type 1 diabetes patients having had the disease for 4–6 years, respectively, could be detected and if discrimination between them could be done. The biorecognition is evaluated with null ellipsometry and the data obtained is related to an internal standard of lactoferrin on each surface. MVDA techniques are used to analyze data.

The suggested method is a qualitative technique and not for quantitative measure. It is intended to be used in order to get a further understanding of global glycosylation alterations of serum proteins in type 1 diabetes.

2. Experimental

2.1. Surface preparation and immobilization

Preparation of microcontact printed gold surfaces with well-defined regions of different chemical functionality: hydrophilic patches separated by a hydrophobic barrier, has been described elsewhere [19–21]. A thorough description of the immobilization procedure of the seven different biotinylated lectins, Table 1, from the species *Lens culinaris*, *Phaseolus vulgaris*, *Ulex europaeus*, *Griffonia simplicifolia*, *Arachis hypogaea*, *Triticum vulgaris* and Concanavalin A (the first four all purchased form Vector and the last three from Sigma) to the microcontact printed surfaces is given in Carlsson et al. [19] and an overview of the immobilization scheme, partly adopted from Schäferling et al. [22], is shown in Fig. 1. The lectins were chosen with regard to their different carbohydrate binding specificities and are readily available. All patches on one surface had the same lectin applied to it.

Table 1
The seven different lectins used in the lectin panel

Lectin	Abbreviation	Specificity	Size (kDa)
Canavalia ensiformis	Con A	α-Man, α-Glc	106.5
Triticum vulgaris	WGA	β-GlcNAc, sialic acid (NeuNAc)	36
Arachis hypogaea	PNA	β-Gal, galNAc	120
Griffonia simplicifolia	GSL-1	α-Gal, α-GalNAc	115
Phaseolus vulgaris agglutinin	PHA	Complex structures	125
Ulex europaeus agglutinin	UEA	α-Fuc	63
Lens culinaris agglutinin	LCA	α-Glc, α-Man	49

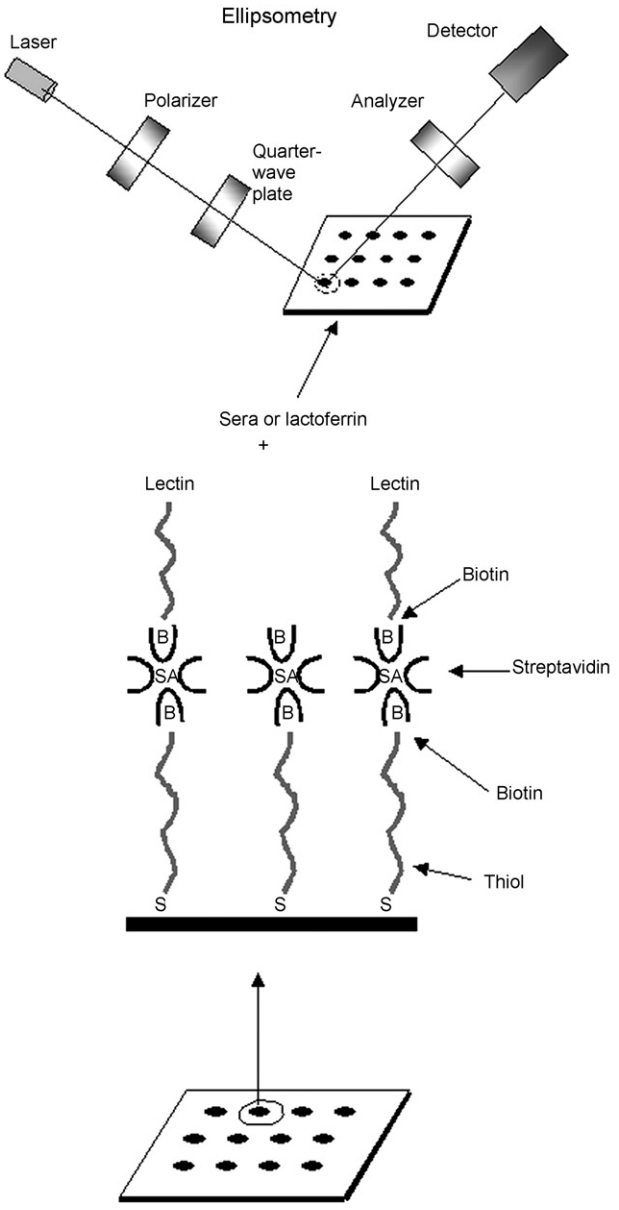

Fig. 1. Schematic presentation of lectin immobilization onto microcontact printed gold surfaces, hydrophobic surfaces with hydrophilic patches. Each hydrophilic patch is incubated with biotin, streptavidin and biotinylated lectin. On one surface the same lectin is immobilized. To the lectin patches serum samples are added. The thickness of bound material in each patch is then measured with null ellipsometry.

2.2. Serum samples

Sera samples from six different healthy persons without type 1 diabetes, from six different newly diagnosed type 1 diabetes patients (day 0) and from six different type 1 diabetes patients having had the disease for 4–6 years were used, making altogether 18 different serum samples investigated. All samples but two healthy were from children (aged 5–18 years old). The healthy samples from children were part of the ABIS-material (All Babies in Southeast Sweden [23]). The protocol of the ABIS study and the collection of serum samples from diabetic patients were approved of by the Research Ethics Committee of the Medical Faculty of Linköping University, Linköping, Sweden.

The 18 serum samples investigated were divided in three measurement occasions. Two sera from each group: healthy, newly diagnosed type 1 diabetes patients (day 0) and type 1 diabetes

patients having had the disease for 4–6 years were used in a double experiment, experiments 1 and 2 with a couple of days in between. Another double experiment was performed a couple of weeks later, experiments 3 and 4 (a couple of days in between), and a third experiment was carried out a couple of months after that, experiments 5 and 6 (a couple of days in between).

Lactoferrin (from bovine colostrum (Sigma)) was added to four patches on each lectin surface. Lactoferrin is used as an internal standard on each surface. A quadruple of each diluted serum was then added to each type of lectin surface (seven different types). Each single experiment used 21 surfaces, three surfaces for each type of lectin. One surface had 12 patches, four used for lactoferrin, four for one serum sample and four for another serum sample (making in total 252 individual patches per experiment). Altogether 126 surfaces with 1512 patches divided in the three measurement occasions, experiments 1–6 were used.

After 2 h of incubation the surfaces were washed with distilled water, blown dry under a stream of nitrogen and the thickness of bound material in each patch of a surface was measured with ellipsometry and presented as a proportion of the average lactoferrin thickness on that particular surface. The ellipsometric thickness of the different lectins varies due to their different size. Lactoferrin, which binds to all the lectins used in the panel, was introduced as an internal standard. Thereby, any varying binding results between surfaces and between days of preparation could to a certain extent be compensated for. Serum and lactoferrin patch outliers on each surface were detected and not included in further calculations. Outliers could for example be a patch damaged by partial drying out or dust particles.

The lactoferrin related thickness data from experiments 1–6 generated a matrix, which was treated with MVDA.

2.3. Null ellipsometry measurements

A null ellipsometer (Rudolph Research Auto EL III bench ellipsometer) equipped with a He–Ne laser (632.8 nm) light source (beam area approximately 1 mm) aligned at an incidence angle of 70° with respect to the surface normal was used in these experiments. The refractive index, n_f, of the adsorbed protein layer was chosen to 1.465 [24].

Polarization changes occurring after deposition of a thin film on the surface together with knowledge of the optical properties of the bare surface are utilized for calculation of the thickness and the refractive index of the deposited film. In null ellipsometry, the polarizing elements (polarizer and analyzer) are rotated until the signal at the detector is zero (null). The angular positions of the polarizer and analyzer then give the ellipsometric angels Δ and ψ, which can be entered into the so called McCrackin algorithm [25] to give the thickness of the layer.

2.4. Data analysis

The lactoferrin related thickness data from experiments 1–6 generated a matrix, which was treated with MVDA techniques, such as principal component analysis (PCA) using SIRIUS 6.5 (Pattern Recognition System A/S, Norway) and artificial neuronal networks (ANN) using Brainmaker (California Scientific Software, USA).

With PCA an overview of a data set is given and patterns in the data can be revealed. PCA explains the variance in the experimental data and reduces the immense data set to plots, score plots, which can easily be used to classify or group the observations (experiments).

The data were also used for making models of prediction using an artificial neuronal net (ANN). This is a non-linear model tolerant to noise and faults and can classify complicated patterns and predict new samples. ANN is a layered structure with an input, at least one hidden and an output neuron layer. For evaluating the prediction capability, cross-validation is often used. Thus, all experiments except for one are used for modeling, the remaining experiment is then used for prediction. This is repeated until all experiments have been predicted. Here a three layered ANN, with one input layer, one hidden layer and one output layer using the learning algorithm back propagation of errors was used to process data. The net consisted of 7 input nodes corresponding to the 7 members in the lectin panel, 6 nodes in the hidden layer and three output nodes corresponding to the three serum classes: healthy, newly diagnosed and having had the disease for 4–6 years. Learning rate and momentum term were set to 0.5 and 0.8, respectively. Thus, a model based on ANN was made to classify unknown serum samples into one of the three serum groups.

3. Results and discussion

In Fig. 2 a typical graph showing the average thickness of serum samples from experiment 1 relative the thickness of the internal standard of lactoferrin for the seven different lectins used in the panel is seen.

PCA score-plots (not shown) were made and studied from data generated from all the six experiments. For all individual experiments, except for experiment 3, clear discriminations between the three groups (healthy, newly diagnosed and having had type 1 diabetes for 4–6 years) were observed. The first principal components (PC1) for all score plots were in the interval 41–43%, and for the second principal components (PC2) in the interval 28–30%, making a total coefficient of determination of up to 70%. The serum samples from healthy persons and type 1 diabetes patients were picked at random from a bank of sera with samples collected at different times and were handled equally. It is not probable that the discrimination between the three groups is due to any non-type 1 diabetic cause such as bacterial infections or difference in age, etc.

A strategy based on an ANN for modeling and class prediction was used for examining and identifying deviating samples. Thus, a model based on an ANN was made to classify unknown serum samples into one of the three serum groups. Using cross validation on data from all six experiments, the number of misclassified samples is rather high (19 out of altogether 90 classifications), especially for predictions of experiment 3 by a model based on the other five experiments.

Using data, excluding experiment 3, the number of misclassifications decreased remarkably, but still a number of samples (7) were classified into the wrong group. It was found out that by removing

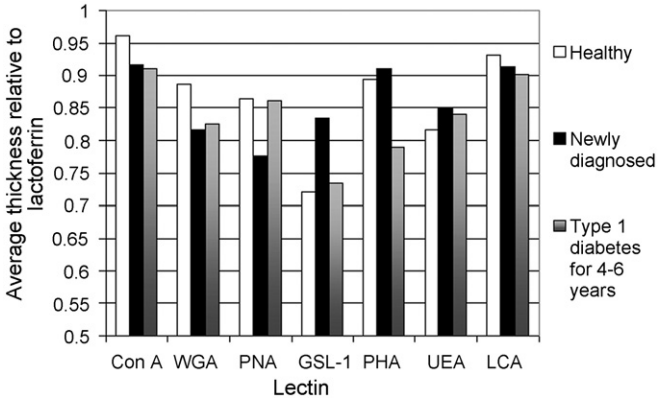

Fig. 2. A typical graph showing the average thickness of serum samples from experiment 1 relative the thickness of the internal standard of lactoferrin for the seven different lectins used in the panel.

data from one of the lectins in the panel, *Arachis hypogaea* (PNA), the results could be further improved. These results indicate that when performing experiments 3 and 4 some problems aroused with the experimental platform and that these problems possibly can be derived to the lectin *PNA*. As can be understood from the experimental section, the preparation of samples entails large effort in manual handling, altogether 1512 patches have to be individually prepared and analyzed. Since one lectin is applied to all patches on one surface, a plausible explanation is that one surface with PNA was altered, which then greatly influenced the results of the whole experiment. Thus, using data with experiment 3 and the lectin PNA left out, cross-validated predictions showed only three misclassifications out of the 90 predictions.

PCA loading plots were performed to elucidate the importance of each lectin. It showed that all lectins were of similar importance, except for experiment 3 and 4, where PNA differed from the other lectins. Due to the limited amount of experiments this result is merely an indication, since normally these kinds of investigations are carried out on larger data sets.

The authors are very well aware of that it is dangerous to leave out experiments that do not fit expected or wanted results. In this case, however, it appeared clear that problems arouse with the experimental platform for experiment 3 and the lectin PNA, and it is thus justified to leave out these experiments.

In Fig. 3a, data from experiments 1, 2, 5 and 6 are shown in the same PCA-plot. Data from experiments 1 and 2 are to the left of the drawn line and data from experiments 5 and 6, to the right. The separation in PC1 between the two double experiments is obviously due to a time dependent parameter of the experimental platform (e.g. storage and possible ageing of lectins, lactoferrin, streptavidin and biotin), since the experiments were performed with 2.5 months in between.

In Fig. 3b, the same data is presented in a PCA-plot with PC2 against PC3. With PC1 left out, no such time separation between the two double experiments as was evident in Fig. 3a can be seen. From these score plots, it is observed that compared to previous plots for experiments 1 and 2 alone with PC1 41% and PC2 30%, the PC1 has increased to 45%, implicating an increased time dependence, and that PC2 has decreased to 20%, implicating increased information in PC3 (16.7%). Thus, it is apparent that there is enough information in PC2 and PC3 to give a separation between the three different groups. The points in the graph representing type 1 diabetes patients having had the disease for 4–6 years are well separated from the other two groups, while there is a slight overlap of some serum samples between the healthy and the newly diagnosed group.

An ANN was also used to examine data. Using cross-validation on all data from experiments 1, 2, 5 and 6, all samples were correctly predicted without any misclassifications into the three different groups. In Fig. 4, the net was modeled and trained during 160 cycles with data from experiments 1, 2 and 5 and then the sera in experiment 6 were predicted. If a discrimination level >0.6 is used all samples are correctly predicted into the three different groups. A similar result was obtained when using experiments 1, 2 and 6 for training and experiment 5 for prediction.

The ANN manages to find a useful model despite the disturbing influence of the time factor on the experimental platform seen in Fig. 3a. Even though there is a slight overlap of some healthy and newly diagnosed serum samples in Fig. 3b, the ANN correctly predicts all samples into the three different serum groups. It is

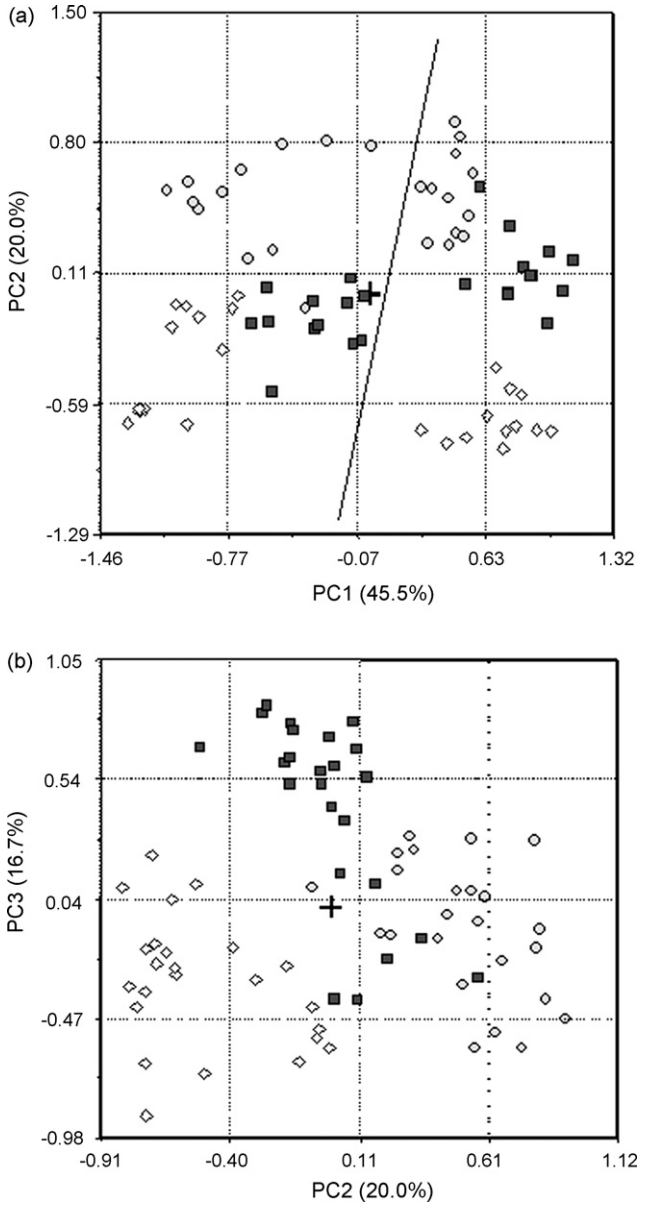

Fig. 3. Score-plots made from data from experiments 1, 2, 5 and 6, showing serum samples from healthy persons (squares), newly diagnosed type 1 diabetes patients (day 0) (circles) and type 1 diabetes patients having had the disease for 4–6 years (diamonds). In (a) PC1 against PC2 is shown. Data from experiments 1 and 2 are to the left of the drawn line and data from experiments 5 and 6 to the right. In (b) PC2 against PC3 is presented.

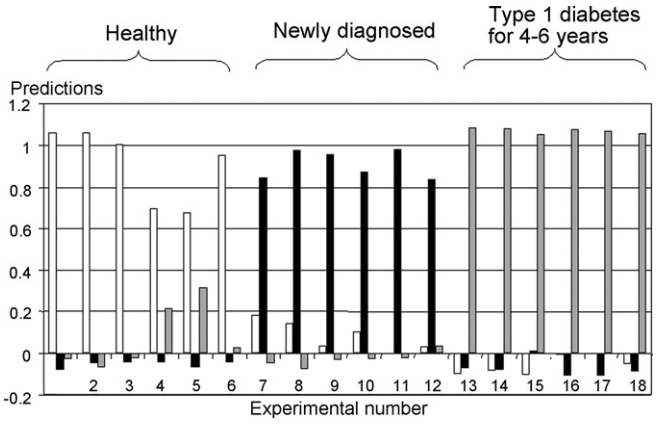

Fig. 4. Prediction of classification of sera from experiment 6 into the three groups healthy (light columns), newly diagnosed (black columns) and having had type 1 diabetes for 4–6 years (grey columns). The ANN model was trained on data from experiment 1, 2 and 5. On the ordinate the predictions are shown and the corresponding experiments are shown on the abscissa.

important to stress, that PCA is based on linear statistics, whilst ANN is based on the search for hidden, unlinear relations. This makes it possible for an ANN to find a useful model for prediction where a statistical based model fails (e.g. based on PLS).

4. Conclusion and future plans

In this paper it was shown that a panel with only seven different lectin types enabled discrimination between sera from healthy persons, newly diagnosed type 1 diabetes patients (day 0) and type 1 diabetes patients having had the disease for 4–6 years. Using an ANN it was possible to correctly categorize unknown serum samples into one of the three groups and correct predictions could be made during a time span of 3 months. The results indicate that there is a measurable global alteration in glycosylation pattern of serum proteins in type 1 diabetic patients compared to healthy subjects. Also, patients having had the disease for a longer period of time show a different glycosylation pattern compared to newly diagnosed type 1 diabetes patients.

We think that an extended lectin panel combined with MVDA has the potential to enable screening for an early prediction of diabetes with the ability to provide diagnostically useful information. It could also be useful for making prognosis of future diabetes related complications.

A future development of the technique is to replace the null ellipsometer with an imaging ellipsometer, making it possible to perform fast and instantaneous measurements and imaging of the surfaces. Furthermore, the problems with the experimental platform will be overcome in the future when the technique has been fully automatized. It would be desirable to increase the number of lectins in the panel and the number of patches per surface by reducing the size of the patches. Also, one surface should contain all the different lectins in the panel to provide an instantaneous image of a given sample.

Acknowledgements

We thank all patients, and children and parents who participated in the ABIS study.

This work was supported by the Swedish Research Council (Vetenskapsrådet) and the Strategic Area for Prevention of Diabetes and its Complications (a joint strategy area for the County Council of Östergötland and Linköping University)

References

[1] J. Axford, Trends Immunol. 22 (2001) 237.
[2] J.N. Arnold, M.R. Wormald, R.B. Sim, P.M. Rudd, R.A. Dwek, Annu. Rev. Immunol. 25 (2007) 21.
[3] E.F. Hounsell, M. Young, M.J. Davies, Clin. Sci. 93 (1997) 287.
[4] http://www.who.int/en/, 2007.
[5] E.H. Baker, D.M. Wood, A.L. Brennan, et al., Proc. Nutr. Soc. 65 (2006) 227.
[6] G.M. Lorenzi, L.M. Delahanty, J.R. Kramer, N.H. White, Diab. Educ. 28 (2002) 735.
[7] M.B. Davidson, Diab. Spect. 14 (2001) 67.
[8] H. Bar-On, G. Nesher, A. Teitelbaum, E. Ziv, J. Diab. Compl. 11 (1997) 236.
[9] D. Chui, G. Sellakumar, R.S. Green, M. Sutton-Smith, T. McQuistan, K.W. Marek, H.R. Morris, A. Dell, J.D. Marth, PNAS 98 (2001) 1142.
[10] Y. Ihara, S. Manabe, M. Kanda, H. Kawano, T. Nakayama, I. Sekine, T. Kondo, Y. Ito, Glycobiology 15 (2005) 383.
[11] S.M. Najjar, J.-P. Broyart, L.T. Hampp, G.M. Gray, Am. J. Physiol. Gastrointest. Liver Physiol. 280 (2001) G104.
[12] D.C.W. Poland, C.G. Schalkwijk, C.D.A. Stehouwer, C.A.M. Koeleman, B. van het Hof, W. van Dijk, Glycoconjugate J. 18 (2001) 261.
[13] M. Grandbois, M. Dettmann, M. Benoit, H.E. Gaub, J. Histochem. Cytochem. 48 (2000) 719.
[14] P. Ertl, S.R. Mikkelsen, Anal. Chem. 73 (2001) 4241.
[15] P. Ertl, M. Wagner, E. Corton, S.R. Mikkelsen, Biosens. Bioelectron. 18 (2003) 907.
[16] Z. Yang, W.S. Hancock, J. Chromatogr. A 1070 (2005) 57.
[17] M. Mecklenburg, J. Svitel, F. Winquist, et al., Anal. Chim. Acta 459 (2002) 25.
[18] J. Carlsson, M. Mecklenburg, I. Lundström, B. Danielsson, F. Winquist, Anal. Chim. Acta 530 (2005) 167.
[19] J. Carlsson, F. Winquist, B. Danielsson, I. Lundström, Anal. Chim. Acta 547 (2005) 229.
[20] A. Kumar, G.M. Whitesides, Appl. Phys. Lett. 63 (1993) 2002.
[21] M. Mrksich, G.M. Whitesides, Trends Biotechnol. 13 (1995) 228.
[22] M. Schäferling, M. Riepl, P. Pavlickova, H. Paul, D. Kambhampati, B. Liedberg, Microchim. Acta 142 (2003) 193.
[23] J. Ludvigsson, M. Ludvigsson, A. Sepa, Ped. Diabetes 2 (2001) 170.
[24] H. Elwing, Biomaterials 19 (1998) 397.
[25] F.L.A. McCrackin, NBS Technical Note 479, 1969, Washington DC.

Talanta 76 (2008) 400–406

Contents lists available at ScienceDirect

Talanta

journal homepage: www.elsevier.com/locate/talanta

Ultrasonic energy as a new tool for fast isotopic ^{18}O labeling of proteins for mass spectrometry-based techniques: Preliminary results

R.J. Carreira[a], R. Rial-Otero[a,1], D. López-Ferrer[b], C. Lodeiro[a], J.L. Capelo[a,*]

[a] REQUIMTE, Departamento de Química, Faculdade de Ciências e Tecnologia, Universidade Nova de Lisboa, Quinta da Torre, 2829-516 Monte de Caparica, Portugal
[b] Biological Science Division, Pacific Northwest National Laboratory, Richland, WA 99352, USA

ARTICLE INFO

Article history:
Received 22 December 2007
Received in revised form 3 March 2008
Accepted 12 March 2008
Available online 21 March 2008

Keywords:
Isotopic labeling
^{18}O
Ultrasonic bath
Protein quantitation

ABSTRACT

Preliminary results regarding fast isotopic labeling of proteins with ^{18}O in conjunction with matrix assisted laser desorption ionization time of flight mass spectrometry technique are presented. Similar $^{16}O/^{18}O$ isotopic labeling ratios were found for the overnight procedure (12 h) and the new fast ultrasonic one (30 min) for the BSA, ovalbumin and α-lactalbumin proteins. The procedure, however, failed to promote double ^{18}O isotopic labeling for the proteins, ovalbumin and α-lactalbumin. Two different sonication frequencies, 35 and 130 kHz, were studied at two different sonication times of 15 and 30 min, being best results obtained with the procedure at 130 kHz of sonication frequency and 30 min of sonication time. For comparative purposes the overnight isotopic ^{18}O labeling procedure was done. In addition, the new fast isotopic labeling procedure was also studied without ultrasonication, in a water bath at 60 °C.

1. Introduction

Protein quantitation is an essential tool for proteomics and systems biology studies, since it helps to understand the function of biological processes, to quantify protein post-translational modifications or to identify diagnosis or prognosis biomarkers, and to develop new drugs [1–3].

Protein quantitation can be done in a relative or absolute manner through mass spectrometry, MS, techniques. MS-based protein quantitative methods can be traced back to the MS stable isotope labeling absolute measurements [4] but, after different improvements in the area, nowadays MS-based strategies for protein relative/absolute quantitation lie mainly into four different approaches, as follows [5]:

(i) in the chemical incorporation or "tagging" approach, proteins are derivatizated with a dedicated reagent in a specific site;
(ii) in the biological/metabolic incorporation approach, cells are cultured in media enriched in stable isotope-containing amino acids which are incorporated to the cell peptides during the growing process;
(iii) in the enzymatic incorporation approach, the protein cleavage is done in ^{18}O-water, thus ^{18}O is incorporated into the C-terminus of peptides and
(iv) in the internal standard approach, a known quantity of an isotopically labeled synthetic peptide is added to the protein digest as internal standard.

The use of ^{18}O-water for isotopic labeling in protein quantitation has its origin in the work of Sprinson and Rittenberg [6]. Enzymatic labeling with ^{18}O during proteolysis cleavage can be used for relative or absolute quantitation [5,7]. In this process, depending on the enzyme used, one or two oxygen atoms from the solvent ($H_2{}^{18}O$) are incorporated into the peptide C-terminus. For relative quantitation, one set of samples is cleaved in ^{18}O-water whilst the other is cleaved in ^{16}O-water. Then, both samples are mixed in equal proportion to ensure that variations due to further sample handling (e.g. losses of peptides) will be paralleled by a proportionate loss of each labeled type (^{16}O or ^{18}O), maintaining in this way the ratio between the two. Relative quantitation is achieved by the measurement of the ratios obtained between the intensities of the labeled to unlabeled peptides [8]. Absolute quantitation can also be done with ^{18}O enzymatic labeling by using standard curves. These curves are done by plotting the protein concentration vs. the ratio obtained between the intensity of a characteristic peptide of the protein and the intensity of an external synthetic peptide used as internal standard, which is also labeled during the protein enzymatic cleavage or later. The internal standard is added in a fixed known quantity to the standards and to the analytical sample. Thus, the intensity ratio of

* Corresponding author. Tel.: +351 212 949 649; fax: +351 212 948 550.
E-mail address: jlcapelom@dq.fct.unl.pt (J.L. Capelo).
URL: http://www.dq.fct.unl.pt/bioscope (J.L. Capelo).
[1] University of Vigo, Faculty of Food Science & Technology, Nutrition & Bromatology Group, Analytical & Food Chemistry Department, E-32400 Orense, Spain.

0039-9140/$ – see front matter © 2008 Published by Elsevier B.V.
doi:10.1016/j.talanta.2008.03.013

the endogenous to synthetic peptide is measured, and the absolute amount of the endogenous peptide can be calculated [9,10]. Enzymatic labeling with ^{18}O-water has the following advantages:

(i) it is of easy labeling;
(ii) all peptides present in the sample are labeled and
(iii) it requires only the presence of ^{18}O-water, avoiding extra-reagents or synthetic steps.

Some drawbacks, however, inherent to this type of labeling need to be overcome. Thus, systematic studies have shown that different types of proteolytic enzymes incorporate different levels of ^{18}O from water during digestion [5]. Ideally, the incorporation of two ^{18}O ($^{18}O_2$), that is, a mass shift of 4 Dalton (Da), would be the minimum needed to obtain appreciable m/z changes in the mass spectrum between samples, avoiding, for instance, the ^{13}C interference or isotopic peak overlapping. The incorporation of a single ^{18}O ($^{18}O_1$), yields a mass increment between each sample of only 2 Da, which is not adequate to produce an appreciable change in m/z, especially for multiply charged species. Furthermore, the procedure for isotopic labeling is a time-consuming approach which can take between 12 and 48 h.

Ultrasound energy has been used in chemistry with the aim to speed up kinetics of chemical reactions [11,12]. Remarkably, ultrasonic energy has been recently reported as a tool for the acceleration of enzymatic protein cleavage from overnight to few minutes [13,14]. However, the potential of ultrasound energy to speed up the ^{18}O enzymatic labeling process and to increase the ratio of ^{18}O incorporation remains unknown.

In this work, we report our preliminary results regarding the acceleration of ^{18}O isotopic labeling joining the enzymatic protein digestion process with ultrasonic energy. With this aim, ^{18}O labeling with ultrasonic energy provided by an ultrasonic bath at 60 °C is studied. The influence of the ultrasonic frequency is also studied by using 35 and 130 kHz ultrasonic transducers. In addition, for comparative purposes the overnight labeling and labeling in water at 60 °C are also done.

2. Experimental

2.1. Apparatus

Protein digestion/labeling was done in safe-lock tubes of 0.5 ml from Eppendorf (Hamburg, Germany). A minicentrifuge, model Spectrafuge-mini, from Labnet (Madrid, Spain), and a minicentrifuge-vortex, model Sky Line, from ELMI (Riga, Latvia) were used throughout the sample treatment, when necessary. Milli-Q natural abundance ($H_2{}^{16}O$) water was obtained from a Simplicity™ 185 from Millipore (Milan, Italy). An ultrasonic bath, model Transsonic TI-H-5, from Elma (Singen, Germany) with control of temperature and amplitude was used.

2.2. Materials and reagents

Bovine serum albumin, BSA (66 kDa, >97%), ovalbumin (45 kDa), α-lactalbumin (14.4 kDa, ≥85%) and trypsin (proteomics grade) used for all experiments, were purchased from Sigma (Steinheim, Germany). Reduction and alkylation of BSA were carried out, respectively, with DL-dithiothreitol (DTT, 99%) and iodoacetamide (IAA) from Sigma. The following reagents were used during sample digestion/labeling: ammonium bicarbonate buffer (AmBic, pH 8.5, ≥99.5%) and formic acid (FA, ~98%) from Fluka (Buchs, Switzerland); $H_2{}^{18}O$ (95 atom%) from ISOTEC™ (Miamisburg, USA). α-Cyano-4-hydroxycinnamic acid (α-CHCA, ≥99.0%), acetonitrile (99.9%) and trifluoroacetic acid (TFA, 99%) were from Fluka, Sigma–Aldrich and Riedel-de Haën (Seelze, Germany), respectively. ProteoMass™ Peptide MALDI-MS calibration kit (MSCAL2) from Sigma was used as mass calibration standard for MALDI-TOF-MS.

2.3. Sample treatment

A stock solution of BSA, ovalbumin and α-lactalbumin (100 pmol/μl) was prepared in AmBic (100 mM) using natural abundance water. Reduction was performed with DTT (10 mM) at 37 °C for 1 h and alkylation was done with IAA (50 mM) at room temperature (RT) for 45 min in the darkness. Then aliquots (10 μl) of the protein solution were taken and diluted to 100 μl with AmBic (100 mM) prepared in natural abundance water or in 95% ^{18}O-enriched water. Trypsin (2%, v/v) was added to these solutions to a final concentration of 0.47 pmol/μl. The substrate to enzyme ratio was 20:1 (mol/mol). Different digestion and labeling procedures were tested:

(i) overnight/labeling (12 h) digestion at 37 °C;
(ii) digestion/labeling at 60 °C in an ultrasonic bath (70% sonication amplitude and 35 kHz sonication frequency) for variable times of 15 and 30 min;
(iii) digestion/labeling at 60 °C in an ultrasonic bath (70% sonication amplitude and 130 kHz sonication frequency) for variable times of 15 and 30 min;
(iv) digestion/labeling at 60° C for variable times of 15 and 30 min.

To stop enzymatic digestion/labeling reactions, 5 μl of formic acid 50% were added. A comprehensive scheme of the sample treatment is presented in Fig. 1.

2.4. MALDI-TOF-MS analysis

Prior to MALDI-TOF-MS analysis, the samples were mixed in a 1:1 ratio with the matrix solution of α-CHCA (10 μg/μl) prepared in Milli-Q water/acetonitrile/TFA (1 ml + 1 ml + 2 μl). Then, 1 μl of each sample was hand-spotted onto a stainless steel well plate of a MALDI-TOF-MS and allowed to dry.

MALDI mass spectra were obtained with a Voyager DE-PRO Biospectrometry Workstation model from Applied Biosystems (Foster City, USA), equipped with a nitrogen laser radiating at 337 nm. Measurements were done in the reflector positive ion mode, with a 20 kV of accelerating voltage, 75.1% of grid voltage, 0.002% of guide wire and a delay time of 100 ns. Two close external calibrations were performed with the monoisotopic peaks of the Bradykinin, Angiotensin II, P14R and ACTH peptide fragments (m/z $[M+H]^+$: 757.3997, 1046.5423, 1533.8582 and 2465.1989, respectively). 250 laser shots were summed per spectrum. The spectra analysis was done with the Data Explorer™ software (version 4.0) from Applied Biosystems.

The following search engines were used to identify the obtained peptide fingerprints: MASCOT [http://www.matrixscience.com/search_form_select.html] and PROTEIN PROSPECTOR [http://prospector.ucsf.edu/]. Search parameters: (i) SwissProt. 2006 Database; (ii) molecular weight (MW) of protein: all; (iii) one missed cleavage; (iv) fixed modifications: carbamidomethylation (C); (v) variable modifications: oxidation (M), $^{18}O_1$ and $^{18}O_2$ label (C-term); (vi) peptide tolerance up to 175 ppm. If the protein identification score is located out of the random region and the protein analyzed scores first, then a match is considered successful.

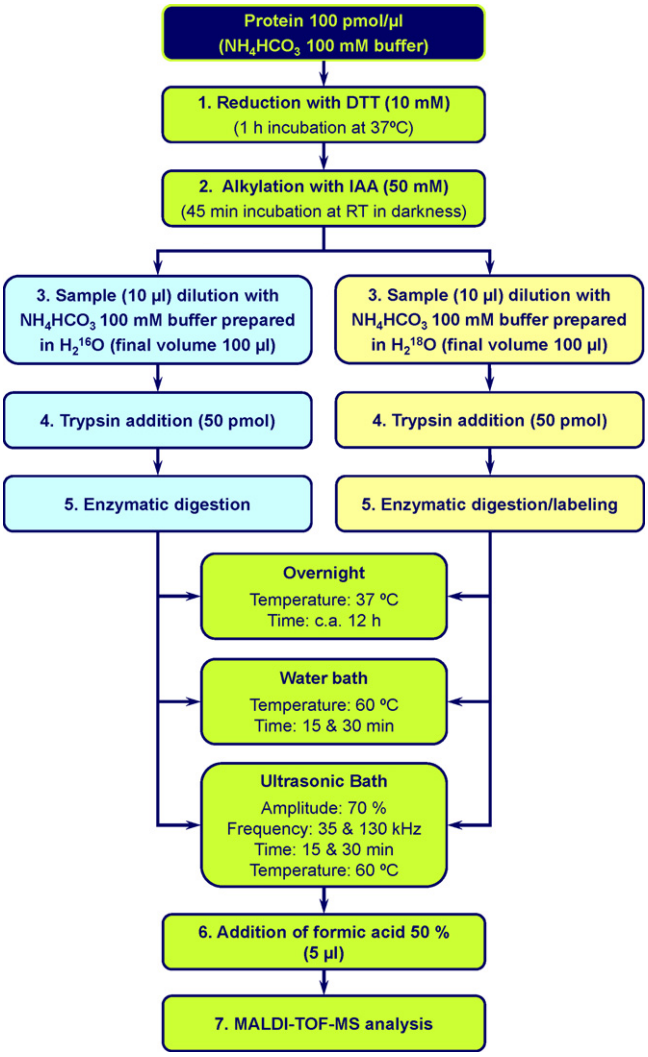

Fig. 1. Comprehensive scheme for the isotopic labeling sample treatment.

2.5. Isotopic peak deconvolution

Isotopic peak deconvolution was done using the deisotope function of the Data Explorer™ software (version 4.0) from Applied Biosystems. This function is an advanced peak filtering method that uses a deisotoping algorithm to determine the relative abundance of multiple components with overlapping isotope distributions [15]. Thus, the deisotope function allows reducing a spectrum to a centroided plot by deconvoluting the monoisotopic peaks from the peak list. For each peak in a spectrum, the software inspects the peak list for the higher theoretical masses and areas associated with additional expected peaks in a theoretical isotopic cluster, relative to the peak in question. Moreover, for comparative purposes in order to test the correct applicability of this function, the mathematical algorithm for deconvolution described by Yao et al. was also used in the first steps of this work [16].

3. Results and discussion

3.1. The isotopic labeling and the deconvolution problem

Fig. 2 presents the MALDI-TOF-MS spectra of the peptide fragment (YLYEIAR)H^+ (m/z = 927 Da) obtained from the tryptic digestion of BSA and acquired under the conditions briefly described in the caption of Fig. 2 (for further details refer to Section 2.3). The peptide (YLYEIAR)H^+ is used throughout this manuscript for explanation purposes because the best isotopic labeling was obtained with this peptide. As it was explained in Section 1, the incorporation of one ^{18}O ($^{18}O_1$) yields a mass increment for each isotopic peak of 2 Da whilst the incorporation of two ^{18}O ($^{18}O_2$) yields a mass increment of 4 Da (see Fig. 2a and b). To avoid isotopic peak overlapping a 100% $^{18}O_2$ labeling should be achieved. The difference in the isotopic patterns due to variable labeling and its consequence for the spectra interpretation can be easily explained through Fig. 2, spectra a–c. Spectrum a, Fig. 2, corresponds to the BSA overnight digestion in ^{16}O-water and, as it can be seen, the isotopic pattern match well with the natural isotopic distribution, as showed in Table 1, with the following main m/z peaks being obtained: 927, 928 and 929 Da. Ideally, as explained before, the isotopic labeling should incorporate two ^{18}O, giving a mass increment of 4 Da for each isotopic peak. Therefore, the following main m/z peaks should be expected 931 Da (=927 + 4), 932 Da (=928 + 4) and 933 Da (=929 + 4) for a 100% of $^{18}O_2$ labeling. Experimentally, however, this does not occur because the yield of double oxygen incorporation is not 100%. This is the reason why spectrum b, Fig. 2, presents m/z peaks at 929 and 930 Da, which should not appear for a 100% of $^{18}O_2$ labeling. The peak at 929 Da observed in Fig. 2b is originated by the incorporation of one ^{18}O to the peptide (YLYEIAR)H^+ (927 + 2) plus the 929 Da peak contribution coming from the unlabeled peptide. The peak at 931 Da has contributions coming from one single ^{18}O incorporation (929 + 2) and from double ^{18}O incorporation to the peptide (YLYEIAR)H^+ (927 + 4). Since there is no way to know the percentage of peptides that were unlabeled, single labeled or double labeled, it is necessary to use complicated mathematical procedures to deconvolute the spectrum [7–9]. Further understanding of this problem is taken from the other spectra present in Fig. 2, where it can be seen different intensities for the peaks of m/z 929 and 931, for the same sample and the same concentration, as a result of the different conditions in which the digestion and the isotopic labeling were done, thus indicating different degrees of labeling (single or double) as a function of the sample treatment.

3.2. Influence of the sample treatment on the ^{18}O labeling ($^{16}O/^{18}O$)

The proteolytic ^{18}O labeling method can be done in two different ways, as explained below. The first approach, named as

Table 1
Theoretical vs. experimental isotopic distribution for the tryptic peptide fragment (YLYEIAR)H^+ from BSA digestion

Mass (m/z) [M+H^+]	Theoretical isotopic distribution[a]	Experimental isotopic distribution[b]	Mass (m/z) after $^{18}O_1$ incorporation	Mass (m/z) after $^{18}O_2$ incorporation
927	100.0	100	929	931
928	53.8	54.1	930	932
929	16.6	15.6	931	933
930	3.7	3.4	932	934

[a] Isotopic distribution calculated with the isotopic calculator function of the Data Explorer™ software (version 4.0) from Applied Biosystems.
[b] Experimental ratios obtained for overnight digested BSA samples. Values were acquired with a MALDI-TOF-MS system in the reflector positive ion mode (n = 2).

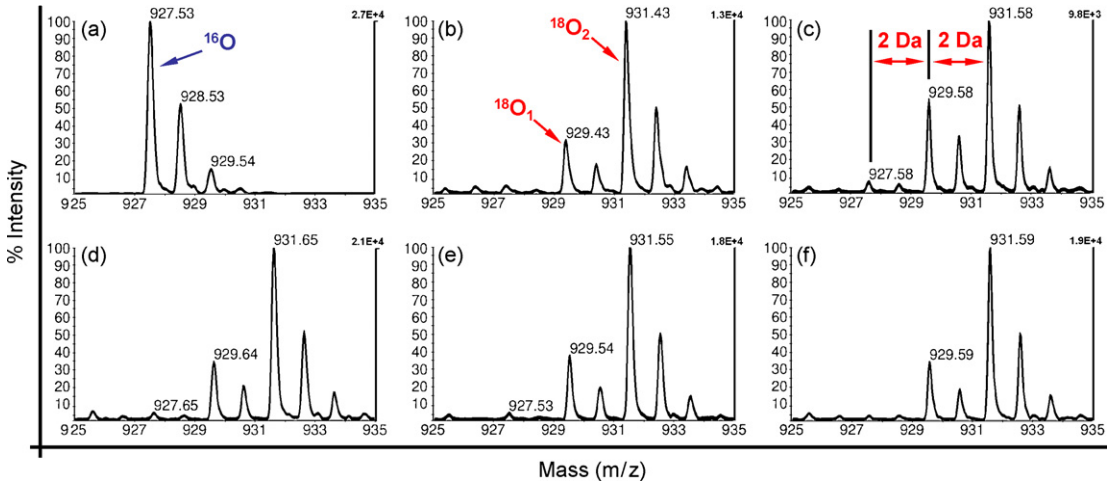

Fig. 2. Reflector positive ion mode MALDI-TOF mass spectra of the peptide fragment (YLYEIAR)H$^+$ obtained in the tryptic digest of BSA. (a) Overnight digestion in 100% $H_2{}^{16}O$ buffer solution at 37 °C (ca. 12 h); (b) overnight digestion in 95 atom% $H_2{}^{18}O$ buffer solution at 37 °C (ca. 12 h); (c) ultrasonic bath digestion in 95 atom% $H_2{}^{18}O$ buffer solution at 60 °C (35 kHz frequency; 70% amplitude; 30 min); (d) ultrasonic bath digestion in 95 atom% $H_2{}^{18}O$ buffer solution at 60 °C (130 kHz frequency; 70% amplitude; 15 min); (e) ultrasonic bath digestion in 95 atom% $H_2{}^{18}O$ buffer solution at 60 °C (130 kHz frequency; 70% amplitude; 30 min) and (f) water bath digestion in 95 atom% $H_2{}^{18}O$ buffer solution at 60 °C (30 min).

"direct labeling", incorporates the ^{18}O at the same time that the enzymatic cleavage is done [8,9]; this is, the enzymatic cleavage is performed in ^{18}O-water, normally at the pH recommended by manufacturers (pH 8.5) to obtain the best efficiency of the enzyme.

The second approach, named as "decoupling procedure", was first reported by Yao et al. [17], and briefly, it decouples the labeling process into two steps, as follows: first, the enzymatic digestion is done in ^{16}O-water, at the recommended pH for the best enzymatic efficiency and then, after ^{16}O-water evaporation, the labeling process takes place in ^{18}O-water at a lower pH (5–6). The ^{18}O labeling decoupling process is based on recent literature, where it is suggested that optimum pH for almost complete two ^{18}O labeling should be shifted toward acidic pHs, compared to the pH range of the enzymes highest activities [7]. Although, the decoupling procedure has the advantage of separating the digestion and labeling steps, allowing their conditions to be optimized separately, in our experiments we decided to use direct labeling as mentioned above, since it was expected a smaller technical variation. In addition, direct labeling is done in one single step facilitating on-line approaches for mass spectrometry.

The ^{18}O labeling process can be divided into two chemical reactions, as follows:

(i) first reaction: amide bond cleavage

$$RC^{16}ONHR' + H_2{}^{18}O \rightarrow [RC^{16}O^{18}O]^- + [H_3NR']^+$$

(ii) second reaction: carboxyl oxygen exchange

$$[RC^{16}O^{18}O]^- + H_2{}^{18}O \rightarrow [RC^{18}O^{18}O]^- + H_2{}^{16}O$$

The first experiments were done to study the influence of ultrasonic energy on the total enzymatic labeling of peptides with ^{18}O. The ratio $^{16}O/^{18}O$ refers to the amount of ^{18}O incorporated in the labeling process, no matter the type of labeling (single or double). Table 2 shows the $^{16}O/^{18}O$ ratios of different peptides obtained from the tryptic digestion of BSA after performing the different sample treatments studied in this work.

Concerning the overnight protocol (12 h), the yield of ^{18}O incorporation all the peptides shown in Table 2 was higher than 95% ($^{16}O/^{18}O$ ratios lower than 0.05).

Regarding ^{18}O incorporation with the treatment with ultrasound at 130 kHz sonication frequency at 60 °C and the treatment with the water bath at 60 °C (no ultrasonication was used), data in Table 2 show that similar results, a labeling efficiency of ca. 90% ($^{16}O/^{18}O$ ratios lower than 0.13), between both methods were obtained. In addition, the yields of incorporation were close to the ones obtained for the overnight protocol, being the labeling slightly worst for the higher peptides. However the labeling efficiency was still ≥90%.

As far as the treatment with 35 kHz sonication time at 60 °C concerns, data showed in Table 2 seems to suggest a dependence of labeling efficiency with the sonication frequency. Thus the ^{18}O incorporation was worst that the one obtained with the same time and the same temperature, but with a sonication frequency of 130 kHz.

On the overall, for the aforementioned treatments, the labeling efficiency was not equally obtained for all peptides. It seems that the labeling yield was dependent of the peptide size. Thus, as showed in Table 2, labeling efficiencies lower than 90% ($^{16}O/^{18}O$ ratios higher than 0.11) were obtained for the peptides (RHPEYAVSVLLR)H$^+$, (LEGYGFQNALIVR)H$^+$ and (KVPQVSTPTLVEVSR)H$^+$, with peak masses of 1439, 1479 and 1639 m/z, respectively; whilst labeling efficiencies higher than 90% ($^{16}O/^{18}O$ ratios lower than 0.11) were observed for the peptides (YLYEIAR)H$^+$ and (ALKAWSVAR)H$^+$ with masses 927 and 1001 m/z, respectively. Interestingly, this problem was not observed when the labeling process was performed overnight. This fact could suggest that the times (15 and 30 min) selected to speed up the enzymatic digestion and labeling with ultrasound or heating at 60 °C were not enough to increase the reaction rates of the enzymatic process. A further explanation can be suggested taking into account that the yields of labeling were similar for the ultrasonic process at 130 kHz sonication frequency at 60 °C and for the water bath digestion at 60 °C. So, although different authors have suggested that ultrasonication can accelerate the enzymatic reactions, little attention has been given to the type of device used to perform such treatment, that can be an ultrasonic bath, such as in this work, or

Table 2
$^{16}O/^{18}O$ ratios of different peptides obtained from the tryptic digestion of BSA, ovalbumin and α-lactalbumin (900 pmol each protein), in the presence of 95% $H_2{}^{18}O$

Protein	Peptide fragment	$[M+H]^+$ (m/z)	Overnight	US bath 35 kHz	US bath 130 kHz	Water bath	Sonication time (min)
BSA	(YLYEIAR)H^+	927.49	0.01 ± 0.02	0.07 ± 0.01	0.03 ± 0.01	0.04 ± 0.00	15
				0.05 ± 0.00	0.02 ± 0.01	0.03 ± 0.03	30
	(ALKAWSVAR)H^+	1001.59	[a]	0.08 ± 0.02	0.03 ± 0.04	0.06 ± 0.01	15
				0.06 ± 0.03	0.06 ± 0.05	0.05 ± 0.03	30
	(RHPEYAVSVLLR)H^+	1439.82	0.04 ± 0.01	0.11 ± 0.02	0.05 ± 0.02	0.08 ± 0.01	15
				0.11 ± 0.02	0.06 ± 0.01	0.07 ± 0.01	30
	(LEGYGFQNALIVR)H^+	1479.80	0.04 ± 0.01	0.31 ± 0.05	0.08 ± 0.01	0.12 ± 0.02	15
				0.23 ± 0.06	0.11 ± 0.04	0.13 ± 0.01	30
	(KVPQVSTPTLVEVSR)H^+	1639.94	0.03 ± 0.02	0.11 ± 0.03	0.08 ± 0.00	0.11 ± 0.02	15
				0.08 ± 0.03	0.08 ± 0.02	0.06 ± 0.05	30
Ovalbumin	(VYLPR)H^+	647.39	0.02 ± 0.02	[b]	0.09 ± 0.00	[b]	30
	(HIATNAVLFFGR)H^+	1345.74	0.03 ± 0.01		0.13 ± 0.01		
	(GGLEPINFQTAADQAR)H^+	1687.84	0.07 ± 0.06		0.11 ± 0.01		
	(ELINSWVESQTNGIIR)H^+	1858.97	0.19 ± 0.17		0.15 ± 0.01		
	(LYAEERYPILPEYLQCVK)H^+	2284.17	0.08 ± 0.03		0.15 ± 0.02		
α-Lactalbumin	(CEVFR)H^+	710.33	0.03 ± 0.00	[b]	0.14 ± 0.01	[b]	30
	(VGINYWLAHK)H^+	1200.65	0.04 ± 0.03		0.14 ± 0.03		
	(EQLTKCEVFR)H^+	1309.66	[a]		0.14 ± 0.01		
	(ILDKVGINYWLAHK)H^+	1669.94	0.09 ± 0.07		0.17 ± 0.01		

Different labeling methods were used in this experimental: overnight (12 h); ultrasonic bath (35 kHz; 70% amplitude, 60 °C, 15 and 30 min); ultrasonic bath (130 kHz; 70% amplitude, 60 °C, 15 and 30 min); water bath (60 °C, 15 and 30 min). Values were acquired with a MALDI-TOF-MS system in the reflector positive ion mode ($n = 2$).

[a] Peptide not present in the spectra. This peptide has a missed cleavage.

[b] Experimental was not done.

an ultrasonic probe [18,19]. Thus, for a given volume of solution, the ultrasonic intensity obtained with an ultrasonic bath is 100 times lower than the ultrasonic intensity obtained with an ultrasonic probe [20]. Therefore, the low yields of ^{18}O labeling observed for the ultrasonication treatment for the peptides of higher masses could be explained taking into account the low sonication intensity of the ultrasonic bath. Thus, in our case, the $^{16}O/^{18}O$ labeling yields observed for the sample treatment with the ultrasonic bath could be linked to the temperature at which the labeling was done rather than to the ultrasonication effects. In fact, the labeling ratios for the treatment with ultrasonic bath at 60 °C and 130 kHz of sonication frequency and with the heating treatment in water at 60 °C without sonication are similar for all BSA peptides. Nevertheless, as we will see below, the $^{18}O_1/^{18}O_2$ labeling efficiencies obtained with both methods were completely different.

Another interesting finding deal with the different yields of isotopic incorporation obtained as a function of the sonication frequency used, as explained above. The ultrasonication bath employed in this work has the possibility of performing two different ultrasonication frequencies of 35 and 130 kHz. As it can be seen in Table 2, the results obtained with the ultrasonication bath at the frequency of 130 kHz and 60 °C are similar to the overnight protocol for all the BSA peptides observed, but the labeling achieved with the 35 kHz sonication frequency was low, specially for the peptide (LEGYGFQNALIVR)H^+. The explanation could be as follows: when ultrasonic energy is provided to a liquid media, an effect known as cavitation occurs. This effect is responsible for the generation of small gas bubbles, which grow in successive cycles, according to the frequency of ultrasound, and when they reach an unstable size they violently collapse. The temperature and pressure near the collapse point can reach values up to 5000 °C and 1000 atm, respectively [21]. This energy is transmitted to the liquid media and the mass transfer processes are enhanced in a more effective manner than when only heat is used. Two types of cavitation can be produced by ultrasound: transient cavitation and stable cavitation. Most of the physical and chemical effects produced by ultrasonication are linked to the collapse of transient cavitation bubbles [21], which are dominant at low frequencies, i.e. 35 kHz. However, as the frequency increases, so it does the fraction of stable cavitation bubbles formed. As the transient cavitation bubbles to stable cavitation bubbles ratio changes, the sonochemical effects are altered. We, therefore, hypothesize that the worst performance of the enzymatic labeling at lower frequencies (i.e. 35 kHz) is directly linked with the increasing number of transient cavitation bubbles formed.

3.3. Influence of the sample treatment on the single to double ^{18}O labeling

The cause of the major variability of the ^{18}O labeling technique applied to quantitative proteomics is the variable incorporation of ^{18}O atoms into peptides, and this variability is directly linked to the second ^{18}O incorporation [7–9]. This is due to the fact that the efficiencies of the two reactions involved in the isotopic labeling with ^{18}O, the amide bond cleavage and the carboxyl oxygen exchange, are different. The first reaction incorporates one ^{18}O in one cycle of the enzymatic reaction, whilst the second reaction needs at least five cycles to have a yield of $^{18}O_2$ incorporation of ca. 98.5% [7]. This reaction is extremely slow under the conditions commonly used leading to variable exchange within the time frame of the proteolytic reaction [17]. The cavitation phenomena generated by ultrasonic energy enhances both of the labeling reactions, but in the second reaction the forward and backward processes are probably both accelerated. In this way it must be stressed out that dedicated literature suggest that ultrasonication in short times can accelerate enzymatic reactions, whilst in longer times it seems that enzymatic inactivation occurs. Thus, Talukder et al. [18] reported an increment in the maximum reaction rate (V_{max}) and unalteration for the Michaelis constant (K_m) when the hydrolytic activity of lipase was enhanced by ultrasonication. Therefore, it is critical to control the carboxyl oxygen exchange reaction (second reaction) as the key strategy in overcoming variability. Table 3 shows data regarding single to double labeling ratios ($^{18}O_1/^{18}O_2$) for the BSA protein obtained with the different sample treatments studied. As it can be seen, the ($^{18}O_1/^{18}O_2$) labeling follow the same pattern that the $^{16}O/^{18}O$ incorporation; this means that the best results were obtained with the overnight protocol ($^{18}O_1/^{18}O_2$ ratio lower then 0.35, that means $^{18}O_2$ incorporation higher than 75%) and, from all the other sample treatments studied, only the acceleration with the ultrasonic bath at 130 kHz sonication frequency at 60 °C showed to be a method of relative success. It is remarkable the fact that the

Table 3
$^{18}O_1/^{18}O_2$ ratios of different peptides obtained from the tryptic digestion of BSA, ovalbumin and α-lactalbumin (900 pmol each protein), in the presence of 95% $H_2{}^{18}O$

Protein	Peptide fragment	$[M+H]^+$ (m/z)	Overnight	US bath 35 kHz	US bath 130 kHz	Water bath	Sonication time (min)
BSA	(YLYEIAR)H^+	927.49	0.32 ± 0.04	1.30 ± 0.16	0.41 ± 0.05	0.80 ± 0.08	15
				0.80 ± 0.23	0.42 ± 0.01	0.51 ± 0.19	30
	(ALKAWSVAR)H^+	1001.59	[a]	1.50 ± 0.33	0.40 ± 0.03	0.12 ± 0.38	15
				0.83 ± 0.18	0.32 ± 0.09	0.55 ± 0.07	30
	(RHPEYAVSVLLR)H^+	1439.82	0.29 ± 0.05	4.33 ± 0.61	0.77 ± 0.07	1.42 ± 0.02	15
				2.11 ± 0.84	0.76 ± 0.01	0.84 ± 0.48	30
	(LEGYGFQNALIVR)H^+	1479.80	0.34 ± 0.04	3.51 ± 0.27	1.15 ± 0.04	1.33 ± 0.23	15
				2.59 ± 0.30	1.21 ± 0.26	1.09 ± 0.21	30
	(KVPQVSTPTLVEVSR)H^+	1639.94	0.30 ± 0.00	24.21 ± 2.17	3.61 ± 0.18	7.77 ± 5.37	15
				21.07 ± 17.47	3.06 ± 0.13	2.63 ± 1.03	30
Ovalbumin	(VYLPR)H^+	647.39	0.36 ± 0.06		2.12 ± 0.30		
	(HIATNAVLFFGR)H^+	1345.74	0.45 ± 0.07		3.89 ± 0.37		
	(GGLEPINFQTAADQAR)H^+	1687.84	0.52 ± 0.06	[b]	3.18 ± 0.48	[b]	30
	(ELINSWVESQTNGIIR)H^+	1858.97	1.02 ± 0.93		[c]		
	(LYAEERYPILPEYLQCVK)H^+	2284.17	0.90 ± 0.87		[c]		
α-Lactalbumin	(CEVFR)H^+	710.33	0.31 ± 0.03		19.38 ± 3.66		
	(VGINYWLAHK)H^+	1200.65	0.39 ± 0.21	[b]	32.25 ± 1.34	[b]	30
	(EQLTKCEVFR)H^+	1309.66	[a]		37.53 ± 13.50		
	(ILDKVGINYWLAHK)H^+	1669.94	5.98 ± 0.43		[c]		

Different labeling methods were used in this experimental: overnight (12 h); ultrasonic bath (35 kHz; 70% amplitude, 60 °C, 15 and 30 min); ultrasonic bath (130 kHz; 70% amplitude, 60 °C, 15 and 30 min); water bath (60 °C, 15 and 30 min). Values were acquired with a MALDI-TOF-MS system in the reflector positive ion mode ($n = 2$).

[a] Peptide not present in the spectra. This peptide has a missed cleavage.

[b] Experimental was not done.

[c] Double labeled peptide was not identified in the MALDI mass spectra.

heating at 60 °C although could promote a $^{16}O/^{18}O$ labeling similar to the ultrasonic process at 130 kHz sonication frequency at 60 °C, failed, however, in promoting double ^{18}O incorporation.

As far as the size of the peptide concerns, the double labeling with the overnight protocol or with the ultrasonic bath at 60 °C and 130 kHz showed to be the most robust procedures, with similar results: the peptides $(YLYEIAR)H^+$ and $(ALKAWSVAR)H^+$ ($m/z = 927$ and 1001, respectively) were labeled with a yield higher than 70% ($^{18}O_1/^{18}O_2$ ratio lower then 0.43). Nevertheless, for the peptides $(RHPEYAVSVLLR)H^+$, $(LEGYGFQNALIVR)H^+$ and $(KVPQVSTPTLVEVSR)H^+$ ($m/z = 1439$, 1479 and 1639, respectively) a double labeling efficiency of about 70% was achieved with the overnight protocol whilst with the ultrasonic protocol (130 kHz and 60 °C) lower double labeling efficiency was obtained and also this efficiency decreased as the peptide size increased. Other authors have also stressed that different peptides may exhibit different relative labeling efficiencies [7]. The reasons for the aforementioned fact, however, are not well understood yet. For instance, Mirgorodskaya et al. [9] reported similar $^{18}O_1/^{18}O_2$ ratios for peptide fragments with masses comprised between 1050.5 and 1385.6 m/z from a RNase tryptic digest, whilst Stewart et al. [8] have found $^{18}O_1/^{18}O_2$ ratios comprised between 25% and 80%, as a function of the peptide-type.

3.4. Application to further proteins

In order to assess the efficiency of the ultrasonic procedure at 60 °C and 130 kHz of sonication frequency to further proteins, the ovalbumin the α-lactalbumin proteins were submitted to the above-mentioned procedure for a time of 30 min. In addition the overnight procedure was also done for comparative purposes. Results are presented in Tables 2 and 3 for ^{16}O to ^{18}O labeling and single to double ^{18}O labeling, respectively.

Regarding ovalbumin, the efficiency of the $^{16}O/^{18}O$ labeling, was similar with both procedures as it can be seen in Table 2. Thus, for the overnight procedure the labeling efficiency was comprised between 84% and 98% ($^{16}O/^{18}O$ ratio comprised between 0.19 and 0.02), whilst for the ultrasonic procedure the incorporation was comprised between 87% and 92% ($^{16}O/^{18}O$ ratio comprised between 0.15 and 0.09). That means a reduction in the sample time needed to perform the isotopic labeling of ca. 12 h when ultrasonication was used. However, the ultrasonication treatment failed in promoting the double oxygen incorporation as showed in Table 3, were it can be seen that for the overnight procedure the double incorporation was comprised between 50% and 73%, ($^{18}O_1/^{18}O_2$ ratio between 1 and 0.36) whilst for the ultrasonic process the double incorporation was comprised between 20% and 32% ($^{18}O_1/^{18}O_2$ ratio between 4 and 2.1).

Concerning protein α-lactalbumin, for the overnight procedure the $^{16}O/^{18}O$ labeling efficiency, was comprised between 65% and 97% ($^{16}O/^{18}O$ ratio comprised between 0.54 and 0.03), whilst for the ultrasonic procedure the incorporation was comprised between 85% and 88% ($^{16}O/^{18}O$ ratio comprised between 0.17 and 0.14). However, the ultrasonication treatment was almost non-effective in promoting the double oxygen incorporation. Thus, the best double incorporation was for the peptide fragment $(CEVFR)H^+$, and it was as poor as 5% ($^{18}O_1/^{18}O_2$ ratio higher than 19). The double incorporation for the same peptide with the overnight protocol was 76% ($^{18}O_1/^{18}O_2$ ratio = 0.31).

4. Future prospects

On the overall, the possibility of speeding up ^{18}O isotopic labeling from 12–48 h to 30 min using ultrasonication with bath and 130 kHz sonication frequency is a reliable approach that deserves further investigation due to the importance of protein quantitation for biomarker discovery and clinical diagnosis either in a relative or absolute manner. It is clearly stated from the data here presented that ultrasonication can accelerate the $^{16}O/^{18}O$ labeling, but it seems to fail in promoting the double ^{18}O incorporation ($^{18}O_2$). However this failing is selective and it depends on the protein. In addition, for the same protein, when the ultrasonication is used, the double ^{18}O incorporation is peptide-selective. Therefore, further research needs to be done focusing on the following variables: regarding ultrasonic energy, it is necessary to establish if the ultrasonic frequency is a variable of main importance linking it with other ultrasonic devices different from the ultrasonic bath, such as the sonoreactor or the ultrasonic probe. Preliminary results

obtained in our laboratory seem to suggest that high differences can be obtained in the ^{18}O incorporation as a function of the ultrasonic device used to speed up the labeling process. Concerning proteins, the sample treatment must be studied linking the ultrasonic efficiency to the physical and chemical characteristics of the protein. In addition, special attention must be paid to the ^{18}O incorporation as a function of the type of peptide.

5. Conclusions

Our preliminary results demonstrate that ultrasonic energy has a great potential to be used to enhance the enzymatic isotopic labeling of peptides with ^{18}O. The time needed to perform the isotopic labeling can be reduced from 12–48 h to 30 min with similar results to the ones obtained with the overnight protocol, depending on the protein.

Similar $^{16}O/^{18}O$ ratios were found for BSA, ovalbumin and α-lactalbumin proteins between the ultrasonic procedure and the overnight one, with a total time used to perform the isotopic labeling of 30 min. However, the $^{18}O_1/^{18}O_2$ labeling ratios obtained were considered acceptable only for the BSA protein.

The fact that sonication frequency (35 kHz vs. 130 kHz) had been found critical for the good performance in accelerating the labeling process, open new ways in re-thinking ultrasonic applications in the analytical laboratory for proteomic purposes. It must be taken into account that most ultrasonic devices used at present, work at low frequencies such as 20, 22, 30 or 35 kHz.

Further research is to date being done in our laboratory to elucidate the key parameters on this new methodology, including the use of different ultrasonic devices with different frequencies of work.

Acknowledgments

R. Rial-Otero and R.J. Carreira acknowledge the postdoctoral grant SFRH/BPD/23072/2005 and the doctoral grant SFRH/BD/28563/2006, respectively, of FCT (Science and Technological Foundation) from Portugal. Dr. J.L. Capelo acknowledges the MALDI-TOF-MS service of the Chemistry Department of the New University of Lisbon (http://www.dq.fct.unl.pt/maldi) for their helpful assistance and valuable suggestions. The research findings here reported are protected by international laws under patent pending PCT/IB2006/052314 and PT 103 303. FCT is also acknowledged for financial support under the project POCI/QUI/55519/2004 FCT-FEDER.

References

[1] M. Hamdam, P.G. Righetti, Mass Spectrom. Rev. 21 (2002) 287–302.
[2] S. Sechi, Y. Oda, Curr. Opin. Chem. Biol. 7 (2003) 70–77.
[3] W.W. Wu, G. Wang, S.J. Baek, R.F. Shen, J. Proteome Res. 5 (2006) 651–658.
[4] A.P. De Leenheer, L.M. Thienpont, Mass Spectrom. Rev. 11 (1992) 249–307.
[5] M. Bantscheff, M. Schirle, G. Sweetman, J. Rick, Bernhard Kuster, Anal. Bioanal. Chem. 389 (2007) 1017–1031.
[6] D.B. Sprinson, D. Rittenberg, Nature 167 (1951) 484.
[7] M. Miyagi, K.C.S. Rao, Mass Spectrom. Rev. 26 (2007) 121–136.
[8] I.I. Stewart, T. Thomson, D. Figeys, Rapid Commun. Mass Spectrom. 15 (2001) 2456–2465.
[9] O.A. Mirgorodskaya, Y.P. Kozmin, M.I. Titov, R. Korner, C.P. Sonksen, P. Roepstorff, Rapid Commun. Mass Spectrom. 14 (2000) 1226–1232.
[10] Y. Oda, K. Huang, F.R. Cross, D. Cowburn, B.T. Chait, PNAS 96 (1999) 6591–6596.
[11] P. Bermejo, J.L. Capelo, A. Mota, Y. Madrid, C. Cámara, Trac-Trend Anal. Chem. 23 (2004) 654–663.
[12] C. Fernandez, C.L. Antonio, R. Conceição, C. Rial-Otero, J.L. Vaz, Capelo, Anal. Chem. 78 (2006) 2494–2499.
[13] D. López-Ferrer, J.L. Capelo, J. Vázquez, J. Proteome Res. 4 (2005) 169–1574.
[14] R. Rial-Otero, R.J. Carreira, F.M. Cordeiro, A.J. Moro, M.G. Rivas, L. Fernandez, I. Moura, J.L. Capelo, J. Proteome Res. 6 (2007) 909–912.
[15] Data Explorer software user's guide, section 3, pp. 45–47.
[16] X. Yao, A. Freas, J. Ramirez, P.A. Demirev, C. Fenselau, Anal. Chem. 73 (2001) 2836.
[17] X. Yao, C. Afonso, C. Fenselau, J. Proteome Res. 2 (2003) 147–152.
[18] M.M.R. Talukder, M.M. Zaman, Y. Hayashi, J.C. Wu, T. Kawanishi, Biocatal. Biotransform. 24 (2006) 189–194.
[19] E. Bracey, R.A. Stenning, B.E. Brooker, Enzyme Microb. Technol. 22 (1998) 147–151.
[20] H.M. Santos, J.L. Capelo, Talanta 73 (2007) 795–802.
[21] T.J. Mason, Sonochemistry, Oxford University Press, Oxford, UK, 1999.

Talanta 76 (2008) 282–287

Contents lists available at ScienceDirect

Talanta

journal homepage: www.elsevier.com/locate/talanta

Separation and determination of abused drugs clenbuterol and salbutamol from complex extractants in swine feed by capillary zone electrophoresis with simple pretreatment

Qian Chen[a,b], Liu-Yin Fan[a,b], Wei Zhang[a,b], Cheng-Xi Cao[a,b,*]

[a] *Laboratory of Analytical Biochemistry and Bioseparation, School of Life Science and Biotechnology, Shanghai Jiao Tong University, 800 Dongchuan Road Minhang, 200240 Shanghai, PR China*

[b] *Key Laboratory of Microbiology Metabolism, Ministry of Educational, School of Life Science and Biotechnology, Shanghai Jiao Tong University, 800 Dongchuan Road Minhang, 200240 Shanghai, PR China*

ARTICLE INFO

Article history:
Received 28 January 2008
Received in revised form 22 February 2008
Accepted 25 February 2008
Available online 4 March 2008

Keywords:
β2-Agonist
Clenbuterol
Salbutamol
Capillary zone electrophoresis
Swine feed

ABSTRACT

A simple but efficient capillary zone electrophoresis (CZE) method was developed for the fast separation and determination of two misused β2-agonists clenbuterol (CLB) and salbutamol (SAL) from complex background extractants existing in swine feed samples. The proper experimental conditions were achieved as 20.0 mmol/l pH 10.5 Na_2HPO_4–NaOH buffer, 20 kV applied voltage, fused-silica capillary of 60.5 cm × 75 μm i.d. (50 cm to detector). Under the proper conditions, the two abused drugs can be online isolated from the complex extractants and the separation between CLB and SAL is good, all of the target analytes can be detected within 4.5 min. The linear response of CLB and SAL concentration ranges from 2.0 to 100.0 μg/ml with high correlation coefficient (R^2 = 0.9990) and (R^2 = 0.9986), respectively. Limit of detection (LOD) and limit of quantification (LOQ) was calculated to be 0.95 and 3.17 μg/ml for CLB, 1.07 and 3.57 μg/ml for SAL. The precision values (expressed as R.S.D.) of intra- and inter-day were 1.24–2.36% and 0.90–3.85% for CLB, 0.47–1.64% and 0.91–3.46% for SAL. Recoveries spiked at levels 5.0, 25.0, 80.0 μg/ml ranged between 93.30% and 104.33% with R.S.D. less than 5%. Finally, the developed method has been applied to the analysis of real swine feed samples and has achieved satisfactory results.

1. Introduction

β2-Agonists are used as drugs for the treatment of bronchial asthma. Then, they are misused by athletes for their potential to improve muscular strength for their significant anabolic effects [1]. β2-Agonists in particular clenbuterol (CLB), salbutamol (SAL) are often illegally used as feed additives for their potential role in increasing muscle mass and reducing body fat in animal species [2]. However, the β2-agonists are steady substances, so they can be easily deposited in both human beings and the edible animal tissue. When using at higher or long-term dose, they are found to have severe poisoning side-effects [3]. The misuse of β2-agonists by athletes has been demonstrated and banned by the International Olympic Committee [4]. Their usages as feed additives for growth promotion in livestock growth, which have resulted in a number of reports of human food poisoning [5] have also been prohibited in many countries.

In order to get adequate monitoring of the therapeutic application and also to control the illegal use of the β2-agonists, several methods have been published to measure their concentration in biological matrixes. These methods include immunoassays [6], HPLC–UV [7,8], LC–MS [9], HPLC–MS [10–12], HPLC–ECD [13,14], HPLC–FD [15,16] and GC–MS [5,17–22]. However, although most of the methods are sensitive, extra extraction and purification of analytes are needed before analysis. All make these methods either laborious and time-consuming, or require highly specialized equipment to improve sensitivity. Thus, simple, accurate and rapid new methods must be developed for the analysis of these compounds.

Capillary electrophoresis (CE) is a widely used technique in separation science on account of its high separation efficiency, small sample volume required, lower cost, and it has become one of the most outstanding separation techniques in the analysis of an increasingly large number of charged species. It also has already become a powerful analytical technique in pharmaceutical and biomedical aspects [23–25]. CE with UV detection (CE–UV) [26–30] has been used to get stereoselective determination and enantiomeric separation of β2-agonists and CE combined with field-amplified online sample stacking [31] has been developed to improve the sensitivity in recent years. However, researches about

* Corresponding author at: School of Life Science and Biotechnology, Shanghai Jiao Tong University, 800 Dongchuan Rd. Minhang, 200240 Shanghai, PR China. Tel.: +86 21 34205682; fax: +86 21 34205820.
E-mail address: cxcao@sjtu.edu.cn (C.-X. Cao).

0039-9140/$ – see front matter © 2008 Elsevier B.V. All rights reserved.
doi:10.1016/j.talanta.2008.02.032

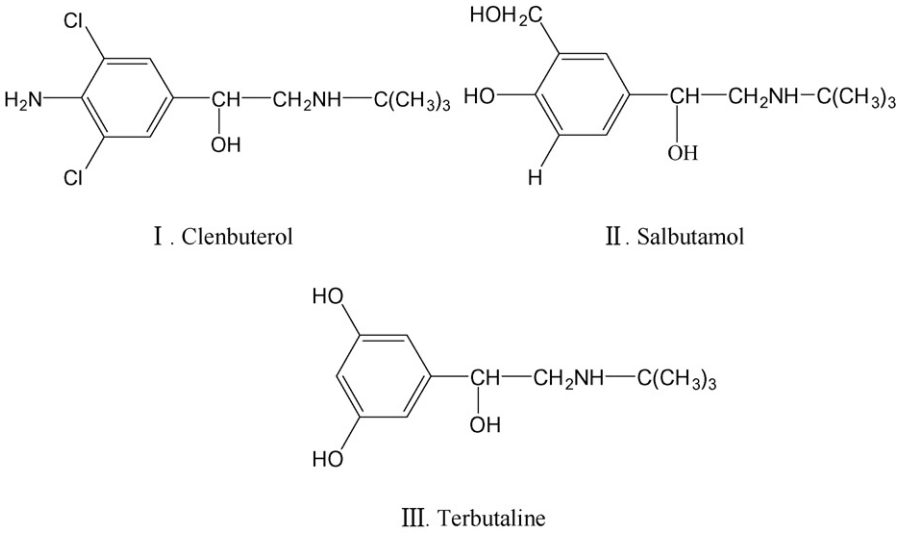

Fig. 1. Chemical structures of clenbuterol, salbutamol and terbutaline.

the determination of β2-agonists in swine feed samples with CE method were relatively few, only Duan et al. [32] has used it for the determination of swine feeds and the analysis time was relatively long. More importantly, the swine feed contains a large number of complex background extractants. The complex background extractants may seriously affect the separation of CLB and SAL, if no proper pretreatment is introduced for the sample purification to remove the background extractants. The removal of extractants is laborious, time-consuming and expansive.

Interestingly, by choosing proper separative conditions of CE, one can simply but efficiently achieve online isolation of the abused drugs CLB and SAL from the complex background extractants existing in the swine feed. Furthermore, the separations of CLB, SAL and terbutaline (internal standards, IS) (Fig. 1) are good, and the appearance of the two abused drugs as well as the IS just located within the sharp clear window of 3–5 min.

Therefore, the main aim of the present work was to report a simple but efficient CE method for the fast separation and determination of abused drugs CLB and SAL in the swine feed sample, including the optimization of proper separative conditions for the abused drugs, the demonstration of validity of the developed analytical method and the actual applications of the developed method for different swine feed samples.

2. Experimental

2.1. Apparatus

A P/ACE MDQ capillary electrophoresis instrument equipped with UV detector (Beckman, Fullerton, CA, USA) was used for the experiments. Electrophoresis was performed in untreated fused-silica capillaries (Yongnian Optical Fiber, Heibei, China), 60.5 cm (effective length 50 cm) × 75 μm i.d. (375 μm O.D.). Data collection, processing, and analysis were performed using system 32-karat software (Beckman) and recorded on an HP personal computer. A 320 pH meter (Mettler-Toledo Instrument Ltd., Shanghai, China) was used to measure the pH of the BGE. An Ultra-pure Water System (SG Ultra Clear system, Wasseraufbereitung und Regenerierstation Gmbh, Germany) was used to produce ultra-pure water. HS-120D ultrasonic cleaner (Ningbo Scientz Biotechnology Co., Ltd., Ningbo, China) was used for extraction. DHG-9070A electrothermal constant temperature drying oven (Yiheng Science and Technology Co., Ltd., Shanghai, China) was used for sample drying.

2.2. Chemicals and reagents

Clenbuterol hydrochloride was purchased from National Institute for the Control of Pharmaceutical and Biological Products (Beijing, China), salbutamol sulfate and terbutaline sulfate were purchased from Dr. Ehrenstorfer GmbH (Augsburg, Germany), all of them had purity higher than 99%. Phosphoric acid (analytical reagent, AR), sodium hydroxide (AR) were purchased from Shanghai Xinhua Chemistry Reagent Company (Shanghai, China). Disodium hydrogen phosphates (AR), sodium dihydrogen phosphate (AR) were purchased from Shanghai N.0.1 Chemistry Reagent Company (Shanghai, China). Hexane (AR) was obtained from the Sinopharm Chemical Reagent Co., Ltd. (Shanghai, China). Acetone (AR) was obtained from Shanghai Linfeng Chemistry Reagent Company (Shanghai, China).

2.3. Standard solution and buffer

Na_2HPO_4–NaOH buffer solution was chosen as the background electrolyte in our experiment. The pH value of the buffer ranged from 9.0 to 11.5 was adjusted by titrating 100.0 mmol/l Na_2HPO_4 with 1.0 mol/l NaOH and was diluted to the required concentrations. The concentrations of the buffer changed from 15.0 to 50.0 mmol/l. The stock standard solutions (1.0 mg/ml) of CLB, SAL and internal standard IS were prepared by dissolving 1.0 mg sample to 1.0 ml ultra-pure water and stored at 4 °C. A series of working standard solutions were further made by diluting the stock standard solutions with running buffer.

100.0, 60.0, 40.0, 30.0, 20.0, 10.0, 5.0 and 2.0 μl of CLB, SAL solution (1.0 mg/ml) and 40.0 μl IS solution (1.0 mg/ml) were added into 1.0 g blank sample, respectively. Corresponding volume of acetone were added afterwards and then the working standards were conducted in accordance with the procedures in Section 2.4. The final concentrations of working standards were 100.0, 60.0, 40.0, 30.0, 20.0, 10.0, 5.0 and 2.0 μg/ml.

2.4. Sample preparation

Finely ground swine feed (1.0 g) were weighed into 25.0 ml centrifuge tubes, and 40.0 μl IS were spiked into the feed samples. Then the feed was put into electrothermal constant temperature drying oven to dry at 50 °C. After that, 3.0 ml acetone and 1.0 mol/l NaOH

mixture (9:1, v:v) was added in to the feed, which would be subjected to supersonic vibration for 5 min. Later, the mixture in the tube was centrifuged at 10,000 rpm (11,180 × *g*) and 5 °C for 10 min. The extraction was repeated for four times and the clear supernatants were combined together and were transferred into a beaker placed at ventilate closet for evaporation. The residues were dissolved in 1.0 ml running buffer, then for defatting the same volume hexane were added. After centrifuging at 10,000 rpm (11,180 × *g*) and 5 °C for 5 min, the organic solvent hexane was then removed and the water phase were collected for analysis. All solutions were stored at 4 °C in a refrigerator until use.

For the analysis of real swine feed samples in Section 3.4.5, 1.0 mg three different feed samples were extracted as mentioned above, without any IS added. Then 40.0 μl of CLB, 40.0 μl SAL solution (1.0 mg/ml) and 40.0 μl IS solution (1.0 mg/ml) were added into 1.0 ml blank sample feed, respectively, to get 40.0 μg/ml CLB, 40.0 μg/ml SAL and 40.0 μg/ml IS.

2.5. CE procedure

HPCE was conducted according to the procedure described below. Before use, the new capillary was conditioned by rinsing with 1.0 mol/l NaOH for 4 min, ultra-pure water for 4 min, 1.0 mol/l HCl for 4 min, ultra-pure water for 4 min, and running buffer for 4 min, with 0.2 psi pressures. Between injections, the capillary was rinsed with the running buffer for 2 min. Detection wavelength was 214 nm. Then the samples were injected in pressure mode at the inlet (0.2 psi, 10 s). Capillary temperature control was maintained at 25 °C with coolant. Data collection, processing, and analysis were performed using system 32-karat software (Beckman).

The resolution R_s was calculated by the equation used in conventional chromatography:

$$R_s = \frac{2\Delta t}{W_1 + W_2}$$

where W_1 and W_2 are peak widths at the baseline and Δt is the difference in migration times.

3. Results and discussions

3.1. Selection of BGE

In the literature [31–34], the normally used BGE for the determination of CLB, SAL and IS in capillary electrophoresis was acidic or neutral citrate buffer, so we first attempted the citrate buffer. The pH 6.5 citrate buffer can repeat the reported baseline separation, but the analysis time was too long. Then, we tried the commonly used Gly–NaOH buffer and Na_2HPO_4–NaOH buffer. The results indicated that all the three substances can be detected within 5 min in Gly–NaOH buffer, but the baseline of Gly–NaOH buffer is bad. The use of Na_2HPO_4–NaOH buffer can achieve good resolution as well as potential for faster determination of the three substances. In addition, the aim of this study was to make preparations for subsequent concentration of the three analytes using moving chemical reaction boundary (MRB) [35–37], thus, we hope that the resolution was large enough and the separation can be performed at alkaline condition (high pH value). Considering on the above results, Na_2HPO_4–NaOH buffer was finally chosen.

3.2. Optimization of extraction

According to the physical and chemical characters of the β2-agonists, they are diffluent in water at acidic environment, and in organic solvent at alkaline environment. So, water, ethyl acetate and acetone were tried as extractant. The interference was severe using water as extractant and the extraction efficiency was low using ethyl acetate as the extractant. The extraction efficiency was acceptable and no interference was found using acetone. So, acetone was chosen as the extractant. Subsequently, we investigated the quantity of 1.0 mol/l NaOH in acetone (5% and 10%, NaOH/acetone, v/v) on extraction, the results indicated that 10% NaOH had better effect on the extraction efficiency. In the later experiment, 10% 1.0 mol/l NaOH (v/v) in acetone solvent was used as the extractant for the sample preparation.

3.3. Optimization of separation conditions

3.3.1. Effect of pH value of buffer

In this experiment, the choice of pH value was very important for the separation of CLB, SAL and IS. The pH values of the buffer were from pH 9.0 to 11.5. We found that pH did not have an obvious influence on the migration time of CLB, SAL and IS. The migration time of CLB and SAL decreased with buffer pH increasing up to 10.5, then increased. But the changes of migration time were all kept within about 2 min. The resolution of CLB and SAL increased with buffer pH increasing up to 11.0, and then decreased at higher pH. The resolution of SAL and IS increased with increasing buffer pH up to 10.0, and then decreased at higher pH till 11, then increased rapidly. Considering on the analysis time and better separation, pH 10.5 was chosen as the optimized pH value.

3.3.2. Effect of buffer concentration

Buffer concentration played an important part in our research to the effect of resolution, peak shape, and electric current. Different concentrations of Na_2HPO_4–NaOH buffer (15.0–50.0 mmol/l) were investigated. The migration times got the lowest when the buffer concentration increased from 15.0 to 20.0 mmol/l, then

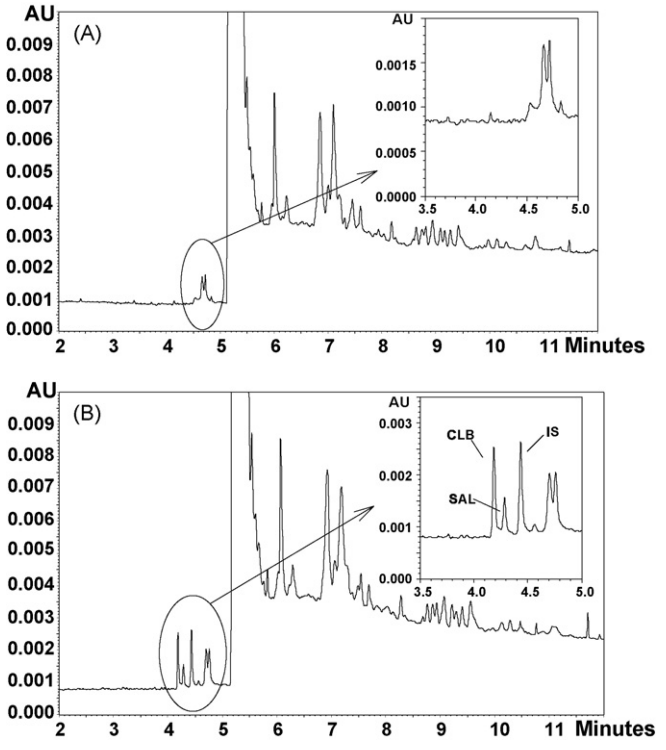

Fig. 2. Electropherograms of feed sample. (A) Blank sample of feed and (B) feed spiked with 40.0 μg/ml CLB, 40.0 ug/ml SAL and 40.0 μg/ml IS. Condition: 15.0 mmol/l Na_2HPO_4–NaOH buffer, 0.2 psi 10 s injection of sample, 15 kV, 60.5 cm capillary (effective length 50 cm), 214 nm wavelength.

increased with the increase of buffer concentration. The resolution of CLB/SAL and SAL/IS were all above 2, which could get good baseline separation. The buffer capacity of 20.0 mmol/l Na_2HPO_4–NaOH was enough, and considering on the compromise of the three substrates resolution and analysis time, finally, the 20.0 mmol/l Na_2HPO_4–NaOH buffer was selected in the following experiments.

3.3.3. Effect of running voltage

Here, the influence of voltage ranging from 10 to 27.5 kV was studied. The experiments unveiled that the applied voltage affected the migration time of them greatly and had great influence on the resolution between the three substances. It was shown that when the voltage increased from 10 to 27.5 kV, the migration times of CLB, SAL and IS decreased steeply from about 9 to 3 min. The resolutions got the maximum when the voltage was 12.5 and 20 kV, considering on the quick analyze as well as the good resolution, the voltage of 20 kV was finally chosen for the further study.

3.3.4. Optimized results

As the results mentioned above, the optimized separation condition was obtained with the background electrolyte containing 20.0 mmol/l Na_2HPO_4–NaOH buffer at pH 10.5, 20 kV applied voltage, 60.5 cm total length (50 cm effective length) and 75 μm i.d. capillary, 214 nm wavelength, 0.2 psi 10 s pressure sample injection, 25 °C coolant.

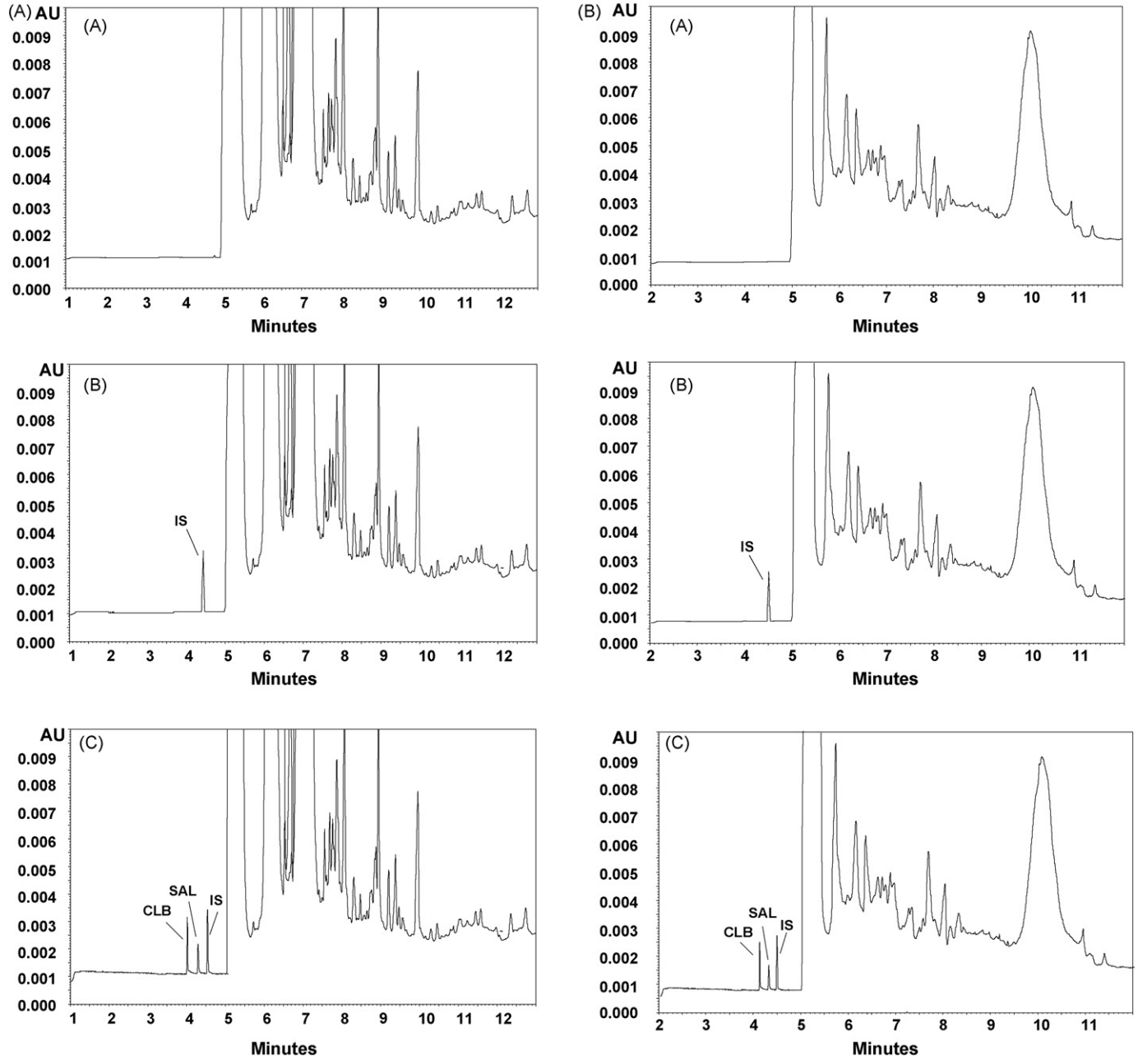

Fig. 3. (a) Electropherograms of feed sample (I). (A) blank sample of feed (B) feed spiked with 40.0 μg/ml IS (C) feed spiked with 40.0 μg/ml CLB, 40.0 ug/ml SAL and 40.0 μg/ml IS. The other conditions were the same as in Fig. 2. (b) Electropherograms of feed sample (II). (A) blank sample of feed (B) feed spiked with 40.0 μg/ml IS (C) feed spiked with 40.0 μg/ml CLB, 40.0 ug/ml SAL and 40.0 μg/ml IS. The other conditions were the same as in Fig. 2. (c) Electropherograms of feed sample (III). (A) blank sample of feed (B) feed spiked with 40.0 μg/ml IS (C) feed spiked with 40.0 μg/ml CLB, 40.0 ug/ml SAL and 40.0 μg/ml IS. The other conditions were the same as in Fig. 2.

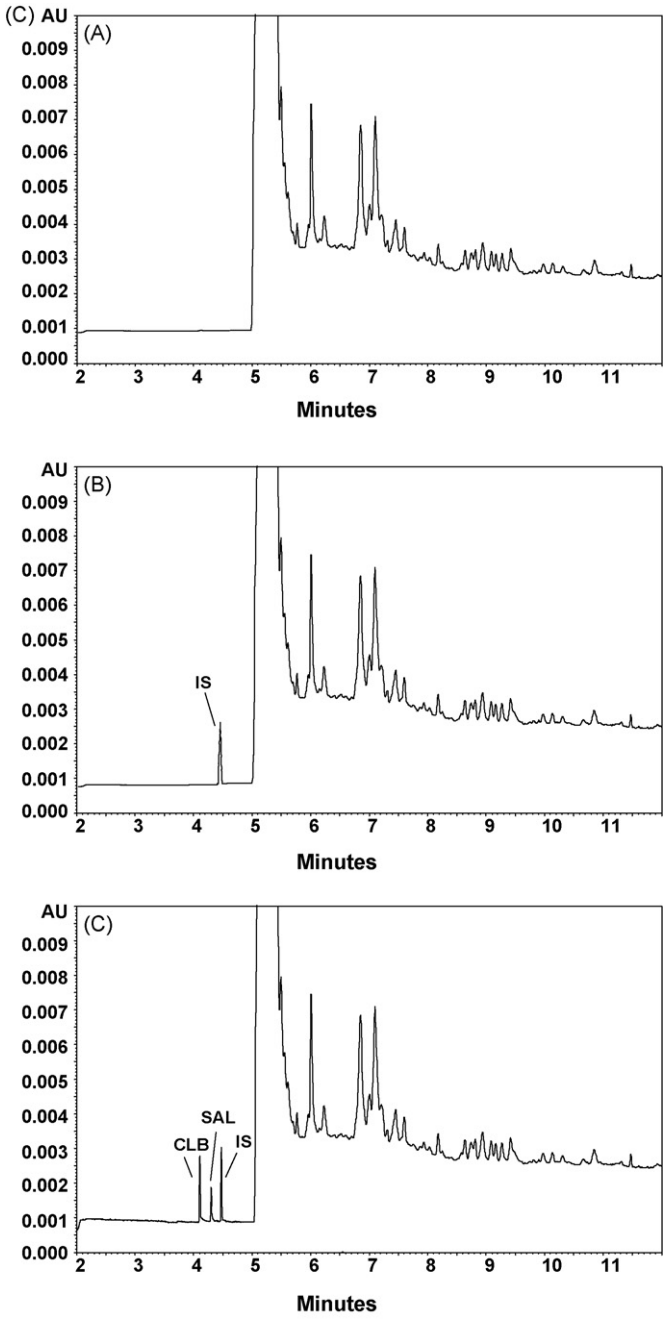

Fig. 3. (*Continued*)

3.4. Validation

In order to validate the feasibility and validity of our developed method in the analysis, routine criteria such as specificity, linearity, precision, accuracy and LOD were assessed as described below.

3.4.1. Specificity of method

The substances contained in swine feed are very complex. It was found that the peaks of CLB, SAL and IS were not interfered under the optimized conditions and they were separated on baseline from other components as shown in Fig. 2. Fig. 2A is the electropherogram of blank sample. Fig. 2B displays the peaks of CLB, SAL and internal standard extracted from the blank sample. It showed good specificity for the determination of the β2-agonists.

3.4.2. Linearity and detection limits

The response of detector was linearly changed with the concentration of standard solutions of CLB, SAL extracted from blank sample in the range of 2.0–100.0 μg/ml. The CLB calibration curves ($y = 0.0217x + 0.0096$, $R^2 = 0.9990$, $n = 7$, y is the ratio of peak area CLB to IS, x is the concentration of CLB, μg/ml) and SAL calibration curves ($y = 0.0192x - 0.0383$, $R^2 = 0.9986$, $n = 7$, y is the ratio of peak area SAL to IS, x is the concentration of SAL, μg/ml) revealed good linear behavior over the investigated concentration range. Taking into account the instrumental noise recorded at 214 nm, the limit of detection (LOD) and limit of quantification (LOQ) was calculated to be 0.95 and 3.17 μg/ml for CLB, 1.07 and 3.57 μg/ml for SAL, respectively, on the basis of a signal-to-noise ratio of 3 and 10.

Table 1
The intra-and inter-day R.S.D. of CLB and SAL under different concentrations ($n = 3$, $r = 5$)

Spiking level (μg/ml)	Intra-day R.S.D. (%)		Inter-day R.S.D. (%)	
	CLB	SAL	CLB	SAL
5	2.35	1.64	3.85	3.46
30	1.35	0.77	2.89	2.44
50	0.24	0.47	0.90	0.91

Table 2
The recovery of CLB and SAL under different concentrations ($n = 3$, $r = 3$)

Spiking level (μg/ml)	Recovery (%)		R.S.D. (%)	
	CLB	SAL	CLB	SAL
5	93.30	104.33	2.96	2.70
25	96.00	102.12	3.14	2.45
80	100.48	99.77	0.24	0.89

3.4.3. Precision

Precision was evaluated by measuring intra- and inter-day relative standard deviations (R.S.D.) of peak areas ratio between samples and internal standard extracted from blank sample. The intra-assay precision was performed by analyzing samples with the interval of 2 h in 1 day for five times at three different concentrations of 5.0, 30.0 and 50.0 μg/ml, and the inter-assay precision were performed over 5 days with the same three concentrations. The results (see Table 1) implied that the operating conditions selected above could provide a stable background with good repeatability.

3.4.4. Accuracy

The recovery experiments were performed on sample with three different concentrations. CLB and SAL standard solution were added to the blank sample and prepared as described in Section 2.4 to achieve the spiking level of 5.0, 25.0 and 80.0 μg/ml. The recovery was calculated using the regression equation from calibration mentioned in Section 3.4.2. The results were all acceptable and given in Table 2.

3.4.5. Analysis of real samples

In order to evaluate the applicability of this method for the determination of CLB in real samples, three kinds of swine feeds were tested. The electropherograms were shown in Fig. 3. The experimental results indicated that no CLB and SAL were detected in the feed.

4. Concluding remarks

The background extractants of swine feed was very complex and may seriously affect the separation of CLB and SAL. In this paper, by choosing proper experimental conditions, the abused drugs of CLB and SAL can be fast separated within 4.5 min, more importantly, under the optimum experimental condition, the appearance of the complex background extractants was behind the appearance of CLB and SAL, which make the complex background extractants have no interference for the determination of CLB and SAL. The validity of the developed method was demonstrated and has been successfully used for the determination of three different bands swine feed samples.

Acknowledgements

The project was supplied by the NSFC (Approved no. 20475036 and 20675051), the national "863" Scientific-technological Key Program (Approved no. 2007AA10Z401), the Shanghai Leading Academic Discipline Project (Approved no. B203) and Shanghai Jiao Tong University.

References

[1] P.M. Clarkson, H.S. Thompson, Sports Med. 24 (1997) 366.
[2] A.P. Moloney, P. Allen, T.V. McHugh, J.F. Quirke, Livest. Prod. Sci. 42 (1995) 23.
[3] Allister Vale, Medicine 35 (2007) 597.
[4] L. Damasceno, R. Ventura, J. Cardoso, J. Segura, J. Chromatogr. B 780 (2002) 61.
[5] F. Ramos, A. Cristino, P. Carrola, T. Eloy, J.M. Silva, M.C. Castilho, M.I.N. Silveira, Anal. Chim. Acta 483 (2003) 207.
[6] A. Prezelj, A. Obreza, S. Pecar, Curr. Med. Chem. 10 (2003) 281.
[7] A. Blomgren, C. Berggren, A. Holmberg, F. Larsson, B. Sellergren, K. Ensing, J. Chromatogr. A 975 (2002) 157.
[8] J.A. Hamann, K. Johnson, D.T. Jeter, J. Chromatogr. Sci. 23 (1985) 34.
[9] H.B. Lee, K. Sarafin, T.E. Peart, J. Chromatogr. A 1148 (2007) 158.
[10] N.G. Knebel, M. Winkler, J. Chromatogr. B 702 (1997) 119.
[11] F. Xu, Z. Zhang, Y. Tian, H. Jiao, J. Liang, G. Gong, J. Pharm. Biomed. Anal. 37 (2005) 187.
[12] L. Hongxia, Z. Shusheng, Z. Xilin, Q. Lingbo, Z. Yufen, Fenxi Huaxue 32 (2004) 801.
[13] A. Koole, J. Bosman, J.P. Franke, R.A. de Zeeuw, J. Chromatogr. B 726 (1999) 149.
[14] M. Zhang, P. Fawcett, J.P. Shaw, J. Chromatogr. B 729 (1999) 225.
[15] D.W. Boulton, J.P. Fawcett, J. Chromatogr. B 672 (1995) 103.
[16] R.E. Bland, R.J.N. Tanner, W.H. Chern, J.R. Lang, J.R. Powell, J. Pharm. Biomed. Anal. 8 (1990) 591.
[17] L. Amendola, C. Colamonici, F. Rossi, F. Botre, J. Chromatogr. B 773 (2002) 7.
[18] B. Bocca, M. Fiori, C. Cartoni, G. Brambilla, J. AOAC Int. 86 (2003) 8.
[19] P. Batjoens, D. Courtheyn, H.F.D. Brabander, J. Vercammen, K.D. Wasch, M. Logghe, J. Chromatogr. A 750 (1996) 133.
[20] M. Thevis, G. Opferman, W. Schanzer, J. Mass Spectrom. 38 (2003) 1197.
[21] M. Weisberger, J.E. Patrick, M.L. Powell, Biomed. Mass Spectrom. 10 (1983) 556.
[22] A. Solans, M. Carnicero, R. de la Torre, J. Segura, J. Anal. Toxicol. 19 (1995) 104.
[23] A.B. Wang, F.Y. Gong, H.F. Li, Y.U.E. Fang, Anal. Chim. Acta 386 (1999) 265.
[24] A.B. Wang, Y.Z. Fang, Electrophoresis 21 (2000) 1281.
[25] M.D. Efstatiade, G.E. Baiulescu, Anal. Lett. 30 (1999) 2755.
[26] C.N. Carducci, S.E. Lucangioli, V.G. Rodríguez, Fernández Otero, J. Chromatogr. A 730 (1996) 313.
[27] C. Gausepohl, G. Blaschke, J. Chromatogr. B 713 (1998) 443.
[28] B. Toussaint, U.R. Tjaden, Ph. Hubert, J. van der Greef, J. Crommen, J. Chromatogr. A 871 (2000) 173.
[29] H.Y. Aboul-Enein, M.D. Efstatiade, G.E. Baiulescu, Electrophoresis 20 (1999) 2686.
[30] B. Toussaint, J. Gysler, P. Hubert, U.R. Tjaden, J. van der Greef, J. Crommen, Biomed. Chromatogr. 14 (2000) 32.
[31] Y. Shi, Y. Huang, J. Duan, J. Chromatogr. A 1125 (2006) 124.
[32] J. Duan, H. Chen, Y. Chen, Chinese J. Chromatogr. 23 (2005) 261.
[33] X. Ji, Z. He, X. Ai, H. Yang, C. Xu, Talanta 70 (2006) 353.
[34] Y. Chen, W. Wang, J. Duan, H. Chen, G. Chen, Electroanalysis 17 (2005) 706.
[35] C.X. Cao, Y.Z. He, M. Li, Y.T. Qian, M.F. Gao, L.H. Ge, S.L. Zhou, L. Yang, Q.S. Qu, Anal. Chem. 74 (2002) 4167.
[36] C.X. Cao, Y.Z. He, M. Li, Y.T. Qian, L. Yang, Q.S. Qu, S.L. Zhou, W.K. Chen, J. Chromatogr. A 952 (2002) 39.
[37] C.X. Cao, W. Zhang, W.H. Qin, S. Li, W. Liu, Anal. Chem. 77 (2005) 955.

Talanta 76 (2008) 479–484

Contents lists available at ScienceDirect

Talanta

journal homepage: www.elsevier.com/locate/talanta

Short communication

Determination of residual oil in diesel oil by spectrofluorimetric and chemometric analysis

Camila N.C. Corgozinho, Vânya M.D. Pasa, Paulo J.S. Barbeira*

Laboratório de Ensaios de Combustíveis, Departamento de Química, ICEx, UFMG, Av. Antonio Carlos 6627, 31270-901 Belo Horizonte, MG, Brazil

ARTICLE INFO

Article history:
Received 9 January 2008
Received in revised form 4 March 2008
Accepted 5 March 2008
Available online 14 March 2008

Keywords:
Adulteration
Diesel oil
Residual oil
Biodiesel
Spectrofluorimetry
Synchronous

ABSTRACT

Multivariate calibration (PLS), principal components analysis (PCA) and linear discriminant analysis (LDA), associated to synchronous spectrofluorimetry, were used to identify and quantify non-transesterified residual vegetable oil in diesel oil with the addition of 2% of biodiesel (B2). The addition of residual oil, one of the easiest ways of adultering fuel, damages engines and leads to tax evasion. Using this method, the samples of diesel oil, B2, and B2 contaminated with residual oil were classified correctly and separated into three well-defined groups. The quantification of residual oil in B2 was carried out in the 0–25% (w/w) band, RMSEC and RMSEP values ranging from 0.26 to 0.48% (w/w) and 1.6–2.6% (w/w), respectively. The method is highly sensitive and efficient to identify and quantify this type of adulterant in which 100% of the samples were correctly classified and the average relative error was approximately 4% in the range 0.5–25% (w/w).

1. Introduction

The commercialization of B2, a mixture of fuel consisting of 2 and 98% (v/v) of biodiesel and diesel oil, respectively, has been carried out by some distributors in Brazil since January 2005 and becomes compulsory in 2008, when B2 will replace automotive diesel oil. The 5% (v/v) concentration of biodiesel in diesel oil is planned for 2013, but this plan may be anticipated if the production of biodiesel meets the demand [1]. The physicochemical characteristics of biodiesel (B100) are very similar to the properties of diesel oil (B0); biodiesel can be mixed with diesel oil in any proportion [2], and the quality of both fuels is monitored through standard assays established by the Brazilian National Petroleum Agency (ANP) [3,4]. Quality control of diesel oil and biodiesel blends must be carried out according to the same technical regulations used to analyze pure diesel oil, and must comply with the same specifications [3]. However, the assays carried out so far do not provide enough evidence in order to conclude that the blend contains biodiesel, and whether the amount of this fuel meets the regulations of the Brazilian legislation [5]. The significant consumption of diesel oil in Brazil is spurred mainly by road cargo transportation which, in 2007, consumed 28.5 billion liters of diesel and 13.0 billion liters of B2. These figures represent 38.1 and 17.3%, respectively, of the Brazilian automotive fuel market [6]. In spite of all the ANP's efforts, fuel adulteration is still frequent in Brazil [5,7–10] and the common illegal practice is the intended adulteration with controlled addition of solvents, which aims at keeping the product within valid legal specifications [11]. Adulteration of fuel has a major influence on engine start-up control, engine heating, acceleration and fuel consumption, and it also increases the emission of particulate material, hydrocarbons and exhaustion gases [12,13]. In addition to the problems related to engine performance and emission of atmospheric pollutants, adulteration also generates tax evasion and gives rise to unfair competition in the market, thus creating a bleak picture for Brazilian economy [8–10].

Adulteration of fuels is also a practice in other countries. In India and Greece, the adulteration of petroleum byproducts has been a serious problem, particularly of diesel oil. Groups of researchers are developing new analytical techniques to detect these frauds which make use of adulterants such as kerosene and cyclohexane, among others [12,14–17]. In Brazil, adulteration of gasoline has been extensively covered by the media, and the addition of a larger amount of anhydrous ethanol exceeding the specifications of Brazilian legislation is one of the most common practices [10], representing 36% of the nonconformities detected in December 2007 [18] by the Fuel Quality Monitoring Program of ANP. However, the addition of light solvents as naphtha and rubber solvent is also observed [9]. Diesel oil is easily adulterated by adding non-transesterified vegetable oil, as edible vegetable oil, or even residual oils.

The characterization of fuels is of fundamental importance in order to carry out an effective quality control, and the development of analytical methodologies to control the quality of biodiesel,

* Corresponding author. Tel.: +55 3134095767; fax: +55 3134096650.
E-mail address: barbeira@ufmg.br (P.J.S. Barbeira).

0039-9140/$ – see front matter © 2008 Elsevier B.V. All rights reserved.
doi:10.1016/j.talanta.2008.03.003

detect adulterations and quantify the amount of biodiesel in blends with diesel oil has been the focus of increasing interest. Infrared spectroscopy (IR) [5,19–21] and high performance liquid chromatography (HPLC) [22] stand out among the techniques used for this type of analysis. These techniques generate multivariate responses for each analyzed sample, as statistical methods for univariated systems may be inadequate for data treatment [23]. Therefore, multivariate calibration and other chemometric techniques have been widely used, associated to conventional analytical methods [5,20,21,24–31] to get maximum information from the obtained data. Among the tools available, partial least squares regression (PLS), principal component regression (PCR) and principal components analysis (PCA) [32,33] are mostly used.

Aliske et al. [19] developed a methodology, using infrared spectrometry, whereby the width and height of the peak corresponding to the carbonyl group of esters are used to quantify biodiesel mixed with diesel in the 0–100% (v/v) band. For the peak area as well as for the peak height methods, approximately 90% of the data are observed within 5% deviation from the fitted function.

Pimentel et al. [20] applied PCA to distinguish pure diesel oil samples from their mixtures with biodiesel and vegetable oil, thus allowing the detection of adulterations. In order to determine the level of biodiesel in diesel oil blends, in the presence of raw vegetable oil, multivariable calibration models based on middle (MID) and near (NIR) infrared spectroscopy were developed. The relative average error for the prediction by an independent set of data was 10.2 and 6.7% for MID and NIR spectral areas, respectively.

PLS and artificial neural network (ANN) combined with FTIR-ATR and FTNIR spectroscopies have been used to design calibration models for the determination of biodiesel content in blends with diesel in the 0–100% (w/w) range [21]. Precisions ranged from 0.06 to 0.53% (w/w) and the coefficients of variation were over 3%.

FTIR and FT-Raman, associated to multivariate calibration, were used to detect the adulteration of B2 and B5 samples with non-transesterified vegetable oil in the 0–5% (w/w) range [5]. From the proposed calibration models, ANN based on FT-Raman provided the best results.

HPLC was used to quantify biodiesel in diesel oil, in the 1–30% (v/v) band, and may also be used to quantify similar levels of oils or fats [22]. The accuracy of the method for soybean oil blends in diesel ranged between 0.4 and 7.5% for the UV detector.

An analytical tool which is becoming important to analyze petroleum byproducts is spectrofluorimetry [15–17,24,34], in which the sample is submitted to a source of excitation and the emission spectrum is recorded. In spectrofluorimetry, the fluorescence intensity of each sample, at a fixed wavelength, is proportional to the concentration of a particular component. The presence of polycyclic aromatic hydrocarbons (PAHs), which have fluorescent properties, make this technique very useful to characterize [15,16,34] and to detect adulterations of petroleum byproducts [15,17,24], to identify and to classify crude oil [25,26,35], to detect polycyclic aromatic hydrocarbons in water [36], and to classify and characterize edible oils [27–31,37]. In conventional spectrofluorimetry, an emission spectrum is obtained by scanning the emission monochromator while the sample undergoes excitation at a fixed excitation wavelength (λ_{EX}) [35,38,39]. Although it has a good applicability in several analytical situations, conventional spectrofluorimetry has some limitations when it comes to complex blends, because the presence of various fluorescent species in the sample can cause interferences, as self-absorption and overlapping of signals [38], thus making this technique inadequate to characterize these kind of samples. An alternative technique to analyze these blends is synchronous fluorescence spectroscopy (SFS). It consists of scanning both the excitation and emission monochromators simultaneously with a fixed wavelength difference ($\Delta\lambda$) between them [35,38,39]. The main advantages of synchronous fluorescence spectroscopy are: formation of narrower and well defined bands, spectral band reduction and the possibility of selecting a $\Delta\lambda$ that increases only the emission intensity of the species under study. This is not achieved by the conventional method [35]. Patra and Mishra [34] used this technique to define the optimized $\Delta\lambda$ for gasoline, diesel oil and kerosene samples. Diesel oil presented spectral characteristics in longer wavelength areas, due to the presence of five- and six-ringed polycyclic aromatic hydrocarbons, maximum synchronous fluorescence intensity at 430 and 520 nm, for $\Delta\lambda$'s of 40 nm [34,38].

The synchronous fluorescence method, based on the combination of excitation and emission wavelengths, has been used to characterize compounds as diesel and kerosene [14], to detect and quantify the adulteration of diesel and gasoline with kerosene [16,17,24], to determine the presence of polycyclic aromatic hydrocarbons in water [36] and in lubricating oil [34] samples.

In the studies developed by Patra and Mishra [16,17], analytical curves based on fluorescence intensity measurements were constructed for quantitative analysis of contamination of diesel by kerosene in the concentration range from 0 to 90% (v/v), using ratios of peak intensity of diesel to kerosene as a function of concentration of kerosene. In another study [24], calibration models were constructed using two multivariate techniques, PCR and PLS, and SFS data of 35 samples with varying composition of gasoline and kerosene. The samples were analyzed with $\Delta\lambda$ of 40 nm and the model was found to be sensitive, detecting even 1% contamination of kerosene in gasoline.

Bearing in mind the high consumption of diesel oil in Brazil, the potential adulteration of this fuel and the damages caused by its commercialization, it is essential to develop methods capable of detecting and quantifying adulterants in diesel oil, and its blends with biodiesel, to help control the quality of these fuels. It is advisable to have a fast and non-destructive method, which does not require a large volume of samples or even sample pretreatment. Therefore, the purpose of this study is to develop a simple and fast analytical method for the identification and quantification of residual oil in B2 samples, using synchronous spectrofluorimetry associated to chemometric techniques, as PLS, PCA and LDA.

2. Experimental

The measurements were carried out on a Shimadzu RF-5301 spectrofluorimeter equipped with a 150 W Xenon lamp and quartz cells with optical path of 1 cm.

Three different samples of metropolitan type B2, collected in gas stations in the state of Minas Gerais, Brazil, were used to prepare the blends with residual oil.

The residual oil, soybean oil used as frying oil in restaurants, was filtered at reduced pressure to extract the solid residues before blending with B2 samples.

To predict the content of residual oil in the B2 samples using PLS, 69 blends were prepared with residual oil concentration ranging from 0.5 to 25% (w/w), with increments of 0.5% (w/w).

In addition to these blends, a group of 16 samples collected in gas stations, composed of 8 samples of pure B2 and 8 samples of pure diesel oil (B0), were used for the principal components analysis and linear discriminant analysis. These analyses were carried out in order to distinguish, in terms of quality, the B2 samples from the contaminated B2 and pure diesel oil samples.

The fluorescent emission spectra of the samples were obtained in synchronous mode, in the 340–800 nm range, maintaining a fixed $\Delta\lambda$ of 40 nm, with excitation and emission slits of 3 nm and scan speed of approximately 20 nm s^{-1}. Nine synchronous emission spectra were drawn for each sample and the averages were used to

build up intensity matrixes, where the rows correspond to samples and the columns to wavelengths.

For the principal components analysis, spectra were organized in a matrix [66 × 460] and the preprocessing used was the covariance matrix, because the emission intensities of the samples were of the same magnitude through all the spectral range.

The first five principal components (PCs) obtained by PCA were used to classify the samples by LDA.

Three calibration models were built using PLS with 69 samples, where 52 were chosen for the calibration model and 17 samples for the prediction set. The samples of the first model had no preprocess (NP), and the data of the remaining models were normalized according to the second peak (NSP), or normalized with a blank sample (NB). The NSP was carried out dividing spectra by synchronous emission intensity corresponding to 480 nm, which corresponds to the second peak and for NB, the spectra of each blend was divided by the spectrum of the pure B2 used for its preparation.

Cross-validation "*leave-one-out*" was the internal validation method used for LDA as well as for PLS. In this method, one sample is removed from the data set and the prediction is made with the model formed by the remaining $n-1$ samples.

MINITAB-14 software (MINITAB Inc.) was used for the chemometric treatment of data.

3. Results and discussion

3.1. Synchronous emission spectra

Fig. 1 shows typical synchronous emission spectra for B2, residual oil and diesel oil samples, obtained with a $\Delta\lambda$ of 40 nm. To determine the optimized $\Delta\lambda$, synchronous emission spectra of the diesel oil samples were obtained for different $\Delta\lambda$. The maximum fluorescence intensity for peak I was found when $\Delta\lambda$ was 40 nm. This is consistent with the optimized value found by Patra and Mishra [34,38] for the diesel oil samples in India. The spectrum of residual oil (curve a) presents an emission overlapping band ranging from 380 to 550 nm, while diesel oil and B2 (curves b and c) present two peaks of greater intensity, at 440 (I) and 480 nm (II), due to the presence of polycyclic aromatic hydrocarbons [34]. In addition, the peak intensities for B2 (curve b) were lower than the peak intensities of diesel oil. This may be caused by the self-quenching effect, because the UV–vis absorption spectra of B2 presents three well-defined absorption bands between 400 and 480 nm, which are not present in the diesel oil and residual oil spectra.

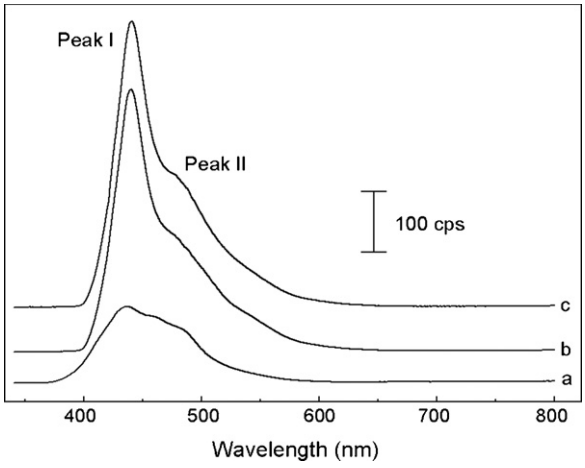

Fig. 1. Synchronous fluorescence spectra of residual oil (a), B2 (b) and diesel oil (c) using $\Delta\lambda$ of 40 nm.

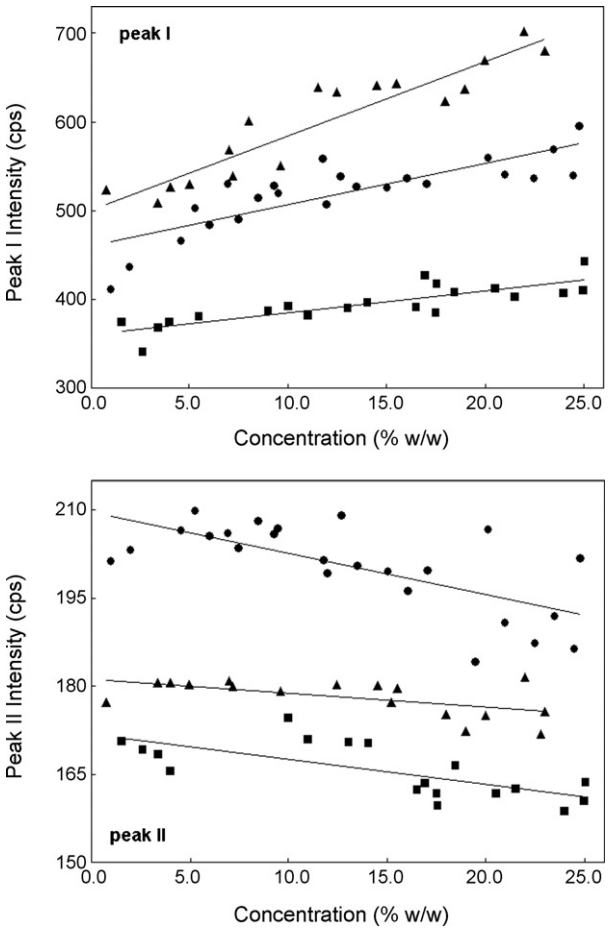

Fig. 2. SFS intensities corresponding to peaks I and II as function of the residual oil concentration added to different B2 samples: (▲) sample 1; (●) sample 2; (■) sample 3.

The addition of residual oil to B2 promotes a significant increase of intensity in peak I, in counts per second (cps), and a moderate reduction of intensity in peak II, as shown in Fig. 2. The increase of intensity in peak I is significantly steeper than the reduction in peak II, although the relation between these variations differs from each other in the three samples of B2 used. Peak I presented an increase ranging from 2.5 to 8.4 cps/% (w/w), and for peak II the average reduction rate ranged from 0.24 to 0.70 cps/% (w/w). The increase of intensity of peak I may be caused by the presence of PAHs in the residual oil [40–43]. High temperatures reached during food frying lead to a complex series of reactions that result in hydrolysis, oxidation, polymerization and pyrolysis of the oil [40]. Organic compounds can be partially cracked to smaller unstable fragments and mostly radicals recombine to give relatively stable PAHs (pyrosynthesis) [41].

Due to slope differences between curves, univariated calibration cannot be used in this data set, as there is no linear correlation between peak intensity and residual oil concentrations suitable for any B2 sample. In this case, another alternative would be the quantification of residual oil in B2 applying multivariate methods to the data, for instance, partial least squares regression.

3.2. Principal components analysis

As stated above, according to the Brazilian legislation [1], in 2008 automotive diesel oil (B0) will be replaced by a blend containing 2% (v/v) of biodiesel (B2). The observance of this law will be con-

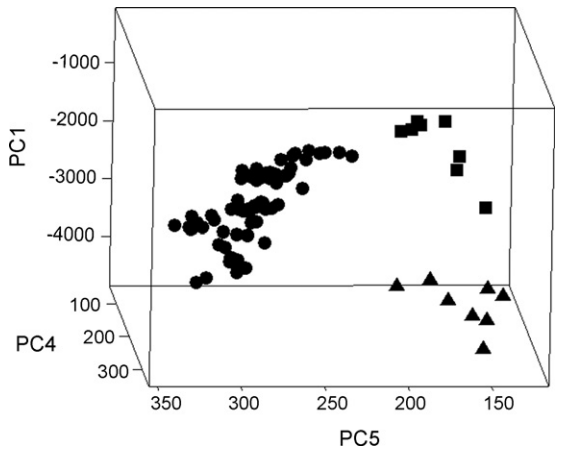

Fig. 3. Principal components analysis of synchronous emission spectra of B2 (■), diesel oil (▲) and mixtures of B2 with residual oil (●).

trolled through inspection procedures, in order to determine the type of fuel commercialized as well as to avoid frauds, such as the commercialization of contaminated B0 and B2 instead of pure B2.

So as to develop an analytical method capable of distinguishing B2 from B0 and from B2 samples contaminated with non-transesterified residual oil, PCA and LDA were applied to the synchronous emission spectra of a set of 85 samples: 8 of B0, 8 of B2 and 69 blends of B2 and residual oil.

It was observed that using both, PCA and synchronous spectrofluorimetry, the B2 samples were separated from its blends as well as from the B0 samples. Five principal components explained 99.8% of the variance of the model (88.2% PC1; 8.7% PC2; 2.0% PC3; 0.5% PC4; 0.4% PC5). The first principal component, PC1, enabled the discrimination between B2 and B0, and the fifth principal component, PC5, separated B0 and B2 from the B2-residual oil blends (Fig. 3). The loadings that most influenced PC1 were wavelengths 400–475 nm (Fig. 4), corresponding to peak I in the synchronous spectrum (Fig. 1).

The linear discriminant analysis classified correctly 100% of the samples using cross-validation (Table 1), thus indicating the high degree of accuracy this method offers to classify these samples. A similar classification was carried out in the past by Pimentel et al. [20], using infrared spectra normalized by the first derivative, where samples of diesel oil were separated from their blends with vegetable oils and biodiesel. However, the method failed in the classification of samples in which the biodiesel/vegetable

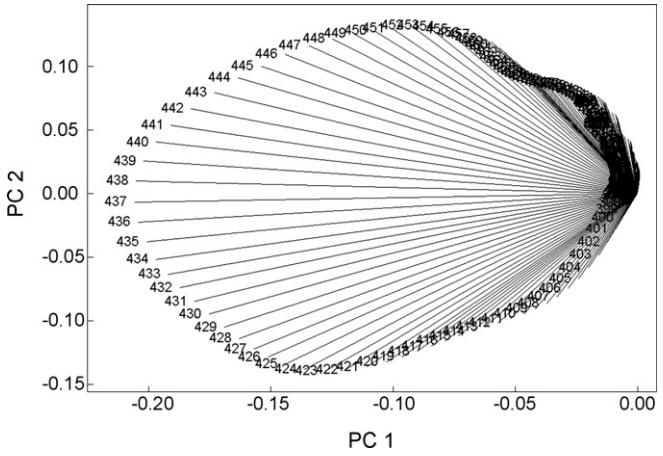

Fig. 4. Loadings plots for the first two principal components.

Table 1
Summary of the classification of the samples with cross-validation[a]

Put into group	True group		
	B2	B2/residual oil	Diesel oil
B2	8	0	0
B2/residual oil	0	74	0
Diesel oil	0	0	8
Total samples	8	74	8

[a] Percentage of samples correctly classified = 100%.

oil and vegetable oil/biodiesel proportions were over five. This does not occur in the method proposed herein, using spectrofluorimetry. Therefore, besides being more sensitive, the use of synchronous spectrofluorimetry has some advantages over infrared spectroscopy: data treatment is simple (spectra do not need any preprocess) and it is cheaper, in addition to accuracy in sample classification and no restrictions regarding biodiesel/vegetable oil proportion. Another interesting aspect of this technique is that it may be carried out "*in loco*", hence making inspection procedures faster.

3.3. Residual oil quantification

In order to quantify the residual oil content in B2, three models of multivariate calibration were built, applying PLS in the spectra of 52 samples. One of the models was built using the original data, that is, with no preprocess (NP). In the remaining models, data was normalized by blank (NB) or by peak II (NSP), as described above.

As synchronous emission spectra are sensitive to slight alterations in B2 samples, in routine analyses it is difficult to obtain a satisfactory blank for the normalization of spectra, due to the unequal compositions of diesel oil produced by different refineries. Although we were aware of this limitation, this preprocess was carried out to verify the influence of blank in data treatment, bearing in mind that peak intensity variations caused by the addition of residual oil are not the same in every sample, as shown in Fig. 2.

The three calibration models were evaluated examining the data dispersion, given by RMSEC values, and the correlation between real and predicted values of the concentrations are shown in Table 2. The correlation coefficient (R) is the intensity measure of the correlation between real values and values predicted by the calibration model. This may reach values from −1 to +1 and the closer to +1 higher the correlation between data. The three models presented high correlation between real and predicted values. The highest correlation was obtained for the NB model, as shown in Fig. 5.

For the three models presented here, the number of variables may be significantly reduced from 460 original variables (wavelengths) to 10 latent variables, which explained from 98.9 to 99.1% of the variances. The amount of factors, or latent variables, used to build the models was determined using "*leave-one out*" cross-validation, which reached the highest R^2 value and whose predictive residual error sum of squares (PRESS) was minimum.

The R^2, or coefficient of determination, is the proportion of variability in y which may be attributed to the variability in x. The

Table 2
Values of root-mean-square error of calibration (RMSEC) and correlation coefficient (R) for predicted vs. reference values plot of the PLS model

Preprocessing method	R	RMSEC (% w/w)	Number of factors	Explained variance (%)
NP	0.9987	0.38	10	98.9
NB	0.9994	0.26	10	99.1
NSP	0.9979	0.48	10	98.9

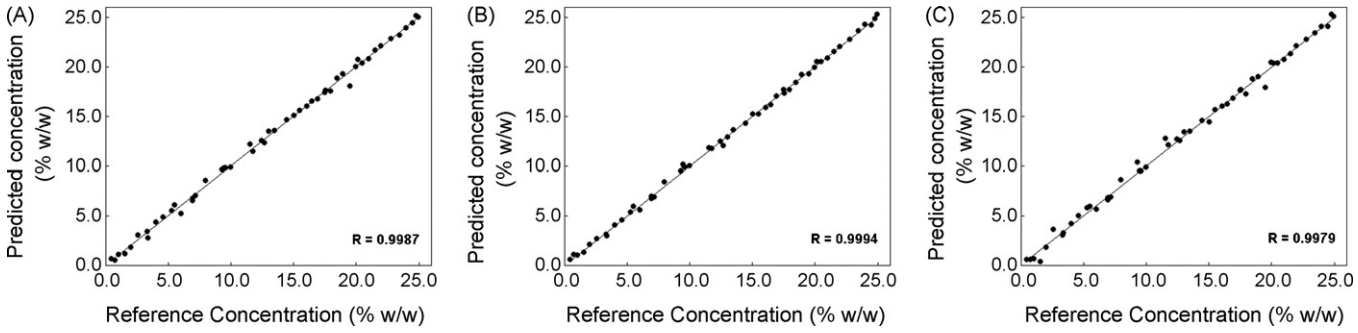

Fig. 5. Reference vs. predicted concentrations for the calibration models (A = NP, B = NB and C = NSP).

predicted R^2, obtained by cross-validation, is the parameter that indicates the accuracy of the model to predict answers to new observations. It may be verified that in the model built with original data the PRESS value was minimum when using 10 factors. This was also observed in the other models.

The RMSEC was obtained from the difference between real (y_r) and predicted (y_p) values of the concentrations of n samples and represents the data dispersion in the calibration model [24]. The lowest RMSEC was found when NB was used, and the highest for NSP, varying from 0.26 to 0.48% (w/w). To compare the variances of the three models and prove if there is a significant difference between them, the test F [44] was applied to the RMSEC values. The calculated F (F_c), for each model, was obtained dividing the square of the highest by the square of the lowest RMSEC value and then, compared to the tabulated F (F_t) with level of significance of 5% ($\alpha = 0.05$) and 51 degrees of freedom. The values found for F_c when comparing models NSP and NB with model NP were 1.61 and 2.06, respectively. As the F_c values were higher than those of F_t (1.59), it may be concluded, with 95% of certainty, that the variances in treatments with preprocess and original data are statistically different. Therefore, the highest accuracy was obtained when using the NB model, which produced RMSEC equal to 0.26% (w/w).

The concentrations of residual oil in an independent prevision set (external validation) composed of 17 blends were established using the three calibration models. The concentrations predicted by the three models were then compared with the real values of the concentrations using the test t [44] in order to check whether the data belonged to the same population group. The values of t (t_{calc}) were calculated from Eq. (1), and compared with the tabulated value ($t_{tab} = 2.12$), for 16 degrees of freedom and 5% ($\alpha = 0.05$) of level of significance, being 0.72, 1.80 and 0.25, for NP, NSP and NB models. As t_{calc} values were lower than those of t_{tab}, it may be concluded, with 95% of certainty, that the predicted concentrations are not statistically different from the real concentrations. This indicates that the three models may be used to predict the content of residual oil in blends containing B2.

Table 3
Results of root-mean-square error of independent prediction (RMSEP) and correlation coefficient for predicted vs. reference values plot of the prediction dataset

Preprocessing method	R	RMSEP (% w/w)	Relative average errors (%)
NP	0.9581	1.82	1.36
NB	0.9099	2.60	1.51
NSP	0.9727	1.60	4.13

$$t_{calc} = \frac{\bar{y}}{s_d}\sqrt{n} \quad (1)$$

where s_d is the standard deviation, n the amount of measures and $\bar{y}$:

$$\bar{y} = \frac{\sum(y_r - y_p)}{n} \quad (2)$$

The root-mean-square error of independent prediction values [24] (RMSEP) for a set of independent samples are shown in Table 3. The lower the RMSEP value, higher the degree of accuracy of the prediction result provided by the calibration model [45].

The mean relative prediction errors (RE) were calculated according to Eq. (3) for the three data sets, and values under 5% were obtained for the quantification of residual oil.

$$RE(\%) = \frac{\sum\left((y'_r - y'_p) \times 100\right)/y'_r}{n} \quad (3)$$

Models NP and NSP presented RMSEP values that, according to test F, are not significantly different and the RE values for these models were equal to 1.36 and 4.13%, respectively. In spite of RE being lower for the model with original data, the normalization through peak II provided lower relative errors, in most samples, compared to the other models. NSP also produced the best correlation between real and predicted values of the concentration (Fig. 6), and was considered the best calibration model for quantification of residual oil in B2 samples.

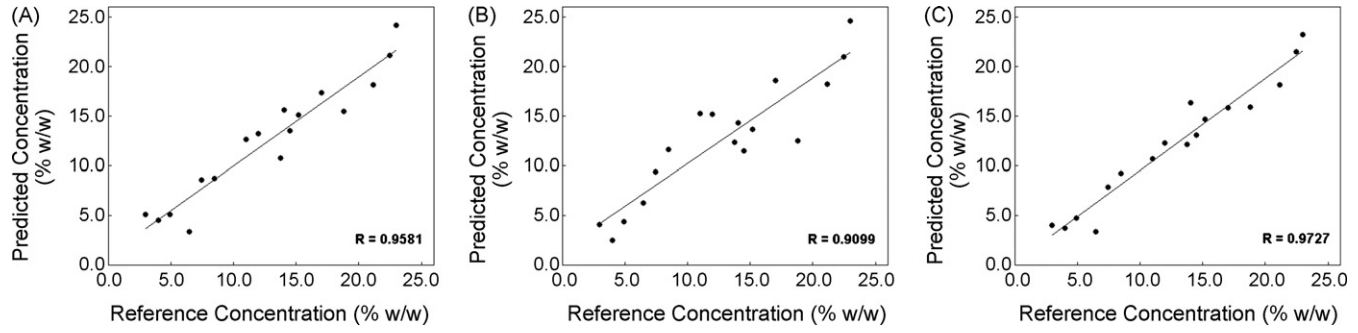

Fig. 6. Reference vs. predicted concentrations for the prediction set (A = NP, B = NB and C = NSP).

When the NB model was used to predict the concentrations of the external validation set, the correlation between real and predicted values was not good, and RMSEP value was the highest, that is, the results were less accurate. Therefore, this proved that in spite of peak intensity variations due to the higher concentration of residual oil, the method is efficient, and there is no need to use a blank in the normalization of data.

4. Conclusions

The recording of synchronous fluorescence spectra of diesel oil, B2, and B2 contaminated with residual oil made possible the correct classification of samples, as well as the separation of these samples in three well-defined groups using linear discriminant analysis and principal components analysis. The method is accurate and reliable to detect a fraud, and can assist the service of inspection and quality control of fuel.

The three calibration models proposed in this work (NP, NSP and NB) showed RMSEC values ranging from 0.26 to 0.48% (w/w) and high correlation between real and predicted concentrations. For the external validation set, the best RMSEP was 1.60% (w/w), and this figure was obtained using the NSP model. This same model reached the highest correlation between real and predicted concentration values in the prevision set, and was the best model for quantification of residual oil in B2.

The methodology described in this paper, synchronous spectrofluorimetry associated to PCA, LDA and PLS techniques, is an efficient tool to classify B2, contaminated B2 and pure diesel oil samples, as well as quantify residual oil in B2 samples. The set studied here, had a correct classification of samples with 100% accuracy and the mean relative error of the quantification of residual oil in B2 was approximately 4%, in the range 0.5–25% (w/w).

The method is simple, fast, does not require pretreatment of the samples, may be carried out "*in loco*", and is cheaper and more sensitive, compared to techniques such as infrared and chromatography.

Acknowledgements

The authors would like to thank CTPetro-FINEP and ANP for their financial support.

References

[1] Ministério das Minas e Energia, Lei No. 11.097 de 13 de Janeiro de 2005, http://www.mme.gov.br.
[2] A. Srivastava, R. Prasad, Renew. Sust. Energy Rev. 4 (2000) 111.
[3] Agência Nacional do Petróleo, Gás Natural e Biocombustíveis, Resolução No. 15 de 17.07.2006, DOU 19.07.2006, http://www.anp.gov.br.
[4] Agência Nacional do Petróleo, Gás Natural e Biocombustíveis, Resolução No. 42 de 24.11.2004, DOU 9.12.2004, http://www.anp.gov.br.
[5] F.C.C. Oliveira, C.R.R. Brandão, H.F. Ramalho, L.A.F. Costa, P.A.Z. Suarez, J.C. Rubim, Anal. Chim. Acta 587 (2007) 194.
[6] Agência Nacional do Petróleo, Gás Natural e Biocombustíveis, Anuário Estatístico, 2007, http://www.anp.gov.br.
[7] L.S.G. Teixeira, F.S. Oliveira, H.C. Santos, P.W.L. Cordeiro, S.Q. Almeida, Fuel 87 (2008) 346.
[8] V.L. Skrobot, E.V.R. Castro, R.C.C. Pereira, V.M. Pasa, I.C.P. Fortes, Energy Fuels 19 (2005) 2350.
[9] R.C.C. Pereira, V.L. Skrobot, E.V.R. Castro, I.C.P. Fortes, V.M.D. Pasa, Energy Fuels 20 (2006) 1097.
[10] F.S. Oliveira, L.S.G. Teixeira, M.C.U. Araujo, M. Korn, Fuel 83 (2004) 917.
[11] P.J.S. Barbeira, Engenharia Térmica 2 (2002) 48.
[12] S. Kalligeros, F. Zannikos, S. Stournas, E. Lois, Energy 28 (2003) 15.
[13] J.A. Santos, Informativo PETROBRAS – Produtos PETROBRAS: Óleo Diesel – Refinaria Gabriel Passos, 5ª edição. (2000).
[14] S. Roy, Sens. Actuators B 55 (1999) 212.
[15] D. Patra, A.K. Mishra, Anal. Chim. Acta 454 (2002) 209.
[16] D. Patra, A.K. Mishra, Analyst 125 (2000) 1383.
[17] A. Taksande, C. Hariharan, Spectrosc. Lett. 39 (2006) 345.
[18] Agência Nacional do Petróleo, Gás Natural e Biocombustíveis, Boletim da Qualidade, Não-conformidades no Brasil, setembro 2007, http://www.anp.gov.br.
[19] M.A. Aliske, G.F. Zagonel, B.J. Costa, W. Veiga, C.K. Saul, Fuel 87 (2006) 1461.
[20] M.F. Pimentel, G.M.G.S. Ribeiro, R.S. Cruz, L. Stragevitch, J.G.A.P. Filho, L.S.G. Teixeira, Microchem. J. 82 (2006) 201.
[21] J.S. Oliveira, R. Montalvão, L. Daher, P.A.Z. Suarez, J.C. Rubim, Talanta 69 (2006) 1278.
[22] T.A. Foglia, K.C. Jones, J.G. Phillips, Chromatographia 62 (2005) 115.
[23] P. Geladi, Spectrochim. Acta B 58 (2003) 767.
[24] O. Divya, A.K. Mishra, Talanta 72 (2007) 43.
[25] O. Abbas, C. Rébufa, N. Dupuy, A. Permanyer, J. Kister, D.A. Azevedo, Fuel 85 (2006) 2653.
[26] J. Li, S. Fuller, J. Cattle, C.P. Way, D.B. Hibbert, Anal. Chim. Acta 514 (2004) 51.
[27] E. Sikorska, T. Górecki, I.V. Khmelinskii, M. Sikorski, J. Koziol, Food Chem. 89 (2005) 217.
[28] K.I. Poulli, G.A. Mousdis, C.A. Georgiou, Anal. Chim. Acta 542 (2005) 151.
[29] F. Guimet, R. Boqué, J. Ferré, J. Agric. Food Chem. 52 (2004) 6673.
[30] F. Guimet, R. Boqué, J. Ferré, F.X. Rius, Anal. Chim. Acta 515 (2004) 75.
[31] F. Guimet, R. Boqué, J. Ferré, Chemom. Intell. Lab. Syst. 81 (2006) 94.
[32] R.G. Brereton, Chemometrics Data Analysis for the Laboratory and Chemical Plant, John Wiley and Sons, England, 2003.
[33] S. Wold, M. Sjostrom, L. Eriksson, Chemom. Intell. Lab. Syst. 58 (2001) 109.
[34] D. Patra, A.K. Mishra, Talanta 53 (2001) 783.
[35] P. John, I. Soutar, Anal. Chem. 48 (1976) 520.
[36] D. Patra, A.K. Mishra, Talanta 55 (2001) 143.
[37] E. Sikorska, A.G. Świgło, I. Khmelinskii, M. Sikorski, J. Agric. Food Chem. 53 (2005) 6988.
[38] D. Patra, A.K. Mishra, Trend Anal. Chem. 21 (2002) 787.
[39] T. Vo-Dinh, Anal. Chem. 50 (1976) 396.
[40] J.B. Rossell, Frying—Improving Quality, Woodhead Publishing Limited, Cambridge, England, 2001.
[41] S. Moret, L.S. Conte, J. Chromatogr. A 882 (2000) 245.
[42] K. Siegman, K. Sattler, J. Aerosol. Sci. 27 (1996) S493.
[43] L. Zhu, J. Wang, Chemosphere 50 (2003) 611.
[44] D.C. Harris, Análise Química Quantitativa, 5th ed., LTC Editora, Rio de Janeiro, 2001.
[45] O. Divya, A.K. Mishra, Anal. Chim. Acta 592 (2007) 82.

Talanta 76 (2008) 327–332

Contents lists available at ScienceDirect

Talanta

journal homepage: www.elsevier.com/locate/talanta

Evaluation of the aquatic passive sampler Chemcatcher for the monitoring of highly hydrophobic compounds in water

A. de la Cal, M. Kuster, M. Lopez de Alda, E. Eljarrat*, D. Barceló

Department of Environmental Chemistry, IIQAB-CSIC, Jordi Girona 18-26, Barcelona 08034, Spain

ARTICLE INFO

Article history:
Received 20 November 2007
Received in revised form 27 February 2008
Accepted 29 February 2008
Available online 15 March 2008

Keywords:
Passive sampling
Water monitoring
PBDE
DDT
DDE
DDD

ABSTRACT

The Chemcatcher passive sampler was primarily developed for the detection and quantification of priority organic pollutants (e.g., polycyclic aromatic hydrocarbons) in water. In the present study, this prototype was evaluated for highly hydrophobic compounds such as the tetrabrominated diphenyl ether BDE-47, the hexabrominated diphenyl ether BDE-153, and the historic pesticide DDT with its main metabolites (DDE and DDD). The sampling device consists basically of a receiving phase with high affinity for organic chemicals which is separated from the environment by a diffusion limiting membrane, both placed in a rigid PTFE body. C18 Empore® disks were evaluated as receiving phase, obtaining a better accumulation when impregnated until saturation with *n*-octanol. As diffusion membrane, low density polyethylene was chosen over polyethersulphone. Once optimized its accumulation capacity for the target compounds, the linear behaviour of this accumulation was investigated and shown to be satisfactory in a period of 15 days. Preliminary uptake rates calculated from that accumulation anticipate the utility of this device for the detection of DDXs and the PBDEs, as calculated limits of detection are lower than usually reported environmental concentrations.

1. Introduction

The most accepted procedure for identifying and quantifying organic pollutants in water is spot sampling followed by extraction and analysis in the laboratory. However, this procedure measures an instantaneous concentration that might not be representative of the average concentration in time. Besides, this type of analysis quantify not only the truly dissolved phase of a chemical, but also that sorbed to particles and in colloidal phase, whose bioavailability, and hence environmental risk, is considered limited. Biomonitoring, directly measuring the accumulation of lipophilic pollutants within living organisms, offers a more time-integrative assessment of contamination and, of course, it measures only the bioavailable fraction. But biomonitoring implies some technical disadvantages. First, a species cannot live anywhere but under some restricted environmental conditions, so that the same species cannot be found or used everywhere. In fact, only a few living beings can survive in highly polluted environments. Moreover, rates of bioaccumulation are influenced by biological factors, and vary even between individuals of the same species. As a result, it is difficult to obtain comparable results. Another inconvenience is that not all chemicals bioaccumulate, because some of them are metabolized by the living organism. On the other hand, the pool of fish or other living beings is not infinite, and, from an ethical point of view, killing living beings is not desirable. In the last few years the European Union (EU) has encouraged the so-called "intelligent testing strategies of chemicals", that promotes the use of alternative devices to living organisms for conducting experimental tests. Passive sampling provides a continuous measure of pollution and overcomes all these difficulties associated to both spot sampling and biomonitoring. Moreover, it offers an important analytical advantage: sample pre-treatment and cleanup are simpler than those required for animal tissues. This way, in the last two decades different types of devices have been shown as promising tools for measuring a wide range of pollutants in water.

The Chemcatcher passive sampling device was developed by Portsmouth University in the frame of an EU project (Standardised Aquatic Monitoring of Priority Pollutants by Passive Sampling, STAMPS). It consists of the basic configuration of aquatic passive samplers being formed by a receiving phase with high affinity for organic chemicals which is separated from the environment by a diffusion limiting membrane. In this case, both the receiving phase and the diffusion membrane are 47 mm diameter disks, loaded on a rigid PTFE body (Fig. 1). It was designed in order to enable its application to several classes of target analytes by simply varying the receiving phase and the membrane in accordance with the compounds affinities. A complete description of the device can be looked up in Kingston et al. [1], Vrana et al. [2]

* Corresponding author. Tel.: +34 934006170; fax: +34 932045904.
E-mail address: eeeqam@cid.csic.es (E. Eljarrat).

0039-9140/$ – see front matter © 2008 Elsevier B.V. All rights reserved.
doi:10.1016/j.talanta.2008.02.049

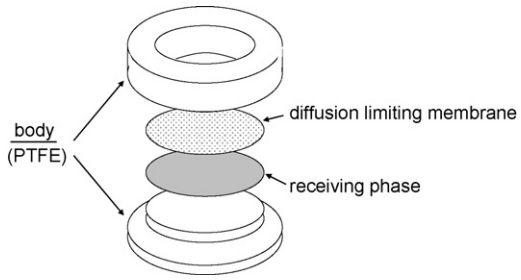

Fig. 1. Chemcatcher general configuration.

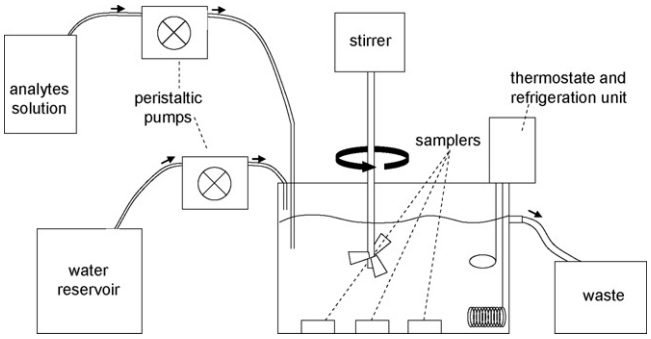

Fig. 2. Schematic drawing of the flow-through system used for laboratory exposure experiments.

or Greenwood et al. [3]. These authors developed the system and calibrated its use for the detection of polycyclic aromatic hydrocarbons (PAHs), polychlorinated biphenyls (PCBs), organochlorine pesticides and triazines. Besides, it has been evaluated for metals [4] and organometals [3].

The objective of the present study is to explore the possibilities of this system for the sampling and subsequent analysis of a selected group of halogenated endocrine disrupting organic contaminants in water: the tetrabrominated diphenyl ether BDE-47 and the hexabrominated diphenyl ether BDE-153, both used as flame retardants, and the historic pesticide DDT and its two main metabolites DDE and DDD (DDXs). Both classes of compounds are subjected to regulation in water in the EU. Polybrominated diphenyl ethers (PBDEs) are included in the list of 33 priority substances in the field of water policy established in the Decision No 2455/2001/EC that amends the Water Framework Directive 2000/60/EC [5]. Besides, for both PBDEs (included in the pentabromodiphenylether mixture) and DDT (DDT total and *p,p′*-DDT) annual average concentrations (in the range 0.0002–0.0005 and 0.01–0.025 $\mu g\,L^{-1}$, respectively) have been proposed for inland and other surface waters [6].

For both groups of compounds, besides the common advantages of passive sampling (e.g. time-integrated measurements), the goal of the use of this kind of methodology is to overcome the analytical difficulties, especially for PBDEs, that arise from their low solubility in water. Although the levels of these compounds are extremely low in water, this medium contributes significantly to the discharge and spread of these pollutants in the environment. In situ concentration onto the receiving phase allows lower quantification limits than usual liquid–liquid or solid phase extraction of water samples. Although semipermeable membrane devices have been successfully used for the assessment of DDXs and PBDEs in water [7,8], usually these devices require laborious and time-consuming separation of lipid matrix components from target analytes using solvent dialysis and size exclusion chromatography [9].

Once that the suitability of the system is verified, a large set of laboratory experiments has to be performed in order to calibrate the device at different environmental conditions (e.g. temperature and turbulence of water).

2. Experimental

2.1. Materials and chemicals

Chemcatcher PTFE devices were supplied by Portsmouth University. C18 Empore® disks were obtained from 3 M (St. Paul, MN, USA). Polyethersulphone (PES) membranes Pall Corporation (East Hills, NY, USA) and low density polyethylene (LDPE) membranes, 40 μm thick, were a gift from Portsmouth University obtained from Fisher Scientific (Loughborough, UK). Sodium sulphate cartridges were purchased from Varian, Inc. (Palo Alto, USA). C18 Isolute cartridges were supplied by Biotage (Hengoed,UK) and Oasis HLB cartridges were supplied by Waters (Mildford, Massachusetts, USA).

All solvents were of gas chromatography quality and supplied by Merck (Darmstadt, Germany) except for octanol which was purchased from Riedel de Haën (Seelze, Germany). HPLC grade water was from Merck (Dramstadt, Germany).

Certified pure standards of the test compounds were used. Solid BDE-47 and BDE-153 congeners were purchased from Cambridge Isotope Laboratories (Andover, MA, USA). PCB-209 ($10\,ng\,\mu L^{-1}$), used as internal standard, and solid DDT isomers and metabolites were purchased from Dr. Ehrenstorfer GmbH (Augsburg, Germany).

2.2. Exposure system

For laboratory exposure experiments, a flow-through system where water temperature and turbulence and the concentrations of the studied analytes can be maintained constant was employed (Fig. 2). It consisted of a 25 L stainless steel tank with an overflow to waste. Distilled water and a solution of the target chemicals in methanol ($30\,\mu g\,L^{-1}$) were continuously supplied to the tank by means of Marprene® tubes and two peristaltic pumps (Watson Marlow, Wilmington, MA, USA) working at velocities high enough to compensate for the losses due to accumulation in the disks and maintain a constant concentration in it ($33\,mL\,min^{-1}$ and $100\,\mu L\,min^{-1}$, respectively). An overhead stirrer (Heidolph, Kelheim, Germany) was used for mixing continuously the water in the exposure tank and controlling the turbulence to which samplers were exposed. The water temperature was maintained constant by using simultaneously a cooling unit (Afora, Barcelona, Spain) and a heating thermostat (SBS, Rubí, Spain) in the tank.

2.3. Chemcatcher configuration optimization

The suitability of different materials was evaluated by comparing the accumulation of each compound onto different configurations of the sampler during an experiment of 48 h at constant concentration, temperature and turbulence. C18 Empore® disks were tested as receiving phase, and PES or LDPE, microporous and non-porous membranes respectively, as diffusion membrane. Before loading the samplers, all disks were conditioned by soaking them in methanol until they were translucent, and then passing 10 mL of methanol followed by 20 mL of HPLC water through them. Disks were then treated in two different ways. Six disks were directly (saturated with water) loaded on the sampler lying on the PTFE disk. Other four disks were completely dried under vacuum during 30 min and then impregnated until saturation with *n*-octanol by adding 1 mL of a solution of octanol in acetone (45%, v/v) and allowing acetone to evaporate. Two of the six water-saturated disks were loaded in the sampler without membrane. Two octanol-saturated disks and two water-saturated disks were covered with a polysulphone membrane and the remaining two disks of each type were covered with a low density polyethylene

membrane (previously washed during 24 h with hexane and dried). In both cases the diffusion limiting membrane was loaded on top of the C18 disk carefully, preventing the formation of bubbles, and they were fixed with the supporting disk of the sampler. After exposure, the samplers were disassembled, the diffusion membrane removed, and the Empore® disks analyzed.

2.4. Calibration experiment

Accumulation of the target compounds in the disks was tested at a high and theoretically constant concentration of the compounds in water of 100 ng L^{-1} each. The theoretical behaviour of this accumulation has been described as an exponential approach to the steady state [10,11]. Nevertheless, during the initial stage of exposure, the uptake and accumulation kinetics of the analytes in the receiving phase should be linear, according to the equation:

$$m(t) = m(0) + C_w R_s t \quad (1)$$

where m represents the mass of analyte in the receiving phase at exposure time t (day) or initial time (0), C_w is the concentration in water during that period (ng L^{-1}) and R_s is the sampling rate of the device, that is, the equivalent extracted water volume per unit of time (L day^{-1}).

The main factors that influence the sampling rate are the sampler configuration, the molecular properties of the analyte and the environmental conditions. The sampling rate is, however, independent of the concentration of the analyte in the water [12]. By this experiment, with known concentration in water, the rate of sampler uptake of each analyte from the water could be calculated for the different environmental conditions tested (temperature and turbulence) and it could be used then, in the field, for quantifying the time-averaged concentration in water during the time that the samplers were immersed. For this purpose, 14 samplers were exposed in the flow-through system at 11 °C during 14 days. The stirrer was used at 20 rpm to mix the fortified water without generate high turbulence. Two samplers were removed every two days for analysis of the accumulated chemicals. Duplicate water samples from the outlet of the tank were taken daily to confirm the concentration to which samplers were exposed.

2.5. Extraction of analytes from disks

Analysis of the accumulated compounds in the receiving phase by ultrasonic solvent extraction consisted of two 5 min extractions, first with 10 mL of acetone and then with 10 mL of a mixture acetone:hexane (1:1, v/v). The extracts were combined, passed through a Na_2SO_4 cartridge and concentrated under N_2 stream until only the octanol remained in the vial. In the case of water-saturated disks the extracts were concentrated until incipient dryness and redissolved with 225 μL of isooctane. After adding the internal standards (25 μL of a solution in octanol or isooctane of PCB-209 and ^{13}C-*p*,*p*′-DDT at 0.4 ng μL^{-1}) the extracts were analyzed by gas chromatography coupled with mass spectrometry detection (GC/MS).

2.6. Extraction of analytes from water

For preventing adsorption of chemicals to the glass walls of the container, the samples were mixed with 30% of methanol just after sampling. Previous to the analyses, samples were filtered through a glass fiber filter (0.45 μm pore size). Afterwards, solid phase extraction (SPE) of the samples was performed with an automated sample processor Aspec XL (Gilson, Middleton, USA) using C18 (500 mg, 3 mL) cartridges. Cartridges were conditioned by passing hexane, followed by dichloromethane, methanol and water HPLC through them (6 mL each, at 1 mL min^{-1}). Once conditioned, 325 mL of sample (250 mL water +30% MeOH) was loaded onto the cartridges at 5 mL min^{-1}. Afterwards, the cartridges were washed with 3 mL of HPLC water at 1 mL min^{-1} and dried under vacuum during 30 min. The cartridges were kept at −20 °C until elution. For elution, methanol, dichloromethane and hexane (3 mL each, 1 mL min^{-1}) were passed through the cartridges. Other solvents (acetonitrile, ethyl acetate) and cartridges (Oasis HLB, 200 mg, 6 mL) were tested, but the best recovery and/or variation was achieved with the above described procedure. The resulting extracts were concentrated down to incipient dryness under nitrogen stream and redissolved with 225 μL of isooctane. 25 μL of a solution in isooctane of PCB-209 and ^{13}C-*p*,*p*′-DDT at 0.1 ng μL^{-1} were added as internal standards prior to the analysis by GC/MS.

2.7. Instrumental analysis

Analysis of extracts was performed following previously described GC/MS methods [13,14]. PBDEs analyses were performed using a gas chromatograph Agilent 6890 coupled to a mass spectrometer Agilent 5973 Network (Agilent Technologies, Inc., Santa Clara, USA). The separation of congeners was achieved using a DB-5 (15 m × 0.25 mm i.d., 0.25 μm) capillary column containing 5% phenyl methyl siloxane. The temperature program was from 140 °C (held during 2 min) to 325 °C (held during 10 min) at 10 °C min^{-1}. Injection was carried out in the splitless mode during 1 min with an injector temperature of 250 °C. Negative chemical ionization (NCI) was used as ionization mode with a source temperature of 250 °C, ionization energy 40 eV and ammonia as reagent gas at a system pressure of 1.9×10^{-4} Torr. Helium was used as the carrier gas at 10 psi. Detection was carried out monitoring the two most abundant isotope peaks from the mass spectra, corresponding to the loss of the bromine ion: m/z = 79 and 81, and m/z 498 and 500 for the internal standard PCB-209.

DDXs analyses were performed with a gas chromatograph GC 8000 series 8060 (Fisons Instruments, Spain) coupled with a mass spectrometer with quadrupole detector MD 800 (Fisons Instruments, Spain). A DB-5 (30 m × 0.25 mm i.d., 0.25 μm) capillary column with 5% phenyl methyl siloxane was used. The temperature program was from 120 °C (held during 1 min) to 200 °C at 5 °C min^{-1}, then from 200 to 220 °C at 1 °C min^{-1} and finally at 8 °C min^{-1} from 220 to 300 °C (held during 5 min). Injection was carried out in the splitless mode during 48 s with an injector temperature of 250 °C. Electronic impact (EI) was used as ionization mode with ionization energy of 70 eV and source temperature of 250 °C. Detection was performed monitoring the three most abundant isotope peaks from the mass spectra of each compound: m/z 246, 248 and 176 for *o*,*p*′-DDE; 246, 248 and 318 for *p*,*p*′-DDE; 235, 237 and 165 for *o*,*p*′-DDD, *p*,*p*′-DDD, *o*,*p*′-DDT and *p*,*p*′-DDT, and m/z 247 and 249 for the internal standard ^{13}C-4,4-DDT.

For the analysis of the disks extracts a slightly modified methodology had to be used due to the high viscosity of the extract solvent octanol. Modifications comprised the application of a pulse of pressure during injection (50 psi), application of a viscosity delay to the syringe time of sampling and injection (7 s) and rising of the initial oven temperature to 120 °C.

Quantification was carried out using PCB-209 and 13 C-4,4-DDT as internal standards for PBDEs and DDXs, respectively.

3. Results and discussion

3.1. Chemcatcher configuration

The accumulation in disk (ng of compound per sampler) was tested with two different membranes and without membrane, and

Table 1
Amount of pollutants accumulated in the disks (ng) under different configurations after being immersed during 48 h in the flow-through system (mean values from $n = 2$)

	Accumulated amount (ng)				
	Without membrane	Polyethylene octanol	Membrane water	Polyethersulfone octanol	Membrane water
BDE-47	30	20	1.85	1.01	0.04
BDE-153	2.7	1.0	0.01	0.11	0.01
o,p′-DDE	25	11	0.6	0.5	0.01
p,p′-DDE	17	7	0.4	0.3	0.06
o,p′-DDD	48	21	1,2	0.9	0.05
p,p′-DDD + *o,p′*-DDT	54	26	1.1	1.0	0.05
p,p′-DDT	56	29	2.5	2.7	0.09

with and without octanol as interstitial solvent. Results obtained are shown in Table 1. As expected, the maximum accumulation occurred onto the disks without coating membrane (2.7–56 ng), whereas the use of a membrane lowered the accumulation 12–270 (LDPE membrane) or 270–2500 (PES membrane) times. Nevertheless, the use of the membrane is mandatory, in order to avoid deterioration of the receiving phase in the aqueous environment, especially due to the biofouling. The diffusion through the tested membranes, and thus accumulation in the disks, was clearly higher (up to 60 times for *o,p′*-DDE) when LDPE was used. Besides, accumulation was found to be up to 100 times higher (BDE-153) when the interstitial space between the receiving sorbent phase and the diffusion membrane is saturated with *n*-octanol. This solvent has a high permeability for the target analytes, so that the internal resistance to mass transfer is decreased. Therefore, the chosen configuration was C18 Empore® disks and low density polyethylene membrane with *n*-octanol as interstitial phase, which is the same that the one used for PAHs and organochlorine compounds with K_{ow} greater than 3 by Vrana et al. [15].

3.2. Disks and water analysis

The optimized procedure for disks analysis yielded recoveries of nearly 100% (89–100%) and maximum relative standard deviations of 5% (1–5%) for all compounds (Table 2). Detection limits ranged from 7.4 to 126.6 pg per disk, where the lowest values were for BDEs and the highest for DDXs.

In the extraction of water, however, no satisfactory recoveries could be achieved for PBDEs. All tested solvents gave similar results, whereas some improvement could be achieved by employing C18 instead of Oasis HLB cartridges. Nevertheless, under the best conditions the recoveries were still very low for both congeners (30% in average). Furthermore, variability, acceptable for BDE-153 (8%), was very high for BDE-47 (49%). For DDXs, recoveries were slightly better (49–55%) but variation was also very high (37–54%). These low recoveries and high variability could be attributed to the high lipophilicity of these chemicals and its consequent sorption to the walls of the containers used. Moreover, we cannot assure either that the concentration measured in the spot water samples does not include part of the chemicals in the colloidal phase or bounded to the dissolved organic mater.

Table 2
Quality control parameters of the analytical method developed for disks

	Recovery (%) (mean of $n = 3$)	Relative standard deviation (%) ($n = 3$)	Limit of detection (pg disk^{-1})
BDE-47	98	4	7.4
BDE-153	98	4	48.9
o,p′-DDE	91	5	31.9
p,p′-DDE	89	5	41.6
o,p′-DDD	89	4	81.0
p,p′-DDD	91	4	85.8
o,p′-DDT	96	2	116.8
p,p′-DDT	100	1	126.6

3.3. Uptake rates

Uptake curves (accumulated analyte against time of exposure) for the studied analytes are plotted in Fig. 3. As could be expected, they were found to be (roughly) linear, with coefficients ranging from 0.76 to 0.88 (slightly better for PBDEs than for DDXs). Preliminary rates of uptake (R_s) were estimated from the division of the slope of the curves by the concentration of each compound in water (see Eq. (1)).

At this point, problems arose from the uncertainty associated to the analysis of water. To the variability of the measured concentration during the length of the experiment (17–36% for PBDEs and 15–22% for DDXs), it has to be added the uncertainty about the recovery of the method that was explained in the previous section. Moreover, measured concentrations (corrected by the recoveries) differed from the theoretical aimed 100 ng L^{-1}: 22–89 ng L^{-1} for PBDEs and 133–288 ng L^{-1} for DDXs.

Possible uptake rates were calculated from both (theoretical and measured) values for each compound. The results of both calculations are shown in Table 3. R_s values ranged between 0.002 and 0.013 L day^{-1} for DDXs and 0.055–0.32 L day^{-1} for PBDEs. Only for BDE-153 the difference between the two values was important (0.251 L day^{-1} from the estimated value and 0.055 L day^{-1} from the theoretical value).

On the other hand, in the same way that it was done for other passive samplers [12,16], an empirical model was derived for the same Chemcatcher configuration used by us (B. Vrana, School of Biological Sciences, University of Portsmouth, Portsmouth, United Kingdom, personal communication). This model allows the calculation of the sampling rate as a function of the hydrophobicity of the compound. In accordance with this model, this configuration of the Chemcatcher favours the uptake of compounds with moderate hydrophobicity (log K_{ow} = 4.0–5.0) showing a higher declination for compounds with high K_{ow} than semipermeable membrane devices (SPMDs) [3]. Table 3 presents the result of the application of this model to the K_{ow} of the analytes studied here. The lowest K_{ow} found in literature [17–19] were used for this calculation so that a maximum limit for sampling rates could be estimated. High sampling rates combined with low instrument detection limits are essential, especially for sampling of non-polar chemicals, due to their

Table 3
Uptake rates R_s (L day^{-1}) estimated in this study and estimated with the model of [2]

	Experimental		Estimated from [2]
	Using measured water concentration	Using theoretical water concentration	
BDE-47	0.317	0.282	0.013
BDE-153	0.251	0.055	0.003
o,p′-DDE	0.002	0.003	0.013
p,p′-DDE	0.001	0.002	0.010
o,p′-DDD	0.003	0.007	0.010
p,p′-DDD + *o,p′*-DDT	0.005	0.013	0.003
p,p′-DDT	0.001	0.004	0.003

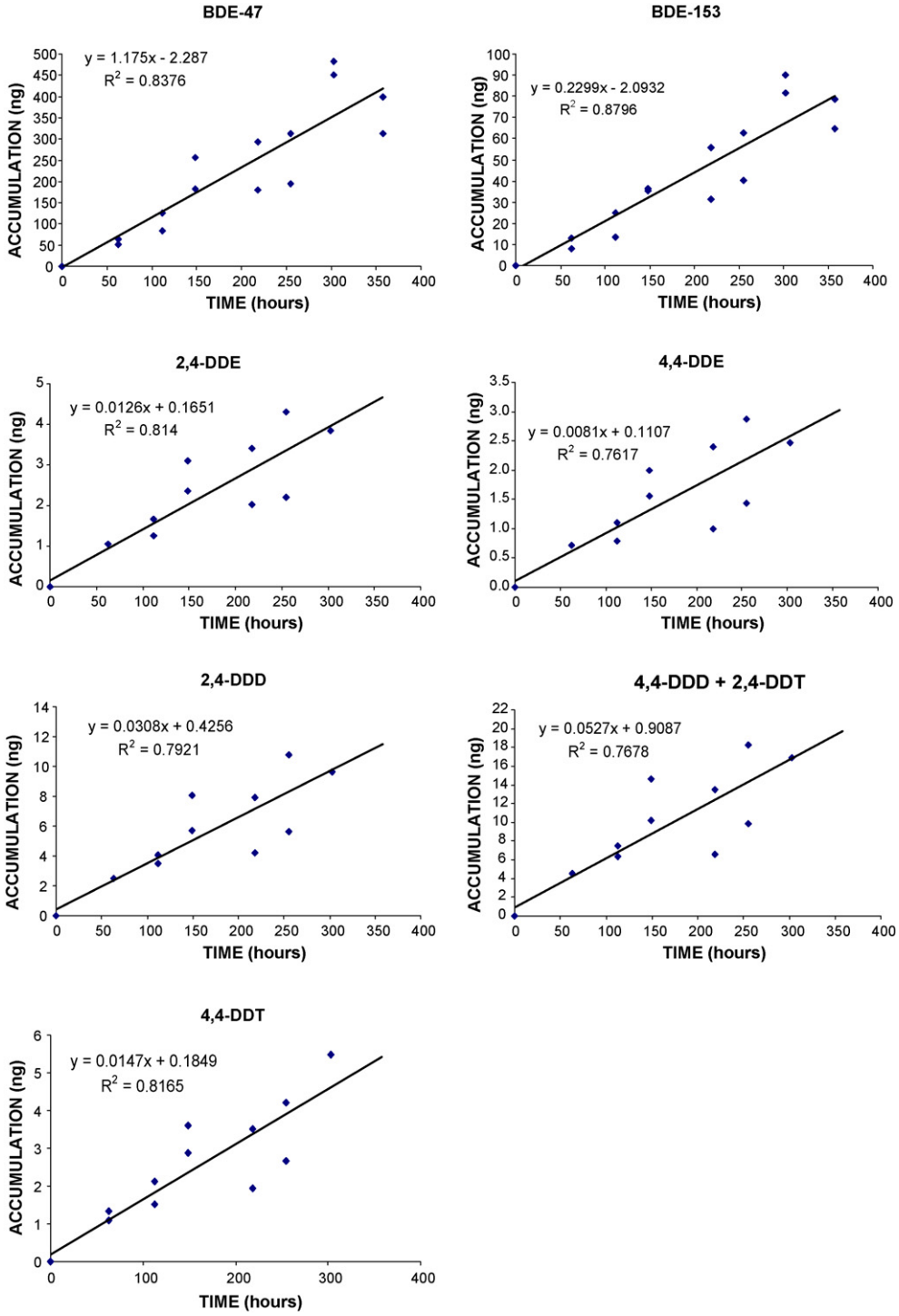

Fig. 3. Uptake curves obtained for the studied chemicals.

extremely low concentration in the water phase. In Table 4 the minimum concentration measurable in water after 15 days of exposure was calculated from the detection limit of the method and the uptake rates of Table 3.

The uptake rates obtained experimentally for the DDXs are not significantly different from those predicted with the model of Vrana et al. [15] and their limits of detection (Table 4) are in the range of 0.16–8.4 ng L^{-1}. Those limits of detections are far below the concentrations commonly detected for these compounds in freshwater (e.g. 92 ng L^{-1} [20], 59 ng L^{-1} [21], 29–270 ng L^{-1} [22]).

For PBDEs, the experimental rates obtained are higher than those for DDXs. This added to the lower detection limits achieved for these compounds as compared with DDXs with the analytical method employed [13,14] yields lower detection limits for PBDEs than for DDXs also when using the Chemcatcher. These uptake rates indicate that concentrations of 2 and 13–59 pg L^{-1} of BDE-47 and BDE-153, respectively, could be detected in 15 days (Table 4). Data about concentrations of PBDEs in water are very scarce in literature. In the San Francisco Estuary BDE-47 reached 180 pg L^{-1}, near wastewater treatment plant effluents whereas BDE-153 was

Table 4
Minimum concentration (pg L^{-1}) measurable in water after 15 days of exposure calculated from the detection limit of the method and the uptake rates of Table 3

	From experimental R_s		From R_s estimated from [2]
	Calculated using the measured water concentration	Calculated using the theoretical water concentration	
BDE-47	1.5	1.7	37.9
BDE-153	13.0	59.3	1087
o,p′-DDE	1063	709	164
p,p′-DDE	2773	1387	277
o,p′-DDD	1800	771	540
p,p′-DDD + *o,p′*-DDT	1333	513	2222
p,p′-DDT	8440	2110	2813

no higher than 10 pg L^{-1} [23]. 158 pg L^{-1} were reported in Lake Michigan for a sum of six PBDE congeners [24]. These concentrations are clearly above the detection limits achieved with the Chemcatcher, which confirms the suitability of the system for the detection of PBDEs. On the other hand, concentration in the Dutch coast calculated from SPMD data (0.1–1 pg L^{-1}) [8] would not be detected by the Chemcatcher according with these limits. It has to be taken into account, besides, that the uptake rates predicted with the model of Vrana et al. [15] suggest a much lower sensitivity.

On the other hand, Vrana et al. [2] found that uptake rates increase with increasing turbulence. As turbulence was not used in this experiment, we can expect higher rates in systems like rivers. Moreover, the sensitivity of the second generation of Chemcatcher (here it was used the first one), has been proved to be higher [3].

4. Conclusions

A recently developed passive sampling device, the Chemcatcher, has been evaluated by the first time for the highly hydrophobic pollutants BDE-47, BDE-153, DDT and metabolites. Accumulation rates calculated here predict the viability of the evaluated configuration of the Chemcatcher for the monitoring of these compounds in environmental water bodies. This possibility means an improvement over traditional water pollution assessment, both over water analysis and over biomonitoring — see Section 1.

On the basis of these preliminary results, future experiments involve the calibration of the system at different water temperatures and turbulences, necessary for the calculation of the time-averaged concentration of the pollutants in water from the amount of accumulated compound in the sampler.

Acknowledgements

This work has been financially supported by the European Union under the STAMPS (EVK1-CT2002–00119) and AQUATERRA (505428) projects and by the Spanish Ministry of Education and Science through the project CEMAGUA (CGL2007–64551/HID) and Acción Complementaria CTM2005-25168-E. This work is also part of the SOSTAQUA Project, leaded by Aguas de Barcelona and founded by CDTI in the framework of the Ingenio 2010 Programme under the CENIT call. Agustina de la Cal acknowledges grant from Departament d'Universitats, Recerca i Societat de la Informació de la Generalitat de Catalunya (2003FI 00092). Marina Kuster acknowledges the I3P Program co-financed by CSIC and European Social Funds for a predoctoral grant. R. Chaler and D. Fanjul are thanked for assistance with the MS work. This work reflects only the author's views and the European Community is not liable for any use that may be made of the information contained therein.

References

[1] J.K. Kingston, R. Greenwood, G.A. Mills, G.M. Morrison, L.B. Persson, J. Environ. Monit. 2 (2000) 487.
[2] B. Vrana, G.A. Mills, E. Dominiak, R. Greenwood, Environ. Pollut. 142 (2006) 333.
[3] R. Greenwood, G. Mills, B. Vrana, I.J. Allan, R. Aguilar, G. Morrison, in: R. Greenwood, G. Mills, B. Vrana (Eds.), Comprehensive Analytical Chemistry, vol. 48, Elsevier, Amsterdam, 2007, pp. 199–229.
[4] L.B. Blom, G.M. Morrison, J. Kingston, G.A. Mills, R. Greenwood, T.J.R. Pettersson, S. Rauch, J. Environ. Monit. 4 (2002) 258.
[5] Decision No 2455/2001/EC of the European Parliament and of the Council of 20 November 2001 establishing the list of priority substances in the field of water policy and amending Directive 2000/60/EC, Official Journal of the European Communities, 15.12.2001, L 331/2.
[6] Commission of the European Communities, Proposal for a Directive of the European Parliament and of the Council on environmental quality standards in the field of water policy and amending Directive 2000/60/EC, Brussels, 2006, COM(2006) 397 final.
[7] J.D. Petty, J.N. Huckins, D.B. Martin, T.G. Adornato, Chemosphere 30 (1995) 1891.
[8] K. Booij, B.N. Zegers, J.P. Boon, Chemosphere 46 (2002) 683.
[9] J.D. Petty, C.E. Orazio, J.N. Huckins, R.W. Gale, J.A. Lebo, J.C. Meadows, K.R. Echols, W.L. Cranor, J. Chromatogr. A 879 (2000) 83.
[10] J.N. Huckins, G.K. Manuweera, J.D. Petty, D. Mackay, J.A. Lebo, Environ. Sci. Technol. 27 (1993) 2489.
[11] J.N. Huckins, J.D. Petty, K. Booij, Monitors of organic chemicals in the environment: Semipermeable Membrane Devices, Springer Verlag, New York, 2006, p. 223.
[12] J.N. Huckins, J.D. Petty, C.E. Orazio, J.A. Lebo, R.C. Clark, V.L. Gibson, W.R. Gala, K.R. Echols, Environ. Sci. Technol. 33 (1999) 3918.
[13] E. Eljarrat, S. Lacorte, D. Barcelo, J. Mass Spectrom. 37 (2002) 76.
[14] A. De la Cal, E. Eljarrat, D. Raldúa, C. Durán, D. Barceló, Chemosphere 70 (2008) 1182.
[15] B. Vrana, G. Mills, R. Greenwood, J. Knutsson, K. Svensson, G. Morrison, J. Environ. Monit. 7 (2005) 612.
[16] D.A. Álvarez, J.N. Huckins, J.D. Petty, T. Jones-Lepp, F. Stuer-Lauridsen, T. Getting, J.P. Goddard, A. Gravell, in: R. Greenwood, G. Mills, B. Vrana (Eds.), Comprehensive Analytical Chemistry, vol. 48, Elsevier, Amsterdam, 2007, pp. 171–197.
[17] E. Braekevelt, S.A. Tittlemier, G.T. Tomy, Chemosphere 51 (2003) 563–567.
[18] H. Kuramochi, K. Maeda, K. Kawamoto, Chemosphere 67 (2007) 1858.
[19] D. Mackay, W.Y. Shiu, K.C. Ma, Illustrated Handbook of Physical–Chemical Properties and Environmental Fate for Organic Chemicals, Chelsea, MI, USA, 1991.
[20] Z.L. Zhang, J. Huang, G. Yu, H.S. Hong, Environ. Pollut. 130 (2004) 249.
[21] S. Tao, B.G. Li, X.C. He, W.X. Liu, Z. Shi, Chemosphere 68 (2007) 10.
[22] K.H. Leong, L.L.B. Tan, A.M. Mustafa, Chemosphere 66 (2007) 1153.
[23] D.R. Oros, D. Hoover, F. Rodigari, D. Crane, J. Sericano, Environ. Sci. Technol. 39 (2005) 33.
[24] R.C. Hale, M. Alaee, J.B. Manchester-Neesvig, H.M. Stapleton, M.G. Ikonomou, Environ. Int. 29 (2003) 771.

Talanta 76 (2008) 309–313

Contents lists available at ScienceDirect

Talanta

journal homepage: www.elsevier.com/locate/talanta

Immobilization of cytochrome *c* on cysteamine-modified gold electrodes with EDC as coupling agent

Karolien De Wael[a,1], Hans Buschop[a], Lina De Smet[b], Annemie Adriaens[a,*]

[a] *Ghent University, Department of Analytical Chemistry, Krijgslaan 281 S12, B-9000 Ghent, Belgium*
[b] *Ghent University, Department of Biochemistry, Physiology and Microbiology, KL Ledeganckstraat 35, B-9000 Ghent, Belgium*

ARTICLE INFO

Article history:
Received 12 December 2007
Received in revised form 19 February 2008
Accepted 26 February 2008
Available online 4 March 2008

Keywords:
Cytochrome *c*
Carbodiimide coupling
EDC
Cross-linking
Film
Voltammetry
Cysteamine

ABSTRACT

Cyclic voltammetry has been applied for the characterization of cross-linked horse heart cytochrome *c* (HHC) on cysteamine-modified gold electrodes. The cross-linking, i.e. amide bond formation, between the proteins was achieved by using 1-ethyl-3-(3-dimethylaminopropyl)-carbodiimide (EDC) as coupling reagent. The optimal conditions for the formation of the HHC film were determined by varying the HHC concentration. In addition the reproducibility, stability and the influence of the scan rate upon these films were investigated with cyclic voltammetry. The protein film stability in a 4-(2-hydroxyethyl)-1-piperazineethanesulfonic acid (HEPES) buffer solution was tested by UV/vis absorption spectroscopy.

1. Introduction

Immobilization of direct electrochemistry of redox proteins on electrodes can provide insight into the electron transfer processes between proteins in real biological systems [1,2]. Apart from this redox-active proteins are potentially useful in the development and fabrication of new kinds of biosensors or bioreactors [3,4]. Such studies can be performed by the so-called "protein film voltammetry", founded by Armstrong et al. [5], in which proteins are either incorporated into various films [6,7] or in which they are cross-linked to each other to form a film. Different types of films occur, including insoluble surfactants [8], hydrogel polymers [9,10] and mesoporous oxide films [11]. They all facilitate the electron transfer between the proteins and the electrode [12,13].

The cross-linking approach of proteins, under investigation in this work, generally leads to the formation of protein films with properties of a hydrogel. The latter are polymeric materials which exhibit the ability to swell in an aqueous solution without dissolving in it [14]. Two kinds of hydrogels can be distinguished: chemically and physically cross-linked hydrogels. The difference between both types is the nature of the cross-link points or junctions: it is either a chemical bond or a physical interaction. In the case of the latter, ionic interactions, hydrophobic associations or coiled-coil interactions appear [15–17]. When covalent bondings are incorporated in the hydrogel, a tight and stable film is formed. To achieve the latter, commonly carbodiimides are used which couple carboxyls to primary amines resulting in the formation of amide bondings. Seminal work in this field using cytochrome *c* as redox protein was published by Collison et al. [18]. In the presence of excess cross-linker, polymerization can occur because all proteins contain carboxyls and amines. In this work, 1-ethyl-3-(3-dimethylaminopropyl)-carbodiimide (EDC) was used as a cross-linking agent. It reacts with carboxylic acids to create an active-ester intermediate. In the presence of an amine nucleophile, an amide bond is formed with the release of an isourea by-product.

Horse heart cytochrome *c* (HHC) is a redox protein which has been mostly studied with respect to direct protein electrochemistry (see [2,4,19] and references therein). It is an important heme-containing metalloprotein which functions as an electron carrier. This redox protein has often been considered as a model system for biological electron transfer [20] and for bioelectrocatalysis [21].

In this paper (part I of our study), we report on the formation of a HHC film, cross-linked by 1-ethyl-3-(3-dimethylaminopropyl)-carbodiimide, on a cysteamine-modified gold electrode surface.

* Corresponding author. Tel.: +32 9 264 48 26; fax: +32 9 264 49 60.
E-mail address: Annemie.Adriaens@UGent.be (A. Adriaens).
[1] Postdoctoral Fellow of the Research Foundation – Flanders, Belgium.

0039-9140/$ – see front matter © 2008 Elsevier B.V. All rights reserved.
doi:10.1016/j.talanta.2008.02.040

The optimal conditions for the formation of the HHC thin-film were determined by varying the HHC concentration. The reproducibility, stability and the influence of the scan rate upon the HCC film were investigated with cyclic voltammetry. The protein film stability in a 4-(2-hydroxyethyl)-1-piperazineethanesulfonic acid (HEPES) buffer solution was tested by UV/vis absorption spectroscopy.

2. Experimental

2.1. Reagents

Horse heart cytochrome *c*, 2-[4-(2-hydroxyethyl)-piperazinyl] ethanesulfonic acid, cysteamine (CYS), sodium hydroxide, sodium dithionite and 1-ethyl-3-(3-dimethylaminopropyl)-carbodiimide were purchased from Sigma–Aldrich. The HEPES buffer solution of 10×10^{-3} mol L^{-1} was set to pH 7.0 using a 0.15 mol L^{-1} NaOH solution.

2.2. Preparation of the modified electrodes

Prior to their first use the gold electrode surfaces, having a diameter of 1.6 mm (BASinstruments, West Lafayette, USA), were scoured briefly on SiC-emery paper 1200 grit to obtain an active surface. To smoothen this relatively rough surface, it was further subjected to sequential polishing using a cloth covered with alumina powder (Buehler, Illinois, USA) of 1, 0.3 and 0.05 μm particle size for, respectively, 5, 10 and 20 min. To remove any adherent Al_2O_3 particles, the electrode surface was rinsed thoroughly with doubly deionized water and cleaned in an ultrasonic bath (Branson 3210) for 2 min.

After being rinsed with water and dried with a nitrogen gas flow, the gold electrodes were incubated in a water solution containing 5 mmol L^{-1} cysteamine (CYS) for 24 h at room temperature, which allowed the adsorption of CYS onto the surface. The modified gold electrodes were rinsed with water to remove any physically adsorbed CYS. In what follows, these modified electrodes are denoted as CYS|Au in the text. To immobilize horse heart cytochrome *c* (HHC) onto CYS|Au, 15 μL of a HHC containing buffer solution (different concentrations: see further) and 5 μL of a 2.5 mol L^{-1} EDC solution were spread onto the surface using a Hamilton syringe and exposed to the air for 2 h at room temperature. The formation of the film occurred while the aqueous phase dried. Finally, these electrodes were washed with the HEPES buffer solution. This electrode is referred to in the text as HHC|EDC|CYS|Au. Important to note is that in order to obtain the typically red coloured HHC film on the electrode surface, it was necessary to expose HHC and EDC to air during the cross-linking process. The latter implied the absence of a cap on top of the electrode so that the buffer solution is able to evaporate out of the formed hydrogel.

2.3. Electrochemical measurements

The basic electrochemical setup consisted of a three-electrode cell using a saturated calomel reference electrode (SCE, $E = 0.244$ V vs. NHE at 298 K, Radiometer, Copenhagen) and a platinum counter electrode. Voltammetry measurements were performed by placing a 20 μL buffer droplet between the tip of the reference electrode and the horizontal working electrode disk (modified from Hagen [21]). A PGSTAT20 potentiostat (ECO Chemie, The Netherlands), controlled by the GPES 4.9005 software package (ECO Chemie, The Netherlands) running on a Pentium II computer, was used to record the voltammetric curves.

2.4. UV/vis measurements

Droplets of the electrochemical experiment were diluted to 20 μL. Absorption spectra of the droplets were recorded using a double beam spectrophotometer (Kontron Uvikon, UK) in the absence and the presence of a few crystals of sodium dithionite. By adding the latter, the native (oxidized) form of cytochrome *c* (ferricytochrome *c*) reduces. The concentration of horse heart cytochrome *c* was determined at 554 nm by deducting the signal of ferricytochrome *c* from the signal of the reduced form (ferrocytochrome *c*). The molar absorption coefficient for the difference between the reduced and oxidized form of cytochrome *c* is 21,400 mol^{-1} L cm^{-1} [22].

3. Results and discussion

In a first experiment the influence of CYS on the direct electrochemistry was investigated. For this two electrodes were prepared: the first one consisted of depositing 15 μL 3.75 mmol L^{-1} HHC and 5 μL 2.5 mol L^{-1} EDC onto a bare gold electrode surface. The second one was first pre-treated with 5 mmol L^{-1} CYS, according to the procedure listed in Section 2, in order to obtain a more hydrophilic and thus a more accessible surface. After that HCC and EDC were deposited in an identical procedure as for the first electrode.

Fig. 1 shows the cyclic voltammetric behaviour of a HHC (3.75 mmol L^{-1})|EDC film immobilized on a bare gold (dotted line) and on a CYS|Au electrode (solid line). In both cases protein film formation can be observed: the observed redox couple can be explained as the oxidation and the reduction of the heme group in the protein. The midpoint potential of the observed process ($E_{1/2,ox} = 0.16$ V vs. SCE) is more positive than the redox potential of native HHC ($E_{1/2,ox} = 0.046$ V vs. SCE) [23,24]. This potential shift towards more positive values reflects mainly the change of heme environment caused by a changed dielectric constant and a variation of solvation properties and can be primarily attributed to

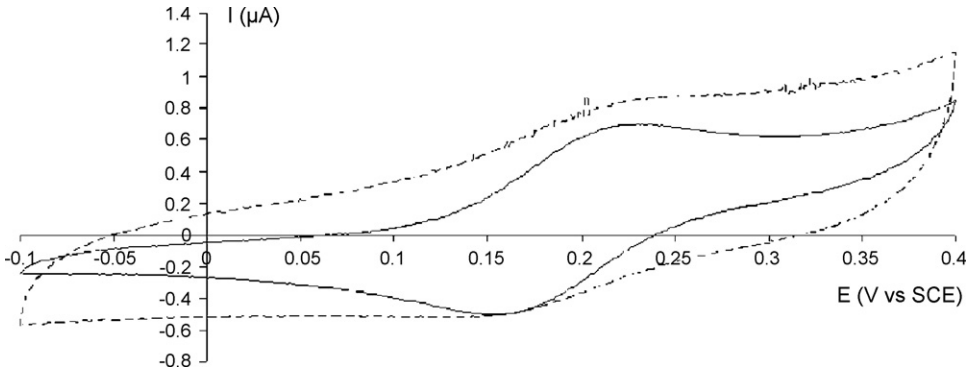

Fig. 1. Current-potential behaviour of a HCC (3.75 mmol L^{-1})|EDC film immobilized on a bare gold (dotted line) and a CYS|Au electrode (solid line).

the covalent bonding between the HHC molecules because of the presence of EDC [25,26]. The latter is responsible for an intermolecular covalent amide bonding. The potential is thus determined by the composition of the adsorbed layer. When the layer would contain the monomeric, native form of HHC, reversible electron exchange can occur. In this situation, the apparent reversibility decreased since the surface was partially covered with polymeric species which can only be oxidized at higher potentials.

The electrochemistry of HHC is governed by the interactions among the protein molecules [26]. Fig. 1 clearly demonstrates that the presence of CYS as an extra linker between the HHC film and the gold electrode causes a more stable background curve. Without CYS, there is no covalent coupling between the gold electrode and the protein film but a redox couple is observed. One can speak of only a physical adsorption of the protein film onto the electrode. Even in the absence of specific interaction or a covalent bond between the protein film and the electrode, the typical electrochemical behaviour of the HHC film is observed. Therefore, and to proof this statement, the use of other electrodes as carrier materials was also investigated. Because HHC has a global positive charge [27], carbon electrodes, which contain negative end groups, were not pre-treated expecting a good interaction between the electrode and the protein film. Indeed, film formation and the typical electrochemical behaviour occurred but the background current was again quite high and the reproducibility was very small. The same could be stated for platinum electrodes. Probably, the lack of a covalent interaction between the protein film and the electrode causes this and makes these bare electrodes not useful as a carrier material.

The amino groups of CYS can react with the HHC molecules through EDC as a coupling agent resulting in a protein film which is covalently adsorbed onto the electrode. It can be stated that CYS facilitates the electron transfer between the electrode and the protein film resulting in a lower background curve. Therefore, only CYS-modified gold electrodes were investigated further.

3.1. Optimization of the modification procedure

In search of the optimal conditions for the creation of a cross-linked HHC film on a gold electrode, the HHC concentration was varied. The concentration study showed us that a minimum HHC concentration of 1.5 mmol L^{-1} is necessary to obtain a HHC film on the electrode. If the concentration of HHC is lower than this value, there will be no visible film formation after 2 h of reaction time between HHC and EDC. This can be explained by the fact that the cytochrome *c* molecules are too low in number and too far away from each other to give rise to a covalent bonding between the different protein molecules. The only covalent bonding that occurs is the monolayer protein formation between the CYS immobilized onto the gold electrode and the HHC molecules in the droplet. There is no intermolecular HHC coupling. A cyclic voltammogram (not shown) of such a monolayer HHC-modified electrode reveals a charge of 6.5×10^{-8} C for the reduction peak of ferrocytochrome *c* corresponding to a surface coverage of 3.37×10^{-11} mol cm^{-2} indicating the formation of a monolayer [28,29].

3.2. Cyclic voltammetry as a function of scan number and scan rate

A few of the first 20 cyclic voltammetric scans recorded at a HHC (3 mmol L^{-1})| EDC|CYS|Au electrode in a HEPES buffer solution are shown in Fig. 2. Regarding the oxidation and reduction process of the iron ion of the heme group, a stable cyclic voltammogram is obtained as of scan 1. Analogous experiments were performed in order to investigate the reproducibility: Fig. 3 shows the cyclic voltammetric behaviour of four independently prepared

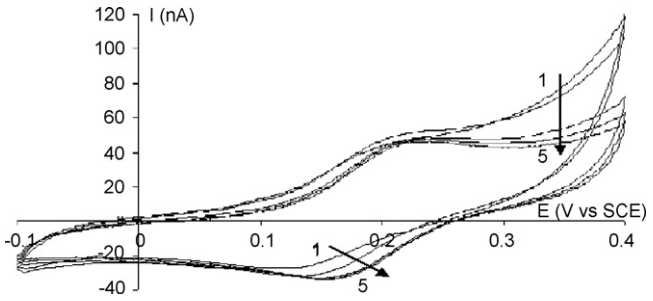

Fig. 2. Successive cyclic voltammograms recorded at a HCC (3 mmol L^{-1})| EDC|CYS|Au electrode in a HEPES buffer solution (pH 7): scan # 1 (1), scan # 2 (2), scan # 10 (3), scan # 15 (4) and san # 20 (5).

HHC (3 mmol L^{-1})|EDC|CYS|Au-modified electrodes. The good correlation between these measurements ($\Delta I = 2$ nA) indicates that with this procedure one can create protein-modified electrodes in a very reproducible way.

The influence of the scan rate on the peak current was investigated to determine the nature of the process. Fig. 4a shows the oxidation and reduction of HHC in a HEPES buffer solution over a wide range of scan rates. The oxidation and reduction peak current for HHC, as well as the peak-to-peak separation, increases linearly with the scan rate from 10 till 150 mV s^{-1}. Integration of the area under the peaks gives nearly constant charge values independent of the scan rate, indicating a quasi-reversible surface-confined thin-film electrochemical behaviour [30]. In the range of explored scan rates, electron diffusion control is observed. Fig. 4b shows the relationship between $\log I_p$ and $\log \nu$. The slope for the redox process is 0.47, indicating a reaction of a particle in solution. The proteins diffuse into the film in which they are immobilized, and the electron transfer process is achieved by exchange of electrons between the bound proteins. Because of the strong interaction between all proteins, the diffusion layer of in the membrane is much thinner than that in solution (on the same time scale). In theory, complete electrolysis of a thin film of material is expected at very low scan rates. However, for thicker film deposits (and for higher scan rates) diffusion control is observed [15,30]. The scan rate for the transition from 'thin-film' behaviour to diffusion characteristics can be predicted by Eq. (1):

$$\nu = \frac{DRT}{\delta^2 F} \quad (1)$$

In this equation the scan rate ν for the transition is obtained from the diffusion coefficient *D*, the gas constant *R*, the temperature *T*, the film thickness δ and the Faraday constant *F*. Knowing that $D_{cytc,membrane} = 2 \times 10^{-14}$ m^2 s^{-1} [31], it could be calculated that for a film thickness of ca. 40 μm, diffusion controlled voltammetric responses are expected. Fig. 5 shows a diagram indicating the char-

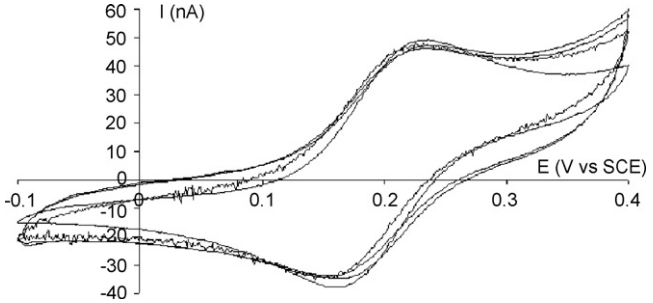

Fig. 3. 20th cyclic voltammogram recorded at four HCC (3 mmol L^{-1})|EDC|CYS|Au electrodes produced by the same procedure.

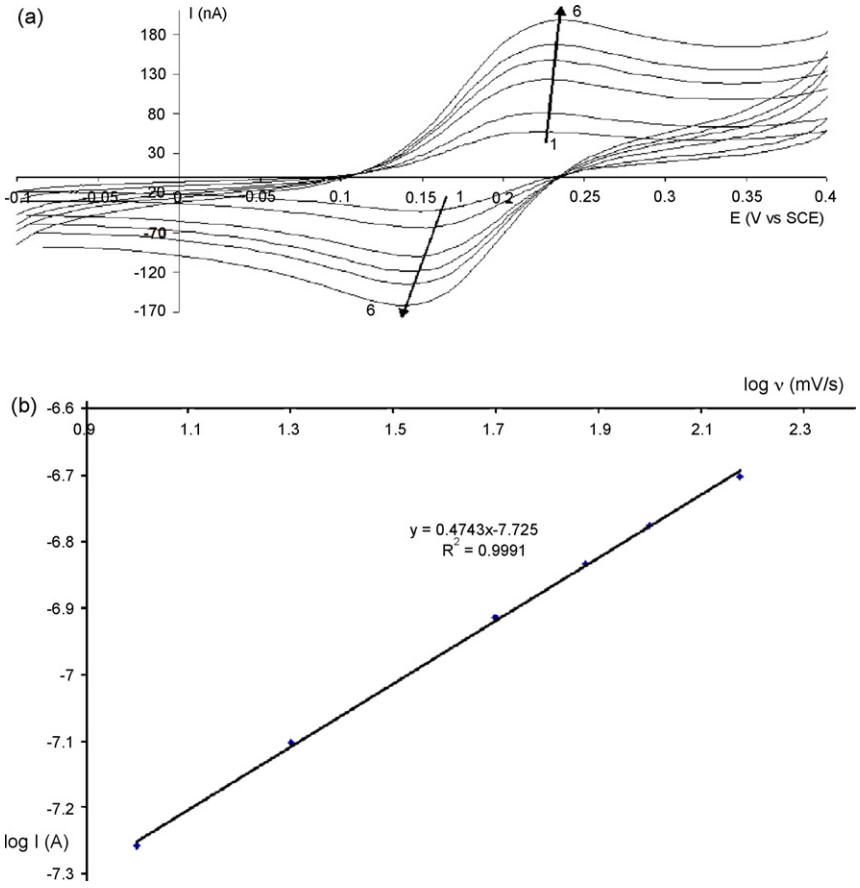

Fig. 4. (a) Current-potential behaviour of a HCC (3 mmol L^{-1})|EDC|CYS|Au electrode in a HEPES buffer solution (pH 7) at different scan rates: 10 (1), 20 (2), 50 (3), 75 (4), 100 (5) and 150 (6) mV s^{-1}. (b) Relationship between log I_p and log ν.

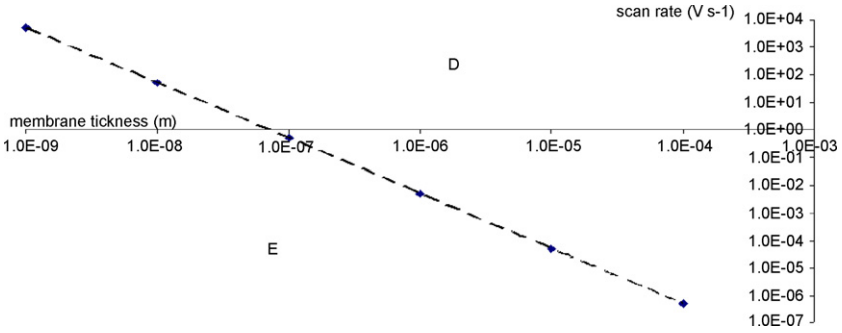

Fig. 5. Plot of the scan rate vs. the membrane thickness (Eq. (1)). The characteristic zones for complete electrolysis (zone E) and for diffusion controlled reactions (zone D) are indicated.

acteristic zones for complete electrolysis (zone E) and for diffusion controlled reactions (zone D) and demonstrates indeed that for film thicknesses of the order of 40 μm, we are working with diffusion controlled reactions.

3.3. Stability study

The protein film stability was tested by storing several HHC (3 mmol L^{-1})|EDC|CYS|Au-modified electrodes in air during several days. Some electrodes were stored at 293 K and others at 277 K. After returning the dry films to the buffer solution, cyclic voltammograms were recorded after 2 and 7 days. Curve 1 in Fig. 6 represents the initial current-potential behaviour of a HHC (3 mmol L^{-1})|EDC|CYS|Au electrode in a HEPES buffer solution. After 7 days of keeping the electrode at a temperature of 277 K, the

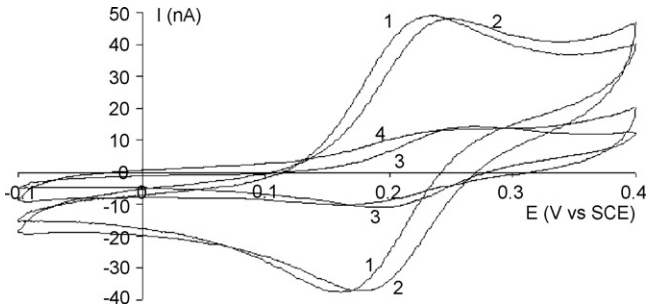

Fig. 6. Current-potential behaviour of a HCC (3 mmol L^{-1})|EDC|CYS|Au electrode in a HEPES buffer solution (pH 7) after 2 (curve 3) or 7 (curve 2,4) days and at room temperature (curve 3,4) or at 277 K (curve 2). Curve 1 represents the initial obtained cyclic voltammogram.

observed cyclic voltammetric behaviour is represented as curve 2. The peak current and the surface under the peak are quite stable for one week. Only a peak potential shift over ca. 20 mV is observed, probably indicating a small reorganization of the protein film or a change in protein conformation [25].

In contrast, when the electrode was kept at 293 K for 2 days, an enormous decrease of the peak current is observed (curve 3). After 7 days, curve 4 was recorded. Based on these results, it is clear that the modified electrodes should be kept at 277 K to retain a stable HHC film.

In order to examine whether the protein film is stable in a HEPES buffer solution or during the electrochemical measurements, the droplet of the buffer solution was collected using a syringe after the electrochemical experiment and was further analyzed using UV/vis. The addition of the buffer solution on the protein film during the voltammetric measurement causes a clear expansion of its volume resulting in the formation of a hydrogel. This looser structure of the film may provide a favourable and mainly aqueous microenvironment for transferring electrons with underlying electrodes. The large buffer content of the hydrogel also increases free volume in the film which facilitates diffusion of target molecules into the hydrogel. This phenomenon has possibilities for the development of an enzymatic sensor.

To determine the HHC concentration in a HEPES droplet, sodium dithionite was added to the droplet in order to reduce all HHC. The latter gives a characteristic UV/vis band at 554 nm [32]. Knowing that its extinction coefficient has a value of 21,400 $mol^{-1}\,L\,cm^{-1}$, an average concentration of 25 $\mu mol\,L^{-1}$, could be calculated in the droplet. The latter implies that only a negligible amount of HHC dissolves in the buffer solution compared to the 3 $mmol\,L^{-1}$ HHC concentration in the film indicating a very stable HHC film. Based on these values, it can be stated that ca. 85% of the initial amount of HHC forms a cross-linked film. The remaining amount of HHC proteins is not covalently bound to the electrode and dissolves in the HEPES buffer solution after contact.

4. Conclusion

The immobilization of a HHC film on a gold electrode, with EDC as coupling agent, has been described in this article. To obtain this protein polymer film, the buffer solution should be able to evaporate out of the hydrogel. It was also observed that the presence of CYS, acting as a covalent linker between the HHC film and the gold electrode, causes a more stable background electrochemical curve. A concentration study showed us that the minimum concentration of HHC to obtain a well-defined protein film is 1.5 $mmol\,L^{-1}$. The stability study made clear that the electrodes stored at 277 K were quite stable in comparison to the ones stored at room temperature.

References

[1] M.F. Chaplin, C. Bucke, Enzyme Technology, Cambridge University Press, Cambridge, UK, 1990.
[2] F.A. Armstrong, G.S. Wilson, Electrochim. Acta 45 (2000) 2623.
[3] D.R. Thevenot, K. Toth, R.A. Durst, G.S. Wilson, Biosens. Bioelectron. 16 (2001) 121.
[4] Y. Wu, S. Hu, Microchim. Acta 159 (2007) 1.
[5] F.A. Armstrong, H.A. Heering, J. Hirst, Chem. Soc. Rev. 26 (1997) 169.
[6] J.F. Rusling, Acc. Chem. Res. 31 (1998) 363.
[7] N. Hu, Pure Appl. Chem. 73 (2001) 1979.
[8] J. Yang, N. Hu, Bioelectrochem. Bioenerg. 48 (1999) 117.
[9] R. Huang, N. Hu, Biophys. Chem. 104 (2003) 199.
[10] H. Zhou, R. Yang, Y. Xu, K. Han, G. Li, Anal. Lett. 38 (2005) 2103.
[11] K.J. McKenzie, F. Marken, M. Opallo, Bioelectrochemistry 66 (2005) 41.
[12] F.A. Armstrong, H.A. Heering, J. Hirsy, Chem. Soc. Rev. 26 (1997) 169.
[13] C. Fan, H. Wang, D. Zhu, G. Wagner, G. Li, Anal. Chem. 73 (2001) 2850.
[14] K. Nam, J. Watanabe, K. Ishihara, Int. J. Pharm. 275 (2004) 259.
[15] T. Wanatabe, A. Ohtsuka, N. Murase, P. Barth, K. Gersonde, Magn. Reson. Med. 35 (1996) 697.
[16] X. Qu, A. Wirsen, A.-C. Albertson, J. Appl. Polym. Sci. 74 (1999) 3186.
[17] C. Wang, R.J. Steward, J. Kopecek, Nature 397 (1999) 417.
[18] M. Collison, E.F. Bowden, M.J. Tralov, Langmuir 8 (1992) 1247.
[19] M. Fedurco, Coord. Chem. Rev. 209 (2000) 263.
[20] K. Miki, T. Ikeda, H. Kinoshita, Electroanalysis 6 (1994) 703.
[21] W.R. Hagen, Eur. J. Biochem. 182 (1989) 523.
[22] T. Ozawa, M. Tanaka, Y. Shimomura, Proc. Natl. Acac. Sci. U.S.A. 77 (1980) 5084.
[23] R.S. Sirohi, M.A. Gensham, J. Electrochem. Soc. 116 (1969) 910.
[24] H.A. Heering, F.G.M. Wiertz, C. Dekker, S. De Vries, J. Am. Chem. Soc. 126 (2004) 11103.
[25] A.V. Krylov, W. Pfeil, F. Lisdat, J. Electroanal. Chem. 569 (2004) 225.
[26] A. Szúcs, M. Novák, J. Electroanal. Chem. 384 (1995) 47.
[27] F.A. Armstrong, P.A. Cox, H. Allen, O. Hill, V.J. Lowe, B.N. Oliver, J. Electroanal. Chem. 217 (2) (1987) 331.
[28] J. Zhou, X. Lu, J. Hu, J. Li, Chem. Eur. J. 13 (2007) 2847.
[29] D.D. Schlereth, J. Electroanal. Chem. 464 (1999) 198.
[30] M. Noel, K.I. Vasu, Cyclic Voltammetry and the Frontiers of Electrochemistry, Aspect Publications, London, 1990.
[31] K.J. McKenzie, F. Marken, Langmuir 19 (2003) 4327.
[32] A.S. Haas, D.L. Pilloud, K.S. Reddy, G.T. Babcock, C.C. Moser, J.K. Blasie, P.L. Dutton, J. Phys. Chem. 105 (2001) 11351.

Talanta 76 (2008) 462–468

Contents lists available at ScienceDirect

Talanta

journal homepage: www.elsevier.com/locate/talanta

Development and validation of an HPLC-method for the determination of alkaloids in the stem bark extract of *Nauclea pobeguinii*

L. Dhooghe[a,*], K. Mesia[a,b], E. Kohtala[a], L. Tona[b], L. Pieters[a], A.J. Vlietinck[a], S. Apers[a]

[a] *Department of Pharmaceutical Sciences, University of Antwerp, Universiteitsplein 1, B-2610 Antwerp, Belgium*
[b] *Faculty of Pharmaceutical Sciences, University of Kinshasa, P.O. Box 212, Kinshasa XI, Congo*

ARTICLE INFO

Article history:
Received 5 November 2007
Received in revised form 20 March 2008
Accepted 25 March 2008
Available online 8 April 2008

Keywords:
Nauclea pobeguinii
Method development
Method validation
HPLC

ABSTRACT

A new method was developed and validated for the quantification of strictosamide in the extract of the stem bark of *Nauclea pobeguinii*. This plant belongs to the Rubiaceae family and is widely used in the African traditional medicine against malaria and malaria-like symptoms. Alkaloids are suspected to be responsible for the antimalarial activity. One of these alkaloids is strictosamide, already reported to be the major constituent in the root bark of this plant. Because strictosamide was not commercially available another alkaloid, ajmalicine HCl, with comparable properties was used as a secondary standard.

The samples of the dried 80% ethanol extract from the stem bark of *N. pobeguinii* were purified on C_{18} solid phase extraction cartridges and analysed using HPLC-UV. The strictosamide used for the validation of the correction factor for response was isolated and purified by means of preparative HPLC and TLC. Although the relative standard deviation (R.S.D.) of 2.6% was still acceptable, the response factor was determined for every analysis based on the ratio of the peak area of strictosamide compared to the peak area of ajmalicine HCl in a concentration of 0.01 mg/ml. The precision of the method according to the time and the concentration, had a R.S.D. value of 2.2% and 2.6%, respectively. The recovery of the method was 92.2% (R.S.D. of 9.4%) which was acceptable.

The method has been proven to be suitable for the determination of alkaloids in the extract of the stem bark of *N. pobeguinii*, according to the ICH guidelines on the validation of analytical methods.

1. Introduction

Malaria, caused by protozoal parasites of the genus *Plasmodium*, the most dangerous one being *P. falciparum*, is still one of the most devastating infectious diseases in the world. The number of lethal cases of malaria is estimated at 1.5–2.5 million annually, especially in developing countries [1]. In view of the limited availability of synthetic drugs in such countries, traditional medicine still has a prominent place in local health care systems, including for the treatment of malaria. In continuation of our work on antimalarial plants used in traditional medicine in DR Congo, we have recently reported on the activity and toxicity of extracts of *Croton mubango*, *Pyrenacantha staudtii* and *Nauclea pobeguinii*. Extracts from the latter plant showed *in vitro* as well as *in vivo* (in rodents) antiplasmodial activity in the absence of obvious toxicity [2–4]. Therefore, it was decided to investigate the active principles from *N. pobeguinii*. This plant is used in DR Congo for the treatment of fever, including fever caused by malaria, and against intestinal worms, abdominal pains, sexual asthenia and gonorrhea [5]. It has been reported that the alkaloid strictosamide was the main constituent of *N. pobeguinii.* Other alkaloids identified from the same plant included angustine, naufoline, angustoline, nauclefine, *O*-acetyl-angustoline and 3,14-dihydroangustine. In addition, two quinovic acid glycosides were reported [6]. Strictosamide, isolated from *Sarcocephalus latifolius* (*Nauclea latifolia*) was characterised as the antiplasmodially active principle from this plant, showing an IC_{50} against *P. falciparum* strains K1 and NF54 of 0.45 and 0.37 μg/ml, respectively [7]. Therefore, awaiting the identification and evaluation of the antiplasmodial activity of minor constituents of *N. pobeguinii*, it was decided to standardise *N. pobeguinii* extracts on strictosamide. Duez et al. compared an HPTLC- and HPLC-method for the assay of strictosamide in the leaves, root and stem bark of *N. latifolia* [8]. Nevertheless the HPLC-method needed optimization and neither method was validated. Indeed, the evaluation of the efficacy of traditional *N. pobeguinii* preparations is only possible if reliable and validated analytical methods are available to investigate their chemical composition. In order to be able to check the quality of such preparations used locally, and with the aim of conducting in a later stage of the work a clinical evaluation of standardised *N. pobeguinii* preparations used in DR Congo, it was decided to develop and

* Corresponding author. Tel.: +32 38202731; fax: +32 38202709.
E-mail address: Liene.Dhooghe@ua.ac.be (L. Dhooghe).

0039-9140/$ – see front matter © 2008 Elsevier B.V. All rights reserved.
doi:10.1016/j.talanta.2008.03.036

validate an analytical method using HPLC for the determination of strictosamide.

2. Experimental

2.1. Reagents

Acetonitrile HPLC far UV, methanol for HPLC, absolute ethanol, diethyl ether, dichloromethane for HPLC, hexane for HPLC, diethylamine, acetic acid for analysis and formic acid for analysis were provided by Acros Organics (Morris Plains, NJ, USA). Distilled water was prepared with a Millipore water purification system (Millipore, Bedford, MA, USA).

The ajmalicine HCl (99.7% purity, determined by argentometric titration) that was used as a secondary standard, was obtained from Sigma–Aldrich (Bornem, Belgium).

2.2. Plant material and extracts

2.2.1. Plant material

The stem bark of *N. pobeguinii* was collected in Sankuru district, DR Congo in January 2002. The plant was identified at the Institut d'Etudes et de Recherches Agronomiques (INERA) from the University of Kinshasa, DR Congo. The plant material was dried at room temperature, reduced to powder using a Thomas Scientific mill (Swedesboro, NJ, USA) with a delivery tube of 2 mm diameter. The powder was stored in the refrigerator until use.

2.2.2. Stem bark extract

The plant material (1900 g) was exhaustively macerated and percolated with 80% ethanol. Macerate and percolate were combined and evaporated *in vacuo*. The resulting dried crude extract (286.96 g) was the subject of this article and from this crude extract the alkaloid enriched fraction was obtained and strictosamide was isolated.

2.2.3. Alkaloid enriched fraction

To obtain an alkaloid enriched fraction, a liquid–liquid extraction was performed. The crude extract (250 g) was dissolved in water and acidified with hydrochloric acid 2% until a pH of 3.0. After washing with chloroform, the water layer was brought to a pH above 9.0 with ammonia 10% and extracted again with chloroform. This organic layer provided the alkaloid enriched fraction (2.64 g) which was used in the accuracy experiments.

2.3. Isolation, identification and purity determination of strictosamide

Strictosamide was isolated from the crude extract using preparative HPLC and TLC. The extract, in a concentration of 10 mg/ml in 80% methanol, was first filtered using a Chromafil AO-45/25 syringe filter (Macherey Nagel, Düren, Germany) and then injected through a 500 μl loop into the Gilson HPLC (Middleton, WI, USA) with pump (Gilson 322), automatic injector (Gilson 234) and UV/VIS detector (Gilson UV/VIS-156) controlled by UniPoint software. For the preparative work a RP18 column was used with 250 mm × 10 mm internal diameter and packed with Nucleosil 100-7 C_{18} AB (Macherey Nagel, Düren, Germany). The guard column was a high performance guard column (10 mm × 10 mm internal diameter and 5 μm particle size) from Grace Vydac (Hesperia, CA, USA). Water was used as solvent A and acetonitrile as solvent B with following gradient: 0 min, 80:20 (A:B); 5 min, 80:20; 15 min, 70:30; 25 min, 70:30; 30 min, 0:100. The flow rate was 3.0 ml/min and the compounds were detected at a wavelength of 226 nm. The major peak at 21 min was repeatedly collected. A last purification step was performed by preparative TLC in order to remove non-UV active co-eluting compounds. RP-18 F_{254_S} plates (10 cm × 20 cm) from Merck (Darmstadt, Germany) were used with water:acetonitrile (1:1) as mobile phase. The spots were observed under UV (254 and 366 nm) and after spraying with phosphomolybdic acid or *p*-anisaldehyde reagent followed by heating at 120 °C. In order to remove all residual solvents, the strictosamide was lyophilised before use.

The isolated compound was confirmed to be strictosamide by NMR spectroscopy using a Bruker DRX-400 instrument (Rheinstetten, Germany), operating at 400 MHz for ^{1}H and 100 MHz for ^{13}C and using CD_3OD as solvent. ^{1}H NMR: δ = 2.04 (ddd, J = 13.9, 13.9, 6.0, 1H), 2.46 (m, 1H), 2.64–2.70 (m, 2H), 2.79 (m, 1H), 2.90–2.98 (m, 1H), 2.95 (m, 1H, of Glc), 3.10 (m, 1H), 3.15–3.30 (m, 3H, of Glc), 3.62 (dd, J = 11.9, 5.8, 1H, of Glc), 3.85 (dd, J = 11.9, 2.1, 1H, of Glc), 4.56 (d, J = 7.9, 1H, of Glc), 4.94 (m, 1H), 5.07 (m, 1H), 5.31 (dd, J = 10.0, 1.8, CH_2 of –$CHCH_2$), 5.36 (dd, J = 17.1, 1.8, CH_2 of –$CHCH_2$), 5.40 (d, J = 1.8, 1H), 5.65 (ddd, J = 17.1, 10.0, 10.0, CH of –$CHCH_2$), 6.99 (ddd, J = 8.1, 8.1, 1.0, 1H), 7.07 (ddd, J = 8.1, 8.1, 1.0, 1H), 7.32 (d, J = 8.1, 1H), 7.37 (s, 1H), 7.38 (d, J = 8.1 Hz, 1H). ^{13}C NMR: δ = 22.12 (C6), 24.96 (C15), 27.36 (C14), 44.77 (C5), 44.80 (C20), 55.14 (C3), 62.63 (C6′), 71.40 (C4′), 74.35 (C2′), 77.98 (C5′), 78.24 (C3′), 98.11 (C21), 100.53 (C1′), 109.27 (C16), 110.35 (C7), 112.27 (C12), 118.68 (C9), 120.16 (C10), 120.52 (C_{18}), 122.50 (C_{11}), 128.72 (C_8), 134.36 (C_{19}), 134.79 (C_2), 137.80 (C_{13}), 149.17 (C_{17}), 167.14 (C_{22}).

Also MS analysis was performed on a linear ion trap mass spectrometer (LXQ; Thermo scientific, Breda, The Netherlands) by infusion of the compound (5 μl/min) added to a solvent flow of 0.5 ml/min 0.1% acetic acid in acetonitrile:0.1% acetic acid (65:35). This was brought into the MS via an ESI source and measured in the positive and negative ion modus. Nebulization was achieved using nitrogen gas at a pressure of 50 psi. The capillary temperature was set at 350 °C. The ESI-MS spectrum recorded in the positive ion mode showed a $[M+H]^+$ peak at m/z 499, which was in agreement with the expected molecular weight of 498 ($C_{26}H_{30}N_2O_8$). MS/MS analysis showed the loss of 162 mass units (peak at m/z 337), corresponding to the loss of the glucosyl moiety. Also in the negative ion mode the corresponding peaks at m/z 497 ($[M-H]^-$) and m/z 335 were observed.

To investigate the purity, the isolate was injected in a concentration of 0.1 mg/ml in an Agilent 1200 HPLC (Eindhoven, the Netherlands) with diode array detector. Chromatograms at different wavelengths were recorded (210, 226, 230, 254, 275, 300 and 325 nm). All peaks were integrated and the area percentage of strictosamide was calculated.

2.4. Method of analysis

2.4.1. Chromatographic conditions

The system used for analysis was an Agilent 1200 series (Eindhoven, the Netherlands) with degasser (G1322A), quaternary pump (G1311A), automatic liquid sampler (G1329A), thermostatted column compartment (G1316A) and diode array detector (G1315O) using ChemStation software. For the HPLC analysis different columns in combination with different solvent systems were tried out. The different columns were: GraceSmart RP18, 5 μm, 250 mm × 4.6 mm (Grace Vydac, Hesperia, CA, USA); LiChrospher RP18 EC, 5 μm, 250 mm × 4.6 mm (Merck, Darmstadt, Germany); Alltima HP C_{18} HL, 3 μm, 150 mm × 3 mm (Grace Davison, Lokeren, Belgium). Solvent system 1: water as solvent A and acetonitrile as solvent B (0 min, 80:20 (A:B); 5 min, 80:20; 15 min, 50:50; 20 min, 0:100). Solvent system 2: water with 0.2% diethylamine and formic acid until pH 3.0 as solvent A and acetonitrile with 0.2% diethylamine as solvent B (0 min, 80:20 (A:B); 5 min, 80:20; 20 min, 60:40; 25 min, 0:100). The flow was adjusted according to the diameter of

the column (a flow of 0.7 ml/min for a diameter of 3 mm; a flow of 1.0 ml/min for a diameter of 4.6 mm).

2.4.2. Sample preparation and purification

Different sample preparation protocols were investigated. Protocol A: dissolve 100 mg crude extract in 50.0 ml methanol; ultrasonicate 15 min; take an aliquot of 5.0 ml and dilute up to 20.0 ml with water. Protocol B: dissolve 100 mg crude extract in 50 ml dilute HCl; ultrasonicate for 30 min; extract three times with 100 ml ethylacetate:hexane (1:1) and discard the organic layer; alkalize the water layer with dilute ammonia; extract one time with 100 ml and two times with 50 ml dichloromethane; keep the organic layer and dry; dissolve again in 50.0 ml methanol 20%; bring 5.0 ml of this solution in a 20.0 ml calibrated flask and fill up with methanol 20%. Protocol C: dissolve 100 mg crude extract in 40 ml methanol; ultrasonicate 15 min; add 10 ml water; extract two times with 50 ml hexane; wash the joint hexane layers with 20 ml methanol 80%; collect all water layers and add methanol 80% until 100.0 ml; bring 10.0 ml of the resulting solution in a 20.0 ml calibrated flask and add water till 20.0 ml. Protocol D: dissolve 100 mg crude extract in 10 ml methanol; ultrasonicate 15 min; dilute with water up to 50.0 ml; bring 5.0 ml on a preconditioned Chromabond SPE C_{18} cartridge (500 mg) of Macherey Nagel (Düren, Germany); wash three times with 6 ml methanol 30%; elute three times with 6 ml methanol 60% and collect in a measuring flask of 20.0 ml; add water until 20.0 ml.

2.4.3. Final method

2.4.3.1. Standard solution. For the standard solution about 10 mg of ajmalicine HCl was accurately weighed into a measuring flask of 50.0 ml. It was dissolved in methanol and sonicated for 15 min. From this solution 1.0 ml was brought in a measuring flask of 20.0 ml and diluted with mobile phase A.

2.4.3.2. Test solution. About 100 mg of crude extract was accurately weighed in a measuring flask of 50.0 ml, 10 ml of methanol was added and ultrasonicated for 15 min. Water was added until 50.0 ml and from this solution 5.0 ml was brought onto a Chromabond SPE C_{18} cartridge preconditioned with methanol and water. The column was eluted with 18 ml methanol 60%. The fraction was collected in a measuring flask of 25.0 ml and brought up to volume with mobile phase A.

2.4.3.3. HPLC conditions. 20.0 μl was analysed by HPLC (0 min, 80:20 (A:B); 5 min, 80:20; 20 min, 60:40; 25 min, 0:100) using 0.2% diethylamine and 0.16% formic acid as solvent system A and 0.2% diethylamine and 0.16% formic acid in acetonitrile as solvent system B. The column used was the GraceSmart RP18, 5 μm, 250 mm × 4.6 mm with a flow rate of 1.0 ml/min. The peaks were detected at 226 nm.

2.5. Method validation

2.5.1. Response function—calibration model

For the calibration model of ajmalicine HCl six solutions in different concentrations were prepared, ranging from 4.24 to 21.20 μg/ml. For strictosamide eight concentration levels were used from 4.27 to 45.79 μg/ml. All solutions were injected twice.

2.5.2. Correction factor for response

For the validation of the correction factor both ajmalicine HCl and strictosamide were injected on three different days. A fresh ajmalicine HCl solution was prepared every day with a concentration of 10.10 μg/ml while the strictosamide concentration was set at 22.90, 10.68 and 45.79 μg/ml, each on a separate day. Every solution was injected six times.

2.5.3. Precision

For the intermediate precision six separate samples (100% or 100 mg) were analysed on 1 day and this was repeated on 2 consecutive days. Every sample was injected once. The secondary standard, used to determine the amount of strictosamide, was freshly prepared each day and injected at the beginning and the end of the sequence. For the repeatability on different concentration levels (linearity of the method) six samples with half the amount (50% or 50 mg) and six samples with twice the amount (200% or 200 mg) were analysed, using the same method.

2.5.4. Accuracy

For the accuracy, a recovery experiment was performed. Different amounts of alkaloid enriched fraction were added to 90% of the crude extract until a total concentration of 100%, 115% or 140% of strictosamide was obtained. About 18 mg of crude extract was weighed into a 10.0 ml measuring flask and 0.5, 1.0 and 2.0 ml of a stock solution of the alkaloid enriched fraction (2.55 mg/ml solution) was added. A 5.0 ml aliquot of this solution was brought onto the SPE column and after eluting, the volume was brought to 25.0 ml. The solutions on the different concentration levels were prepared in triplicate and each solution was injected once.

2.5.5. Specificity

To test the specificity, the peak purity of ajmalicine HCl and strictosamide was investigated using the HPLC with diode array detector.

3. Results and discussion

In general, in order to determine the amount of an active component or a marker compound present in a crude extract or in thereof derived preparations, using a chromatographic technique such as HPLC, reference material that serves as an external standard is required. For the analysis of *N. pobeguinii* preparations, the standard substance of choice would be strictosamide reference material with known purity. Since strictosamide is not commercially available, every laboratory willing to perform this analysis would first need to isolate and fully characterize a sufficient amount of pure substance. This kind of practice is economically and practically unjustifiable rendering the developed and validated method worthless and useless.

An elegant way to overcome the problem of lack of reference material or of high price quotes of pure plant compounds is to use a secondary standard, i.e. a commercially available, related compound. There are three possibilities when using a secondary standard: (1) the amount of strictosamide can be calculated with respect to the secondary standard as such, yielding a relative amount of strictosamide; (2) making a correction for the difference in molecular weight; since the difference in detector response between both substances is neglected in the latter case, the most correct way is (3) to use a correction factor, yielding an absolute result.

The work performed in order to develop and validate an HPLC-method for the determination of strictosamide in *N. pobeguinii* crude extract (preparation procedure described in Section 2.2.2) using ajmalicine HCl as a secondary standard is outlined in the following sections. The first step was to isolate an amount of pure strictosamide allowing the determination of the appropriate correction factor. In the development of a suitable analytical method the chromatographic conditions and the sample preparation and

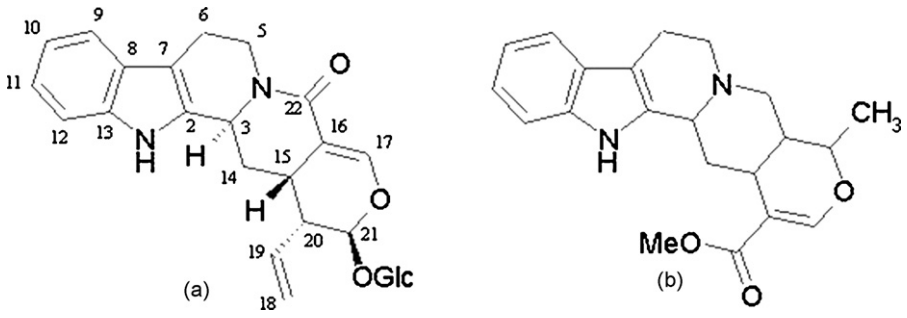

Fig. 1. The structures of strictosamide (a) and ajmalicine (b).

purification procedure were investigated and optimised. As a last step the final method was validated in order to prove the suitability for its purpose.

3.1. Isolation, identification and purity determination of strictosamide

Strictosamide was isolated from the dried stem bark of *N. pobeguinii* using the procedure outlined in Section 2.3 of the experimental part. The isolated compound was confirmed to be strictosamide, an indol alkaloid containing a glucosyl moiety (Fig. 1a), which has been reported as the main alkaloid from *N. pobeguinii* by Zeches et al. [6]. The ^{1}H, ^{13}C, DEPT-135 and DEPT-90 NMR spectra were recorded, as well as its mass spectrum. The NMR data were in good agreement with the assignments listed by Erdelmeier et al. for strictosamide isolated from *Nauclea orientalis* [9].

Purity analysis was performed by means of HPLC. No other peaks were present at other wavelengths, not even at 210 nm. After integration of all of the peaks at 226 nm, a purity of 90% of strictosamide was calculated by means of the normalization method. This was taken into account in the calculations for the analysis and the validation.

3.2. Method development

3.2.1. Chromatographic conditions

Because strictosamide is not commercially available, ajmalicine HCl was used as a secondary standard (Fig. 1b). This alkaloid has similar physicochemical properties and also has the same maximum absorption wavelength as strictosamide. Due to the alkaline nature of this compound developing a proper method was a challenge. Different columns and several solvent systems, listed in Section 2.4.1, were tested in order to obtain a nice peak shape for ajmalicine HCl and to separate the different peaks in the crude extract.

The second generation columns containing extra-pure silica, i.e. GraceSmart RP18 and Alltima HP C_{18} HL, seemed to give the best results particularly with respect to the peak shape. In fact, when using the LiChrospher RP18 EC containing a less pure silica material, no peak for ajmalicine HCl could be observed. The performance of the other columns was comparable suggesting that not the high carbon load but the quality of the silica was the determining characteristic. Based on these conclusions and due to economical reasons, the GraceSmart RP18 column was implemented in the final method.

Solvent system 1, containing pure water and acetonitrile, nicely separated the alkaloid compounds and was used in the beginning but after a while it seemed that ajmalicine HCl was remaining in small amounts on the column. Further optimisation lead to solvent system 2 in which formic acid to avoid ionised hydroxyl groups, and diethylamine to mask the remaining ionised groups, were added so no ajmalicine HCl was captured. In the final solvent system formic acid was also added to the organic layer to keep its concentration equal during the whole run in order to prevent the column from bleeding (pH range for stability was 1.5–10.5). The latter change in mobile phase had a negative effect on the separation of the different compounds of the crude extract. The gradient had to be adapted in order to keep a good separation of the peaks due to the alkaloids in the crude extract, as described in the final method (Section 2.4.3). The resulting chromatograms of the extract (a) and of the standard (b) are shown in Fig. 2. Ajmalicine HCl in the reference solution eluted after 18.5 min and strictosamide in the sample solution after 20.5 min.

3.2.2. Sample preparation and purification

In order to dissolve all compounds from the crude extract, different solubility parameters were tested. Different solvents (water, methanol), concentrations (100:0; 80:20; 20:80; 0:100) and ultrasonication times (5, 15, 30 and 60 min) were tried out. Results showed that dissolving in water was more difficult and needed a longer sonication time than dissolving the sample in methanol. Based on these conclusions a first simple and fast sample preparation protocol was designed: protocol A (Section 2.4.2) in which the crude extract was dissolved in pure methanol by sonication during 15 min and analysed after a fourfold dilution. Since a crude extract, in this case an 80% ethanol extract of a plant, contains a broad range of compounds with different structures and thus different polarity and UV absorbance, it is always necessary to investigate whether or not all compounds elute from the stationary phase. A convenient way is to use thin layer chromatography with multiple development and a range of detection methods (UV254/366; spray reagents). This study revealed that non-UV absorbing compounds remained on the starting spot. In order to increase the column life time it was necessary to remove all column blocking compounds from the sample solution before injecting it into the HPLC. Different liquid–liquid extraction methods (protocols B and C) were tested. Protocol B showed a great loss of strictosamide. Possibly this alkaloid, containing a glucose, has different properties and for this reason this extraction scheme, normally used to purify alkaloids, could not be used. Protocol C could remove some column blocking lipids but also showed a high loss of strictosamide because of a poor separation of the layers. Changing the methanol concentration from 80% to 20% could not improve the results. In the end the use of Chromabond SPE C_{18} cartridges (protocol D) seemed to be more effective and time saving. The volumes and methanol concentrations in the washing/eluting steps were tested to obtain the best results. The washing/eluting steps were thoroughly investigated so no alkaloids would be eliminated in order to be able to determine the total alkaloids in the extract if necessary. Since the washing step with methanol 30% in protocol D caused the loss of the first elut-

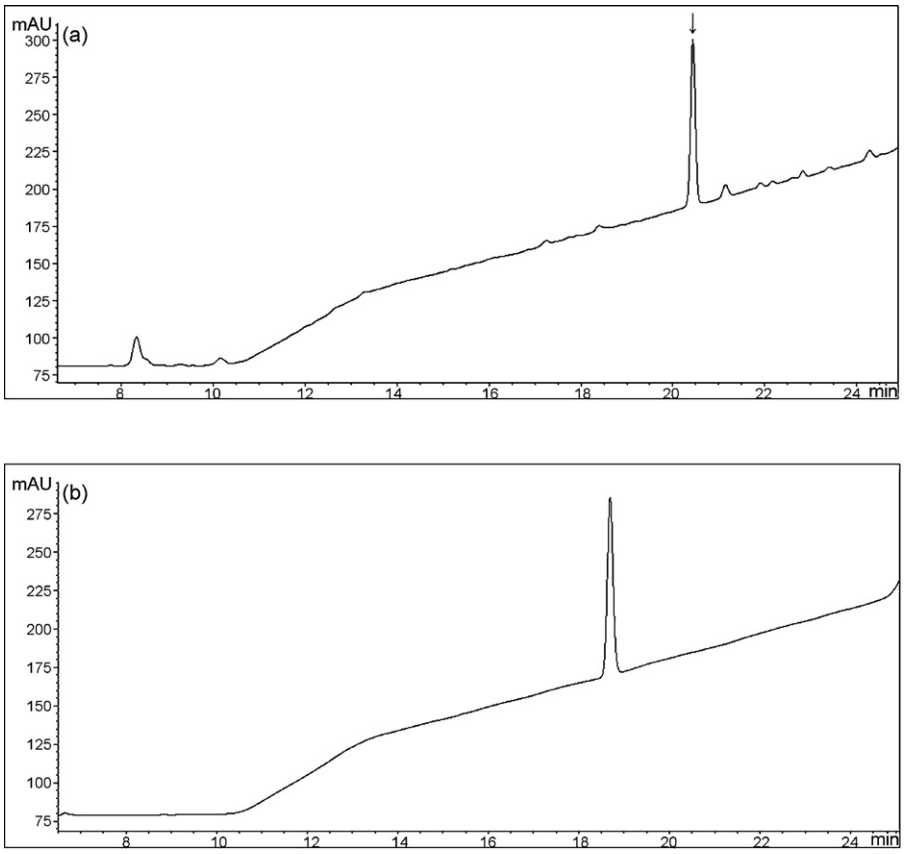

Fig. 2. (a) Chromatogram of the crude extract of the stem bark of *N. pobeguinii*, after purification on a C_{18} solid phase extraction cartridge, in a concentration of 0.4 mg/ml. 20.0 μl was injected in an HPLC system with GraceSmart RP18 column (5 μm, 250 mm × 4.6 mm). The flow was 1.0 ml/min and following gradient was used: 0 min, 80:20 (A:B); 5 min, 80:20; 20 min, 60:40; 25 min, 0:100. The solvent system was water (A) and acetonitrile (B) both containing 0.2% diethylamine and 0.16% formic acid. The peaks were detected at 226 nm. Strictosamide is marked with an arrow. (b) Chromatogram of the standard ajmalicine HCl in a concentration of 0.01 mg/ml using the same chromatographic conditions.

ing alkaloids, this step was omitted in the final method (Section 2.4.3). Using this sample preparation protocol the extract could be injected into the HPLC for analysis.

3.2.3. Final method

The amount of strictosamide was determined in the crude extract using ajmalicine HCl as standard. The test solution was first cleaned up using a Chromabond SPE C_{18} cartridge before injecting it into the HPLC. A second generation column with extra-pure silica was used in combination with formic acid and diethylamine in the solvent system to obtain a nice peak shape for ajmalicine HCl. The gradient was adjusted in order to separate all peaks of the alkaloids in the extract. The detailed protocol is described in Section 2.4.3.

3.3. Validation

The method was validated according to the ICH guidelines [10,11]. The experimental design of the investigation of the different characteristics is described in detail in Section 2.5.

3.3.1. Response function—calibration model

The linearity for ajmalicine HCl and strictosamide was investigated. The least square lines and the correlation coefficients were calculated. The regression lines were constructed and inspected. The slope and the intercept of the calibration curves were evaluated by means of the Student's *t*-test and the residuals were graphically examined. The results are shown in Table 1.

For ajmalicine HCl the results were all good. Graphical examination of the regression line and the residuals proved that the method was linear. The correlation coefficient was at least 0.99. The slope of the curve was significant and the point (0, 0) fell within the calibration curve.

Concerning strictosamide the model was proven linear after graphical evaluation of the regression line and the residuals. The correlation coefficient was also acceptable. Although the slope of the curve was significantly different from zero, the origin did not fall within the calibration curve. This means that a single point calibration is not justified and for every analysis a calibration curve for strictosamide should be constructed.

3.3.2. Correction factor for response

The correction factor for the response is calculated for every injection ($C_p/A_p \times A_s/C_s$) using the concentration (C) and area (A) of the primary (p) standard, strictosamide, and secondary (s) standard, ajmalicine HCl. An analysis of variance (ANOVA) single factor was performed and by means of the *F*-test the difference between the results and the linearity of the correction factor for response

Table 1
Overview of the linearity data of ajmalicine HCl and strictosamide

	Ajmalicine HCl	Strictosamide
Correlation coefficient	0.9985	0.9997
Slope ± standard error	43,733,985 ± 533,040	17,748,102 ± 84,227
Intercept ± standard error	−15,752 ± 7221	23,696 ± 1911
Confidence interval (95%)	−31,842–337	19,598–27,794
Range (μg/ml)	4.24–21.20	4.27–45.79
Number of standards (in duplicate)	6	8

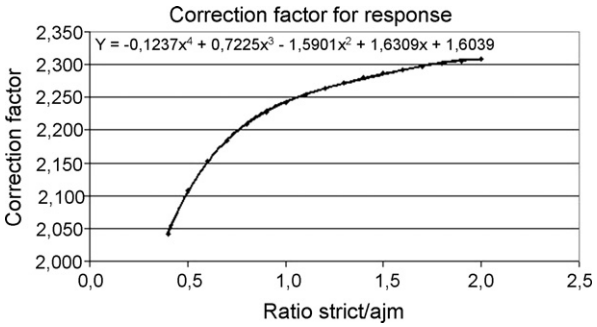

Fig. 3. Graph used for the determination of the correction factor for response according to the ratio of the peak area of strictosamide to the peak area of ajmalicine HCl in a concentration of 0.01 mg/ml.

were investigated. The averages of the correction factors for each day were, respectively, 2.33, 2.23 and 2.35. The overall mean was 2.30 with a relative standard deviation (%R.S.D.) of 2.61%. The calculated *F*-value was 33.61 which was much higher than the critical *F*-value of 3.68. Although the %R.S.D. is smaller than 5% and the mean correction factor could be applicable, this would contribute to a bigger error to the analysis of the extract. Also the calibration curve of strictosamide was linear but did not contain the point (0, 0) which also resulted in a difference in correction factor in function of the concentration. For this reason a graph and its corresponding equation were developed to determine the correction factor for each analysis according to the ratio of the peak area of strictosamide to the peak area of ajmalicine HCl in a concentration of 10 μg/ml (Fig. 3). Following equation can be used:

$$y = -0.1237x^4 + 0.7225x^3 - 1.5901x^2 + 1.6309x + 1.6039$$

in which x is the peak area ratio and y the correction factor that should be used.

3.3.3. Precision

The mean, the standard deviation, %R.S.D. and the 95% confidence interval for every day and every concentration level were calculated. For the evaluation of the repeatability the within-day and within-level mean square were calculated. The intermediate precision was estimated using the overall mean, standard deviation, %R.S.D. and the between-day or between-level mean square. The results were evaluated by means of an ANOVA single factor. To test the homogeneity of variance between the different days or the different concentration levels, a Cochran's test was performed (C was calculated). All results are summarized in Table 2.

The Cochran's test revealed that the variation on the different days and on the different levels were equal: the calculated *C*-value was always smaller than the critical *C*-value. Although the calculated *F*-value was higher than the critical *F*-value, $R.S.D._{between}$ was lower than 5% and thus the method is still acceptable and the results obtained on the different days and different concentration levels are not significantly different. This was also concluded after graphical inspection of the results, meaning that no dependency on time or concentration on the results could be observed. The concentration of strictosamide determined by this method was 5.6% (w/w).

Table 2
Precision on different days and different concentration levels

	Day 1	Day 2	Day 3	50%	200%
Repeatability					
Number of replicates	6	6	6	6	6
Mean content (%)	5.53	5.47	5.66	5.56	5.78
Standard deviation (%)	0.06	0.09	0.08	0.10	0.10
R.S.D. (%)	1.05	1.73	1.33	1.85	1.82
MS_{within}	0.006			0.008	
Intermediate precision					
Number of groups	3			5	
Number of replicates	6			6	
Overall mean (%)	5.55			5.60	
$R.S.D._{between}$ (%)	2.21			2.63	
$MS_{between}$	0.06			0.09	
C/C_{crit}	0.50	0.71		0.28	0.51
F_{calc}/F_{crit}	10.02	3.68		11.40	2.76

Table 3
Results of the recovery experiment

Concentration	X_{after} (μg/ml)	X_{before} (μg/ml)	X_{added} (μg/ml)	Recovery (%)
100%	22.37	19.61	3.43	80.6
	23.12	20.05	3.43	89.4
	22.89	20.22	3.43	78.0
115%	24.94	18.88	6.86	88.2
	25.98	19.44	6.86	95.3
	26.78	19.77	6.86	102.1
140%	32.86	19.33	13.72	98.6
	35.74	22.11	13.72	99.4
	34.35	20.88	13.72	98.2

X_{after} is the concentration of strictosamide determined in the final sample solution. It was calculated using the resulting peak area and the correction factor. X_{before} is the concentration of strictosamide in the weighed crude extract (containing 5.6% strictosamide). X_{added} is the concentration of strictosamide in the alkaloid enriched fraction (containing 13.4% strictosamide) that was added. The recovery was calculated using following formula: $(X_{after} - X_{before})/X_{added} \times 100$.

3.3.4. Accuracy

Since the available amount of pure strictosamide was insufficient for conducting a recovery study, an alkaloid enriched fraction was prepared (see Section 2.2.3). The amount of strictosamide in the alkaloid enriched fraction was determined according to the final method, using 20 mg as sample size. The mean alkaloid content was 13.4% (w/w) ($n = 3$). In order to check whether these results were obtained under the repeatability conditions, calculations according to the ISO norm "Accuracy (trueness and precision) of measurement methods and results—Part 6: Use in practice of accuracy values" [12] were performed. The actual range (1.45) was smaller than the critical range of 2.21 indicating that these results are acceptable. Using this enriched fraction the recovery experiment was performed. The recovery was calculated for each of the individually prepared samples ($n = 9$). All results are shown in Table 3.

The mean recovery, the %R.S.D. and the 95% confidence interval were calculated. A mean recovery of 92.2% with %R.S.D. of 9.4% was obtained. The confidence interval ranged from 85.6% to 98.9%. Based on these results the recovery was considered to be significantly different from 100% and exceeds the general acceptance limits for the accuracy so this should be explicitly mentioned with every result obtained with this method. This is still acceptable considering the complexity of the method and the small amounts of strictosamide added. Looking at the results obtained at the different concentration levels separately, it can be concluded that the results at the highest level were close to 100% and the results at the lowest level were the most deviant. The reason the overall recovery differed from 100% was therefore not due to the loss of analyte, since then the reverse observations would have occurred (i.e. lower recovery at higher level of addition). The low recovery could be explained by the small amounts of strictosamide added at the lower levels.

3.3.5. Specificity

The peak purity was investigated by inspecting the UV-spectra in the beginning, at the apex and at the end of the peaks of strictosamide and ajmalicine HCl. No deviations were seen.

4. Conclusion

An HPLC-method was developed to determine the amount of strictosamide and other alkaloids in the stem bark extract of *N. pobeguinii*. Due to the complexity of the crude extract and in order to eliminate column blocking compounds a cleaning step was included in the sample preparation protocol. The best solution was to use Chromabond SPE C_{18} cartridges. Because strictosamide was not commercially available, another alkaloid with similar properties was used as a secondary standard: ajmalicine HCl. This alkaline compound made it obligatory to use a second generation column and to use a solvent system with formic acid and diethylamine in order to obtain a nice peak shape.

The method was validated according to the ICH guidelines. The model was shown to be linear but because of the calibration curve of strictosamide, which was not going through (0, 0), and because of the different correction factors for response in function of the concentration, a graph was made to calculate the correction factor to be used according to the peak area ratio of strictosamide and ajmalicine HCl. The accuracy and the precision were acceptable. The developed method is suitable for the preparation of standardised extracts of the stem bark of *N. pobeguinii*. These extracts will be used in a clinical study for the treatment of malaria in order to prove its efficacy.

Acknowledgement

This work was supported in part by the Special Fund for Research of the University of Antwerp.

References

[1] T. Efferth, Planta Med. 73 (2007) 299.
[2] L. Tona, R.K. Cimanga, K. Mesia, C.T. Musuamba, T. De Bruyne, S. Apers, N. Hermans, S. Van Miert, L. Pieters, J. Totté, A.J. Vlietinck, J. Ethnopharmacol. 93 (2004) 27.
[3] L. Tona, K. Mesia, N.P. Ngimbi, B. Chrimwami, K. Okond'Ahoka, T. Cimanga, S. De Bruyne, N. Apers, J. Hermans, L. Totté, A.J. Pieters, Vlietinck, Ann. Trop. Med. Parasit. 95 (2001) 47.
[4] L. Tona, N.P. Ngimbi, M. Tsakala, K. Mesia, K. Cimanga, S. Apers, T. De Bruyne, L. Pieters, J. Totté, A.J. Vlietinck, J. Ethnopharmacol. 68 (1999) 193.
[5] G.K. Mesia, G.L. Tona, O. Penge, M. Lusakibanza, T.M. Nanga, R.K. Cimanga, S. Apers, S. Van Miert, J. Totté, L. Pieters, A.J. Vlietinck, Ann. Trop. Med. Parasit. 99 (2005) 345.
[6] M. Zeches, B. Richard, L. Gueye-M'Bahia, L. Le Men-Olivier, C. Delaude, J. Nat. Prod. 48 (1985) 42.
[7] P. Abreu, A. Pereira, Nat. Prod. Lett. 15 (2001) 43.
[8] P. Duez, A. Milcamp, M. Lompo, P. Guissou, M. Hanocq, J. Planar Chromat. – Mod. TLC 7 (1994) 5.
[9] C.A.J. Erdelmeier, A.D. Wright, J. Orjala, B. Baumgartner, T. Rali, O. Sticher, Planta Med. 57 (1991) 149.
[10] ICH, Text on validation of analytical procedures—ICH Harmonised Tripartite Guideline, 1994.
[11] ICH, Validation of analytical procedures: methodology—ICH Harmonised Tripartite Guideline, 1996.
[12] Belgian Institute for Normalisation (BIN), NBN ISO 5725-6, 1996.

Talanta 76 (2008) 441–447

Contents lists available at ScienceDirect

Talanta

journal homepage: www.elsevier.com/locate/talanta

Selectivity of solid-contact Ag potentiometric sensors based on thiacalix[4]arene derivatives

G.A. Evtugyn*, I.I. Stoikov, S.V. Belyakova, E.E. Stoikova, R.V. Shamagsumova, A.Yu. Zhukov, I.S. Antipin, H.C. Budnikov

A.M. Butlerov' Chemistry Institute, Kazan State University, Kremlevskaya Street, 18, Kazan, 420008, Russia

ARTICLE INFO

Article history:
Received 4 September 2007
Received in revised form 17 March 2008
Accepted 21 March 2008
Available online 28 March 2008

Keywords:
Potentiometric sensor
Thiacalixarene
Host–guest complexation
Silver determination

ABSTRACT

Potentiometric sensors based on glassy carbon electrode covered with polyaniline and thiacalix[4]arenes containing amidopyridine, morpholide, pyrrolidide and hydrazide functional groups in cone, partial cone and 1,3-alternate conformations have been developed and applied for determination of Ag^+ ions in the range from 1.0×10^{-2} to 4.0×10^{-7} M and limits of detection from 1×10^{-7} to 3.5×10^{-8} M. The sensitivity of Ag^+ detection decreases in the following range of thiacalix[4]arene substituents: morpholide > pyrrolidide > amidopyridine > hydrazide. Potentiometric selectivity coefficients predominantly showed binding of Ag^+, Hg(II) and Fe(III) ions over other transient and alkali metals. The influence of functional groups and conformation of receptor on the selectivity of the sensor response was investigated. As shown, selectivity and sensitivity of Ag^+ determination depends on the steric accessibility of the binding site and flexibility of the receptor structure. For Fe(III) ions, changes of the sensor potential are also determined by their implementation in redox reactions of polyaniline.

1. Introduction

The interest to the development of novel potentiometric sensors and their application in biology, medicine, environmental monitoring, industry and agriculture is currently stimulated by the advantages they possess, i.e. low cost, simple operation, flexible production, a wide range of concentrations to be determined, adequate sensitivity and selectivity [1]. Current research activity in this area includes the construction of maintenance-free sensors with high stability of the response and diverse selectivity toward analytes [2,3]. This can be achieved by combination of novel neutral ionophores with conducting polymers which provide ion-to-electron transduction and can be used as a matrix for incorporating the specific receptors or other additives entrapped into the polymer film due to electrostatic interactions.

Polyaniline (PANI) [4–7], polythiophene derivatives [8–11], polypyrrole [7,11–14] polyanisidine [7], polycarbazole [15] were investigated in the assembly of solid-contact potentiometric sensors. For PANI, strong pH-sensitivity of its potential can limit its sensor applications. However, the use of additional polymeric membranes with lipophilic salts and PANI incapsulation as well as introduction of substituents at nitrogen atom of the polymeric chain partially diminish the pH dependence of the response and increase its reversibility [16–20].

Among other ionophores, substituted calixarenes and their thioanalogs have been intensively investigated in the past two decades as recognition elements toward inorganic ions and some organic species [21–23]. The calixarene moiety establishes pre-determined coordination of the binding sites and hence makes it possible to control the reactivity and selectivity of the receptors toward various organic and inorganic compounds. Thus the calix[4]arenes containing pendant ether, ester, amide and ketonic groups as well as mono- and bis-calix(crowns) exhibit a selective response toward alkali-earth metal ions [24–27]. The introduction of sulfur and nitrogen atoms into the substituents increases the interaction of the calixarenes with soft transient metals (Ag, Pb and Hg). Disubstituted arylamide [28] and tetrasubstituted carboxyphenyl azo [29] calix[4]arenes show selective binding of Pb(II) ions. In comparison with parent calixarenes, thiacalixarenes offer additional opportunities for binding metal ions which can also coordinate at bridging sulfur atoms [30]. Recently, a number of substituted thiacalixarenes with π-coordinating centers was characterized in terms of potentiometric selectivity for Ag(I) determination. The detection limit of 3×10^{-11} M was found for bridged thiacalixarenes in potentiometric measurements [31]. Unsubstituted thiacalix[4]arene and *p-tert*-butylthiacalixarene were deposited by vacuum evaporation onto the gold electrode and active part of ISFET and used for Cu(II) determination [32–34]. Sulfonated thiacalixarene derivatives were applied for pre-column concentration of Ni(II) in the pres-

* Corresponding author.
E-mail address: Gennady.Evtugyn@ksu.ru (G.A. Evtugyn).

0039-9140/$ – see front matter © 2008 Elsevier B.V. All rights reserved.
doi:10.1016/j.talanta.2008.03.029

ence of other transient metals in ion-pair reversed phase HPLC [35]. Cd(II)-selective sensors have been fabricated by involvement of *p-tert*-butylthiacalix[4]arene and thiacalix[4]arene in poly(vinyl chloride) membrane [36].

The selectivity of metal ion binding by thiacalixarenes with *O*,*S*,*N*-ligating and π-coordinate groups was investigated also by picrate extraction and NMR titration in organic solvents. Preferable silver extraction was described with disubstituted thiacalixarens with alkoxy groups [37] and tetrasubstituted thiacalixarenes with amido- and carbamoylmethoxy functions [38]. (Thia)calix[4](*O*,*S*,*N*)crowns were found to be stronger binders than the π-coordinate molecules and thiacalixarene receptors were generally superior to calixarenes [38].

The following progress in the development of selective receptors on thiacalixarene platform can be related to the regio- and stereoselective functionalization of thiacalixarene precursors. Recently, one-step methods for the synthesis of tetrasubstituted thiacalix[4]arenes based on the alkylation of hydroxy-groups at the lower rim of a macrocycle by appropriate α-halogencarbonylic compounds in the presence of alkali metal ions were described [39–41]. Due to the templating effect of the metal cation, selected conformational isomers, i.e. *cone*, *partial cone* and *1,3-alternate*, can be obtained with high yield. Some of the products obtained, e.g. tetrakis(hydroxycarbonylmethoxy)-thiacalix[4]arene, are used for further modification to introduce functional groups with high complexation abilities toward metal ions. This approach was successfully applied for the synthesis of (2-pyridyl)-carbamoylmethoxy derivative of thiacalix[4]arene which showed selective binding of Ag^+, Fe^{3+} and Hg^{2+} ions [42]. The receptor was used in the assembly of the thin-film solid-contact potentiometric sensor based on glassy carbon electrode covered with PANI [42].

In this work, the potentiometric selectivity of various Ag(I) selective receptors based on tetrasubstituted *N*-containing thiacalix[4]arenes was investigated to establish the effect of substituents and macrocycle conformation on the response of the solid-contact potentiometric sensor.

2. Experimental

2.1. Chemicals

p-tert-Butylphenol used for synthesis of tetraacid derivative of thiacalix[4]arene and aniline for electropolymerization were purchased from "EcRos", Russia. Prior to use, aniline was distilled under vacuum and stored under argon at 4 °C. All other chemicals were of analytical-reagent grade. Metal nitrates and sulfates used for selectivity investigation were dissolved in bidistilled water, and mercury nitrate in 0.1 mol L^{-1} nitric acid.

2.2. Thiacalix[4]arene receptor synthesis

The thiacalixarene derivatives investigated (structures see (1)) were synthesized from the tetraacid derivative of thiacalix[4]arene, i.e. 5,11,17,23-tetra-*tert*-butyl-25,26,27,28-tetrakis (hydroxylcarbonylmethoxy)-2,8,14,20-tetrathiacalix[4]arene obtained as described elsewhere [43].

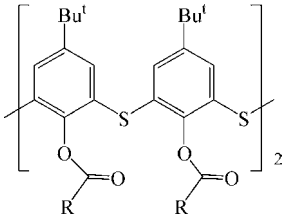

(1)

Functional group of the substituent	R	Stereoisomer		
		Cone	*Partial cone*	*1,3-Alternate*
2-Pyridylamido	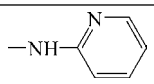	**1a**	**1b**	**1c**
Morpholide	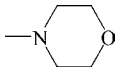	**2a**	**2b**	**2c**
Pyrrolidide	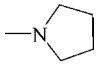	**3a**	**3b**	**3c**
Hydrazide	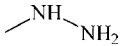	**4a**	**4b**	**4c**

Briefly, appropriate isomers, i.e. *cone*, *partial cone* or *1,3-alternate*, of tetracid derivative (1 g, 1.05×10^{-3} mol) were mixed with $SOCl_2$ (10 mL, 0.084 mol). The mixture was refluxed for 1.5 h, then the excess of $SOCl_2$ was evaporated and 50 mL of amine solution in dichloromethane (3.36×10^{-3} mol of pirrolidine, morpholine, 2-aminopyridine or hydrazine sulfate + 5 mL of triethylamine, 0.04 mol) were added and left overnight stirring. After that, the reaction was stopped with HCl. The organic layer was separated, dried (mol. sieves, 3 Å) and evaporated in vacuum. The remainder was crystallized from the ethyl alcohol/methylene chloride. Synthesis and physicochemical characteristics of 2-pyridylamido derivative (*1,3-alternate*, **1c**) were described in [42] and hydrazides in [44].

5,11,17,23-Tetra-*tert*-butyl-25,26,27,28-tetrakis[(2-pyridyl)-carbamoyl-methoxy]-2,8,14,20-tetrathiacalix[4]arene *cone* (**1a**). Yield: 1.95 g (70%). mp: 245 °C. ^{1}H NMR (300 MHz, 373 K, $CDCl_3$,) δ 10.59 (s, 4H; NH), 7.39 (s, 8H; ArH), 8.26–8.23, 7.99–7.96, 7.56–7.50, 6.95–6.90 (m, 16H; PyH), 5.15 (s, 8H; OCH_2CO), 1.11 (s, 36H, $(CH_3)_3C$). ^{13}C NMR(75 MHz, $CDCl_3$) δ 167.4, 157.6, 151.1, 147.9, 147.7, 137.8, 135.1, 128.3, 119.6, 114.4, 75.1, 34.3, 31.1. IR (KBr) λ_{max} 1698, 2870, 2962, 3288. MS (ESI): calcd for $[M]^+$ m/z = 1256.4, found m/z = 1256.5, $[M+Na]^+$ m/z = 1279.4, found m/z = 1279.3 El. anal. calcd for $C_{68}H_{72}N_8O_8S_4$: C, 64.94, H, 5.77, N, 8.91, S, 10.20. Found: C, 64.87, H, 5.65%, N, 8.90, S, 10.34.

5,11,17,23-Tetra-*tert*-butyl-25,26,27,28-tetrakis[(2-pyridyl)-carbamoyl-methoxy]-2,8,14,20-tetrathiacalix[4]arene *partial cone* (**1b**). Yield: 2.27 g (82%). mp: 226 °C. ^{1}H NMR (300 MHz, 373 K, $CDCl_3$,) δ 9.22 (s, 1H; NH), 9.94 (s, 2H; NH), 10.66 (s, 1H; NH), 8.34–8.22, 8.01–7.33, 7.04–6.91 (m, 16H; PyH), 7.96 (s, 2H, ArH), 7.74 (s, 2H, ArH), 7.57 (d, J = 2.5 Hz, 2H, ArH), 7.47 (d, J = 2.5 Hz, 2H, ArH), 5.26 (d, J = 15.2 Hz; 4H, OCH_2CO), 5.24 (s, 2H; OCH_2CO), 5.00 (s, 2H; OCH_2CO), 4.96 (d, J = 15.2 Hz; 4H, OCH_2CO), 3.81 (s, 2H; OCH_2CO), 1.31 (s, 9H, $(CH_3)_3C$), 0.98 (s, 18H, $(CH_3)_3C$), 0.95 (s, 9H, $(CH_3)_3C$). ^{13}C NMR(75 MHz, $CDCl_3$) δ 167.3, 167.2, 166.0, 157.8, 150.8, 148.3, 148.1, 148.1, 148.0, 137.9, 137.8, 137.7, 136.5, 135.5, 133.8, 131.9, 128.3, 127.6, 127.4, 127.3, 119.9, 119.7, 119.6, 114.2, 114.0, 113.8, 75.4, 73.5, 71.3, 34.5, 34.3, 34.2, 31.2, 30.8, 30.6. IR (KBr) λ_{max} 1253, 1700, 2870, 2961, 3287, 3374, 3457. MS (ESI): calcd for $[M]^+$ m/z = 1256.4, found m/z = 1256.4, $[M+Na]^+$ m/z = 1279.4, found m/z = 1279.3. El. anal. calcd for $C_{68}H_{72}N_8O_8S_4$: C, 64.94, H, 5.77, N, 8.91, S, 10.20. Found: C, 64.41, H, 5.73, N, 8.45, S, 9.82.

5,11,17,23-Tetra-*tert*-butyl-25,26,27,28-tetrakis[(*N*-morpholidocarbonyl)-methoxy]-2,8,14,20- tetrathiacalix[4]arene *cone* (**2a**). Yield: 1.20 g (93%). mp: 258 °C. ^{1}H NMR (300 MHz, 373 K, $CDCl_3$,) δ 7.30 (s, 8H; ArH), 5.34 (s, 8H; OCH_2CO), 3.71–3.68 (m, 16H; $-CH_2OCH_2-$), 3.60–3.57 (m, 16H; $-N(CH_2CH_2)_2O$), 1.08 (s, 36H, $(CH_3)_3C$). ^{13}C NMR(75 MHz, $CDCl_3$) δ 166.1, 156.8, 146.4, 132.2, 127.4, 67.8, 66.6, 45.90, 41.9, 34.2, 31.9. IR (KBr) λ_{max} 1253, 1662, 2857, 2961. MS (ESI): calcd for $[M+Na]^+$ m/z = 1251.5, found m/z = 1251.4. El. anal. calcd for $C_{64}H_{84}N_4O_{12}S_4$: C, 62.52;

H, 6.89; N, 4.56; S, 10.43. Found: C, 62.42; H, 6.99; N, 4.56; S, 10.26.

5,11,17,23-Tetra-*tert*-butyl-25,26,27,28-tetrakis[(*N*-morpholidocarbonyl)methoxy]-2,8,14,20-tetrathiacalix[4]arene *partial cone* (**2b**). Yield: 1.06 g (82%). mp: 149 °C. ^{1}H NMR (300 MHz, 373 K, $CDCl_3$) δ 7.76 (s, 2H, ArH), 7.60 (d, J = 2.5 Hz, 2H; ArH), 7.59 (s, 2H; ArH), 7.06 (d, J = 2.5 Hz, 2H, ArH), 5.24 (s, 2H; OCH_2CO), 4.80 (d, J = 12.5 Hz; 4H, OCH_2CO), 4.78 (s, 2H; OCH_2CO), 4.55(d, J = 12.5 Hz; 4H, OCH_2CO), 3.82–3.22 (m, 32H, $-N(CH_2CH_2)_2O$), 1.38 (s, 9H; $(CH_3)_3C$), 1.31 (s, 9H; $(CH_3)_3C$), 1.06 (s, 18H; $(CH_3)_3C$). ^{13}C NMR(75 MHz, $CDCl_3$) δ 166.1, 156.8, 146.3, 132.1, 127.4, 67.7, 66.5, 45.9, 41.9, 34.2, 31.1. IR (KBr) λ_{max} 1260, 1654, 2859, 2904, 2960. MS (ESI): calcd for $[M+Na]^+$ m/z = 1251.5, found m/z = 1251.3. El. anal. calcd for $C_{64}H_{84}N_4O_{12}S_4$: C, 62.52; H, 6.89; N, 4.56; S, 10.43. Found: C, 62.11; H, 6.95; N, 4.36; S, 10.58.

5,11,17,23-Tetra-*tert*-butyl-25,26,27,28-tetrakis[(*N*-morpholidocarbonyl)methoxy]-2,8,14,20-tetrathiacalix[4]arene *1,3-alternate* (**2c**). Yield: 0.98 g (76%). mp: 255 °C. ^{1}H NMR (300 MHz, 373 K, $CDCl_3$) δ 7.51 (s, 8H; ArH), 4.68 (s, 8H; OCH_2CO), 3.62 (m, 16H; $-CH_2OCH_2-$), 3.35–3.22 (m, 16H; $-N(CH_2CH_2)_2O$), 1.26 (s, 36H; $(CH_3)_3C$). ^{13}C NMR(75 MHz, $CDCl_3$) δ 166.1, 156.8, 146.3, 132.1, 127.4, 67.7, 66.5, 45.9, 41.9, 34.2, 31.1. IR (KBr) λ_{max} 1265, 1651, 2860, 2905, 2959. MS (ESI): calcd for $[M+Na]^+$ m/z = 1251.5, found m/z = 1251.3. El. anal. calcd for $C_{64}H_{84}N_4O_{12}S_4$: C, 62.52; H, 6.89; N, 4.56; S, 10.43. Found: C, 62.34; H, 6.98; N, 4.49; S, 10.29.

5,11,17,23-Tetra-*tert*-butyl-25,26,27,28-tetrakis[(*N*-pyrrolididocarbonyl)methoxy]-2,8,14,20-tetrathiacalix[4]arene *cone* (**3a**). Yield: 1.03 g (84%). mp: 248 °C. ^{1}H NMR (300 MHz, 373 K, $CDCl_3$) δ 7.27 (s, 8H; ArH), 5.21 (s, 8H; OCH_2CO), 3.62 (t, J = 6.8 Hz, 8H, $-N(CH_2CH_2)_2$), 3.44 (t, J = 7.0 Hz, 8H, $-N(CH_2CH_2)_2$), 2.00–1.79 (m, 16H; $-N(CH_2CH_2)_2$), 1.07 (s, 36H; $(CH_3)_3C$). ^{13}C NMR (75 MHz, $CDCl_3$) δ 166.8, 157.9, 145.3, 133.9, 128.7, 72.0, 45.4, 33.7, 30.9, 26.0, 23.8. IR (KBr) λ_{max} 1268, 1653, 2871, 2963. MS (ESI): calcd for $[M+Na]^+$ m/z = 1187.5, found m/z = 1187.4. El. anal. calcd for $C_{64}H_{84}N_4O_8S_4$: C, 65.82; H, 7.01; N, 4.87; S, 11.16. Found: C, 65.49; H, 7.38; N, 4.65; S, 11.03.

5,11,17,23-Tetra-*tert*-butyl-25,26,27,28-tetrakis[(*N*-pyrrolididocarbonyl)methoxy]-2,8,14,20-tetrathiacalix[4]arene *partial cone* (**3b**). Yield: 1.16 g (95%). mp: 255 °C. ^{1}H NMR (300 MHz, 373 K, $CDCl_3$,) δ 7.85 (s, 2H; ArH), 7.62 (d, J = 2.4 Hz; 2H, ArH), 7.55 (s, 2H; ArH), 7.02 (d, J = 2.4 Hz; 2H, ArH), 4.95 (s, 2H; OCH_2CO), 4.70 (s, 2H; OCH_2CO), 4.65 (d, J = 14.5 Hz; 4H, OCH_2CO), 4.71 (d, J = 14.5 Hz; 4H, OCH_2CO), 3.57–3.42 (m, 12H; $-N(CH_2CH_2)_2$), 3.31–3.24 (m, 4H; $-N(CH_2CH_2)_2$), 1.94–1.73 (m, 16H; $-N(CH_2CH_2)_2$), 1.39 (s, 9H; $(CH_3)_3C$), 1.29 (s, 9H; $(CH_3)_3C$), 1.05 (s, 18H; $(CH_3)_3C$). ^{13}C NMR (75 MHz, $CDCl_3$) δ 167.5, 165.5, 165.7, 159.1, 157.8, 157.7, 146.1, 146.0, 144.1, 134.8, 134.6, 134.2, 133.9, 128.3, 128.1, 126.7, 72.9, 70.6, 67.5, 46.2, 45.8, 45.6, 45.4, 45.2, 34.2, 33.9, 33.9, 31.2, 31.1, 31.0, 26.1, 24.0, 23.9, 23.8. IR (KBr) λ_{max} 1260, 1653, 2871, 2961. MS (ESI): calcd for $[M+Na]^+$ m/z = 1187.5, found m/z = 1187.3. El. anal. calcd for $C_{64}H_{84}N_4O_8S_4$: C, 65.82; H, 7.01; N, 4.87; S, 11.16. Found: C, 65.80; H, 7.26; N, 4.76; S, 11.39.

5,11,17,23-Tetra-*tert*-butyl-25,26,27,28-tetrakis[(*N*-pyrrolididocarbonyl) methoxy]-2,8,14,20-tetrathiacalix[4]arene *1,3-alternate* (**3c**). Yield: 1.10 g (90%). mp: 272 °C. ^{1}H NMR (300 MHz, 373 K, $CDCl_3$,) δ 7.53 (s, 8H; ArH), 4.56 (s, 8H; OCH_2CO), 3.47 (t, J = 6.0 Гц, 8H, $-N(CH_2CH_2)_2$), 3.03 (t, J = 6.0 Гц, 8H, $-N(CH_2CH_2)_2$), 1.82–1.68 (m, 16H; $-N(CH_2CH_2)_2$), 1.24 (s, 36H; $(CH_3)_3C$). ^{13}C NMR (75 MHz, $CDCl_3$) δ 165.9, 157.6, 146.0, 132.4, 127.9, 69.9, 45.8, 34.1, 31.1, 26.2, 23.9. IR (KBr) λ_{max} 1260, 1653, 2872, 2953. MS (ESI): calcd for $[M+Na]^+$ m/z = 1187.5, found m/z = 1187.3. El. anal. calcd for $C_{64}H_{84}N_4O_8S_4$: C, 65.82; H, 7.01; N, 4.87; S, 11.16. Found: C, 65.64; H, 7.36; N, 4.65; S, 11.29.

2.3. Potentiometric sensor preparation

Glassy carbon electrode of 3 mm in diameter was mechanically polished to a mirror like surface and rinsed with acetone, KOH and H_2SO_4. After that, the electrode was conditioned in 0.2 M H_2SO_4 at +0.1 V for 3 min followed by the potential cycling between −0.2 and +1.0 V at 40 mV s^{-1} for 10 min. After cleaning, the electrode was placed into the solution of 0.07 M aniline in 0.2 M H_2SO_4 and the potential was scanned between −0.3 and +0.8 V at 50 mV s^{-1}. Five cycles of potential scanning were used to obtain a dense continuous polymer film. Voltammetric experiments were conducted using AUTOLAB PGSTAT 302 (Ecochemie, The Netherlands). After the polyaniline formation, 10 μL of 1.0×10^{-3} M thiacalix[4]arene receptor solution in chloroform were placed onto the electrode and let dry at room temperature. When stored in dry conditions, the potentiometric sensor was conditioned before measurement in the supporting electrolyte for 10 min. Non-conditioned sensors showed much slower response toward Ag^+ ions and often larger potential drift. All the measurements were conducted at least three times and the average EMF values were calculated. Between measurements, the electrodes were treated with 0.01 M EDTA for 5 min followed by 5 min conditioning in supporting electrolyte. Signal recovery for at least 10 consecutive measurements of 2×10^{-4} M $AgNO_3$ was about 95–98%.

2.4. Potentiometric measurements

All the measurements were performed at room temperature 23 ± 2 °C. The reference Ag/AgCl electrode was separated from the measurement cell by a salt bridge filled with 0.1 M $NaNO_3$. The cell set up for the EMF measurement was as follows: glassy carbon, polyaniline, thiacalix[4]arene receptor|test solution|salt bridge (0.1 M $NaNO_3$)||3 M KCl|AgCl, Ag. The EMF was measured in a stirring solution with the digital ionometer Ecotest-001 ("Econix-Expert", Moscow, Russia) connected to PC. The unbiased potentiometric selectivity coefficients $\log K_{Ag/Me}$, were determined by the separate solution method (SSM) with 0.01 M solutions of Ag^+ and interfering ions [1] in accordance with Eq. (2)

$$\log K_{Ag/Me} = \frac{zF(E^0_{Me} - E^0_{Ag})}{RT} \quad (2)$$

where E^0_{Me} and E^0_{Ag} are the EMF values measured for the interfering ion, Me^{z+}, and Ag^+, respectively, and extrapolated to unit activity and z is the charge of the primary ion. The activities of ions were calculated from the modified form of the Debye–Hückel equation [45]. In some cases, a mixed solution method (MSM) was used for calculation of potentiometric selectivity coefficients.

3. Results and discussion

3.1. Analytical performance of thiacalixarene based potentiometric sensors

All the potentiometric sensors developed exhibit a sharply defined reproducible response toward 1×10^{-2} to $n \times 10^{-8}$ M Ag^+ in the pH range of its hydrolytic stability (pH 1–7). The content of the surface layer, i.e. the number of the cycles of potential scanning for aniline electropolymerization and the amount of thiacalixarene receptor per electrode, was optimized previously [42] with **1c** receptor and confirmed here for other substituted thiacalix[4]arenes investigated. After five cycles of potential cycling, a uniform fine-grained film of PANI is formed. In accordance with AFM images, PANI forms rounded clusters of 50–150 nm aggregates evenly distributed along the surface. Nearly full covering

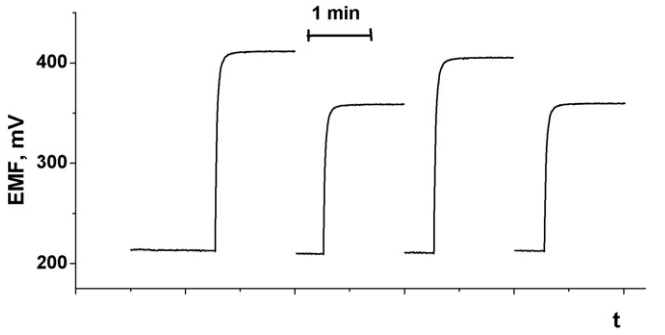

Fig. 1. The repeated response of the sensors with receptor **3a** toward alternating injection of 5×10^{-4} and 5×10^{-5} M $AgNO_3$. The potential was not recorded during the time when the electrode was treated with EDTA solution and solutions replacement (ca. 10 min).

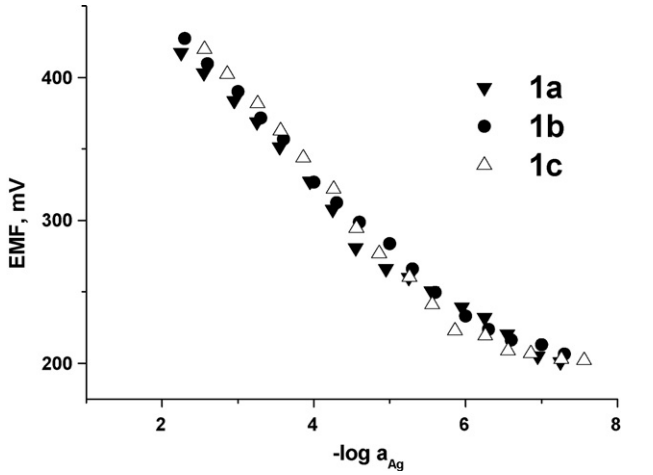

Fig. 2. The determination of Ag^+ ions with the potentiometric sensor contained polyaniline and thiacalix[4]arenes **1a–c** (140 nmol cm^{-2}), 1.0×10^{-3} M Na_2SO_4, pH 6.5.

of the electrode with PANI layer is also confirmed by well reproducible pH response of the sensor in the pH range from 1.0 to 5.0 with the slope of about 55.6 ± 1.2 mV per pH unit. The thiacalix[4]arene coverage smoothes the pH dependence of the potential and decreases its slope to 50 ± 2 mV for 50–70 nmol cm^{-2} and down to 35 ± 3 mV for 100–140 nmol cm^{-2}. Probably, the partial suppression of the pH-sensitivity of PANI potential is caused by basic features of amino groups of the thiacalix[4]arene substituents. All the following experiments were performed with 140 nmol cm^{-2} of thiacalix[4]arene. This loading provides quite stable response toward metal ions with a drift of about 0.1 mV s^{-1} in the measurement series. Lower amounts of the receptor do not form a dense film on the PANI layer. This results in a much higher deviation of the signal in a series of the sensors. Higher loading increases the response time from 12–20 s in optimal conditions to about 1 min and even more because of the decay of conductivity of the surface layer and its permeability for electrolyte ions. Again, this is followed by an increase in the confidence interval both for the EMF value measured and Ag^+ concentration calculated from the calibration curve.

The reproducibility of the response for four consecutive injections of 5×10^{-4} and 5×10^{-5} M $AgNO_3$ on the same sensor is shown on Fig. 1 for **3a** as an example.

The deviation of the background potential value between the measurements did not exceed 5 mV and the recovery of the response to the same Ag^+ concentration not less as 95%. The drift of the potential tends to increase with the number of measurements from initial 0.1–0.2 mV s^{-1} to about 1 mV s^{-1} for sixth measurement. Between measurements, the sensor was recovered after 5 min treatment with 0.01 M EDTA. For six different sensors, the R.S.D. was about 4.3–6.5% in the same conditions. The accuracy of EMF measurement depended on the response time, i.e. the longer the response the higher its R.S.D. value. This makes it possible to conclude that the deviation of the signal is mainly related to the diffusional limitations of the access of the binding site within the surface layer. In the series of measurements each sensor provides at least 15 measurements with the maximum total shift of the background potential of about 50 mV.

The calibration curves of Ag^+ ion obtained for the sensors modified with **1a–c** are presented as an example in Fig. 2.

All the conformational isomers show similar response to Ag^+ ion with the slope of the linear piece of the curve from −57 to −62 mV. The limit of Ag^+ detection calculated from S/N = 3 ratio was found to be $(2.5–8) \times 10^{-8}$ M. The analytical performance of thiacalix[4]arene based sensors is summarized in Table 1. The response time was determined as the time after the injection of 5.0×10^{-4} M $AgNO_3$ which is required to reach its stationary value with the drift equal to 0.1 mV s^{-1} after the injection.

Although the difference in the characteristics of Ag^+ determination seems rather small, the sensitivity of Ag^+ detection decreases in the following range of thiacalix[4]arene substituents: morpholide > pyrrolidide > amidopyridine > hydrazide. Pyrrolidine derivative **3c** gave the lowest limit of detection whereas hydrazide **4b** (*partial cone*) the biggest one. The limits of Ag^+ detection observed are lower than most reported for other S-containing calixarene derivatives. Thus, di- and tetrasubstituted calix[4]arenes

Table 1
Analytical performance of thiacalix[4]arene based potentiometric sensors for Ag^+ determination

Compound	Limit of detection (M)	Concentration range (M)	Calibration slope (mV)	Response toward 2.0×10^{-4} M $AgNO_3$	
				Response time (s)	R.S.D. (%)[a]
1a	5.0×10^{-8}	1×10^{-2} to 4×10^{-7}	−57	20	2.0
1b	7.0×10^{-8}	1×10^{-2} to 2×10^{-7}	−55	20	2.3
1c	2.5×10^{-8}	1×10^{-2} to 5×10^{-7}	−62	20	1.4
2a	5.5×10^{-8}	2×10^{-2} to 8×10^{-7}	−62	35	3.2
2b	7.0×10^{-8}	2×10^{-2} to 1×10^{-6}	−68	25	2.2
2c	5×10^{-8}	$2 \times 10^{-2}$to 2×10^{-6}	−70	20	2.5
3a	3.5×10^{-8}	1×10^{-2} to 4×10^{-7}	−62	20	1.6
3b	4.0×10^{-8}	1×10^{-2} to 2×10^{-7}	−62	22	1.8
3c	2.0×10^{-8}	1×10^{-2} to 5×10^{-7}	−65	23	1.6
4a	6.0×10^{-8}	1×10^{-2} to 6×10^{-7}	−58	30	1.6
4b	1.0×10^{-7}	2×10^{-2} to 1×10^{-6}	−56	25	1.8
4c	4×10^{-8}	1×10^{-2} to 4×10^{-7}	−56	30	1.6

[a] Three measurements with the same sensor, 0.01 M EDTA treatment (5 min) between the measurements.

Table 2
Selectivity coefficients $\log(K_{Ag/M})$ of potentiometric sensor with thiacalix[4]arene receptors **(1–4)a–c** by SSM method

Ion	PANI[a]	1a	1b	1c	2a	2b	2c	3a	3b	3c	4a	4b	4c
H	–			3.11			3.50			4.67			4.11
K	2.60[a]	4.80	3.96	4.95	4.77	3.11	4.43	4.68	4.39	4.39	6.53	4.92	4.85
Na	2.80[a]	4.45	4.60	5.26	5.16	5.04	3.95	4.30	4.19	3.63	6.28	5.41	5.67
Cu(II)	4.04	4.63	3.30	3.90	4.75	4.61	5.10	5.40	4.70	4.01	5.62	6.31	5.79
Cd	4.20	6.00	4.44	5.90	5.34	5.70	5.16	4.90	5.83	4.38	7.10	6.90	6.30
Hg(II)[b]	0.50[a]	−1.62	−1.62	−1.78	−0.72	−1.78	−1.79	0.30	0.65	1.25	0.74	0.05	2.76
Fe(III)	−1.20	0.20	3.48	−0.67	−0.23	−0.50	0.26	1.54	0.59	0.06	0.30	0.35	1.20

[a] Calculated from the data presented in [42].
[b] Measurements in 0.1 M nitric acid.

with thioetheric groups in PVC membrane provided the detection of $10^{-4.5}$ M Ag^+ [46]. Mono- and dibenzothiazolyl substituted calix[4]arenes showed limits of detection down to 10^{-5} M [47]. However, recently reported bridged thiacalixarene derivatives made it possible to detect down to 3×10^{-11} M Ag^+ [31]. Some other ionophores used in solid-contact potentiometric sensors also showed higher sensitivity of their Ag^+ response (e.g. Cu(II) *o*-xylylene bis(*N*,*N*-diisobutyldithiocarbamate) [48], poly(3-octylthiophene) [49]) which is predominantly in nanomolar concentration range. It should be mentioned that these results were obtained with composite membranes containing besides conductive polymers additional ionic sites (lipophilic salts) dispersed in inert polymeric matrices. This is hardly possible to do with the format of the surface layer deposition described in this work, but probably this will improve the analytical performance of similar solid-contact sensors exploiting the receptors synthesized.

Within the conformers of the same structure, better analytical characteristics of Ag^+ detection were obtained with *1,3-alternates*. Based on the conformer structure and the content of the surface layer, it could be assumed that *1,3-alternate* is coordinated on the PANI layer in such a manner that one couple of the substituents interacts with the positively charged amino groups of PANI. The second couple on the opposite side of the macrocycle moiety is transversely directed to the electrode plane. Such an orientation is most favorable for the interaction with metal ions not only due to better accessibility of the binding site but also due to the partial shielding of the PANI charge hindering the transfer of the metal ions from the bulk solution to the electrode surface. Other conformers, e.g. *cone* or *partial cone* are preferably placed on the PANI layer with functional groups parallel to the electrode so that their interaction with Ag^+ ions is less effective than that of *1,3-alternate*. Although the receptor loading is rather high to form multi-layered structure on the electrode surface, mutual interactions partially retain the specific orientation of the functional groups of thiacalix[4]arene conformers.

3.2. Selectivity of Ag^+ determination

The unbiased potentiometric selectivity coefficients $\log K_{Ag/Me}$ determined by the separate solution method are presented in Table 2. All the thiacalix[4]arenes selectively bind Ag^+ ions over to other alkali and most transient metal ions tested. Fe(III) and Hg(II) ions override the Ag^+ effect. These ions are partially hydrolyzed in aqueous solutions and their notations, i.e. Fe(III) and Hg(II), involve all the forms of the ions present in solution.

Also, the selectivity of the response toward H^+ ions was determined for *1,3-alternates* which were shown to largely affect the pH-sensitivity of the potential in comparison with other stereoisomers. The efficiency of Ag^+ binding predominates the pH-sensitivity of PANI so that the appropriate selectivity coefficients were similar to those of alkali metals.

The comparison of the coefficients obtained with those recalculated from data presented in [42] shows that hydrazides **4a–c**, and mainly *1,3-alternate*, are most selective receptors which improves the selectivity of PANI toward alkali and transient metals. In addition to them, other receptors also improve the selectivity of PANI toward selected ions, preferably, Hg(II) and Fe(III) but to a less extent considering the whole pool of the metals tested. It should be also mentioned that the receptors suppress the pH-sensitivity of the PANI response and make it possible to extend the conditions of response measurements.

As regards the potentiometric sensors developed, Hg(II) most effectively competes with Ag^+ for the binding site of the receptor. Only hydrazide derivatives **4a–c** show a selective signal toward Ag^+. This is probably due to the specific interactions between the hydrazide groups and Hg(II) species followed by partial oxidation of the substituents by nitric acid. Selectivity coefficients of other metals were determined in aqueous solutions and no evidence of receptor instability was observed. Irreversible interaction of **4a–c** with Hg(II) was confirmed by a much lower recovery of the sensor signal. The treatment of the sensors with complexing agents (EDTA, NaCl) resulted in an appreciable shift of their background potential. Hence, the lifetime of the sensors comprising thiacalix[4]arenes **4a–c** was much shorter than that of the other sensors developed. The effect of Hg(II) on the sensor response was less reversible and reproducible (R.S.D. about 3.4–4.5%) than that of other metals within the whole receptor series. For hydrazide derivatives, the drift of the background potential limited the use of appropriate sensor to four consecutive measurements. All the other thiacalix[4]arenes were quite stable both in neutral media and in the presence of nitric acid and showed approximately similar values of potentiometric selectivity in both media.

The increase of the amounts of thiacalix[4]arene results in the regular improvement of the selectivity. This influence is less pronounced for the metals with a rather high $\log K_{Ag/Me}$ value. Thus, for Cu(II) ions, the $\log K_{Ag/Cu}$ value increases by 30% of its value when the concentration of thiacalix[4]arenes changes from 70 to 150 nmol cm^{-2}. The following increase of the thiacalix[4]arene loading does not affect the selectivity but increases the R.S.D. of potentiometric selectivity from 4% (140 nmol cm^{-2}) to 10% (360 nmol cm^{-2}). For Hg(II), the increase of the thiacalix[4]arene loading also improves the selectivity of the signal, but in favor of Hg(II). The $\log K_{Ag/Hg}$ value decays from −0.15 (70 nmol cm^{-2}) to −0.6 (280 nmol cm^{-2} and higher) (see Fig. 3 for **2b** as an example). This coincides well enough with the primary role of host–guest complexation in the signal generation. The higher the surface concentration of the receptor the bigger the difference in the binding of primary and interfering ions.

The behavior of Fe(III) differs from that of most other metals investigated. First, the calibration plots of Fe(III) showed a much higher slope of a linear piece which was observed in a rather narrow interval of its concentration (Fig. 4).

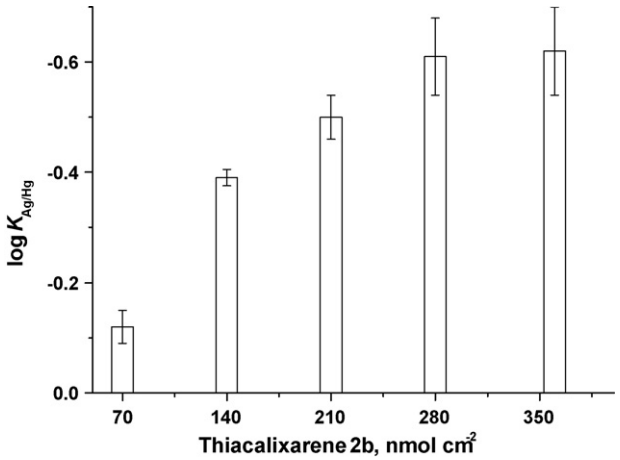

Fig. 3. The dependence of the potentiometric selectivity coefficients log($K_{Ag/Hg}$) on the surface concentration of **2b** receptor.

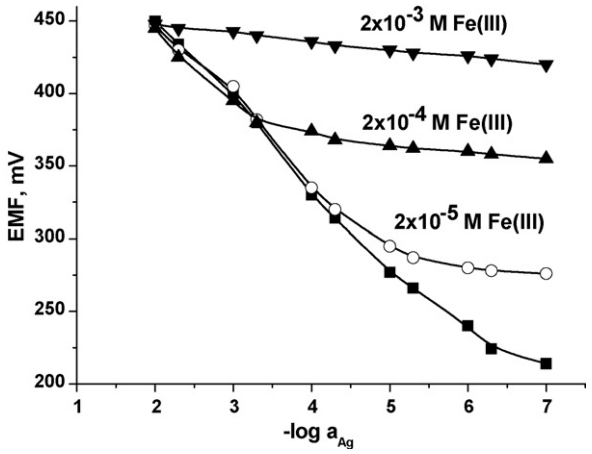

Fig. 5. Interfering effect of Fe^{3+} ions on the Ag^+ signal of potentiometric sensor containing **2c** receptor.

In the presence of Ag^+ ions, the concentration range of the Fe(III) determined is shortened in accordance with the competition of both ions for the binding sites of thiacalix[4]arene receptors. The potentiometric selectivity log $K_{Ag/Fe}$ does not change regularly with the conformation of the receptor and its surface concentration as that calculated for other interfering metals. Contrary to other ions, the highest value of log $K_{Ag/Fe}$ in the series of thiacalix[4]arenes with the same substituents was observed mainly for *partial cone* which provided better conditions for the inclusion of a rather large ion with the highest charge ($z = 3$). Negative values observed for morpholide derivative **2a** (*cone*) and **2b** (partial cone) can be related to the kinetic effects. Potentiometric sensors with these receptors change their potential rather slowly (see Table 1). Contrary to this, Fe(III) showed the shift of the sensor potential in 8–12 s for all the receptors investigated. For this reason, the saturation of the surface layer with Fe(III) ions diminishes their interaction with Ag^+. Many of these specific features can be due to the direct influence of Fe (III) on the redox potential of PANI which preferably exists in the reduced non-doped state in neutral media. In this respect, the maximum shift of the EMF, observed on calibration curves (more than 400 mV, see Fig. 4) corresponds to the difference in standard redox potentials of Fe(III)/Fe(II) and that of PANI. Thiacalix[4]arene receptors alter the access of Fe(III) ions to the PANI and its reactivity in appropriate redox reactions. This mechanism is also proved by the dependence of the potential of polyaniline covered electrode on the Fe(III) concentrations in absence of any thiacalix[4]arene receptors. The initial potential of the electrode after its contact with Fe(III) can be effectively recovered after 10 min treatment with hydroquinone solution.

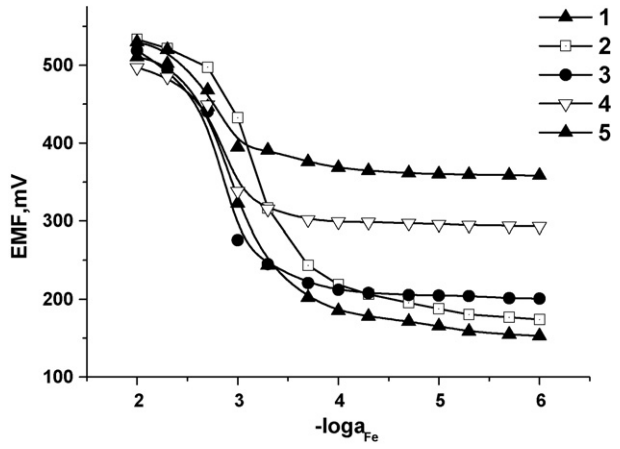

Fig. 4. Variation of the sensor signal with Fe(III) activity in the presence of Ag^+ ions. Potentiometric sensor includes **3c** (140 nmol cm^{-2}). 1.0×10^{-3} M Na_2SO_4, pH 6.5. $AgNO_3$ 0 M (1), 1×10^{-6} M (2), 1×10^{-5} M (3) 1×10^{-4} M (4) 5×10^{-4} M (5).

The influence of Fe(III) and Hg(II) on the sensor signal toward Ag^+ ions in mixed runs measurements diminishes the linear piece of the calibration curve whereas its slope remains about the same in accordance with Nikolsky Eq. (3).

$$\mathrm{EMF} = \mathrm{Const} + S \log \left[a_{\mathrm{Ag}} + \sum K_{\mathrm{Ag/Me}} a_{\mathrm{Me}}^{1/z_{\mathrm{Me}}} \right], \quad (3)$$

in which S is the sensitivity of determination [29]. Fig. 5 illustrates the interfering effect of Fe(III) on the signal of the sensor containing the morpholide functional group **2c** (*1,3-alternate*). The potentiometric selectivity coefficients calculated from the variation of the signal with the interfering ion concentration in the presence of constant amounts of Ag^+ ions coincided well with those obtained by the separate solution method. Thus, for Fe(III) ions $K_{Ag/Me}$ (MSM) varied from 0.08 to 1.2 and for Hg(II) from 0.01 to 10. This indicates that primary and interfering ions interact with the components of the surface layer (thiacalix[4]arene receptor and polyaniline) quite independently and do no affect each other.

The influence of the redox sensitivity of PANI on the sensor potential is considered much stronger than the pH-sensitivity [16]. To quantify this effect, the dependence of the sensor potential on the ratio of $Fe(CN)_6^{3-}/Fe(CN)_6^{4-}$ was investigated. For PANI itself, the slope of the dependence was quite similar to that of pH-sensitivity (55 ± 2 mV for the interval of log[$Fe(CN)_6^{3-}/Fe(CN)_6^{4-}$] from 1 to 4) at pH 5.1. For potentiometric sensors contained *1,3-alternates*, the potentiometric slopes of appropriate curves diminished to 25–35 mV. This is sufficiently lower than the effect of additional ionic sites in PVC membranes investigated earlier but gives a chance to avoid interfering effect of matrix component while the sensors are used for the Ag detection in real samples.

In accordance with the results obtained, the interaction of transient metals with thiacalixarene receptors on the sensor surface differs from that described in the bulk solution. First, no evidence of the formation of the complexes with the stoichiometry different from 1:1 was observed. Parallel investigation with picrate extraction indicated inclusion of two and even three metal ions in the host–guest complex when thiacalix[4]arenes with the same substituents form *partial cone* and *1,3-alternate* configuration. Probably, steric effects change the interaction of metal ions with potential binding sites on the sensor surface. For the same reason,

the substituents with flexible structure (hydrazides) and conformations (*1,3-alternate*) have an advantage in approaching primary and interfering ions. On the one hand, this results in the improvement of the analytical characteristics of Ag^+ determination. On the other hand, this increases interfering influence of Hg(II) and Fe(III) which predominantly bind thiacalixarenes due to their higher charge and faster kinetics. Based on the similar behavior of thiacalix[4]arene investigated and literary data, it can be assumed that transient metals are coordinated near the bridging sulfur atoms of the macrocycle promoting the effect of the nitrogen atoms of the substituents (4).

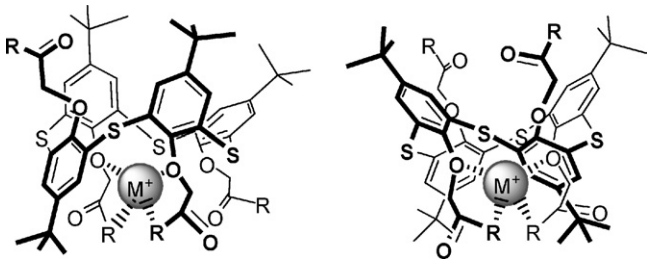

(4)

Contrary to that, alkali metals are primarily coordinated by carbonyl oxygen atoms. This provides the predominant binding of soft transient metals (Hg and Ag) over alkali metals observed for all the receptors investigated. As regards Fe(III) ions, their effect on the sensor potential is partially established by involvement in polyaniline redox equilibria altered by host–guest complexation.

4. Conclusion

The use of the thiacalix[4]arene receptors with nitrogen containing functional groups in the assembling solid-contact potentiometric sensors provides a high sensitivity and selectivity of Ag^+ determination. The sensitivity of Ag^+ detection decreases in the following range of thiacalix[4]arene substituents: morpholide > pyrrolidide > amidopyridine > hydrazide. The investigation of the sensor response by separate solution methods and in mixed runs predominantly showed the binding of soft transient metals, i.e. Ag^+ and Hg(II), over alkali metals. The selectivity of interactions is primarily determined by the accessibility of macrocyle binding site for metal ions. *1,3-altrernate* gave bigger values of potentiometric selectivity for most thiacalixarenes because of its pre-determined orientation on the sensor surface due to the interaction with polyaniline layer. The low selectivity of the signal toward Fe(III) ions is related to its interaction with polyaniline mediated by an appropriate receptor on its surface. The high efficiency of redox reactions as well as fast kinetics give Fe(III) an advantage over Ag^+ in changing the potential of the sensor.

The dependence of the potentiometric selectivity on the conformation of thiacalixarene receptors and their functional groups makes it possible to change directly the analytical performance of potentiometric sensor in accordance with the nature and amounts of interfering ions in the sample matrix.

Acknowledgements

Financial support of RFBR (05-03-33162-a) and of joint program of CRDF and Ministry of Education and Science of Russian Federation "BRHE" (REC-007, BP2M07) is gratefully acknowledged.

References

[1] E. Bakker, E. Pretsch, Angew. Chem. 46 (2007) 5660.
[2] E. Pretsch, Trends Anal. Chem. 26 (2007) 46.
[3] E. Bakker, Y. Qin, Anal. Chem. 78 (2006) 3965.
[4] T. Lindfors, A. Ivaska, Anal. Chim. Acta 404 (2000) 111.
[5] T. Lindfors, A. Ivaska, Anal. Chim. Acta 437 (2001) 171.
[6] H. Karami, M.F. Mousavi, Talanta 63 (2004) 743.
[7] J.E. Zachar, R. Toczyłowsk, R. Pokrop, M. Zagórska, A. Dybko, W. Wróblewski, Sens. Actuators B 101 (2004) 207.
[8] J. Bobacka, A. Lewenstam, A. Ivaska, Talanta 40 (1993) 1437.
[9] T.A. Bendikov, T.C. Harmon, Anal. Chim. Acta 551 (2005) 30–36.
[10] M. Ocypa, A. Michalska, K. Maksymiuk, Electrochim. Acta 51 (2006) 2298.
[11] Z. Mousavi, J. Bobacka, A. Ivaska, Electroanalysis 17 (2005) 1609–1615.
[12] A.A. Khan, Inamuddin, M.M. Alam, Reactive Funct. Polym. 63 (2005) 119.
[13] K.-K. Shiu, F.-Y. Song, K.-W. Lau, J. Electroanal. Chem. 476 (1999) 109.
[14] A.R. Zanganeh, M.K. Amini, Electrochim. Acta 52 (2007) 3822.
[15] P.C. Pandey, R. Prakash, G. Singh, I. Tiwari, V.S. Tripathi, J. Appl. Polym. Sci. 75 (2000) 1749.
[16] T. Lindfors, S. Ervelä, A. Ivaska, J. Electroanal. Chem. 560 (2003) 69.
[17] T. Lindfors, A. Ivaska, J. Electroanal. Chem. 531 (2002) 43.
[18] T. Lindfors, A. Ivaska, J. Electroanal. Chem. 535 (2002) 65.
[19] T.V. Shishkanova, I. Sapurina, J. Stejskal, V. Král, R. Volf, Anal. Chim. Acta 553 (2005) 160.
[20] T. Lindfors, C. Kvarnström, A. Ivaska, J. Electroanal. Chem. 518 (2002) 131.
[21] Z. Asfari, V. Bohmer, J. Harrowfield, J. Vicens (Eds.), Calixarenes, Kluver Academic Publishers, Netherlands, 2001, p. 2001.
[22] R. Ludwig, N.T.K. Dzung, Sensors 2 (2002) 397.
[23] K.M. O'Connor, D.W.M. Arrigan, G. Svehla, Electroanalysis 7 (2005) 205.
[24] A. Dondoni, A. Marra, M. Rossi, M. Scoponi, Polymer 45 (2004) 6195.
[25] Y. Choi, H. Kim, J.K. Lee, S.H. Lee, H.B. Lim, J.S. Kim, Talanta 64 (2004) 975.
[26] N. Zine, J. Bausells, F. Vocanson, R. Lamartine, Z. Asfari, F. Teixidor, E. Crespo, I.A. Marques de Oliveira, J. Samitier, A. Errachi, Electrochim. Acta 51 (2006) 5075.
[27] I. Dumazet-Bonnamour, H. Halouani, F. Oueslati, R. Lamartine, C. R. Chimie 8 (2005) 881.
[28] L. Chen, J. Zhang, W. Zhao, X. He, Y. Liu, J. Electroanal. Chem. 589 (2006) 106.
[29] J. Lu, R. Chen, X. He, J. Electroanal. Chem. 528 (2002) 33.
[30] N. Iki, S. Miyano, J. Inclusion Phenom. Macrocyclic Chem. 41 (2001) 99.
[31] Z. Szigeti, A. Malon, T. Vigassy, V. Csokai, A. Gr¨un, K. Wygladacz, N. Ye, C. Xu, V.J. Chebny, I. Bitter, R. Rathore, E. Bakker, E. Pretsch, Anal. Chim. Acta 572 (2006) 1.
[32] M. Ben Ali, C. Bureau, C. Martelet, N. Jaffrezic-Renault, R. Lamartine, H. Ben Ouada, Mater. Sci. Eng. C 7 (2000) 83.
[33] M. Ben Ali, N. Jaffrezic-Renault, C. Martelet, H. Ben Ouada, J. Davenas, M. Charbonnier, Mater. Sci. Eng. C 14 (2001) 17.
[34] M. Ben Ali, R. Ben Chabanne, F. Vocanson, C. Dridi, N. Jaffrezic, R. Lamartine, Thin Solid Films 495 (2006) 368.
[35] H. Matsumiya, T. Ishida, N. Iki, S. Miyan, Anal. Chim. Acta 478 (2003) 163.
[36] V.K. Gupta, A.K. Jain, R. Ludwig, G. Maheshwari, Electrochim. Acta 53 (2008) 2362.
[37] X. Ha, Z. Pan, L. Wang, X. Shi, Spectrochim. Acta A 59 (2003) 2419.
[38] V. Csokai, A. Grün, B. Balázs, A. Simon, G. Tóth, I. Bitter, Tetrahedron 62 (2006) 10215.
[39] N. Morohashi, H. Katagiri, N. Iki, Y. Yamane, C. Kabuto, T. Hattori, S. Miyano, J. Org. Chem. 68 (2003) 2324.
[40] L.I. Gafiullina, I.S. Vershinina, I.I. Stoikov, I.S. Antipin, A.I. Konovalov, J. Struct. Chem. 46 (2005) 25.
[41] I.I. Stoikov, O.A. Omran, S.E. Solovieva, S.K. Latypov, K.M. Enikeev, A.T. Gubaidullin, I.S. Antipin, A.I. Konovalov, Tetrahedron 59 (2003) 1469.
[42] G.A. Evtugyn, I.I. Stoikov, S.V. Beljyakova, R.V. Shamagsumova, E.E. Stoikova, A.Yu. Zhukov, I.S. Antipin, H.C. Budnikov, Talanta 71 (2007) 1720.
[43] N. Iki, N. Morohashi, F. Narumi, T. Fujimoto, T. Suzuki, S. Miyano, Tetrahedron Lett. 40 (1999) 7337.
[44] I.I. Stoikov, R.Z. Nasibullin, V.A. Smolentsev, L.I. Gafiullina, A.Yu. Zhukov, J.B. Puplampu, I.S. Antipin, A.I. Konovalov, Mendeleev Commun. 16 (2006) 248.
[45] R.P. Buck, E. Linder, Pure Appl. Chem. 66 (1994) 2527.
[46] E. Malinowska, Z. Brzozka, K. Kasiura, R.J.M. Egberink, D.N. Reinhoudt, Anal. Chim. Acta 298 (1994) 245.
[47] L. Chen, H. Ju, X. Zeng, X. He, Z. Zhang, Anal. Chim. Acta 437 (2001) 191.
[48] N. Rubinova, K. Chumbimuni-Torres, E. Bakker, Sens. Actuators B 121 (2007) 135.
[49] K.Y. Chumbimuni-Torres, N. Rubinova, A. Radu, L.T. Kubota, E. Bakker, Anal. Chem. 78 (2006) 1318.

Talanta 76 (2008) 320–326

Contents lists available at ScienceDirect

Talanta

journal homepage: www.elsevier.com/locate/talanta

Optimization of polymeric triiodide membrane electrode based on clozapine–triiodide ion-pair using experimental design

Khalil Farhadi*, Morteza Bahram, Donya Shokatynia, Floria Salehiyan

Department of Chemistry, Faculty of Science, Urmia University, Urmia, Iran

ARTICLE INFO

Article history:
Received 7 November 2007
Received in revised form 26 February 2008
Accepted 27 February 2008
Available online 7 March 2008

Keywords:
Coated graphite
Central composite design
Triiodide ion-selective electrode
Clozapine
Ascorbic acid
Potentiometry

ABSTRACT

Central composite design (CCD) and response surface methodology (RSM) were developed as experimental strategies for modeling and optimization of the influence of some variables on the performance of a new PVC membrane triiodide ion-selective electrode. This triiodide sensor is based on triiodide–clozapine ion-pair complexation. PVC, plasticizers, ion-pair amounts and pH were investigated as four variables to build a model to achieve the best Nernstian slope (59.9 mV) as response. The electrode is prepared by incorporating the ion-exchanger in PVC matrix plasticized with 2-nitrophenyl octal ether, which is directly coated on the surface of a graphite electrode. The influence of foreign ions on the electrode performance was also investigated. The optimized membranes demonstrate Nernstian response for triiodide ions over a wide linear range from 5.0×10^{-6} to 1.0×10^{-2} mol L^{-1} with a limit of detection 2.0×10^{-6} mol L^{-1} at 25 °C. The electrodes could be used over a wide pH range 4–8, and have the advantages of easy to prepare, good selectivity and fast response time, long lifetime (over 3 months) and small interferences from hydrogen ion. The proposed electrode was successfully used as indicator electrode in potentiometric titration of triiodide ions and ascorbic acid.

1. Introduction

Due to the vast application in the various field of analysis, there has been continued growth in the number of ion-selective electrodes (ISEs) especially PVC membrane-based electrodes for a variety of substances. These electrodes can be prepared by incorporating any of the many ion-exchanger or neutral-sequestering agents within a plasticized PVC matrix, and used as very useful tools for clinical, chemical and environmental analysis [1,2]. Due to the importance of selective monitoring of triiodide in direct measurements and end point recognition in titrations of some important oxidizing and reducing agents, several sensors have been described in the literatures [3–7].

The parameters that affect the performance of a polymeric membrane electrode are usually the PVC, plasticizers, ion-pair amounts and pH value. Successful sensing the analyte with a constructed electrode depends on the selection of suitable electrode composition and operating conditions, e.g. pH. Therefore, it is important to determine the operating parameters at which the response reaches its optimum. Usually the Nernstian behavior has been noticed as an important characteristic especially when the proposed electrode was used in theoretical studies [3–12]. One way to obtain the optimum results is response surface methodology (RSM) [13].

The optimization of the influencing parameters using "one variable-at-a-time" optimization method required many experiments. Furthermore there are maybe interactions between the investigated parameters. The total number of requires experiments can be reduced using experimental design technique. It is essential that an experimental design methodology will be very economical for extracting the maximum amount of complex information, saving significant experimental time as well as material used for analyses and personal costs [13]. Such designs have been applied to the optimization of different process [14–18].

In this work, fabrication of an ISE based on triiodide–clozapine ion-pair was optimized using CCD. The chemical structure of clozapine is shown in Fig. 1. The goal of the proposed work was to describe in detail the factor's effect, by modeling the slope of calibration curve as a response. The influence of each of the factors and their interactions could be well identified for the responses screened. The use of an experimental design, as mentioned, enabled a subsequent benefit in terms of labor time and number of experience to optimize the conditions. The main purpose of this study was to perform the central composite design as a novel procedure in order to investigate the effect of PVC, plasticizers, ion-pair amount and pH in order to build a model to achieve the best Nernstian slope

* Corresponding author. Tel.: +98 441 2972170; fax: +98 441 3443442.
E-mail addresses: khfarhadi@yahoo.com, kh.farhadi@urmia.ac.ir (K. Farhadi).

0039-9140/$ – see front matter © 2008 Elsevier B.V. All rights reserved.
doi:10.1016/j.talanta.2008.02.043

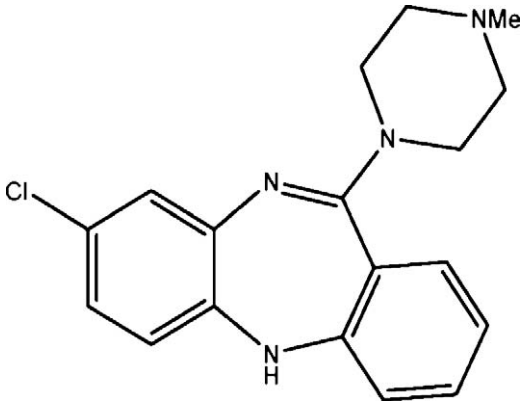

Fig. 1. The structure of clozapine (CLZ).

(59.9 mV) as response. Also, the characteristic performance and analytical application of the proposed sensors have been studied in this article.

2. Experimental

2.1. Apparatus

All potentiometric and pH measurements were made at 25 ± 1 °C using a digital WTW multilab 540 Ionalyzer (Germany). Ag/AgCl reference electrodes were purchased from Azar Electrode Company (Urmia, Iran). The absorption spectra were recorded on a LKB (United Kingdom) model 4054 UV–vis spectrophotometer using 10-mm quartz cells.

2.2. Reagents

Reagent grade 2-nitrophenyl octyl ether (NPOE) and high relative molecular weight PVC were purchased from Aldrich and Fluka companies and used as received. Chloroform and all of salts (all from Merck) were of highest purity available and used without further purification. Standard solutions and buffers were prepared using doubly distilled water. Working standards of clozapine was prepared from Tehran-Shimi (Tehran, Iran) pharmaceutical company.

2.3. Preparation of ion-pairs

0.5 g of clozapine powder was completely dissolved in 20 mL of HNO_3 0.1 mol L^{-1}. A 25 mL of 1.0×10^{-2} mol L^{-1} triiodide solution was slowly added to this solution with continuous stirring until precipitation was completed. The resulting brown clozapine–triiodide ion-pair precipitate was separated by filtration, washed thoroughly with distilled water and dried at 40 °C. The composition of the formed ion-pair was confirmed by a chemical analysis as well as UV–vis spectroscopy.

2.4. Electrode preparation

The membranes were fabricated by dissolving the powdered PVC, NPOE and ion-pair complex in 5 mL of THF. The resulting mixture was transferred into a glass dish of 2-cm diameter. The THF was slowly evaporated until an oily concentrated mixture was obtained. A polished graphite electrode (3-mm diameter and 10-mm length) was dipped into the membrane solution, then removed and allowed to dry. This operation was repeated several times so that a globular membrane of about 1 mm thickness around the graphite electrode was obtained. The electrode was finally conditioned by soaking in 1.0×10^{-2} mol L^{-1} triiodide solution for 24 h and had to be stored in the same solution when not in use.

Table 1
The variables and values used for central composite design (CCD)

Variable	Name	Factor levels				
		−2 (low)	−1	0	+1	+2 (high)
*F*1	PVC (g)	0.024	0.027	0.030	0.033	0.036
*F*2	Plasticizer (g)	0.064	0.067	0.070	0.073	0.076
*F*3	Ion-pair	0.001	0.0026	0.0051	0.0076	0.01
*F*4	pH	2	4	6	8	10

2.5. Statistical software

Essential Regression and Experimental Design for Chemists and Engineers (EREGRESS), as a MS Excel Add-In software [19,20], was used to design the experiments and to model and analyze the results.

2.6. Central composite design

Central composite design (CCD) was used to optimize the fabrication of an ISE based on triiodide–clozapine ion-pair. Four independent factors, namely the PVC (*F*1), plasticizers (*F*2) and ion-pair (*F*3) amounts and pH (*F*4) were studied at five levels with three repeats at the central point, using a circumscribed central composite design. For each of the four studied variables, high (coded value: +2) and low (coded value: −2) set points were selected as shown in Table 1. Also Tables 2 and 3 show the coded and real values of designed experiments based on CCD methodology achieved using EREGRESS software.

Table 2
List of experiments in the CCD for model optimization (coded values)

Design points	Factor levels				Response	
	*F*1	*F*2	*F*3	*F*4	−Slope (mV)	R^{2} [a]
1	−1	−1	−1	−1	32.8	0.9734
2	0	2	0	0	41.5	0.9944
3	0	0	0	−2	35	0.9754
4[b]	0	0	0	0	48.1	0.7959
5	−1	1	−1	1	38.2	0.9762
6	−1	1	1	−1	46.8	0.9961
7[b]	0	0	0	0	48.1	0.7959
8	−1	−1	1	1	36.3	0.6805
9	−1	1	−1	−1	35.4	0.969
10	1	−1	1	−1	42.2	0.9765
11	−1	−1	1	−1	37.4	0.8979
12	1	−1	−1	1	39.1	0.9335
13	1	−1	−1	−1	36.4	0.965
14	0	0	0	2	47.7	0.9767
15[b]	0	0	0	0	48.1	0.7959
16	1	1	1	−1	38.8	0.9884
17	−1	−1	−1	1	50.4	0.996
18	2	0	0	0	39.9	0.9857
19	1	1	1	1	41.4	0.9712
20	1	1	−1	−1	36.9	0.9611
21	−1	1	1	1	56.6	0.993
22	1	1	−1	1	36.9	0.9611
23	0	−2	0	0	37.9	0.991
24	1	−1	1	1	39.8	0.9855
25	0	0	−2	0	39.4	0.997
26	−2	0	0	0	37.8	0.9998
27	0	0	2	0	40.5	0.9934

[a] Squared regression coefficient.
[b] Three times replicates of center points.

Table 3
List of randomly designed experiments, observed responses and predicted ones using constructed model

Number of run	*F*1	*F*2	*F*3	pH	Observed response[a]	Predicted response[a]
1	0.024	0.07	0.0051	4	57.3	57.4
2	0.03	0.07	0.0026	6	55.6	51.4
3	0.024	0.067	0.0026	6	57.8	54.5
4	0.027	0.07	0.0026	8	54.6	52.3
5	0.027	0.067	0.0026	2	60.2	59.7
6	0.036	0.07	0.0076	8	43.4	45.5
7	0.033	0.076	0.0076	8	10.7	0
8	0.01	0.033	0.0076	6	12.1	30
9	0.01	0.033	0.0076	4	12.1	30.3
10	0.033	0.07	0.0076	10	48.4	46.9

[a] Slope of calibration curve (−slope, mV).

Polynomial equations, response surface and central design for a particular response are produced using EREGRESS. For an experimental design with four factors, the model including linear, quadratic and cross-terms can be expressed as

$$\text{response} = b0 + b1F1 + b2F2 + b3F3 + b4F4 + b5F1F1 + b6F2F2 + b7F3F3 + b8F4F4 + b9F1F2 + b10F1F3 + b11F1F4 + b12F2F3 + b13F2F4 + b14F3F4 \quad (1)$$

Within Eq. (1), *F*1–/*F*4 are the variable parameters, and *b*0–/*b*14 are the coefficient values obtained through MLR using EREGRESS. The response surface plots were obtained through a statistical process that described the design and the modeled CCD data. Response surface methodologies graphically illustrate relationships between parameters and responses and are the way to obtain an exact optimum [19,21–24].

The statistical significance of the predicted models was evaluated by the analysis of variance (ANOVA) and least squares techniques. The ANOVA consists in determining which of the factors significantly affect the response variables in study, using a Fisher's statistical test (*F*-test). The significance and the magnitude of the estimated coefficients of each variable and all their possible interactions on the response variables were determined. Such coefficients for each variable represents the improvement in the response, that is, to expect as the variable setting is changed from low to high. Effects with less than 95% of significance, effects with a *p*-value higher than 0.05, were discarded and pooled into the error term and a new analysis of variance was performed for the reduced model. Note that the *p*-value represents a decreasing index of the reliability of a result [19]. Replicates ($n = 3$) of the central points were performed to estimate the experimental error.

3. Results and discussion

3.1. Study of the reaction between clozapine and I_3^- ions

Clozapine, 8-chloro-11-(4-methyl-1-piperazinyl)-5*H*-dibenzo-[*b*,*e*]-[1,4]-diazepine (CLZ) (Fig. 1) a tricyclic dibenzodiazepine neuroleptic with a piperazinyle side chain, is used for the treatment of positive and negative symptoms of schizophrenic patients who do not respond well to traditional neuroleptic drugs [25].

In preliminary experiments, we found that there is a specific interaction between the I_3^- ion and an acidic solution of clozapine, so that the protonated form of clozapine ($CLZH^+$) was immediately precipitated in the presence of excess I_3^- ions. The obtained results from the determination of unreacted I_3^- ions in a filtrated solution and also assay of clozapine in obtained precipitate clearly indicated that an ion-pair with a ratio of 1:1 was formed.

$$(CLZH)^+_{aq} + I^-_{3(aq)} \rightleftharpoons (CLZH)I_{3(s)}$$

In order to obtain a clue about the interaction mechanism of I_3^- ions and protonated clozapine, the UV–vis spectra of the CLZ, ion-pair and triiodide ions in mixture solution of acetonitrile–chloroform were recorded (Fig. 2). As can be seen, the ion-pair solution (Fig. 2B) has two sharp peaks at 293 and 365 nm, which are characteristic of triiodide free (or solvent separated) ions (Fig. 2C) [26]. Thus, due to the stability and insolubility of the resulting ion-pair in aqueous solutions, it was tested as a suitable anion sensory in construction of a new PVC-based membrane-coated graphite triiodide ISE.

3.2. Central composite experimental design

The slope of calibration curve and squared regression coefficient for each electrode were collected as responses in order to optimize four independent factors, namely the PVC (*F*1), plasticizers (*F*2) and ion-pair (*F*3) amount and pH (*F*4). Tables 1 and 2 present the levels of coded and actual experimental variables that were tested. Table 2 also presents the corresponding response of each run. In order to prevent over-fitting, 10 randomly designed electrodes (Table 3) that have not been used in model construction were consequently evaluated with the model coefficients.

The aims of this CCD strategy were: (i) to maximize the slope of calibration curve; (ii) to determine which variables have a higher impact on the slope of calibration curve; (iii) to give an insight on the robustness of the method close to the optimum conditions; (iv) eventually show interactions between variables.

In order to find the important factors and build a model to optimize the procedure, we started with a full quadratic model including all terms as in Eq. (1). To obtain a simple and yet a realistic model, the insignificant terms ($p > 0.05$) were eliminated from the model through 'backward elimination' process. Using all 15 parameters presented in Eq. (1) for modeling the response (slope/mV) showed a relatively good fit and R^2 for calibration close to 0.85 was achieved. Although adjusted R^2 as well R^2 for prediction were very

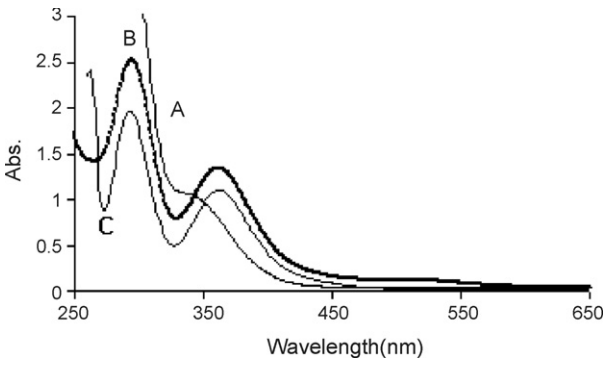

Fig. 2. Absorption spectra of (A) CLZ, (B) $(CLZH)I_3$ and (C) triiodide ion (as KI_3) in mixture solution of chloroform–acetonitrile.

Table 4
Some characteristics of the constructed models

Response	Slope
R^2[a]	0.991
R^2 adjustment	0.978
R^2 for prediction	0.925
Regression equations	Slope = $b0 + b1F2 + b2F3 + b3F1F3 + b4F1F4 + b5F2F3 + b6F2F4 + b7F3F3 + b8F3F4 + b9F4F4 + b10F2F3F4 + b11F1F2F3 + b12F1F3F3 + b13F2F2F4 + b14F1F2F4 + b15F1F1F4$

[a] Squared regression coefficient.

low (<0.1). Some of these 15 regressor variables are insignificant or at least have low significance and should be eliminated from the model. Since R^2 always decreases when a regressor variable is eliminated from a regression model, in statistical modeling the adjusted R^2, which takes the number of regressor variables into account, is usually selected [19,27]. Also R^2 for prediction, which indicates the predictive power of the model, is chosen for the same reason. This parameter was approximated using *prediction error sum of squares* or PRESS that was calculated from residuals, which are based on a regression model with one data point removed. So, R^2, adjusted R^2, and R^2 for prediction together are very convenient to get a quick impression of the overall fit of the model and the predictive power based on one data point removed. In a good model, these parameters should not be too different from each other. However, for small data sets, it is very likely that every data point is influential. In these cases, a high value for R^2 for prediction cannot be expected [19]. By the elimination of insignificant parameters from Eq. (1), calibration R^2 decreased finally to 0.75 but adjusted R^2, and R^2 for prediction increased nearly to 0.6 and 0.41, respectively. This fact shows low overall fit and also poorness of constructed model for prediction.

For instance, when performing a curve fit of scientific data using a polynomial model, it is always possible to increase the R^2 by adding higher order terms. Ultimately, this leads to a very complicated fitted curve which basically just connects the dots in our graph. Such a model with a very impressive R^2 close to 1 might perform very poorly in predicting new data (*over-fitted model*). Therefore, the procedure of adding new regressor(s) should be handled carefully. This means that only necessary parameters should be added to the model. Adding the cubic regressors and tri-way interaction parameters increased R^2 of prediction and R^2 adjustment dramatically and also improved the model fitness (calibration R^2). Repeated forward and backward stepwise regression was employed to generate the equations for this purpose at confidence level 95%. A reduced model using significant linear, quadratic and cubic interaction parameters was obtained finally (Table 4).

For this case, the adjusted R^2 were well within the acceptable limits and there was not large differences between R^2 values which revealed that the experimental data shows a good fit with the third-order polynomial equations (see Table 4). As stated before 10 randomly designed samples that have not been used in model construction were evaluated with the model coefficients. Table 3 shows the observed and predicted responses for these randomly designed electrodes. As can be seen there are good agreement between observed and predicted responses that shows a predictive model has been constructed.

The plots of predicted response versus calculated ones (Fig. 3) showed that the residual values were low. This allows us to further use the response surface methodology as a predictive tool to obtain responses over the whole parameter uncertainty range. By using the standardized data, the quality of significant coefficients can be provided from the size of the coefficients. On the other hand R^2, R^2 adjusted and R^2 predicted can be used to evaluate model fitness [19]. The significant coefficients are presented in Table 5 as real values and standardized modeling. The non-significant ones have been eliminated based on ANOVA and corresponding p-values (not shown).

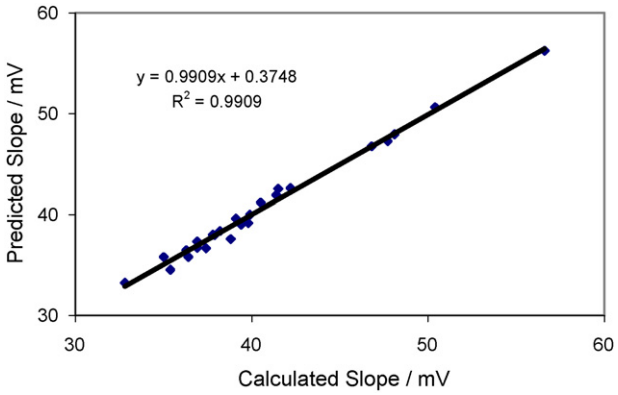

Fig. 3. Plot of predicted slope *vs.* the calculated ones.

From the constructed models (regard to Tables 4 and 5) the following results could be obtained:

- Plasticizer amount ($F2$) and ion-pair ($F3$) affect significantly the response of ISE by both linear and quadratic variables.
- The model showed that PVC amount ($F1$) and pH ($F4$) are not lonely significant parameter at confidence level 95% but have significant interaction in conjunction with plasticizer amount ($F2$) and ion-pair ($F3$) more or less.
- As Tables 4 and 5 show the main quadratic and cubic interaction parameters are $F1F3$ ($b3 = 551.62$) and $F1F2F3$ ($b11 = -488.85$) which is probably related to high chemical interaction between PVC ion-pair and PVC–plasticizer ion-pair adducts, respectively.

3.3. Response surface and selection of optimum conditions

In order to gain insight about the effect of each variable, the three-dimensional (3D) plots for the predicted responses were also formed, based on the model function to analyze the change of response surface. For example Fig. 4 shows some of response surface plots that show the 3D plots relationship between two variables and slope of calibration curve while other variables were kept in center levels. As shown in Fig. 4 there was non-linear relation between response and variables $F1$–$F4$, because the surface plots of response showed curves. It has been shown in Tables 4 and 5 that several squared terms and quadratic or cubic interaction parameters are statistically significant.

Table 5
Constants and coefficients for the constructed quadratic models (for equation presented in Table 4)

	Uncoded values	Standardized values
$b0$	−260.38	41.09
$b1$	3751.38	11.55
$b2$	−169776.84	−396.46
$b3$	7674821.85	551.62
$b4$	−2327.79	−140.76
$b5$	2070959.34	348.08
$b6$	2248.90	307.70
$b7$	2938876.95	74.23
$b8$	−13503.77	−236.89
$b9$	−0.40	−9.364
$b10$	188403.33	236.74
$b11$	−94758752.82	−488.85
$b12$	−110904207.98	−84.80
$b13$	−35821.79	−356.14
$b14$	63352.95	271.56
$b15$	−41405.23	−85.20

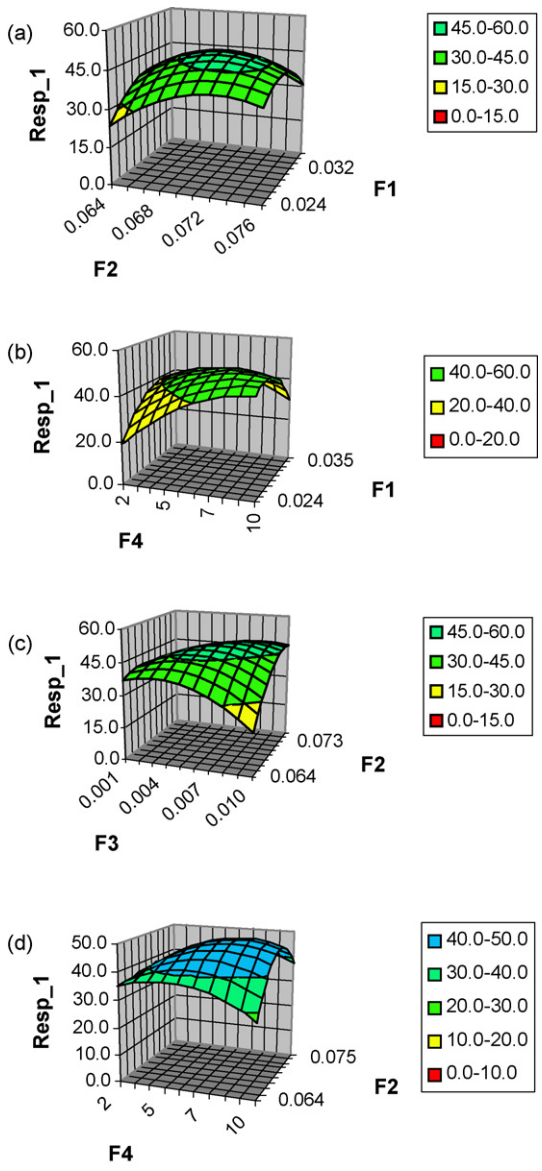

Fig. 4. Response surface and counter plot of slope modeling: the PVC (*F*1), plasticizers (*F*2) and ion-pair amount (*F*3) and pH (*F*4).

The surface plots (Fig. 4) show the pronounced effect of plasticizer (*F*2) as well as ion-pair amount (*F*3) on the slope of calibration curve (*Y*). The results also showed that PVC amount (*F*1) has a moderate interaction effect with plasticizer (*F*2) and also with ion-pair amount (*F*3). It is clear from Fig. 4 that pH is a low-significant factor (at least at the range 4–8). The overall overview of presented figures and the coefficients of Tables 4 and 5 clearly show the non-linear relation between response and variables and interaction between variables as well.

The selection of optimized method conditions is possible from the response surface plots (Fig. 4). These results demonstrate that all the response surfaces have a flat optimum. Therefore, response (*Y*) surface optimization could be found depending on the PVC (*F*1), plasticizers (*F*2) ion-pair (*F*3) amount and pH (*F*4) according to the following equations:

$$\left[\frac{\partial Y}{\partial F1}\right]_{F2,F3,F4} = 0 \quad (2)$$

Table 6
Optimum conditions obtained by response surface modeling

	Variable name	Optimum values	Selected optimum values
*F*1	PVC (g)	0.027–0.029	0.028
*F*2	Plasticizer (g)	0.07–0.074	0.073
*F*3	Ion-pair	0.006–0.009	0.008
*F*4	pH	7–9 (low effect)	8

$$\left[\frac{\partial Y}{\partial F2}\right]_{F1,F3,F4} = 0 \quad (3)$$

$$\left[\frac{\partial Y}{\partial F3}\right]_{F1,F2,F4} = 0 \quad (4)$$

$$\left[\frac{\partial Y}{\partial F4}\right]_{F1,F2,F3} = 0 \quad (5)$$

Response optimization results of the non-linear polynomial model are shown in Table 6. The slope of 59 mV at the optimal parameters of *F*1 (0.028 g), *F*2 (0.073), *F*3 (0.008 g) and *F*4 (pH 8) has been achieved. Note that if the criterion is fabricating an ISE with Nernstian response, the conditions that meet this requirement have been achieved by this optimization procedure and presented in Table 6 for the constructed model. The proposed method showed an excellent repeatability using the optimum values obtained through a CCD.

3.4. EMF response characteristics and selectivity of electrodes

The responses of the optimized triiodide ion-selective electrode based on triiodide–clozapine ion-pair to other common inorganic anions are shown in Fig. 5. As seen, all anions tested showed no considerable responses in the concentration range 1.0×10^{-5} to 1.0×10^{-2} mol L^{-1} towards triiodide ions because of their very weak interactions with membrane. However, the membrane sensors show high selectivity for triiodide ion with Nernstian behavior over the activity range 2.0×10^{-1} to 5.0×10^{-6} mol L^{-1} with a limit of detection 2.0×10^{-6} mol L^{-1} at 25 °C.

The potentiometric selectivity coefficients are clearly the most important characteristics of a sensor especially critical in direct potentiometric measurements [28]. Umezawa et al. have been collected the potentiometric selectivity coefficients for inorganic anions reported during 1988–1998 [29]. It is well known that the selectivity of an ion-pair complex-based membrane electrode

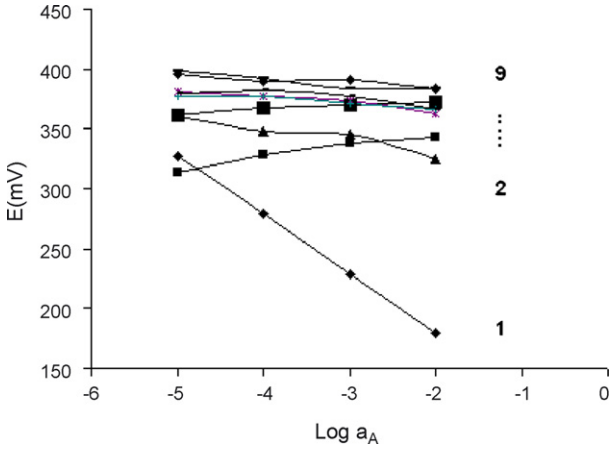

Fig. 5. Potential response of membrane electrode based on clozapine–triiodide ion-pair to various anions, (1) I_3^-; (2) Cl^-; (3) SCN^-; (4) IO_3^-; (5) CH_3COO^-; (6) NO_2^-; (7) $C_2O_4^{2-}$; (8) SO_4^{2-}; (9) Br^-.

Table 7
Selectivity coefficient (log $K_{A,B}^{Pot*}$) of various interfering anions

Anions	log $K_{A,B}^{Pot}$
IO_3^-	−2.72 ± 0.20
NO_3^-	−3.59 ± 0.17
SCN^-	−3.62 ± 0.20
CH_3COO^-	−3.80 ± 0.10
Cl^-	−2.84 ± 0.20
NO_2^-	−3.00 ± 0.12
Br^-	−2.60 ± 0.20
$C_2O_4^{2-}$	−4.15 ± 0.25
SO_4^{2-}	−3.18 ± 0.20

* Average of three replicate measurements ($X \pm$ S.D.).

depends on the selectivity of the ion exchange process at the membrane–sample solution interface, the mobility of the respective ions in the membrane and hydrophobic interactions between the primary ion and the organic membrane. The selectivity of the proposed electrodes to other anions was investigated by the matched potential method (MPM) [30–33]. According to the MPM, the selectivity coefficient is defined as the activity ratio of the primary ion (A) and the interfering ion (B) that gives the same potential change in a reference solution. Thus, one should measure the change in potential upon changing the primary ion activity. Then the interfering ion would be added to an identical reference solution until the same potential change is obtained. The selectivity coefficient, $K_{A,B}^{Pot}$, is determined as expression $K_{A,B}^{Pot} = \Delta A/a_B$ where $\Delta A = a_A^{'} - a_A$, a_A is the initial primary ion activity and a'_A the activity of A in the presence of interfering ion, a_B. The obtained selectivity coefficients are summarized in Table 7. As seen, much of diverse anions used could not significantly disturb the functioning of the proposed triiodide ion-selective membrane electrodes. It should be noted that the concentration of triiodide ion used, as a primary ion in the determination of selectivity coefficients was 1×10^{-4} mol L^{-1}.

3.5. Response time and lifetime of proposed electrode

For analytical applications, the response time of a sensor is an important factor. The average time required for the I_3^- selective membrane electrodes to rich a potential within ±1 mV of final equilibrium value after successive immersion of a series of I_3^- ion solutions, each having a 10-fold difference in concentration were measured. The static response time for the PVC-membrane electrodes obtained were less than 10 s over all linear concentration range. The potentials remained constant for more than 2 min, after which a very slow divergence was observed. The membrane electrodes were very stable and could be used over a period of 2 months without any considerable change in response characteristics.

3.6. Comparison of the characteristics of proposed electrodes with the reported triiodide ISE in literature

In Table 8, the analytical performance of the proposed membrane electrodes based on clozapine–triiodide ion-pair complex has been compared with previously reported for triiodide ion-selective membrane electrodes based on charge transfer complexes of 2,4,6,8-tetraazabicyclo[3.3.0]octane [4] and crown ethers [5] with iodine, tetrachlorophenylporphyrinato Mn(III) acetate [8,9], 5,10,15,20-tetraphenylporphyrinato Mn(III) [3], 2,2-[4,4-diphenylmethane-bis-(nitromethylidyne)] Cu(II) [6], 2,2-[4,4-diphenylmethane-bis-(nitromethylidyne)] Fe(III) [6] and *N*,*N*-1,2-propylene-bis-(5-methyl salicylidene iminato) copper(II) [7]. As seen, the ionophore used in this work shows a lower somewhat similar, in most cases, or even superior, in some cases, to the sensors prepared previously. However, wider linear range and a fully Nernstian response slope (in most cases) are two important advantageous of the proposed electrode. It is worth mentioned that though the selectivity of proposed ion-exchanger electrodes toward triiodide ion is relatively low in comparison to that of previously reported electrodes, the independent of the potential response of the proposed electrodes in a wide pH range; specially in acidic media, a very short static response time as well as facility preparation and purification of the ionophores are the silent performance over the reported sensors.

4. Analytical applications

Titrations based on iodine are the easiest, most rapid and accurate methods in chemical and pharmaceutical analysis. Potentiometric triiodide sensors can be used as suitable indicator electrodes in end-point detection of iodometric and iodimetric titrations, which has advantages to starch indicator reagent and Pt indicator electrode. Because of some disadvantages in application of starch as an indicator in visual titrations such as the instability of starch in cold water, formation of water insoluble complexes between starch and iodine and also drift of the end-point in dilute solutions, the use of the proposed triiodide sensors in determination of a number of important chemical, environmental as well as pharmaceutical organic molecules can improve the accuracy of the obtained results. Moreover, the ability of triiodide sensor in direct determination of the activity of triiodide ion in solution and in the presence of other redox reagents similar to triiodide ion, causes its application not only as an indicator electrode in end point detection of both iodometric and iodimetric titrations, but also in determining of thermodynamic and kinetic parameters of the complexation reactions between triiodide and different reagents (e.g. ion-pairing reactions).

The proposed triiodide membrane sensor was applied for the determination of triiodide in solutions. The sample solutions were determined by potentiometric titration using standard sodium

Table 8
Comparison of the analytical characteristics of triiodide selective electrodes

Reference	Slope (mV/decade)	Linear range (mol L^{-1})	Detection limit (mol L^{-1})
[3]	−87.2	1.0×10^{-5}–1.0×10^{-3}	3.0×10^{-6}
[4]	−54.8	3.5×10^{-6}–5.0×10^{-2}	2.0×10^{-6}
[5]	−59.7	1.0×10^{-5}–1.0×10^{-1}	5.6×10^{-6}
[6]	−60.0	8.0×10^{-6}–6.0×10^{-1}	4.0×10^{-6}
[6]	−60.0	1.0×10^{-5}–5.0×10^{-1}	6.0×10^{-6}
[7]	−61.4	4.0×10^{-5}–7.0×10^{-1}	1.0×10^{-5}
[8]	−66.5	7.9×10^{-6}–1.0×10^{-1}	6.0×10^{-6}
[9]	−59.6	7.0×10^{-6}–1.0×10^{-2}	5.0×10^{-6}
This work	−59.9	5.0×10^{-6}–1.0×10^{-2}	2.0×10^{-6}

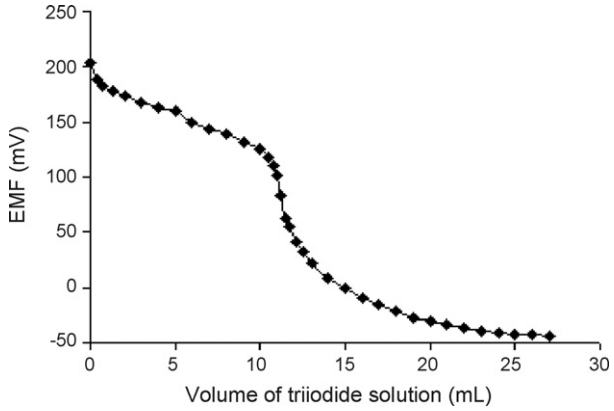

Fig. 6. Potentiometric titration curve for 10 mL of 4.25×10^{-3} mol L^{-1} ascorbic acid solution (pH was fixed in 3 using phosphate buffer) with 3.54×10^{-3} mol L^{-1} triiodide standard solution using the proposed sensor as an indicator electrode.

thiosulfate solution as titrant and proposed sensor as indicator electrode. Also, the applicability of the proposed membrane indicator electrodes were tested in direct potentiometric titration of ascorbic acid with standardized solution of iodine. A sample of the obtained potentiometric curves from the titration of ascorbic acid using proposed electrode is shown in Fig. 6. As seen, the amount of ascorbic acid in the solutions can be accurately determined from the resulting titration curve providing a sharp end point. Also, the proposed electrode was used as an indicator electrode in iodimetric titration of ascorbic acid in injection samples (500 mg ascorbic acid/5 mL) and the obtained results were compared with official method [34]. The obtained results indicated a reasonably fair agreement between the present and official methods.

5. Conclusions

This study shows the use of an experimental design enabled a subsequent benefit in terms of labor time and number of experience to optimize the conditions for the construction of a new PVC membrane-coated graphite triiodide ISE. By using central composite design and subsequently response surface methodology: (i) the slope of calibration curve was maximized; (ii) the variables that have a higher impact on the slope of ISE calibration curve was determined; (iii) the optimum conditions were obtained and (iv) the possible interactions between variables were shown. The proposed membrane electrode based on clozapine–triiodide ion-pair complex may provide an attractive alternative for determination of I_3^- ions using potentiometric methods. The wide dynamic concentration range, low detection limit, fast response time and high selectivity would make these sensors suitable for measuring the concentration of triiodide in various samples, without the need for pre-treatment steps and without significant interaction from other anionic species present in the samples. The repeatability of sensor at optimum conditions was investigated and successfully used as indicator electrode in potentiometric titration of triiodide ions and ascorbic acid.

References

[1] G.J. Movdy, B.B. Saud, J.D.R. Thomas, Sel. Electrode Rev. 10 (1988) 71.
[2] M.E. Meyerhoff, M.N. Opdyche, Adv. Clin. Chem. 25 (1986) 1.
[3] H. Suzuki, H. Nakagawa, M. Mifune, Y. Saito, Anal. Sci. 9 (1993) 351.
[4] S. Sadeghi, G.R. Dashti, Anal. Chem. 74 (2002) 2591.
[5] A. Rouhollahi, M. Shamsipur, Anal. Chem. 71 (1999) 1350.
[6] S. Sadeghi, M. Gafarzadeh, M.A. Naseri, H. Sharghi, Sens. Actuator B 98 (2004) 174.
[7] S. Sadeghi, F. Fathi, A.A. Esmaeili, H. Naeimi, Sens. Actuator B 114 (2006) 928.
[8] K. Farhadi, H. Shaikhlouei, R. Maleki, H. Sharghi, M. Shamsipur, Bull. Korean Chem. Soc. 23 (2002) 861.
[9] K. Farhadi, H. Shaikhlouei, R. Maleki, M. Shamsipur, H. Sharghi, J. Chin. Chem. Soc. 49 (2002) 861.
[10] K. Farhadi, R. Maleki, M. Shamsipur, Electroanalysis 14 (2002) 760.
[11] K. Farhadi, R. Maleki, Anal. Sci. 18 (2002) 133.
[12] K. Farhadi, R. Maleki, Anal. Lett. 37 (2004) 1063.
[13] M. Kincl, S. Turk, F. Vrecer, Int. J. Pharm. 291 (2005) 39.
[14] X. Zhang, R. Wang, X. Yang, J. Yu, Chemometr. Intell. Lab. Syst. 89 (2007) 45.
[15] A. Avila, E.I. Sanchez, M.I. Gutierrez, Chemometr. Intell. Lab. Syst. 77 (2005) 247.
[16] P. Vanloot, J.-L. Boudenne, L. Vassalo, M. Sergent, B. Coulomb, Talanta 73 (2007) 237.
[17] M. Capella-Perio, D. Bose, M.F. Rubert, J. Esteve-Romero, J. Chromatogr. B 839 (2006) 95.
[18] C. Goncalves, J.J. Carvalho, M.A. Azenha, M.F. Alpendurada, J. Chromatogr. A 1110 (2006) 6.
[19] D.D. Stephan, J. Werner, R.P. Yeater, Essential Regression and Experimental Design for Chemists and Engineers, MS excel add in software package (1998–2001).
[20] I. Bulacov, J. Jirkovsky, M. Muller, R.B. Heimann, Surf. Coat. Technol. 201 (2006) 255.
[21] A.M. Siouffi, R. Phan-Tan-Luu, J. Chromatogr. A 892 (2000) 75.
[22] T. Lundstedt, E. Seifert, L. Abramo, B. Thelin, A. Nystrom, J. Pettersen, R. Bergman, Intell. Lab. Syst. 42 (1998) 3.
[23] P.W. Araujo, R.G. Brereton, Trends Anal. Chem. 15 (1996) 63.
[24] P.A.J. Rosa, A.M. Azevedo, M.R. Aires-Barros, J. Chromatogr. A 1141 (2007) 50.
[25] M.G. Choc, F. Hsuan, G. Honigfeld, Pharm. Res. 7 (1990) 347.
[26] M. Mizuno, J. Tanaka, J. Harada, J. Phys. Chem. 85 (1981) 1789.
[27] T. Sivakumar, R. Manavalan, C. Muralidharan, K. Valliappan, J. Pharm. Biomed. Anal. 43 (2007) 1842.
[28] E. Bakker, E. Pretsch, P. Buhlmann, Anal. Chem. 72 (2000) 1127.
[29] Y. Umezawa, K. Umezawa, B. Philippe, N. Hamada, H. Aoki, J. Nakanishi, M. Sato, K.P. Xiao, Y. Nishimura, Pure Appl. Chem. 74 (2002) 923.
[30] V.P. Gadzepko, G.D. Christian, Anal. Chim. Acta 164 (1984) 279.
[31] Y. Umezawa, K. Umezawa, H. Sato, Pure Appl. Chem. 67 (1995) 507.
[32] Y. Umezawa, CRC Handbook of Ion Selective Electrodes; Selectivity Coefficients, CRC Press, Boca Raton, 1990.
[33] E. Bakker, Electroanalysis 9 (1997) 7.
[34] British Pharmacopoeia,Version 3, Incorporating the Requirements of the 3rd edition of the European Pharmacopoeia 1997 as Amended by Supplement, 1999.

Talanta 76 (2008) 373–381

Contents lists available at ScienceDirect

Talanta

journal homepage: www.elsevier.com/locate/talanta

Wavelet neural networks to resolve the overlapping signal in the voltammetric determination of phenolic compounds

Juan Manuel Gutiérrez [a], Albert Gutés [b], Francisco Céspedes [b], Manuel del Valle [b,*], Roberto Muñoz [a]

[a] Bioelectronics Section, Department of Electrical Engineering, CINVESTAV, 07360 Mexico DF, Mexico
[b] Sensors & Biosensors Group, Department of Chemistry, Universitat Autònoma de Barcelona, Edifici Cn, 08193 Bellaterra, Spain

ARTICLE INFO

Article history:
Received 13 November 2007
Received in revised form 7 March 2008
Accepted 12 March 2008
Available online 21 March 2008

Keywords:
Voltammetry
Signal resolution
Wavelet neural network
Phenols

ABSTRACT

Three phenolic compounds, i.e. phenol, catechol and 4-acetamidophenol, were simultaneously determined by voltammetric detection of its oxidation reaction at the surface of an epoxy-graphite transducer. Because of strong signal overlapping, Wavelet Neural Networks (WNN) were used in data treatment, in a combination of chemometrics and electrochemical sensors, already known as the electronic tongue concept. To facilitate calibration, a set of samples (concentration of each phenol ranging from 0.25 to 2.5 mM) was prepared automatically by employing a Sequential Injection System. Phenolic compounds could be resolved with good prediction ability, showing correlation coefficients greater than 0.929 when the obtained values were compared with those expected for a set of samples not employed for training.

1. Introduction

Wavelet Transform (WT) proposed by Grossmann and Morlet [1] has become a useful decomposition tool in a wide variety of applications throughout mathematics, science and engineering; in the last years, it has emerged as an interesting option in the chemistry field [2,3] because of its ability to compress or denoise data. WT is used to represent a signal, $f(x)$, using a linear combination of a set of basis functions which are the scaled and translated versions of a main function named mother wavelet [4]. The fundamental idea of the transform is to analyze data at different resolutions and to reveal aspects that other signal analysis techniques can overlook [1]. WT signal processing compresses the signal by removing useless features; in this way, modeling becomes computationally less demanding.

On the other hand, Artificial Neural Networks (ANNs) are powerful modeling tools for deriving meaning from complex or imprecise data; their superior performance makes them interesting in tasks of approximation, pattern recognition or multivariate calibration methods that are too complex to be attempted by either humans or other computer techniques [5–9]. An ANN is an information processing model that is inspired by the physiology of animal nervous systems. It is composed of a large number of highly interconnected processing elements (neurons) working in parallel to solve specific problems [10–12].

The stepwise coupling of WT and ANN has been proposed as a strategy for the non-stationary signal processing, mainly when it is conformed by a great amount of input data [13,14]. The purpose of WT is to compact the signal, representing it by means of a reduced set of coefficients. On the other hand, the artificial neural network is the one in charge to map the set of coefficients into the sought information. Nevertheless, for the development of this strategy, a large effort is required to obtain the optimal configurations of WT and ANN. First, it is necessary to determine which wavelet mother function to use plus the maximum level of compaction that better preserves the information; secondly, one needs to find the ANN type and structure to properly interpret the compacted signal. Evidently, this implementation requires the setup and fine tuning of the two processes separately.

In order to solve this disadvantage, a novel processing strategy that combines wavelets with neural networks has been recently proposed. This successful synthesis of theories has generated a new class of networks called Wavelet Neural Networks (WNNs) [15]. The distinct feature of these networks is that they use wavelet functions as the activation functions of hidden layer neurons. Using theoretical features of wavelet transform, network construction methods could be developed [16].

There are a few works related with the WNN and its application in chemistry; most of them make use of these networks in QSAR predictions such as: inclusion complexation constants of cyclodex-

* Corresponding author. Tel.: +34 93 5811017; fax: +34 93 5812379.
E-mail address: manel.delvalle@uab.es (M. del Valle).

0039-9140/$ – see front matter © 2008 Elsevier B.V. All rights reserved.
doi:10.1016/j.talanta.2008.03.009

trins [17], programmed-temperature retention values of naphtas [18], solubility of polycyclic aromatic hydrocarbons [19], critical micelle concentrations of Gemini surfactants [20] or solubility of anthraquinone dyes [21]. Besides, WNN have been employed to build response models, for example in the differential pulse adsorptive stripping voltammetric determination of Cu(II) ion [22].

Signals originated in voltammetry can be seriously overlapping records having non-stationary characteristics [23]; the resolution and quantification of overlapping peaks in this kind of signals is a difficult task in electroanalysis [24]. Additionally, voltammograms may contain hundreds of measures that demand a preprocessing stage to extract the most relevant information prior to the use of a calibration model. Different methods such as multiple linear regression (MLR), principal component regression (PCR), partial least squares (PLS) and principal component analysis (PCA) have been used to tackle this problem [25,26].

The present work is aimed to the development of a processing strategy based on WNN to build a multivariate model that describes a complex overlapping voltammogram; the application is the resolution of mixtures of three phenolic compounds, and in this way, to quantify them more efficiently than with other conventional methods. These signal processing tools are of paramount importance for the development of electronic tongue systems which employ voltammetric sensors.

2. Theory

The first approach to a WNN model makes sense if the inversion formula of WT defined by Eq. (1) is seen like the sum of the products between the wavelet coefficients and the family of daughter wavelets (Eq. (2)). This last definition is known as inverse WT Strömberg's equation [16].

$$f(x) = \frac{1}{C_\psi}\int_{-\infty}^{\infty}\int_{-\infty}^{\infty} W_f(s,t)\frac{1}{\sqrt{|s|}}\psi\left(\frac{x-t}{s}\right)\frac{ds\,dt}{s^2} \tag{1}$$

where C_ψ is a constant that depends only on $\psi(x)$.

$$f(x) = \sum_{s=-\infty}^{\infty}\sum_{t=-\infty}^{\infty} w_{s,t}\psi_{s,t}(x) \tag{2}$$

The WNN is based on the similarity found between this definition and the output for a hidden layer in a multilayer perceptron (MLP) network structure [1]. The compact system of functions located in the hidden layer allows MLPs with only three layers (one input layer with no activation function, one hidden layer with non-linear activation function and one output linear layer) to approximate any arbitrary and continuous function [27,28]. The predetermined precision is defined by the characteristics of the family function used as well as by the convergence error. In the development of WNNs, a MLP structure with three layers is usually considered because both analysis and implementation are simpler.

Orthogonal wavelets are related with theory of multiresolution analysis and usually cannot be expressed in an informal context; these must fulfill with stringent orthogonal conditions. On the other hand, wavelet frames are constructed by simple operations of translation and dilation and are the easiest to use [16,23,29]. Although many wavelet applications use orthogonal wavelet bases, others work better with redundant wavelet families. The redundant representation offered by wavelet frames has demonstrated to be good both in signal denoising and in compression [30,31].

In this way, a signal $f(x)$ can be approximated by generalizing a linear combination of daughter wavelets $\psi_{s,t}(x)$ derived from its mother wavelet $\psi(x)$, this family of functions defined as:

$$M_c = \left\{ \frac{1}{\sqrt{|s_i|}}\psi\left(\frac{x-t_i}{s_i}\right), \quad t_i, s_i \in \Re, \quad s_i > 0 \right\} \tag{3}$$

where the translation t_i and the scaling s_i are real numbers in $\Re$.

The family of functions M_c is known as a continuous frame of $L^2(\Re)$ if there exists two constants A and B that fulfills the condition [32]:

$$A||f(x)||^2 \le \sum_{s,t} |\langle f(x), \psi_i(x)\rangle|^2 \le B||f(x)||^2 \quad \text{with} \quad A > 0, \quad B < \infty \tag{4}$$

In order to model multivariable processes, the use of multidimensional wavelets is necessary. Multidimensional wavelets are obtained from the product of P monodimensional wavelets, $\psi(a_{ij})$, of the form:

$$\Psi_i(x) = \prod_{j=1}^{P}\psi(a_{ij}) \quad \text{where} \quad a_{ij} = \frac{x - t_{ij}}{s_{ij}} \tag{5}$$

where t_{ij} and s_{ij} are the translation and scaling vectors, respectively.

2.1. WNN algorithm

The WNN architecture shown in Fig. 1 corresponds to a feed-forward MLP architecture with multiple outputs. The output $y^n(r)$ (where n is an index, not a power) depends on the connection weights $c_i(r)$ between the output of each neuron and the rth output of the network, the connection weights $w_j(r)$ between the input data and each output, an offset value $b_0(r)$ useful when adjusting functions that has a mean value other than zero, the nth input vector x^n and the wavelet function Ψ_i of each neuron. The approximated signal of the model $y^n(r)$ can be represented by Eq. (6):

$$y^n(r) = \sum_{i=1}^{K} c_i(r)\Psi_i(x^n) + b_o(r) + \sum_{j=1}^{P} w_j(r)x_j^n \quad \{i, j, K, P\} \in Z \tag{6}$$

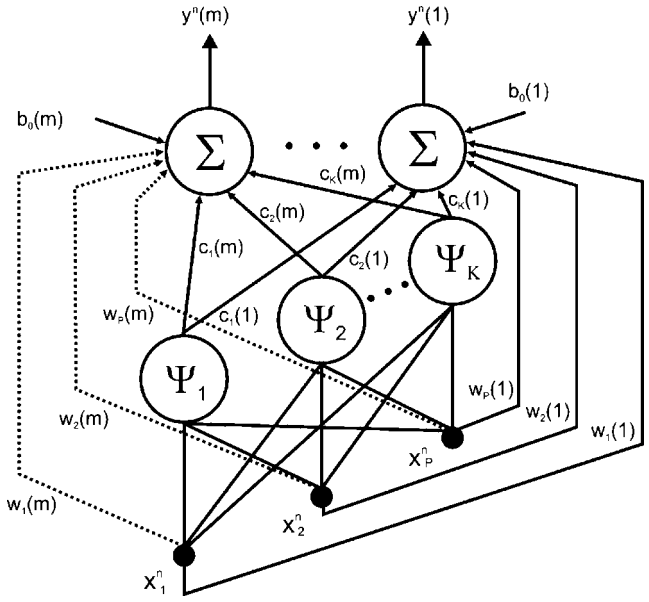

Fig. 1. WNN model. x_j^i denotes the jth current value of the ith voltammogramm, and $y^i(m)$ the sought information for each concentration compound.

where $r = 1,2,\ldots,m$, with $m \in Z$, represent the number of outputs, and subindexes i and j stand for the ith neuron in the hidden layer and the jth element in the input vector, x^n, respectively, K is the number of wavelet neurons and P is the length of input vector, x^n. With this model, a P-dimensional space can be mapped to a m-dimensional space ($R^P \rightarrow R^m$), allowing the network to predict a value for each output $y^n(m)$ when the nth voltammogram x^n is input to the trained network.

The basic neuron will be a multidimensional wavelet $\Psi_i(x^n)$ which is built using the definition (5), where scaling (s_{ij}) and translation (t_{ij}) coefficients are the adjustable parameters of the ith wavelet neuron. With this mathematical model for the wavelet neuron, the network's output becomes a linear combination of several multidimensional wavelets [15,33–35].

Some functions have been proposed in the implementation of WNN [36–38]. In the present work, the mother wavelet used as activation function corresponds to the first derivative of a Gaussian function defined by $\psi(x) = xe^{-0.5x^2}$. This function has demonstrated to be an effective function for the implementation of WNN [15].

The training procedure consists in the error *backpropagation*. This method, proposed by Rumelhart et al. [39], is an iterative algorithm that allows training of multilayer networks. The algorithm looks for the minimum of the error function from the set of training vectors. In our application, the weights change once when all the vectors have been entered to the network (after one epoch). In this way, the training process tries to diminish the difference between the outputs of the network and the expected values. The difference is evaluated according to the *Mean Squared Error* (*MSE*) function defined by Eq. (7):

$$J(\Omega) = \frac{1}{2}\sum_{n=1}^{N}\sum_{r=1}^{m}(y^n_{\text{exp}}(r) - y^n(r))^2 = \frac{1}{2}\sum_{n=1}^{N}\sum_{r=1}^{m}(e^n(r))^2 \quad (7)$$

where $y^n(r)$ is the rth output of the network and $y^n_{\text{exp}}(r)$ is the rth real value related to the input vector x^n.

Since the proposed model is of multivariable character, we define:

$$\Omega = \{b_0(r), w_j(r), c_i(r), t_{ij}, s_{ij}\} \quad (8)$$

as the set of parameters that will be adjusted during training.

These parameters must change in the direction determined by the negative of the output error function's gradient:

$$-\frac{\partial J}{\partial \Omega} = \frac{1}{N}\sum_{n=1}^{N}\sum_{r=1}^{m} e^n(r)\frac{\partial y^n(r)}{\partial \Omega} \quad \text{where} \quad \frac{\partial y^n(r)}{\partial \Omega} = \left.\frac{\partial y}{\partial \Omega}\right|_{x=x^n} \quad (9)$$

In order to obtain a weighted error that diminishes the time of training, the value $1/N$ in Eq. (9) is a term that averages the error with the number, N, of inputs vectors. The index m corresponds to the number of outputs.

The changes in network parameters are calculated at each iteration according to $\Delta\Omega = \mu(\partial J/\partial\Omega)$, where μ is a positive real value known as *learning rate*. With these changes the variables contained in Ω are updated using:

$$\Omega_{\text{new}} = \Omega_{\text{old}} + \Delta\Omega \quad (10)$$

where Ω_{old} represents the current values and $\Delta\Omega$ represents the changes.

Two conditions may stop the training process; one is to exceed a number of epochs and the other to reach the convergence error, selected as a sufficiently small number to assure consistent results.

2.2. Initialization of network parameters

An important issue during training is the initialization of network parameters, because convergence may depend on them. Traditional initialization where all the parameters are assigned with a small random value (as usually done with ANN) is not appropriate because it makes some wavelets too local, the training too slow and the error convergence difficult to be reached. Initialization reported by Oussar et al. [40], used before in a similar model [23], was found appropriate: considering a range in input vectors defined by the domain $[x_{j,\min}, x_{j,\max}]$, then the initial values of the ith neuron for translation and scaling parameters are set to $t_{ij} = 0.5(x_{j,\min} + x_{j,\max})$ and $s_{ij} = 0.2(x_{j,\min} + x_{j,\max})$, respectively, to guarantee that wavelets will not concentrate on localities of the input universe. The weights are proposed to have random initial values since its initialization is less critical than translation and scaling variables.

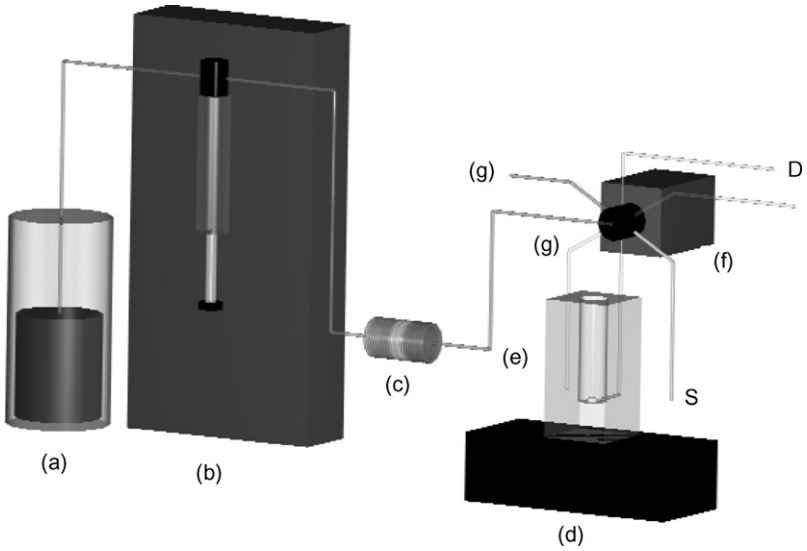

Fig. 2. Sequential Injection System used for the automated electronic tongue. (a) Diluting solution, (b) bi-directional microburette, (c) holding coil, (d) magnetic stirrer, (e) mixing cell, (f) selection valve (with 1 input and 6 outputs), (g) standard solution. D: to the detector, S: sample.

3. Materials and methods

3.1. Reagents

All reagents used were of analytical reagent grade. Doubly distilled water was used throughout. For the preparation of the three phenolic standard solutions, the right amount of the pure substances (Fluka) was dissolved in KCl (Merck) 0.1 M to ensure high electrical conductivity.

3.2. Apparatus

A Sequential Injection Analysis (SIA) automated flow system was used to prepare randomly defined standards from stock solutions and to perform the voltammetric measurements. The SIA system used in this determination is shown in Fig. 2. A bi-directional microburette (Precision Syringe drive/2 Module, Hamilton, Switzerland) equipped with a syringe of 2.5 ml (Hamilton) was used as the pumping device. The selection valve was a motorised MVP valve with a 6 way valve head, HVXM 6-5 (Hamilton). PTFE tubing (Bioblock, France) with 1 mm i.d was used to connect the different SIA components and as holding coil. Connections were attained with fittings for low-pressure chromatography. A specially designed mixing cell, made in Perspex, was used in sample preparation. Automatic stirring was used to assure homogeneity. The whole SIA system was controlled with in-house software programmed in BASIC (Quick-Basic, Microsoft, USA). Different independent text files provided the possibility of performing different sequences of liquid handling, ensuring versatility in the function of sample and/or standard solution preparation. A complete description of the developed SIA system can be found in the literature [41].

Measurements were developed using an Autolab/PGSTAT20 electrochemical system (Ecochemie, Netherlands). Reference electrode consisted in a double-junction electrode (90-02-00 model, Thermo Orion, USA). Stainless steel used as a constitutional part of the measuring cell was considered as counter electrode. Working electrode consisted in a home-made epoxy–graphite transducer, of general use in our laboratories [42].

3.3. Hardware and software environment

Data processing was performed by a AMD Turion™ 64 X2 computer. The WNN algorithm was written in MATLAB (Math Work, Natick, MA, version 7.0) by the authors and it employed the Neural Network Toolbox (V 4.0.6) for the development of ANN models. As said before, SI control was achieved by homemade software in BASIC (Quick-Basic, Microsoft, USA).

3.4. Procedures

3.4.1. Automated preparation of standards

A total amount of 89 standard solutions, an equivalent number to previous studies similar to this [41], were prepared automatically by the SI system, as demanded by specific files entered to the control program. For doing so, different volumes of stock solutions were taken, diluted appropriately and homogenized in the mixing cell. Concentration values for each standard were defined by a random number generator, through in-house software that generates the appropriate files used by the control software. By doing this, a total independence of concentrations was achieved. This fact assured us that training was not conditioned by the previous prepared solution, so memory effects, trends or drifts were minimized. The scheme of a large set of randomly generated standards was preferred over a smaller set with concentrations defined according to a factorial design. This is because, in our automated system, it does not represent to increase the experimental effort, and a larger training data set improves the confidence of the neural model [43]. Moreover, this totally random sequence in sample preparation ensures the total independence between data points. Phenolic compounds concentration varied from 0.25 to 2.5 mM for the three analytes. Fig. 3 plots the distribution of the standards in a three-dimensional space, where each point represents a triad of concentrations.

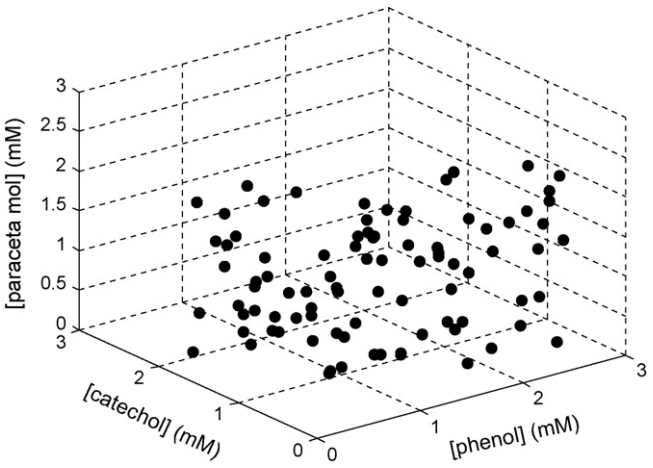

Fig. 3. Three-dimensional space of the automatically generated training standards. Each point corresponds to the triad of concentrations of the three phenolic compounds.

Each solution pumped into the detection cell was measured by linear scan voltammetry. Scans were performed from 0 to 1.15 V with a potential step of 10 mV, and a scan rate of 100 mV/s. Obtained currents depend on applied potential as well as concentrations of phenols. One reduced voltammogram of 36 current values was taken for each sample, after suppressing first 7 baseline values of the voltammogram and subsampling the rest of acquired currents, keeping one out of every three. Measured currents were in the interval 1.8–273 μA. Fig. 4 displays some voltammograms of prepared solutions having one of the considered compounds in majority, where the high degree of overlapping is manifest.

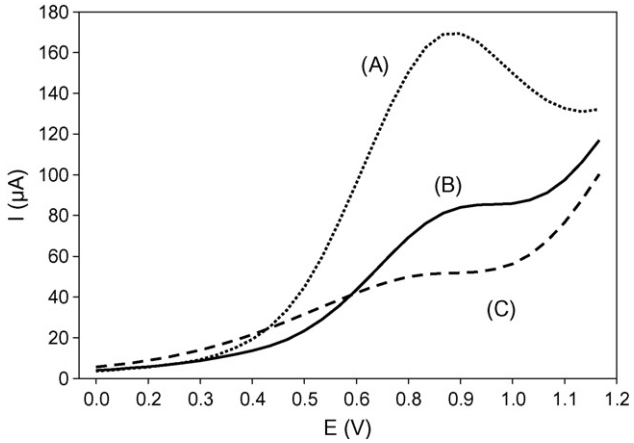

Fig. 4. Examples of voltammetric signals used. For each determination, three different phenolic compounds were mixed in a single solution by the SIA system. Similar overlapped signals are obtained, even for mixtures with different predominant compounds; concentrations (mM) of the three mixtures are (phenol, cathechol, and paracetamol): (A) 0.268, 0.048, and 2.528; (B) 2.013, 0.050, and 1.019; (C) 2.056, 0.429, and 0.212.

3.4.2. Programming

The information contained in the voltammetric signal is related with the concentration of each component under study, so that, it constitutes the input data for training and testing the WNN. On the other hand, the phenolic concentrations constitute the targets to be modeled. The task of the WNN will be to map each voltammogram represented by x^n to a point of the three-dimensional space of concentration identified by $y^n(r)$. In order to obtain this, WNN structures with a single hidden layer having 1–3 neurons and three outputs were programmed and trained to obtain the concentration of each compound. Other structures with more neurons in the hidden layer were not tested because the proposed architectures allowed to obtain satisfactory results.

3.4.3. Processing

From the 89 generated standard solutions, the input data is a voltammetric matrix of dimension [36, 89], and the target is a [36, 89] matrix (phenol, catechol and paracetamol concentrations). The input data and targets were normalized to an interval of [−1, 1] and randomly separated in two sets; two thirds of the data were used for training and the remaining third for testing.

It is known that the prediction capability in a network depends on the samples chosen for the test space. To minimize this inconvenient, the final trained model was evaluated using a cross validation method.

4. Results and discussion

4.1. WNN training

The expected output error was programmed to reach a value of 0.025 mM, evaluated by $2/NJ(\Omega)$, where $J(\Omega)$ is the MSE defined in Eq. (7); we denote this error as *Mean Squared Training Error*. Network parameters were initialized as described previously. The learning rate and the maximum number of training epochs were set to 0.005 and 10,000, respectively. In all cases, the training error was reached within less iterations than the allowed maximum. Larger values of the learning rate parameter were not used, because oscillations in the network output may impede convergence whereas smaller values may reduce speed in reaching it [23].

The selection of the number of neurons in the hidden layer was made according previous experience [23]; there, it was shown that the increase of the number of neurons in the hidden layer did not improve performance and generalization of the WNN [23]. In this way, only networks with three neurons or less in its hidden layer were evaluated.

4.2. WNN testing

Fig. 5 shows the comparative graphs between real concentrations for the three phenolic compounds and those predicted with a WNN model having a single neuron in its hidden layer, for training and testing subsets in one of the calculated cases. For further validation and to see how WNN is affected by random initialization, ten replicate training processes were performed with the same architecture, employing a *k*-fold cross validation that select the test set each time at random form from the original data universe (10 different training processes using 10 samples for the test subset and the rest for training). Table 1 summarizes this information, showing average values for each replicate's obtained versus expected comparison line plus the correlation coefficients. Slope (m) and intersection (b) that defines the comparison line $y = mx + b$ that best fits the data altogether with the error for a 95% of confidence interval are shown for each one of the networks.

In order to compare the performance of different WNN structures, architectures with 2 and 3 neurons in the hidden layer were analyzed using the same data sets and also using *k*-fold cross validation. The different results were recorded, and the comparison lines constructed for each case. Table 1 also includes the results obtained for the 2-neuron and 3-neurons architectures. Uncertainties indicated for each parameter correspond to the 95% confidence interval of the 10-replicate evaluation. From these results, it is possible to observe that the case presented before in graphic detail is only an average case from the almost infinite training possibilities and that, by increasing the number of neurons in the hidden layer, the performance of the trained model was not improved.

4.3. Conventional ANN modeling

In order to validate the WNN modeling performance, results were compared to simple ANN models trained with the same data sets used before. In this case, each voltammogram was entered directly into the ANN structure (36-neuron input layer) with an associated target of the three phenol concentrations corresponding to the particular sample.

Optimization of the ANN architecture comprised variation of the transfer function in the hidden and output layers, as well as selection of the number of neurons in the hidden layer. The modeling used Bayesian regularization algorithm, which does not make use of an internal validation stage and does not require an extra subset for this purpose [44].

ANN learning was monitored through the residual values calculated between the expected and the obtained concentrations for each compound, using the Root Mean Square Error (RMSE). The training process was stopped when the fitness degree of RMSE

Table 1
Linear regression parameters ($y = mx + b$) for the mean of the 10 *k*-fold cases of WNN uncertainly intervals calculated at the 95% confidence level employing architectures with one, two and three neurons in the hidden layer

	1 neuron			2 neurons			3 neurons		
	m	b	R	m	b	R	m	b	R
Phenol									
Training	1.013 ± 0.100	−0.018 ± 0.159	0.936	1.012 ± 0.102	−0.017 ± 0.162	0.934	1.012 ± 0.100	−0.018 ± 0.159	0.936
Testing	0.853 ± 0.145	0.225 ± 0.206	0.918	0.849 ± 0.146	0.225 ± 0.207	0.917	0.852 ± 0.145	0.228 ± 0.204	0.919
Catechol									
Training	1.006 ± 0.065	−0.006 ± 0.077	0.971	1.007 ± 0.068	−0.006 ± 0.077	0.968	1.006 ± 0.065	−0.006 ± 0.077	0.971
Testing	1.079 ± 0.122	−0.097 ± 0.149	0.961	1.088 ± 0.123	−0.107 ± 0.151	0.961	1.086 ± 0.124	−0.105 ± 0.152	0.960
Paracetamol									
Training	1.003 ± 0.107	−0.003 ± 0.080	0.972	1.003 ± 0.064	−0.003 ± 0.081	0.972	1.003 ± 0.063	−0.003 ± 0.080	0.972
Testing	0.991 ± 0.112	−0.034 ± 0.152	0.961	0.994 ± 0.111	−0.039 ± 0.151	0.962	0.991 ± 0.111	−0.034 ± 0.151	0.962

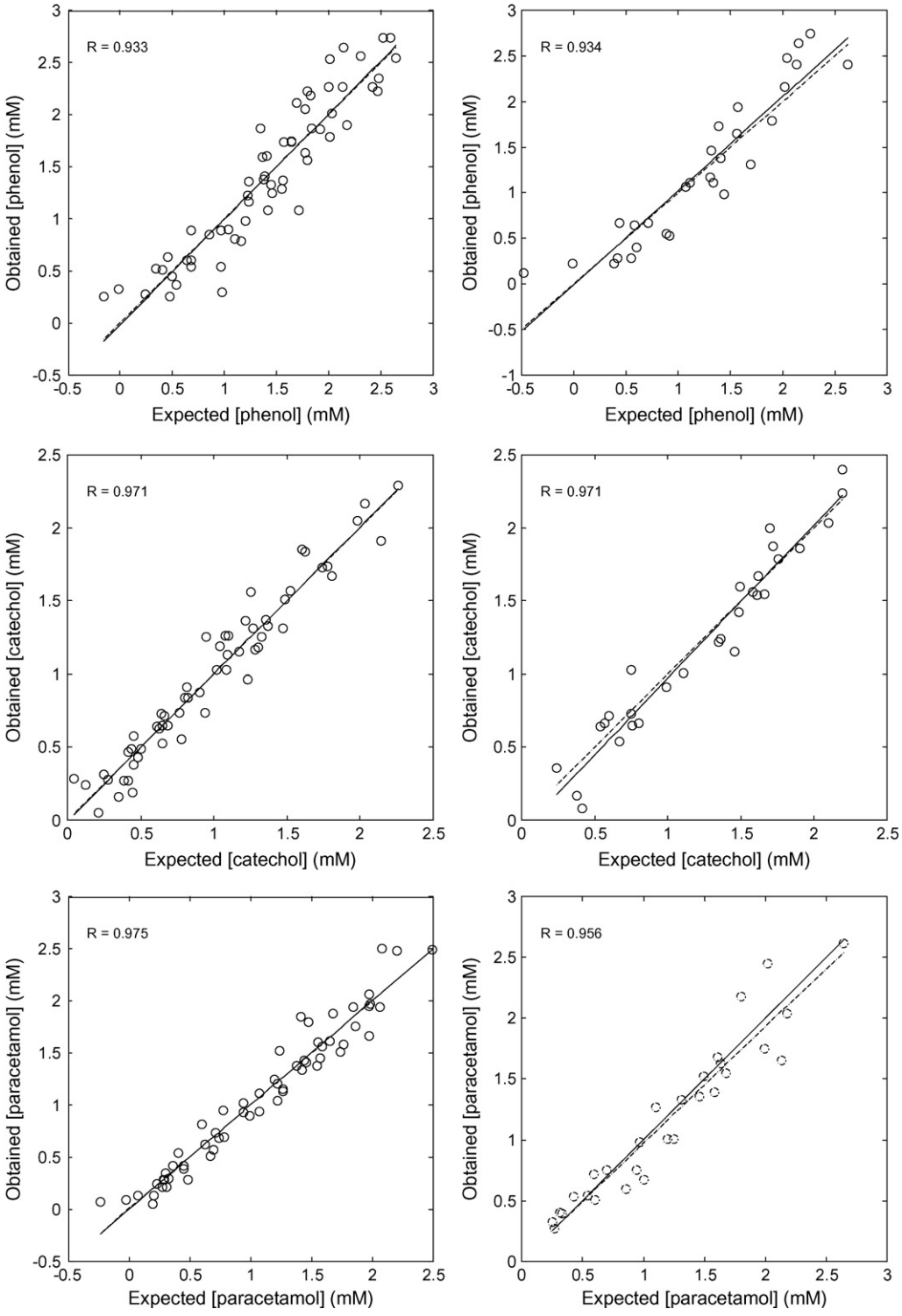

Fig. 5. Comparison between expected results and those obtained using a WNN with one neuron in the hidden layer. The graphs correspond to the three species under study. The dashed line corresponds to ideality ($y = x$) and the solid line is the regression of the comparison data. Plots on the left correspond to training and plots on the right to testing.

was achieved or the maximum numbers of epochs were completed (6000 epochs).

A study of the ANN architecture was performed in order to optimize the quantification of the three phenols. Networks with more than one hidden layer were not considered as preview experience and reports have shown that is possible to obtain an appropriate level of modeling using only one hidden layer [10–14]. After preliminary evaluations of transfer functions used in the hidden and output layers, combinations of tan-sigmoidal (Tansig), sat-lineal (Satlin), pure-lineal (Purelin) and log-sigmoidal (Logsig) were tested in order to obtain the combination of hidden/output transfers function offering the lowest RMSE. The best model was obtained using a network with an architecture $36 \times 3 \times 3$ that used the Tansig transfer function in the hidden layer and the Purelin

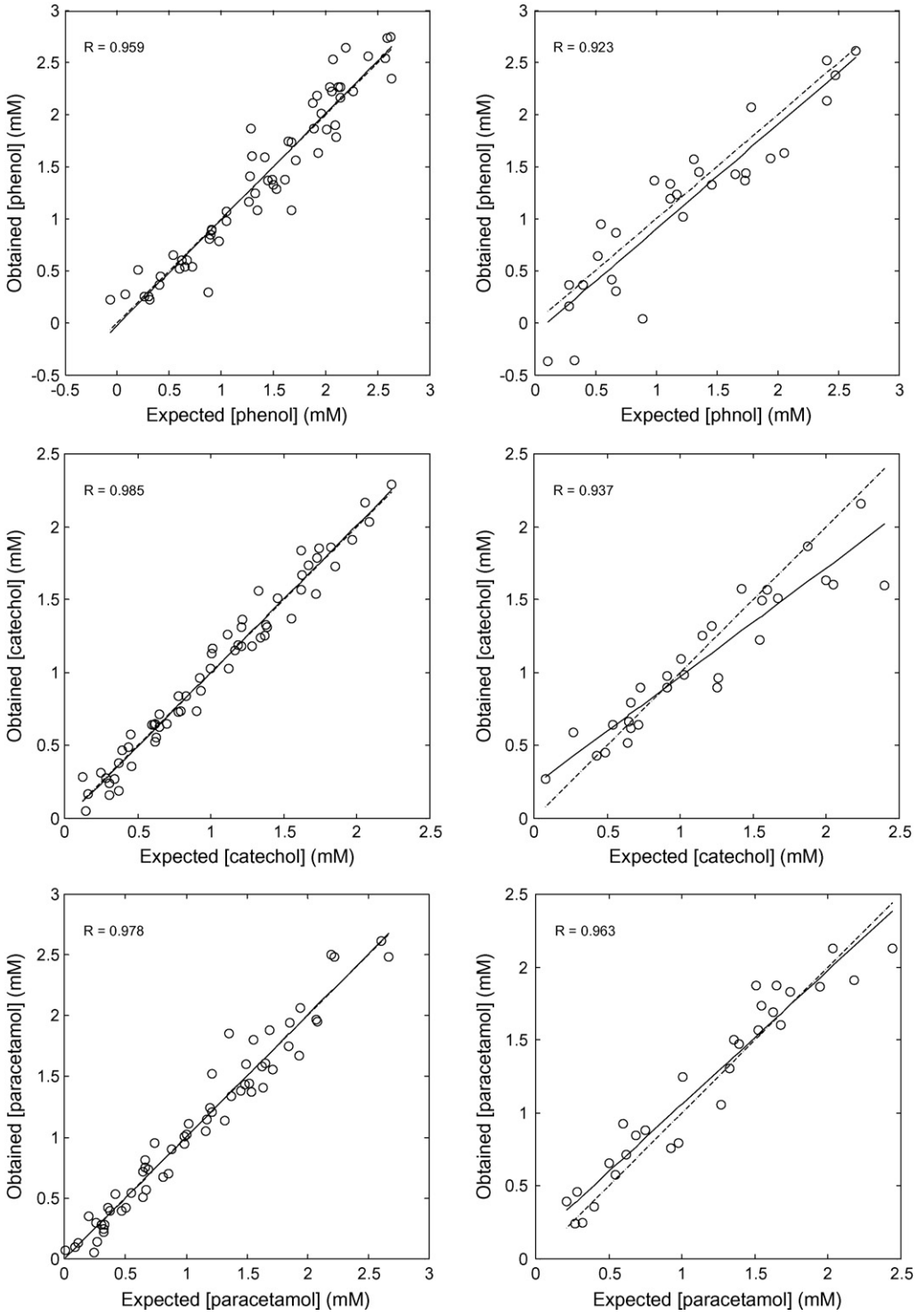

Fig. 6. Comparison between expected results and those obtained with the ANN. The graphs correspond to the three species under study. The dashed line corresponds to ideality ($y = x$) and the solid line is the regression of the comparison data. Plots on the left correspond to training and plots on the right to testing.

function in the output layer. The corresponding results are shown in Fig. 6 while Table 2 contains the information of the comparison line obtained versus expected concentrations, $y = mx + b$ that best fits the data.

4.4. Comparison of WNN and ANN models

The performance obtained with the proposed WNN architecture was better than that ANN using Bayesian regularization algorithm. In the case of the WNN, the correlation values (R) were greater than 0.9 both for training and testing sets, and for the three determined phenols. Although the correlation values for training are slightly better in the ANN case, the values for testing using WNNs were always the best, a much more significant feature, as it is more interesting to generalize than to memorize the data.

In both cases, the proper choice of the number of hidden neurons used is an important task to obtain the desired prediction models. With the use of a WNN model, this selection is easier. Neurons in

Table 2
Linear regression parameters ($y = mx + b$) obtained with training and testing data sets using the ANN with three outputs and three neurons in the hidden layer

Compound	Training			Testing		
	m	b	R	m	b	R
Phenol	1.017 ± 0.079	−0.025 ± 0.125	0.959	1.003 ± 0.165	−0.103 ± 0.237	0.923
Catechol	1.011 ± 0.046	−0.012 ± 0.054	0.985	0.746 ± 0.110	0.225 ± 0.141	0.937
Paracetamol	1.004 ± 0.056	−0.004 ± 0.072	0.978	0.918 ± 0.101	0.139 ± 0.132	0.963

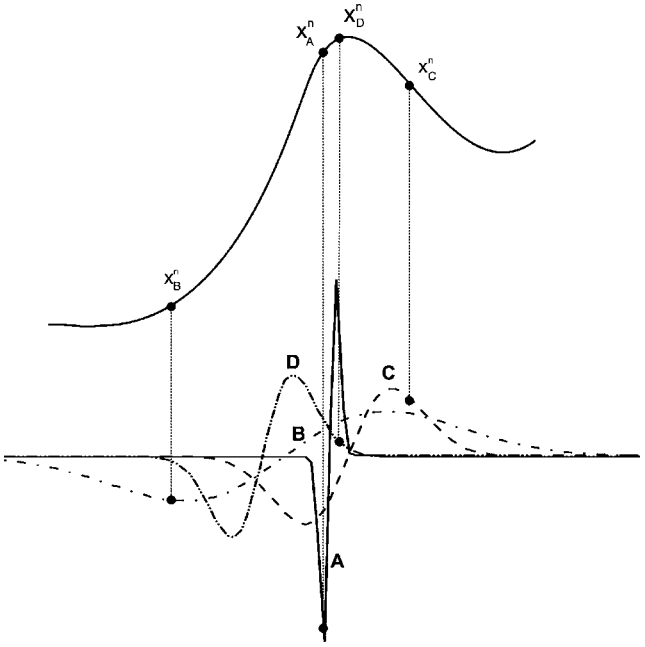

Fig. 7. Some points in a voltammetric signal represented by a set of wavelet functions. (a) Less scaled wavelet. (b) Most scaled wavelet. (c and d) Scaled and translated versions of a wavelet among the space defined by the voltammogram.

the hidden layer have wavelet activation functions with different resolutions, providing this wavelets locally responsive information about the input. This inherent property allows to reduce the number of neurons in the architecture. Fig. 7 is a representation of the wavelet's family, obtained once the WNN training was finished; in this graph, each input point is approximated by means of a point pertaining to the daughter wavelet of the generated family that represents the total input space.

Using frames to generate daughter wavelets, it is possible to approximate any continuous nonlinear mapping at any resolution, for the highest this may be. In the WNN there is one weight w_i for each ith data point contained in the set of voltammograms x_i^n. After training the network, the set $\{w_j(r)\}$ establishes which points in a voltammogram contribute more significantly to the quantification of the chemical species. Although when increasing the number of neurons in the WNN architecture one would expect a better generalization of the input space, we believe that it also means an increase in the redundancy of wavelets that represent the original signals. The reason for the surprisingly good results from using a single neuron in the hidden layer, are thought then, to be due to the reduction of the redundancy between families generated by neighbor neurons. As was observed with the phenols study case, such a single neuron architecture improved the generalization of the trained model.

5. Conclusions

The selected case here showed the satisfactory quantification of the three phenols (phenol, catechol and paracetamol) from a strongly overlapped voltammetric signal. WNNs have shown to be a valid chemometric tool for signal extraction and quantification. Training process was successfully accomplished, showing the good characteristics of the WNN for modeling complex input–output relationships. In this case, voltammograms, analytical signals that due to its complexity normally require a stage of feature extraction prior to any modeling or pattern recognition. In this way, WNN adjusted the parameters for a family of wavelet functions that best fitted the shapes and frequencies of the voltammetric signals. Obtaining a family of wavelets (that represents the original voltammogram) may also be exploited for qualitative identification of electrochemical species, due to the linear characteristics of the multidimensional wavelets in the WNN's architecture.

Acknowledgements

This work was supported by Spanish Agency AECI with the framework of the proyect A/012192/07 (AMALENG) and CONACyT (Mexico) within the project 43553. Mobility of researchers was possible though the Alfa network BioSenIntg (Alfa II-0486-FCFA-FCD-FI, European Union).

References

[1] Y. Meyer, Wavelets: Algorithms and Applications, Society for Industrial and Applied Mathematics, SIAM, Philadelphia, PA, 1994.
[2] A.K.-M. Leung, F. Chau, J. Gao, Chemometr. Intell. Lab. Syst. 43 (1998) 165.
[3] S. Xue-Guang, A. Kai-Man, C. Foo-Tim, Acc. Chem. Res. 36 (2003) 276.
[4] G. Kaiser, A Friendly Guide to Wavelets, Birkhäuser, Boston, MA, 1994, p. 300.
[5] R.G. Brereton, Analyst 122 (1997) 1521.
[6] A. Cladera, J. Alpízar, J.M. Estela, V. Cerdà, M. Catasús, E. Lastres, L. García, Anal. Chim. Acta 350 (1997) 163.
[7] A.A. Ensafi, T. Khayamian, M. Atabati, Talanta 57 (2002) 785.
[8] W. Guo, P. Zhu, H. Brodowsky, Talanta 44 (1997) 1995.
[9] C. Bessant, S. Saini, Anal. Chem. 71 (1999) 2806.
[10] J. Gallardo, S. Alegret, R. Muñoz, M. De Roman, L. Leija, P.R. Hernández, M. del Valle, Anal. Bioanal. Chem. 377 (2003) 248.
[11] F. Despagne, D.L. Massart, Analyst 123 (1998) 157R.
[12] M. Bos, A. Bos, W.E. Van der Linden, Analyst 118 (1998) 323.
[13] L. Moreno-Baron, R. Cartas, A. Merkoçi, S. Alegret, J.M. Gutiérrez, L. Leija, P.R. Hernández, R. Muñoz, Anal. Lett. 38 (2005) 2189.
[14] L. Moreno-Baron, R. Cartas, A. Merkoci, S. Alegret, M. del Valle, L. Leija, P.R. Hernandez, R. Munoz, Sens. Actuators B113 (2006) 487.
[15] Q. Zhang, A. Benveniste, IEEE Trans. Neural Netw. 3 (1992) 889.
[16] M. Akay, in: M. Akay (Ed.), Biomedical Signal Processing. IEEE Press Series on Biomedical Engineering, Wiley-IEEE Press, Piscataway, NJ, 1997, p. 739.
[17] L. Liu, Q. Guo, J. Chem. Inf. Comput. Sci. 39 (1999) 133.
[18] X. Zhang, J. Qi, R. Zhang, M. Liu, Z. Hu, H. Xue, B. Fan, J. Comput. Chem. 25 (2001) 125.
[19] T. Khayamian, M. Esteki, J. Supercrit. Fluids 32 (2004) 73.
[20] Z. Kardanpour, B. Hemmateenejad, T. Khayamian, Anal. Chim. Acta 531 (2005) 285.
[21] R. Tabaraki, T. Khayamian, A.A. Ensafi, J. Mol. Graph. 25 (2005) 46.
[22] T. Khayamian, A.A. Ensafi, A. Bendivi, Talanta 69 (2006) 1176.
[23] A. Gutés, F. Céspedes, R. Cartas, S. Alegret, M. del Valle, J.M. Gutierrez, R. Muñoz, Chemometr. Intell. Lab. Syst. 83 (2006) 169.
[24] L. Nie, S. Wu, J. Wang, L. Zheng, X. Lin, L. Rui, Anal. Chim. Acta 450 (2001) 185.
[25] M.C. Ortiz, J. Arcos, L. Sarabia, Chemometrics Intell. Lab. Syst. 34 (1996) 245.
[26] R.G. Brereton, Analyst 125 (2000) 2125.
[27] K. Hornik, Neuronal Netw. 2 (1989) 359.
[28] F. Scarcelli, A.C. Tsoi, Neural Netw. 11 (1998) 15.
[29] C.E. Heil, D.F. Walnut, SIAM Rev. 31 (1989) 628.
[30] I. Daubechies, A. Grossmann, Y. Meyer, J. Math. Phys. 27 (1986) 1271.
[31] I. Daubechies (Ed.), Ten Lectures on Wavelets, SIAM, Philadelphia, PA, 1992.
[32] T. Kugarajah, Q. Zhang, IEEE Trans. Neural Netw. 6 (1995) 1552.
[33] M. Cannon, J.E. Slotine, Neurocomputing 9 (1995) 293.

[34] S.G. Mallat, IEEE Trans. Pattern Anal. Mach. Intell. 11 (1989) 674.
[35] J. Zhang, G.G. Walter, Y. Miao, W.N.W. Lee, IEEE Trans. Signal. Process. 43 (1995) 1485.
[36] Q.X. Guo, L. Liu, W.S. Cai, Y. Jiang, Y.C. Liu, Chem. Phys. Lett. 290 (1998) 514.
[37] X. Zhang, J. Qi, R. Zhang, M. Liu, Z. Hu, H. Xue, B. Fan, Comput. Chem. 25 (2001) 125.
[38] H. Zhong, J. Zhang, M. Gao, J. Zheng, G. Li, L. Chen, Chemometr. Intell. Lab. Syst. 59 (2001) 67.
[39] D.E. Rumelhart, G.E. Hilton, R.J. Williams, in: D.R. Rumelhart, J.L. McClelland (Eds.), Parallel Distributed Processing: Explorations in the Microstructures of Cognition, vol. 1, Foundations, MIT, Cambridge MA, 1986 (Chapter 8).
[40] Y. Oussar, I. Rivals, L. Personnaz, G. Dreyfus, Neurocomputing 20 (1998) 173.
[41] A. Gutés, F. Céspedes, S. Alegret, M. del Valle, Talanta 66 (2005) 1187.
[42] F. Céspedes, S. Alegret, Trends Anal. Chem. 19 (2000) 276.
[43] V. Pravdova, M. Pravda, G. G: Guilbault, Anal. Lett. 35 (2002) 2389.
[44] H. Demuth, M. Beale, Neural Network Toolbox, User's guide. Version 4, The Mathworks Inc., Natick, MA, 2005.

Talanta 76 (2008) 301–308

Contents lists available at ScienceDirect

Talanta

journal homepage: www.elsevier.com/locate/talanta

Determination of trace metals by anodic stripping voltammetry using a bismuth-modified carbon nanotube electrode

Gil Ho Hwang[a], Won Kyu Han[a], Joon Shik Park[b], Sung Goon Kang[a,*]

[a] Department of Materials Science and Engineering, Hanyang University, 17 Haengdang-dong, Seongdong-gu, Seoul 133-791, Republic of Korea
[b] Nano-mechatronics Research Center, Korea Electronics Technology Institute, 68 Yatap, Bundang, Seongnam, Kyunggi 463-816, Republic of Korea

ARTICLE INFO

Article history:
Received 28 November 2007
Received in revised form 26 February 2008
Accepted 26 February 2008
Available online 4 March 2008

Keywords:
Carbon nanotubes
Bismuth film
Screen printing
Anodic stripping voltammetry
Heavy metal

ABSTRACT

A bismuth-modified carbon nanotube electrode (Bi-CNT electrode) was employed for the determination of trace lead, cadmium and zinc. Bismuth film was prepared by in situ plating of bismuth onto the screen-printed CNT electrode. Operational parameters such as preconcentration potential, bismuth concentration, preconcetraion time and rotation speed during preconcentration were optimized for the purpose of determining trace metals in 0.1 M acetate buffer solution (pH 4.5). The simultaneous determination of lead, cadmium and zinc was performed by square wave anodic stripping voltammetry. The Bi-CNT electrode presented well-defined, reproducible and sharp stripping signals. The peak current response increased linearly with the metal concentration in a range of 2–100 μg/L. The limit of detection was 1.3 μg/L for lead, 0.7 μg/L for cadmium and 12 μg/L for zinc (S/N = 3). The Bi-CNT electrode was successfully applicable to analysis of trace metals in real environments.

1. Introduction

In stripping voltammetry, mercury has been widely used as the working electrode owing to its remarkable analytical properties. However, the toxicity of mercury restricts the continued use of mercury as an electrode material and intensive researches have been attempted to introduce mercury-free sensors. Bismuth, known as an environmentally friendly material, is considered as the best alternative material due to its comparable performance to mercury for the electrochemical analysis [1–5]. The advantageous stripping performance of bismuth is based on its fusing alloy formation with other metals [6].

Carbon nanotubes (CNTs) have received increasing attention due to their high electrical conductivity, high surface area, significant mechanical strength and good chemical stability [7–10]. Recently, numerous investigations have been carried out to explore the potential applications of CNTs such as hydrogen storage [11], quantum wires [12], electron field emission sources [13] and electronic devices [14]. Moreover, in an analytical procedure, the electrochemical use of CNTs as the electrode material could greatly enhance the voltammetric response of organic and inorganic analytes [15–17]. Liu et al. reported that CNT nanoelectrode array with a bismuth film offered an excellent electrochemical sensing platform for voltammetric analysis [18]. But, this method is laborious and relatively time-consuming due to the CNTs growth and passivation layer formation.

In this study, we prepared the CNT electrode by screen-printing technique. This technique was well established for the production of low cost, reproducible and sensitive electrochemical sensors. Screen-printed sensors have been widely used for environmental, biomedical and industrial monitoring [19,20]. The electrochemical characteristics of CNT electrode were compared with glassy carbon, activated carbon and graphite electrodes. For the determination of lead, cadmium and zinc, the CNT electrode was modified with in situ plated bismuth film and the performance of the bismuth-modified CNT electrode (Bi-CNT electrode) was evaluated in synthetic solutions and real samples of river water.

2. Experimental

2.1. Apparatus

All electrochemical experiments were performed with the CHI model 750 potentiostat (CH instruments) interfaced with a personal computer. A conventional three-electrode cell configuration was employed for the voltammetric measurements. A CNT electrode (3-mm diameter disk) was used as the working electrode, with SCE (Fisher Scientific) and platinum mesh (Alfa Aesar) for the reference and the counter electrode, respectively.

* Corresponding author. Tel.: +82 2 2220 0404; fax: +82 2 2296 4560.
E-mail address: skang@hanyang.ac.kr (S.G. Kang).

0039-9140/$ – see front matter © 2008 Elsevier B.V. All rights reserved.
doi:10.1016/j.talanta.2008.02.039

Table 1
The effects of additions of some interferents on the stripping response of 100 μg/L lead, cadmium and zinc

Additives (μg/L)	Peak current decrease (%)		
	Pb	Cd	Zn
Copper			
100	17.2	2.3	85.6
200	25.5	20.4	90.1
400	65.5	71.2	100
Tin			
100	1.2	0.7	3.2
200	0.5	2.5	0.5
400	2.1	1.0	3.8
Benzene			
20	1.2	0.9	91.3
50	7.6	8.7	83.6
100	10.3	19.1	80.7
1000	17.9	29.5	83.8
Xylene			
20	2.4	9.2	85.6
50	31.1	12.9	100.0
100	32.5	19.4	100.0
1000	34.9	60.4	100.0
PDDA			
100	1.6	2.1	100.0
400	4.4	37.3	100.0
2000	2.8	43.9	100.0
Triton X-100			
100	0.2	8.5	17.2
400	39.0	41.9	70.9
2000	51.4	45.2	82.0
SDS			
100	0.4	1.7	3.2
400	1.2	2.3	4.1
2000	1.4	2.6	4.4
PSS			
100	−19.6	−21.0	−152.9
400	−36.3	−33.2	−247.0
2000	−2.7	2.7	46.4

Positive values are related to the decrease of the peak current and negative values are related to the increase of the peak current.

2.2. Reagents

All chemicals used in this study were of analytical reagent grade and used without further purification. Bismuth, lead, cadmium and zinc standard stock solutions (1000 mg/L, atomic absorption standard solution) were obtained from Kanto Chemical. Sodium acetate and acetic acid were purchased from Aldrich. 0.1 M acetate buffer (pH 4.5) was used as supporting electrolyte. Carbon nanotubes (MWNT), carbon, glassy carbon, activated carbon and graphite were supplied by Aldrich. Epoxy and silver paste was obtained from Sungji Tech. Deionized water (∼18 MΩ cm) was used throughout.

2.3. Electrode preparation

CNTs, glassy carbon, activated carbon and graphite pastes were prepared by mixing with a binder (SJ-52-1, Sungji Tech) using a pestle and mortar. The solid contents of the pastes were 15, 25 and 30 wt.%, respectively. Commercially available silver and epoxy paste were used to form the metallic connection and insulating layer, respectively. First, silver paste was printed on the alumina plate to form the metallic connection and then the alumina substrate was baked on the hot plate at 130 °C for 30 min. The same baking procedure was repeated for each screen-printing step. After cooling it at room temperature, CNT paste served as a working electrode was formed onto the silver layer. Finally, the epoxy paste was printed over the sensor strip except the silver electrical connection and sensing area (3-mm diameter disk).

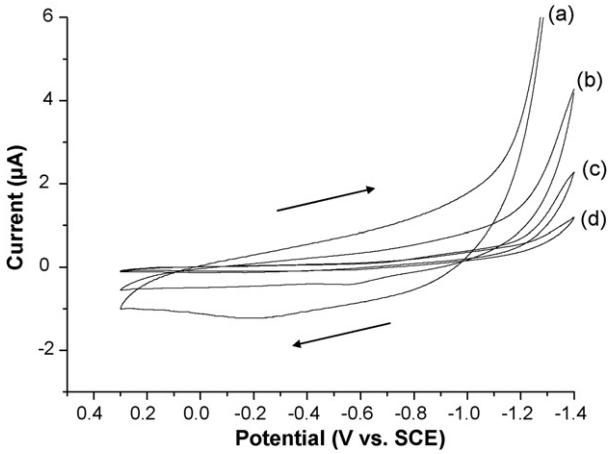

Fig. 1. Cyclic voltammograms of different carbon electrodes in 0.1 M acetate buffer (pH 4.5): (a) CNT, (b) glassy carbon, (c) activated carbon and (d) graphite. Supporting electrolyte: 0.1 M acetate buffer (pH 4.5); scan rate: 10 mV/s.

2.4. Procedure

All measurements were carried out in 0.1 M acetate buffer (pH 4.5) containing 1000 μg/L of bismuth. A preconcentration potential of −1.4 V (vs. SCE) was applied to the working electrode under stirring conditions. The stirring was stopped and after 10 s equilibration time, the square wave anodic stripping voltammograms were recorded between −1.4 and 0.3 V (frequency: 50 Hz, pulse height: 50 mV, step increment: 5 mV). The electrode was cleaned for 30 s at 0.3 V to remove the residual metals and bismuth film under stirring conditions. After recording the background voltammograms in 0.1 M acetate buffer (pH 4.5) containing 1000 μg/L of bismuth, lead, cadmium and zinc standard solutions were added to the cell as required and the measurements were repeated five times. All experiments were performed at room temperature.

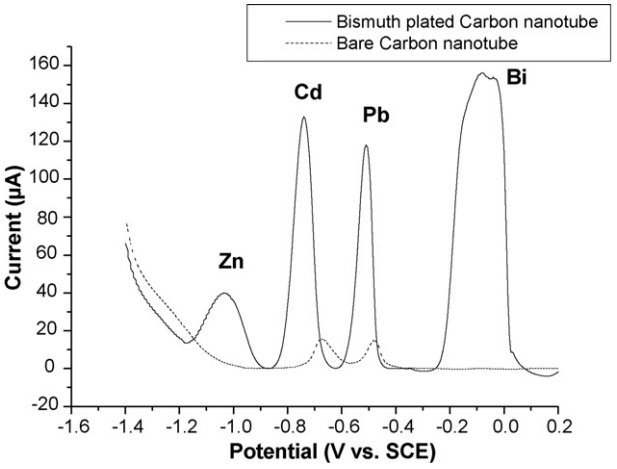

Fig. 2. Anodic stripping voltammograms of 100 μg/L lead, cadmium and zinc at bare carbon nanotube and in situ plated bismuth film on carbon nanotube. Supporting electrolyte: 0.1 M acetate buffer (pH 4.5); deposition potential: −1.4 V; deposition time: 300 s; frequency: 50 Hz; pulse height: 50 mV; step increment: 5 mV.

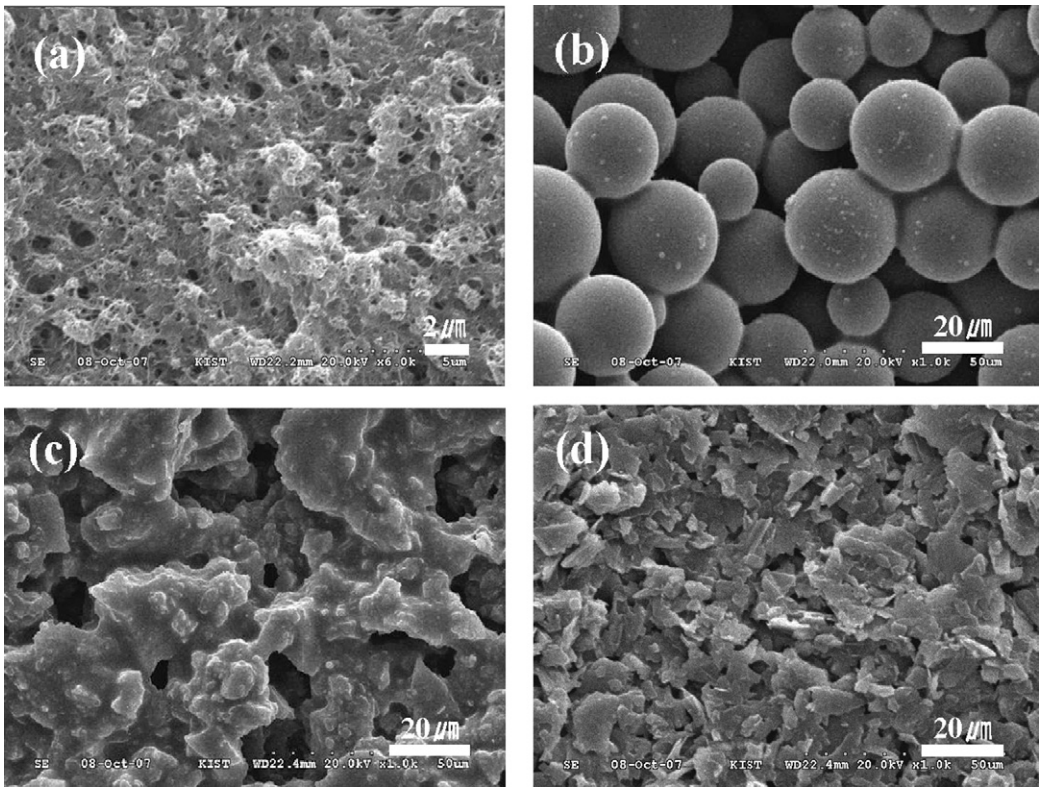

Fig. 3. SEM images of different carbon electrodes: (a) CNTs, (b) glassy carbon, (c) activated carbon and (d) graphite.

3. Results and discussion

3.1. Sensitivity of different carbon materials

The capacitance and sensitivity of different carbon materials (CNTs, activated carbon, glassy carbon, graphite) were compared by the measurement of cyclic voltammetry and anodic stripping voltammetry in 0.1 M acetate buffer solution (pH 4.5).

Fig. 1 shows the cyclic voltammograms of different carbon materials under the above-mentioned conditions. The background current of the CNTs increased rapidly below −1.1 V, while glassy carbon, activated carbon and graphite exhibited the lower background current and more negative hydrogen evolution potential than the CNTs. These results indicate that CNTs cannot be applicable for the determination of zinc since they had the narrow potential window and their hydrogen evolution potential was more positive than the reduction potential of zinc (around −1.3 V). However, when the bismuth film was plated on the CNT electrode, the voltammetric analytical curve of the electrode depended on the bismuth film on the substrate. The potential window of the bismuth was limited between its oxidation potential and hydrogen evolution potential. In general, traces of most heavy metals except for zinc can be determined using the bismuth film successively as their redox potential is more negative than the oxidation potential of bismuth and more positive than their hydrogen evolution potential. Although CNTs themselves might restrict the potential window due to their more positive hydrogen evolution potential, in these experiments, zinc was successfully determined at the Bi-CNT electrode (Fig. 2). Therefore, CNTs could be used as the substrate for bismuth film, which is suitable for the determination of most heavy metals including zinc.

In Fig. 1, the CNTs produced the relatively high background current. The charge of the double layer and faradaic processes are the contributing factors to the background current [21]. Since no significant redox peaks were observed in cyclic voltammograms, the charge of the double layer, which is proportional to the surface area, was the main contributing factor. The background current was enlarged about 3–10 times in CNTs compared to the other substrate materials. The increase of the surface area at the CNTs could be attributed to the larger quantities of active sites on it.

Fig. 3 displays SEM images of the different carbon electrodes. Individual particles were homogeneously distributed throughout the electrode surface. CNTs revealed three-dimensional bush-like networks as the most unique property of the CNTs and they had a much larger real surface area than the apparent geometric area (Fig. 3). This increase of surface area resulted in the enhancement of the capacitance at the CNT electrode.

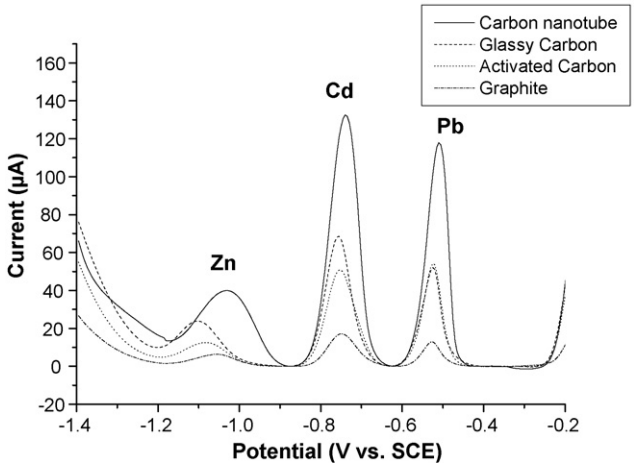

Fig. 4. Anodic stripping voltammograms of 100 μg/L lead, cadmium and zinc at in situ plated bismuth film on different carbon electrodes. Other conditions as in Fig. 2.

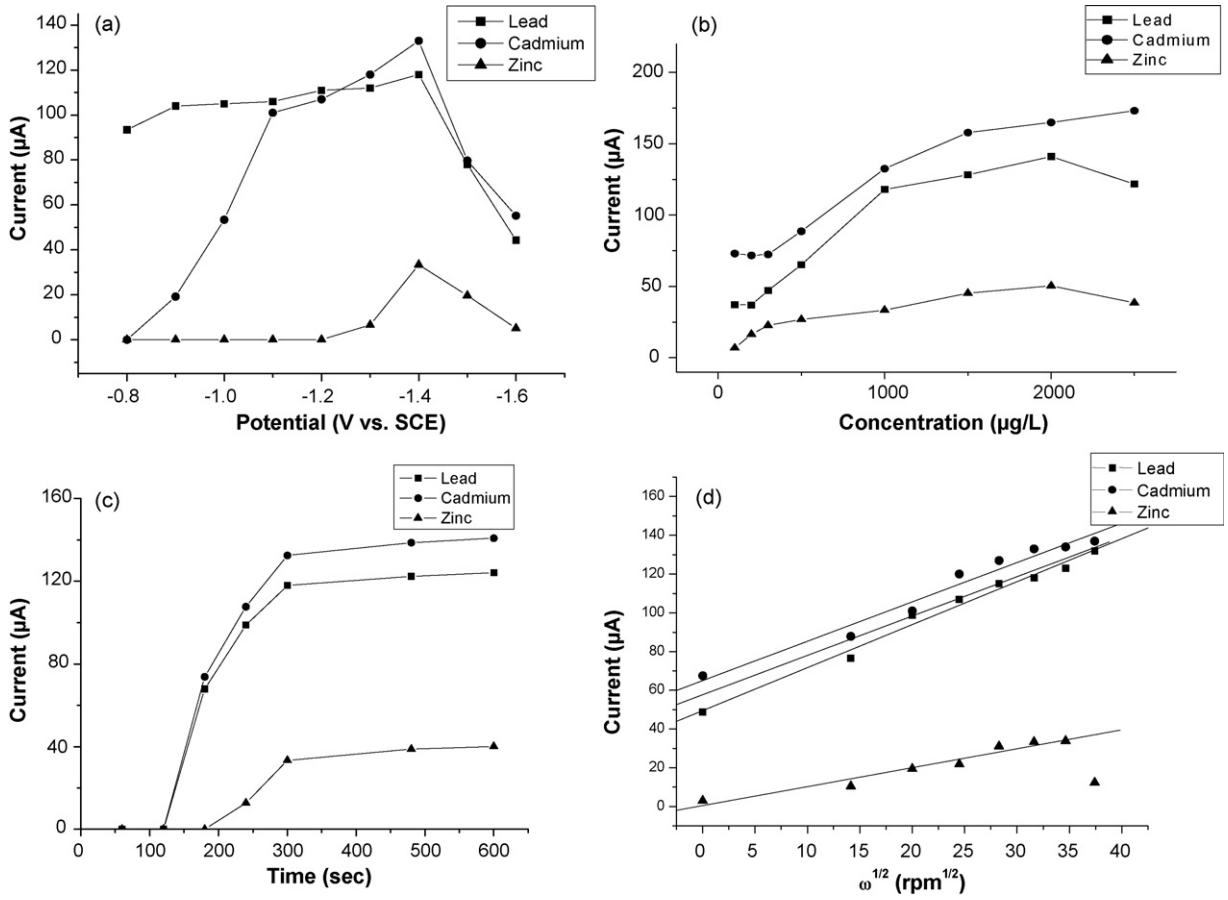

Fig. 5. Effect of the preconcentration potential (a), bismuth ion concentration (b), preconcentration time (c) and rotation speed during preconcentration (d) on the stripping peak current. Other conditions as in Fig. 2.

Stripping voltammograms of different carbon electrodes on which bismuth was in situ plated are illustrated in Fig. 4. Stripping voltammograms were obtained in 0.1 M acetate buffer solution (pH 4.5) containing 100 μg/L of lead, cadmium and zinc. For the comparison of the resulting voltammograms of each electrode, the baselines were fitted. Hydrogen evolution, which determined the potential window, occurred at about −1.2 V on these electrodes. Although the bismuth plated graphite electrode produced the flattest baseline among them, the Bi-CNT electrode exhibited the sharpest and the highest peak current. And the sensitivity of the electrodes decreased in the order of glassy carbon, activated carbon and graphite electrode. The sensitivity of the Bi-CNT electrode was two times higher than that of glassy carbon. The sensitivity could be dependent on paste preparation conditions and reactivity of the electrodes. However, it was clear that the CNT-based electrode had much better sensitivity than the other electrodes for anodic stripping voltammetry.

3.2. Effect of experimental variables

3.2.1. Preconcentration potential

As shown in Fig. 5(a), the stripping responses of cadmium and zinc were found to occur at potential more negative than −0.8 and −1.3 V, respectively. As the preconcentration potential became more negative, the peak current of cadmium and zinc increased up to −1.4 V. The lead peak current did not increase significantly and it was unaffected by the preconcentration potential due to its more positive reduction potential. The evolution of hydrogen gas from the CNT electrode surface started to occur at −1.2 V and could damage the bismuth film when more negative potential was applied. This explains the significant stripping signal decreases below −1.4 V. For this reason, zinc could be measured within a very narrow range of −1.3 to −1.4 V. A potential of −1.4 V was thus chosen as optimum preconcentration potential.

3.2.2. Bismuth concentration

The thickness of the bismuth film depended on its ion concentration and preconcentration time. Although it has been reported that the increase of bismuth film thickness resulted in the background current increase at negative potentials, where the zinc peak appeared [22], it was not obviously observed. As expected, higher bismuth concentration caused the more negative hydrogen overpotential and bismuth film thickness did not affect the peak potential of lead, cadmium and zinc.

In Fig. 5(b), lead and cadmium peak currents increased rapidly over 200 and 300 μg/L of bismuth ion concentration, respectively. As lead has more positive reduction potential than cadmium and zinc, lead can be determined at lower bismuth concentration. At high bismuth concentration, peak current reached a plateau corresponding to the saturation of bismuth film on the CNT electrode [23]. An excess concentration of bismuth ions did not lead to a substantial increase in sensitivity over the bismuth concentration of 1000 μg/L. Thus, bismuth concentration of 1000 μg/L was selected.

3.2.3. Preconcentration time

In Fig. 5(c), the peak currents were not observed at all until 120 s. Lead and cadmium peak currents increased rapidly with the preconcentration time in the time interval from 120 to 300 s, while

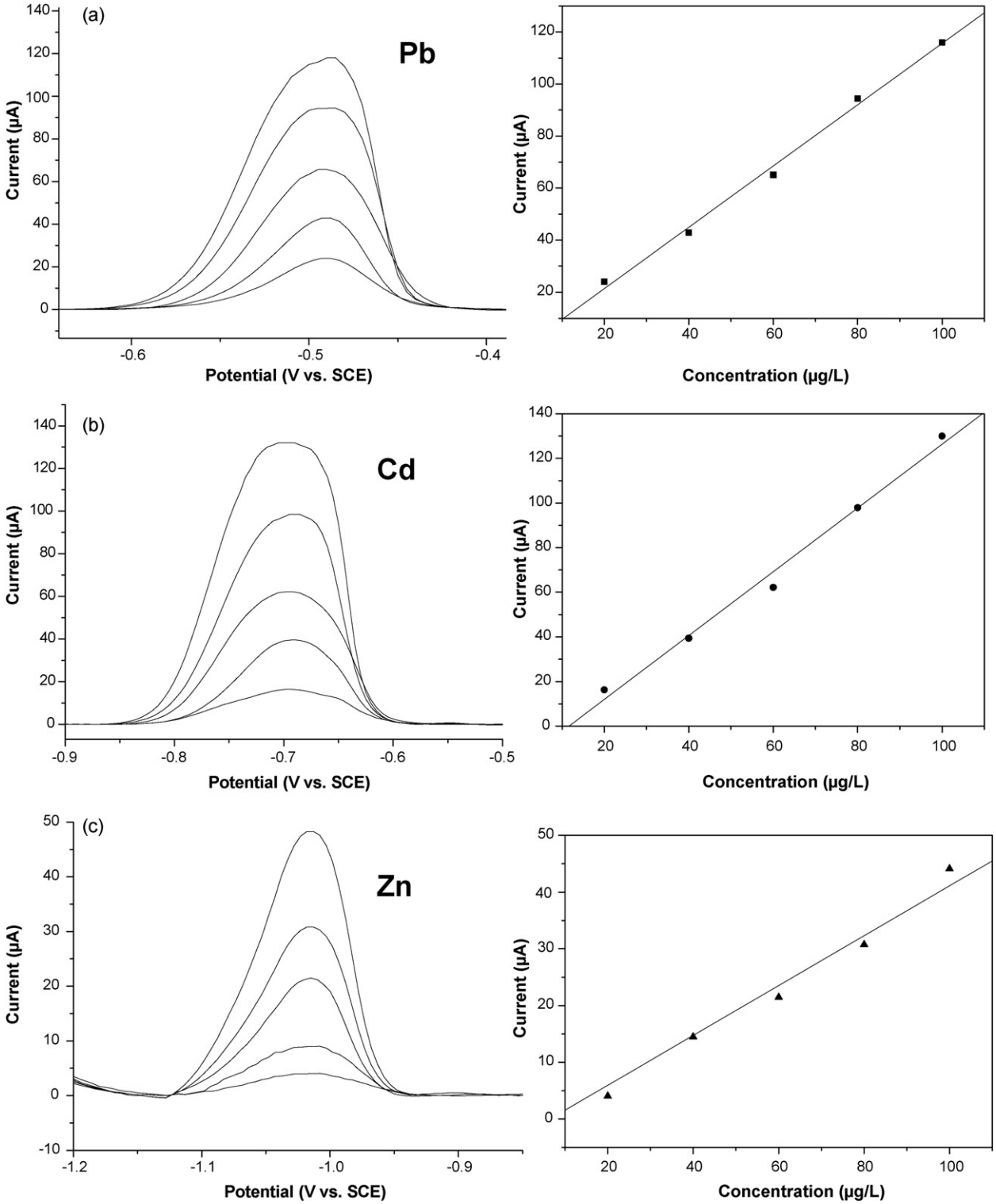

Fig. 6. A series of voltammograms for increasing concentration of lead (a), cadmium (b) and zinc (c) obtained with Bi-CNT electrode. Other conditions as in Fig. 2.

the zinc peak current started to increase after 180 s. It is considered that both lead and cadmium, which have more positive reduction potential than zinc, competed with zinc and suppressed the zinc peak. For the long preconcentration time above 300 s, the current response of all the electrodes attained constant values because of the excess deposition of bismuth film on the CNT electrode, similar to the influence of bismuth ion concentration. Metal ions were preconcentrated for 300 s for further experiments.

3.2.4. Rotation speed during preconcentration step

The mass transport behavior during preconcetration step was investigated by varying the rotation speed in the range of 0–1400 rpm as shown in Fig. 5(d). As indicated in the Levich equation, the plot of the stripping current showing the mass transport behavior was linear with the square root of the electrode rotation speed (lead: $i = 4.9499\text{E}{-5} + 2.21933\text{E}{-6}\omega^{1/2}$, $R = 0.993$; cadmium: $i = 6.50285\text{E}{-5} + 2.03079\text{E}{-6}\omega^{1/2}$, $R = 0.984$;

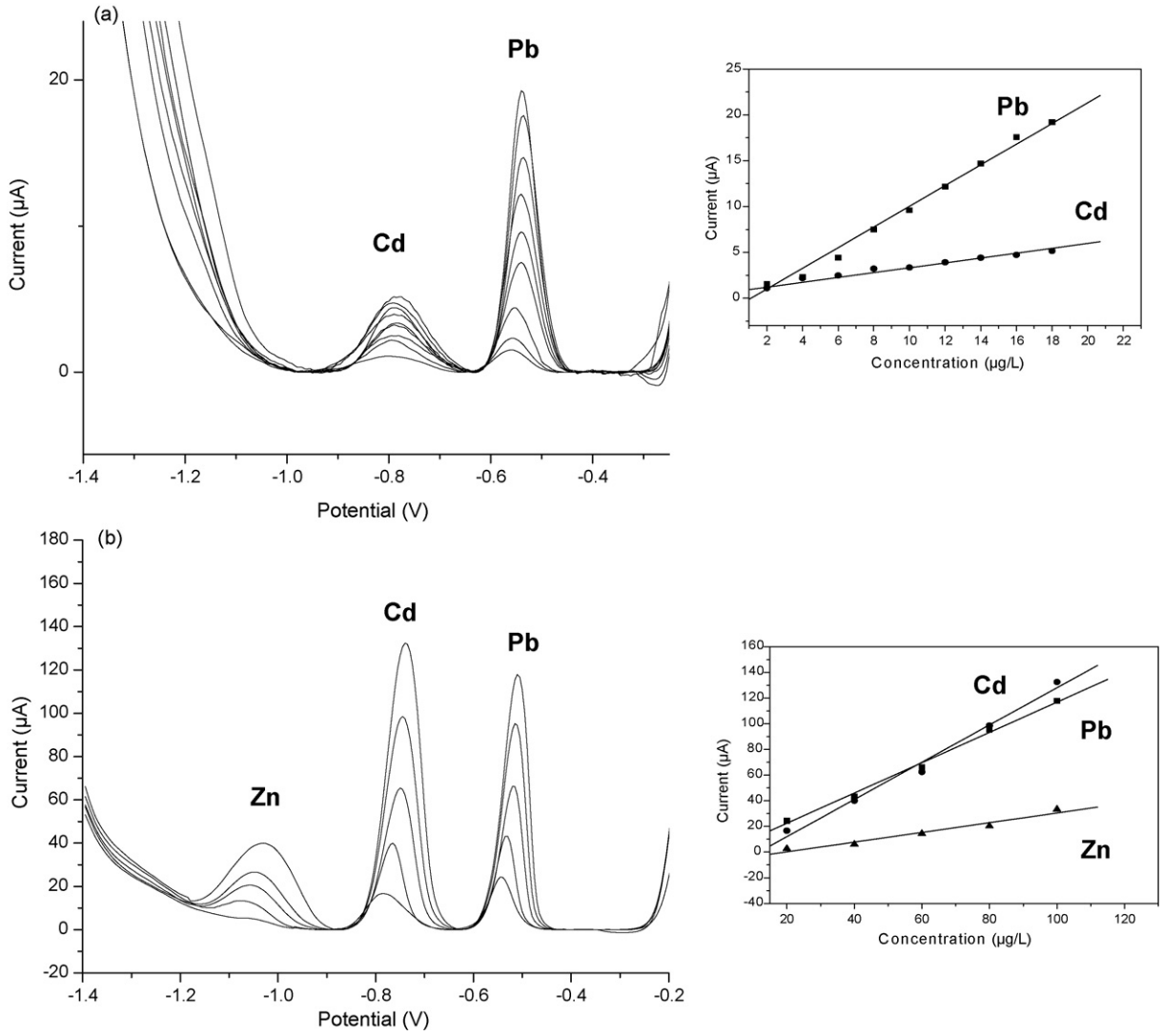

Fig. 7. A series of voltammograms for simultaneous determination of lead, cadmium and zinc obtained with Bi-CNT electrode. Other conditions as in Fig. 2: (a) 2–18 μg/L and (b) 20–100 μg/L.

zinc: $i = 5.22492E{-}7 + 9.77396E{-}7\omega^{1/2}$, $R = 0.976$). While the stripping peak currents for lead and cadmium continuously increased with rotation speed, the sudden drop of peak current was observed for zinc. Unfortunately, higher rotation speed than 1400 rpm could not be applied due to the allowable maximum rotation speed of the equipment. But, since very high rotation speeds increased the risk of the bismuth film being mechanically damaged, preconcentration was performed at 1000 rpm.

3.3. *Interference*

The interference of some metal ions, organic material and surfactants on the stripping voltammetric measurements were examined in 0.1 M acetate buffer containing lead, cadmium and zinc of 100 μg/L (Table 1).

In general, copper has a large influence on the stripping response at bismuth electrode due to the competition between bismuth ions and copper ions at the active sites of the surface. In the absence of copper, well-defined lead, cadmium and zinc peaks were observed. But, the addition of copper ions strongly influenced the stripping responses at even equal concentration. When 400 μg/L of copper ions was added, stripping responses of lead and cadmium were decreased by 65.5% and 71.2%, respectively, and zinc was completely suppressed. Tin is usually known as an interfering material for the determination of lead since its stripping peak overlaps with lead stripping peaks. However, the addition of tin ions to 400 μg/L did not affect the stripping responses of lead, cadmium and zinc.

The addition of benzene and xylene seriously suppressed the stripping response of trace metals even at low concentrations. Zinc was more sensitive than lead and cadmium. The addition of xylene at the concentration of 50 μg/L completely suppressed the zinc signal.

The presence of surfactants had a profound effect on the stripping response. They adsorbed on the sensing electrode and partially blocked the electrode surface, resulting in low and broad peaks [24].

As expected, additions of the cationic surfactant PDDA (poly(diallyldimethylammonium chloride)) and neutral surfactant Triton X-10 caused a severe deterioration in the stripping response. In the presence of PDDA, the zinc stripping response was completely suppressed while the lead stripping response remained unaffected. At a concentration of 2000 μg/L of PDDA, the suppression of the stripping response for lead and cadmium were 2.8% and 43.9% and zinc was not determined at all. It is assumed that PDDA, which has the size exclusion properties [25], suppressed the per-

Table 2
Determination results in real samples

	Lead (μg/L)		Cadmium (μg/L)		Zinc (μg/L)		Copper (μg/L)	Chromium (μg/L)	Manganese (μg/L)
	ICP-MS	SWASV	ICP-MS	SWASV	ICP-MS	SWASV	ICP-MS	ICP-MS	ICP-MS
Sample 1	9.5 ± 0.10	N.D.	8.6 ± 0.31	7.8 ± 0.37	2.3 ± 0.08	N.D.	4.8 ± 0.06	5.5 ± 0.07	2.1 ± 0.03
Sample 2	12.1 ± 0.19	13.2 ± 0.71	9.4 ± 0.17	8.4 ± 0.42	4.3 ± 0.19	N.D.	4.6 ± 0.18	5.2 ± 0.22	2.5 ± 0.09

N.D.: not detected; SWASV: square wave anodic stripping voltammetry.

meation of cadmium and zinc while lead, which has smaller ion size than cadmium and zinc, could permeate through polymers. Triton X-100 caused the significant interference to all three metal ions with the distortion of stripping peaks.

In general, it is known that the anionic surfactants exhibit weaker suppression [26,27] and their interference can be easily prevented by Nafion coating [28]. In this study, anionic surfactant sodium dodecyl sulfate (SDS) did not suppress the stripping current. Surprisingly the stripping current was dramatically increased with the addition of PSS (poly(sodium 4-styrenesulfonate)). First of all, the zinc peak current greatly enhanced about 2.5 times in the presence of 400 μg/L PSS. At the high concentration of 2000 μg/L PSS, stripping voltammograms presented 50% loss of zinc peak while lead and cadmium peak currents were slightly varied. PSS has ion-exchange and permselectivity properties and the target analyte diffuses selectively throughout the electrode surface. Thus, PSS adsorbed on the CNT electrode surface made a high sensitivity of stripping analysis. It has been reported that the PSS coating onto glassy carbon improved the formation of mercury film as well as the sensitivity of the stripping voltammetric determination [29,30].

3.4. Calibration data

The separate and simultaneous measuring of lead, cadmium and zinc was performed as shown in Figs. 6 and 7, respectively. The resulting stripping voltammograms for lead and cadmium exhibited no differences in peak height and peak position. However, stripping response of zinc for separate measurement was 1.5 times higher that that for simultaneous measurement. Kirgoz et al. reported that the simultaneous determination of zinc with lead and cadmium was difficult due to the competition of these metals [31]. A series of stripping voltammograms at low concentration (2–18 μg/L) are shown in Fig. 7(a) and at high concentration (20–100 μg/L) in Fig. 7(b). The inset shows the calibration plot of lead, cadmium and zinc. Each point on these curves is an averaged value of five repeated measurements. The peak current increases linearly with the metal concentration with a slope of 1.197 and 0.378 $\mu A\,\mu g^{-1}\,L^{-1}$ for lead and for zinc (correlation coefficients: 0.996 and 0.979 for lead and cadmium, respectively). Calibration curves for cadmium had two different slopes in the range of 2–18 and 20–100 $\mu g\,L^{-1}$ (slope at low concentration: 0.22184 $\mu A\,\mu g^{-1}\,L^{-1}$, slope at high concentration: 1.45 $\mu A\,\mu g^{-1}\,L^{-1}$, correlation coefficients: 0.987 and 0.994). The limit of detection was 1.3 μg/L for lead, 0.7 μg/L for cadmium and 12 μg/L for zinc on the basis of the response for 2 μg/L lead and cadmium and for 20 μg/L zinc solution following a 5 min accumulation (S/N = 3).

3.5. Application to real environments

For the purpose of practical applicability, real water samples were collected from two different sites along the Joongrang stream and bismuth-modified carbon nanotube electrode was employed for the determination of lead, cadmium and zinc in river samples. Water samples were filtered with a 0.45 μm membrane (purchased from Millipore) and adjusted to pH 4.5 using sodium acetate and acetic acid. After that, the anodic stripping peak current was recorded for the determination of lead, cadmium and zinc with the addition of their standard solutions to the sample solution under the same condition. These results were compared with ICP-MS measurement (Table 2). ICP-MS was performed with ELAN 6100 (PerkinElmer Sciex) using internal standards. The lead and cadmium concentrations were in good agreement with the results found in the ICP-MS measurement and zinc was not determined.

4. Conclusions

The possibility of the Bi-CNT electrode for the determination of cadmium, lead and zinc was investigated in this study. CNTs exhibited superior performance compared to commonly used glassy carbon, activated carbon and graphite. As CNTs had more active sites as shown in the results of cyclic voltammetry, they were more electrochemically sensitive than other carbon materials. In spite of the more positive hydrogen evolution potential of the CNT electrode compared to the other carbon electrodes, the determination of zinc could be successfully carried out owing to the in situ plated bismuth film. Preconcentration potential, bismuth concentration, preconcentration time and rotation speed during preconcentration were optimized to obtain highest sensitivity. The simultaneous determination of lead, cadmium and zinc was made by square wave anodic stripping voltammetry. The Bi-CNT electrode with a well-defined stripping response could be successfully applied to the determination of trace metals in real samples. However, the stripping response was more seriously tolerated by the additives than previously reported results by other research. Zinc could not be determined in the presence of copper, xylene and PDDA even at low concentration.

References

[1] E.A. Hutton, J.T. Elteren, B. Ogorevc, M.R. Smyth, Talanta 63 (2004) 849.
[2] G. Kefala, A. Economou, M. Sofoniou, Talanta 68 (2006) 1013.
[3] J. Wang, J. Lu, S.B. Hocevar, P.A.M. Farias, Anal. Chem. 72 (2000) 3218.
[4] J. Wang, D. Lu, S. Thongngamdee, Y. Lin, O.A. Sadik, Talanta 69 (2006) 914.
[5] A. Economou, A. Voulgaropoulos, Talanta 71 (2007) 758.
[6] J. Wang, J. Lu, U.A. Kirgoz, S.B. Hocevar, B. Ogorevc, Anal. Chim. Acta 434 (2001) 29.
[7] P.M. Ajayan, Chem. Rev. 99 (1999) 1787.
[8] A. Peigney, Ch. Laurent, E. Flahaut, R.R. Bacsa, A. Rousset, Carbon 39 (2001) 507.
[9] M.M.J. Treacy, T.W. Ebbesen, J.M. Gibson, Nature 381 (1996) 678.
[10] P.M. Ajayan, T.W. Ebbesen, T. Ichihashi, S. Iijima, K. Tanigaki, H. Hiura, Nature 362 (1993) 522.
[11] P. Chen, X. Wu, J. Lin, K.L. Tan, Science 285 (1999) 91.
[12] S.J. Tans, M.H. Devoret, H. Dai, A. Thess, R.E. Smalley, L.J. Geerligs, C. Dekker, Nature 386 (1997) 474.
[13] B.B. Gao, G.Z. Yue, Q. Qiu, Y. Cheng, H. Shimoda, L. Fleming, O. Zhou, Adv. Mater. 13 (2001) 1770.
[14] J. Li, Q. Zhang, D. Yang, J. Tian, Carbon 42 (2004) 2263.
[15] W. Huang, W. Hu, J. Song, Talanta 61 (2003) 411.
[16] J.B. He, X.Q. Lin, J. Pan, Electroanalysis 17 (2005) 1681.
[17] G.P. Jin, J.B. He, Z.B. Rui, F.S. Meng, Electrochim. Acta 51 (2006) 4341.
[18] G. Liu, Y. Lin, Y. Tu, Z. Ren, Analyst 130 (2005) 1098.
[19] H.D. Goldberg, R.B. Brown, D.P. Liu, M.E. Meyerhoft, Sens. Actuator B: Chem. 21 (1994) 171.
[20] S. Laschi, I. Palchetti, M. Mascini, Sens. Actuator B: Chem. 114 (2006) 460.
[21] N.S. Lawrence, R.P. Deo, J. Wang, Electroanalysis 17 (2005) 65.
[22] G. Kefala, A. Economou, A. Voulgaropoulos, M. Sofoniou, Talanta 61 (2003) 603.
[23] I. Svancara, L. Baldrianova, E. Tesarova, S.B. Hocevar, S.A.A. Elsuccary, A. Economou, S. Sotiropoulos, B. Ogorevc, K. Vytras, Electroanalysis 18 (2006) 177.
[24] C. Gouveia-Caridade, C.M.A. Brett, J. Electroanal. Chem. 592 (2006) 113.

[25] H. Dautzenbert, U. Schuldt, D. Lerche, H. Woehlecke, R. Ehwald, J. Membr. Sci. 162 (1999) 165.
[26] T.W. Lee, K.C. Chung, J.M. Park, Electroanalysis 14 (2002) 833.
[27] S.B. Hocevar, B. Ogorevc, J. Wang, B. Pihlar, Electroanalysis 14 (2002) 1707.
[28] Z. Hu, C.J. Seliskar, W.R. Heineman, Anal. Chim. Acta 369 (1998) 93.
[29] S.C.C. Monterroso, H.M. Carapuca, A.C. Duarte, Talanta 65 (2005) 644.
[30] L.S. Rocha, J.P. Pinheiro, H.M. Carapuca, Langmuir 22 (2006) 8241.
[31] U.A. Kirgoz, S. Marin, M. Pumera, A. Merkoci, S. Alegret, Electroanalysis 17 (2005) 881.

Talanta 76 (2008) 365–368

Contents lists available at ScienceDirect

Talanta

journal homepage: www.elsevier.com/locate/talanta

Determination of chloride in admixtures and aggregates for cement by a simple flow injection potentiometric system

Jaroon Junsomboon [a], Jaroon Jakmunee [a,b,*]

[a] Department of Chemistry, Faculty of Science, Chiang Mai University, Chiang Mai 50200, Thailand
[b] Institute for Science and Technology Research and Development, Chiang Mai University, Chiang Mai 50200, Thailand

ARTICLE INFO

Article history:
Received 5 February 2008
Received in revised form 7 March 2008
Accepted 10 March 2008
Available online 16 March 2008

Keywords:
Flow injection
Potentiometry
Chloride
Cement

ABSTRACT

A simple flow injection system using three 3-way solenoid valves as an electric control injection valve and with a simple home-made chloride ion selective electrode based on Ag/AgCl wire as a sensor for determination of water soluble chloride in admixtures and aggregates for cement has been developed. A liquid sample or an extract was injected into a water carrier stream which was then merged with 0.1 M KNO_3 stream and flowed through a flow cell where the solution will be in contact with the sensor, producing a potential change recorded as a peak. A calibration graph in range of 10–100 mg L^{-1} was obtained with a detection limit of 2 mg L^{-1}. Relative standard deviations for 7 replicates injecting of 20, 60 and 90 mg L^{-1} chloride solutions were 1.0, 1.2 and 0.6%, respectively. Sample throughput of 60 h^{-1} was achieved with the consumption of 1 mL each of electrolyte solution and water carrier. The developed method was validated by the British Standard methods.

1. Introduction

Reinforced concrete is a concrete with incorporating of reinforcement bars (rebars) to strengthen a material that would otherwise be brittle. Typically, concrete has high resistance to compressive stresses (about 4000 psi), but not to tension, while steel has high strength in tension. The reinforced concrete structures can support 300–500 times their combined weight [1]. The alkaline chemical environment of concrete can protect steel from corrosion. However, chloride (Cl^-) content in concrete plays important role on quality of reinforced concrete, therefore, Cl^- induces depassivation of the steel rebars and initiation of the corrosion process leading to degradation of the structure. Chloride in concrete comes from cement, aggregate materials and water used for creating concrete, or by diffusion of Cl^- from outside of the structure through pore water in concrete. Determination of Cl^- in materials for concrete is necessary. Aggregate materials could be analyzed according to the British Standard (BS 812: Part 117: 1988), by mean of back titration of silver nitrate used in precipitation of Cl^- by using thiocyanate as titrant [2]. Referring to BS EN 480-10:1997, Cl^- in admixtures for concrete, mortar and grout was determined by potentiometric titration with precipitation as silver chloride, monitoring of end point by using ion selective electrode (ISE) [3]. However, these methods are tedious, slow and consume large amounts of reagents, not suitable for analysis a large number of samples. New method which is faster, less chemical consumption and has higher degrees of automation would be needed. Several flow based methods have been reported for determination of Cl^- using different detection principles [4–17]. Spectrophotometric detection based on reaction of Cl^- with mercuric thiocyanate to release SCN^- to form complex with Fe^{3+} has been widely used [4–8]. Turbidity measurement due to formation of AgCl [9,10] or absorbance measurement of chloranilate released from silver chloranilate solid phase reactor [11] was also proposed to avoid using of toxic mercury compound. By new flow techniques, e.g., sequential injection (SI) [6], FI with reagent immobilized on solid phase [7], and multisyringe flow injection (MSFI) [8], the amounts of toxic mercury reagent could be reduced several orders. Potentiometric detection was also popularly used in flow system for Cl^- determination, which provided the same sensitivity as the spectrophotometric one [12–17]. A simple home-made Cl^- ISE as in wire [17] or tubular [14,15] format, or a commercial Cl^- ISE [12] has been employed in different flow techniques.

In this paper, we developed a simple FI system using three 3-way solenoid valves as an electronic control injection valve and with a simple home-made Cl^- ISE based on Ag/AgCl wire as a sensor for determination of water soluble Cl^- in admixtures and aggregates for cement. The Cl^- ISE could be prepared by oxidation of a jewelry grade Ag wire electrochemically or chemically and could be used for at least 3 months by storage in 3 M KCl. A linear calibration graph plotting between peak height (mV) versus logarithms of

* Corresponding author at: Department of Chemistry, Faculty of Science, Chiang Mai University, Chiang Mai 50200, Thailand. Tel.: +66 5394 1909; fax: +66 5394 1910.
E-mail address: scijjkmn@chiangmai.ac.th (J. Jakmunee).

0039-9140/$ – see front matter © 2008 Elsevier B.V. All rights reserved.
doi:10.1016/j.talanta.2008.03.006

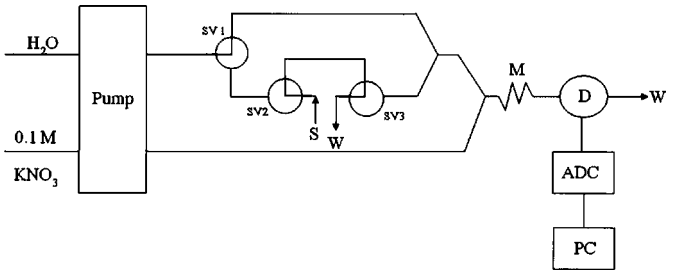

Fig. 1. FI manifold of flow injection potentiometric detection of chloride; SV1-3 = solenoid valves, S = standard/sample, W = waste, M = mixing coil, D = detector, ADC = analog to digital converter unit, and PC = personal computer (injection valve is in loading position).

Cl^- concentration in range of 10–100 mg L^{-1} was obtained with a detection limit of 2 mg L^{-1}. Relative standard deviation in range of 0.6–1.2% was observed. Sample throughput of 60 h^{-1} was achieved with the consumption of 1 mL each of 0.1 M KNO_3 electrolyte solution and water carrier.

2. Experimental

2.1. Chemicals

All chemicals used were of analytical reagent grade. Deionized water (obtained by a system of Milli-Q, Millipore, Sweden) was used throughout. A chloride standard stock solution (1000 mg L^{-1}) was prepared by dissolving 0.1648 g of sodium chloride (Merck, Darmstadt, Germany) in water and making up to a volume of 100 mL in a volumetric flask. A potassium nitrate stock solution (0.10 M) was prepared by dissolving 5.05 g of potassium nitrate (Merck, Darmstadt, Germany) in 500 mL of water. A ferric chloride solution (0.5 M) in 1 M hydrochloric acid was prepared by dissolving 8.11 g of $FeCl_3$ anhydrous (Merck, Darmstadt, Germany) in 100 mL of 1 M HCl.

2.2. Potentiometric flow through cell and Cl^- ISE

A potentiometric flow through cell was fabricated from a Perspex plastic block, similar to the previous reported [17], by cutting and drilling to form channels for inserting a Ag/AgCl wire working electrode (WE) and a Ag/AgCl reference electrode (RE) (3 M KCl) (MW-2030, BAS, Indiana, USA), and for solution inlet and outlet.

A silver wire (0.5 mm in diameter) obtained from a local jewelry shop was used for preparation of a Ag/AgCl electrode. The wire was polished and cleaned just before immerging it into a solution of 0.5 M ferric chloride in 1 M hydrochloric acid, to form a AgCl film on the electrode. The electrode was then washed with water and used as a working electrode by assembling into the flow through cell described above. The electrode was placed in 3 M KCl solution after used and can be last long more than 3 months.

2.3. FI manifold

The FI system used is schematically depicted in Fig. 1. It consisted of a peristaltic pump (Ismatec, Switzerland), a 3-way connector and three 3-way solenoid valves (Biochemvalve, USA) connecting to be an injection valve (see Fig. 1), a flow through cell with Ag/AgCl electrodes connecting to a home-made potentiometer, an analog to digital converter unit for data recording with relevant software (PowerChrom280, eDAQ, Australia) and a computer. Data acquisition was controlled by eDAQ chart software and eDAQ FIA extension software was used for data analysis. Sample loading or injection was performed manually by switching electrical switch for applying power to the solenoid valves. All tubings used were of PTFE tubing of inner diameter of 0.5 mm, except Tygon pump tubing (Saint-Gobain Performance Plastics, USA).

2.4. Procedures

The water carrier and 0.1 M KNO_3 solution were propelled with constant flow rate of 1 mL min^{-1} each, to attain a stable baseline recording on the computer. While the injection valve was at loading position (see Fig. 1), a standard/sample was filled in a sample loop (100 μL), then by turn on the switch to change all three solenoid valves to another position (injection valve turn to injecting position), the solution in the sample loop was injected into the system and flowed to the flow cell to monitor for potential difference between WE and RE as the zone passed the WE, recording as a peak. A calibration graph was a plot of the peak height obtained as a function of the logarithm value of concentration of the Cl^- standard. Chloride concentration in a sample was evaluated from the calibration graph.

Aggregate sample preparation was carried out following the standard method [2], briefly, soak 2 kg of aggregates (particle size <20 mm) in 2 kg of deionized water for 24 h and take the supernatant for analysis.

Admixture sample was prepared following the standard method [3], briefly, accurately weigh 10 g of a liquid admixture sample and dilute with deionized water to obtain Cl^- concentration within about the middle range of the calibration graph (dilution about 2–5 times).

3. Results and discussion

3.1. Preparation of Ag/AgCl wire Cl^- ISE and condition for FI system

The Ag/AgCl wire could be prepared by oxidation of a Ag wire electrochemically or chemically using ferric chloride in HCl. Effect of oxidation time on sensitivity of the electrode was investigated. The produced Ag/AgCl electrodes were tested for theirs performance by using FIA system described in Section 2.3. After preliminary studies (described below), some parameters were fixed, i.e., concentration of KNO_3 electrolyte solution of 0.1 M, flow rate of water carrier and the electrolyte solution of 1 mL min^{-1} each line, injection volume of 100 μL and mixing coil of 50 cm. A series of Cl^- standard solutions was injected into the systems and a calibration graph (a plot of peak height (Y) versus logarithm of Cl^- concentration (X)) was obtained for each electrode. By electrooxidation of Ag wire in a 0.1 M HCl for 0.5–3 h to produce AgCl coated Ag wire, the resulted electrode gave closely response to Cl^- ion in concentration range of 3.6–3550 mg L^{-1}, with slope of 49.8–55.4 mV/decade. The electrode was tested for its durability by placing it in a 3 M KCl solution, which was vigorously stirred using magnetic stirrer and the potential of the electrode was recorded versus a Ag/AgCl reference electrode for a period of 17 h. It was found that the potential of the electrode was only slightly change during this period.

Despite the Cl^- ISE prepared by this method worked well, the voltage supplier is needed for electrooxidation of Ag, so the preparation of the electrode by chemical oxidation [17] was tried. The clean Ag wire was dipped into a solution containing 0.5 M $FeCl_3$ and 1.0 M HCl for 1–24 h. The electrode was tested for determination of Cl^- in range of 10–100 mg L^{-1}, which was expected to be found in samples. It was found that the comparable slopes of calibration graphs (58.1–60.3 mV/decade) were obtained with good linearities ($r^2 > 0.999$), indicating that the dipping time does not affect on sensitivity of the electrode. Dipping time of ≥24 h was

Table 1
Analytical features of the developed FI potentiometric method versus some reported methods

Method	Principle	Sample	Linear range (mg L^{-1})	LOD (mg L^{-1})	R.S.D. (%)	h^{-1}	Ref.
FI spect	Cl^--$Hg(SCN)_2$-Fe^{3+}	Water	0–50	3	2.5	37	[6]
FI spect	$Hg(SCN)_2$ impregnated on epoxy resin bead	Water	2.0–7.8	0.5	2.2	100	[7]
MSFI spect	Cl^--$Hg(SCN)_2$-Fe^{3+}, use small amounts of reagent	Water	1–40	0.2	0.8	130	[8]
SI turbidity	Forming of AgCl precipitate	Ground, surface, wastewater	2–400	2	3.7	57	[9]
FI spect	Release of chloranilate from silver chloranilate solid phase reactor	Water	0.5–100	0.3	1.1	80	[11]
SI poten	On-line dialysis, tubular Ag/AgCl electrode	Electroplating bath	3550–35500	–	–	40	[14]
FI poten	Ag/AgCl electrode with on-line dialysis	Milk and coconut water	4–1000	0.4	1.2	90	[16]
SI-LAV poten	Ag/AgCl electrode	Water	3.6–28.4, 28–298	3.6	0.7–1.3	50	[17]
FI poten	Ag/AgCl wire	Cement aggregates and admixtures	10–100	2	0.6–1.2	60	This work

Spect = spectrophotometry, poten = potentiometry, FI = flow injection, SI = sequential injection, MSFI = multisyringe flow injection, and LAV = lab-at-valve.

selected for electrode preparation to ensure a good sensitivity and long time stability of the electrode.

Effect of purity of Ag wire was investigated by using a high purity Ag wire (diam. 0.25 mm, >99.99%, Sigma–Aldrich) to prepare the Ag/AgCl electrode. It was found that the sensitivity obtained from this electrode is comparable to that of preparing from Ag wire from jewelry shop, usually called Sterling silver which has purity of 92.5% Ag (slopes of calibration graphs were 58.9 and 58.7 mV/decade, respectively).

Effect of electrode contacting area was investigated by dipping Ag wire at different depth (0.5–2.0 cm) for 24 h and the resulted ISE were tested using FIA system as described above. It was found that the length of Ag/AgCl electrode did not affect on sensitivity of Cl^- determination (electrode slopes in range of 58.2–59.9 was observed). However, a broader peak was observed for the longer electrode, thus an electrode length of 1.5 cm which gave a calibration graph of $Y = 59.9X - 24.7$, $r^2 = 0.9996$) was selected for further experiment. By keeping the electrode in a solution of 3 M KCl after used, stability of the electrode was good for longer than 3 months, with slope of calibration graph changing from ~59 to ~53 mV/decade.

Carrier and KNO_3 electrolyte solutions flow rate in range of 1–4 mL min^{-1} and length of mixing coil in range of 20–80 cm were studied, by injecting of 50 mg L^{-1} Cl^- into the system. It was found that only slightly different in peak height was observed for all flow rate and mixing coil length studied. A flow rate of 1 mL min^{-1} and mixing coil length of 50 cm were selected. Effect of pH of 0.1 M KNO_3 solution was investigated and found that similar peak heights were obtained in pH range of 1–8 and shorter peaks were observed at pH higher than 10. This has been explained that Ag_2O was formed on the electrode surface at high pH, lead to diminishing of electrode sensitivity [18]. A KNO_3 solution without adjusting pH was selected. According to the theory, the potential obtained by ISE depends on temperature, however, all experiments were carried out in an air condition room of about 25 ± 1 °C, thus no significant variation due to temperature change was observed.

Table 2
Chloride contents in cement aggregates and admixtures found by the FI potentiometric and standard methods

Sample	Chloride content (%, w/w)	
	FI–potentiometry[a]	Standard method[b]
Admixtures		
1	0.0109 ± 0.0003	0.01
2	0.0113 ± 0.0003	0.01
3	0.0076 ± 0.0002	0.01
4	0.0141 ± 0.0003	0.01
5	0.082 ± 0.003	0.08
6	0.093 ± 0.002	0.09
Aggregates		
1	0.0010 ± 0.0001	<0.01
2	0.0080 ± 0.0001	<0.01
3	0.0010 ± 0.0001	<0.01
4	0.0013 ± 0.0001	<0.01
5	0.0014 ± 0.0001	<0.01
6	0.0068 ± 0.0003	0.01
7	0.0069 ± 0.0004	0.01

[a] Mean of triplicate results.
[b] BS EN 480-10: 1997 [3] was applied for admixture samples, BS 812: Part 117: 1988 Method A [2] was applied for aggregates samples.

3.2. Analytical characteristics

Under the selected condition as described above although the linear range may be extended to higher concentration up to at least 1000 mg L^{-1} Cl^-, a linear calibration graph in the concentration range of 10–100 mg L^{-1} Cl^- ($Y = 58.8X - 18.9$, $r^2 = 0.9996$) was constructed. By using low concentration range, the appropriate dilution of sample solution was made, thus gave advantages in terms of minimizing interference effect and matching of viscosity of the sample to the carrier solution. A detection limit (3 times the standard deviation of the blank/slope of analytical curve) of 2 mg L^{-1} Cl^- was achieved. Relative standard deviations for 7 replicates injecting of 20, 60 and 90 mg L^{-1} chloride solutions were 1.0, 1.2 and 0.6% respectively. Recoveries were found to be 99.7–102.6% for spiking of Cl^- to the sample at concentrations of 20–90 mg L^{-1}. Performance of the developed method which used a home-made Cl^- ISE was compared with other methods as shown in Table 1. The developed method provided comparable performance to the reported methods but it is simpler, cheaper, consumed smaller amounts of non-toxic and inexpensive chemicals (1 mL each of water and 0.1 M KNO_3 per injection).

According to literatures [18,19], some halides (I^- and Br^-), sulfide, cyanide and some metal ions (Fe^{3+} and Al^{3+}) are the interferences in Cl^- determination by this kind of ISE in acidic medium, but not the other common ions, e.g., NO_3^-, NO_2^-, CO_3^{2-}, SO_4^{2-} and PO_4^{3-}. Effects of NO_2^-, CO_3^{2-}, SO_4^{2-} and PO_4^{3-} on the proposed method where performed in neutral medium were studied by spiking each ion into 50 mg L^{-1} Cl^- solution. It was found that NO_2^-, CO_3^{2-}, SO_4^{2-} and PO_4^{3-} at least up to 100 mg L^{-1} did not interfere (causing a change in peak height of less than 5%). Effects of I^-, Br^-, S^{2-}, Fe^{3+} and Al^{3+} have also been investigated. It was found that I^-, Br^- and S^{2-} seriously interfere, but Fe^{3+} and Al^{3+} up to 500 mg L^{-1} caused a change in peak height of less than 5%. By injecting a series of I^-, Br^- or S^{2-} standard solutions (10–100 mg L^{-1}), calibration graphs of $Y = 70.8X - 25.7$ ($r^2 = 0.998$), $Y = 70.2X + 14.5$ ($r^2 = 0.998$)

or $Y = 96.5X - 16.1$ ($r^2 = 0.989$), respectively, were obtained. However, these ions are usually present in the sample at relatively low concentrations compared to Cl^- and do not significantly interfere.

3.3. Application to real samples

The system was applied to cement aggregate and admixture samples. The samples were prepared as described in Section 2.4. The contents of Cl^- in the samples were calculated using a calibration graph ($Y = 57.6X - 23.3$, $r^2 = 0.9994$) and were found in range of 8–113 mg L^{-1}, which were converted to % (w/w) of Cl^- in samples as summarized in Table 2. The analysis of aggregate samples by titrimetric standard method [2] and admixture samples by potentiometric titration standard method [3] was also carried out for comparison. The standard methods are applied for determination of total halides, except F^-, reported as Cl^- content. The Cl^- contents obtained from the proposed method were in good agreement with those from the standard methods, evaluating by *t*-test at 95% confidence level [20]. It should be noted that the proposed method has lower detection limit (0.0002%, w/w), so it can determine lower level of Cl^- in samples with good precision. It is also faster and consumed smaller amounts of reagents. The permission level of Cl^- in concrete admixtures by Thai Industrial Standard (TIS 733–2530) is 0.20 ± 0.01%, while British Standard is 0.10%. The application of the method could be extended to analysis of water used in preparing of cement.

4. Conclusion

A simple Cl^- ISE and FI potentiometric method have been developed for the determination of water soluble Cl^- content in aggregates and admixtures for concrete. In comparison to the standard methods, the developed method provided agreeable results, moreover it is lower cost, lower reagent consumption, faster and has lower detection limit. The system gave linear range of 10–100 mg L^{-1} Cl^-, detection limit of 2 mg L^{-1} Cl^-, relative standard deviation of 0.6–1.2% and sample throughput of 60 h^{-1}, which are comparable to the previous flow based systems, but with simpler in instrumentation and no use of toxic or expensive chemicals.

Acknowledgements

We thank the Center for Innovation in Chemistry: Postgraduate Education and Research Program in Chemistry (PERCH-CIC), the Commission on Higher Education (CHE) and the Thailand Research Fund (TRF) for financial support.

References

[1] http://en.wikipedia.org/wiki/Reinforced_concrete (access on 26/1/2008).
[2] British Standard: testing aggregates, Part 117: method for determination of water soluble chloride salts (BS 812: Part 117: 1988, Method A), British Standard Institution, 1988.
[3] British Standard: admixtures for concrete, mortar and grout – Test Methods – Part 10: determination of water soluble chloride content (BS EN 480 – 10: 1997), British Standard Institution, 1997.
[4] J.F. Liu, Y.D. Feng, G.B. Jiang, J. AOAC Int. 84 (2001) 1179.
[5] J.F. Liu, G.B. Jiang, Talanta 54 (2001) 329.
[6] J.F. van Staden, S.I. Tlowana, Fresenius J. Anal. Chem. 371 (2001) 396.
[7] C.R. Silva, H.J. Vieira, L.S. Canaes, J.A. Nobrega, O. Fatibello-Filho, Talanta 65 (2005) 965.
[8] F. Maya, J.M. Estela, V. Cerda, Talanta 74 (2008) 1534.
[9] R.B.R. Mesquita, S.M.V. Fernandes, A. Rangel, J. Environ. Monitor. 4 (2002) 458.
[10] M. Zenki, Y. Iwadou, Talanta 58 (2002) 1055.
[11] V.G. Bonifacio, L.C. Figueiredo-Filho, L.H. Marcolino, O. Fatibello-Filho, Talanta 72 (2007) 663.
[12] A. Andrade-Eiroa, J.A. Erustes, R. Forteza, V. Cerda, J. Lima, Anal. Chim. Acta 467 (2002) 25.
[13] A.M. Pimenta, A.N. Araujo, M. Conceição, B.S.M. Montenegro, C. Pasquini, J.J.R. Rohwedder, I.M. Raimundo-Júnior, J. Pharm. Biomed. Anal. 36 (2004) 49.
[14] J.E. da Silva, M.F. Pimentel, V.L. da Silva, M.D. Montenegro, A.N. Araujo, Anal. Chim. Acta 506 (2004) 197.
[15] A.N. Araujo, M. Montenegro, L. Kousalova, H. Sklenarova, P. Solich, R.P. Olmos, Anal. Chim. Acta 505 (2004) 161.
[16] I.S. da Silva, E.M. Richter, C.L. do Lago, I.G.R. Gutz, A.A. Tanaka, L. Angnes, Talanta 67 (2005) 651.
[17] J. Jakmunee, L. Patimapornlert, S. Suteerapataranon, N. Lenghor, K. Grudpan, Talanta 65 (2005) 789.
[18] W. Frenzel, Fresenius J. Anal. Chem. 335 (1989) 931.
[19] T. Altunbulduk, H. Meier zu Koecker, W. Frenzel, Fresenius J. Anal. Chem. 351 (1995) 593.
[20] G.D. Christian, Analytical Chemistry, 6th ed., Wiley, New York, USA, 2004.

Talanta 76 (2008) 382–388

Contents lists available at ScienceDirect

Talanta

journal homepage: www.elsevier.com/locate/talanta

A new fully automated on-line digestion system for ultra trace analysis of mercury in natural waters by means of FI-CV-AFS

K. Leopold [a,*], L. Harwardt [a], M. Schuster [a], G. Schlemmer [b]

[a] Technische Universität München, Arbeitsgruppe für Analytische Chemie, Lichtenbergstrasse 4, D-85747 Garching, Germany
[b] Analytik Jena AG, Konrad-Zuse-Strasse 1, D-07745 Jena, Germany

ARTICLE INFO

Article history:
Received 14 November 2007
Received in revised form 4 March 2008
Accepted 12 March 2008
Available online 21 March 2008

Keywords:
Total mercury determination
Flow injection (FI)
On-line digestion
Atomic fluorescence spectrometry (AFS)
Cold vapor (CV)
Natural water samples

ABSTRACT

A fully automated flow injection (FI) system utilizing the extraordinary oxidation power of bromine monochloride (BrCl) for the transformation of dissolved mercury species to Hg^{2+} and oxidation of dissolved organic carbon (DOC) has been developed and coupled to cold vapor (CV) atomic fluorescence spectrometry (AFS) for highly sensitive mercury detection. The system can be applied to natural waters, sea water as well as freshwater and provides a detection limit as low as 16 pg Hg l^{-1} from a sample volume of 7 ml. The relative standard deviation is about 4–10%. A 3-fold measurement of one sample is completely processed within 15 min. Dissolved organic carbon, chloride and iodide ions are tolerated in concentrations of 15 mg DOC l^{-1}, >21 g Cl^- l^{-1}, and 10 mg I^- l^{-1}. Validation of the proposed method yielded a good recovery of total mercury in a moorland water sample and in the certified reference material ORMS-3, river water. Investigation of eight real water samples with mercury concentrations in the range of 0.3–1.4 ng l^{-1} also confirmed the suitability of the proposed method.

1. Introduction

Mercury is one of the most toxic elements that may severely affect human health. Hydrosphere plays an important role, since aquatic organisms accumulate mercury species [1]. Fish and aquatic mammals, as later members of the food chain, can have mercury concentrations up to 10^6 times higher than the ambient water [2,3]. Therefore, this is the main source for human mercury exposure. Mercury content in natural waters varies in a wide concentration range: very low concentrations of sub ng l^{-1} can be found in open ocean water [4,5], values of about 5 ng l^{-1} or less can be found in non-contaminated freshwaters [6], whereas humic lakes and particle rich river waters often have elevated concentrations of 10–20 ng l^{-1} [7] and contaminated waters can have up to some μg l^{-1}.

For correct determination of total mercury in natural water samples, oxidation or digestion is strongly recommended. Especially in freshwater samples, more than 90% of the mercury species are complexed by organic matter [7]. Accepted standard methods [e.g. 8,9] for total mercury determination in natural water samples follow oxidation with bromine monochloride in a batch procedure that takes at least 12 h. Apart from the long sample preparation time, unfavorable contamination risk arises from this procedure, since solutions containing BrCl act as Hg sink and take up Hg from the environment (containers, ambient air). This may not only lead to systematic errors but also to high measurement variation. Hence, the advantages of a closed system are obvious. For the investigation of sea water samples, flow injection devices were proposed, e.g. by Wurl et al. [10,11], using BrCl solution as oxidant in combination with UV radiation. Bloxham et al. [12] used BrCl solutions as oxidant in a heated reaction coil. These flow injection (FI) systems were coupled to cold vapor-atomic absorption spectrometry (CV-AAS) and allow for detection limits of 0.1 and 25 ng Hg l^{-1}, respectively.

In freshwaters, e.g. lake water, 94–99% of inorganic mercury and 72–97% of methyl mercury are complexed by dissolved humic matter [13], whereas in sea water the proportion of mercury bound to humic matter is very low due to high chloride ion concentrations which stabilize Hg species by ionic interactions. Furthermore, the proportion of organomercury in marine waters is typically less than 5% of total mercury [14] (only the Mediterranean waters show a "mercury anomaly" with organomercury contents of up to 30% of total mercury [15]) and total dissolved organic carbon (DOC) contents in marine waters are usually less than 0.5 mg l^{-1} [16], whereas in freshwater lakes and rivers organomercury proportion is up to about 30% [7] and DOC content is up to 10 mg l^{-1} [16]. Therefore, oxidation for total mercury determination is more demanding in natural freshwaters. An approach for on-line oxidation in river water was made by Elsholz et al. [17]. Here the authors determined

* Corresponding author. Tel.: +49 89 28913764; fax: +49 89 28913186.
E-mail address: kerstin.leopold@lrz.tum.de (K. Leopold).

0039-9140/$ – see front matter © 2008 Elsevier B.V. All rights reserved.
doi:10.1016/j.talanta.2008.03.010

elevated mercury concentrations in a range from 20 to 1000 ng l^{-1} by means of the standard addition method.

In this work, a fully automated flow injection system for on-line oxidation coupled to cold vapor-atomic fluorescence spectrometry (CV-AFS) is described, providing for the first time determination of total mercury in the ultra trace range (pg Hg l^{-1}) in water samples with high DOC and organomercury contents, such as moorland water. In contrast to existing methods, particular attention has been paid to the presence of DOC and methylmercury. Consequently, all parameters of the FI system – working ranges, samples volume, reagent concentrations, reaction coil lengths and temperatures – were studied in detail. Validation of the method was performed by comparison of the values obtained by the proposed method with the values obtained by standard EPA method 1631 (for the determination of total Hg in water samples) in a moorland water sample. In addition, recovery of total mercury was investigated in the certified reference material ORMS-3, a river water sample.

2. Experimental

2.1. Instrumentation and experimental setup

Mercury analysis was performed with a *mercur* atomic fluorescence spectrometer (Analytik Jena AG, Jena, Germany) equipped with an integrated flow injection system for cold vapor generation and additional mercury enrichment on a gold collector [18]. Measurement of samples with unknown mercury concentration should first be performed without using that built-in enrichment procedure in order to exclude overload and contamination of the system. Mercury resonance fluorescence is detected at a wavelength of 253.7 nm. The developed FI system for on-line oxidation was coupled to the FI system of the *mercur* and was controlled by personal computer with additional software configured by Analytik Jena AG. The FI-manifold for on-line oxidation consists of peristaltic pumps (HS 60, Analytik Jena AG), magnetic valves (6606, Bürkert GmbH & Co. KG, Ingelfingen, Germany), a heatable reactor (self-made) and a gas–liquid separator (Analytik Jena AG). The reactor consists of a 3-m braided reaction coil (RC1 in Fig. 1) with an inner diameter of 1 mm which is placed in a sand-filled aluminum cylinder (wall thickness 0.5 mm, inner diameter of cylinder 50 mm, height of cylinder 40 mm) for better heat dissipation. The aluminum cylinder is placed on a heating mat (36 V, 100 mm × 100 mm; Telemeter electronic GmbH, Donauwörth, Germany) to acquire the temperature of 70 °C for the oxidation reaction.

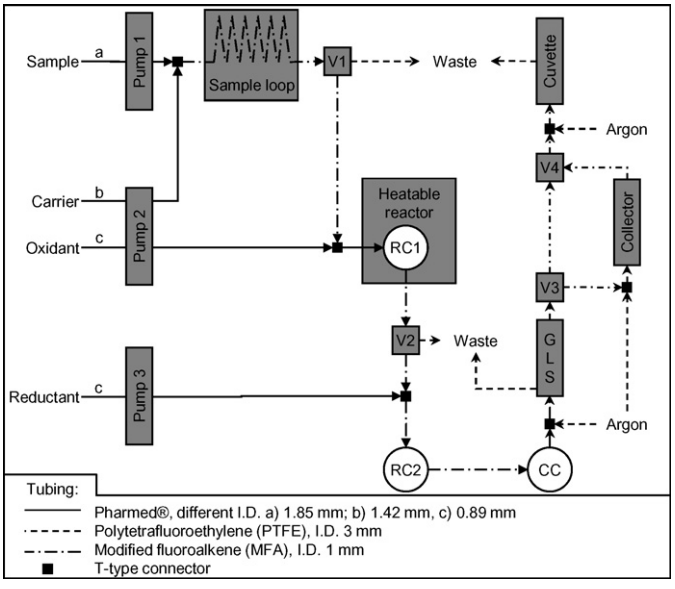

Fig. 1. Scheme of the developed FI-CV-AFS system for measurement of ultra traces of mercury in freshwater samples (sample loopm, 9.0 m MFA coil corresponding to 7 ml sample; RC1, 3.0 m MFA reaction coil for on-line oxidation placed in a heatable reactor consisting of in an aluminum cylinder filled with sand; RC2, 0.3 m MFA reaction coil for chemical reduction of Hg^{2+} to Hg^0; CC, 0.3 m MFA cooling coil; GLS, gas–liquid-separator; V, magnetic valve).

The connections between the valves, the pump tubes, and other parts of the system were made of polytetrafluoroethylene (PTFE) and/or modified fluoroalkene (MFA) tubes with an inner diameter of 3 or 1 mm, respectively. Pharmed® pump tubes (LIQUID-scan GmbH & Co. KG, Überlingen, Germany) were used for the transport of all aqueous solutions including BrCl solutions with a durability of 3–4 months when used daily. Fig. 1 shows a scheme of the combined FI-CV manifold. Tables 1 and 2 summarize the optimized operation steps of the FI system, with and without mercury enrichment, respectively.

Dissolved organic carbon in real water samples and stock DOC solution was measured as non-particular organic carbon (NPOC) with a TOC analyzer (High TOC II, Elementar Analysensysteme, Hanau, Germany) using the EN 1484 DEV H3 method. This method provides a detection limit of 1.0 mg l^{-1} and a S.D. of 10%.

2.2. Processing of the sample solutions in the FI-CV system

For sample volume management, a loop with a volume of 7 ml was chosen. Before processing a new sample, the loop was once filled with the sample solution which was then passed to waste. Rinsing and filling the sample loop for a 3-fold measurement therefore requires a sample volume of about 34 ml in total. Subsequently the sample and the oxidant (4% (v/v) of BrCl stock solution) are mixed and moved to the 70 °C hot reactor, in which the on-line oxidation and decomposition takes place. Within the next step, the remaining oxidant is destroyed by hydroxylamine which is added to the tin(II) chloride reductant solution used for the chemical reduction of Hg^{2+} to Hg^0. These reactions take place in a second reaction coil (RC2 in Fig. 1; length 0.3 m, inner diameter 1 mm). Before the solution reaches the gas–liquid separator (GLS), in which an argon gas stream purges the elemental mercury off from the solution, a cooling step in an ice water bath (cooling coil 0.3 m, inner diameter 1 mm; CC in Fig. 1) is performed. This cooling is necessary for effective gas–liquid separation; otherwise the warm sample solution forms condensate drops which may leave the separator and reach the gas way and so interfere the Hg fluorescence measurement. After cold vapor generation, the *mercur* system provides two alternatives: for samples with Hg concentrations ≥15 ng Hg l^{-1}, the cold vapor stream is directly subjected to AFS measurement (cf. FI steps given in Table 1). For samples with Hg concentrations, <15 ng Hg l^{-1} enrichment of Hg^0 on a gold collector is used (cf. FI steps given in Table 2).

2.3. Cleaning procedures and chemicals

The analysis of ubiquitously occurring mercury in the pg to ng l^{-1} range requires special operations ensuring extremely low mercury contents of the ambient air and the used chemicals and vessels. Therefore, the entire instrumental setup was built up in a clean room class 100 and all high-purity materials and chemicals were kept in this clean room.

The cleaning of vessels and tools was adapted according to the Hg concentrations to be handled. For the handling of solutions with mercury contents >2.5 μg l^{-1}, glass vessels were used and cleaned with nitric acid steam in a steaming apparatus (quartz glass steaming apparatus, H. Kuerner Analysetechnik, Rosenheim, Germany) for at least 6 h and then kept in a clean bench under a laminar stream

Table 1
FI-CV procedure steps for on-line oxidation and CV-AFS measurement without enrichment

Step	Action	Time interval in second from start	Flow rate of S/C/O/R in ml min^{-1}	Valve position	Ar flow rate in ml min^{-1}	
					GLS	Cuvette
1	Load of sample coil[a]	0–45	S: 11.2	V1 to waste V2 idle V3 idle V4 idle	–	–
2	Auto zero measurement[a] Transport of sample Reactions (on-line digestion, CV generation)[b]	46–105	C: 7.6 O: 2.0 R: 2.5	V1 to RC1 V2 to RC2 V3 to V4	250	
2	Rinsing of FI system	106–200	C: 7.6 O: 2.0 R: 2.5	V1 to RC1 V2 to RC2 V3 to V4 V4 to cuvette	250	
3	Purging of cuvette	201–215	–	(V1 idle) (V2 idle) V3 to V4 V4 to cuvette	–	250

S, sample; C, carrier; O, oxidant; R, reductant; GLS, gas–liquid separator.
[a] Auto zero measurement in time interval 46–50 s from start.
[b] AFS measurement (read of signal) in time interval 65–105 s from start.

of particle-poor air. For Hg concentrations <2.5 μg l^{-1}, the vessels were treated with a BrCl solution (1% (v/v)) for at least 24 h. After removing the BrCl solution, the vessels were rinsed with ultra pure water (UPW) three times and the whole procedure was repeated subsequently. Glass vessels were heated to 250 °C for at least 12 h in a drying oven. After cooling down to room temperature, the vessels were put in plastic bags and kept in closed boxes in the clean room until use. Perfluoroalkoxy (PFA) vessels were filled with UPW, closed and kept in a clean bench until use.

All reagents were purchased in the highest purity commercially available and some of them were further purified by cleaning procedures described in the following. Ultra pure water (at least 18.2 MΩ) was obtained from a Milli-Q-Gradient system (Millipore, Billerica, USA). The mercury contamination of hydrochloric acid (p.a., Merck, Darmstadt, Germany) was strongly reduced by adding 0.1 g of $NaBH_4$ (p.a., Merck, Darmstadt, Germany) to 400 ml of hydrochloric acid and purging the solution for 12 h with nitrogen (120 ml min^{-1}) which was additionally purified by passing it over a self-made activated carbon/sulphur column (activated carbon: granulate, 2.5 mm, Merck, Darmstadt, Germany; sulphur: elemental sulphur for external pharmaceutical application, Merck). The glass column (h. 180 mm; i.d. 550 mm) is filled with 500 ml of the carbon/sulphur mixture (sulphur content ~3 wt.%) and has a sintered-glass filter. Potassium bromate and potassium bromide (both p.a., Merck, Darmstadt, Germany) were pre-treated by heating the salts to 240 °C for 2 h before use. Sodium chloride and potassium iodide (both p.a., Merck) were pre-treated by heating the salts to 240 °C for 12 h.

For the preparation of stock BrCl solution, 4.32 g of KBr were dissolved in 400 ml of hydrochloric acid. In a fume hood, 6.08 g of $KBrO_3$ were then added slowly under constant stirring. This process generates free halogens (Cl_2, Br_2, BrCl), which are released from the bottle. Therefore, the solution was allowed to stir for another hour in the loosely capped bottle before the lid was tightened. The resulting saturated BrCl solution was used as stock solution for the preparation of oxidant solution (dilutions are further given as % (v/v) of the saturated stock solution) and as reagent for the cleaning procedures. The stock solution was stored for a maximum of 1 week.

The reductant solution was freshly prepared before use by dissolving 11.9 g of $SnCl_2{\cdot}2H_2O$ (p.a., Hg max. 10^{-6}%, Merck, Darmstadt, Germany) and 5 g of hydroxylamine hydrochloride (p.a., Hg max. 10^{-6}%, Merck, Darmstadt, Germany) in 500 ml of 3.6% (w/v) hydrochloric acid.

Table 2
FI-CV procedure steps for on-line oxidation and CV-AFS measurement with enrichment

Step	Action	Time interval in seconds from start	Flow rate of S/C/O/R in ml min^{-1}	Valve position	Ar flow rate in ml min^{-1}		
					GLS	Collector	Cuvette
1	Load of sample coil[a]	0–45	S: 11.2	V1 to waste V2 idle V3 idle V4 idle	–	–	
2	Transport of sample Reactions (on-line digestion, CV generation) Enrichment	46–200	C: 7.6 O: 2.0 R: 2.5	V1 to RC1 V2 to RC2 V3 to collector V4 to cuvette	250		–
3	Purging of cuvette & collector	201–215	–	(V1 idle)		250	
4	Auto zero measurement	216–220		(V2 idle)	–		250
5	Thermodesorption[a]	221–240		V3 to collector			
6	Cooling and purging of collector and cuvette[a]	241–280		V4 to cuvette			

S, sample; C, carrier; O, oxidant; R, reductant; GLS, gas–liquid separator.
[a] AFS measurement (read of signal) in time interval 221–255 s from start.

Diluted hydrochloric acid (0.5% (v/v)) was used as carrier solution.

For the preparation of humic acid stock solution, 110 mg of humic acid sodium salt (Roth, Karlsruhe, Germany) was dissolved in 100 ml of UPW. The dissolved organic carbon content of the resulting solution was measured to be 342 mg DOC l^{-1}. Stock solutions of sodium chloride and potassium iodide were prepared by dissolving 35 g of NaCl in 200 ml of UPW and 65.4 mg of KI in 100 ml of UPW, respectively.

Mercury stock standard solutions of 10 mg Hg l^{-1} were prepared weekly from commercially available standard solutions (Mercury(II)nitrate, 1000 mg l^{-1}, Merck, Darmstadt, Germany; methylmercurychloride, 1000 mg l^{-1}, Alfa Aesar, Karlsruhe, Germany) by dilution in hydrochloric acid (0.5% (v/v)). Solutions with mercury contents lower than 10 mg Hg l^{-1} were freshly prepared every day by gradual dilution of stock mercury solution in hydrochloric acid (0.5% (v/v)).

Model solutions were prepared by the addition of appropriate amounts of different stock solutions to mercury standard solutions about 2 h before measurement.

Remaining contamination of the tubing and chemicals add up to a blank value of 0.00610 ± 0.00009 (fluorescence intensity) after enrichment of mercury vapor on a gold collector (sample, UPW, $n = 10$; fluorescence intensity for 0.1 ng Hg l^{-1}, 0.00661 ± 0.00002). Blank values in model solutions caused by the addition of matrix substances were carefully investigated and given results were corrected when necessary.

2.4. Sampling, storage, and sample pre-treatment

The seven investigated real freshwater samples from lakes and rivers were all taken in August 2007 in South Germany and Southern France (cf. Table 5). The sampling was performed with PFA containers, which were rinsed three times with the sample, before they were completely filled and locked under water in order to exclude ambient air. All water samples were taken 1 m from the shore line in a depth of about 0.02 m. The samples were filtered through 0.45 μm polycarbonate filters (VWR, Darmstadt, Germany) and stored in PFA containers at 4 °C in the clean room, protected from light. Potential contamination of the used filters was checked by a blank test that confirmed the absence of mercury. For analysis of mercury, 250 μl hydrochloric acid were added in a 50-ml glass flask and filled up to volume with the filtered sample.

The sea water sample was taken in the North Sea (near estuary of the River Elbe) and was collected in January 2007 by the *Bundesamt für Seeschifffahrt und Hydrographie* (BSH, Hamburg, Germany). The sampling was performed with PFA containers in a depth of about 11 m by using a dipper with automated sealing controlled by a ship board crane. Filtration (0.45 μm) of the sea water samples was performed on-site immediately after collection.

The certified reference material ORMS-3 (elevated mercury in river water) was purchased from the National Research Council Canada (NRC-CNRC, Ottawa, Canada) and handled according to the recommendation given in the certificate.

3. Results and discussion

3.1. Optimization of the flow injection analysis system

The optimization of the proposed on-line oxidation system was performed by the use of mercury model solutions and addition of matrix constituents occurring in nature in various concentrations. For this purpose either $MeHg^+$ standard solutions or mixtures of $MeHg^+$ and Hg^{2+} standard solutions (1:1) were used so as to allow for different chemical behaviors (e.g. complexation) of the different mercury species. In a first approach, the key parameters of the on-line oxidation system were optimized with less demanding model solutions and relatively high Hg concentrations (20–100 ng Hg l^{-1}) in order to observe clear trends (Section 3.1.1). For this purpose, AFS measurement without enrichment was chosen. In the following, the system was adapted for natural water samples with lower Hg concentrations, elevated dissolved organic carbon contents and higher concentrations of other matrix constituents occurring in nature which may cause problems in the chemical reaction with BrCl (Section 3.1.2). Here, measurement was performed after Hg enrichment on the built-in collector of the AFS instrument.

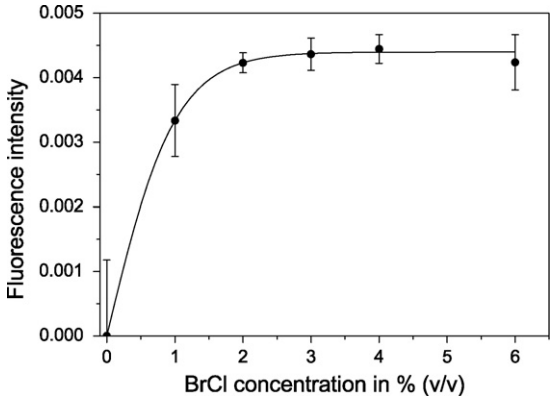

Fig. 2. On-line methylmercury decomposition by oxidation with different BrCl concentrations (c(Hg) = 100 ng l^{-1}; $n = 3$).

3.1.1. Optimization of key parameters

In a first series of experiments, the key parameters – BrCl concentration, reaction temperature and time – were optimized in order to achieve optimal decomposition results. A methylmercury standard solution (100 ng Hg l^{-1}) in ultra pure water was therefore decomposed on-line by use of the oxidant BrCl in different concentrations from 0% to 6% of the stock solution. The achieved fluorescence signals are given in Fig. 2 and show – as expected – no signal appearance without BrCl and rising signal strength within increasing BrCl concentration from 1% to 3% (v/v) BrCl. A constant signal intensity is observed from up about 3% (v/v) BrCl. For ensuring complete decomposition, a concentration of 4% BrCl was used for further experiments. The optimization of the reaction temperature for on-line decomposition was examined within a range of 25–70 °C. For this purpose, methylmercury standard solu-

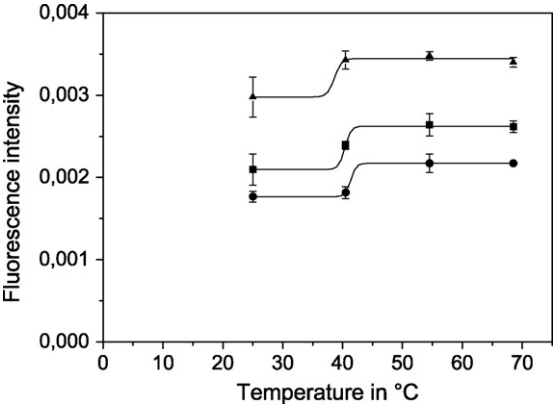

Fig. 3. On-line methylmercury decomposition by BrCl oxidation at different temperatures (c(BrCl) = 4% (v/v); c(Hg): (●) 20 ng l^{-1}; (■) 30 ng l^{-1}; (▲) 50 ng l^{-1}, respectively).

tions were used with a concentration of 20, 30 and 50 ng Hg l^{-1}, respectively, and decomposed in a reaction coil of 1.5-m length in the heated reactor. Fig. 3 shows the received fluorescence signals at reaction temperatures of 25, 40, 55 and 70 °C. Apparently, higher signals are achieved above a temperature of 40 °C and in the temperature range from 55 to 70 °C no further increase of the signal intensities is observed. Therefore, all further experiments were performed at a temperature of 70 °C. Variations of the reaction coil length (0.5–2.0 m) and thus of the reaction time did not show any influence when investigating the model solution. The found parameters are suitable for non-contaminated water samples, whereas for water samples with, e.g. elevated DOC the system was adapted as follows.

3.1.2. Adaptations for more demanding samples

In the following series of experiments, the on-line decomposition was tested in mercury model solutions containing known concentrations of interfering matrix components. It is well known that the ionic mercury species occurring in natural waters, such as $MeHg^+$ and Hg^{2+}, are strongly complexed by organic matter. Therefore, it is very important, in particular for the investigation of freshwater samples with DOC contents of up to 10 mg DOC l^{-1} [16], that the developed on-line decomposition achieves quantitative decomposition and/or release of the complexed Hg species. In this context, again the concentration of BrCl solution is very important. Therefore, in a first experiment, the fluorescence signal intensity of a mixture of methyl mercury and mercury standard solution ($MeHg^+$:Hg^{2+}, 1:1) in 10 mg DOC l^{-1} was investigated in dependence of the applied BrCl concentration. A commercially available sodium salt of humic acid was used as model substance for DOC. From a concentration of 0–3% (v/v) BrCl, the signal intensity increases clearly but remains almost constant with further increase (see Fig. 4). Therefore, BrCl concentration was kept at 4% (v/v) in all further experiments.

Moreover, the influence of DOC content was examined within a concentration of up to 50 mg l^{-1} using the above-found parameters (oxidant concentration 4% (v/v) BrCl; temperature 70 °C; reaction coil length 1.5 m). However, it was observed that these parameters do not lead to quantitative decomposition. Since further increase of oxidant concentration and temperature could probably have a negative impact on the lifetime of the tubing, connectors and valves of the FIA system, the reaction time was prolonged. Lengthening the reaction coil for oxidation from 1.5 to 3.0 m – and so doubling the retention time – leads to quantitative Hg determination in solutions with up to 15 mg DOC l^{-1} (cf. Fig. 5). Only at a concentration

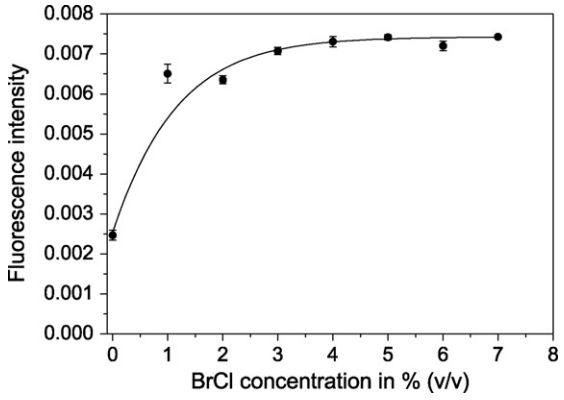

Fig. 4. On-line decomposition of a mixture of methylmercury, inorganic mercury and dissolved organic carbon (DOC) as model solution for oxidation with different BrCl concentrations ($MeHg^+$:Hg^{2+} = 1:1; $c(Hg_t)$ = 5 ng l^{-1}; c(DOC) = 10 mg l^{-1}; n = 3).

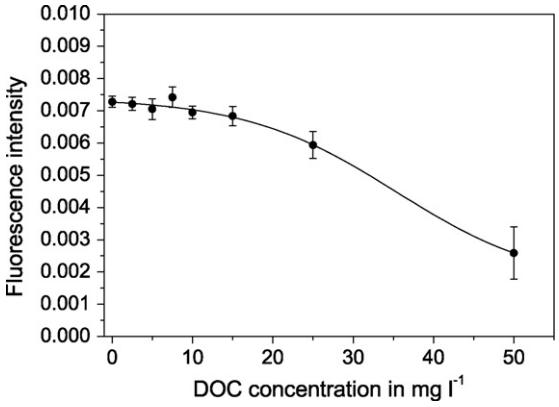

Fig. 5. Influence of dissolved organic carbon on the fluorescence signal intensity for total mercury determination in a mixture of methylmercury and inorganic mercury standard solution (c(BrCl) = 4% (v/v); $MeHg^+$:Hg^{2+} = 1:1; $c(Hg_t)$ = 5 ng l^{-1}; n = 3).

of 25 mg DOC l^{-1} or higher the signal intensity decreases clearly. But in practice, DOC concentrations over 15 mg l^{-1} do not occur in natural waters [16] and can only be found in waste waters or in strongly contaminated waters that are not subject of the investigations in the present work.

Naturally occurring inorganic species such as chloride and iodide may also interfere the on-line oxidation with BrCl. High concentrations of Cl^- ions, which are only found in sea water (~19 g l^{-1}) [16], possibly influence the reaction equilibria of the oxidation reaction. Iodide ions, another constituent of sea water (~50 μg l^{-1}), influence redox reactions even in low concentrations and were also

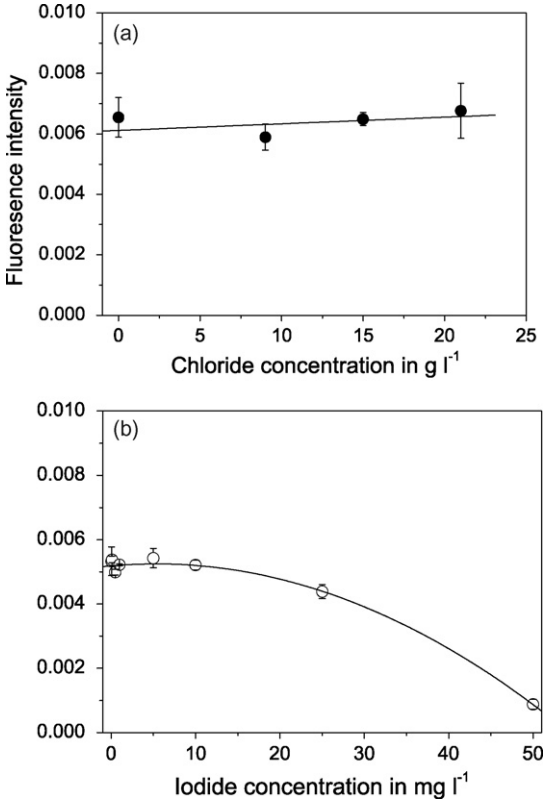

Fig. 6. Influence of (●) chloride and (○) iodide (respectively) on the fluorescence signal intensity for total mercury determination in a mixture of methylmercury and inorganic mercury standard solution (c(BrCl) = 4% (v/v); $MeHg^+$:Hg^{2+} = 1:1; $c(Hg_t)$ 5 ng l^{-1}; n = 3).

Table 3
Optimized parameters and maximum tolerated matrix compounds for the new developed FI-CV-AFS method

Parameter	Optimum/found value
Oxidant	4% (v/v) BrCl in HCl
Reaction temperature (°C)	70
Reaction coil length (m)	3
Max. tolerated DOC (mg l^{-1})	15
Tolerated Cl^- (g l^{-1}, at least)	21
Max. tolerated I^- (mg l^{-1})	10

Table 4
Analytical data for total mercury determination with the developed FI-CV-AFS method

Analytical data	Obtained values
Sample volume for 3-fold measurement (ml)	34
Analysis time for 3-fold measurement (min)	15
Typical calibration range (ng Hg l^{-1})	0.02–15
Calibration function (n_c = 15)	$y = 4.99 \times 10^{-3}$; $x + 6.12 \times 10^{-3}$
Regression coefficient, R^2	0.9943
Detection limit as derived from the calibration function (pg Hg l^{-1}) [18]	16

investigated as potentially interferent. Fortunately, both inorganic species are tolerated in concentrations which are clearly higher than the naturally occurring concentrations. Fig. 6 reveals that chloride and iodide ions are tolerated in concentrations up to at least 21 g Cl^- l^{-1} and 10 mg I^- l^{-1}.

In order to show the applicability of the proposed method in occurrence of all matrix components, eight different natural water samples and a certified reference material were investigated (cf. Sections 3.2 and 3.3).

3.1.3. Summary of optimized parameters and resulting analytical data

In Table 3 the found parameters and maximum tolerated interferent concentrations for on-line digestion are listed. Calibration experiment using these parameters and the enrichment procedure leads to a detection limit of only 16 pg Hg l^{-1} and R.S.D. of about 4%. The limit of detection (LOD) was calculated from the confidence interval of a calibration function in the range from 0.02 to 0.1 ng Hg l^{-1} (LOD: two times the confidence interval at Hg concentration of "0" extrapolated from the linear regression) [19]. In contrast to the often used "3σ-method" for estimation of the detection limit the applied method uses more measurement data (all pairs of variates of the calibration function) and therefore provides more reliable information. This sensitivity offers the opportunity to investigate even uncontaminated open sea water. The analytical data are summarized in Table 4.

3.2. Validation

A validation experiment was performed with the certified reference material ORMS-3, a river water sample with a certified value of 12.7 ± 1.1 ng Hg l^{-1}. The found concentration of 11.40 ± 0.39 ng Hg l^{-1} (number of replicates $n = 3$; significance level $P = 95\%$) determined by means of the proposed on-line oxidation method lie within the certified value range. In addition, the analytical accuracy of the proposed method was checked by comparison of the obtained Hg value with the value found by application of a standard method—EPA method 1631 for the determination of Hg traces in water. For ORMS-3 this is in a very good accordance (11.39 ± 0.70 ng Hg l^{-1}; $n = 3$, $P = 95\%$). Furthermore, a real water sample with very high demand on oxidation power due to its extremely high DOC content of 14.5 mg l^{-1} was chosen for comparison. Here too, the obtained value of 1.39 ± 0.14 ng Hg l^{-1} found by the use of EPA method 1631 corresponds very well to the Hg concentration found by application of the proposed on-line digestion method (1.38 ± 0.06 ng Hg l^{-1}).

3.3. Investigation of natural water samples

Several natural water samples were examined for their total mercury content, using the developed FIA system. In all samples, the content of DOC was determined additionally. The found values are summarized in Table 5.

The DOC contents of the river, lake and the estuary sea water samples are all in a close concentration range from 2.0 to 3.9 mg l^{-1}, only the moorland water sample "Deininger Moor" shows – as expected – a clearly higher value of 14.5 mg DOC l^{-1}. Besides, the Hg content of the moorland water is the highest value observed (1.38 ng l^{-1}). This is reasonable, since humic rich waters mobilize Hg from the sediment and particle charge more easily [20]. Comparing the three river water with the three lake water samples, it is remarkable that the Hg concentrations found in the rivers (0.68–1.07 ng Hg l^{-1}) are somewhat higher than the values found in the lakes (0.27–0.51 ng Hg l^{-1}). Obviously, the examined lakes have a very low geogenic background due to their geographical location (very close to the foothills of the Alps). By contrast, the investigated rivers flow through partially industrialized and/or inhabited areas and so may have slightly higher contamination. Nevertheless, compared to, e.g. river water flowing through very industrialized areas (e.g. the River Elbe shows values up to 160 ng Hg l^{-1} [17]), all found Hg concentrations are in the range of geogenic background concentrations and/or minor contamination. A good summary of measured mercury contents in natural freshwaters in the past decade is given in Ref. [21]. Here, the found mercury concentrations for clearwater lakes range between 0.5 and 2.0 ng Hg l^{-1}, for humic rich lakes between 2 and 10 ng Hg l^{-1} and in river water between 1 and 20 ng Hg l^{-1} in the absence of local pollution. So, the concentrations found in this work are all within these concentration ranges. This applies also to the sea water sample with a total Hg content of

Table 5
Results for DOC measurement and total mercury determination by FI-CV-AFS method in different natural freshwater samples collected in August 2007 in South Germany and Southern France ($n = 3$; $P = 95\%$).

Sample type	Sampling site	Sample name	Total Hg in ng l^{-1}	DOC in mg l^{-1}
River water	The River Rhine, riverbank near Mannheim, Germany	The Rhine	0.89 ± 0.11	2.5
	The River Moselle, riverbank near Bernkastel-Kues, Germany	The Moselle	0.68 ± 0.11	3.6
	The River "La Garonne", riverbank near Buzet-sur-Baise, France	La Garonne	1.07 ± 0.12	2.0
Lake water	Starnberger Lake, lakeside in Starnberg, Germany	Starnberger Lake	0.27 ± 0.09	3.9
	Feringa Lake, lakeside near Ismaning, north of Munich, Germany	Feringa Lake	0.33 ± 0.09	2.8
	Echinger Lake, lakeside near Eching, north of Munich, Germany	Echinger Lake	0.51 ± 0.07	2.6
Moorland water	Deininger Lake, lakeside near Deining, south of Munich, Germany	Deininger Moor	1.38 ± 0.06	14.5
Sea water	North Sea, estuary of the River Elbe, Germany	North Sea	0.75 ± 0.09	2.3

0.75 ng Hg l^{-1} which is reasonable compared to the value of reactive Hg measured by the *Bundesamt für Seeschifffahrt und Hydrographie* (Hamburg, Germany) which is 0.73 ng Hg l^{-1}.

4. Conclusion

The developed fully automated FI-CV-AFS method is a fast and simple method for the correct and precise analysis of total mercury contents in natural water samples. This was confirmed by the high tolerable concentrations of dissolved organic carbon and halogens, the successful validation experiments and the application of the method to the investigation of eight different natural water samples. The new on-line procedure enables a high sample throughput of 13 measurements h^{-1} with a very low detection limit of 16 pg Hg l^{-1}, which makes the method suitable for Hg monitoring.

Acknowledgments

The authors are very grateful to the Deutsche Forschungsgemeinschaft (DFG) for their generous financial support. The authors also thank Analytik Jena AG for the provision of apparatus and equipment and owe Thomas Labatzke and Klaus-Christian Friese a debt of gratitude for technical support and providing special software. Further, the authors are very grateful to Dr. Brigitte Helmreich (Lehrstuhl und Laboratorien für Siedlungswasserwirtschaft; TUM) for performing the DOC measurements.

References

[1] D.M. Orihel, M.J. Paterson, P.J. Blanchfield, R.A. Bodaly, H. Hintelmann, Environ. Sci. Technol. 41 (14) (2007) 4952–4958.
[2] R.P. Mason, F.M.M. Morel, H.F. Hemond, Water, Air Soil Pollut. 80 (1995) 775–787.
[3] R.P. Mason, W.F. Fitzgerald, in: W. Bayens, R. Ebinghaus, O. Vasiliev (Eds.), Global and Regional Mercury Cycle: Sources, Fluxes and Mass Balance, Kluwer Academic Publishers, Dordrecht, 1996, pp. 249–272.
[4] D. Cossa, J.-M. Martin, J. Sanjuan, Deep-Sea Res. Part II: Top. Stud. Oceanogr. 44 (1997) 721.
[5] R.P. Mason, K.R. Rolfhus, W.F. Fitzgerald, Mar. Chem. 61 (1998) 37.
[6] N. Bloom, Can. J. Fish. Aquat. Sci. 46 (7) (1989) 1131–1140.
[7] M. Meili, in: A. Sigel, H. Sigel (Eds.), Metal Ions in Biological Systems. Vol. 34: Mercury and its Effect on Environment and Biology, Marcel Dekker Inc., New York, 1997, pp. 21–51 (Chapter 2).
[8] W.A. Telliard, United States Environmental Protection Agency, Federal Register, vol. 67, no. 209 EPA-821-R-01-033 Method 1631 Revision C, 2001.
[9] European Standard EN 13506, 2001 (RefNrEN 13506:2001).
[10] O. Wurl, O. Elsholz, R. Ebinghaus, Talanta 52 (2000) 51–57.
[11] O. Wurl, O. Elsholz, R. Ebinghaus, Anal. Chim. Acta 438 (2001) 245–249.
[12] M.J. Bloxham, S.J. Hill, P.J. Worsfold, J. Anal. Atom. Spectrosc. 11 (1996) 511–514.
[13] R.J.M. Hudson, S.A. Gherini, C.J. Watras, D.B. Porcella, in: C.J. Watras, J.W. Huckabee (Eds.), Mercury Pollution—Integration and Synthesis, Lewis Publishers, Boca Raton, FL, 1994, pp. 473–523.
[14] R.P. Mason, K.A. Sullivan, Deep-Sea Res. Part II: Top. Stud. Oceanogr. 46 (1999) 937.
[15] D. Cossa, M. Coquery, in: A. Saliot (Ed.), Handbook of Environmental Chemistry, vol. 5, Springer, 2005, pp. 177–208.
[16] E. Worch, Wasser und Wasserinhaltsstoffe, Teubner Verlag, Stuttgart, 1997.
[17] O. Elsholz, C. Frank, B. Matyschok, F. Steiner, O. Wurl, B. Stachel, H. Reincke, M. Schulze, R. Ebinghaus, M. Hempel, Fresenius J. Anal. Chem. 366 (2) (2000) 196–199.
[18] T. Labatzke, G. Schlemmer, Anal. Bioanal. Chem. 378 (2004) 1075–1082.
[19] W. Funk, V. Dammert, G. Donnevert, Qualitätssicherung in der Analytischen Chemie, VCH, Weinheim, 1992.
[20] D. Wallschlaeger, M.V.M. Desai, R.-D. Wilken, Water Air Soil Pollut. 90 (3/4) (1996) 507–520.
[21] M. Meili, in: A. Sigel, H. Sigel (Eds.), Metals Ions in Biological Systems: Mercury and its Effects on Environment and Biology, vol. 34, Marcel Dekker Inc., New York Basel Hong Kong, 1997, pp. 21–51.

Talanta 76 (2008) 276–281

Contents lists available at ScienceDirect

Talanta

journal homepage: www.elsevier.com/locate/talanta

Rapid quantitative analysis of phenazine-1-carboxylic acid and 2-hydroxyphenazine from fermentation culture of *Pseudomonas chlororaphis* GP72 by capillary zone electrophoresis

Hai-Ming Liu[a], Xue-Hong Zhang[a], Xian-Qing Huang[a], Cheng-Xi Cao[b], Yu-Quan Xu[a,*]

[a] *Key Laboratory of Microbial Metabolism, Ministry of Education and College of Life Science and Biotechnology, Shanghai Jiaotong University, Dongchuan Road 800, Minhang District, Shanghai 200240, PR China*

[b] *Laboratory of Analytical Biochemistry and Bioseparation, School of Life Science and Biotechnology, Shanghai Jiaotong University, Shanghai 200240, PR China*

ARTICLE INFO

Article history:
Received 9 January 2008
Received in revised form 22 February 2008
Accepted 25 February 2008
Available online 4 March 2008

Keywords:
Antibiotics
Phenazine-1-carboxylic acid
2-Hydroxyphenazine
Capillary zone electrophoresis
Pseudomonas chlororaphis GP72

ABSTRACT

Natural phenazines in secondary metabolites of bacteria have been receiving increasing attention in recent years due to their potential usage as antibiotics. In the present study, a rapid and reliable capillary zone electrophoresis (CZE) method was developed and validated for monitoring for the first time dynamic phenazine-1-carboxylic acid (PCA) and the 2-hydroxyphenazine (2-OH-PHZ) production of *Pseudomonas chlororaphis* GP72 during the entire fermentation cycle. The paper begins with the optimization of separate conditions for 2-OH-PHZ and PCA together with phenazine (PHZ), which is used as internal standard. The optimized conditions are: 10 mM, pH 7.3 phosphate buffer, a fused-silica capillary with a total length of 49 cm × 75 μm ID, 375 μm OD with an effective length of 40 cm, 25 kV, 13 mbar 10 s pressure sample injection and 25 °C air-cooling. The three compounds could be separated within 2 min under optimized conditions. The validation of the newly developed study shows the linear response of 2-OH-PHZ and PCA ranging from 10 to 250 μg mL^{-1} with high correlation coefficient (r = 0.9997 and 0.9993, n = 7), low limits of detection (0.47 and 0.38 μg mL^{-1}) and quantification (1.56 and 1.28 μg mL^{-1}), respectively. Good precision values for intra- and inter-day detection and acceptable individual recovery ranges for 2-OH-PHZ and PCA are indicated. The newly developed method was also validated through monitoring dynamic PCA and 2-OH-PHZ production of *P. chlororaphis* GP72 during an 84 h growth cycle.

1. Introduction

More than 6000 phenazine-containing compounds have been identified and reported during the last two centuries, including those synthetic analogues for the discovery of new anti-infective agents. Fewer than 100 are of natural origin [1]. Both soil habitants and marine microorganisms are known to produce phenazine natural products with antibiotic effects. These classes of metabolites are particularly interesting due to their biological activities including broad-spectrum antimicrobial, antifungal, physical, and electrochemical effects. Some of these natural products have already been used as antitumor, antimalaria, and antiparasitic agents [2–4].

Phenazine natural products are isolated as secondary metabolites, which primarily come from *Pseudomonas*, *Streptomyces* [5–8] and a few other genera from soil or marine habitats. Some well-known phenazine compounds have been originally and mostly found in best-studied fluorescent pseudomonad, such as phenazine-1-carboxylic acid (PCA), pyocyanin (PYO), phenazine-1-carboxamide (PCN), 1-hydroxyphenazine (1-OH-PHZ), 2-hydroxyphenazine-1-carboxylic acid (2-OH-PCA) and 2-hydroxyphenazine (2-OH-PHZ) [1,4,9–11]. Except for *Pseudomonas fluorescens*, which only produce PCA, phenazine-producing fluorescent pseudomonad typically synthesizes two or more phenazines, such as PCA, 1-OH-PHZ and PYO in *Pseudomonas aeruginosa* PAO1 [12]; PCA and PCN in *Pseudomonas chlororaphis* PCL1391 [13]; PCA, 2-OH-PCA and 2-OH-PHZ in *P. chlororaphis* 30–84 [14]; and so on. These kinds of phenazine-producing strains prove to be excellent biocontrol agents in further studies [15–17].

Previous methods of analysis and quantification of phenazines include the use of thin layer chromatography (TLC), high performance liquid chromatography (HPLC), and even liquid chromatography–mass spectrometry (LC–MS) to determine metabolites in either fermentation broth or serum. Taunk and Mital described a method for detection of 5,10-dihydrophenazines by TLC [18]. O'Connor et al. applied LC for the determination of phenazines together with clofazimine in serum and tissue [19].

* Corresponding author. Tel.: +86 21 34204854; fax: +86 21 34204051.
E-mail address: xuyq@sjtu.edu.cn (Y.-Q. Xu).

0039-9140/$ – see front matter © 2008 Elsevier B.V. All rights reserved.
doi:10.1016/j.talanta.2008.02.034

Based on this method, Watson et al. developed a method for determining pyocyanin and 1-hydroxyphenazine [20]. With more and more natural phenazine products discovered from the secondary metabolites of some pseudomonad, Fernandez et al. used HPLC to separate PYO, 1-OH-PHZ and PCA in the supernatant cultures of *P. aeruginosa*, Which does not almost need any treatment [21]. Delaney et al. described a method for the separation and quantification of PCA, 2-OH-PCA and 2-OH-PHZ in the fermentation broth of *P. chlororaphis* 30–84 with gradient elution in reverse phase HPLC [22]. More recently, we also developed a method for the detection and quantification of PCA and 2-OH-PHZ in the fermentation broth of *P. chlororaphis* GP72 [23]. Although these methods gave good separation resolution of phenazine compounds, they still hold some obvious disadvantages, such as complex procedures, expensive consumption of flow phase, longer separation time (nearly half an hour) and pollution of organic reagents. All of these problems can almost be solved with high performance capillary electrophoresis (HPCE) [24–26].

Until now, no electrophoretic method has been developed for the determination of phenazines, which is of both agricultural and medical importance in the fermentation broth of bacterial strains. Thus, we describe a CZE method for the rapid quantitative analysis of the antifungal metabolites of PCA and 2-OH-PHZ from the fermentation broth of *P. chlororaphis* GP72. Method development includes optimization of parameters affecting the separation process, such as applied voltage, buffer ionic strength, and buffer pH value. Investigation on the reliability of this method includes specificity, selectivity, linearity, accuracy, and precision. The LOD and LOQ of this method are also determined in the present study.

2. Experimental

2.1. Instrumentation

All capillary-based experiments are performed with an ACS2000 HPCE apparatus (Beijing Cailu Scientific Inc., Beijing, China). This instrument consists of a digital electric power supply (up to voltage 30 kV) with a UV detector performing wavelength scanning from 190 to 740 nm. Detection wavelength has been set at a maximum absorbance wavelength of 254 nm by an automatic wavelength scanning of PHZ, 2-OH-PHZ, and PCA with the UV detector in CE apparatus. The operating system is Windows XP professional SP2 with a HW-2000 chromatography workstation (Qianpu Software Co. Ltd., Nanjing, China). The room temperature is maintained at 25 °C. A fused-silica capillary of total length 49 cm × 75 μm ID, 375 μm OD with an effective length of 40 cm (Factory of Yongnian Optical Fiber, Hebei, China) is used throughout the following process of analysis. An Ultra-pure Water System (SG Ultra Clear System, Wasseraufbereitung und Regenerierstation GmbH, Germany) is used to generate ultra-pure water with a specific conductivity of 0.055 μs cm^{-1} for analysis.

2.2. Reagents and standard preparation

Authentic PCA and 2-OH-PHZ standard samples were purified from the secondary metabolites of *P. chlororaphis* GP72. The purity and molecular structures of these two standards were determined by elemental analysis, ultraviolet absorbent spectrum scanning, mass spectrum with electrospray ionization and ^{1}H and ^{13}C nuclear magnetic resonance (NMR) [23]. Potassium phosphate (analytical grade AR) and sodium phosphate dibasic (analytical grade AR) were purchased from Bio Basic Inc. (Markham Ontario, Canada). Sodium hydroxide, hydrochloric acid, methanol (MeOH, HPLC grade) and the internal standard of PHZ (analytical grade AR) were purchased from Shanghai Chemistry Reagent Company (Shanghai, China). The stock concentration of the internal standard was 1000 μg mL^{-1}. A series of phosphate buffers with different pH values and concentrations was prepared. The pH values of the buffers ranged from 7.0 to 8.0 and the concentrations from 5 to 25 mmol L^{-1}. Standard solutions were prepared based on the following procedure. A series of samples with different concentrations of PCA and 2-OH-PHZ plus PHZ was added into blank fermentation liquor and extracted in accordance with the procedure described in Section 2.4. The final concentrations of PCA and 2-OH-PHZ were 10, 20, 25, 50, 75, 100, and 250 μg mL^{-1}, respectively and with a final concentration of PHZ as 50 μg mL^{-1}.

2.3. Bacterial fermentation conditions

P. chlororaphis GP72 was used in the present study. The standard fermentation process consisted of pre-culture in a 250 mL conical flask containing 50 mL of King's B medium (KMB) [27] at 28 °C for 10 h. A portion (7.5 mL) of this culture was inoculated into 150 mL of KMB and pigment producing medium (PPM) [28] in 500 mL conical flasks, cultivating at 28 °C for 84 h to quantify the production of PCA and 2-OH-PHZ.

2.4. Extraction procedures

PCA, 2-OH-PHZ, as well as PHZ could be well extracted from the fermentation broth of strain *P. chlororaphis* GP72 with chloroform. For PCA and 2-OH-PHZ extraction, 180 μL bacterial cultures plus 27 μL internal standard (PHZ, 1000 μg mL^{-1}) were adjusted to pH 2.0 with 1 M HCl, were mixed well with 540 μL chloroform, and were centrifuged at 12,000 × *g* for 5 min. Finally 500 μL of the chloroform phase was dried under vacuum after discarding the upper layer, and then it was used for HPCE analysis similar to the method established previously [29]. The residue after dryness in the tube was dissolved with MeOH and diluted to 500 μL with running buffer for CZE analysis. All solutions were stored at 4 °C in a refrigerator until use.

2.5. Capillary conditioning

Prior to first use, a new fused-silica capillary (49 cm × 75 μm ID, 375 μm OD with effective length 40 cm) was pressure-rinsed with 0.1 M NaOH for 30 min, followed by water for 10 min, and then finally 0.1 M HCl for 30 min. The capillary was then rinsed with water for 10 min and finally rinsed with running buffer for 30 min. Pressure injection of the sample was chosen, and the pressure was set at 13 mbar with the injection time controlled at 10 s. The capillary was rinsed with running buffer for 5 min between each injection. The running buffer was replaced every 10 injections in order to avoid migration time drift. The daily rinsing sequence includes pressure rinsing the capillary with 0.1 M NaOH for 10 min, followed by water for 5 min, and buffer for 15 min. The capillary was stored in water when not in use.

3. Results and discussion

The primary purpose of this study is to develop a rapid and effective method for monitoring the dynamic variation of both PCA and 2-OH-PHZ during the fermentation process of *P. chlororaphis* GP72. First, the PHZ is chosen as an internal standard to reduce errors brought by the operations in different injections due to its similar chemical structure, and physical and chemical properties to both PCA and 2-OH-PHZ (Fig. 1). Furthermore it is a very common and cheap commercial product nowadays. The phosphate buffer was selected as background electrolyte after having been compared

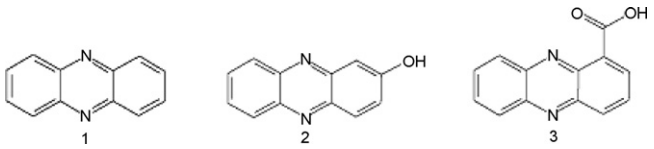

Fig. 1. Chemical structures of (1) phenazine (PHZ), (2) 2-hydroxyphenazine (2-OH-PHZ), (3) phenazine-1-carboxylic acid (PCA).

with several commonly used running buffers. After that, the CZE separation conditions were optimized for the three compounds. Finally, the newly developed method was validated during whole fermentation process.

3.1. Optimization of CE separation conditions

3.1.1. Effect of applied voltage

The applied voltage plays an important role in migration time, current strength and resolution. Normally, the ideal separation can be obtained by using a voltage as high as possible, not only to obtain the best separation, but also to finish the process in the shortest time possible. However, high voltages lead to high Joule heat, which is known to affect electroosmotic flow (EOF). The applied voltage ranges from 5 to 30 kV. The migration time of the three compounds is inversely proportional to the applied voltage (data not shown). All migration time can be controlled within 2 min with voltage supplied above 25 kV. However, at 30 kV, the current is too high, resulting in high Joule's heating, poor peak resolution, and bad peak shapes. Therefore 25 kV was chosen as the final applied voltage.

3.1.2. Effect of pH value

PH value is of key importance in peak resolutions among PHZ, 2-OH-PHZ, and PCA. Increasing the pH value from 7.0–8.0 results in increasing the resolution between PHZ and 2-OH-PHZ while decreasing the resolution for 2-OH-PHZ and PCA (Fig. 2). PHZ and 2-OH-PHZ cannot be separated well under the pH value of 7.0, and for 2-OH-PHZ and PCA, at 8.0. The migration time differs a little with the increasing pH value (data not shown). Considering both resolutions in the two groups, the best resolution of the three compounds should be obtained when the pH value of the running buffer is controlled at 7.3, and the final migration time for PHZ, 2-OH-PHZ and PCA is 1.26, 1.62, and 1.95 min individually under this condition.

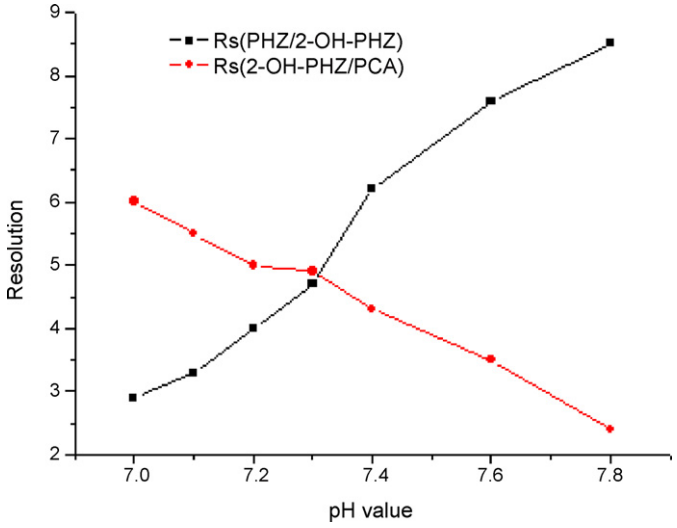

Fig. 2. Resolution of PHZ, 2-OH-PHZ and PCA with pH value ranging from 7.0–8.0. *Conditions*: 10 mM, pH 7.0–7.8 phosphate buffer, a fused-silica capillary with a total length of 49 cm × 75 μm ID, 375 μm OD, with an effective length of 40 cm, 13 mbar 10 s pressure sample injection, and 25 °C air-cooling room temperature.

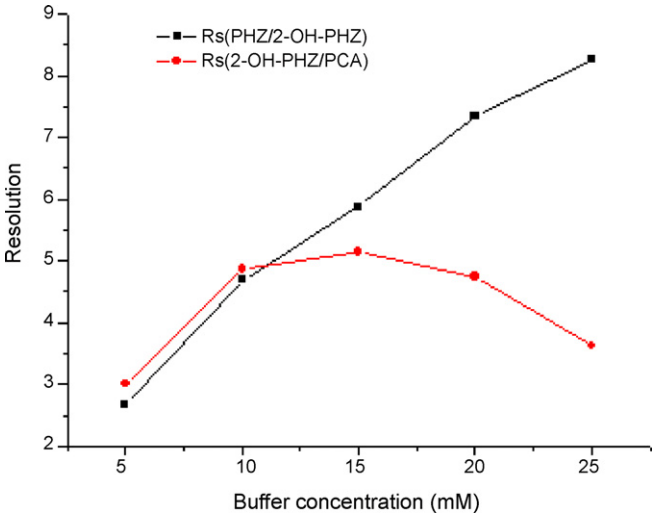

Fig. 3. Resolution of PHZ, 2-OH-PHZ and PCA with buffer concentration ranging from 5 to 25 mM. *Conditions*: 5–25 mM, pH 7.3 phosphate buffer, a fused-silica capillary with a total length of 49 cm × 75 μm ID, 375 μm OD, with an effective length of 40 cm, 13 mbar 10 s pressure sample injection and 25 °C air-cooling room temperature.

3.1.3. Effect of buffer concentration

The buffer concentration has obvious influence on peak resolutions, migration times, peak shapes, and detection noise. With the buffer concentration ranging from 5–25 mM, the resolution of PHZ and 2-OH-PHZ increases quickly, while the opposite trend is obtained for that of 2-OH-PHZ and PCA (Fig. 3). The migration time decreases while the buffer concentration increases (data not shown). At the same time, the current increases rapidly with the increasing buffer concentration. The resolution of 2-OH-PHZ and PCA decreases quickly when the buffer concentration reaches above 10 mM, possibly due to high Joule's heating. Although we can also obtain good separation of these compounds and lower current with the buffer concentration controlled at 5 mM, the 5 mM buffer gives poorer buffering ability. A comparative study on the optimization process suggests that we choose 10 mM as the final buffer concentration, yielding to an acceptable current ranging from 65–70 μA.

3.1.4. Optimized separation conditions

The final optimized separation condition is listed as follows: 10 mM, pH 7.3 phosphate buffer, a fused-silica capillary of total length 49 cm × 75 μm ID, 375 μm OD, with effective length 40 cm, 25 kV, 13 mbar 10 s pressure sample injection, and 25 °C air-cooling for room temperature control.

3.2. Validation of the developed method

3.2.1. Specificity

PHZ, 2-OH-PHZ, and PCA, which are extracted from the fermentation broth with chloroform have been detected repeatedly with different pH values, buffer concentrations, and applied voltage to determine the specificity of the method prior to use. No other peaks are detected under such different conditions. It is important for us to be sure of the purity of the peaks in electropherogram under optimized separation condition before monitoring dynamic antibiotic production during a complete growth cycle. As shown in Fig. 4, panel A shows the electropherogram of blank fermentation broth extracts. No obvious peak is detected. Panels B, C,

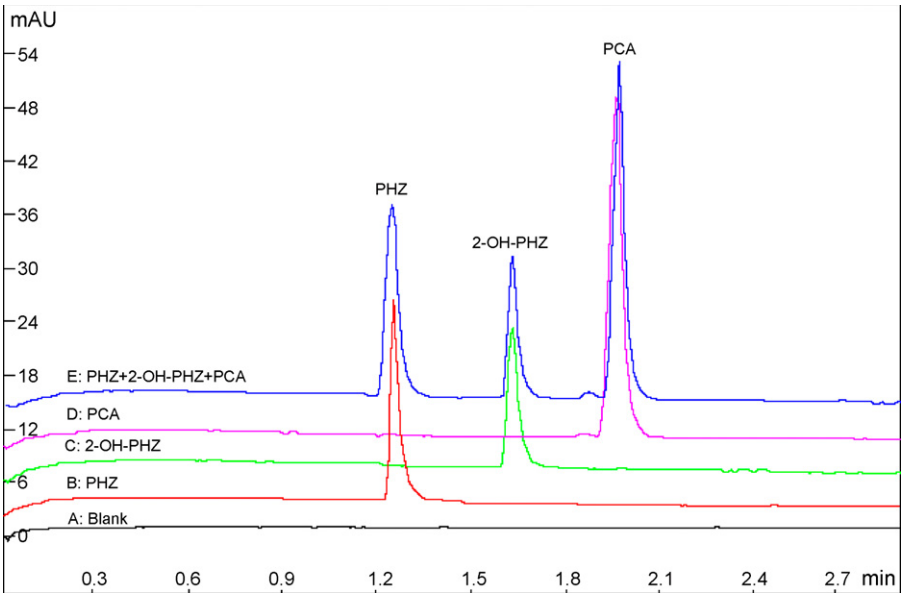

Fig. 4. Electrophoregrams of phenazine compounds in CZE: (A) blank fermentation broth; (B) internal standard PHZ extracted from fermentation broth; (C) 2-OH-PHZ extracted from fermentation broth; (D) PCA extracted from fermentation broth (E) PHZ, 2-OH-PHZ and PCA extracted from the fermentation broth in buffer. *Conditions*: 25 kV, 10 mmol L^{-1}, pH 7.3 phosphate buffer.

and D prove the unique peak detected in the electropherogram representing PHZ, 2-OH-PHZ, and PCA, which are extracted from the fermentation broth individually. Panel E displays the electropherogram of the three compounds extracted together from the fermentation broth with symmetrical peak shape, good resolution, and quick migration time. All the electropherograms appearing in Fig. 4 indicate the specificity of the optimized method for detecting phenazine compounds in the fermentation broth of *P. chlororaphis* GP72.

3.2.2. Linearity

The linearity of the developed method has been checked with a series of different concentrations of 2-OH-PHZ and PCA together with the internal standard PHZ (50 μg mL^{-1}) extracted from the fermentation broth. The gradients of 2-OH-PHZ and PCA concentrations (10, 20, 25, 50, 75, 100, 250 μg mL^{-1}) are used to construct a calibration curve to determine the linearity ratio of linear response for the analytes and the internal standard versus concentration of the analytes (data not shown). The correlation

Table 1
Precision data for 2-OH-PHZ ($n = 6$)

2-OH-PHZ	Sample concentration (μg mL^{-1})	Mean t_m (min)	S.D. (t_m)	R.S.D. t_m (%)	Mean peak area ratio	S.D.	R.S.D. (%)	Confidence intervals (CI)
Intra-day	10	1.625	0.021	1.29	0.0917	0.002	2.18	0.0901–0.0928
	20	1.618	0.017	1.05	0.1548	0.005	3.23	0.1492–0.1631
	25	1.623	0.015	0.92	0.1927	0.003	1.56	0.1901–0.1984
	50	1.614	0.022	1.36	0.3548	0.009	2.54	0.3308–0.3772
	75	1.621	0.019	1.17	0.5124	0.023	4.49	0.4693–0.5307
	100	1.626	0.034	2.09	0.6448	0.007	1.09	0.6215–0.6667
Inter-day	10	1.628	0.019	1.17	0.0949	0.002	2.11	0.0915–0.0966
	20	1.626	0.027	1.66	0.1616	0.009	5.57	0.1557–0.1783
	25	1.621	0.016	0.99	0.2005	0.011	5.49	0.1872–0.2119
	50	1.609	0.031	1.93	0.3513	0.020	5.69	0.3316–0.3727
	75	1.617	0.033	2.04	0.5029	0.018	3.58	0.4852–0.5337
	100	1.623	0.028	1.73	0.6421	0.016	2.49	0.6139–0.6638

Table 2
Precision data for PCA ($n = 6$)

PCA	Sample concentration (μg mL^{-1})	Mean t_m (min)	S.D. (t_m)	R.S.D. t_m (%)	Mean peak area ratio	S.D.	R.S.D. (%)	Confidence intervals (CI)
Intra-day	10	1.966	0.031	1.58	0.5672	0.008	1.41	0.5581–0.5773
	20	1.958	0.017	0.87	0.7385	0.019	2.57	0.7112–0.7606
	25	1.965	0.029	1.48	0.8339	0.013	1.56	0.8115–0.8510
	50	1.953	0.034	1.74	1.3383	0.048	3.59	1.2597–1.3865
	75	1.961	0.018	0.92	1.7817	0.017	0.95	1.7579–1.8041
	100	1.967	0.036	1.83	2.2865	0.056	2.45	2.2167–2.3599
Inter-day	10	1.971	0.019	0.96	0.5591	0.014	2.50	0.5327–0.5716
	20	1.966	0.011	0.56	0.7427	0.012	1.62	0.7301–0.7611
	25	1.957	0.024	1.23	0.8329	0.013	1.56	0.8161–0.8499
	50	1.951	0.013	0.67	1.3171	0.018	1.37	1.2849–1.3375
	75	1.949	0.021	1.08	1.7992	0.019	1.06	1.7726–1.8221
	100	1.955	0.027	1.38	2.2497	0.069	3.07	2.1247–2.3036

Table 3
The recovery of 2-OH-PHZ and PCA under different conditions ($n = 4$)

Sample concentration ($\mu g\,mL^{-1}$)	Mean peak area ratio of 2-OH-PHZ and PHZ		Recovery of 2-OH-PHZ (%)	Mean peak area ratio of PCA and PHZ		Recovery of PCA (%)
	Extraction from fermentation broth	Resolving in buffer directly		Extraction from fermentation broth	Resolving in buffer directly	
10	0.092	0.093	98.77 ± 2.17	0.551	0.561	98.35 ± 2.03
50	0.333	0.342	97.28 ± 1.25	1.275	1.322	96.42 ± 1.88
150	0.943	0.999	94.33 ± 2.01	3.016	3.247	92.89 ± 1.24
250	1.529	1.652	92.56 ± 3.69	4.801	5.233	91.75 ± 3.31

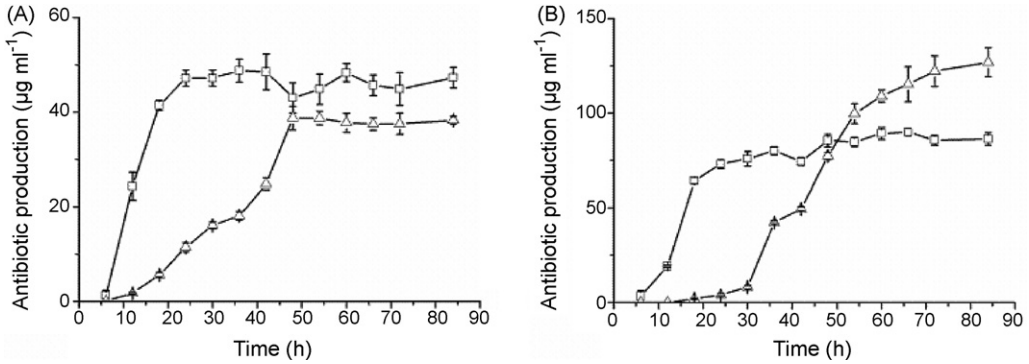

Fig. 5. Dynamic antibiotic curve of *P. chlororaphis* GP72 during the entire 84 h growth cycle. The graph shows the concentration-time profile of both 2-OH-PHZ and PCA in the fermentation process both in KMB (Fig. 5A) and PPM (Fig. 5B) analyzed with the newly defined CE method. Conditions are the same as those in Fig. 3.

coefficient for 2-OH-PHZ and PCA is 0.9997 and 0.9993 ($n = 7$), respectively.

3.2.3. Precision

The precision of the newly developed method has been evaluated according to inter- and intra-day standard deviations (S.D.) and the relative standard deviations (R.S.D.) of both migration time and peak areas ratio between the analytes and the internal standard. Calculations of S.D. and R.S.D. of both migration time and peak areas ratio are based on six replicate injections of the five different concentrations of the analytes. Confidence limits are set up for five different standard concentrations. All the values are within the intervals. Intra-day values are calculated based on six replicate injections of the five different concentrations within a day, while inter-day values are evaluated with six replicate injections of the same standard concentration in 5 days. The final precision data for 2-OH-PHZ and PCA are listed in Tables 1 and 2. Precision studies imply the stable separation conditions and good repeatability of this method.

3.2.4. Accuracy

A set of recovery experiments has been done to check the accuracy of the new method based on four different standard concentrations of both 2-OH-PHZ and PCA. Four standard concentrations (10, 50, 150, 250 $\mu g\,mL^{-1}$) of analytes together with internal standard PHZ (50 $\mu g\,mL^{-1}$) have been prepared as described above. The recovery of the method is calculated by the ratio value of analytes and PHZ extracted from the fermentation broth to that resolving in running buffer directly. The recovery data sets for 2-OH-PHZ and PCA are listed in Table 3. All of these data are within acceptable ranges for monitoring fermentation process.

3.2.5. Limits of detection and quantification

A series of standard solutions with concentration ranging from 0.5–5 $\mu g\,mL^{-1}$ has been prepared and analyzed six times to be sure of the exact limits. The limits of detection for 2-OH-PHZ and PCA are 0.47 $\mu g\,mL^{-1}$ and 0.38 $\mu g\,mL^{-1}$, respectively by setting the signal-to-noise ratio to 3:1. Meanwhile, the limits of quantification for 2-OH-PHZ and PCA are 1.56 $\mu g\,mL^{-1}$ and 1.28 $\mu g\,mL^{-1}$, respectively by setting the signal-to-noise ratio to 10:1. The limits of detection and quantification of this method are shown at a very low level. This result suggests that it should be a very sensitive method. It also implies the possibility of detecting the phenazine compounds through microanalysis of environmental samples.

3.2.6. Quantification of 2-OH-PHZ and PCA production over 84 growth curves

After optimization and validation of the newly developed method, we use this method to monitor 2-OH-PHZ and PCA production of *P. chlororaphis* GP72 during a complete growth cycle. The bacteria fermentation and extraction procedures are in accordance with the methods described before (See Sections 2.3 and 2.4). At the same time, cell growth was also monitored (data not shown) consistent with the cell culture conditions done previously [20]. Sampling was performed every 12 h until 84 h when production of PCA and 2-OH-PHZ started to become stable. As it is in agreement with that detected with HPLC in the previous study [23], the dynamic curves of both 2-OH-PHZ and PCA production are shown in Fig. 5. In the KMB medium (Fig. 5A), the production of PCA reaches 48.55 $\mu g\,mL^{-1}$ after 24 h of cultivation, and it reaches its maximum at 78.26 $\mu g\,mL^{-1}$ after 60 h of cultivation. At the same time, the production of 2-OH-PHZ reaches 37.98 $\mu g\,mL^{-1}$, while in the PPM medium (Fig. 5B), PCA begins to accumulate after 6 h of incubation and quickly reaches 127.40 $\mu g\,mL^{-1}$ after 24 h of cultivation, and then it further increases slowly to 151.50 $\mu g\,mL^{-1}$ after 48 h, while 2-OH-PHZ begins to accumulate in the PPM medium after 18 h of cultivation. It reaches its maximum of 196.20 $\mu g\,mL^{-1}$ after 72 h of culture due to appropriate conversion conditions. In comparison with the previously established method [23], this application provides us with a more rapid, simple and accurate method to mon-

itor dynamic production of phenazine compounds from bacterial fermentation process.

4. Conclusion

In the present study, we develop a simple and rapid method for the separation and quantification of 2-OH-PHZ and PCA during the entire fermentation process. With all kinds of natural phenazines discovered from newly found biocontrol agents and more synthetic phenazine analogues for potential drug discovery [1,30], rapid and sensitive detection methods for these compounds are an emergent need. In the current work, we provide a CZE method allowing for the efficient and accurate detection of the phenazine secondary metabolites of *P. chlororaphis* GP72 during the entire growth cycle. The paper also shows the possibility of its potential use in various kinds of samples due to its high sensitivity, accuracy and precision. Further research should therefore be focused on CE and CE–MS analysis of phenazine compounds in clinical and environmental samples.

References

[1] J.B. Laursen, J. Nielsen, Chem. Rev. 104 (2004) 1663.
[2] D.V. Mavrodi, W. Blankenfeldt, L.S. Thomashow, Annu. Rev. Phytopathol. 44 (2006) 417.
[3] J.R. Kerr, Infect. Dis. Rev. 2 (2000) 184.
[4] J.M. Turner, A.J. Messenger, Adv. Microb. Physiol. 27 (1986) 211.
[5] H. Umezawa, S. Hayano, K. Maeda, Y. Ogata, Y.J. Okami, J. Antibiot. 4 (1951) 34.
[6] S. Chatterjee, E.K.S. Vijayakumar, C.M.M. Franco, R. Maurya, J. Blumbach, B.N.J. Ganguli, J. Antibiot. 48 (1995) 1353.
[7] K. Pusecker, H. Laatsch, E. Helmke, H.J. Weyland, J. Antibiot. 50 (1997) 479.
[8] C. Maul, I. Sattler, M. Zerlin, C. Hinze, C. Koch, A. Maier, S. Grabley, R.J. Thiericke, J. Antibiot. 52 (1999) 1124.
[9] T.F.C. Chin-A-Woeng, G.V. Bloemberg, B.J.J. Lugtenberg, New. Phytol. 157 (2003) 503.
[10] U. Beifuss, M. Tietze, in: J.H. Mulzer (Ed.), Natural Products Synthesis II—Targets, Methods, Concepts, vol. 2, 2005, p. 77.
[11] A. Price-Whelan, L.E. Dietrich, D.K. Newman, Nat. Chem. Biol. 2 (2006) 71.
[12] D.W. Essar, L. Eberly, A. Hadero, I.P. Crawford, J. Bacteriol. 172 (1990) 884.
[13] T.F. Chin-A-Woeng, G.V. Bloemberg, I.H. Mulders, L.C. Dekkers, B.J. Lugtenberg, Mol. Plant–Microbe Interact. 13 (2000) 1340.
[14] L.S. Pierson III, L.S. Thomashow, Mol. Plant–Microbe Interact. 5 (1992) 330.
[15] R.J. Cook, L.S. Thomashow, D.M. Weller, D. Fujimoto, M. Mazzola, Proc. Natl. Acad. Sci. 92 (1995) 4197.
[16] S. Gurusiddaiah, D.M. Weller, A. Sarkar, R.J. Cook, Antimicrob. Agents Chemother. 29 (1986) 488.
[17] L.S. Thomashow, D.M. Weller, R.F. Bonsall, L.S. Pierson, Appl. Environ. Microbiol. 56 (1990) 908.
[18] P.C. Taunk, R.L. Mital, J. Chromatogr. 60 (1971) 433.
[19] R. O'Connor, J.F. O'Sullivan, R. O'Kennedy, J. Chromatogr. B Biomed. Appl. 681 (1996) 307.
[20] D. Watson, J. MacDermot, R. Wilson, P.J. Cole, G.W. Taylor, Eur. J. Biochem. 159 (1986) 309.
[21] R.O. Fernandez, R.A. Pizarro, J. Chromatogr. A 771 (1997) 99.
[22] M.S. Delaney, D.V. Mavrodi, R.F. Bonsall, L.S. Thomashow, J. Bacteriol. 183 (2001) 318.
[23] H.M. Liu, Y.J. He, H.X. Jiang, H.S. Peng, X.Q. Huang, X.H. Zhang, L.S. Thomashow, Y.Q. Xu, Curr. Microbiol. (2007) 302.
[24] S. Hjerten, Chromatogr. Rev. 9 (1967) 122.
[25] J.W. Jorgenson, K.D. Lukacs, J. Chromatogr. 27 (1991) 1551.
[26] J.W. Jorgenson, K.D. Lukacs, Science 222 (1983) 266.
[27] E.O. King, M.K. Ward, D.E. Raney, J. Lab. Clin. Med. 44 (1954) 301.
[28] A.J. Kluyver, J. Bacteriol. 72 (1956) 406.
[29] H.M. Liu, D.X. Dong, H.S. Peng, X.H. Zhang, Y.Q. Xu, Arch. Microbiol. 185 (2006) 91.
[30] D. Haas, G. Défago, Nat. Rev. Micro. 3 (2005) 307.

Talanta 76 (2008) 413–418

Contents lists available at ScienceDirect

Talanta

journal homepage: www.elsevier.com/locate/talanta

Silanizing agent for semipermanent wall coating in micellar electrokinetic capillary chromatography

Zhi Luo, Shumin Wang, Lei Zhou, Zhide Hu*

Department of Chemistry, Lanzhou University, Tianshui Road 298#, Lanzhou 730000, PR China

ARTICLE INFO

Article history:
Received 14 December 2007
Received in revised form 13 March 2008
Accepted 17 March 2008
Available online 1 April 2008

Keywords:
Silanizing agent
Semipermanent coating
Amino acid
Chloro(dodecyl)dimethylsilane
Laser-induced fluorescence

ABSTRACT

In this paper, the long-chained, silanizing agent chloro(dodecyl)dimethylsilane (CDDS) was investigated as a semipermanent coating in micellar electrokinetic capillary chromatography (MEKC). CDDS coating had great stability due to the formation of covalent bonding with the silanol groups on the surface of fused-silica capillary and remained stable for over 100 min after removal of the rinse step of CDDS solution. Anionic surfactant sodium dodecyl sulfate (SDS) could aggregate at this CDDS coating by the hydrophobic group and formed a SDS layer which could increase the electroosmotic flow (EOF). The separation was performed with the running buffer composed of 60 mM sodium tetraborate, 12 mM SDS at pH 9.9, with the applied voltage of 20 kV and capillary temperature 25 °C. The effect of the coating agent was investigated by the analysis of amino acids. Compared with previous no-coating method, the EOF increases from 4.34×10^{-4} cm^2 V^{-1} s^{-1} to 7.02×10^{-4} cm^2 V^{-1} s^{-1}. Migration time reproducibility was less than 0.97% R.S.D. from run to run and less than 1.56% R.S.D. from day to day.

1. Introduction

Capillary electrophoresis (CE) is a powerful tool for the separation of solutes ranging from small ions to biological molecules such as amino acids [1,2], proteins [3] and DNA [3,4]. However, the separation of proteins by CE is not always possible. Basic analytes, such as basic proteins, have the interaction with silanol groups on the surface of fused-silica capillaries, which greatly increase band broadening and peak tailing. So, it is necessary to manipulate the surface charge of the capillary to prevent wall adsorption of proteins.

Numerous types of coatings have been developed to reduce the protein adsorption. These coatings can be broadly classed as permanent covalently bonded coatings [5–7]; semipermanent coatings [8–13], such as many polymers and strongly adsorbed molecules; and dynamic wall coatings where a dynamic equilibrium exists between the adsorbed reagent on the wall and dissolved reagent in the electrolyte [14–16]. All of these approaches have been successful in both electroosmotic flow (EOF) control and reducing protein adsorption.

Silanizing agent was firstly used in capillary coating procedure described by Hjertén in 1985 [17]. The chemistry for this pioneering work bases on a monolayer with polymerizable functional groups that is chemically attached to the silica surface through SiO_2–O–Si–C linkage. Since 1985, numerous papers have been published about polymerizable functional groups covalently bonded to the silica surface, such as methacryloxypropyl through SiO_2–O–Si–C linkage [17,18], methacryloxypropyl through SiO_2–Si–C linkage [19], and vinyl through SiO_2–Si–C [20]. However, these permanent covalently bonded coatings have the drawbacks of complicated synthesis and limited pH stability. Recently, a number of semipermanent coatings have been introduced, such as DDAB [21], DLPC [22] and CTAB/SDS [13], which are based on double-chained surfactants. Besides, Xie reported the small molecular-mass silanizing agent hexamethydisilazane (HMDS) as semipermanent coating for capillary electrophoresis, which relies on covalent bonding attached to the silica surface, and achieved a good effect [23]. These coatings overcome the complicated synthesis, and separations are performed with no-coating agent in the run buffer.

Silanizing agent chloro(dodecyl)dimethylsilane (CDDS) has a simple molecular structure and can react with silanol groups on the surface of capillary under a mild condition, a process similar with HMDS. According to this principle, CDDS used as wall coating in CE is feasible. Fig. 1 shows the molecular structure of CDDS.

Micellar electrokinetic capillary chromatography (MEKC) was selected for the CE analysis since it is capable of separating both neutral and charged analytes and therefore may accommodate different classes of chemical constituents present in a single sample [24–26]. Besides, the hydrophobic group of anionic surfactant

* Corresponding author. Tel.: +86 931 8912540; fax: +86 931 8912582.
E-mail addresses: luozh03@lzu.cn (Z. Luo), huzd@lzu.edu.cn (Z. Hu).

0039-9140/$ – see front matter © 2008 Elsevier B.V. All rights reserved.
doi:10.1016/j.talanta.2008.03.035

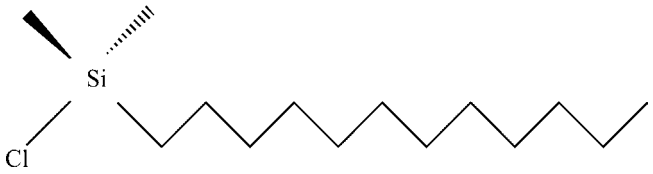

Fig. 1. The molecular structure of CDDS.

sodium dodecyl sulfate (SDS) can attach to the surface of the CDDS layer and formed a SDS layer, which can improve the EOF. In this paper, we firstly explore the use of CDDS as semipermanent coatings in MEKC. The stability of EOF in capillary coated with CDDS was investigated in MEKC by laser-induced fluorescence detection, as tested with nine kinds of amino acids after derivatization with 4-chloro-7-nitrobenzo-2-oxa-1,3-diazol.

2. Experimental

2.1. Apparatus

Experiments were performed on a P/ACE MDQ capillary electrophoresis system (Beckman Coulter) equipped with a LIF detector using a 32 Karat software (Version 5.0 Beckman). The excitation was performed at 488 nm and a 520-nm band-pass filter was used for emission. Unless otherwise noted, the data acquisition rate was 4 Hz. The capillary was untreated fused silica (Yongnian Photoconductive Fiber Factory, Hebei, China) with an inner diameter of 75 μm and total length 50.2 cm, and were thermostated at 25.0 °C. New capillary was pretreated by rinsing with 1.0 M HCl for 20 min, 0.5 M NaOH for 20 min and distilled water for 15 min.

Fourier transformed infrared spectroscopy (FTIR) was used to acquire transmittance spectra with a Nicolet NEXUS 670 FT-IR in the spectral range of 400–4000 cm^{-1}. Atomic force microscope (AFM) images were obtained with SPM Nanoscope IIIa (Digital Instruments, USA). The AFM substrates were polished fused-silica plates (Zhongkekaite, Lanzhou, China). The silica substrates were cleaned by heating in hot H_2SO_4:H_2O_2 (70:30, v/v) solution ("piranha solution") for 4.0 h followed by rinsing thoroughly with distilled water. The procedure for coating CDDS was the same as that for the capillary columns.

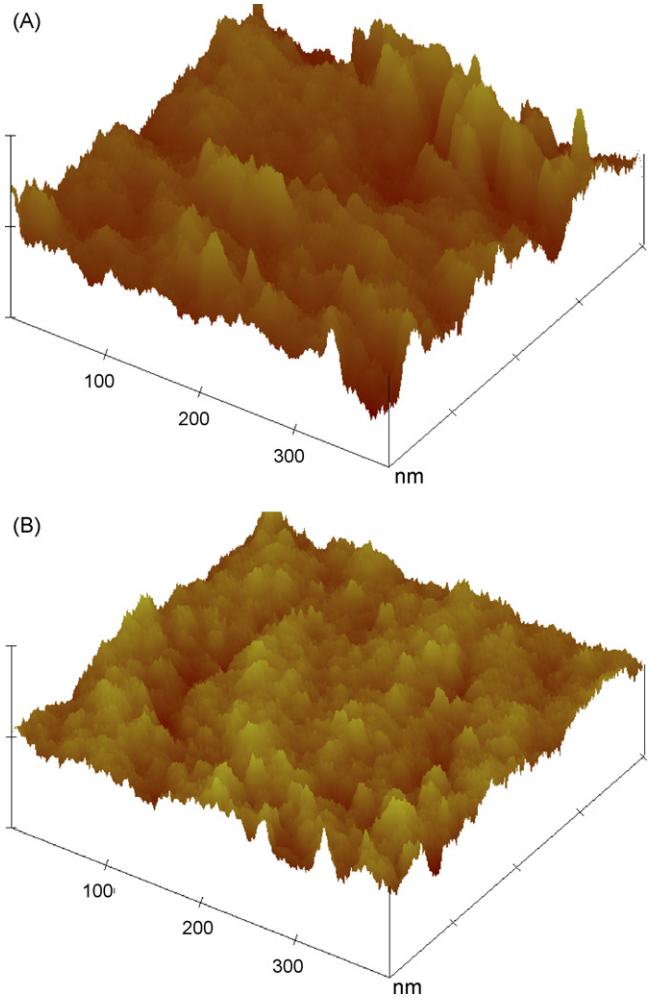

Fig. 2. AFM images (400 nm × 400 nm) of fused-silica plates: (A) bare fused-silica plate and (B) fused-silica plate rinsed with 1% CDDS solution.

2.2. Chemicals

Standard amino acids were obtained from Gansu Institute for Control of Pharmaceuticals, China. 4-Chloro-7-nitrobenzo-2-oxa-

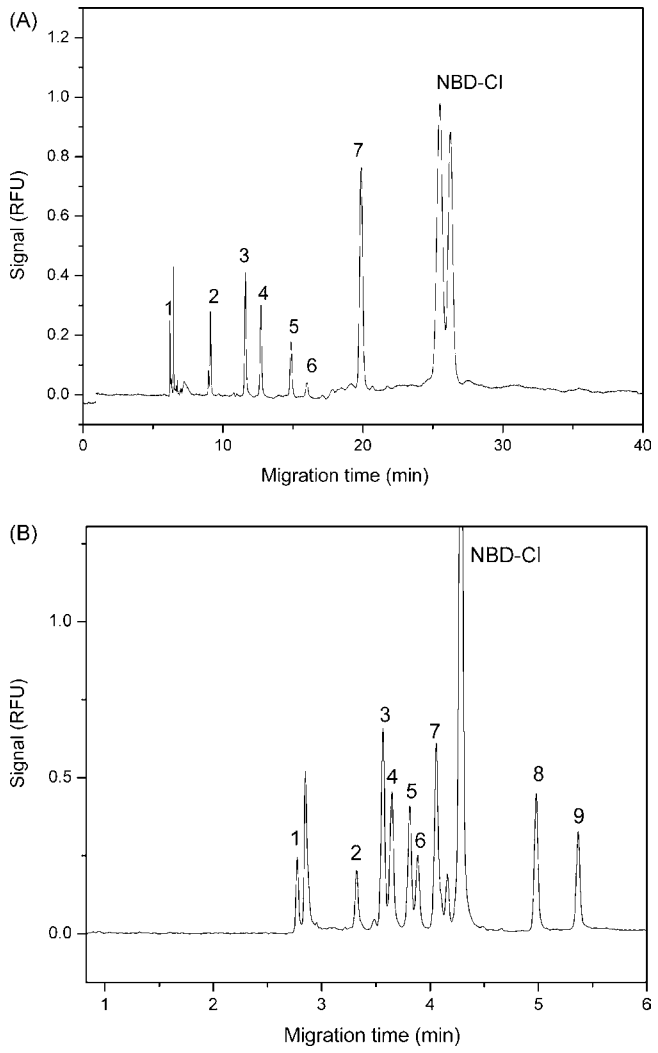

Fig. 3. Electrophoregrams for the standards: (A) detecting on a bare fused-silica capillary; (B) detecting on a coated capillary. Peak identification: (1) arginine; (2) proline; (3) valine; (4) phenylalanine; (5) alanine; (6) threonine; (7) glycine; (8) glutamic acid; (9) aspartic acid. Conditions: 40 cm × 75 μm i.d. capillary; 20 kV; pH 9.9; 12 mM SDS, 60 mM $Na_2B_4O_7$.

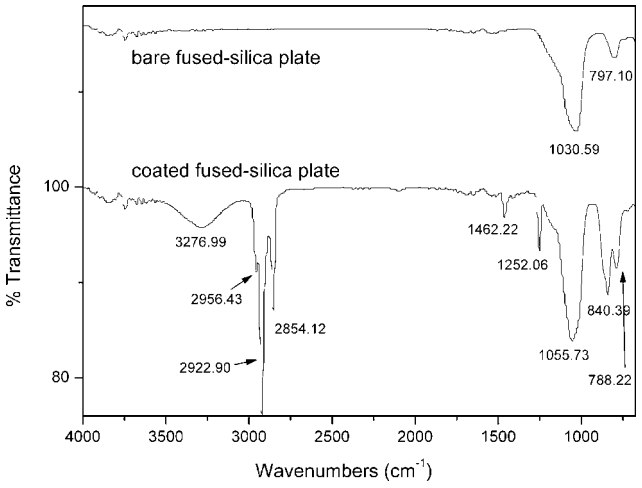

Fig. 4. FTIR spectrum of the CDDS coating on the fused silica.

1,3-diazol (NBD-Cl) was the product of Tokyo Kaser Kogyo Co., Ltd. (Japan). CDDS was provided by Tokyo Kaser Kogyo Co., Ltd. and diluted directly 100 times with ethanol. No difference was observed between fresh and aged CDDS solutions ($n < 7$ days). The pH of all buffers was adjusted with analysis-grade sodium hydroxide. Celesse Angel Amino Acids Oral Solution was used as received from Kang'erjia Pharmaceutical Store (Lanzhou, China).

2.3. Coating studies

New capillaries (total length 50.2 cm, 40 cm to the detector) were treated prior to its first coating by rinsing (20 psi) with 1.0 M HCl for 20 min, 0.5 M NaOH for 20 min, distilled water for 15 min, acetonitrile for 5 min, CDDS solution for 15 min, respectively. Between two runs, the capillary was rinsed (20 psi) with distilled water for 1 min, acetonitrile for 1 min, CDDS solution for 2 min and run buffer for 1 min. At the end of each day, the capillary was rinsed (20 psi) with acetonitrile for 1 min and CDDS solution for 2 min, which was in favor of keeping good reproducibility.

2.4. Solutions and sample preparation

The running buffers employed for the separation were prepared by mixing appropriate volumes of 100 mM sodium tetraborate solution and 200 mM SDS. Before use, all buffers were adjusted accurately to the desired pH value with 1.0 M and 0.1 M HCl or 1.0 M and 0.1 M NaOH, and filtered through a 0.45 membrane filter.

A standard amino acid mixture was prepared by mixing nine amino acids. The concentration of each amino acid is 0.19 mM, respectively. Celesse Angel Amino Acids Oral Solution was diluted 100 times with distilled water and directly derivatization for analysis.

2.5. Derivatization procedure

According to the pervious derivatization method [23], a 40 μl of 0.19 mM standards or samples was transferred to a 1.5 ml plastic tube containing 360 μl of 30 mM NBD-Cl solutions and 600 μl of 40 mM $Na_2B_4O_7$ buffer solution. The blank solutions were prepared by mixing 600 μl $Na_2B_4O_7$ buffer solution, 40 μl distilled water and 360 μl NBD-Cl solution. The derivatization reaction was processed at 60 °C for 20 min. Prior to the analysis, the derivatization solutions were diluted with 40 mM derivatization buffer (pH 8.4) to the desired concentrations.

2.6. EOF measurement

No neutral market was used to measure the EOF in this method, so the EOF mobility was calculated by the abrupt change of electric current [27].

$$\mu_{EOF} = \frac{L^2}{V[(t_1 + t_2)/2]} \quad (1)$$

where L and V are the total length of the capillary and the separation voltage, respectively; t_1 and t_2 is the start and the end time of the abrupt change of current.

3. Results and discussion

3.1. AFM images of CDDS on fused silica

AFM has been used to image surfaces coated with different compounds to more directly determine their coating morphology [28–30]. To determine whether this silanizing agent coating bonds on the capillary surface as semipermanent coating during CE, we employed AFM imaging to observe the silanizing agent coating by rinsing the capillary with CDDS solution. Fused-silica plates were used as the imaging substrate to mimic the inside wall of a capillary. The AFM images of blank fused-silica plate and CDDS rinsed fused-silica plate are shown in Fig. 2. The CDDS image shows many small particles coating on the 400 nm × 400 nm surface. Comparing Fig. 2A and B, it is clear that there is a layer of compound coating on the bare fused-silica capillary, which result in shortening of the migration time of analytes. According to the structure of CDDS, there is only Si–Cl bond that can react with the surface of the fused-silica plates. Therefore, the film showed in Fig. 2B is CDDS coating, which should be a monolayer. The roughness surface scanned by the AFM is probably caused by the aggregates of CDDS molecule. Fig. 3 shows the electrophoregrams of amino acids with no-coating capillary and coating capillary. In Fig. 3A, the detection time was shortened greatly after coating the fused-silica capillary with CDDS that nine amino acids were detected within 5.5 min. Compared to Fig. 3B, Glu and Asp were not detected within 30 min. Thus, the comparison of Fig. 3A and B suggests that the CDDS coating has bonded to the silica substrate.

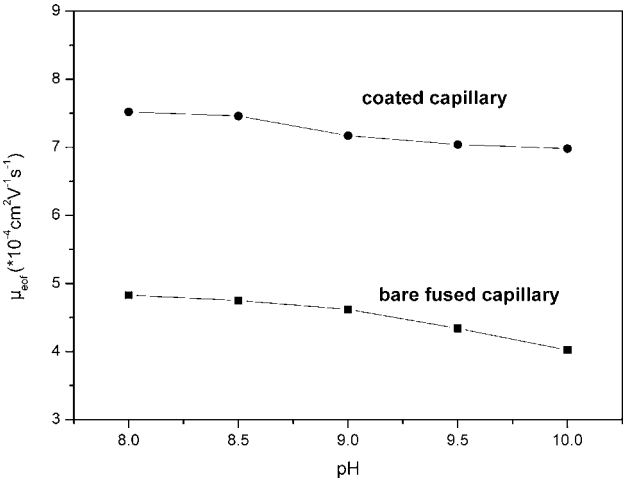

Fig. 5. Effect of pH on EOF. Conditions: 40 cm × 75 μm i.d. capillary; 20 kV; 12 mM SDS, 60 mM $Na_2B_4O_7$. The semipermanent coating was prepared by rinsing with 1% CDDS solution between two runs.

Table 1
Repeatability of migration times of Glu and Asp in different solvents[a]

Solvent	Amino acids	Migration time (min)			R.S.D. (%)
		1st run	6th run	Average	
Ethanol	Glu	5.208	5.250	5.229	0.31
	Asp	5.621	5.662	5.642	0.31
2-Propanol	Glu	5.658	5.717	5.685	0.34
	Asp	6.121	6.188	6.155	0.35
Heptane	Glu	5.642	5.787	5.726	0.87
	Asp	6.104	6.263	6.203	0.90

[a] Conditions: 40 cm × 75 μm i.d. capillary; 20 kV; pH 9.9; 12 mM SDS, 60 mM $Na_2B_4O_7$.

3.2. FTIR spectrum of the CDDS on fused silica

Fig. 4 shows the spectral range of 650–4000 cm^{-1} of bare fused-silica plate and coated fused-silica plate. In the spectra of bare fused-silica plate, the absorption band at 797.10 cm^{-1} originates form symmetrical Si–O–Si stretching [31], while the band at 1030.59 cm^{-1} comes from asymmetrical Si–O–Si stretching. After CDDS coated on the fused-silica plate, the bands at 2854.12–2956.43 cm^{-1} of the C–H and the band at 1462.22 cm^{-1} of the asymmetrical stretching vibration of $–CH_3$ were found in the FTIR spectrum. Compared to the spectra of bare fused-silica plate and coated fused-silica plate, the band of asymmetrical Si–O–Si stretching transferred from 1030.59 cm^{-1} to 1055.73 cm^{-1} because of the induction effect of CDDS group. This indicates that CDDS bonded with the silanol groups on the surface of the fused-silica plate.

3.3. Selection of solvent in CDDS solutions

The solvent in CDDS solutions was selected among acetonitrile, ethanol, *n*-propanol and heptane. In order to investigate the effect of the solvents, 12 mM SDS and 60 mM $Na_2B_4O_7$ were used, and the pH value was adjusted to 9.9. It was observed that CDDS could not dissolve into acetonitrile, but it could dissolve in ethanol and 2-propanol due to the reaction with alkyl group, and could dissolve in heptane due to the hydrophobic group. Table 1 shows the repeatability of migration times of Glu and Asp in ethanol, 2-propanol and heptane. It is seen that the repeatability of migration times is better when using ethanol: the R.S.D. values of the migration times were 0.31% ($n = 6$), while 0.34–0.35% for 2-propanol and 0.87–0.90% for heptane. Furthermore, ethanol, as CDDS solvents, produced shorter time than 2-propanol and heptane. Thus, ethanol was selected as the solvent for CDDS in this experiment.

3.4. Effect of pH on EOF

In this paper, the direction of the EOF is consistent with that of the apparent electrophoretic mobility, so the variety of the apparent electrophoretic mobility can reflect the variety of the EOF. The relationship between electrophoretic mobility and ion strength is described by the following equation [32,33]:

$$\mu = \frac{e}{3 \times 10^7 |Z| \eta C^{1/2}} \quad (2)$$

where e, Z, η and C are the surplus electric charge, the ion strength, the viscosity of the solvent and the concentration of the buffer, respectively. Vindevogel and Sandra have discussed the relationship between the pH of buffer and the EOF in previously work [34]. Under the condition of $Na_2B_4O_7$ buffer, increasing the pH tend to increase ionic strength, thereby decreasing the electrophoretic mobility and the EOF. Fig. 5 illustrates the same decreasing trend for bare-silica capillary and coated capillary.

In contrast, Fig. 5 also shows that a coated capillary shows only a 7.2% decrease in the EOF value when the buffer pH is increased from 8 to 10 in the concentration of 12 mM SDS and 60 mM $Na_2B_4O_7$, while the bare-silica capillary shows 16.8% decrease in the EOF value. With CDDS coatings, the zeta potential responsible for the EOF is dictated by the surface charge of the SDS layer, which has SO_4^{2-} group that the variety of pH less affects the negative charge around the SO_4^{2-} group. Thus, the EOF is less affected by the pH in coated capillary, compared to bare fused capillary.

3.5. Stability of CDDS semipermanent coating

The stability of CDDS coating can be determined by monitoring the variety of the EOF after removal of the excess CDDS solution from the capillary. Specifically, the capillary was first rinsed with CDDS solution for 10 min at high pressure. The excess CDDS solution was then rinsed from the capillary by a 1 min high-pressure (20 psi) rinse of running buffer. The EOF mobility was calculated by Eq. (1) according to the abrupt change of current. Fig. 6A shows the consecutive amino acids separations performed on CDDS capillary. From Fig. 6A, the EOF was monitored after removal of the excess CDDS solution from the capillary. It can be seen that the migration time slightly increases over 17 runs (6 min/run). The EOF has decreased 14.7% over 110 min from 7.02×10^{-4} cm^2 V^{-1} s^{-1} to

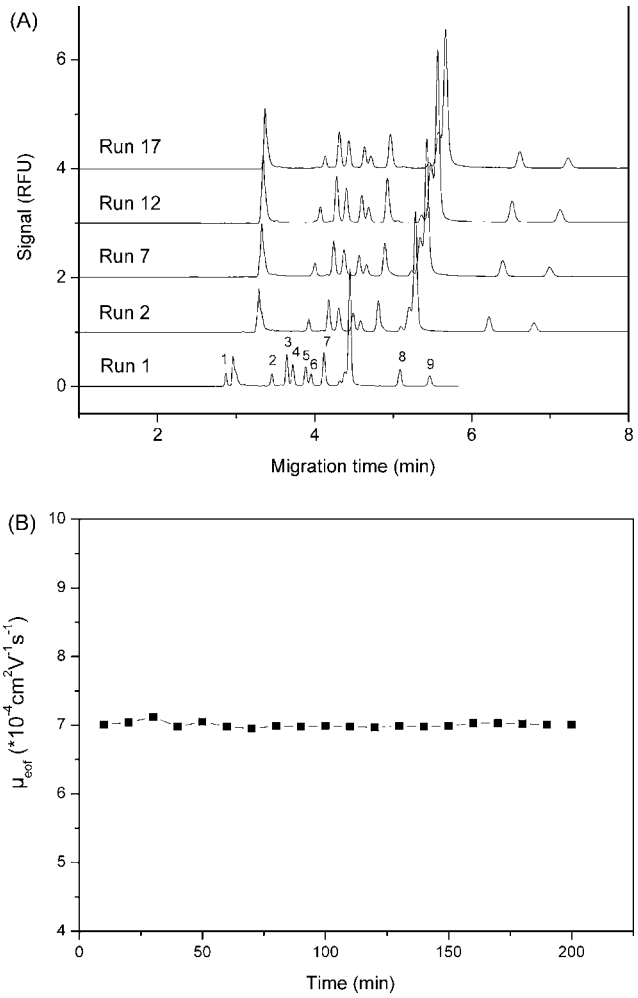

Fig. 6. (A) Consecutive amino acids separations performed on CDDS capillary without rinsing buffer between runs; (B) stability of EOF with rinsing the capillary with CDDS solution between runs. Conditions: 40 cm × 75 μm i.d. capillary; 20 kV; pH 9.9; 12 mM SDS, 60 mM $Na_2B_4O_7$.

Table 2
Regression data, reproducibility, recovery, content and detection limit of nine amino acids of sample on a CDDS/SDS coating capillary by using the second-order derivative electrophoregram[a]

Amino acids	Regression equations[b]	Ranges (μM)	Correlation coefficients	Migration time (% R.S.D.)		LOD (nM)
				Run to run	Day to day	
Arg	$Y = 0.057x + 0.00007$	0.057–1.14	0.9992	0.51	0.92	0.21
Pro	$Y = 0.073x - 0.00029$	0.057–1.14	0.9994	0.77	1.02	0.27
Val	$Y = 0.022x - 0.00107$	0.057–1.14	0.9999	0.68	1.16	0.08
Phe	$Y = 0.036x + 0.00052$	0.057–1.14	0.9969	0.71	1.12	0.14
Ala	$Y = 0.039x - 0.00032$	0.057–1.14	0.9991	0.72	1.22	0.15
Thr	$Y = 0.050x - 0.00035$	0.057–1.14	0.9995	0.73	1.20	0.19
Gly	$Y = 0.024x + 0.00033$	0.057–1.14	0.9980	0.74	1.16	0.09
Glu	$Y = 0.031x - 0.00053$	0.057–1.14	0.9987	0.90	1.48	0.12
Asp	$Y = 0.044x - 0.00008$	0.057–1.14	0.9994	0.97	1.56	0.16

[a] Conditions: 40 cm × 75 μm i.d. capillary; 20 kV; pH 9.9; 12 mM SDS, 60 mM $Na_2B_4O_7$.
[b] Y is the peak height (RFU) while x is the concentration of corresponding amino acid (μM).

$5.99 \times 10^{-4} cm^2 V^{-1} s^{-1}$. This indicates that the CDDS semipermanent coating has a good stability on the capillary wall due to the covalent bond attaching to the silica surface.

Fig. 6B displays the EOF with consecutive 20 runs (10 min for each run). During this process, the capillary was rinsed with the CDDS solution between two runs. From Fig. 6B, excellent reproducibility was observed in 20 runs—with the EOF value varied only 2.4% over 200 min. Thus, according to the EOF of Fig. 6B, the CDDS covalent layer can be reproduced on-line by a rinse-coating cycle.

3.6. CDDS semipermanent coating for amino acid analysis

To evaluate the quantitative applicability of the CDDS coating, the amino acids standards and Celesse Angel Amino Acids Oral Solution were analyzed after derivatization under the selected conditions described above on a coated capillary. The derivatization reagent could react with the amino acid and eliminate the positive charge from part of the amino acid, leaving an anionic solute at pH 9.9 of the run buffer. Thus, both hydrophobic and hydrophilic (repulsion from the micelle) interactions would occur with the micelle. Compared to the bare fused-silica capillary, the migration time was greatly decreased because of the enhancement of EOF by the CDDS coating capillary. When making the standard working curve, we found it difficult to integrate some target peaks due to the partial resolution. Therefore, quantitative analysis was obtained by employing the second-order derivative electropherogram. It has been proved that the second-order derivative electropherogram is a good determination method when the components are partially separated [23,35,36]. Table 2 shows the analytical data of the amino acids standards based on the second-order derivative electropherogram (Fig. 7). The detection limit (LOD, based on signal to noise, S/N = 3) of amino acids is in the range of 0.08–0.27 nM and the sensitivity is slightly better than those of HMDS/SDS (LOD 0.25–0.63 nM)

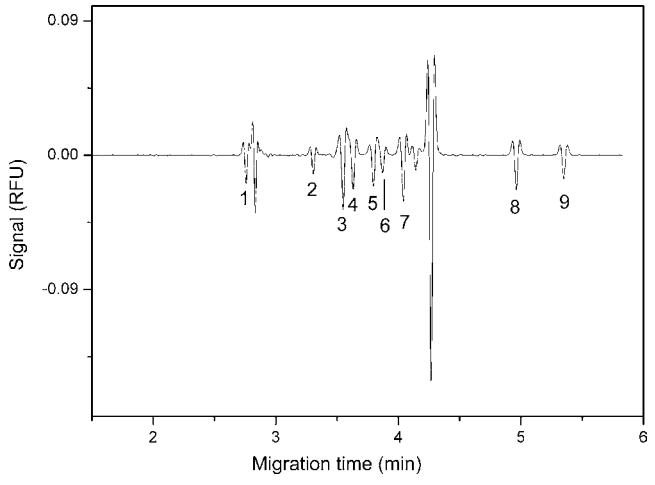

Fig. 7. The second-order derivative electrophoregram of standards detected on the coated capillary. Peak identification: (1) arginine; (2) proline; (3) valine; (4) phenylalanine; (5) alanine; (6) threonine; (7) glycine; (8) glutamic acid; (9) aspartic acid. Conditions: 40 cm × 75 μm i.d. capillary; 20 kV; pH 9.9; 12 mM SDS, 60 mM $Na_2B_4O_7$.

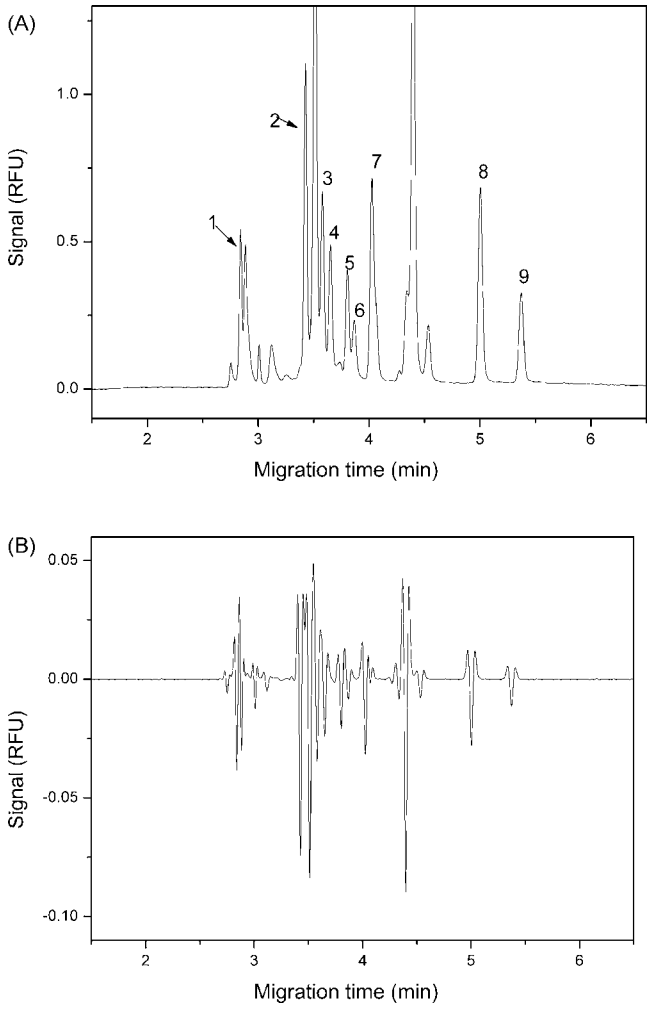

Fig. 8. Electrophoregrams for the samples: (A) for the Celesse Angel Amino Acids Oral Solution using CDDS/SDS coating; (B) the second-order derivative electropherogram of Celesse Angel Amino Acids Oral Solution. Peak identification: (1) Arg; (2) Pro; (3) Val; (4) Phe; (5) Ala; (6) Thr; (7) Gly; (8) Glu; (9) Asp. Conditions: 40 cm × 75 μm i.d. capillary; 20 kV; pH 9.9; 12 mM SDS, 60 mM $Na_2B_4O_7$.

Table 3
Determination of the amino acids in the Celesse Angel Amino Acids Oral Solution

Peak number	Amino acids	Content (μg/ml)	Recovery (%)
1	Arg	0.699	108.4 ± 3.3
2	Pro	0.381	101.3 ± 3.4
3	Val	0.405	101.4 ± 2.7
4	Phe	0.401	104.9 ± 1.9
5	Ala	0.264	91.8 ± 1.9
6	Thr	0.205	101.4 ± 1.4
7	Gly	0.211	99.5 ± 2.6
8	Glu	0.640	86.6 ± 3.4
9	Asp	0.463	90.8 ± 2.1

Conditions: 40 cm × 75 μm i.d. capillary; 20 kV; pH 9.9; 12 mM SDS, 60 mM $Na_2B_4O_7$.

[16]. The run-to-run reproducibility of the migration times of the nine amino acids ranged from 0.51% to 0.97% R.S.D. (n = 16) and the day-to-day reproducibility was 0.92–1.56% R.S.D. (3 days). Fig. 8A shows the separation of Celesse Angel Amino Acids Oral Solution. It was observed that some amino acids were not baseline separated and hardly quantitatively analyzed, so the second-order derivative electrophoregram (Fig. 8B) was introduced. The content and recoveries for these amino acids were determined and are listed in Table 3. With the CDDS coating, the recovery of amino acids is 86.6–108.4%, which is reasonable that the derivatization was continuative when the detection was running.

4. Conclusion

AFM image obviously showed that CDDS coating can covalently bond on the surface of the capillary by rinsing the capillary with CDDS solution and forms a monolayer flat. CDDS semipermanent coating had great stability on the surface of fused-silica capillary due to the formation of covalent bonding. It remained stable for over 100 min after removal of the rinse step of CDDS solution. Migration time reproducibility was less than 0.97% R.S.D. for run to run and less than 1.56% R.S.D. for day to day. This CDDS coating effectively shortened the analysis time of amino acids (within 5.5 min) in MEKC mode due to the enhancement of the EOF, and the sensitivity is slightly higher than that of HMDS with laser-induced fluorescence. This proposed method shows an important application of silanizing agent as semipermanent coating for capillary electrophoresis.

References

[1] T. Soga, D.N. Heiger, Anal. Chem. 72 (2000) 1236.
[2] C.L. Schultz, M. Moini, Anal. Chem. 75 (2003) 1508.
[3] S. Hu, N.J. Dovichi, Anal. Chem. 74 (2002) 2833.
[4] S.D. Mendonsa, M.T. Bowser, J. Am. Chem. Soc. 126 (2004) 20.
[5] J.K. Towns, F.E. Regnier, J. Chromatogr. 516 (1990) 69.
[6] G. Kleindienst, C.G. Huber, D.T. Gjerde, L. Yengoyan, G.K. Bonn, Electrophoresis 18 (1998) 262.
[7] H. Wan, M. Ohman, L.G. Blomberg, J. Chromatogr. A 924 (2001) 59.
[8] Y.J. Yao, K.S. Khoo, M.C.M. Chung, S.F.Y. Li, J. Chromatogr. A 680 (1994) 431.
[9] E. Cordova, J. Gao, G.M. Whitesides, Anal. Chem. 69 (1997) 1370.
[10] C.A. Lucy, R.S. Underhill, Anal. Chem. 68 (1996) 300.
[11] K.K.C. Yeung, C.A. Lucy, Anal. Chem. 69 (1997) 3435.
[12] N.E. Baryla, C.A. Lucy, Anal. Chem. 72 (2000) 2280.
[13] C.Z. Wang, C.A. Lucy, Electrophoresis 25 (2004) 825.
[14] P. Sedláková, J. Svobodová, I. Mikšík, H. Tomás, J. Chromatogr. B 841 (2006) 135.
[15] C. Lanz, U. Marti, W. Thormann, J. Chromatogr. A 1013 (2003) 131.
[16] N. Naruishi, Y. Tanaka, T. Higashi, S.I. Wakida, J. Chromatogr. A 1130 (2006) 169.
[17] S. Hjertén, J. Chromatogr. 347 (1985) 191.
[18] Z.J. Tan, V.T. Remcho, Anal. Chem. 69 (1997) 581.
[19] M. Chiari, M. Nesi, J.E. Sandoval, J.J. Pesek, J. Chromatogr. A 717 (1995) 1.
[20] K.A. Cobb, V. Dolnik, M. Novotny, Anal. Chem. 62 (1990) 2478.
[21] J.E. Melanson, N.E. Baryla, C.A. Lucy, Anal. Chem. 72 (2000) 4110.
[22] J.M. Cunliffe, N.E. Baryla, C.A. Lucy, Anal. Chem. 74 (2002) 776.
[23] J.P. Xie, X.F. Chen, J.Y. Zhang, J.Q. Liu, J.N. Tian, X.G. Chen, Z.D. Hu, J. Pharm. Biomed. Anal. 36 (2004) 1.
[24] H. Watarai, Chem. Lett. 231 (1991) 391.
[25] K.D. Altria, J. Chromatogr. A 892 (2000) 171.
[26] G.B. Li, X.G. Chen, M.C. Liu, Z.D. Hu, Analyst 123 (1998) 1501.
[27] Q.F. Li, X.Y. Zhang, H.Y. Zhang, X.G. Chen, M.C. Liu, Z.D. Hu, Chin. J. Chem. 19 (2001) 581.
[28] X.Y. Huang, L.J. Doneski, M.J. Wirth, Anal. Chem. 70 (1998) 4023.
[29] N.E. Baryla, J.E. Melanson, M.T. Mcdermott, C.A. Lucy, Anal. Chem. 73 (2001) 4558.
[30] A. Cifuentes, J.C. Diez-Masa, J. Fritz, D. Anselmetti, A.E. Bruno, Anal. Chem. 70 (1998) 3458.
[31] G. Guiu, P. Grange, Bull. Chem. Soc. Jpn. 67 (1994) 2716.
[32] G.J.M. Bruin, J.P. Chang, R.H. Kuhlham, K. Zegers, J.C. Kraak, J. Chromatogr. 471 (1989) 429.
[33] W. Nashabeh, Z.E. Rassi, J. Chromatogr. 514 (1990) 57.
[34] J. Vindevogel, P. Sandra, J. Chromatogr. 588 (1991) 483.
[35] J.Y. Zhang, Z.D. Hu, X.G. Chen, Talanta 65 (2005) 986.
[36] A.J. Chen, J.Y. Zhang, C.H. Li, X.F. Chen, X.G. Chen, Z.D. Hu, J. Sep. Sci. 27 (2004) 569.

Talanta 76 (2008) 458–461

Contents lists available at ScienceDirect

Talanta

journal homepage: www.elsevier.com/locate/talanta

Real-time monitoring of double-stranded DNA cleavage using molecular beacons

Changbei Ma, Zhiwen Tang, Xiqin Huo*, Xiaohai Yang, Wei Li, Weihong Tan

State Key Laboratory of Chemo/Biosensing and Chemometrics, College of Chemistry and Chemical Engineering, Biomedical Engineering Center, Key Laboratory for Bio-Nanotechnology and Molecular Engineering of Hunan Province, Hunan University, Yuelu-Qu District, Changsha 410082, Hunan, PR China

ARTICLE INFO

Article history:
Received 13 December 2007
Received in revised form 18 March 2008
Accepted 21 March 2008
Available online 8 April 2008

Keywords:
Molecular beacon
Real-time monitoring
Restriction endonuclease
DNA cleavage

ABSTRACT

Traditional methods to assay enzymatic cleavage of DNA are discontinuous, time-consuming and laborious. Here, we report a new approach for real-time monitoring of double-stranded DNA cleavage by restriction endonuclease based on nucleic acid ligation using molecular beacon. Upon cleavage of DNA, the cleavage product can be ligated by DNA ligase, which results in a fluorescence enhancement of the molecular beacon. This method permits real-time monitoring of DNA cleavage and makes it easy to characterize the activity of restriction endonuclease and to study the cleavage reaction kinetics.

1. Introduction

The DNA cleavage reactions catalyzed by restriction endonucleases are important in cellular processes, such as DNA replication, recombination and repair [1]. They also play significant roles in a variety of biotechnologies such as cloning, genetic analysis and genotyping. To assay the cleavage efficiency of these enzymes, several traditional methods such as gel electrophoresis, filter binding, high-performance liquid chromatography (HPLC) and enzyme-linked immunosorbent assay (ELISA) [2–5] are commonly used. All these methods, however, are discontinuous, time-consuming, laborious and usually require isotope labeling. There have been many recent efforts for the development of fluorescence assays which are based on fluorescence resonance energy transfer (FRET) for DNA cleavage [6–13]. These assays are continuous and real-time. However, up to now all of them have been designed only for doubly labeled DNA substrates with fluorophores, might interfere with the kinetic behavior of the restriction endonucleases. Furthermore, the potential for achieving high sensitivity through FRET has not been fully realized. Therefore, there is a great demand for continuous, convenient, sensitive assays for these reactions.

In this paper, a novel method is described for real-time monitoring of double-stranded DNA cleavage by using molecule beacons (MBs). Since they were first reported in 1996 [14], MBs have become a class of probes widely used in chemistry, biology, biotechnology, and medical sciences for biomolecular recognition, due in part to their high sensitivity and excellent specificity [15,16]. MB is not only a useful tool for DNA/RNA studies, but also a promising probe for monitoring DNA–protein interactions [17–19]. Previously, we have developed a method for real-time monitoring of nucleic acid ligation and phosphorylation using MB [20–22]. In this work, we further extend this new strategy for real-time monitoring of double-stranded DNA cleavage by restriction endonuclease based on nucleic acid ligation. Here, Rsa I endonuclease that recognizes the GTAC sequence was chosen as an example. This approach is simple, rapid, sensitive, and without requirement for doubly labeled DNA substrates.

2. Experimental

2.1. Reagents and materials

The MB probe: 5′-TAMRA-CGATGCCGTGTCTTGTAGTTCCCGTCG CATCG-DABCYL-3′, oligonucleotide (Oligo) A: 5′-GACGAGAGGTA-CAAGACACG-3′, Oligo B: 5′-CTTGTACCTCTCGTC-3′ and Oligo D: 5′-GACGGGAACT-3′ were synthesized by Dalian Takara Bio Inc. (Dalian, China), and the T4 DNA ligase was purchased from the same company. The Rsa I endonuclease was purchased from MBI Fermentas (Lithuania). The $MgCl_2$ and ATP were purchased from Amresco (Solon, OH). All other reagents were of analytical-reagent grade. Deionized water was obtained through a Nanopure InfinityTM

* Corresponding author. Tel.: +86 731 8821566; fax: +86 731 8821566.
E-mail address: ocslab@hnu.cn (X. Huo).

0039-9140/$ – see front matter © 2008 Elsevier B.V. All rights reserved.
doi:10.1016/j.talanta.2008.03.038

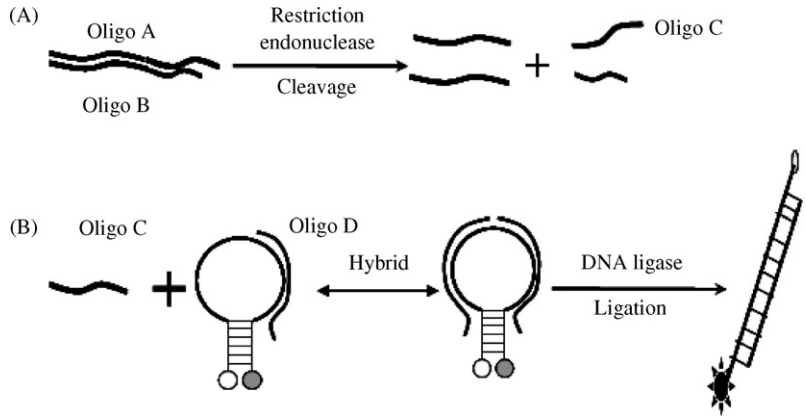

Fig. 1. Schematic of real-time monitoring of DNA cleavage by restriction endonuclease using molecular beacon (A) DNA cleavage by restriction endonuclease; (B) the cleavage product hybridizes with the MB and can be ligated by DNA ligase, which restores the quenched fluorescence of the MB.

ultrapure water system (Barnstead/thermolyne Corp., Dubuque, IA).

2.2. Fluorescence measurement

All fluorescence measurements were carried out on an F2500 (Hitachi, Japan) with excitation at 521 nm and emission at 578 nm for TAMRA labeling at 5′ end of MB as a fluorophore. Each experiment was carried out in a final volume of 100 μL and incubated at 37 °C by an aqueous thermostat (Amersham) for about 8 min to a steady status before the addition of DNA ligase, after which the sample incubated until the fluorescence reached equilibrium again, then Rsa I endonuclease was introduced into the solution and stirred for 4 s, and the fluorescence intensity of sample was recorded synchronously.

2.3. Real-time monitoring of DNA cleavage

Two samples were prepared: sample A contained MB, Oligo A, Oligo B and Oligo D; sample B only contained MB. The concentrations of MB and oligos were 250 nM and 300 nM, respectively. Assays were carried out in a buffer consisting of 50 mM Tris–HCl (pH 8.0), 5 mM $MgCl_2$, 1.0 mM DTT and 500 μM ATP. In the real-time monitoring experiment of the DNA cleavage, the aforementioned two samples were incubated at 37 °C with the sequential addition of 1.4 units of DNA ligase and 40.0 units of Rsa I endonuclease.

2.4. Activity assay of Rsa I endonuclease

In the assay of Rsa I endonuclease activity experiments, samples were prepared containing 200 nM MB, 250 nM Oligo A, 250 nM Oligo B, 250 nM Oligo D and buffer (50 mM Tris–HCl (pH 8.0), 5 mM $MgCl_2$, 1.0 mM DTT, 500 μM ATP). Before the addition of Rsa I endonuclease at various concentrations (1–320 units/ml), 1.4 units of DNA ligase was introduced into each sample. The cleavage velocities of samples were evaluated by analyzing the time courses respectively.

3. Results and discussion

3.1. The experimental principle

The principle of this approach is illustrated in Fig. 1. The Oligo A and Oligo B are designed to hybridize with each other to form a DNA duplex containing the Rsa I endonuclease recognition site. Upon cleavage, the resulting Oligo C which is complementary with 3′ half part of MB's loop is expected to dissociate readily from the duplex. The Oligo C together with Oligo D, can hybridize with the MB's loop to form a ligatable nick and ligated by DNA ligase, resulting in the complete opening of MB and leading to a full fluorescence restoration. Thus, the DNA cleavage reaction by Rsa I endonuclease can be monitored in real-time based on this principle.

3.2. Real-time monitoring of double-stranded DNA cleavage

The fluorescence intensity of these samples was monitored and the time courses were plotted in Fig. 2. As illustrated in Fig. 2, after the addition of DNA ligase and Rsa I endonuclease, there was no fluorescence change in curve B (corresponding to sample B). This result implied that MB's conformation was not affected by DNA ligase and Rsa I endonuclease. The only factor that could affect the conformation of MB altering its fluorescence was the presence of the target DNA hybridizing with MB. In sample A represented by curve A, after the addition of DNA ligase, the fluorescence did not change. After the addition of Rsa I endonuclease, the fluorescence was enhanced rapidly, implying MB's hybridization with the target DNA. According to the mechanism demonstrated in Fig. 1, the DNA cleavage reaction took place, and the newly produced DNA could "open" the MB by hybridizing with the loop

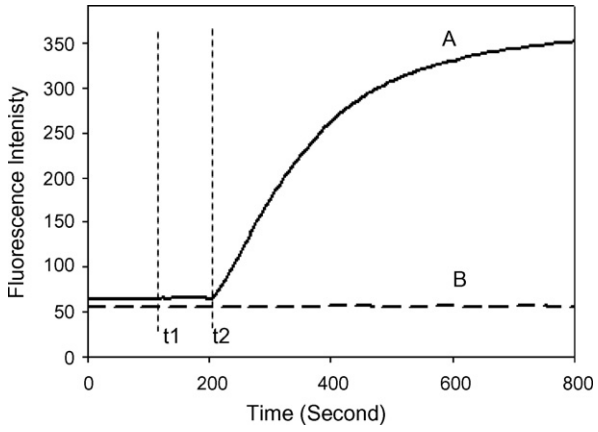

Fig. 2. Monitoring of the Rsa I endonuclease activity in real-time. The curves A and B represent the time courses of samples A and B, respectively. At time *t*1, DNA ligase was added into the samples; while at time *t*2, Rsa I endonuclease was added.

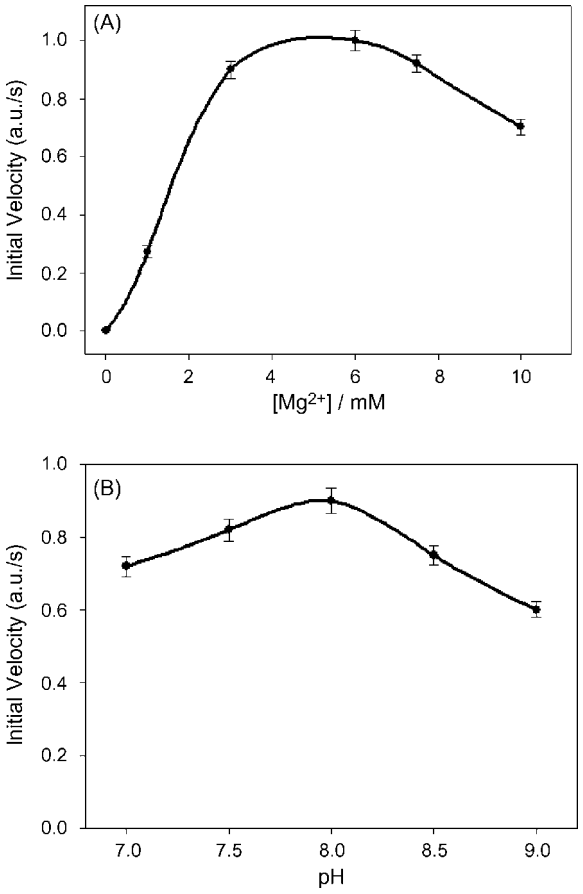

Fig. 3. Effect of Mg^{2+} and pH. Assays were carried out at 37 °C in a final volume of 100 μL. The amounts of DNA ligase and Rsa I endonuclease were 1.4 units and 40.0 units, respectively. The experiments were performed in triplicate.

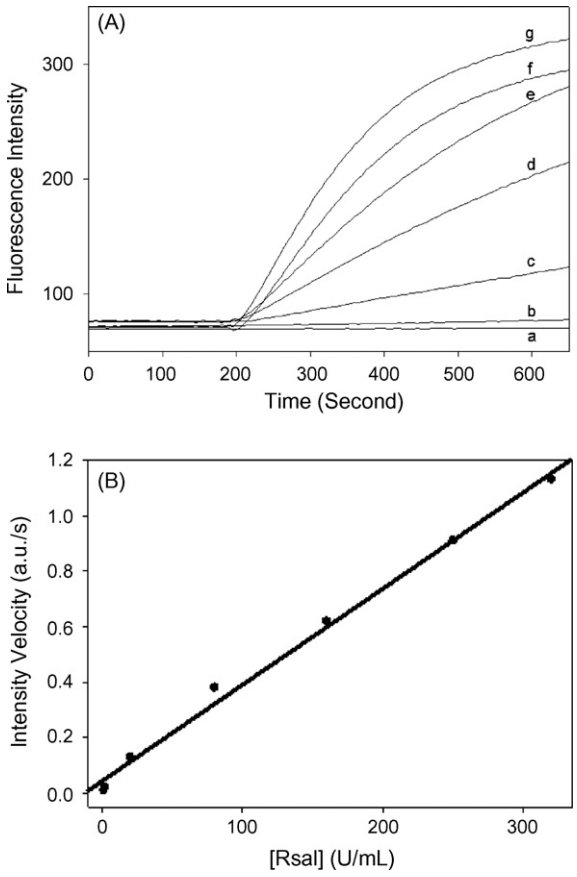

Fig. 4. (A) Time courses of real-time monitoring of DNA cleavage process catalyzed by various Rsa I endonuclease concentrations: (a) 1 unit/ml; (b) 2 units/ml; (c) 20 units/ml; (d) 80 units/ml; (e) 160 units/ml; (f) 250 units/ml; (g) 320 units/ml. (B) Relationship between initial reaction velocity and concentration of Rsa I endonuclease. Assays were carried out at 37 °C in a final volume of 100 μL under optimized conditions (50 mM Tris–HCl (pH 8.0), 5.0 mM $MgCl_2$, 1.0 mM DTT and 500 μM ATP).

of MB. Based upon the above data, DNA cleavage reactions by Rsa I endonuclease can be monitored in real-time by this novel approach.

3.3. Optimization of the experimental conditions

To obtain the optimum conditions for this assay, the effects of Mg^{2+} and pH have been investigated as they are important factors influencing enzyme activity. As shown in Fig. 3A, the initial velocity of DNA cleavage reached its maximum at an Mg^{2+} concentration of 5.0 mM and then declined when the concentration of Mg^{2+} increased. So, 5.0 mM was chosen in our experiments hereafter. According to Fig. 3B, the initial velocity of DNA cleavage increased at pH 7.0–8.0, reached its maximum at pH 8.0, and then declined at pH 8.0–9.0. Therefore, pH 8.0 was selected for further study. Thus, the method developed here is convenient and accurate in detecting the effects of various catalytic conditions on DNA cleavage reactions. It will enable a better understanding of the enzymatic reactions performed under various conditions.

3.4. Assay of Rsa I endonuclease

Applied with these optimum conditions (pH 8.0 and 5.0 mM Mg^{2+}), a series of reactions using various concentrations of Rsa I endonuclease have been carried out. The time courses are shown in Fig. 4A. The result manifests that, as Rsa I endonuclease concentration was increased, the fluorescence enhancement rate was increased. Within the enzyme concentration ranging from 1.0 unit/ml to 320 units/ml, a good linear correlation ($r^2 = 0.9932$) between initial velocity of fluorescence enhancement and Rsa I endonuclease concentration was observed (Fig. 4B). The detection limit was 1.0 unit/ml. The assay avoids any indirect and time-consuming problems arising from stopping the reaction, such as in gel electrophoresis methods. And real-time monitoring avoids any subsequent detection and analysis step, so it shortens the detections time for each sample. So the real-time assay we have developed here is convenient, quick and sensitive, and has a wide dynamic range, which makes it a useful method to analyze the Rsa I endonuclease activity.

4. Conclusion

In conclusion, we have developed a novel, sensitive, continuous fluorescence assay method to monitor the cleavage of double-stranded DNA by restriction endonuclease based on nucleic acid ligation using MB. This assay used MB DNA probes to perform the signal transduction. Under optimized conditions, Rsa I endonuclease analysis could be realized within 5 min with a detection limit down to 1.0 unit/ml without the need for labeling of DNA substrates. This method permits real-time monitoring of DNA cleavage and makes it easy to characterize the activity of endonucleases and to study the cleavage reaction kinetics.

Acknowledgements

This work was partially supported by National Key Basic Research Program of China (2002CB513110), Key Project of Natural Science Foundation of China (90606003), Major International (Regional) Joint Research Program of Natural Science Foundation of China (20620120107), Natural Science Foundation of China (20475015), Key Technologies Research and Development Program (2003BA310A16), Key Project of International Technologies Collaboration Program of China (2003DF000039).

References

[1] A. Pingoud, A. Jeltsch, Nucleic Acids Res. 29 (2001) 3705.
[2] A.P. Sharp, B. Sugden, J. Sambrook, Biochemistry 12 (1973) 3055.
[3] A. Jeltsch, A.M. Pingoud, Methods Mol. Biol. 160 (2001) 287.
[4] A. Alves, T. Ruter, R. Geiger, A. Fliess, G. Mass, A. Pingoud, Biochemistry 28 (1989) 2678.
[5] A. Jeltsch, A. Fritz, J. Alves, H. Wolfes, A. Pingoud, Anal. Biochem. 213 (1993) 234.
[6] S.S. Ghosh, P.S. Eis, K. Blumeyer, K. Fearon, D.P. Millar, Nucleic Acids Res. 22 (1994) 3155.
[7] T.R. Waters, B.A. Connolly, Anal. Biochem. 204 (1992) 204.
[8] P.C. Ray, A. Fortner, G.K. Darbha, J. Phys. Chem. B 110 (2006) 20745.
[9] J.J. Li, R. Geyer, W. Tan, Nucleic Acids Res. 28 (2000) e52.
[10] K. Eisenschmidt, T. Lanio, A. Jeltsch, A. Pingoud, J. Biotechnol. 96 (2002) 185.
[11] S.P. Lee, M.L. Censullo, M.G. Kim, J.R. Knutson, M.K. Han, Anal. Biochem. 227 (1995) 295.
[12] S.P. Lee, D. Porter, J.G. Chirikjian, J.R. Knutson, M.K. Han, Anal. Biochem. 220 (1994) 377.
[13] E.S. Roddy, M. Price, A.G. Ewing, Anal. Chem. 75 (2003) 3704.
[14] S. Tyagi, F.R. Kramer, Nat. Biotechnol. 14 (1996) 303.
[15] S. Tyagi, D.P. Bratu, F.R. Kramer, Nat. Biotechnol. 16 (1998) 49.
[16] W. Tan, K. Wang, T.J. Drake, Curr. Opin. Chem. Biol. 8 (2004) 547.
[17] C. Ma, Z. Tang, K. Wang, W. Tan, J. Li, W. Li, Z. Li, X. Yang, H. Li, L. Liu, Anal. Biochem. 353 (2006) 141.
[18] C. Ma, Z. Tang, K. Wang, W. Tan, X. Yang, W. Li, Z. Li, H. Li, X. Lv, Chem. BioChem. 8 (2007) 1487.
[19] C. Ma, Z. Tang, K. Wang, W. Tan, X. Yang, W. Li, Z. Li, X. Lv, Anal. Biochem. 363 (2007) 294.
[20] Z. Tang, K. Wang, W. Tan, J. Li, L. Liu, Q. Guo, X. Meng, C. Ma, S. Huang, Nucleic Acids Res. 31 (2003) e148.
[21] L. Liu, Z. Tang, K. Wang, W. Tan, J. Li, Q. Guo, X. Meng, C. Ma, Analyst 130 (2005) 350.
[22] Z. Tang, K. Wang, W. Tan, C. Ma, J. Li, L. Liu, Q. Guo, X. Meng, Nucleic Acids Res. 33 (2005) e97.

Talanta 76 (2008) 259–264

Contents lists available at ScienceDirect

Talanta

journal homepage: www.elsevier.com/locate/talanta

Determination of cationic surfactants in pharmaceutical disinfectants using a new sensitive potentiometric sensor

Dubravka Madunić-Čačić[a], Milan Sak-Bosnar[b,*], Olivera Galović[b], Nikola Sakač[b], Ružica Matešić-Puač[b]

[a] Saponia Chemical, Pharmaceutical and Foodstuff Industry, M.Gupca 2, HR-31000 Osijek, Croatia
[b] Department of Chemistry, Josip Juraj Strossmayer University of Osijek, F. Kuhača 20, HR-31000 Osijek, Croatia

ARTICLE INFO

Article history:
Received 21 November 2007
Received in revised form 18 February 2008
Accepted 20 February 2008
Available online 4 March 2008

Keywords:
Surfactant sensor
PVC membrane
Cationic surfactant
Potentiometric titration
Pharmaceuticals

ABSTRACT

A new sensitive potentiometric surfactant sensor was prepared based on a highly lipophilic 1,3-didecyl-2-methyl-imidazolium cation and a tetraphenylborate antagonist ion. This sensor was used as a sensing material and incorporated into the plasticized PVC-membrane. The sensor responded fast and showed a Nernstian response for investigated surfactant cations: cetylpyridinium chloride (CPC), hexadecyltrimethylammonium bromide (CTAB) and Hyamine with slope 59.8, 58.6 and 56.8 mV/decade, respectively. The sensor served as an end-point detector in ion-pair surfactant potentiometric titrations using sodium tetraphenylborate as titrant. Several technical grade cationic surfactants and a few commercial disinfectant products were also titrated, and the results were compared with those obtained from a two-phase standard titration method.

The sensor showed satisfactory analytical performances within a pH range of 2–11, and exhibited excellent selectivity performance for CPC compared to all of the organic and inorganic cations investigated. The influence of the nonionic surfactants on the shape of titration curves was negligible if the mass ratio of ethoxylated nonionic surfactants and cationic surfactants (EONS:CS) was not greater than 5.

1. Introduction

Cationic surfactants account for only 5–6% of the total surfactant production. However, they are extremely effective for some specific uses because of their peculiar properties. Their positive charge allows them to adsorb on negatively charged substrates, while most solid surfaces are at neutral pH. This capacity confers to them an antistatic behavior and a softening action for fabric and hair rinsing. The positive charge enables them to operate as flotation collectors, hydrophobating agents, corrosion inhibitors, and solid particle dispersants. Many cationic surfactants are also used as bactericides. They are used to clean and aseptize surgery hardware, to formulate heavy-duty disinfectants for domestic and hospital use, and to sterilize food bottles or containers, particularly in the dairy and beverage industries. Cationic and anionic surfactants have usually been determined by two-phase titration [1], but this technique suffers from a large number of drawbacks such as the limitation of application to strongly colored and turbid samples, the toxicity of the organic chlorinated solvent used, the formation of emulsion during titration that can disturb visual end-point detection, and the numerous matrix interferences.

These limitations are overcome by the use of ion-selective electrodes in direct potentiometry or as indicators in potentiometric surfactant titration. Potentiometric titrations involve reaction with an oppositely charged ion (ion-pair formation). An Al-wire electrode coated with plasticized PVC membrane was developed for potentiometric titration of cationic and ampholytic surfactants using the solution of sodium tetraphenylborate as titrant [2,3]. Denter et al. investigated a commercial liquid membrane PVC body electrode for the determination of cationic surfactant in a comparative study [4]. Buschmann and Schulz proposed a method for the potentiometric titration of cationic and zwitterionic surfactants with sodium tetraphenylborate (TPB) using the PVC membrane-based electrode as an end-point indicator [5]. Due to increasing use of cationic surfactants (corrosion inhibitors, flotation reagents, softeners in textile and detergent industries, disinfectants in pharmacy, medicine and cosmetics, etc.), considerable interest for the application of cationic surfactant-sensitive electrodes has been seen in recent years [6–13].

Several ion-pair based sensing materials have been used for potentiometric determination of cationic surfactants in some pharmaceutical formulations. Cetylpyridinium–iodomercurate PVC

* Corresponding author. Tel.: +385 31 495 530; fax: +385 31 495 549.
E-mail address: msbosnar@kemija.unios.hr (M. Sak-Bosnar).

0039-9140/$ – see front matter © 2008 Elsevier B.V. All rights reserved.
doi:10.1016/j.talanta.2008.02.023

membrane ion selective electrode was used for the determination of cetylpyridinium cation in mouthwash [14]. Amodiaquine, an antimalarial drug prophylactic, can be potentiometrically determined using a polymeric membrane electrode based on the cationic drug and sodium tetraphenylborate or potassium tetrakis(4-chlorophenyl) borate ion-pair [15]. A PVC-membrane sensor based on *s*-benzylthiuronium tetraphenylborate was used as an end-point indicator by potentiometric titration of CPC in some mouth wash preparations [16]. The capillary electrophoresis method was developed for the determination of cationic surfactants and benzethonium and cetylpyridinium ions, which are commonly used as preservatives in various pharmaceutical and cosmetic products [17]. The surfactant to dye binding degree (SDBD) method was extended to the determination of cationic surfactants in pharmaceuticals [18–20].

Cationic surfactants can be determined in environmental samples using ion-sensitive field effect transistor (ISFET) devices [21], flow injection analysis [22], and spectrophotometry [23]. Spectrofluorimetry [24] and optical sensors [25] can also be used for their determination.

In this study, a PVC-plasticized liquid type ionic surfactant sensitive membrane was prepared based on 1,3-didecyl-2-methylimidazolium–tetraphenylborate (DMI–TPB) as a sensing ion-pair element and *o*-nitrophenyloctylether (*o*-NPOE) as a plasticizer. The sensor was applied for potentiometric titration of the commonly used pure and technical grade cationic surfactants, as well as for cationic surfactant content in several pharmaceutical and household disinfectant formulations.

2. Experimental

2.1. Reagents and materials

The standard solutions of sodium dodecylsulfate (DDS) (c = 4 mM) and sodium TPB (c = 5 mM) were used as titrants. Hyamine 1622 (benzethonium chloride, diisobutylphenoxyethoxyethyldimethylbenzylammonium chloride), cetylpyridinium chloride (CPC), 1,3-didecyl-2-methylimidazolium chloride (DMIC), and hexadecyltrimethylammonium bromide (CTAB) were used for sensor response characteristics measurements and for potentiometric titrations.

All of the above-mentioned chemicals were of reagent grade quality and supplied by Fluka. The following technical grade cationic surfactants were used for investigations too: alkyldimethylbenzylammonium chloride (ADBAC); alkyldimethylbenzylammonium bromide (ADBAB); didecyldimethylammonium chloride (DDAC); triethanolamine di-esterquat methosulfate (TDM); dihydrogenated tallowethyl hydroxyethylammonium methosulfate (DTHM).

The sensor membrane was composed of *o*-nitrophenyloctylether (*o*-NPOE) as plasticizer, high molecular weight poly(vinyl chloride) (PVC) (both the *o*-NPOE and PVC were from Fluka, Switzerland), and an isolated ion-exchange complex as a sensing material (1.0%).

2.2. Preparation of the PVC membrane sensor

2.2.1. Preparation of the DMI–TPB ion-exchange complex

The DMI–TPB ion-exchange complex was prepared by dropwise addition of 10 mL of a 0.01 M sodium tetraphenylborate solution to 10 mL of a 0.01 M DMIC solution. The mixture was magnetically stirred for 30 min. The white precipitate was extracted with three portions of dichloromethane, 30 mL each. The extracts were collected and washed with three portions of water, of 50 mL each, and dried with anhydrous sodium sulfate. The solvent was evaporated at room temperature and the precipitate was dissolved in 10-mL mixture of diethylether:methanol (1:1) by use of an ultrasonic bath. The solvent was evaporated at −18 °C and the isolated precipitate was used as a sensing material for membrane preparation.

2.2.2. Sensor preparation

The plasticizer:PVC ratio was 3:2. One hundred and eighty milligrams of the mixture were dissolved in 2-mL tetrahydrofuran using an ultrasonic bath for homogenization. Then the clear solution was carefully poured into a glass ring (i.d. 24 mm, lower side ground flat, Fluka) which was fixed tightly on a glass plate. After curing, small disks (i.d. 7 mm) were punched from the cast film and mounted in a Philips electrode body IS-561 (Glasblaeserei Moeller, Zurich, Switzerland). A mixture of sodium chloride (c = 0.1 M) and sodium dodecylsulfate solution (c = 0.001 M) was employed as the internal filling solution. A few preliminary titrations were used as a preconditioning procedure before using the sensor as an indicator in quantitative titrations.

Between measurements, the sensor was kept in distilled water. The lifetime of the sensor was several months. A silver/silver(I) chloride reference electrode (Metrohm, Switzerland) in sodium chloride solution (c = 3 M) was used as one reference.

2.3. Apparatus

The all-purpose titrators 751 GPD Titrino and 794 Basic Titrino (Metrohm, Switzerland), combined with Metrohm 806 Exchange units (Metrohm, Switzerland), were used as dosing elements to perform potentiometric titrations. The solutions during titrations were magnetically stirred using the 727 Ti Stand (Metrohm, Switzerland).

The Titronic Basic piston burette was combined with the Handylab pH 12 (both manufactured by Schott Geraete GmbH, Germany) and controlled by a PC using self-programmed software to measure the response characteristics of dynamic response time and interferences.

2.4. Procedure

The sensor response toward Hyamine, DMIC, CPC and CTAB was investigated at constant ionic strength (0.01 M Na_2SO_4) using incremental analyte addition. The volume of solution used for titration varied between 25 and 50 mL, depending on the sample nature and expected surfactant concentration.

All measurements and titrations were performed at room temperature using a magnetic stirrer without ionic strength and pH adjustment. The titrator was programmed to work in MET (monotonic equivalent point titration) Mode with dosing increments of 0.1 mL, equilibrium time 20 s, and signal drift 5 mV/min. The titrator was also programmed to work in DET (dynamic equivalent point titration) Mode with signal drift 5 mV/min and equilibrium time 60 s. The wait time before the start of titration varied between 30 and 60 s, depending on the sample nature and surfactant concentration.

3. Results and discussion

3.1. Response characteristics

The electromotive force of the membrane sensor assembly when dipped in the solution of cationic surfactant (CS) being investigated is given by the Nernst equation:

$$E = E^0 + S \log a_{CS^+} \quad (1)$$

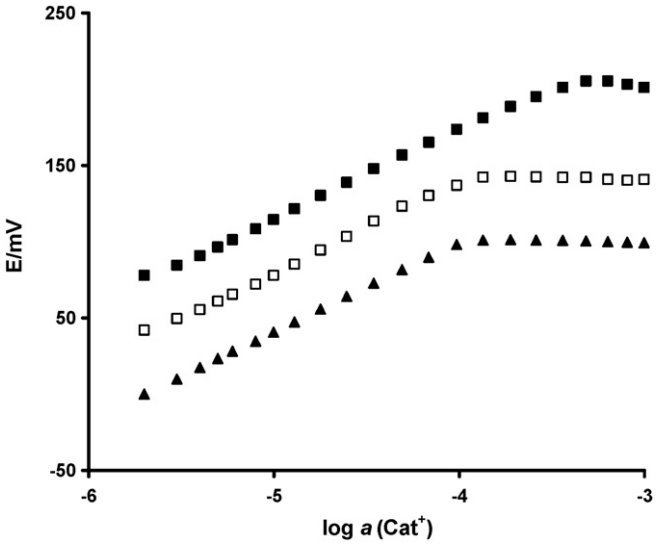

Fig. 1. Response characteristics of DMI–TPB surfactant sensor toward Hyamine (■), CPC (□) and CTAB (▲).

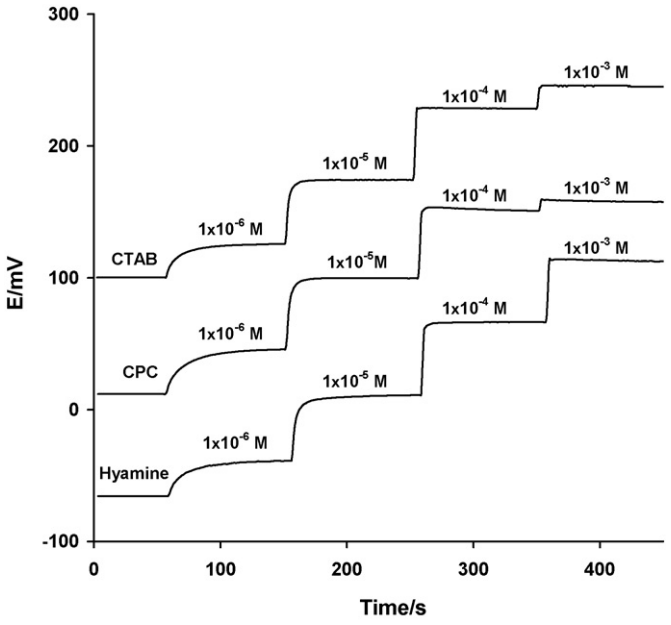

Fig. 2. Dynamic response characteristics of DMI–TPB surfactant sensor in Hyamine, CPC and CTAB solutions.

where E^0 is the constant potential term, S is the sensor slope, and a_{CS^+} is the activity of surfactant cation. The response characteristics of a DMI–TPB surfactant sensor in solutions of Hyamine, CTAB and CPC are shown in Fig. 1. The slope values and correlation coefficients were calculated from the linear region of the calibration graphs on the five series of measurements using linear regression analysis. The detection limits were estimated according to the IUPAC recommendations [26]. The sensor showed Nernstian response to all of the tested cationic surfactants. The deviations from linearity at the lower concentration level are caused by gradual dissolution of the ion-pair complex from the membrane and by the micelle formation at the higher concentration level. Agreement between several sensor coating procedures was satisfactory concerning analytical performances of the sensors. Statistical evaluation of the sensor characteristics is given in Table 1.

The dynamic response of the DMI–TPB surfactant sensor was also evaluated. As shown in Fig. 2, the sensor reached 95% of its equilibrium response for CPC ion within 13 s for the concentration change 1×10^{-6} M → 1×10^{-5} M, 5 s for the concentration change 1×10^{-5} M → 1×10^{-4} M, and 2 s for the concentration change 1×10^{-4} M → 1×10^{-3} M. The corresponding values for the Hyamine and CTAB cations for the same concentration changes were 36, 6 and <3 s and 10, 4 and <3 s, respectively.

3.2. Potentiometric titration

3.2.1. Titrant selection

The standard solutions of DDS and TPB, both of $c = 4$ mM, were tested as titrants for potentiometric titration of cationic surfactants.

The following pure cationic surfactants were used as analytes: Hyamine 1622; CPC; DMIC; CTAB. The resulting titration curves exhibited sharp inflexions for both titrants (Fig. 3), with magnitudes as follows: DMIC > CPC > CTAB > Hyamine. However, those obtained using sodium TPB exhibited higher potential jump at the equivalence point, thus sodium TPB was used in further investigations. The large potential changes at the equivalence point (300–400 mV, depending on the analyte nature) using TPB as titrant enabled high accuracy and sensitivity in cationic surfactant determination.

3.2.2. Titration of technical grade cationic surfactants

The main application of the sensor described was for indication of the end-point in ion-pair surfactant potentiometric titrations. The cationic surfactant (CS^+ = analyte determined) reacts during titration with the anionic surfactant (AS^- = titrant), accompanied by formation of a water insoluble (1:1) ion-pair CS^+AS^- (ion-exchange or ion-pair complex), which dissociates as follows:

$$CS^+AS^- \rightleftharpoons CS^+ + AS^- \quad (2)$$

For the above equilibrium, the solubility product is defined as:

$$K_{sp} = a(CS^+)\,a(AS^-) \quad (3)$$

where $a(CS^+)$ and $a(AS^-)$ are activities of the corresponding surfactant ions.

Before the equivalence point, the change (decrease) of sensor potential responded to the change of cationic surfactant concentration as shown in Eq. (1). After the equivalence point (all the cationic surfactant is precipitated), the increase of anionic surfactant concentration in solution is evident.

Table 1
Response characteristics of DMI–TPB-based liquid membrane sensor selective to the cationic surfactants given together with ±95% confidence limits

Parameters	Cationic surfactants		
	CTAB	CPC	Hyamine 1622
Slope (mV/decade)	58.6 ± 0.4	59.8 ± 0.9	56.8 ± 1.2
Correlation coefficient (r)	0.9999	0.9992	0.9972
Detection limit (M)	1.4×10^{-6}	4.6×10^{-6}	2.9×10^{-6}
Useful conc. range (M)	2×10^{-6} to 1×10^{-4}	5×10^{-6} to 1×10^{-4}	4×10^{-6} to 4×10^{-4}

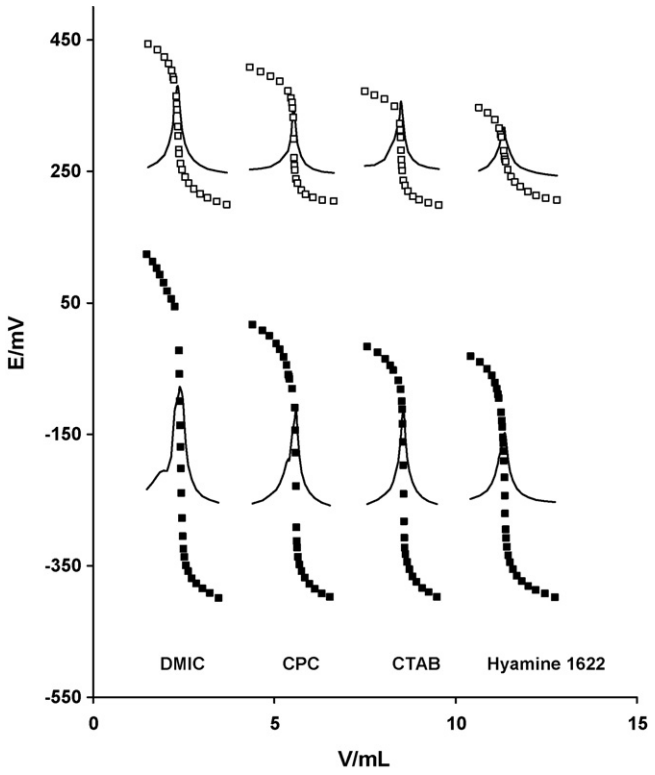

Fig. 3. Potentiometric titration curves and their first derivatives of a few cationic surfactants solutions ($c = 4 \times 10^{-3}$ M) with sodium tetraphenylborate (■) and sodium dodecylsulfate (□) using DMI–TPB surfactant sensor as indicator. Here and in later figures some curves are displaced laterally or vertically for clarity.

From Eq. (3), $a(CS^+) = K_{sp}/a(AS^-)$, and after insertion into Eq. (1), the following sensor response is obtained:

$$E = E^0 + S \log \frac{K_{sp}}{a(AS^-)} \quad (4)$$

which after rearrangement yields:

$$E = \text{const} - S \log a(AS^-) \quad (5)$$

where const = $E^0 + S \log K_{sp}$.

From Eq. (5) it follows that after the equivalence point, the sensor responds to the change of anionic titrant (anionic response). Further addition of anionic titrant after the equivalence point causes further decrease of the sensor potential E. It can be also concluded from Eq. (5) that the magnitude of the inflexion at the equivalence point is strongly dependent on the solubility product value. The lower K_{sp} value causes the higher potential change at the equivalence point, resulting in a more sensitive surfactant determination.

The standard solution of TPB was used as the titrant in the determination of cationic surfactants forming the water insoluble (1:1) complexes. The several technical grade cationic surfactants were titrated potentiometrically using the new DMI–TPB membrane sensor as a surfactant sensor for end-point determination. The results of the determinations of some of the most frequently used surfactants, compared with those obtained using a commercial surfactant sensor and two-phase titration method, showed no significant difference (Table 2). The equivalence points for all potentiometric titrations were calculated from the derivative curves.

3.2.3. Titration of commercial products

Six cationic surfactant-based commercial disinfectant products were potentiometrically titrated using the new DMI–TPB sensor as an indicator. Cationic surfactants declared in the products investigated were CPC and ADBAC. Disinfectant for hospital use C contained a synergistic mixture of *n*-octyl-dimethylbenzylammonium chloride, Hyamine 1622 and methylbenzethonium chloride. The results of cationic surfactant content in the disinfectants for hospital use B and C were expressed in M due to lack of the corresponding average molecular mass data, although the quantitative composition of product C (each cationic surfactant content) was declared. No pH or ionic strength adjustment was made. The pH values of samples varied between 6 and 9. Their potentiometric titration curves and the corresponding first derivatives exhibited clearly defined inflection and enabled unambiguous equivalence point detection. The results (Table 3) were compared to those obtained using a commercial surfactant electrode and exhibited satisfactory mutual agreement.

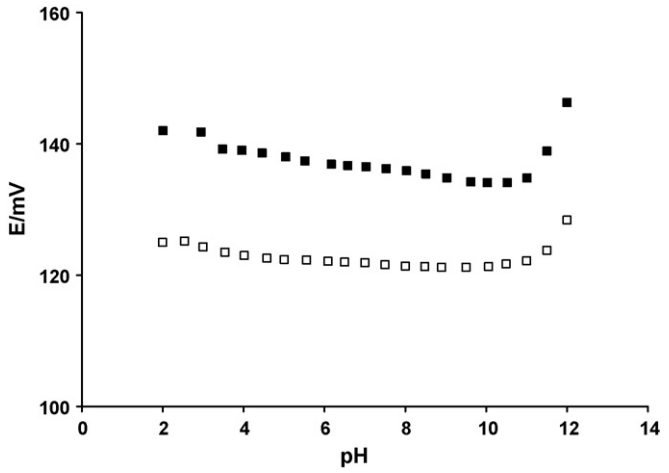

Fig. 4. The influence of pH value on the potentiometric response of DMI–TPB surfactant sensor in the solutions of CPC: (■) 5 mM; (□) 0.5 mM.

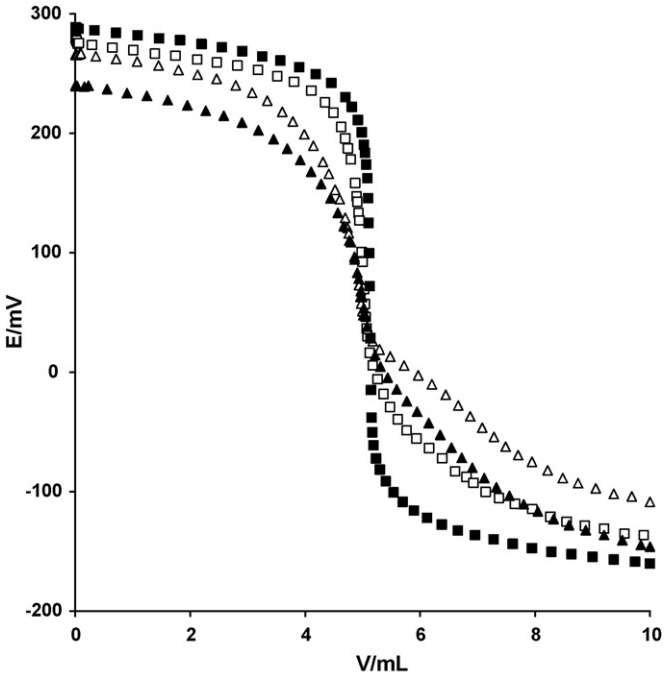

Fig. 5. Influence of EONS nature (EO groups number) at fixed CPC:EONS molar ratio 1:2 on the shape of titration curves of CPC using TPB as titrant and DMI–TPB surfactant sensor as indicator. EONS investigated: (■) CPC only; (□) 5 EO; (▲) 10 EO; (△) 12 EO.

Table 2
Results of potentiometric titrations of some technical grade cationic surfactants using sodium TPB ($c = 5 \times 10^{-3}$ M) as titrant and DMI–TPB surfactant sensor as an indicator, in comparison with the results obtained with a commercial surfactant sensor and standard two-phase titration method

Surfactant used	Surfactant content[a]				
	DMI–TPB sensor		Commercial sensor		Two-phase titration[b]
	Found (%)	R.S.D. (%)	Found (%)	R.S.D. (%)	Found (%)
DDAC	52.83	0.51	51.50	0.71	52.42
ADBAC 1	50.03	0.99	51.11	0.31	50.87
ADBAC 2	53.25	0.79	53.67	0.48	53.94
Hyamine 1622	98.36	0.58	98.27	0.54	98.59
CTAB	95.41	0.54	95.68	0.57	95.90
CPC	97.52	0.24	97.36	0.22	98.23

[a] Average of five determinations.
[b] Average of three determinations.

Table 3
Results of potentiometric titrations of six disinfectant products using sodium TPB ($c = 5 \times 10^{-3}$ M) as titrant and DMI–TPB surfactant sensor as an indicator, in comparison with the results obtained with commercial sensor

Product	Cationic surfactant content[a]			
	DMI–TPB sensor		Commercial sensor	
	Found (%)	R.S.D. (%)	Found (%)	R.S.D. (%)
Mouthwash A	0.0554	0.99	0.0536	1.02
Mouthwash B	0.0584	0.94	0.0564	0.97
Disinfectant for food industry	4.3360	0.96	4.3690	0.89
Disinfectant for hospital use A	5.0230	0.34	5.0040	0.12
	Found (M)	R.S.D. (%)	Found (M)	R.S.D. (%)
Disinfectant for hospital use B	0.1510	0.23	0.1505	0.19
Disinfectant for hospital use C	0.00373	0.79	0.00351	0.73

[a] Average of five determinations.

3.3. Interferences

3.3.1. The influence of pH

The sensor potential stability was investigated over a wide pH range in order to simulate the practical titration conditions of different formulated products of varying acidity and alkalinity. The investigations were performed in Hyamine 1622 and CPC solutions at two concentration levels: 0.4 and 4 mM. The pH values were adjusted with solutions of NaOH and H_2SO_4 ($c = 1$, 0.1 and 0.01 M). The surfactant solutions investigated contained 0.1 M of Na_2SO_4 to provide measurements at constant ionic strength. The sensor potential readings were maintained within ±1 mV. There were no significant sensor potential deviations within the pH range of 2–11, which indicates the applicability of the sensor in strongly acidic and alkaline conditions (Fig. 4). The shapes of titration curves and the magnitude of the potential change at the inflection point, at different pH values, further confirmed the above statement (not shown).

3.3.2. The influence of nonionic surfactants

The ethoxylated nonionic surfactants (EONSs) can be a component part of cationic surfactants (CSs) based on formulated products. The widely used class of nonionics are alkoxylated alcohols, which under certain circumstances may exhibit slightly anionic character. Therefore its influence on the potentiometric titration of cationic surfactants was investigated.

Five different EONS containing 5, 6, 10, 12 and 25 ethoxy groups (EO), were separately added in different molar proportions to the solution of CPC, one of the most frequently used cationic surfactants. It can be concluded that the titration curves are seriously disturbed for the EONS:CS molar ratio greater than 3 (corresponding mass ratio 6.6). This value depends on the number of EO groups in the EONS molecule. The EONS with higher EO content influence the shape of the titration curves more strongly (Fig. 5). Practical surfactant-based products are rarely formulated with EONS:CS mass ratios greater than 2. Therefore, it can be concluded that EONS do not interfere seriously with potentiometric titration of CS in common products.

3.3.3. Determination of selectivity coefficients

The influence of the interferents on the response of the cationic surfactant sensor described is defined by the Nikolskii–Eisenman equation:

$$E = E^0_{CS^+_{det}} + \frac{RT}{F} \ln[a_{CS^+_{det}} + K^{pot}_{CS^+_{det} CS^+_{int}} a_{CS^+_{int}}] \quad (6)$$

where $K^{pot}_{CS^+_{det} CS^+_{int}}$ is the selectivity coefficient, $a_{CS^+_{det}}$ and $a_{CS^+_{int}}$ are the activities of analyte (determined) ion (det) and interfering ion (int), respectively.

Table 4
Potentiometric selectivity coefficients for different inorganic and organic cations measured with DMI–TPB surfactant sensor

Interference, M	$K^{pot}_{CS,M}$
Ammonium	3.1×10^{-5}
Sodium	5.1×10^{-5}
Potassium	2.8×10^{-5}
Magnesium	7.7×10^{-5}
Calcium	4.8×10^{-5}
Zinc	2.1×10^{-5}
Monoethanolamine	Less than 10^{-5}
Triethanolamine	Less than 10^{-5}
Tetraethylammonium	1.3×10^{-5}
Tetrabutylammonium	2.6×10^{-3}
Benzyltrimethylammonium	1.8×10^{-5}
Benzyltriethylammonium	7.1×10^{-5}

CPC was used as the primary (analyte) ion, concentration of the interfering cation was $c = 0.02$ M.

The mixed solution method [27] was used for measurement of selectivity coefficients, because it yields more realistic data than the separate solution method for the systems investigated. The sensor response was measured in a series of solutions of varying primary (determined) ion activity $a_{CS^+_{det}}$ and fixed interfering ion activity $a_{CS^+_{int}}$. The selectivity coefficients were then estimated graphically, which is a very subjective and rough method. The more reliable method involved fitting the Nikolskii–Eisenman equation (used as a model) to the experimental data obtained by the mixed solution method. By using Solver, an analysis tool incorporated into Microsoft Excel, the minimal sum of squared residuals was calculated by varying the values of E^0, S and $K^{pot}_{CS^+_{det}CS^+_{int}}$.

The selectivity coefficients of some potentially interfering inorganic and organic cations that are usually present in products were determined for the DMI–TPB ion-pair-based sensor (Table 4). For all selectivity measurements, CPC was used as the primary ion in the range of 10 μM to 10 mM, while the concentration of the interfering ion was 20 mM.

The new DMI–TPB ion-pair-based sensor exhibited excellent selectivity performances for CPC for all organic and inorganic cations investigated.

4. Conclusions

A new liquid membrane potentiometric surfactant sensitive sensor was prepared. It was based on a highly lipophilic 1,3-didecyl-2-methyl-imidazolium cation and tetraphenylborate as antagonist ion and was used as a sensing material and incorporated into the plasticized PVC-membrane. The sensor showed a Nernstian response for all the investigated surfactant cations: 59.8 mV/decade between 5×10^{-6} and 1×10^{-4} M for CPC; 58.6 mV/decade between 2×10^{-6} and 1×10^{-4} M for CTAB; 56.8 mV/decade between 4×10^{-6} and 4×10^{-4} M for Hyamine. The sensor responded very fast and reached 95% of its equilibrium response for the concentration change 1×10^{-5} M → 1×10^{-4} M (the range usually used in potentiometric titration) within 4–6 s for all the cationic surfactants investigated.

The main application of the sensor described is the indication of the end-point in ion-pair surfactant potentiometric titrations. The frequently used cationic surfactants of analytical and technical grades were successfully titrated and the results were evaluated using a commercial surfactant electrode.

Several commercial disinfectant products containing various cationic surfactants were potentiometrically titrated using the new DMI–TPB sensor as an indicator. The results, compared to those obtained using a commercial surfactant electrode with the standard two-phase titration method, exhibited satisfactory mutual agreement.

The resulting potentiometric titration curves from all the investigations revealed analytically usable inflexions, enabling reliable equivalence point detection using the first derivative method. The sensor displayed satisfactory analytical performances within a pH range of 2–11. The influence of the widely used class of nonionic surfactants on the shape of titration curves was negligible if the mass ratio of EONS:CS was not greater than 5. The selectivity coefficients were determined by fitting the Nikolskii–Eisenman equation to the experimental data obtained by the mixed solution method. The sensor exhibited excellent selectivity performances for CPC over all organic and inorganic cations investigated.

Acknowledgements

The authors gratefully acknowledge the financial support of the Croatian Ministry of Science, Education and Sports given to project No. 291-0580000-0169. The authors are also indebted to Prof. Dr. Bozidar Grabaric for fruitful discussion, careful reading, and correction of the final version of the type-script.

References

[1] V.W. Reid, G.F. Longman, E. Heinerth, Tenside 4 (1967) 292.
[2] K. Vytras, M. Dajkova, V. Mach, Anal. Chim. Acta 127 (1981) 165.
[3] K. Vytras, J. Kalous, J. Symersky, Anal. Chim. Acta 177 (1985) 219.
[4] U. Denter, H.J. Buschmann, E. Schollmeyer, Tenside Surf. Det. 28 (1991) 333.
[5] N. Buschmann, R. Schulz, Tenside Surf. Det. 29 (1992) 128.
[6] S. Alegret, J. Alonso, J. Bartrol, J. Baro-Roma, J. Sanchez, M. del Valle, Analyst 119 (1994) 2319.
[7] M. Gerlache, Z. Sentürk, J.C. Vire, J.M. Kauffmann, Anal. Chim. Acta 349 (1997) 59.
[8] A.I. Kulapin, A.M. Mikhailova, E.A. Materova, Russ. J. Electrochem. 34 (1998) 382.
[9] Y.M. Issa, S.S. Badawy, W.F. El-Hawary, M.S. Ashour, Electroanalysis 11 (1999) 1063.
[10] C. Baillarger, A. Mayaffre, M. Turmine, P. Letellier, H. Suquet, Electrochim. Acta 39 (1994) 813.
[11] S. Matysik, F.M. Matysik, J. Mattusch, W.D. Einicke, Electroanalysis 10 (1998) 98.
[12] R. Matesic-Puac, M. Sak-Bosnar, M. Bilic, B.S. Grabaric, Electroanalysis 16 (2004) 843.
[13] M.A. Plesha, B.J. Van Wie, J.M. Mullin, D.A. Kidwell, Anal. Chim. Acta 570 (2006) 186.
[14] M.N. Abbas, G.A.E. Mostafa, A.M.A. Homoda, Talanta 53 (2000) 425.
[15] T. Kimbeni Malongo, B. Blankert, O. Kambu, K. Amighi, J. Nsangu, J.-M. Kauffmann, J. Pharm. Biomed. Anal. 41 (2006) 70.
[16] G.A.E. Mostafa, J. Pharm. Biomed. Anal. 41 (2006) 1110.
[17] N. Öztekin, F.B. Erim, J. Pharm. Biomed. Anal. 37 (2005) 1121.
[18] A. Pedraza, M.D. Sicilia, S. Rubio, D. Perez-Bendito, Anal. Chim. Acta 522 (2004) 89.
[19] E.M. Costi, M.D. Sicilia, S. Rubio, D. Perez-Bendito, Anal. Chim. Acta 577 (2006) 257.
[20] A. Pedraza, M.D. Sicilia, S. Rubio, D. Perez-Bendito, Analyst 131 (2006) 81.
[21] L. Campanella, L. Aiello, C. Colapicchioni, M. Tomassetti, Anal. Lett. 30 (1997) 1611.
[22] K. Agrawal, G. Agnihotri, K. Shrivas, G.L. Mundhara, K.S. Patel, P. Hoffmann, Microchim. Acta 147 (2004) 273.
[23] S. Li, S. Zhao, Anal. Chim. Acta 501 (2004) 99.
[24] J. Liu, X. Wang, L. Wang, Microchim. Acta 151 (2005) 123.
[25] T. Masadome, T. Takahashi, Anal. Lett. 40 (2007) 441.
[26] G.G. Guilbault, R.A. Durst, M.S. Frant, H. Freiser, E.H. Hansen, T.S. Light, E. Pungor, G. Rechnitz, N.M. Rice, J.J. Rohm, W. Simon, J.D.R. Thomas, Pure Appl. Chem. 48 (1976) 127.
[27] S.H. Hoke, A.G. Collins, C.A. Reynolds, Anal. Chem. 51 (1979) 859.

Talanta 76 (2008) 475–478

Contents lists available at ScienceDirect

Talanta

journal homepage: www.elsevier.com/locate/talanta

Short communication

Improvements in cobalt determination by thermospray flame furnace atomic absorption spectrometry using an on-line derivatization strategy

Geraldo Domingues Matos [1], Marco Aurélio Zezzi Arruda *

Universidade Estadual de Campinas, Unicamp, Institute of Chemistry, Department of Analytical Chemistry, Group of Spectrometry, Sample Preparation and Mechanization-GEPAM, P.O. Box 6154, 13084-862 Campinas, SP, Brazil

ARTICLE INFO

Article history:
Received 19 December 2007
Received in revised form 26 February 2008
Accepted 2 March 2008
Available online 18 March 2008

Keywords:
On-line derivatization
Thermospray
Cobalt
Sediment

ABSTRACT

An on-line derivatization strategy was developed for improving cobalt sensitivity using thermospray flame furnace atomic absorption spectrometry (TS-FF-AAS) as the analytical technique. This strategy involves the generation of a volatile cobalt compound, providing better sample vaporization efficiency. The effect of sodium diethyldithiocarbamate (DDTC) as complexing agent on the integrated absorbance signal was evaluated. Parameters including the pH of complex formation, complex concentration and volume, sample volume, flame gas composition and tube atomization configuration were optimized. A wide linear range (from 23 $\mu g\,L^{-1}$ to 3 $mg\,L^{-1}$; $r^2 = 0.9786$) was obtained, with the best one ($r^2 = 0.9992$) attained from 23 to 400 $\mu g\,L^{-1}$ with a sample throughput of 30 h^{-1}. The improvement in the detection power was 17-fold when compared to FAAS, which provides 7 $\mu g\,L^{-1}$ as the limit of detection when considered TS-FF-AAS technique. A relative standard deviation ($n = 10$) of 4% for a cobalt solution containing 50 $\mu g\,L^{-1}$ was attained, and the accuracy of the procedure was evaluated through certified reference materials (IAEA-SL-1, lake sediment; and ISS-MURST-A1, Antarctic marine sediment). Good agreement between the results at the 95% confidence level was observed.

1. Introduction

The thermospray flame furnace atomic absorption spectrometry (TS-FF-AAS) technique proposed by Gáspár and Berndt [1] provides a simple and efficient sample introduction, because the entire sample reaches the atomizer (commonly a nickel tube), as well as efficient sample nebulization due to the good heating capacity of the ceramic capillary and the nebulization mechanism involved [2]. In view of such characteristics, some applications can be found in the literature, with their sensitivities sometimes being comparable to ETAAS [3].

Although the power of detection obtained with this technique is promising, an important drawback is related to the low temperature produced by the flame from FAAS equipment, making the TS-FF-AAS technique somewhat restricted to volatile elements. To augment the applicability of this technique, while maintaining its main advantage (power of detection), the use of a derivatization strategy [4,5] can be an effective way for solving/minimizing this drawback. This strategy is used to allow more volatile compound formation (commonly organometallics) than when the element is in its free form, which results in better limits of detection [6,7]. Thus, by changing the chemical form, those refractory species can be determined even at lower atomization temperatures. As an example, Tao and Kumamaru [6] reported the vaporization of refractory species, such as Al, Cr and V in the complexed form by using 8-hydroxyquinoline, where the vaporization temperatures did not excide 1000 °C, when ETV-ICP OES was applied.

Some complexing agents including 1-phenyl-3-methyl-4-benzoyl-pyrazolone (PMBP), 1-(2-pyridylazo)-2-naphthol (PAN) and sodium diethyldithiocarbamate (DDTC) have also been used in the electrothermal atomic absorption spectrometry (ETAAS) due to characteristics as lower vaporization temperatures as well as their use as chemical modifiers and/or extracting reagents [8–10].

In view of the difficulty to work with refractory analytes at low atomization temperature, the main objective of this work was to enhance the applicability of TS-FF-AAS for such analytes. Cobalt was taken as the example and the development of a fast, simple procedure with good power of detection for its determination in sediment samples (certified reference materials) by TS-FF-AAS based on an on-line derivatization system was then proposed.

* Corresponding author. Fax: +55 19 35213023.
E-mail address: zezzi@iqm.unicamp.br (M.A.Z. Arruda).
[1] Present address: Universidade Federal da Bahia (UFBA), Institute of Chemistry, 40170-290 Salvador, BA, Brazil.

0039-9140/$ – see front matter © 2008 Elsevier B.V. All rights reserved.
doi:10.1016/j.talanta.2008.03.001

2. Experimental

2.1. Apparatus

A PerkinElmer Model AAnalyst 300 flame atomic absorption spectrometer equipped with deuterium lamp background correction was used for cobalt determination. A cobalt hollow cathode lamp (PerkinElmer Co., Norwalk, USA), operated at 10 mA was used. The wavelength (240.7 nm) and slit (0.2 nm) conditions were those recommended by the manufacturer. All data acquisition was made in the peak area mode ($n = 3$).

A Digimed DM20 pH meter was used to adjust the pH of solutions. A Provecto Analítica microwave oven, model DGT100 Plus (Provecto Analítica, Jundiaí, Brazil) was employed for microwave-assisted decomposition of the samples. The on-line derivatization comprised a homemade injector-commutator and an Ismatec Model IPC-12 peristaltic pump (Ismatec, Glattzbrugg, Switzerland) with Tygon® tubes for propelling the solutions.

2.2. Reagents and solutions

Deionized water (18.2 MΩ cm) from a Milli-Q system (Millipore, Molsheim, France) was used to prepare all solutions. Nitric and hydrochloric sub-boiled acids, and hydrofluoric acid were used for sample decomposition. Reference solutions were freshly prepared from appropriate dilution of 1000 mg L^{-1} cobalt stock solution (Tec-Lab, Jundiaí, Brazil). Sodium diethyldithiocarbamate (JT Baker, Phillipsburg, USA) was employed as complexing agent. HNO_3 and NaOH solutions were used for pH adjustment.

2.3. Analytical procedure

The TS-FF-AAS system comprised a nickel tube (10 cm long with 10 mm i.d.) that was positioned on a standard burner head (through a stainless steel support) and a ceramic capillary (0.5 mm i.d. and 10 cm long). The nickel tube had six holes at the bottom for allowing a partial flame gases introduction into the nickel tube, as well as a hole positioned at 90° to the bottom holes where the ceramic capillary was introduced. This capillary was used for sample introduction into the nickel tube. A lab-made methacrylate injector-commutator was used for both complex formation and its transport towards the atomizer. Water was used as carrier and pumped at 1 mL min^{-1} flow rate with the peristaltic pump. The schematic diagram of the system is shown in Fig. 1. The volume of the complexing agent was divided into two loops, the sample being inserted between these volumes to obtain better mixing. All data obtained were based on the integrated absorbance signal during 60 s (maximum time allowed by the spectrometer software).

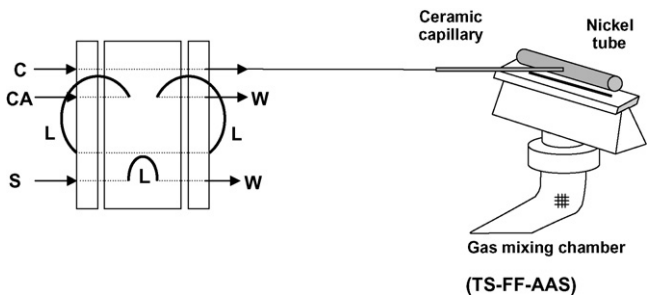

Fig. 1. Schematic diagram of the on-line derivatization system for cobalt determination by TS-FF-AAS. C: Carrier, CA: complexing agent, L: loop, S: sample, W: waste.

Based on metals found in sediment certified reference materials, concomitant tests were carried out from binary solutions. In this way, Cr(III), Cu(II), Mg(II), Mn(II), Ni(II), Pb(II) and Zn(II) were then evaluated in the 1:1, 1:10 and 1:100 analyte:concomitant concentration ratios.

For accuracy evaluation, two certified reference materials IAEA-SL-1 (trace and minor elements in lake sediment) and ISS-MURST-A1 (Antarctic marine sediment) were selected. For sample preparation, a microwave-assisted acid decomposition was carried out. Five milliliters of *aqua regia* ($HCl:HNO_3$ 3:1, v/v) + 2 mL conc. HF were added to *ca.* 200 mg certified reference materials in Teflon flasks. The program used comprised five steps: (1) 3 min at 200 W, (2) 5 min at 400 W, (3) 5 min at 600 W, (4) 20 min at 700 W and (5) 2 min at 80 W [11]. Fifty milligrams of H_3BO_3 was added to the obtained solutions for HF elimination, and the mixture was heated on a hot plate near to dryness. After cooling, deionized water was added to the resulting solution, the pH was then adjusted to 3 using a 0.1 mol L^{-1} NaOH solution, and the volume was completed to 25 mL in calibrated flasks. Blank solutions were prepared accordingly.

3. Results and discussion

In order to properly attain the derivatization, the complexing agent (DDTC) was evaluated considering its effect on peak shape. All studies were carried out using 2 mg L^{-1} Co, 0.1% (w/v) DDTC and 400 μL of sample and complexing volumes. It is interesting to comment that the referred cobalt concentration was chosen due to low cobalt signals obtained in the initial stages of this work. The pH of complex formation was first studied. Only slight variations in the analytical signal were verified over the 2–5 pH range. These results indicated good robustness for the complexation pH. At lower pH (<2), there was a decrease (*ca.* 48%) in the analytical signal, and from pH 2 to 5, only slight variations (*ca.* 10%) on the cobalt analytical signals were observed. In this way, a pH value of 3 was then chosen for the Co-DDTC formation.

The effect of the DDTC concentration on the integrated absorbance signal was studied within 0.005–2% (w/v) range. By increasing the complexing agent concentration from 0.005 to 0.1% (w/v), the integrated absorbance was also increased. However, at DDTC concentration higher than 0.1% (w/v) a decrease in the analytical signal was observed (from 27%). This result can be explained due to the high background signal when higher DDTC concentrations were used. In this way, a concentration of 0.1% (w/v) DDTC was selected for further experiments.

Sample and DDTC volumes were investigated in the 100–500 μL volume range (Fig. 2), and a threefold increase in the integrated absorbance was obtained over this volume range. However, when 500 μL sample volume was used, a double peak in the signal profile was observed. Additionally, no significant variation (*ca.* 3%) on increasing the complexing agent volume was observed. Thus, a volume of 400 μL was chosen for both DDTC and sample due to the best signal profile and the highest integrated absorbance obtained.

Experiments were carried out to evaluate the flame gas composition effect on the integrated absorbance signal (Fig. 3). It was the most important parameter due to its great influence on analytical response, whose signal was increased up to two orders of magnitude when the air flow rate ranged from 10 to 17 L min^{-1}. Using the FAAS recommended conditions from the manufacturer (2/10 L min^{-1} acetylene/air flow rate), the same analytical signal was also obtained for TS-FF-AAS, even using the derivatization system. Thus, the study of acetylene/air ratios became necessary to improve cobalt detectability in the TS-FF-AAS. Comparing the signal obtained using 2/10 L min^{-1} with that one using 2/17 L min^{-1}

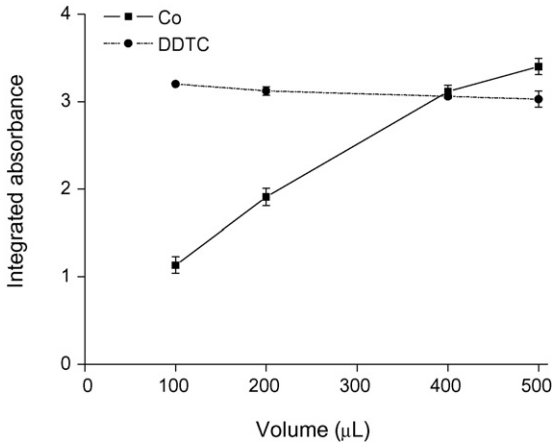

Fig. 2. Effect of sample and DDTC volumes on the integrated absorbance signal. Operating conditions: 2 mg L^{-1} cobalt solution at pH 3; 0.1% (w/v) DDTC; 2/17 flame gases composition (acetylene/air); 1 mL min^{-1} carrier fluid flow rate.

acetylene/air flow rate an increase in the analytical signal (96%) was verified. Through Fig. 3, a higher integrated absorbance signal using 2 L min^{-1} acetylene flow rate can be observed. A decrease (*ca.* 42%) in the cobalt detectability can also be observed when 4 L min^{-1} acetylene flow rate was used. In this way, 2/17 L min^{-1} acetylene/air composition was selected for further experiments. These results pointed out the most effective cobalt atomization condition in an oxidizing environment, when compared to that condition commonly recommended for FAAS.

The total area of the holes in the nickel tube was another important parameter for cobalt determination by TS-FF-AAS. Tubes with different total hole areas were investigated (0, 19, 43, 67, 91 and 115 mm^2). It is important to comment that in the initial experiments, a nickel tube with 19 mm^2 total hole area was used. This parameter is as important as the flame gas composition, which also led to an analytical signal increase of 2.4 orders of magnitude for cobalt measurements by TS-FF-AAS. Using tubes without holes, no analytical signal was observed, indicating that the cobalt atomization is much more dependent on the atomization environment than the temperature itself. By increasing the total hole area, an increase in the analytical signal was observed. However, this area cannot be increased at will, since the analytical signal decreased *ca.* 40% with a 91 mm^2 total hole area. When larger hole areas are provided, the amount of flame that penetrates into the interior of the atomizer increases, making its internal environment similar to the flame commonly used in the FAAS. Thus, the amount of flame directly affects the internal environment of the nickel tube, changing it to a more or less oxidant environment (depending on the hole area). This effect can also be seen with hole areas above 67 mm^2, since a decrease in the analytical signal was detected. In this way, the amount of flame into the tube is an important parameter, which directly influences the analytical response. These studies showed that the best result was obtained using tube with 67 mm^2 total hole area, producing a twofold larger signal when compared to that obtained with 19 mm^2, used previously. It is interesting to point out that these results are in agreement with those obtained when the flame gas composition was evaluated (a more oxidizing environment for cobalt atomization was necessary).

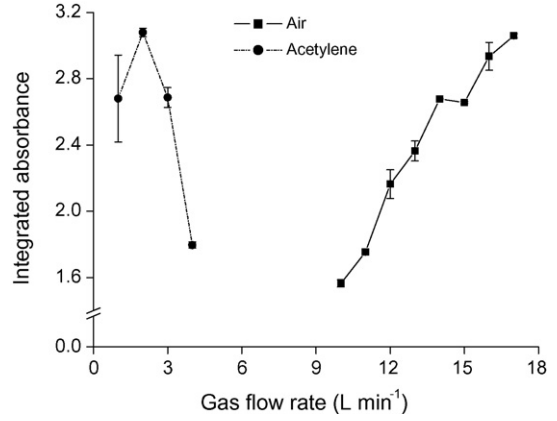

Fig. 3. Influence of the gas flame compositions on the integrated absorbance signal. Operating conditions: 2 mg L^{-1} cobalt solution at pH 3; 400 μL sample and DDTC volumes; 0.1% (w/v) DDTC; 1 mL min^{-1} carrier fluid flow rate.

Table 1
Results obtained ($\bar{x} \pm$ S.D.) for cobalt determination ($n = 3$) in certified reference materials

Sample	Certified value (μg g^{-1})	Found value (μg g^{-1})
IAEA-SL-1[a]	19.8 ± 1.5	20.3 ± 1.0
ISS-MURST-A1[b]	6.87 ± 0.34	6.54 ± 0.27

[a] Trace and minor elements in lake sediment.
[b] Antarctic marine sediment.

The concomitant effect on cobalt determination (500 μg L^{-1} concentration) was investigated using analyte:concomitant ratios of 1:1, 1:10 and 1:100. Interference was only observed for magnesium at 50 mg L^{-1} concentration (100-fold concentration higher than the analyte ones), which provided a decrease of *ca.* 50% in the analytical signal.

Under the optimized conditions, the figures of merit were then obtained. Limits of detection (three times the standard deviation of the blank/slope) and quantification (10 times the standard deviation of the blank/slope) were determined using 10 blank measurements, and the values obtained were 7 and 23 μg L^{-1}, respectively. A wide linear range (from 23 μg L^{-1} to 3 mg L^{-1}; $r^2 = 0.9786$) was obtained, with the best one ($r^2 = 0.9992$) attained from 23 to 400 μg L^{-1}. The repeatability (4% RSD) was determined from 10 measurements of 50 μg L^{-1} cobalt solution, and a sample throughput of 30 h^{-1} was obtained. The sensitivity and limit of detection were respectively 191- and 17-fold better than the conventional FAAS.

It is interesting to comment that there is only one application of TS-FF-AAS for cobalt determination in the literature [12], which reports 2.1 μg L^{-1} as limit of detection. However, this value was obtained employing a cloud point preconcentration procedure and a sample volume 50 times larger than that reported here.

By comparing the proposed derivatization strategy with that one without derivatization, the analytical signals obtained (based on peak area mode) on both cases and using 2 mg L^{-1} cobalt concentration were 6.141 (after the optimization) and 0.225, respectively.

To check the accuracy of the proposed method, cobalt determination in sediment samples (certified reference materials) was carried out. The certified reference materials analyzed were IAEA-SL-1 (trace and minor elements in lake sediment) and ISS-MURST-A1 (Antarctic marine sediment). The cobalt quantification in soil and sediment samples is of great importance for environmental contamination monitoring. However, as low concentrations are found in such samples, the cobalt quantification is not appropriate by conventional FAAS. This inconvenience is related to the limit of quantification obtained by conventional FAAS (*ca.* 400 μg L^{-1}). The value found by the proposed procedure was 23 μg L^{-1}. Thus, the on-line derivatization strategy coupled to TS-FF-AAS demonstrated a good alternative for cobalt determination, when low concentrations are present in such samples.

Table 1 shows the analytical results obtained. From these results, a good correlation between the values obtained by the proposed procedure and certified values was observed, demonstrating the applicability of the procedure for cobalt determination in sediment samples.

4. Conclusions

The strategy proposed in this work to enhance the applicability of the TS-FF-AAS was a good alternative for cobalt determination as well as the drawbacks for less volatile species were overcome. In this way, employing the TS-FF-AAS and a derivatization system, the cobalt determination was successfully carried out, attaining the initial purpose of this work.

The most influenced parameters that affect the performance of the method were the gas flame composition and total hole area in the nickel tube. The complex formed provided better volatilization efficiency, showing a good sensitivity (191-fold higher than that obtained with FAAS). This increase allowed the method to be applied to sediment samples.

Finally, such strategy can also be an alternative for other refractory elements, when considering TS-FF-AAS as analytical technique.

Acknowledgements

The authors thank the Fundação de Amparo à Pesquisa do Estado de São Paulo, FAPESP (São Paulo, Brazil), Coordenação de Aperfeiçoamento de Pessoal de Nível Superior, CAPES (Brasília, Brazil) and the Conselho Nacional de Desenvolvimento Científico e Tecnológico, CNPq (Brasília, Brazil) for financial support and fellowships. We also thank Carol H. Collins for language assistance.

References

[1] A. Gáspár, H. Berndt, Spectrochim. Acta B 55 (2000) 587.
[2] M.L. Brancalion, E. Sabadini, M.A.Z. Arruda, Anal. Chem. 79 (2007) 6527.
[3] E.R. Pereira-Filho, H. Berndt, M.A.Z. Arruda, J. Anal. At. Spectrom. 17 (2002) 1308.
[4] J.R. Castilho, J.M. Mir, C. Bendicho, J. Anal. At. Spectrom. 4 (1989) 105.
[5] M.S. Jiménez, J.R. Castilho, J. Anal. At. Spectrom. 12 (1997) 1397.
[6] S. Tao, T. Kumamaru, J. Anal. At. Spectrom. 11 (1996) 111.
[7] M.S. Black, R.F. Browner, Anal. Chem. 53 (1981) 249.
[8] Y.L. Wu, B. Hu, T.Y. Peng, Z.H. Liao, Z.C. Jiang, Talanta 55 (2001) 841.
[9] S.Z. Chen, D.B. Lu, Talanta 64 (2004) 140.
[10] Z.F. Fan, Z.C. Jiang, F. Yang, B. Hu, Anal. Chim. Acta 510 (2004) 45.
[11] F.L. Alves, W.F. Jardim, S. Cadore, M.A.Z. Arruda, P. Smichowski, J. Marrero, Quim. Nova 24 (2001) 756.
[12] G.L. Donati, C.C. Nascentes, A.R.A. Nogueira, M.A.Z. Arruda, J.A. Nóbrega, Microchem. J. 82 (2006) 189.

Talanta 76 (2008) 432–440

Contents lists available at ScienceDirect

Talanta

journal homepage: www.elsevier.com/locate/talanta

New method for removal of spectral interferences for beryllium assay using inductively coupled plasma atomic emission spectrometry

Sherrod L. Maxwell III[a,*], Maureen A. Bernard[a], Matthew R. Nelson[b], Linda D. Youmans[b]

[a] Washington Savannah River Company, Analytical Labs, Building 735-B, Aiken, SC 29808, USA
[b] Washington Savannah River Company, Building 772-F, Aiken, SC 29808, USA

ARTICLE INFO

Article history:
Received 6 February 2008
Received in revised form 19 March 2008
Accepted 20 March 2008
Available online 28 March 2008

Keywords:
Beryllium analysis
Rapid spectral interference removal
Ion exchange

ABSTRACT

Beryllium (Be) has been used widely in specific areas of nuclear technology. Frequent monitoring of air and possible contaminated surfaces in U.S. Department of Energy (DOE) facilities is required to identify potential health risks and to protect U.S. DOE workers from beryllium-contaminated dust. A new method has been developed to rapidly remove spectral interferences prior to beryllium measurement by inductively coupled plasma atomic emission spectrometry (ICP-AES) that allows lower detection limits. The ion exchange separation removes uranium (U), plutonium (Pu), thorium (Th), niobium (Nb), vanadium (V), molybdenum (Mo), zirconium (Zr), tungsten (W), iron (Fe), chromium (Cr), cerium (Ce), erbium (Er) and titanium (Ti). A stacked column consisting of Diphonix Resin® and TEVA Resin® reduces the levels of the spectral interferences so that low level Be measurements can be performed accurately. If necessary, an additional anion exchange separation can be used for further removal of interferences, particularly chromium. The method has been tested using spiked filters, spiked wipe samples and certified reference material (CRM) standards with high levels of interferences added. The method provides very efficient removal of spectral interferences with very good accuracy and precision for beryllium on filters or wipes. This new method offers improvements over other separation methods that have been used by removing large amounts of all the significant spectral interferences with greater simplicity and effectiveness. The effective removal of spectral interferences allows lower method detection limits (MDL) using inductively coupled atomic emission spectrometry. A vacuum box system is employed to reduce analytical time and reduce labor costs.

1. Introduction

Beryllium (Be) has been used widely in specific areas of nuclear technology because of its ability to reflect neutrons and its efficiency in the production of neutrons when exposed to alpha emitters [1]. Exposure to beryllium particulate at very low levels can lead to an immune response known as beryllium sensitization, or to chronic beryllium disease (CBD). The U. S. Department of Energy (DOE) promulgated the Chronic Beryllium Disease prevention program in 1999 (10CFR Part 850) to protect DOE workers from beryllium-contaminated dust. This requires frequent monitoring of air and possible contaminated surfaces in U.S. DOE facilities to identify potential health risks. Samples which include filters and wipes are digested and analyzed. The current analytical method of choice is inductively coupled plasma atomic emission spectrometry (ICP-AES) [2]. A discussion of alternate techniques and the advantages and disadvantages of each is provided by Brisson et al. [3]. A number of elements can interfere spectrally with the beryllium measurement by ICP-AES. Spectral interference correction software is used at the ICP-AES, but at higher levels of interferences and very low level beryllium the spectral interferences can cause significant errors. A rapid separation method to remove spectral interferences is needed to allow accurate measurement of beryllium at low levels to meet method detection limit (MDL) requirements. The U.S. DOE Beryllium Rule established an action level of 0.2 $\mu g/cm^3$ with accuracy of ±25% [4]. Air samplers vary in collection time, so results are reported in μg Be/sample. It is up to the customer to determine if a lab method detection limit meets their needs. For the purposes of this study, a target reporting limit of 0.01 μg/filter sample was established that will meet current SRS (Savannah River Site) customer needs. An empirical action level of 0.2 $\mu g/100\,cm^2$ for surface wipes was established by the DOE as a criterion for release of equipment to the public or "non-beryllium" areas. For the purposes of this

* Corresponding author. Tel.: +1 803 952 7473; fax: +1 803 952 7881.
E-mail address: sherrod.maxwell@srs.gov (S.L. Maxwell III).

0039-9140/$ – see front matter © 2008 Elsevier B.V. All rights reserved.
doi:10.1016/j.talanta.2008.03.032

study, a target reporting limit of 0.03 μg/wipe sample was established.

ICP-AES can be used to meet customer requirements, but the presence of spectral interferences adversely affects the accuracy at the lower reporting levels. There is an increasing trend toward lower and lower action levels [3], thus the need for effective removal of interferences when using ICP-AES to allow the minimum detection limit possible to be reached.

PG Research Foundation (Darien, IL, USA) has developed a beryllium separation method for Eichrom Technologies (Darien, IL, USA) using Be Resin® to remove spectral interferences, but this method can be affected by large amounts of interferences that can significantly reduce Be retention on the resin. In these cases one or more guard columns may also be needed prior to Be Resin® to remove large amounts of spectral interferences. Additional guard columns would likely add time and expense. Fluoride, if present, must also be complexed with boric acid to prevent Be losses using the Be Resin® method. Time to adjust each sample to pH 2 using an indicator is also required [2]. The U.S. Department of Energy Y12 National Security Complex uses a simpler pass-through approach using LN-3 Resin® (bis (2,4,4-trimethylpentyl) phosphinic acid extractant, Eichrom Technologies) to remove only some of the spectral interferences. LN-3 Resin® will retain uranium (U), niobium and molybdenum under the digestion conditions used (dilute sulphuric–nitric acid mixture), while allowing Be to pass through. Vanadium, however, a severe spectral interference, is not retained using this method. If vanadium is present, the Be Resin® method must be used after LN-3 Resin®, increasing the time and cost for this analysis [5].

A new method has been developed in the Savannah River Site (SRS) 735-B Environmental Bioassay Laboratory to remove spectral interferences prior to beryllium measurement by inductively coupled plasma atomic emission spectrometry. The ion exchange separation removes uranium (U), plutonium (Pu), thorium (Th), niobium (Nb), vanadium (V), molybdenum (Mo), zirconium (Zr), tungsten (W), iron (Fe), chromium (Cr), cerium (Ce), erbium (Er) and titanium (Ti). The spectral interferences tested were based on the list in Table 1, which were taken from the interference tables given in PerkinElmer WinLab32 software v.2.0 (PerkinElmer Life And Analytical Sciences Inc., Waltham, MA, USA). This list is very similar to what was tested by Philip Horwitz et al. [2]. Plutonium removal was also tested because of radiological as well as spectral overlap concerns [6]. Erbium removal was also tested because it can have a spectral overlap with zirconium, and therefore can cause an erroneous interference correction for beryllium based on "apparent" zirconium that is actually erbium. To minimize matrix effects from easily ionized elements such as Ca, Al, Mg and Na, a robust plasma at high RF power (1400 W), a low-flow GemCone™ Nebulizer, a large bore alumina injector, and internal standards (Y or Sc) were employed. In addition, alkali (Cs) at several hundred ppm was added to minimize easily ionized element effects. The typical beryllium emission lines used are also shown in Table 1: Be-313.042 nm (intensity 64,000) and Be-313.107 nm (intensity 41,000). The Be emission line 234.846 nm (intensity 11,500) can also be used, but it has an interference from iron at 234.811 nm with intensity 530. Since iron is usually present in Be samples, particularly wipes, removal of iron was also tested. The SRS lab typically examines results using all three lines to determine whether the spectral interference corrections have been effective.

A stacked column made of 5 ml of Diphonix Resin® and 2 ml of TEVA Resin® reduces the levels of the spectral interferences significantly. Using this approach, Be is not affected by large amounts of interferences that can reduce Be recovery in methods where it is first retained and then eluted from a resin. Instead of retaining beryllium ions to separate interferences, the beryllium is passed through the Diphonix Resin®–TEVA Resin® column and the interferences are removed on the resins. An optional anion resin column separation can also be used to remove additional chromium if needed.

Table 1
Potential spectral interferences for Be determination by ICP-AES[a]

Analyte	Peak (nm)	Intensity
U	312.879	6.0
Zr	312.917	400.0
Nb	312.964	22.0
U	312.973	15.0
Zr	312.976	550.0
Th	312.997	10.0
V	313.027	1020.0
Ce	313.033	50.0
Be[b]	313.042	64000.0
U	313.056	6.0
U	313.073	0.0
Nb	313.079	2200.0
Ti	313.079	150.0
Ce	313.087	65.0
Th	313.107	27.0
Be[b]	313.107	41000.0
Tm	313.126	Not listed
U	313.132	8.0
Hf	313.181	20.0
U	313.199	15.0
Cr	313.206	1000.0
Zr	313.207	7.0
Th	313.226	5.0
Mo	313.259	1800.0
Ce	313.259	30.0

[a] As listed in PerkinElmer WinLab32 software v.2.0.
[b] Commonly used peaks for determining beryllium by ICP-AES.

Diphonix Resin® is similar to Be Resin® in retention performance, but much less expensive. In the new SRS method, Diphonix Resin® is used to remove spectral interferences instead of retaining the beryllium. Diphonix is a resin with geminally substituted diphosphonic acid groups chemically bonded to a styrene-divinylbenzene matrix, that was developed by Argonne National Laboratory and the University of Tennessee [7–9]. Diphonix Resin® is used in the SRS Environmental Bioassay Lab (EBL) to recover and measure actinides in fecal samples [10]. Diphonix Resin® has a very high retention for uranium, plutonium, thorium, vanadium, iron, erbium and cerium even in the presence of dilute hydrofluoric acid.

Other spectral interferences are removed on TEVA Resin®, which is a resin-coated with a liquid ion exchanger (Aliquat-336 ™) [11]. The retention of niobium, titanium, molybdenum, zirconium, and tungsten as anionic fluoride complexes on quaternary amine anion exchange resin is well known [12–15]. Retention of hafnium, niobium and zirconium fluoride complexes using Aliquat-336™ extractant has also been documented [16]. TEVA Resin® retains niobium, titanium, molybdenum, zirconium, and tungsten from dilute hydrofluoric acid–hydrochloric acid solutions. Hafnium removal was not tested due to its relatively low intensity at 313.181 nm (intensity 20) and because it is typically not found it air filter or wipe samples at SRS, but it should also be removed on TEVA Resin® as a fluoride complex. Thulium (Tm) was also not tested because it is unlikely to be present. Tm is likely to follow the behavior of fellow rare earth elements cerium and erbium, which are retained on Diphonix Resin®. The filter digestion method already employed at SRS uses nitric acid, hydrochloric acid, hydrofluoric acid and hydrogen peroxide. Since fluoride is present, utilizing fluoride complexing to form anionic complexes with key spectral interferences was a logical approach to consider. Resins are not reused in the new SRS method to ensure no cross-contamination of samples. Additional reasons they are not reused are that some elements such as uranium and thorium are very difficult to remove from Diphonix

Resin® (reducing capacity with continued use), and TEVA Resin® (an extractant-coated resin) may show degradation with multiple uses.

A 0.20 M HF–0.1 M HCl solution was used in the new column separation, following evaporation steps to convert to this acid matrix. Uranium, plutonium, thorium, cerium, erbium, vanadium, chromium (partial) are retained on Diphonix Resin®, while niobium, titanium, molybdenum, zirconium, and tungsten are retained on TEVA Resin® as fluoride complexes. In 0.20 M HF–0.1 M HCl, beryllium forms a fluoride complex anion that will pass through the Diphonix Resin® column. Without fluoride ions present, Be^{+2} cations would be retained on Diphonix Resin® under low acid conditions. Be also passes through TEVA Resin® when 0.20 M HF–0.1 M HCl is used as the eluant. The concentration of chloride ions present is high enough to reduce beryllium ion retention on TEVA Resin®, while niobium, titanium, molybdenum, zirconium, and tungsten are still strongly retained. Chromium has different valence states and forms different cationic, neutral and anionic complexes [17]. As a result, Diphonix Resin® removes a fraction of the chromium present, but not all of the chromium depending on the extent of chromium complexing with fluoride.

If more effective chromium removal is required, the sample may be further purified using an anion exchange resin separation using 0.2 M HF. Under these conditions, Be is retained while chromium passes through the anion resin. Be can be eluted using 1 M HCL–0.25 M HF. If the 234.861 nm emission line is used when residual Cr is present (since this line is not significantly affected by Cr), the additional anion resin separation is not required.

The new method was tested using spiked filters, spiked wipe samples and certified reference material (CRM) standards with and without high levels of spectral interferences added.

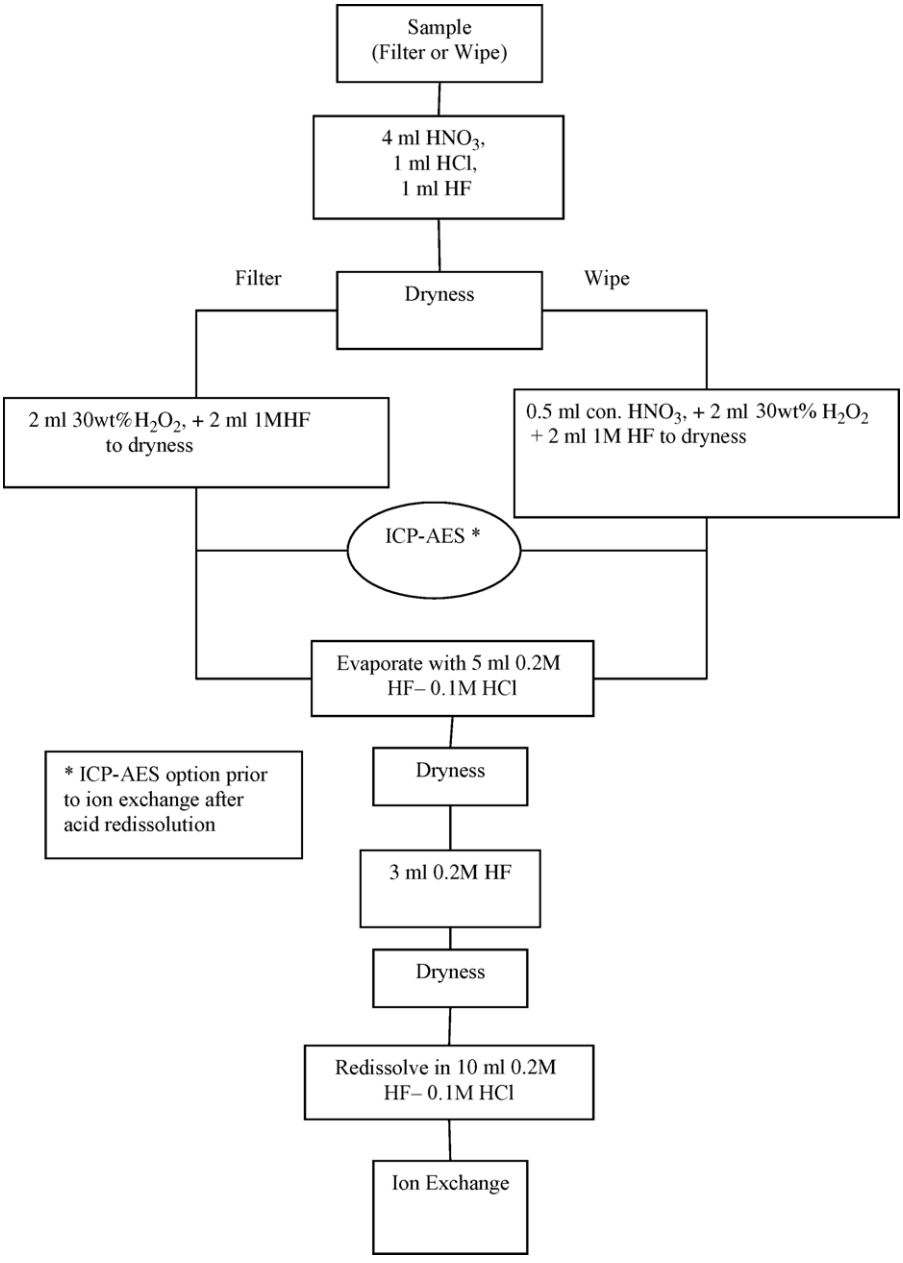

Fig. 1. Sample digestion to prepare for ion exchange.

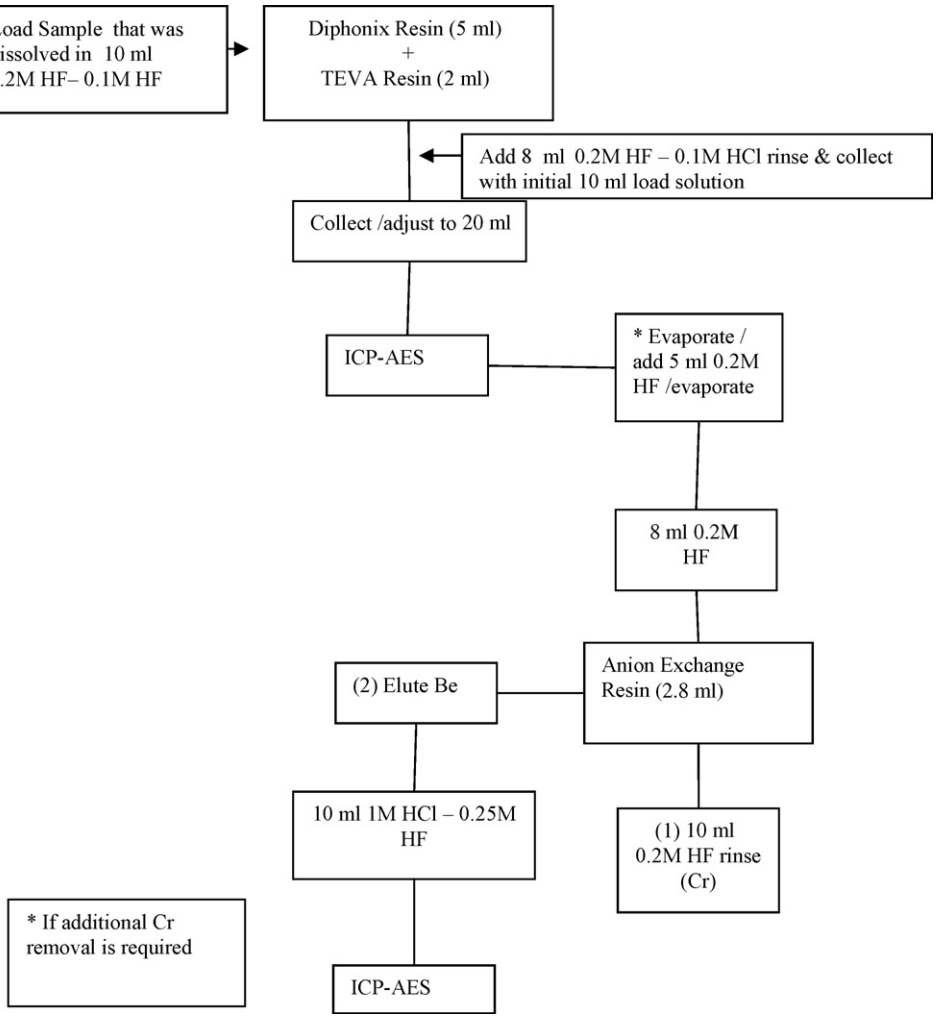

Fig. 2. Ion exchange removal of spectral interferences.

2. Experimental

2.1. Reagents

The resins employed in this work are TEVA Resin® (Aliquat-336™), Diphonix Resin® (100–200 mesh) and anion resin (1-X8, chloride form, 100–200 mesh) available from Eichrom Technologies Inc. (Darien, IL, USA). Nitric acid and hydrochloric acid were high purity-grade acids (Optima™-Fisher Scientific Inc.). Hydrofluoric acid and hydrogen peroxide were reagent grade (Fisher Scientific Inc.). All water was obtained from a Milli-Q2™ water purification system. Element standards (1000 or 10,000 parts per million Be, Cr, Nb, Mo, Ti, Fe, U, Th, Ce, Er, V, Zr, W) were obtained

Table 2
Instrument operating conditions and operating parameters for PerkinElmer Optima 3000XL

RF power	1400 W
Nebulizer flow	0.75 l/min
Auxillary flow	0.5 l/min
Plasma flow	15 l/min
Sample pump flow	1.5 ml/min
Plasma viewing	Axial
Processing mode	Area
Auto integration (min–max)	5–20 s
Read delay	30 s
Rinse	90 s
Replicates	3
Background correction	1–2 points
Nebulizer GemCone™	Low-flow
Nebulizer Chamber	Cyclonic
Injector	Alumina, 2 mm

Table 3
Average removal results for spectral interferences

Interference (ppm)	Added (ppm)	Measured (%)	Removal
Iron[a]	1000	0.039	99.996
Uranium	300	0.112	99.963
Niobium	100	ND	~100
Molybdenum	100	0.002	99.998
Vanadium	100	0.003	99.997
Zirconium	100	0.082	99.918
Tungsten	100	0.010	99.990
Thorium	50	ND	~100
Plutonium	34.4	0.000048	99.999
Titanium	100	0.736	99.964
Cerium	50	ND	~100
Erbium	100	ND	~100
Chromium	100	50.01	49.99
Chromium[b]	100	8.98	91.02

$N = 10$. ND = none detected. Added ppm added to have this level interference in 20 ml at ICP-AES.

[a] Fe has similar removal at 2500 ppm.

[b] Additional anion exchange to remove more Cr.

Table 4
Be average recovery results (wipes)—interferences added

Emission line (nm)	Be added (ppb)	Be measured after IEX (ppb)	Recovery (%)	Bias (%)	R.S.D. (%)	After anion exchange	Recovery (%)	Bias (%)	R.S.D. (%)
234.861	1.00	1.07	107.29	7.29	7.28	N/A	N/A	N/A	N/A
313.042	1.00	1.60	159.75	59.75	14.79	1.06	105.50	5.50	13.54
313.107	1.00	1.61	161.25	61.25	18.85	1.18	117.61	17.61	10.86

$N = 12$.

from High Purity Standards (Charleston, SC, USA). A plutonium standard solution (0.53 g Pu/L) was prepared in the SRS F/H laboratory using a plutonium stock solution that was characterized by controlled potential coulometry in that laboratory using ISO 12183:2005, "Controlled Potential Coulometric Assay of Plutonium". Certified reference material filter standards traceable to the National Institute of Standards and Technology (Gaithersburg, MD, USA) were obtained from High Purity Standards (Charleston, SC, USA).

2.2. Procedures

2.2.1. Column preparation

TEVA Resin® cartridges containing 2 ml of each resin were obtained from Eichrom Technologies Inc. Small particle size (50–100 μm) resin was employed, along with a vacuum extraction system (Eichrom Technologies). Diphonix Resin® columns (5 ml) and anion resin columns (2.8 ml) were prepared from a water slurry (~1:1 water:resin) using small Fast Rad Columns (Environmental Express Inc., Mount Pleasant, SC, USA) and a 24 column vacuum box.

2.2.2. Sample preparation

Fig. 1 shows a flow chart of the sample preparation method prior to ion exchange. Filters (37 mm mixed cellulose ester filters, Environmental Express Inc., Mount Pleasant, SC, USA) and wipes (15 cm × 15 cm Ghostwipes®, Environmental Express Inc., Mount Pleasant, SC, USA) were placed in 150 ml digestion tubes (Environmental Express Inc., Mount Pleasant, SC, USA), Be and/or spectral interferences were added to each tube. Four milliliters of 15.7 M nitric acid (HNO_3) and 1 ml of 12 M hydrochloric acid (HCl) were added to each tube. After the reaction subsided, 1 ml of 28 M hydrofluoric acid (HF) was added to each digestion tube. The digestion tubes were placed on a Hot Block heating system (Environmental Express Inc., Mount Pleasant, SC, USA) and heated at ~95 °C until the samples reached complete dryness. Wipes were a medium dark color when digested to dryness on this initial step. For filters, 2 ml of 30 wt% hydrogen peroxide and 2 ml of 1 M HF were then added to each digestion tube. For wipes, 0.5 ml of 15.7 HNO_3 was added and the tube was swirled to fully contact the wipe residue. Then 2 ml of 30 wt% hydrogen peroxide and 2 ml of 1 M HF were added to each wipe digestion tube. The digestion tubes were heated to dryness. For wipes, care was given to ensure the wipe residue was not overheated at dryness and to prevent charring and overheating at this step. A light color wipe residue was obtained at dryness by minimizing heating after dryness was reached. Five milliliters of 0.2 M HF–0.1 M HF was added to each tube and heated to dryness. Three milliliters of 0.2 M HF was added to each digestion tube and heated to dryness. Samples were redissolved in 10 ml of 0.2 M HF–0.1 M HCl, heating filters for ~6 min and wipes for ~8 min to redissolve.

2.2.3. Column separation

Fig. 2 shows a flow chart of the ion exchange method using Diphonix Resin® and TEVA Resin® cartridges. Fifty milliliters centrifuge tubes were used to collect rinse or final purified fractions. Each stacked Diphonix Resin®–TEVA Resin® column was conditioned using 8 ml of 0.2 M HF–0.1 M HCl. This solution was discarded. The redissolved filter or wipe samples in 10 ml of 0.2 M HF–0.1 M HCl were loaded onto the Diphonix Resin®–TEVA Resin® columns at ~1 drop per second and the purified solution was collected in labeled 50 ml tubes. The digestion vessel was rinsed well with 3 ml of 0.2 M HF–0.1 M HCl, capping the vessels and swirling vigorously. After the initial load solution has passed through the columns, the rinse solutions were added and allowed to drain at ~1 drop per second. Eight milliliters of 0.2 M HF–0.1 M HCl was added to each column and allowed to drain at ~1–2 drops per second. The tubes were removed and the volume was adjusted to 20 ml with deionized water. It should be noted that when samples analyzed on an ICP-AES without an HF resistant nebulizer the volume

Table 5
Be average recovery results (air filters)—interferences added

Emission line (nm)	Be added (ppb)	Be measured after IEX (ppb)	Recovery (%)	Bias (%)	R.S.D. (%)	After anion exchange	Recovery (%)	Bias (%)	R.S.D. (%)
234.861	5.00	4.76	95.11	−4.89	3.97	N/A	N/A	N/A	N/A
313.042	5.00	5.30	105.97	5.97	5.99	4.91	98.13	−1.87	3.85
313.107	5.00	5.18	103.53	3.53	4.72	4.94	98.87	−1.13	3.86

$N = 6$.

Table 6
BeO filter recovery results—interferences added

	BeO CRM filters		0.2 μg Be/filter		
		Be added (ppb)	Be measured after IEX (ppb) 234.861 nm	Recovery (%)	Bias (%)
1	BeO filter	10	8.35	83.50	−16.50
2	BeO filter	10	8.37	83.70	−16.30
3	BeO filter	10	8.44	84.40	−15.60
4	BeO filter	10	8.27	82.7	−17.30
Average				83.58	−16.42
%R.S.D.				0.84	
	BeO bias-No IEX		SRS F/H lab		−21.87
	BeO bias-No IEX		SRS EBL lab		−14.80

Table 7
Be recovery results at report limit—filters

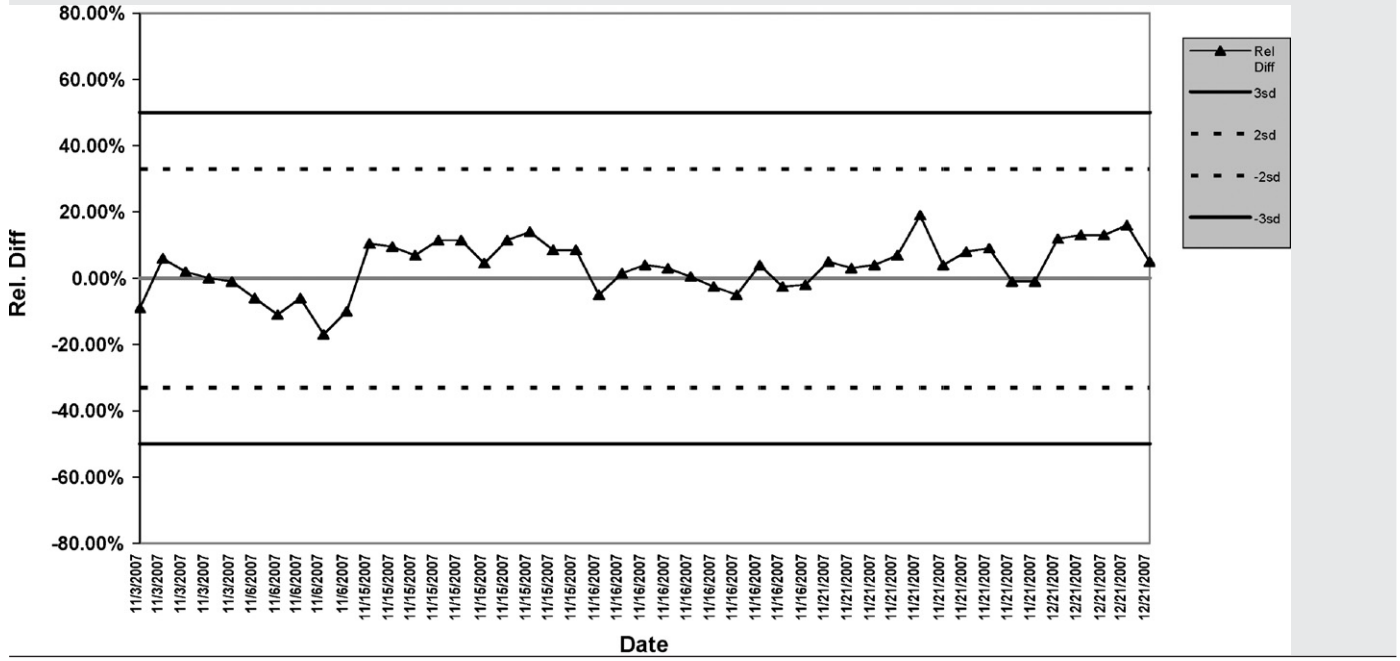

maybe adjusted to 20 ml with 0.8 M boric acid instead of water. Blanks were analyzed with the spiked samples but blank subtraction was not performed per typical protocol for beryllium analysis at SRS.

An additional anion exchange removal is not typically required. But if additional removal of chromium was needed, a 10 ml aliquot of the initial purified solution was evaporated to dryness in a digestion tube on the Hot Block system. Five milliliters of 0.2 M HF were added and evaporated to dryness. The samples were redissolved in 8 ml of 0.2 M HF, warming for ~5 min to redissolve each sample. Anion resin columns (2.8 ml resin) were placed on the vacuum box and conditioned by adding 5 ml of 0.2 M HF at ~1 ml/min. Redissolved samples were loaded to the Anion resin columns at ~1 ml/min. Three milliliters of 0.2 M HF was added to each digestion vessel to rinse the tube and this rinse was added to each column. Ten milliliters of 0.2 M HF were added to each column and allowed to drain at 1–2 ml/min. The rinse solutions were discarded and new labeled tubes were placed in the vacuum box. Be was eluted from the Anion resin using 10 ml of 1 M HCl–0.25 M HF at 1–2 ml/min.

2.3. Apparatus

A Hot Block heating system (Environmental Express, Mount Pleasant, SC) was used to digest filters and wipes at 95 °C. Polycarbonate vacuum boxes with 24 positions (Eichrom Technologies, Darien, IL, USA) and a rack to hold 50 ml plastic tubes were used. A

Table 8
Be recovery results at report limit—wipes

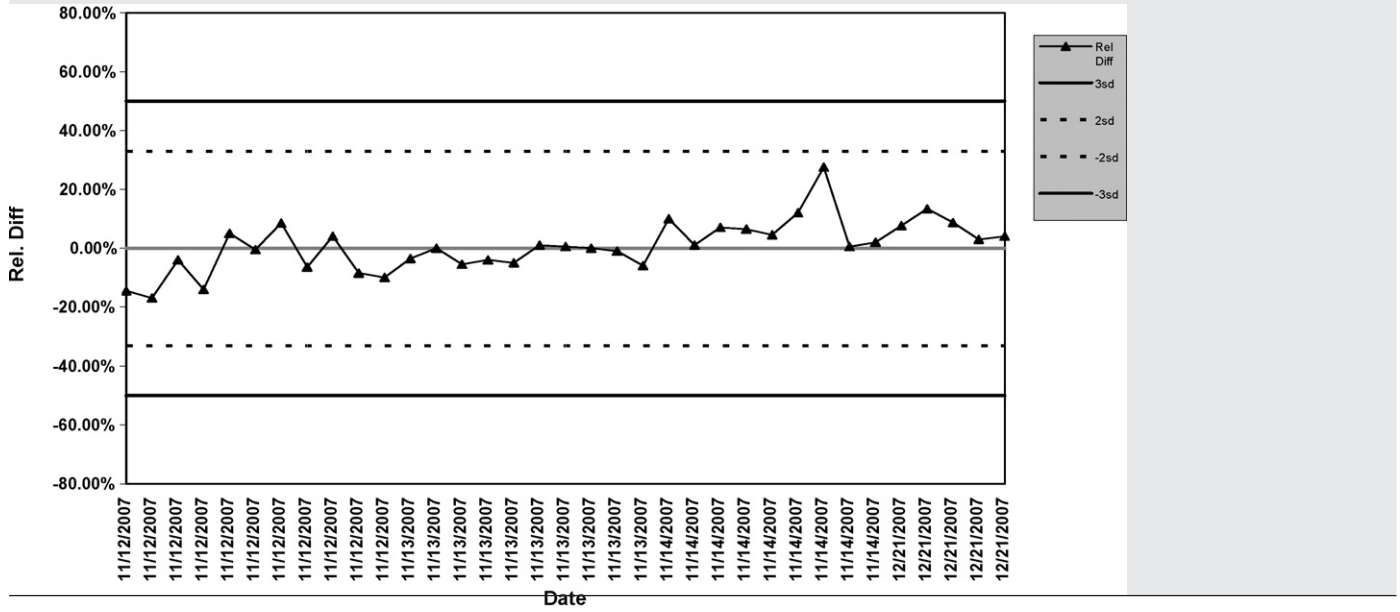

Perkin Elmer 3000 XL simultaneous axial ICP-AES with an echelle polychromator, segmented-array charge-coupled detector (SCD) cyclonic spray chamber, and low-flow GemCone™ (cross-flow) Nebulizer was used to perform the elemental measurements. The instrument operating conditions are given in Table 2. The acid matrix used for calibration standards was 2% HNO_3–5% HCl. A conditioning solution of 2% HNO_3–5% HCl–0.5% HF was applied to condition the sample introduction system prior to calibration. Matrix-matched blank solutions containing a 0.2 M HF–0.1 M HCl acid solution were also used in batch sequences to condition the ICP-AES prior to sample measurements.

3. Results and discussion

The results in Table 3 show the average spectral interference removal results for spiked Be wipes and filters. Spectral interference measurements were performed using the Perkin Elmer 3000 XL simultaneous axial ICP-AES, except for plutonium, which was measured using an Agilent 7500 inductively coupled mass spectrometer (Agilent Technologies, Tokyo, Japan). The interference levels added are based on a final dilution volume of 20 ml. The data in Table 3 shows that the removal for spectral interferences is very good. Uranium removal was 99.963% at the 300 ppm U level. Pu removal was greater than 99.999%. Chromium removal is shown with and without additional anion exchange. It should be noted that the 234.861 nm emission line for Be, which is not significantly impacted by Cr, can be used to measure Be with only minimal interference correction applied. Although its sensitivity is slightly less than the 313.042 nm and 313.107 nm emission lines, the customer-requested report limits (RL) of 0.01 μg Be per filter sample and 0.03 μg/wipe sample can be met using the 234.861 nm line when needed. Iron was also tested at the 2500 μg/ml level and was removed down to the same level of iron shown in this table. The iron removal is extremely efficient and makes the use of the 234.861 nm beryllium emission line feasible, since iron has a very adverse impact on the 234.861 nm line.

Table 4 shows the average Be Recovery results for spiked Be wipes based on 12 measurements using the 234.861 nm, 313.042 nm and the 313.107 nm emission lines. The interference levels added were based on a final dilution volume of 20 ml. Be was added at the 1 ppb level at the ICP-AES, equivalent to 0.02 μg Be/sample. The results using the 234.861 nm line were not affected by Cr levels shown in Table 1, with minimal interference correction applied. The performance limits for Be testing and accreditation by the American Industrial Hygiene Association (AIHA) are ±25%. The average Be recovery for the 234.861 nm line was 107.29%, with a relative standard deviation of 7.28%. The slight positive bias may be due to the uncertainty at this level close to the report limit, a minimal effect from the residual Cr or to the slightly different acid matrix (0.2 M HF–0.1 M HCl) from the calibration standards (2% HNO_3–5% HCl). This is well within the AIHA performance limits, however, even at this very low level. The Be results using the 313.042 nm and 313.107 nm lines show a significant positive bias due the residual Cr present (+59.75% and +61.25%, respectively), illustrating the bias effect that occurs at very low levels. After anion exchange to remove most of the residual Cr, the Be recoveries using the 313.042 nm and 313.107 nm lines were 105.50% and 117.61%, respectively, within performance limits.

Table 5 shows the average Be Recovery results for certified reference material Be air filters from High Purity Standards (Charleston, SC, USA) based on six measurements using the 234.861 nm, 313.042 nm and the 313.107 nm emission lines. The interference levels added were based on a final dilution volume of 20 ml. Be in these CRM air filters was 5.0 ppb level at the ICP-AES, equivalent to 0.10 μg Be/sample. The results using the 234.861 nm, 313.042 nm

Table 9
Summary of MDL and RL results for Be filter method

Analyzed	17 October 2007	17 October 2007	17 October 2007	15 November 2007	15 November 2007	15 November 2007	16 November 2007	16 November 2007	16 November 2007
ppb	1	1	1	1	1	1	1	1	1
Be emission line, nm	234.861	313.042	313.107	234.861	313.042	313.107	234.861	313.042	313.107
Average	1.12206	1.07341	1.02602	1.46648	0.80707	1.09679	1.12479	0.99870	0.99605
Standard Deviation	0.031843	0.038831	0.036713	0.049504	0.040893	0.026412	0.031859	0.046317	0.034562
MDL, ppb Be	0.090	0.110	0.104	0.140	0.115	0.075	0.090	0.131	0.097
Report limit [MDL × 5], ppb Be	0.449	0.548	0.518	0.698	0.577	0.373	0.449	0.653	0.487
Report limit [MDL × 5 × 0.020 l], μg Be/filter	0.009	0.011	0.010	0.014	0.012	0.007	0.009	0.013	0.010

$N = 10$.

Table 10
Summary of MDL and RL results for Be wipes method

Analyzed	13 November 2007	13 November 2007	13 November 2007	14 November 2007	14 November 2007	14 November 2007
ppb	1	1	1	1	1	1
Be emission line, nm	234.861	313.042	313.107	234.861	313.042	313.107
Average	0.96218	1.02472	0.97656	1.05410	1.05407	1.07881
Standard Deviation	0.033457	0.029333	0.026731	0.095662	0.094815	0.083318
%Recovery	96.218	102.472	97.656	105.41	105.41	107.88
MDL, ppb Be	0.094	0.083	0.075	0.277	0.275	0.241
Report limit [MDL × 5], ppb Be	0.472	0.414	0.377	1.385	1.373	1.206
Report limit [MDL × 5 × 0.020 l], μg Be/wipe	0.009	0.008	0.008	0.028	0.027	0.024

and 313.107 nm lines were not significantly affected by Cr levels shown in Table 1, with minimal interference correction applied. The average Be recovery for the 234.861 nm line was 95.11%, with a relative standard deviation of 3.97%. The average Be recovery for the 313.042 nm line was 105.97%, with a relative standard deviation of 5.99%. The average Be recovery for the 313.107 nm line was 103.53%, with a relative standard deviation of 4.72%. This is well within the AIHA performance limits, even at this very low level. After anion exchange to remove most of the residual Cr, the Be recoveries using the 313.042 nm and 313.107 nm lines are 98.13% and 98.87%, respectively, also well within performance limits.

Table 6 shows the average Be Recovery results for CRM BeO filters from High Purity Standards (Charleston, SC, USA) based on four measurements using the 234.861 nm emission line at the 0.2 μg Be/filter level. The average Be bias was −16.42% using the new ion exchange method, with a relative standard deviation of 0.84%. These results are within the AIHA performance limits of ±25%. The routine SRS digestion method does not use ion exchange. This routine method also shows a negative bias in two different labs at SRS, indicating a problem with the digestion of BeO itself or the CRM BeO filters. The SRS F/H Lab has seen an average negative bias of −21.87% and the SRS EBL lab has seen a negative bias of −14.80% using the routine method. This data supports that the problem is not with the ion exchange separation, but instead with the difficulty in completely digesting BeO. It is important to note, however, that the BeO results using this method meet the AIHA performance limits of ±25%.

Table 7 summarizes Be spike recovery results at or near the report limit of 0.01 μg Be/filter, using the 313.107 nm line, without interferences added, analyzed using the ion exchange method. The plot includes data at the 0.01 μg Be and 0.02 μg Be/filter levels. The average bias for 20 data points at the 0.01 μg Be/filter level was 2.56% with a 8.96% relative standard deviation. The average bias for 25 data points at the 0.02 μg Be/filter level was 4.65% with a 6.0% relative standard deviation. The administrative control limits shown in Table 7 for results near the report limit were set at ± 50% (± 3 S.D.).

Table 8 summarizes Be spike recovery results at or below the report limit of 0.03 μg Be/wipe, using the 313.107 nm line, without interferences added, analyzed using the ion exchange method. The plot includes data from the 0.02 μg Be and 0.03 μg Be/wipe levels. The average bias for 29 data points at the 0.02 μg/wipe level, less than the 0.03 μg/wipe report limit, was 0.45% with an 8.8% relative standard deviation. The average bias for 5 data points at the 0.03 μg/wipe level was 7.33% with a 4.2% relative standard deviation. The administrative control limits shown in Table 8 for results near the report limit were set at ± 50% (± 3 S.D.).

Table 9 summarizes method detection limit and report limit data for filters, while Table 10 summarizes the MDL and RL data for wipes. The data shows that the required Be filter report limit of 0.01 μg Be/filter and the Be wipes report limit of 0.03 μg Be/wipes can be met using the new ion exchange method. The method detection limit was calculated by measuring the standard deviation of the measurement at 1 ppb Be and multiplying that value times the *t*-table value for 9° of freedom. The report limit for the method was calculated by multiplying the MDL by a factor of five. The report limit per sample was calculated by multiplying the RL (ppb) by the 0.02 l dilution volume.

The ion exchange steps using Diphonix Resin® and TEVA Resin® take about 1–1.5 h for a batch of 20 samples. If the additional anion resin separation is required to lower Cr levels, an additional 1.5 h of ion exchange time is required after about ∼2 h evaporation step. It is anticipated that the anion resin separation will only be used rarely, but it is available if needed. The filtering of the samples through ion exchange also filters out any residual organic material which can clog the ICP-AES nebulizer. By performing the ion exchange, accuracy and precision at very low levels of Be are very good, often with less errors associated with spectral interference corrections, which are effective but sometimes have large uncertainties.

Samples may also be analyzed by the ICP-AES first to see whether ion exchange is required. If a 10 ml aliquot (out of an initial 20 ml digest volume) is later reprocessed for ion exchange removal of interferences, an additional evaporation step to lower the final volume after ion exchange back to 10 ml may be required to maintain a report limit of 0.01 μg Be/sample or less.

Be measurement is typically performed by comparing all three emission lines to ensure there are no adverse impact due to spectral interferences. The 313.107 nm and 313.042 nm lines are preferred due to higher sensitivity, but this work shows that the 234.861 nm emission line can be used if necessary to meet the 0.01 μg/sample target limit set for this work.

Although more expensive to operate than ICP-AES, inductively coupled mass spectrometry provide even lower detection limits than ICP-AES. Inductively coupled plasma mass spectrometry (ICP-MS) is such a sensitive analytical technique that introducing high levels of other metals found on surface wipes is often not desired [3]. The new ion exchange method can also likely be applied to Be assay by inductively coupled plasma mass spectrometry to prevent introduction of high levels of metallic impurities into the ICP-MS.

The spectral interference removal was found to be highly effective using a simple pass-through approach to remove a wide range of spectral interferences. Only chromium showed any significant levels after applying the single pass Diphonix Resin®–TEVA Resin® approach. An additional anion exchange separation was demonstrated to lower Cr such that beryllium measurements could be accurately made at very low levels, but it was shown when the 234.861 nm beryllium line was used the additional anion exchange removal step was not required. The previous report limit capability for Be in air filters and wipes was 0.05 μg/sample. As a result of the new ion exchange method developed at SRS, the capability has been significantly improved, lowering the air filter report limit to 0.01 μg/filter and 0.03 μg/wipe.

4. Conclusions

A new method has been developed to remove spectral interferences prior to beryllium (Be) measurement by inductively coupled plasma atomic emission spectrometry. The method is a simple, single pass method that effectively removes spectral interferences and allows accurate low level Be measurement using ICP-AES. The ion exchange separation removes uranium (U), plutonium (Pu), thorium (Th), niobium (Nb), vanadium (V), molybdenum (Mo), zirconium (Zr), tungsten (W), iron (Fe), chromium (Cr), cerium (Ce), erbium (Er) and titanium (Ti). A stacked column consisting of Diphonix Resin® and TEVA Resin® reduces the levels of the spectral interferences so that accurate low level Be measurements can be performed. If necessary, an additional anion exchange separation can be used for further removal of interferences, particularly chromium. The method has been tested using spiked filters, spiked wipe samples and certified reference material standards with high levels of interferences added. The method provides a high level of removal for spectral interferences with very good accuracy and precision for beryllium. The ion exchange method can also be applied to Be assay by inductively coupled plasma mass spectrometry to prevent introduction of high levels of metallic impurities into the ICP-MS.

Acknowledgments

This work was performed under the auspices of the Department of Energy, DOE Contract No. DE-AC09-96SR18500. The authors wish to acknowledge William P. Baker, Roslyn Cooke, Erika Lee, Marcia Gibson, Matt Hammett, Perry Miller, James Pearre and Shirley Riley for their assistance with this work.

References

[1] T.P. Taylor, et al., J. Environ. Sci. Health A: Environ. Sci. Eng. Toxicol. Hazard Subst. Control A 38 (2003) 439.
[2] E. Philip Horwitz, et al., Talanta 67 (2005) 873.
[3] M.J. Brisson, et al., J. Environ. Monit. 8 (2006) 605.
[4] U.S. Code of Federal Regulations, Fed. Regist., 64 (8th December), 1999, 68854.
[5] E. Philip Horwitz et al., Enhanced Beryllium Sample Preparation: How To Improve The Results Of The Instrument You Already Have, Pittcon 2006, Orlando, FL, March 13, 2006.
[6] Mary Gopalkrishnan, et al., Talanta 44 (1997) 169–176.
[7] E. Philip Horwitz, et al., Solvent Extr. Ion Exc. 11 (1993) 943.
[8] E. Philip Horwitz, et al., Solvent Extr. Ion Exc. 11 (1993) 967.
[9] E. Philip Horwitz, et al., Sep. Sci. Technol. 32 (1997) 1.
[10] S.L. Maxwell III, et al., J. Radioanal. Nucl. Chem. 250 (1) (2001) 117.
[11] S.L. Maxwell III, Separation and Preconcentration of Actinides by Extraction Chromatography Using a Supported Liquid Anion Exchanger: Application to the Characterization of High-level Nuclear Waste Solutions, Co-authors: E. Philip Horwitz, M.L. Dietz, R. Chiarizia, H. Diamond from Argonne National Lab; Matthew Nelson from WSRC, Analytica Chimica Acta, 310 (1995) 63.
[12] J.P. Faris, Anal. Chem. 32 (1960) 520.
[13] L. Danielson, Acta Chem. Scand. 19 (1965) 5.
[14] K.A. Kraus, et al., J. Am. Chem. Soc. 77 (1955) 3972.
[15] K.A. Kraus, et al., J. Am. Chem. Soc. 82 (1960) 339.
[16] Z. Szeglowski et al., Study on Adsorption of Zr, Hf and Nb as Homoloques of Super-Heavy Elements on the Films Prepared on Some Liquid Ion Exchangers on the Surface of Some Foils, Report No. 1918/C, The Henryk Niewodniczanski Institute of Nuclear Physics, January 2003, www.ifj.edu.pl/reports/2002.html.
[17] J. Braz, et al., J. Braz. Chem. Soc. 15 (1 (January/February)) (2004).

Available online at www.sciencedirect.com
ScienceDirect
Talanta 76 (2008) 241–245
Talanta
www.elsevier.com/locate/talanta

Simultaneous determination of inorganic anions and cations in explosive residues by ion chromatography

Hong-Bo Meng [a,c], Tian-Ran Wang [b], Bao-Yuan Guo [b], Yuki Hashi [b], Can-Xiong Guo [a], Jin-Ming Lin [c,*]

[a] *Faculty of Science, Beijing University of Chemical Technology, Beijing 100029, China*
[b] *State Key Laboratory of Environmental Chemistry and Ecotoxicology Research Center for Eco-Environmental Sciences, Chinese Academy of Sciences, P.O. Box 2871, Beijing 100085, China*
[c] *Department of Chemistry, Tsinghua University, Beijing 100084, China*

Received 11 November 2007; received in revised form 22 January 2008; accepted 25 January 2008
Available online 5 February 2008

Abstract

A non-suppressed ion chromatographic method by connecting anion-exchange and cation-exchange columns directly was developed for the separation and determination of five inorganic anions (sulfate, nitrate, chloride, nitrite, and chlorate) and three cations (sodium, ammonium, and potassium) simultaneously in explosive residues. The mobile phase was composed of 3.5 mM phthalic acid with 2% acetonitrile and water at flow rate of 0.2 mL/min. Under the optimal conditions, the eight inorganic ions were completely separated and detected simultaneously within 16 min. The limits of detection (S/N = 3) of the anions and cations were in the range of 50–100 μg/L and 150–320 μg/L, respectively, the linear correlation coefficients were 0.9941–0.9996, and the R.S.D. of retention time and peak area were 0.10–0.29% and 5.65–8.12%, respectively. The method was applied successfully to the analysis of the explosive samples with satisfactory results.

Keywords: Non-suppressed ion chromatography; Simultaneously; Inorganic explosive residues; Phthalic acid

1. Introduction

Ion chromatography (IC) was an important technique for the ionic compound determination. IC has excellent repeatability and extensive appliance in water quality controlling [1–5], atmosphere monitoring [6], food security [7–9], pharmaceutical [10–12], including forensic science [13,14].

Simultaneous determination of inorganic ions was very important to meet the need of real field determination. However, in most cases, anions and cations are usually determined separately using different separation systems with different types of columns and conditions. The determination of anions and cations needs more time to balance the two different columns. Thus, data on the ionic composition of a sample can be obtained either by two parallel analyses on two different ion chromatographs, or by two consecutive analyses of the same sample with one instrument but with different columns and under different eluent conditions. Sometime, the amount of samples, such as the real field samples or the bio samples, was slightness not enough to be determined under twice runs. Therefore, the IC methods for the simultaneous determination both anions and cations were developed in the recent years by connecting two columns in series via a single six-port switching valve [15–17], or assembling two switching six-port valves and two detectors on flow system with two ion-exchange columns for the determination of both anions and cations [18]. Although the method which directly connected ion-exclusion/cation-exchange columns was reported in some papers [19–21], the method of directly connecting anion exchange/cation exchange in the determination was less reported. It was difficult to choose one single proper eluent for the two columns connected sequentially.

Other methods were available to determine inorganic explosive residues, such as capillary electrophoresis [13,14,22], and traditional chemical method [23]. Capillary electrophoresis has limits of poor reproducibility and sensitivity, and traditional chemical method is easily interfered by other ions existing in the

* Corresponding author. Tel.: +86 10 62792343; fax: +86 10 62792343.
E-mail address: jmlin@mail.tsinghua.cn (J.-M. Lin).

0039-9140/$ – see front matter © 2008 Published by Elsevier B.V.
doi:10.1016/j.talanta.2008.01.054

sample matrix and of low credibility and accuracy. Hence, ion chromatography was the suitable analytical method to determine inorganic ions.

In recent years, increasing illegal uses of inorganic explosives have been observed. These inorganic explosive are easy to be synthesized, the starting materials such as inorganic salt are readily available at low cost and with excellent performance. Hence, the inorganic explosive has extensive application in different fields including industry, agriculture, irrigation military and so on. At the same time, occurrences of many explosions including terroristic explosions were also caused by inorganic explosive.

The most widely used inorganic explosives in the world were ammonium nitrate explosive, potassium chlorate explosive and black powder. After the blast of these inorganic explosives, some major ion residues of these explosives left behind from the blast. The residue ions of ammonium nitrate were mostly NO_3^- and NH_4^+; the residue ions of potassium chlorate explosive mostly were Cl^-, ClO_3^-, K^+, Na^+; the residue ions of black powder mostly were K^+, Na^+, NO_3^-, SO_4^{2-}. The species of ions are the most important evidence used to identify the nature and source of the explosive. Hence, it is necessary to find out a method that can determine the ions and then to deduce the type of inorganic explosive.

In the present study, simultaneous determination of inorganic explosive residue ions by anion-exchange column and cation-exchange column connected directly in series without any switch valves was established. This method was successfully applied to determine the real samples, which was very important for evaluating the type of inorganic explosive. This method was simple, sensitive and cost-effective, and it could be applied in other areas.

2. Experimental

2.1. Apparatus

The separation of the inorganic explosive residues was performed on the Shimadzu (Kyoto, Japan) PIA-1000 with the following devices: column oven, one pump, manual 10 μL injector and non-suppressed conductivity detector. The PIA-1000 is suitable for real-time determination of real sample in explosion site or installation at location with limited space due to its low weight (15 kg), small cubage (26 cm × 42 cm × 30 cm) and supplied powder by dc battery or automobile battery. The chromatography data were saved directly onto a floppy disk and then processed using Shimadzu Class-VP software (Version 6.13 SP1). Anion-exchange/cation-exchange simultaneous chromatography separation of anions and cations was carried out using Shim-pack IC-A3 column (i.d. 150 mm × 4.6 mm, 5 μm particle size, functional group was quaternary ammonium group that has hydrophobic characteristics) and shim-pack IC-C3 column (i.d. 100 mm × 2.0 mm, 7 μm particle size, functional group was hydroxyl group that has hydrophilic characteristics) directly connected in series as shown in Fig. 1. The experimental conditions for ion chromatography were as follows: column temperature: 35 °C, eluent flow rate: 0.2 mL/min, injection volume: 10 μl, detector polarity: +.

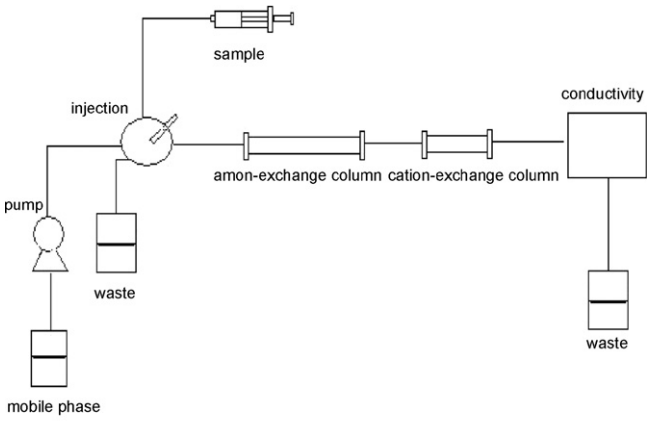

Fig. 1. Experiment apparatus. Anion-exchange/cation-exchange columns directly connected in series.

2.2. Reagents

All chemicals used for the preparation of standard solutions of desired anions, cations and eluent (phthalic acid) were of analytical grade or higher. Methanol and acetonitrile used are of HPLC grade. The stock solution was prepared by dissolving these agents in methanol. And then, this solution was diluted to the desired concentration. All standard solutions were stored in 100 mL volumetric flask and kept under refrigeration at 4 °C. Deionized water (>18 MΩ) was used for the preparation of standard solutions and eluent. The mobile phase consisted of 3.5 mM phthalic acid with 2% acetonitrile as the additive, pH adjusted by Tris, and it was degassed in ultrasonic bath for 20 min before use. The real sample analyzed was provided by Ministry of Public Security of the People's Republic of China, and was filtered by 0.45 μm filters before analysis.

3. Result and discussion

3.1. Eluent conditions

In non-suppressed ion chromatography, weak acids were usually employed as the eluent for simultaneous separation of anions and cations for their low background conductivity. Some weak acids, such as phthalic acid [7], sulfosalicylic acid [16,19], tartaric acid [17], were commonly used in non-suppressed system as the eluent for simultaneous determination of anions and cations.

In the present study, the group of anion-exchange column functional was hydrophobic, and that of cation-exchange column functional was hydrophilic. If the eluent had no hydrophobic group, the anion-exchange column cannot adsorb the eluent for ion exchange with inorganic anions, and the same reason is for cation-exchange column. Therefore, the eluent of both hydrophobic group and hydrophilic group should be chosen. Phthalic acid has been chosen as the eluent to determine anions

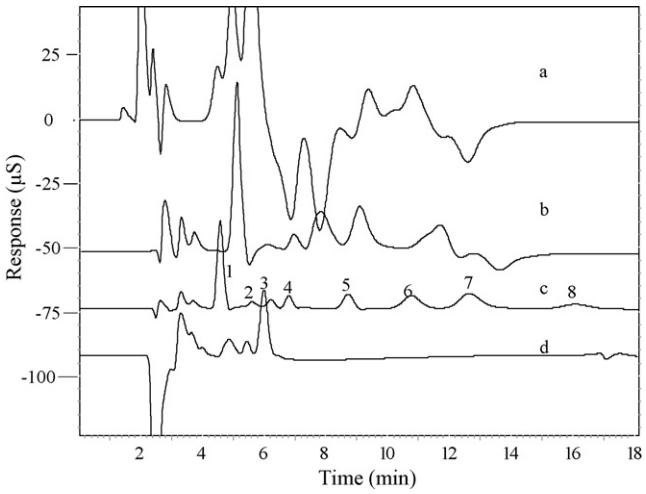

Fig. 2. Effect of eluent pH. Column: shim-pack ICA3 (150 mm × 4.6 mm i.d.) and shim-pack IC-C3 (100 mm × 2 mm i.d.). Column temperature: 35 °C. Inject volume: 10 μl. Eluent flow rate: 0.2 mL/min. (a) pH 3.0, (b) pH 3.5, (c) pH 4.0 and (d) pH 4.5. Peak identities: (1) Cl^-, (2) NO_2^-, (3) ClO_3^-, (4) NO_3^-, (5) SO_4^{2-}, (6) Na^+, (7) NH_4^+ and (8) K^+.

and cations simultaneously, considering that phthalic acid contains strong hydrophobic benzene ring and hydrophilic hydroxyl group.

3.2. Effect of pH of eluent

The pH of eluent was the most important factor to separate and determine inorganic anions and cations, especially polycarboxylic acids as the eluent. The exchangeable ions of eluent depend on pH, since the eluents for non-suppressed ion chromatography were hydroxy acid that mostly possess several pK_a values. Under different pH, hydroxy acid ions appear to be different ionic species, which offer different ion-exchange abilities. Therefore, the adjusting pH could control the quantity of the exchangeable ions of the eluent. The pH affects both the retention time and resolution of ions, especially for divalent ions. Phthalic acid was a binary weak acid, which has two pK_a's (pK_{a_1} = 2.95, pK_{a_2} = 5.41). In the present study, the pH range of 3–5 was investigated according to the pH tolerance range of the columns (pH 3–7 for the anion-exchange column, and pH 2–5 for cation-exchange column). As shown in Fig. 2, when pH of the eluent was 3.0, two big system peaks appeared, peaks hard to identify and possess poor resolution. With the increase in the pH, peak shapes and resolutions improved. However, when pH was higher than 4.5, ions peaks overlapped and the resolution and peak shape become poorer than those under pH 4.0. Therefore, pH 4.0 was selected in the following experiments.

3.3. Effect of phthalic acid concentration

The effect of phthalic acid concentration in eluent on the retention time of anions and cations was investigated as well. As shown in Fig. 3, SO_4^{2-} could be eluted by the eluent, until the phthalic acid concentration was higher than 2.5 mM. With the concentration of phthalic acid increasing, the retention time

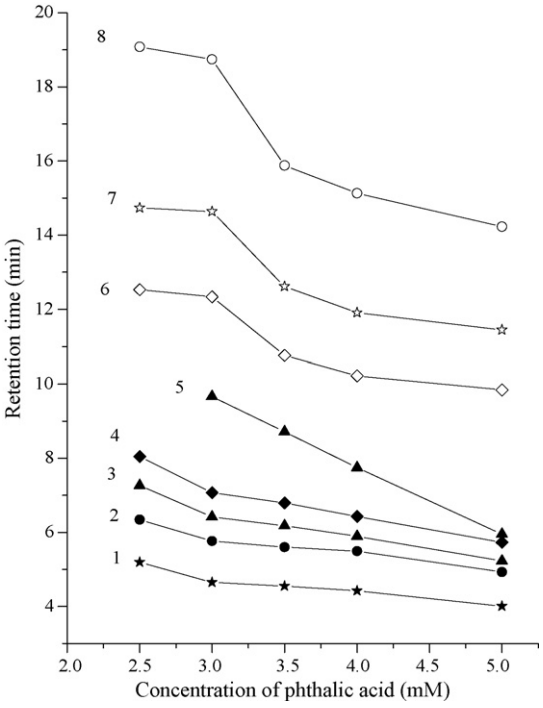

Fig. 3. Effect of phthalic acid concentration on retention time of inorganic ions.

of ions decreased, especially for the divalent ions SO_4^{2-}, which was more influenced by the ion-exchange effect. At the same time, the resolution of inorganic ions also decreased as the phthalic acid concentration increased. In conclusion, the retention time and resolution of anions and cations both decreased with the increase of the phthalic acid concentration. The peak of inorganic cations was wider than that of anions because the phthalic acid of ion-exchange ability for cations was not strong as anions.

The background conductance increased with concentration of phthalic acid in the eluent (231 μS/cm for a 2.5 mM eluent, 261 μS/cm for a 3 mM eluent, 296 μS/cm for a 3.5 mM, 329 μS/cm for a 4 mM eluent, and 399 μS/cm for a 5 mM eluent). The increase of the phthalic acid concentration of the phthalic acid caused decrease in the sensitivity of conductivity detection. Therefore, the low phthalic acid concentration should be chosen. Taking the retention time, the resolution and the sensitivity into consideration, the optimal concentration of phthalic acid was 3.5 mM. The corresponding chromatography was shown in Fig. 4.

3.4. Effect of additive in the mobile phase

Some organic solvents, such as acetonitrile, methanol, can effectively improve resolution, peaks shape and retention time. Addition of eluent has been known to be very effective to improve resolutions and peaks shape. The influence of acetonitrile on the retention time of anions and cations was also investigated in the present work. Acetonitrile can occupy the hydrophobic position of ion-exchange resin, and reduce the non-ion-exchange reaction of target inorganic ions and ion-exchange resin, at the same time; acetonitrile possesses hydrophobic char-

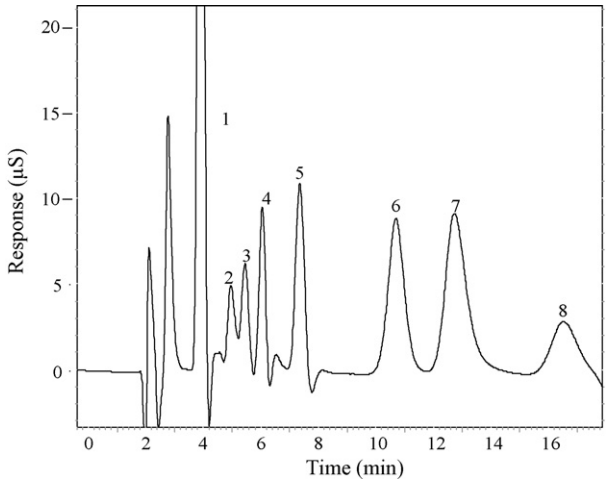

Fig. 4. Anion-exchange/cation-exchange chromatography of inorganic ions by eluent with 3.5 mM phthalic acid. pH:4.0; (1) Cl^-, (2) NO_2^-, (3) ClO_3^-, (4) NO_3^-, (5) SO_4^{2-}, (6) Na^+, (7) NH_4^+ and (8) K^+. Other conditions are as in Fig. 2.

acter, and increases the hydrophobicity of eluent [24]. The resolution, peaks shape and retention time were affected by the two factors simultaneously. As shown in Fig. 5, the retention time of cations became more shorter, and the retention time of anions became more longer. Resolution and peaks shape of anions and cations all became more and more better along with the increasing acetonitrile volume. Acetonitrile has no significant effect on retention time of monovalent anions and cations, but the divalent anion SO_4^{2-} increased significantly. When acetonitrile was added to 8% (v/v), SO_4^{2-} and Na^+ were not

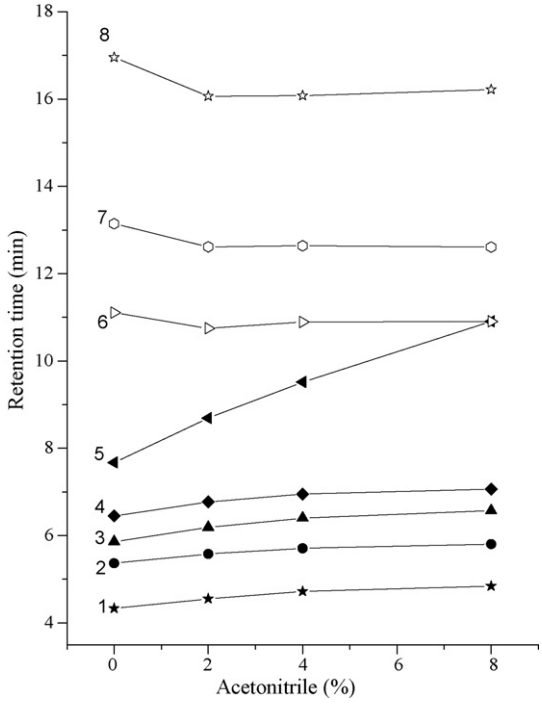

Fig. 5. Effect of volume percentage acetonitrile in 3.5 mM phthalic acid eluent on retention time of inorganic ions. (1) Cl^-, (2) NO_2^-, (3) ClO_3^-, (4) NO_3^-, (5) SO_4^{2-}, (6) Na^+, (7) NH_4^+ and (8) K^+. Other conditions are as in Fig. 2.

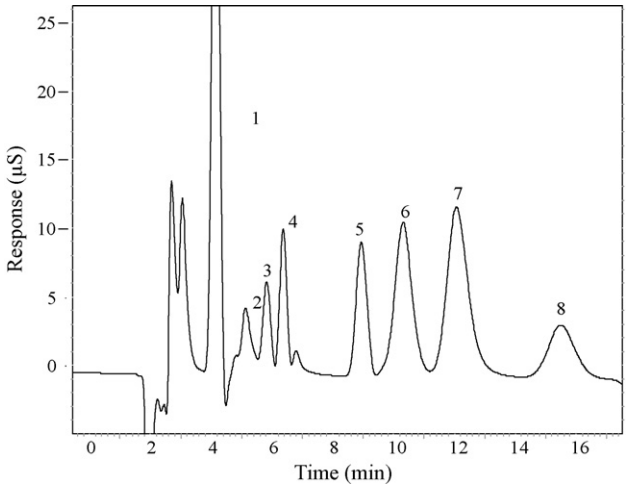

Fig. 6. Anion-exchange/cation-exchange chromatography of inorganic ions by eluent with 3.5 mM phthalic acid, 2%acetonitrile, anion-exchange/cation-exchange connect order. Eluent pH: 4.0; (1) Cl^-, (2) NO_2^-, (3) ClO_3^-, (4) NO_3^-, (5) SO_4^{2-}, (6) Na^+, (7) NH_4^+ and (8) K^+. Eluent conductivity: 293 μS/cm. Other conditions are as in Fig. 2.

separated. Hence, 2% acetonitrile was added in the eluent as the optimal amounts of additive.

3.5. Effect of the order of ion-exchange columns in series

The order of the columns connected has slight effect on the peak shapes, but has no effect on retention time. The cation-exchange column connects follow anion-exchange column show slightly better performance on peak shape than vice versa. Two types connect have similar retention time. The cations slightly retained in anion-exchange column and passed thorough the anion-exchange column quickly. The anions have the same retention behavior in cation-exchange column. Hence, the order of ion-exchange columns connect was not the major factor influence separate and determine inorganic ions. The cation-exchange column follow anion-exchange column was chosen in this study.

As shown in Fig. 6, simultaneous determination of inorganic anions and cations by connecting anion-exchange/cation-exchange columns was obtained within 16 min using an eluent composed of 3.5 mM phthalic acid, 2% acetonitrile, pH 4.0.

3.6. Analytical performance characteristics

The calibration graphs of these anions and cations were obtained by plotting peak areas versus concentration at the optimal conditions of anion-exchange/cation-exchange chromatography system. The concentration of anions and cations were in the range of 0.1–20 mg/L for anions and cations (NO_2^-, ClO_3^-, NO_3^-, SO_4^{2-}, NH_4^+, K^+), and 0.28–57.6 mg/L for Cl^-, 0.16–32.60 mg/L for Na^+, as shown in Table 1. The limits of detection (LODs, S/N = 3) and recovery were also given in Table 1. The reproducibility was evaluated by six consecutive runs at the concentration of 5 mg/L. The R.S.D. of retention time and peak area were 0.10–0.29% and 5.65–8.12%, respectively. The poorer reproducibility for peak

Table 1
LODs, correlation coefficient (r^2) and the retention time (t_R) of anions and cations obtained from the optimum chromatography condition as in Fig. 6

Analyte	LODs (μg/L)	r^2	t_R (min)	Recovery (%)
Cl^-	115	0.9972	4.63	108
NO_2^-	300	0.9984	5.66	104
ClO_3^-	300	0.9989	6.30	94.8
NO_3^-	50	0.9984	6.87	104
SO_4^{2-}	70	0.9996	8.82	109
Na^+	320	0.9989	10.65	91
NH_4^+	150	0.9994	12.47	82
K^+	300	0.9941	15.82	109

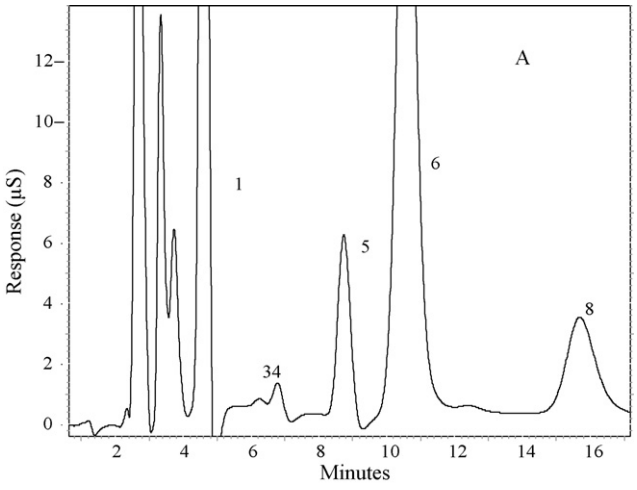

Fig. 7. Anion-exchange/cation-exchange chromatography of anions and cations in the inorganic explosive residues from Ministry of Public Security of the People's Republic of China. Other conditions are as in Fig. 2.

areas was because of the manual injection and inaccurate integration.

3.7. Application to inorganic explosive residues

The validated method was successfully applied to the simultaneous separation and determination of inorganic explosive residues. It is important for forensic analysis to evaluate the types of explosives. Fig. 7 illustrates the chromatogram of explosive residues taken from several explosion sites by Ministry of Public Security of the People's Republic of China, major anions and cations (Cl^-, NO_3^-, SO_4^{2-}, Na^+ and K^+) were determined in these samples. The nature of NO_2^- is instable, so the content of NO_2^- in the soil is too slightly to be detected. The data for three samples are summarized in Table 2.

Table 2
Determination of major anions and cations concentration in inorganic explosive residues ($n = 3$)

Analyte	Inorganic explosive residues (mg/L)		
	Sample 1	Sample 2	Sample 3
Cl^-	19.926 (±0.52%)	1.787 (±0.36)	26.427 (±0.42)
NO_2^-	n.d.[a]	n.d.	n.d.
ClO_3^-	0.462 (±0.32%)	n.d.	n.d.
NO_3^-	0.764 (±0.07%)	4.142 (±0.09)	71.269 (±0.05)
SO_4^{2-}	6.051 (±0.56%)	14.096 (±0.5)	42.303 (±0.61)
Na^+	38.589 (±0.62%)	3.382 (±0.71)	22.259 (±0.59)
NH_4^+	n.d.	1.312 (±0.37)	n.d.
K^+	7.837 (±0.26%)	1.731 (±0.38)	10.470 (±0.37)

[a] Not detected.

4. Conclusion

Anion-exchange column and cation-exchange column were connected directly for the simultaneous separation and determination of anions and cations which was usually found in inorganic explosive. The optimized eluent containing 3.5 mM phthalic acid, 2% acetonitrile, pH 4.0, showed good performance for the simultaneous determination of anions and cations of the inorganic explosive residues within 16 min. The methods developed could meet the need of the simultaneous determination of the field conditions, as a portable IC instrument was used in the present investigation.

References

[1] Z.L. Chen, M. Megharaj, R. Naidu, Talanta 72 (2007) 1842.
[2] Y.J. Liu, S.F. Mou, Microchem. J. 75 (2003) 79.
[3] R. Li, W.L. Lee, T. Takeuchi, Talanta 72 (2007) 1625.
[4] P. Miskaki, E. Lytrad, L. Kousouris, P. Tzoumerkas, Desalination 213 (2007) 182.
[5] K. Zhang, Y.S. Wang, T.X. Wen, Y. Meslmani, F. Murray, Atmos. Res. 84 (2007) 67.
[6] K.J. Yoshkawa, M. Okamura, M. Inokuchi, S. Akio, Talanta 72 (2007) 305.
[7] S.N. Walford, J. Chromatogr. A 956 (2002) 187.
[8] Z. Yan, Y.Y. Guo, M.L. Ye, F.S. James, J. Chromatogr. A 1085 (2005) 143.
[9] Z.F. Chen, B.W. Darvell, V.W.-H. Leung, Arch. Oral Biol. 49 (2004) 863.
[10] L. Valentin-Blasini, B.C. Blount, A. Delinsky, J. Chromatogr. A 1155 (2007) 40–46.
[11] B.S. Yu, Q.G. Yuan, L.H. Nie, S.Z. Yao, J. Pharm. Biomed. 25 (2001) 1027–1032.
[12] H.E. Aribi, Y.J.C.L. Blanc, S. Antonsen, T. Sakuma, Anal. Chim. Acta 567 (2006) 39.
[13] J.M. Doyle, B.R. McCord, J. Chromatogr. B 714 (1998) 105.
[14] T. Kishi, J. Nakamura, H. Arai, Electrophoresis 19 (1998) 3.
[15] S.R. Aari-Nordhaus, J.M. Anderson Jr., J. Chromatogr. 549 (1991) 257.
[16] R. Saari-Nordhaus, L. Nair, J.M. Anderson Jr., J. Chromatogr. 602 (1992) 127.
[17] A. Muhammad, W.L. Lee, T. Toyohide, Talanta 71 (2007) 1470.
[18] K.J.B.A. Karim, J.Y. Jin, T. Takeuchi, J. Chromatogr. A 995 (2003) 153.
[19] K. Tanaka, K. Ohta, P.R. Haddad, J.S. Fritaz, A. Miyanaga, W.Z. Hu, K. Hasebe, J. Chromatogr. A 884 (2000) 167.
[20] M. Mori, K. Tanaka, M.I.H. Helaleh, Q. Xu, M. Ikedo, Y. Ogura, S. Sato, W.Z. Hu, K. Hasebe, P.R. Haddad, J. Chromatogr. A 997 (2003) 219.
[21] M. Mori, K. Tanaka, T.I.M. Satori, W.Z. Hu, H. Itabashi, J. Chromatogr. A 1118 (2006) 51.
[22] J.P. Hutchinson, C.J. Evenhuis, C. Johns, A.A. Kazarian, M.C. Breadmore, M. Macka, E.F. Hilder, R.M. Guijt, G.W. Dicinoski, P.R. Haddad, Anal. Chem. 79 (2007) 7005.
[23] E.T. Urbansky, Crit. Rev. Anal. Chem. 30 (2000) 311.
[24] X.J. Ding, S.F. Mou, J. Chromatogr. A 897 (2000) 205.

Talanta 76 (2008) 338–346

Contents lists available at ScienceDirect

Talanta

journal homepage: www.elsevier.com/locate/talanta

A simple and rapid high performance liquid chromatographic method with fluorescence detection for the estimation of fexofenadine in rat plasma—Application to preclinical pharmacokinetics

Shriram M. Pathak*, A. Ranjith Kumar, P. Musmade, N. Udupa

Department of Pharmaceutical Quality Assurance, Manipal College of Pharmaceutical Sciences, Manipal-University, Manipal 576104, Karnataka, India

ARTICLE INFO

Article history:
Received 29 January 2008
Received in revised form 29 February 2008
Accepted 29 February 2008
Available online 13 March 2008

Keywords:
Fexofenadine
Bioanalytical method validation
Rat plasma
Preclinical pharmacokinetics

ABSTRACT

A sensitive high performance liquid chromatographic (HPLC) method involving fluorescence detection was developed for the determination of fexofenadine (FEX), known to have low oral bioavailability, in rat plasma. In order to understand the effect of various chromatographic factors on the separation of analytes and to simultaneously optimize the resolution and analysis run time, a response surface method was used. The chromatographic separation was achieved using a Supelco C_{18}-DB (250 mm × 4.6 mm I.D./5 μm particle size) column with mobile phase comprising of ammonium acetate buffer and acetonitrile (63:37, v/v), delivered isocratically at a flow rate of 1.0 mL min^{-1}. Diphenhydramine was used as an internal standard (I.S.). The statistical evaluation of the method was examined and the method was found to be precise and accurate with a linearity range of 1–500 ng mL^{-1} ($r > 0.9980$). The intra- and inter-day precision studies showed good reproducibility with coefficients of variation (C.V.) less than 12.26%. The advantages of our method are small sample volume (100 μL), short time of analysis (13 min) and a simple sample extraction and clean-up as compared to the previously published methods. The established method provides a reliable bioanalytical methodology to carry out FEX pharmacokinetics in rat plasma.

1. Introduction

The absorption of drugs via oral route is a subject of intense and continuous investigation in the field of biopharmaceutical research. Low and variable bioavailability is still considered to be one of the main reasons for terminating further development of many oral pharmaceutical products. Presently, it is becoming increasingly evident that intestinal transporters play an important role in the oral absorption of compounds, with both efflux transporters such as P-glycoprotein (P-gp) and influx transporters such as the organic anion transporting polypeptide (OATP), altering the pharmacokinetics of various drugs and particularly associated with poor bioavailability in co-ordination with gut wall metabolism [1–3]. Thus, a deep insight and thorough understanding of these transporters and their physiological and biochemical role in effluxing drugs is worthwhile in order to improve the bioavailability of drugs. Such investigations begin from preclinical models and find their way to clinical models. Consequently, a rapid and reliable analytical tool is the heart of such investigations.

Fexofenadine (FEX) is a non-sedating antihistamine that is chronically administered for the relief of allergy symptoms. FEX (Fig. 1a) has been identified as a substrate of P-gp and OATP based on several in-vitro and in-vivo studies [4,5]. Approximately 95% of an oral dose of FEX is recovered in urine and feces as unchanged drug. Only 5% of the oral dose of FEX is metabolized, making it an ideal probe to assess the total activity of these transporter proteins in preclinical study models [6]. Such preclinical pharmacokinetic investigations involve many samples to be analyzed in order to obtain reliable conclusions and, that is why, the development of more rapid and reliable analytical method is of great interest.

The pharmacokinetic studies of FEX in rats have shown relatively low bioavailability when this compound was administered orally (a single oral dose of 10 mg kg^{-1} body weight yielded the highest plasma level of 20–25 ng mL^{-1}) [7]. Taking into account this fact, a quantification limit of 1 ng mL^{-1} is required for a single dose design pharmacokinetic study of FEX. To best of our knowledge, none of the previously published high performance liquid chromatographic (HPLC) methods using ultraviolet (UV) or fluorescence detection had such a lower limit of quantification [8–11]. Also, these methods are mainly designed for human biological samples in a relatively large volume, typically 0.5–1.0 mL human plasma. Consequently, in case of mouse/rat studies, only one or two blood samples can be taken from each animal for measurement by these

* Corresponding author. Fax: +91820 2571998.
E-mail address: shriram.pathak@manipal.edu (S.M. Pathak).

0039-9140/$ – see front matter © 2008 Elsevier B.V. All rights reserved.
doi:10.1016/j.talanta.2008.02.047

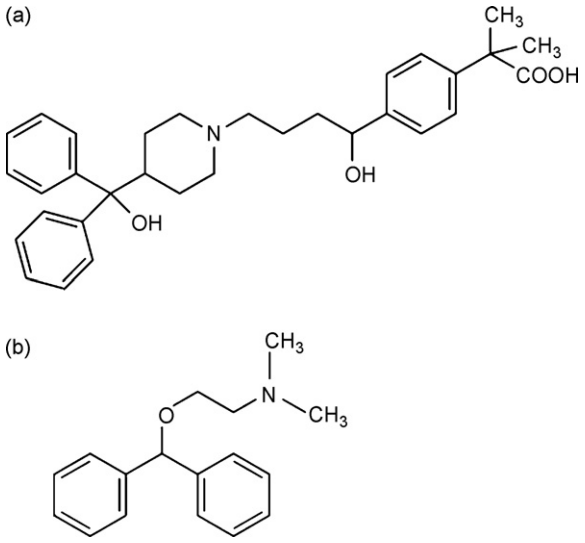

Fig. 1. Chemical structures of fexofenadine (a) and diphenhydramine (b) as an internal standard.

HPLC methods. This situation makes it impossible to get a desired set of blood samples from one small animal to perform a pharmacokinetic study. Also, the sensitivity obtained was lower with nonclinical samples because of both, the lower sample volumes obtained, and, the higher concentrations of UV absorbing endogenous compounds with similar retention times.

A bioanalytical method for the quantitation of FEX using fluorescence detection has been reported by Uno et al. [12]. Although, the limit of quantification (LOQ) of this method is 1 ng mL^{-1}, a large volume of plasma sample (1 mL) is needed for analysis. Moreover, the described method is gradient and needs a long chromatographic elution time (~17 min), which is not suitable for processing multiple samples in a limited amount of time for preclinical pharmacokinetic studies.

Recently, many methods using HPLC coupled with mass spectrometric detection have also been published, which are much more specific and sensitive analytical techniques [13,14]. However, these methods are not affordable for most laboratories because of their specialty requirement and high equipment cost.

Under the scope of this view, the aim of our research work was to develop a more precise, accurate, rugged and reliable method for FEX determination in rat plasma that proves to be of immense use for carrying out the preclinical pharmacokinetic studies efficiently in terms of small processing volume, very low concentration and a relatively short run time.

Taking into account the polar nature of the analyte, solid-phase extraction has been proven to be an effective and highly preferred technique in most of the published methods. However, these methods are time consuming, require a large processing volume and are not affordable in most of the research laboratories, as commercially available columns for solid-phase extraction are relatively expensive, especially for the study of pharmacokinetics where many samples are to be collected and treated.

A simple protein precipitation prior to solvent extraction with acetonitrile guaranteed a high absolute recovery (>80%) and good purification from matrix interference. The described method was found equally competent as solid-phase extraction with respect to sensitivity, extract cleanliness and analyte recovery.

We have developed an isocratic method and a response surface method was used to optimize the experimental conditions aimed at achieving a short analysis time without losing resolution. Further, this research work exploits the high selectivity and sensitivity of fluorescence detector to develop and validate a method for the determination of FEX in rat plasma. In addition to this, pharmacokinetics of FEX was studied in a rat model that were administered a single oral dose of 10 mg fexofenadine per kg body weight, in order to validate the method with real samples.

2. Experimental methodology

2.1. Reagents and materials

Fexofenadine hydrochloride, 4-[1-hydroxy-4-[4-(hydroxydiphenylmethyl)-1-piperidinyl] butyl]-α, α-dimethylbenzeneacetic acid hydrochloride, (99.50%, as is basis) was supplied by Wockhardt Limited (Aurangabad, India). Diphenhydramine (99.02%, as is basis) was supplied by IPCA Labs (Mumbai, India). HPLC-grade reagents such as acetonitrile and methanol were purchased from Rankem Chemicals (Delhi, India). Analytical grade reagents such as ammonium acetate, glacial acetic acid and trichloroacetic acid (20%) were purchased from Merck (Mumbai, India). HPLC-grade water was produced in the laboratory by a Milli-Q purification system (Millipore Corp., Vienna, Austria).

2.2. Apparatus

The analysis was carried out on a Shimadzu LC-10 series chromatographic system (Shimadzu Corporation, Kyoto, Japan). More precisely, the system consisted of a model SCL-10A controller unit, a model DGU-2A degasser unit, two LC-10AT piston pumps, SIL-10AD refrigerated autosampler and a model RF-10AXL fluorescence detector. System control, data acquisition and processing were performed with a PC-Pentium IV Processor personal computer operated with Microsoft Windows NT version 4.0 and Shimadzu CLASS-VP version 6.12 SP1 chromatography software with the system suitability option installed. Standard substances were weighed on AY 220 Shimadzu analytical balance. A glass vacuum-filtration apparatus (Alltech Associates) was employed for the filtration of buffer solution using 0.45 μm filters obtained from Pall Life Sciences. Degassing of the mobile phase was performed by sonication in Oscar Micro clean-103 Ultrasonic bath. Sanyo ultra low temperature freezer (Leicestershire, UK) was used to store the study samples. A model Genie-2 Spinix vortex mixer, a REMI C24 refrigerated centrifuge (REMI, India) and TurboVap LV Evaporator (Caliper Life Sciences, Hopkinton, MA, USA) were employed for sample pretreatment.

2.3. Chromatography

The mobile phase consisting of a mixture of ammonium acetate buffer (containing 7.708 g of ammonium acetate and 1.0 mL of triethylamine per liter, pH adjusted to 5.6 with acetic acid) and acetonitrile in the ratio 63:37 (v/v) was delivered isocratically at a flow rate of 1.0 mL min^{-1}. Following its preparation, the mobile phase was filtered under vacuum through a 0.45 μm membrane filter and ultrasonically degassed prior to use. The chromatographic separation was achieved by a Supelco516 C_{18}-DB column (250 mm × 4.6 mm I.D./5 μm particle size, Sigma–Aldrich, Missouri, USA). Diphenhydramine (Fig. 1b) was used as an internal standard (I.S.). The column temperature was maintained constant at 25 °C using a thermostatically controlled column oven. Fluorescence measurements were done at 220 nm excitation and 280 nm emission wavelengths with spectral bandwidth and the response time constant set at 18 nm and 1.5 s, respectively. The sensitivity of the detector was set at "Medium". The chromatographic run time for each analysis was 13.0 min.

2.4. Peak characteristics

The peak retention factor (k) for both the drug and I.S. was calculated from $k = (t_R - t_0)/t_0$, where t_R and t_0 are the retention times of the peak of interest and the solvent front, respectively. The separation factor (α) was estimated from $\alpha = k_2/k_1$, where k_1 and k_2 are the retention factors of the drug and I.S., respectively. A useful and practical measurement of peak shape, the peak asymmetry factor, A_s, was calculated at 10% of the peak height. The resolution factor (R_s) was calculated by $R_s = 1/4\ (\alpha - 1)\ (N^{1/2})\ (k'/1 + k')$, where N is the column plate number and k' is the average retention factor for the two bands. The column plate number was determined using the formula, $N = 5.54(t_R/w_h)^2$, where w_h is the bandwidth at 50% of the peak height.

2.5. Preparation of standard solutions

FEX was dissolved in methanol to prepare a primary stock solution at a concentration of 1000 μg mL^{-1}. Corrections to the theoretical concentration were performed according to the degree of standard substance impurities. Intermediate stock solutions (100 and 10 μg mL^{-1}), in duplicate, were prepared from the primary stock solution. Primary and intermediate stock solutions were kept at 4 °C and remained stable for at least 15 days. Working stock solutions of FEX were prepared using a mixture of methanol–acetate buffer, 50:50, v/v (diluent). The I.S. working solutions were prepared in a similar manner, providing finally a plasma concentration of 250 ng mL^{-1}. The intermediate stock solutions were prepared weekly, while working stock solutions used for the calibration curves were prepared daily.

Calibration standards in plasma (1, 5, 10, 25, 50, 100, 250, and 500 ng mL^{-1}) samples were prepared by spiking blank rat plasma with 10 μL of working stock solutions of FEX. Quality control (QC) samples at four different levels were independently prepared at concentrations of 1 ng mL^{-1} (LOQ-QC, same concentration as the lowest non-zero standard), 15 ng mL^{-1} (LQC, Low QC), 150 ng mL^{-1} (MQC, Medium QC) and 450 ng mL^{-1} (HQC, High QC) of FEX in the same manner. The quality control samples were prepared from a stock solution that was different from the one used to generate standard curve samples. These quality control samples were used to investigate intra- and inter-run variations.

2.6. Sample preparation

The plasma samples were stored in freezer at −20 °C until use and allowed to thaw at room temperature before processing. FEX and internal standard (diphenhydramine) were extracted from 100 μL of plasma by protein precipitation with 2 mL of 0.25% trichloroacetic acid in ice-cold acetonitrile. The mixture was vortexed for 1 min and centrifuged at 2500 × g for 10 min. The organic phase was collected and evaporated to dryness in a water bath at 55 °C under a gentle stream of nitrogen. The dried residue was reconstituted with 100 μL of diluent and vortexed for 1 min. The supernatant was transferred entirely into a 250 μL vial-insert and a volume of 50 μL was injected into the HPLC system.

2.7. Validation of the method

Validation of the developed method allowed us to confirm the linearity over the tested concentration range and to assess precision (repeatability and intermediate precision), trueness, and selectivity of the analytical method. To validate these different criteria, two kinds of plasma samples were prepared: calibration and validation samples corresponding to QC samples used in the routine analysis. The validation range was selected on the basis of the preliminary experiments to cover the expected FEX concentrations in the animal studies. These concentrations were between 1 and 500 ng mL^{-1} in the rat plasma.

2.7.1. Selectivity

Selectivity is generally defined as the lack of interfering peaks at the retention times of the assayed drug and the internal standard in the chromatograms. The selectivity of the assay was investigated by processing and analyzing (a) blanks prepared from six independent lots of control plasma and (b) a group of potentially co-administrated drugs with FEX as P-gp/OATP modulators during drug interaction studies in rats (e.g. verapamil, talinolol, propranolol, quinidine, digoxin, phenol red, antipyrine and saquinavir) in a final concentration of 5 μg mL^{-1} in plasma. The retention times for these drugs under the chromatographic conditions for the FEX assay were determined. The method is selective if the response of interfering peaks at the retention time of drug is less than 20% of mean response of six extracted LOQ-QC samples.

2.7.2. Linearity

The linearity of an analytical procedure is its ability (within a given range) to obtain test results which are directly proportional to the concentration (amount) of analyte in the sample. The linearity of assay for the test compounds was evaluated with a total of eight calibration standards over the concentration range 1–500 ng mL^{-1}. Calibration curves were constructed by linear least-squares regression analysis plotting of peak-area ratios (FEX/I.S.) versus the drug concentrations. The linearity of the calibration curve was tested and evaluated using both linear and polynomial regression model of internal standard calibration (ISTD) curve. Coefficients of calibration equation and the correlation coefficient were expressed. The calibration model was accepted, if (a) coefficient of correlation was greater than or equal to 0.98; (b) residuals were within ±20% at the lower limit of quantification and within ±15% at all other calibration levels; (c) no two consecutive calibration curve standards fail to meet the above acceptance criteria; and (d) at least 2/3 of the standards meet this criterion. Five calibration curves were prepared to ensure that the regression model was the most accurate for quantitative purposes. These standard curves were used to determine the concentrations of the QCs and to back calculate the relative error (residuals) for each point in the standard curve.

2.7.3. Detection and quantification limits (sensitivity)

The detection limit (LOD) was defined as the lowest concentration level resulting in a peak area of three times the baseline noise. The ratio of signal size to that of noise was calculated by equation $2H/h$, where H is the height of the peak corresponding to the component concerned in a chromatogram obtained with the prescribed reference solution and h is the range of the background noise in the chromatogram obtained after the injection of a blank.

The limit of quantification (LOQ) was determined as the lowest concentration on the standard calibration curve that provided a peak area with a signal-to-noise ratio higher than 10 with a precision ≤20% and accuracy of 80–120% of its nominal value.

2.7.4. Assay precision and accuracy

The precision of an analytical procedure expresses the closeness of agreement between a series of measurements obtained from multiple sampling of the same homogeneous sample, while, the accuracy of an analytical method describes the closeness of the test results obtained by the method to the true (nominal) value of the analyte. Accuracy, intra- and inter-day precisions of the method were determined for FEX according to FDA guidance for bioanalytical method validation [15]. The run consisted of a calibration curve plus six replicates of each QC sample (LOQ-QC,

LQC, MQC and HQC) on the same day. The inter-day accuracy and precision were assessed by the analysis of six samples (two samples per day at each level of four QC samples) on three different days. The accuracy (%bias) was calculated from the mean value of observed concentration (C_{obs}) and the nominal concentration (C_{nom}) as follows: accuracy (%bias) = $[(C_{obs} - C_{nom})/C_{nom}] \times 100$. The percent coefficient of variation, C.V. (%), was calculated from the observed concentrations as follows: precision, C.V. (%) = [standard deviation (S.D.)/C_{obs}] × 100.

The accuracy determined at each concentration level must be within ±15% of the respective nominal value except at LOQ-QC where it must be within ±20% of the nominal value. The precision around the mean value must not exceed 15% of the C.V. except for LOQ-QC where it must not exceed 20% of the C.V.

2.7.5. Recovery

The trueness of an analytical procedure refers to the closeness of agreement between a conventionally accepted value and a mean experimental one. Trueness was expressed as percentage recovery of the target value and assessed by means of validation standards in the matrix at three independent concentration levels, LQC, MQC and HQC. Recovery was calculated by comparing the mean peak area of an extracted sample ($n = 3$) to the one obtained after the direct injection of a solution with the same drug concentration.

$$\text{Absolute \% recovery} = \frac{\text{Mean peak area response of extracted samples at LQC, MQC or HQC level}}{\text{Mean peak area response of nonextracted samples at LQC, MQC or HQC level}} \times 100$$

2.7.6. Stability tests

The stock solution stability of FEX and I.S. was tested at room temperature for 12 h and upon refrigeration (4 °C) for 15 days period. Considering the sensitivity of FEX to light as demonstrated in number of studies, the fluorescence-induced photodegradation of the drug in mobile phase was studied using spectrofluorimeter. The standard solution (250 ng mL^{-1}) was transferred into a quartz cuvette and irradiated with fluorescent radiation. The photodecomposition was determined by measuring the emission at 280 nm after excitation at 220 nm wavelength. The stability of FEX during the analysis was also evaluated by injecting the same samples ($n = 5$) at the beginning and end of irradiation. In addition, a peak purity analysis was performed on irradiated solutions using a shimadzu photodiode-array detector.

The drug stability in a biological fluid is a function of the storage conditions, the chemical properties of the drug and the matrix. The stability procedures should evaluate the stability of the analytes in biological fluids after long-term (frozen at the intended storage temperature and conditions) and short-term (bench top, room temperature and conditions) storage, and after going through freeze and thaw cycles and the analytical process. Twenty-four hours autosampler stability of plasma sample extracts at 4 °C was determined for analyte as well as I.S.

The long-term stability of FEX in rat plasma was assessed by performing the experiment after 30 days of storage at −20 °C. Freeze–thaw stability of FEX (LQC, MQC and HQC) in rat plasma samples was determined for three freeze–thaw cycles. The samples were thawed at the room temperature without any assistance, and then kept in the freezer (−20 °C) for minimum of 12 h before taking out for the next thawing. The post-preparative short-term room temperature stability of FEX in processed samples left at ambient temperature was followed for 24 h. The concentration of FEX after each storage period was related to the initial concentration as determined for the samples that were freshly prepared. The criterion for an acceptable stability of compounds in plasma samples under different storage conditions is that the relative recovery of the drug should be at least 90% of the initial concentration.

2.8. Pharmacokinetic application of the developed HPLC method

To validate the method with real samples, a trial was undertaken to determine FEX in the plasma samples of healthy rats ($n = 6$), that were administered a single dose of fexofenadine hydrochloride orally. The study was conducted in accordance with the ethical guidelines for investigations in laboratory animals and was approved by the Institutional Animal Ethics Committee (IAEC), Manipal-University. All procedures and the care of the rats were in accordance with institutional guidelines for animal use in research. Rats were housed in plastic cages on corn-cob bedding in a temperature controlled room (20 ± 2 °C) with a 12 h light/dark cycle.

Male Wistar rats, 250 ± 10 g, fasted overnight with free access to water for at least 12 h, were dosed orally by gavages with 10 mg kg^{-1} body weight of fexofenadine suspended in 1.0% (w/v) carboxy methyl cellulose aqueous solution as a vehicle. Rats were divided into six groups ($n = 6$) based on the time of blood sampling having five animals each. The control groups received the vehicle only. The blood samples (approximately 200 μL) were collected from the suborbital vein in heparinized tubes at control and 0.25, 0.50, 0.75, 1.00, 1.25, 1.50, 2.00, 3.00, 4.00, 6.00 and 8.00 h after the administration. Samples were immediately centrifuged at 2500 × *g* for 10 min and the plasma was frozen at −20 °C and stored until analysis. The estimation of FEX in all the samples was undertaken within 24–48 h of blood collection by the method described above in Section 2.6. The samples were also prepared by spiking blank rat plasma at three concentration levels (LQC, MQC, HQC) and analyzed as the quality control points incorporated into the series after every three to four pharmacokinetic samples during the routine measurements.

2.8.1. Calculation of pharmacokinetic parameters

The pharmacokinetic parameters were calculated by using a non-compartmental approach. The area under the plasma concentration–time curve after oral administration, AUC, was calculated using the linear trapezoidal rule up to the last measured plasma concentration and extrapolated to infinity, $AUC_{0-\infty}$, using a correction term, namely $C_p(\text{last})/\lambda_z$, where $C_p(\text{last})$ denotes either the observed or predicted concentration at the last sample time and λ_z is the first order rate constant associated with the terminal (log-linear) portion of the curve and is estimated via linear regression of time versus log concentration. The area under the first-moment curve to the last measured plasma concentration, AUMC, was also calculated using the linear trapezoidal rule and the addition of the concentration term after the last measured point ($t(\text{last})$) to infinity, namely, $t(\text{last})C_p(\text{last})/\lambda_z + C_p(\text{last})/\lambda_z$. The terminal elimination half-life, $t_{1/2}$, was determined by dividing ln 2 by λ_z.

2.8.2. Statistics

All values were expressed as mean ± S.D., unless otherwise stated. Statistical differences were assumed to be reproducible when $p < 0.05$ (two-tailed *t*-test).

3. Computer modeling

The SPSS program (SPSS Inc., Chicago, IL, USA) was used for the nonlinear regression analysis of the data and for obtaining the empirical mathematical model that represents the response surface. A surface plot was produced by Sigmaplot-10, a contouring and three-dimensional surface mapping software program (Wpcubd, GmbH, Germany).

4. Results and discussion

4.1. Selection of the chromatographic parameters

FEX is an amphoteric compound with a carboxylic acid group (pK_{a_1} = 4.25) and a tertiary amino group (pK_{a_2} = 9.53). Being amphoteric in nature, it remains in ionic form in the entire pH range, and, this makes its retention difficult on reversed-phase columns. In the acidic pH range, the carboxylic acid group is protonated and therefore not charged. The compound, therefore, bears just one positive charge. In the intermediate pH range, both, the carboxylic acid group and the amino group, are ionized. Due to the fact that there is now a dual charge on the molecule, the retention time is intermediate. In alkaline pH range, the amino group is deprotonated, the molecule bears only a single negative charge and, thus, the retention increases again. Hence, in chromatographic reversed-phase separation, both hydrophobic and ionic interactions will take part. This is in compliance with the observation reported [16] that the functional dependence of retention factor on pH of mobile phase differs from the ideal sigmoidal shape of predicted hydrophobic interactions, indicating additional donor–acceptor interactions. These interactions of protonated amino group moiety with residual silanol groups of stationary phase in acidic media often cause problems in chromatographic determination of FEX in the presence of I.S., manifesting mainly with bad peak shape (peak broadening and tailing), low efficiency of separation and insufficient resolution. Consequently, optimizing chromatographic conditions to obtain desired retention and adequate resolution in a short time were critical factors in the method development process.

Since HPLC utilizes a wide selection of chromatographic factors, optimization of the experimental conditions is a complicated process. Hence, a systematic approach such as experimental design to optimize chromatographic separations is more essential. This is because traditional HPLC method development techniques are time and energy consuming and uneconomical; further, they may not necessarily yield methods that would meet suitability requirements during validation. Therefore, the optimization of the method was performed using an interpretative strategy, and more specifically, 3^2 factorial design that supplied data to obtain a fitted polynomial model for drawing a response surface in all the variable space.

The selection of factors for the optimization was based on preliminary experiments, prior knowledge from literature and certain instrumental limitations.

The manipulation of mobile phase pH is a technique that works well for ionizable compounds, because the retention characteristics of ionizable compounds are a function of pH of mobile phase. Moreover, in order to obtain efficient separation for polar compounds containing ionizable groups, a significant percentage of a buffer (%*B*) should be present in the mobile phase. The buffer serves a dual role—it controls the pH of the separation system and also provides competitive ions for ionic interactions. Preliminary studies were conducted to check the effect that mobile phase pH and buffer: organic ratio had on analytes' retention and resolution. As can be seen in Fig. 2, pH had a detrimental effect on FEX and diphenhydramine separation, since differences in the degree of ionization change elution order and modify resolution. Therefore, the key factors selected for optimization process were pH and %*B*. The experimental domain of the selected variables is reported in Table 1. The criteria for the selection of the optimum separation conditions included the achievement of the optimum separation of the analytes in the mixture within minimum time. Hence, based

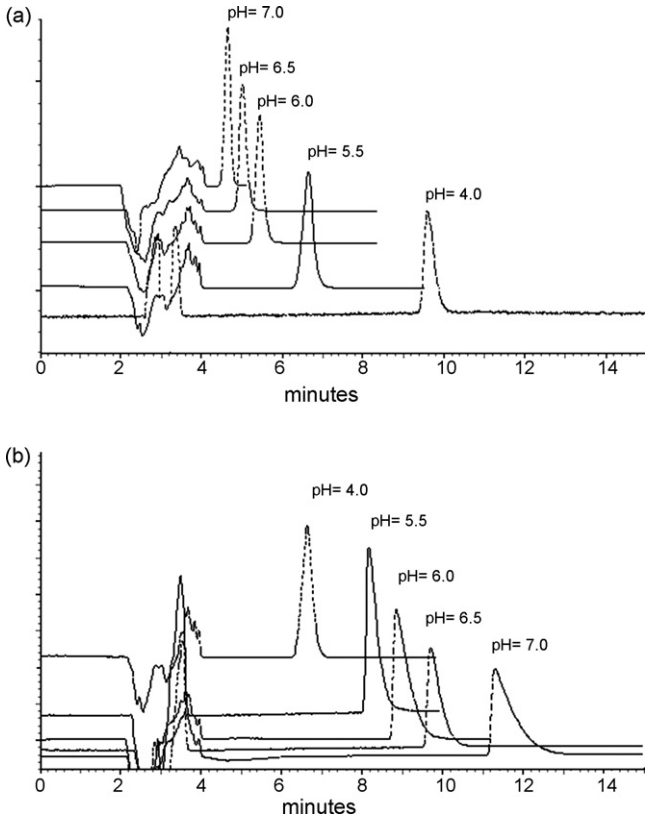

Fig. 2. Overlaid chromatograms of test solutions at different mobile phase pH showing retention behavior of FEX (a) and I.S. (b).

Table 1
Chromatographic parameters and range investigated during optimization process

Variable factor	Optimized value	Range investigated
pH	5.6	4.0–7.0
Buffer percentage (%*B*)	63%	55–65%

Table 2
Experimental and predicted values for different chromatographic response variables at various experimental conditions

Exp. no.	Levels of independent variables		Responses		
	pH (x_1)	%*B* (x_2)	t_R	k	R_s
1	7.0	55	3.22 (3.32)	0.24 (0.28)	13.45 (13.41)
2	7.0	60	4.65 (4.45)	0.79 (0.71)	11.54 (11.62)
3	7.0	65	5.28 (5.38)	1.03 (1.07)	10.45 (10.41)
4	5.5	55	5.04 (4.84)	0.94 (0.86)	6.94 (7.02)
5	5.5	60	5.43 (5.83)	1.09 (1.24)	6.47 (6.32)
6	5.5	65	7.62 (7.42)	1.93 (1.85)	4.91 (4.99)
7	4.0	55	7.80 (7.90)	2.00 (2.04)	0.40 (0.36)
8	4.0	60	8.29 (8.09)	2.19 (2.11)	−0.02 (−0.06)
9	4.0	65	9.59 (9.69)	2.69 (2.73)	−2.08 (−2.12)

Table 3
Reduced response models and adjusted r^2 values

Response	Regression model	Adjusted r^2
R_s	$-328.20 + 45.47x_1 + 11.29x_2 + 1.68x_1^2 - 0.10x_2^2 - 1.64x_1x_2 - 0.02x_1x_2^2 - 0.03x_2x_1^2$	0.9999
k	$119.82 - 23.71x_1 - 3.54x_2 + 0.74x_1^2 + 0.03x_2^2 + 0.62x_1x_2 - 0.004x_1x_2^2 - 0.01x_2\,x_1^2$	0.9897
t_R	$314.73 - 61.77x_1 - 9.20x_2 + 1.94x_1^2 + 0.07x_2^2 + 1.62x_1x_2 - 0.01x_1x_2^2 - 0.03x_2x_1^2$	0.9896

on the results, it was decided that the following chromatographic responses needed to be optimized if validation of the method was to be successful: the retention time of FEX (t_R), retention factor of FEX (k) and resolution between analyte and I.S (R_s).

Table 2 reveals the levels of each factors studied for finding out the optimum values and responses. All experiments were performed in a randomized order to minimize the effects of uncontrolled variables that may introduce bias on the measurements.

The coefficients of the second-order polynomial model were estimated by nonlinear regression. The relationship between a particular chromatographic parameter and the corresponding chromatographic response and r^2 values are shown in Table 3. As it can be seen, the interaction term with the largest absolute coefficient among the fitted models is x_1 (pH). It is, however, important for the response surface study to consider also the factors whose coefficients are statistically insignificant.

In order to gain a better understanding of the results, the predicted models are presented in Fig. 3a–c. The analysis produces three-dimensional graphs by plotting the response models against two of the factors, pH and *%B*. These graphs show how the response changes as each factor moves from a chosen reference point. The surface plot allows the entire range of conditions to be explored, including combinations that were not experimentally demonstrated, indicating that the optimal experimental conditions correspond to pH 5.6 and to 63% of *B*. In the optimized conditions of the mobile phase, the resolution of FEX and I.S. peaks was to the baseline and the compounds were eluted in about 12.0 min with respective retention times of 7.7 and 10.2 min using a Supelco516 C_{18}-DB 250 mm column (Fig. 4a). Resolution and retention factor for FEX were 5.09 and 1.98, respectively (Table 4).

4.2. Sample preparation

The role of sample preparation continues to be an important area for method development since the increased acceptance of high-throughput instrumentation has shifted the analysis bottle-

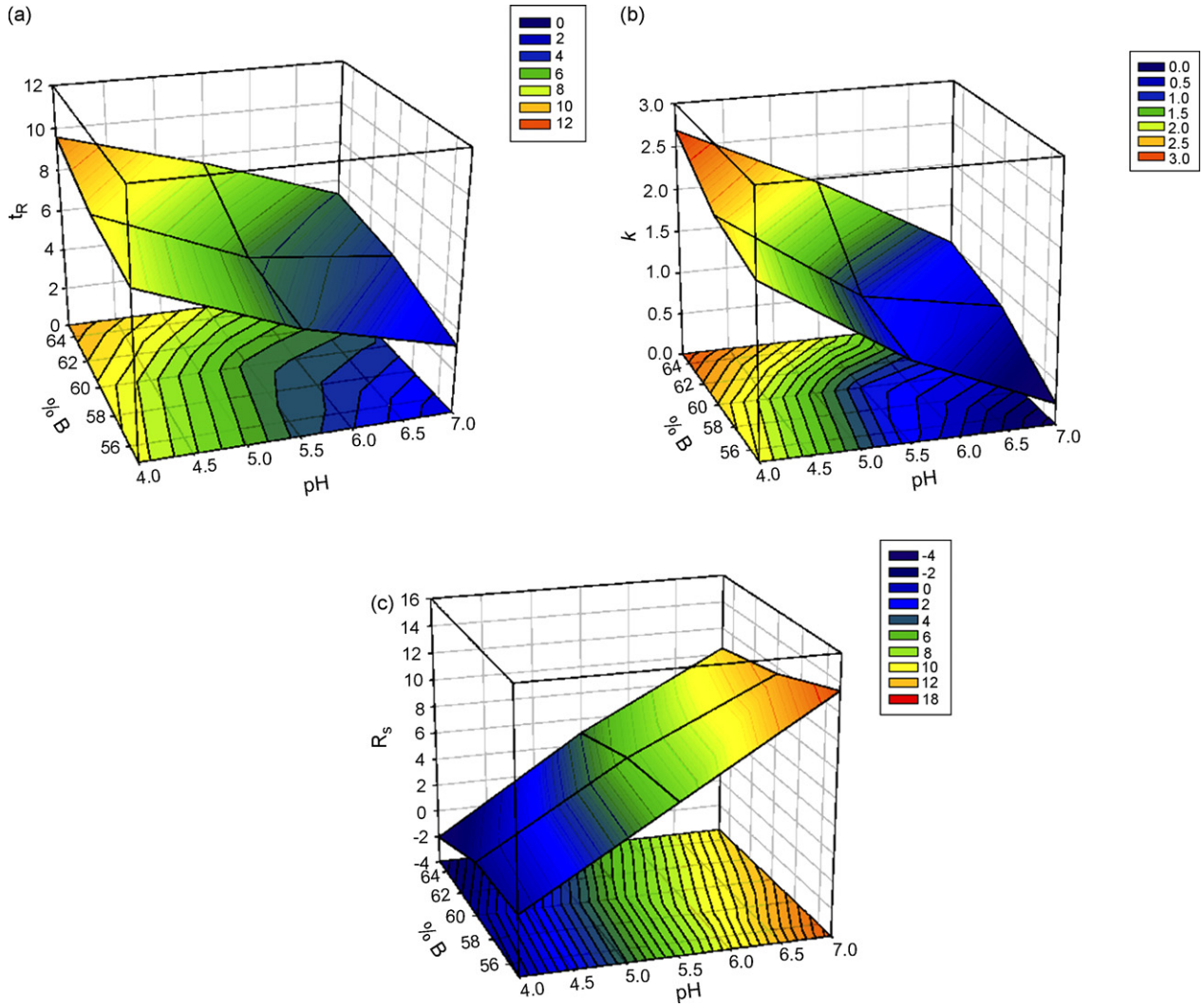

Fig. 3. Three-dimensional plots of the response surface representing the variation of the chromatographic responses: (a) t_R (retention time); (b) k (retention factor); and (c) R_s (resolution), as a function of pH and percentage of buffer (*%B*).

Table 4
Chromatographic separation characteristics of FEX analyzed under optimized assay conditions mentioned above in Section 4.1

Analyte	Area C.V. (%)[a]	Width at 50% height (min)	Plate number (USP)	Retention factor	Asymmetry (10%)	Resolution factor (USP)
FEX	0.22	0.22	6928	1.98	1.12	–
I.S.	0.41	0.33	5266	2.91	1.16	5.09

[a]Six replicate injections.

neck backward towards sample preparation. The determination of FEX in plasma, due to its physico-chemical properties: such as the high degree of ionization and the large polar surface area (124 $A^{\circ 2}$), has always been an analytical challenge for bioanalysts and numerous methodologies have been reported in the literature in recent years.

Taking into account the polar nature of the analyte, solid-phase extraction has been proven to be an effective and highly preferred technique in almost all published methods. However, it is time consuming, needs personal manipulation and when a large number of samples have to be measured, it is a potential source of errors. Also, most of these methods needed relatively large volumes of sample (≥0.250 μL) and/or lacked sensitivity. Consequently, their application in pharmacokinetic studies in small laboratory animals is unsatisfactory. Therefore, we evaluated various protein precipitation methods for sample preparation to make easier and speed up the analysis. Trials on the partitioning of FEX and I.S. between an alkaline or acidic solution and an organic solvent showed that the substances could be quantitatively extracted from blood plasma when acidified. A 0.1% trichloroacetic acid in cold acetonitrile was used for this purpose. Employing a combination of cold acetonitrile and acidic pH for protein precipitation resulted in a high recovery of analyte without increase in endogenous peaks. The detection of FEX by this method is sensitive enough for pharmacokinetic studies in rats dosed as low as 10 mg per kg. No interfering peaks from the endogenous substances were observed in any of the plasma samples. Diphenhydramine was selected as an I.S. because of high recovery and suitable retention time. Furthermore, the assay as described, gives satisfactory validation results with the use of diphenhydramine as the I.S. Both, system pressure and column performance, remained stable after the analysis of a large number of validation samples. Carryover effect of endogenous material or FEX from previous injections was not observed during study.

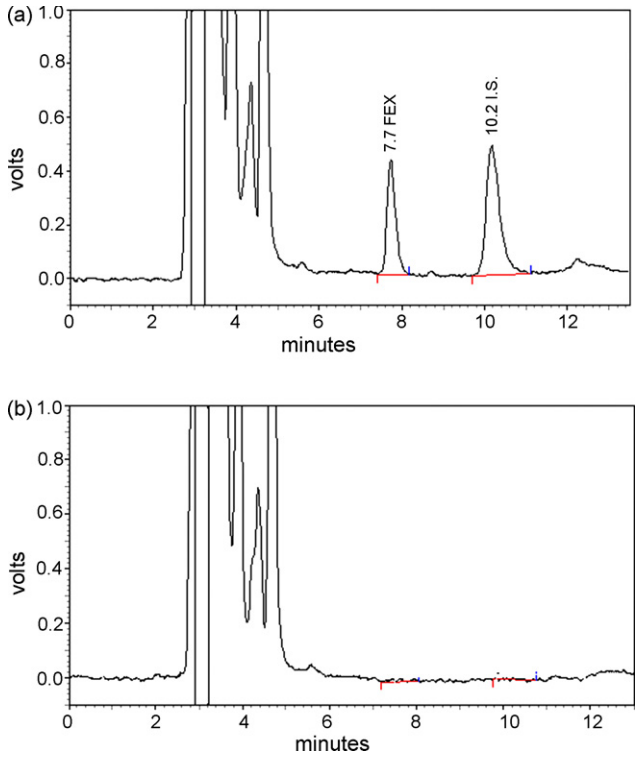

Fig. 4. Chromatograms obtained from (a) a plasma sample spiked with 100 ng mL^{-1} FEX and (b) a drug free blank rat plasma. Spiked concentration of diphenhydramine (I.S.) is constant throughout (250 ng mL^{-1}).

4.3. Method validation

4.3.1. Selectivity

No interference peak was detected in the eluting positions of FEX and the I.S. in six blank plasma samples. A typical chromatogram for the blank plasma sample is shown in Fig. 4b. The common drugs, which are administered concurrently with FEX during drug interaction studies in rats, were injected separately and found not to interfere with both analyte and I.S. retention times.

4.3.2. Linearity, limit of detection and limit of quantitation

During the method validation, five sets of calibration standards were prepared and analyzed on five different days, each calibration curve originating from a new set of extractions (Table 5). The mean regression equation of five standard curves was: $y = (0.0029 \pm 0.0002)x + (0.0266 \pm 0.0029)$, where y is the peak area ratio of FEX to the I.S. and x is the plasma concentration of FEX. The calibration curve was linear over the concentration range of 1–500 ng mL^{-1} with a mean correlation coefficient of 0.9990.

The Lower limit of quantification was found to be 1 ng mL^{-1} with an accuracy (%bias) and precision (C.V.) not exceeding 20%. The limit of detection (LOD) considering a signal-to-noise ratio 3:1 was estimated to be 0.75 ng mL^{-1}.

4.3.3. Accuracy and precision

The accuracy and precision of the method were evaluated with QC samples at concentrations of 1, 15, 150 and 450 ng mL^{-1}. The intra- and inter-day accuracy and precision values of the assay method are shown in Table 6. The precision of the method was calculated as the percent coefficient of variation, C.V.(%), of the concentrations determined in all replicates. The intra-day C.V. (%) for FEX was below 11.7%. All inter-day C.V. (%) were below 12.26%. The accuracies were determined by comparing the mean calculated concentration to the spiked target concentration of the quality control samples. The intra- and inter-day accuracies for FEX were found to be within 95.87% and 108%, respectively, of the target values.

Table 5
Inter-day precision in the slope, intercept and correlation coefficient (r) of standard curves (r = 0.9992–0.9997)

Day	Slope	Intercept	r
1	0.0031	0.0261	0.9998
2	0.0026	0.0301	0.9988
3	0.0028	0.0265	0.9978
4	0.0029	0.0221	0.9996
5	0.0030	0.0280	0.9988
Mean ± S.D.	0.0029 ± 0.0002	0.0266 ± 0.0029	0.9990 ± 0.0008
C.V. (%)	6.68	11.10	0.08

Table 6
Intra- and inter-day accuracy and precision of FEX determination at four concentration levels ($n = 6$)

QC sample	Concentration (ng mL^{-1})	Mean measured concentration (ng mL^{-1}) ± S.D.	Accuracy (%)	Precision (C.V.%)
Intra-day				
LLOQ	1.00	1.08 ± 0.12	108.00	11.22
LQC	15.00	14.70 ± 1.48	98.00	10.07
MQC	150.00	148.38 ± 11.38	98.92	7.67
HQC	450.00	450.36 ± 38.12	100.08	8.46
Inter-day				
LLOQ	1.00	1.06 ± 0.13	106.00	12.26
LQC	15.00	14.38 ± 1.57	95.87	10.92
MQC	150.00	153.50 ± 15.07	102.33	9.82
HQC	450.00	435.15 ± 41.69	96.70	9.58

4.3.4. Extraction efficiency

The mean extraction recovery of FEX at the three concentrations was 83.76% (LQC), 85.23% (MQC) and 81.79% (HQC), respectively (Table 7). The extraction recovery of diphenhydramine (internal standard) was 78.50%.

4.3.5. Stability

The stock solution of FEX was stable at least for 15 days when stored at 4 °C (the concentration of the analyte was within 99.17–102.70% of the initial concentration). The I.S. stock solution was stable atleast for 30 days at 4 °C (the concentration was found within 99.02–100.05% of initial concentration). The stability of these standard solutions at room temperature and under laboratory neon tubes access for a minimum for 12 h was equally proved. Degradation with a degree of only 3.2% was observed in solutions of FEX without protection from laboratory light.

The stability of FEX in plasma was investigated by using spiked QC samples at three concentration levels (low, medium, high). FEX in plasma samples proved to be stable for a minimum of 1 month when stored at −20 °C. The freeze and thaw cycles did not change the concentration levels of analyte significantly. The concentration of FEX in processed samples (15, 150 and 450 ng mL^{-1}) was found to be 99.7%, 99.2% and 98.7%, respectively of the nominal value after three freeze–thaw cycles. The stability of spiked plasma samples at room temperature was examined by comparing the data of the samples analyzed immediately with those at 4, 10 and 24 h after sample preparation. The residual percentage of FEX in plasma stored at room temperature for 24 h ranged from 97.5% to 103%, of the initial concentration. Twenty-four hour autosampler stability results of plasma sample extracts at 4 °C indicated no significant change in the concentration levels of the respective analyte (e.g. more than 15%).

The percentage of fluorescence-induced photodegradation of FEX was assessed by the comparison of chromatographic peak areas of the samples at the beginning to that obtained at the end of irradiation. Only 1.2% degradation was observed, which indicated that FEX was stable enough under fluorescence detection. In addition, the resulting UV spectra of the irradiated samples matched with that of the control and the peak purity index indicated a homogeneous peak in all cases (data not shown).

Table 7
Absolute recovery of FEX from plasma ($n = 3$)

Sample	Concentration (ng mL^{-1})		Recovery (%)	C.V. (%)
	Added	Found (mean ± S.D.)		
LQC	15.00	12.56 ± 0.78	83.76	6.21
MQC	150.00	127.85 ± 10.04	85.23	7.85
HQC	450.00	368.06 ± 18.22	81.79	4.95

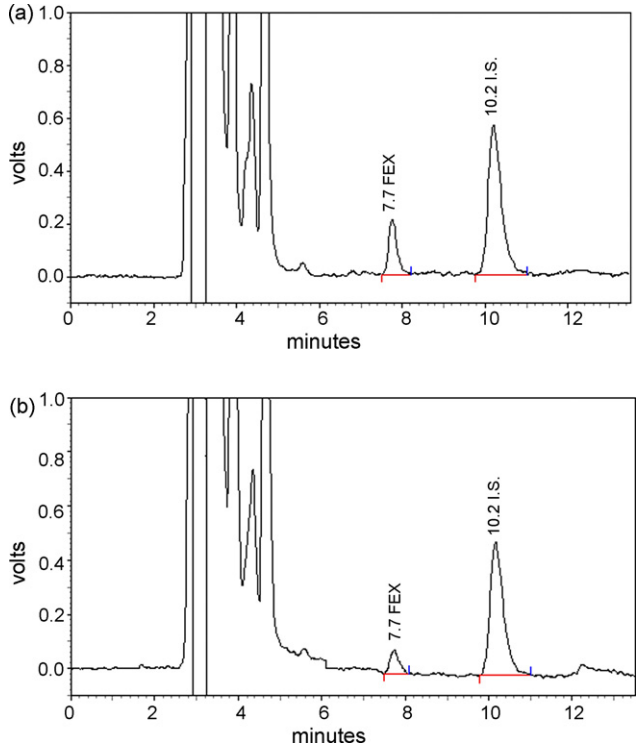

Fig. 5. Representative chromatograms of plasma samples collected from one animal at (a) 0.75 h and (b) 2.0 h after a single oral dose of 10 mg of FEX per kg of body weight.

5. Application of the method

This validated method was applied to monitor the plasma concentration of FEX in rats that were administered a single oral dose

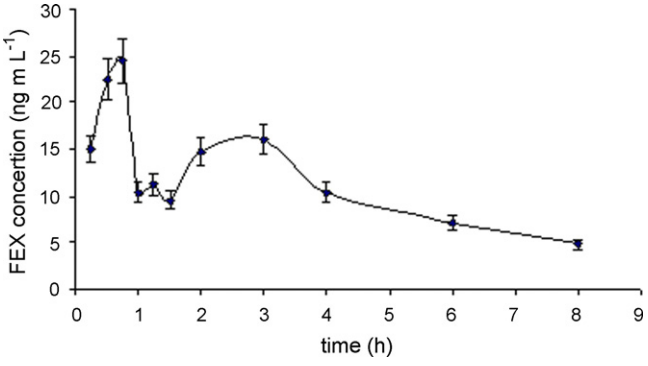

Fig. 6. Mean (±S.D.) plasma concentration–time profile of FEX in the plasma of healthy rats ($n = 6$) that were administered a single oral dose of 10 mg of FEX per kg of body weight.

Table 8
Pharmacokinetic characteristics of FEX in the plasma of healthy rats ($n = 6$), that were administered a single oral dose of 10 mg of fexofenadine per kg of body weight

FEX pharmacokinetic parameter values (mean ± S.D.)[a]		
$AUC_{0-\infty}$	($ng\,h\,mL^{-1}$)	90.81 ± 10.88
C_{max}	($ng\,mL^{-1}$)	24.45 ± 3.55
T_{max}	(h)	0.75 ± 0.05
λ_z	(h^{-1})	0.22 ± 0.11
$t_{1/2}$	(h)	3.12 ± 0.58
Cl_{app}	($mL\,h^{-1}$)	0.03 ± 0.08

[a] Each value represents the mean ± S.D. of six experiments.

of 10 mg fexofenadine per kg of body weight. The representative chromatograms obtained from one animal at 0.5 h and 2.5 h after drug administration are shown in Fig. 5a and b, respectively. A first peak at 0.75 h ($24.45 \pm 3.55\,ng\,mL^{-1}$) and a secondary peak at 2.8 h ($16.22 \pm 2.89\,ng\,mL^{-1}$) can be observed. The area under the curve ($AUC_{0-\infty}$) and the maximum plasma concentration (C_{max}) were determined to be 90.81 $ng\,h\,mL^{-1}$ and 24.45 $ng\,mL^{-1}$, respectively. Therefore, this method had adequate sensitivity for the determination of FEX in rat plasma. The mean (±S.D.) plasma concentration–time profile of FEX in rats ($n = 6$) is shown in Fig. 6. The pharmacokinetic parameters derived from these data are presented in Table 8.

6. Conclusion

In conclusion, a reproducible, accurate, and precise isocratic HPLC method with fluorescence detection was developed for the determination of FEX in rat plasma. This study evaluated the applicability of a designed experiment at the fine-tuning stage in reversed-phase high performance liquid chromatographic (HPLC) method development. Results indicated that once the mobile phase that provides reasonably good retention and resolution has been identified, the strategy of using a designed experiment is advantageous over the conventional one-factor-at-a-time approach since it would enable the analyst to optimize important responses, including run time with a minimum number of experiments. The developed method holds upper hand over other methods reported in literature so far in terms of both, simplicity, as well as sensitivity. The small sample volume (100 μL) required makes it possible to study the full pharmacokinetic profile in individual small animals, like the rat. The validity of the method was studied and the method was found to be precise and accurate with a linearity range from 1 to 500 $ng\,mL^{-1}$ ($r > 0.9980$). The intra- and inter-day precision studies showed good reproducibility with coefficients of variation less than 12.26%. Further studies are ongoing in our laboratory to characterize the transporters involved and their role in absorption of FEX.

References

[1] J.R. Kunta, P.J. Sinko, Curr. Drug Metab. 5 (2004) 109.
[2] H. Suzuki, Y. Sugiyama, Eur. J. Pharm. Sci. 12 (2000) 3.
[3] V.J. Wachera, L. Salphatib, L.Z. Benetb, Adv. Drug Deliv. Rev. 20 (1996) 99.
[4] M. Cvetkovic, B. Leake, M.F. Fromm, G.R. Wilkinson, R.B. Kim, Drug Metab. Dispos. 27 (1999) 866.
[5] G.K. Dresser, D.G. Bailey, B.F. Leake, U.I. Schwarz, P.A. Dawson, D.J. Freeman, Clin. Pharmacol. Ther. 71 (2002) 11.
[6] ALLEGRA (Fexofenadine Hydrochloride) Product Information. Physician's Desk Reference, 57th ed., Thomson Corporation, 2003.
[7] A.V. Kamath, M. yao, Y. zhang, S. chong, J. Pharm. Sci. 94 (2005) 233.
[8] T. Radhakrishna, G.O. Reddy, J. Pharm. Biomed. Anal. 29 (4) (2002) 755.
[9] A.R. Breier, J. Menegola, C.S. Paim, M. Steppe, E.E.S. Schapoval, J. AOAC Int. 87 (2004) 1093.
[10] J.E. Coutant, P.A. Westmark, P.A. Nardella, S.M. Walter, R.A. Okerholm, J. Chromatogr. 570 (1991) 139.
[11] S. Surapaneni, S.K.W. Khalil, J. Liq. Chromatogr. 17 (1994) 2419.
[12] T. Uno, N. Yasui-Furukori, T. Takahata, K. Sugawara, T. Tateishi, J. Pharm. Biomed. Anal. 35 (2004) 937.
[13] I. Fu, E.J. Woolf, B.K. Matuszewski, J. Pharm. Biomed. Anal. 35 (2004) 837.
[14] U. Hofmann, M. Seiler, S. Drescher, M.F. Fromm, J. Chromatogr. B 766 (2002) 227.
[15] Guidance for industry: Bioanalytical Method Validation, US Department of Health and Human Services, Food and Drug Administration, Center for Drug Evaluation and Reserch (CDER), Center for Biologics Evaluation and Research (CBER), May 2001.
[16] J. Barbosa, R. Berges, V. Sanz-Nebot, J. Chromatogr. A 823 (1998) 411.

Talanta 76 (2008) 295–300

Contents lists available at ScienceDirect

Talanta

journal homepage: www.elsevier.com/locate/talanta

The cyclic renewable mercury film silver based electrode for determination of molybdenum(VI) traces using adsorptive stripping voltammetry

Robert Piech*, Bogusław Baś, Władysław W. Kubiak

Faculty of Materials Science and Ceramics, AGH University of Science and Technology, 30-059 Kraków, al. Mickiewicza 30, Poland

ARTICLE INFO

Article history:
Received 15 November 2007
Received in revised form 21 February 2008
Accepted 26 February 2008
Available online 4 March 2008

Keywords:
Molybdenum
Trace analysis
Amalgam
Mercury film electrodes
Stripping voltammetry

ABSTRACT

The new cyclic renewable mercury film silver based electrode (Hg(Ag)FE), applied for the determination of molybdenum(VI) traces using differential pulse adsorptive cathodic stripping voltammetry (DP AdSV) is presented. The Hg(Ag)FE electrode is characterized by very good surface reproducibility (≤2%) and long-term stability (more than 2 thousand measurement cycles). The preparation of the Hg(Ag)FE is very simple and its operation may be controlled automatically. The effects of various factors such as: preconcentration potential and time, pulse height, step potential and supporting electrolyte composition are optimized. The calibration graph is linear from 2 nM (192 ng L^{-1}) to 200 nM (19 μg L^{-1}) for an accumulation time of 15 s, with correlation coefficient of 0.9995. For a Hg(Ag)FE with a surface area of 3.5 mm^2 the detection limit for an accumulation time of 60 s is as low as 8 ng L^{-1}. The repeatability of the method at a concentration level of the analyte as low as 2.4 μg L^{-1}, expressed as R.S.D. is 1.3% (n = 7). The proposed method was successfully applied and validated by studying the certified reference material TMRAIN-95 and simultaneous recovering of Mo(VI) from spiked water and sediment samples.

1. Introduction

Molybdenum has an important role in enzymatic redox reaction. In biological systems, molybdenum is an essential constituent of enzymes, which catalyze redox reactions, e.g. oxidation of aldehydes, xanthine, and other purines [1,2], and reduction of nitrates and molecular nitrogen [3–5]. Molybdenum plays an important role in a wide variety of plants and animals particularly ruminants and is an essential trace element in plant nutrition. Some lands are barren for lack of this element in the soil. Typically deficiency symptoms of molybdenum in animals are poor hatchability, weak chicks, and poor feathering [6]. Delayed puberty, reduced growth rate and reduced egg production are typical toxicity symptoms of molybdenum in animals [7]. Molybdenum also affects self purification processes of natural water and is valuable as a catalyst in the refining of petroleum [8]. High soil and water molybdenum levels can intensify nitrate toxicity. Since the concentration of molybdenum in plants, water and soil is generally at parts per billion levels, therefore, a sufficiently sensitive method is required for the determination of molybdenum.

The most common methods for the trace determination of molybdenum such as spectrophotometry [9], neutron activation analysis [10], atomic absorption spectrometry [11], X-ray fluorescence spectrometry [12], and first-derivative synchronous solidphase spectrofluorimetry [13] require preconcentration procedures such as coprecipitation, solvent extraction, ion exchange, or adsorption on activated carbon. Electroanalytical procedures allow the necessary preconcentration of the analyzed element in situ, which is not possible with the other analytical techniques. Many electroanalytical procedures have been proposed for the determination of trace amounts of molybdenum.

In particular, several adsorptive stripping voltammetric (AdSV) procedures have been developed for the determination of trace molybdenum. These include the use of different complexing agents such as Toluidine Blue [14], oxine [15–17], chloranilic acid [18], methyl thymol blue [19], cupferron [20,21], a-benzoin oxime [22–24], 1,10-phenanthroline [25], dihydroxynaphthalene [26], *p*-cresol derivative [27], resorcinol derivative [28], cetyltrimethylammonium bromide [29], methyl orange [30], 8-hydroxyquinoline [14], a-benzoin oxime [31], pyrogallol red [32], and mandelic acid [33].

Authors in most works dealing with voltammetric determination of molybdenum mostly use the HMDE as the working electrode. Only in a few cases other electrodes such as the bismuth-film electrode [34], the glassy carbon electrode [35], modified carbon paste electrodes [29,36] were used.

The HMDE is the electrode of preference due to its high sensitivity, reproducibility and linearity. However, the toxicity of mercury

* Corresponding author. Tel.: +48 12 6172473; fax: +48 12 6341201.
E-mail address: rpiech@agh.edu.pl (R. Piech).

0039-9140/$ – see front matter © 2008 Elsevier B.V. All rights reserved.
doi:10.1016/j.talanta.2008.02.038

limits the usage of the mercury electrodes in the analytical practice and excludes them from the out-of-laboratory applications. The problem of limiting the amount of mercury or its soluble salts needed for the analytical procedure can be solved with the help of a renewable silver amalgam film electrode. The principle of working and first proposal of a construction of the (Hg(Ag)FE) was described in, Ref. [37].

In this work differential pulse adsorptive cathodic stripping voltammetry (DP AdSV) is applied for the trace molybdenum(VI) determination in the presence of chloranilic acid as a complexing agent [18]. The presentation of the optimized methodology of the voltammetric determination of molybdenum(VI) by application of cylindrical mercury film electrode formed on the silver wire, refreshed before each measurement, is the main purpose of this paper. The validation and recovery of the method was evaluated by use certified reference material and by use of spiked water and sediment samples. Potential interference from selected cations, humic materials and surface-active substances was determined using commercially supplied humic acid and Triton X-100.

2. Experimental

2.1. Measuring apparatus and software

A multipurpose Electrochemical Analyzer M161 with the electrode stand M164 (both MTM-ANKO, Poland) were used for all voltammetric measurements. The classical three-electrode quartz cell, volume 20 mL, consisting of a homemade cylindrical silver based mercury film electrode, refreshed before each measurement and with a surface area of 1–12 mm^2, as the working electrode, a double junction reference electrode Ag/AgCl/KCl (3 M) with replaceable outer junction (3 M KCl) and a platinum wire as an auxiliary electrode. The results obtained with the film electrode were then compared with corresponding values obtained using the Hanging Mercury Drop Electrode M163 (MTM-ANKO). pH measurements were performed with laboratory pH-meter. Solid material was digested with a Uniclever II microwave digestion system (Plazmatronika, Poland). Liquid samples were mineralized using a UV-digester (Mineral, Poland). Stirring was performed using a magnetic bar rotating at approximately 500 rpm. All experiments were carried out at room temperature. The MTM-ANKO *EAGRAPH* software enabled electrochemical measurements, data acquisition and advanced processing of the results.

2.2. Chemicals and glassware

All reagents used were of analytical grade. HNO_3 (Merck, Suprapur®), mercury GR for polarography (Merck). 0.01 M standard stock solutions of molybdenum(VI) were prepared by dissolving the sodium salt $Na_2MoO_4{\cdot}2H_2O$ (Aldrich). Solutions with lower molybdenum concentrations were made weekly by appropriate dilution of the stock solution. A fresh 0.01 M solution of chloranilic acid (Aldrich) was prepared every two weeks by dissolving chloranilic acid in water. Certified reference materials, rain water TMRAIN-95 was obtained from the National Water Research Institute, Canada. Triton X-100 (Windsor Laboratories Ltd., UK) and humic acid (sodium salt, Aldrich). A 0.1% solution of humic acid was prepared by dissolving the primary (original) reagent in water distilled from quartz with addition of 10 μL of 10% NH_3. The silver base for the film electrode was prepared from polycrystalline silver wire with a diameter of 0.5 mm, and of 99.99% purity (Goodfellow Science Park, England). Prior to use, glassware was cleaned by immersion in a 1:1 aqueous solution of HNO_3, followed by copious rinsing in distilled water.

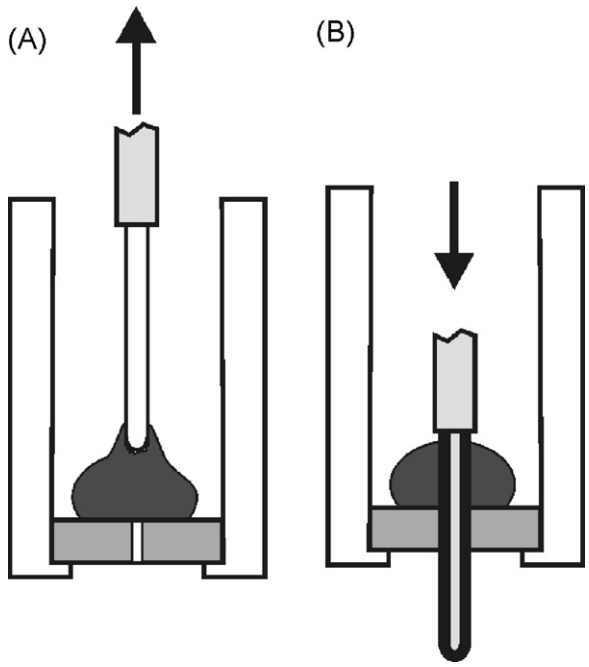

Fig. 1. The principle of mechanical refreshing of the mercury film silver based electrode. The Hg(Ag)FE used in our experiments: (A) refreshing configuration, (B) configuration ready for measurement.

2.3. Construction of the cyclic renewable mercury film electrode Hg(Ag)FE

The cyclic renewable mercury film silver based electrode was described in Refs. [37,38]. The simple construction of the applied electrode that allows the mercury film to be refreshed before each measurement, a procedure essential for its performance, is given in Fig. 1. The procedure of refreshing the outer mercury film involves two steps (Fig. 1A) pulling up the silver electrode base inside the electrode body, through the mercury chamber and then (Fig. 1B) pushing it back outside the electrode body. In comparison to pure mercury, the liquid amalgam allows the electrode to function in a stable manner for a great number of regeneration cycles and, furthermore, to stay usable for an extended period of several months, which was proved in a previously published paper [37].

2.4. Standard procedure of measurements

Quantitative measurements were performed using differential pulse adsorptive cathodic stripping voltammetry and the standard addition procedure. The procedure of refreshing the mercury film Hg(Ag)FE electrode was carried out before each measurement. A potential of −1.10 V was applied to condition the electrode prior to the refreshing step. An Hg(Ag)FE electrode conditioned in this way was used to determine molybdenum(VI) in the supporting electrolyte: 40 μL HNO_3 (1:10) + 100 μL chloranlilic acid (0.01 M) and water (total volume 10 mL) contained in a quartz voltammetric cell. The potential of the electrode was changed in the following sequence: conditioning potential −1.10 V for 7 s, accumulation potential E_{acc} = 0.00 V for t_{acc} = 30 s and starting potential −0.250 V for 3 s. During the accumulation step molybdenum(VI) was adsorbed while the solution was being stirred (ca. 500 rpm.) using a magnetic stirring bar. Then, after a rest period of 5 s a differential pulse voltammogram was recorded in the cathodic direction from −0.250 V to −0.850 V. The other experimental parameters were as follows: step potential, 4 mV; pulse potential, 30 mV; time

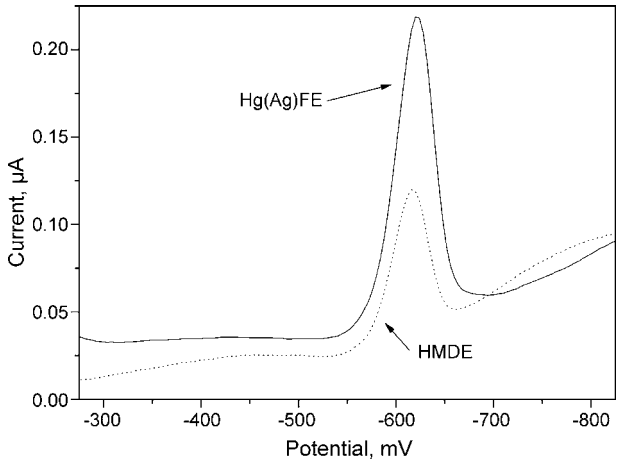

Fig. 2. Comparison of voltammograms obtained for 25 nM molybdenum(VI) in 100 μM chloranilic acid and HNO_3 (pH of base electrolyte 2.5) for HMDE and Hg(Ag)FE electrode. The electrode areas were 3.5 mm^2 for the (Hg(Ag)FE) and 1.8 mm^2 for the HMDE. Instrumental parameters: ΔE = 30 mV, E_s = 4 mV, t_w = 10 ms. Preconcentration potential E_{acc} = 0.00 V and time t_{acc} = 30 s. Stirring rate, 500 rpm.

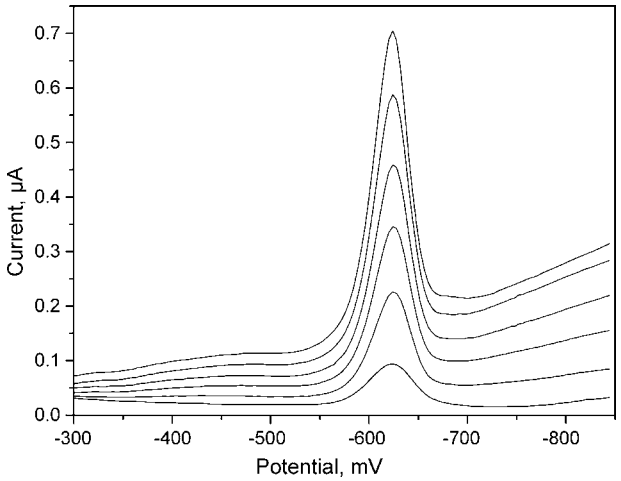

Fig. 3. Voltammograms obtained for electrode surface area: 1.7 mm^2, 3.5 mm^2, 5.3 mm^2, 7.1 mm^2, 8.9 mm^2 and 10.7 mm^2 for 25 nM molybdenum(VI) in 100 μM chloranilic acid and HNO_3 (pH of base electrolyte 2.5). All other conditions as in Fig. 2.

step potential, 30 ms (10 ms waiting +20 ms sampling time). The measurements were carried out from deaerated solutions.

2.5. Sample preparation

2.5.1. Water

For DP AdSV determination of Mo(VI) in and tap water samples, 40 mL of the sample were transferred directly into a quartz tube. For each sample, 20 μL of HNO_3 (conc.) were added. Acidified water samples were digested by UV irradiation for 2 h.

2.5.2. Sediment

For DP AdSV molybdenum determination in the sediments, about 250 mg of dried sample was weighed and transferred into a high pressure Teflon container and treated with 4 mL of nitric acid and 2 mL of perchloric acid. The vessel was then placed into a microwave oven. Digestion of the samples was carried out with the following program: 15 min under microwave irradiation 10 min cooling time, 5 min waiting time. Digested samples were placed on a heated plate in order to evaporate. The sample solutions were cooled to room temperature and transferred quantitatively into volumetric flasks (10 mL) and filled up to the mark with four times distilled water.

3. Results and discussion

3.1. Renewable film electrode Hg(Ag)FE

Adsorptive stripping voltammetric techniques are applicable for measuring ultra traces of molybdenum(VI). So far, one of the most sensitive methods are based on the adsorption of a complex of molybdenum with chloranilic acid on a hanging mercury electrode [18,39]. This is due to its high sensitivity, reproducibility and linearity. However, the use of mercury has to be avoided because of its toxicity, especially in the case of environmental analysis. The problem of the limitation of mercury or its soluble salts from the analytical procedure can be solved with the help of Hg(Ag)FE. Signals obtained for Hg(Ag)FE as compared to HMDE are in Fig. 2. Molybdenum peak current is similar for the Hg(Ag)FE vs. the HMDE electrode (for comparable geometrical sizes of surfaces of working electrodes). The peak potentials were similar for both electrodes. The halfway width of the molybdenum(VI) peak current was 45 mV for both electrodes. The obtained precision for n = 7 was 1.3%. The surfaces of solid electrodes are usually much larger than those of mercury drop electrodes. When using the Hg(Ag)FE electrode the surface of the working electrode may easily be varied in a wide range. For a surface area of 1.7 mm^2, the molybdenum peak current was 81 nA and grew linearly as the surface of the working electrode increased in size. For a surface area of 10.7 mm^2, the peak current was 550 nA (Fig. 3). The parameters of the linear growth of peak current vs. surface of working electrode are: slope, 51.6 ± 0.5 (nA mm^{-2}), and correlation coefficient r = 0.999. For further study, a 3.5 mm^2 surface area was applied.

In the case of the electrode with no refreshable mercury layer the signal from the molybdenum decreased significantly after each registration.

3.2. Influence of DPV parameters on technique on molybdenum(VI) peak

The important parameters of the DPV technique are pulse amplitude (ΔE), potential step amplitude (E_s) and pulse duration which consist of the sampling time (t_s) and the waiting time (t_w). The former define time when current is measured and the latter is time elapsing from leading edge of the pulse to the moment when starts current measurement. Longer waiting time cause lower measured current and better ratio of faradaic to capacitive current. Consequently, these parameters were investigated. To optimize the conditions for molybdenum measurements, the following instrumental parameters were systematically varied: ΔE in the range 10–100 mV (both positive and negative mode), E_s in the range 1–6 mV and t_w from 10 ms to 80 ms (t_s = const = 10 ms).

For a pulse amplitude of 10 mV the molybdenum(VI) peak current was equal to 72 nA and increased with increasing pulse amplitude. The best results were obtained for an amplitude of 30 mV (the peak current was ~180 nA). Higher pulse amplitude (>30 mV) caused major growth of the background current. The increase in pulse amplitude from 10 mV to 100 mV caused the peak potential to shift from −615 mV to −635 mV and from −605 mV to −530 mV for negative pulse amplitude, respectively (peak currents were similar for both negative and positive values). For further work, the pulse amplitude of 30 mV was applied.

Changes of the step potential cause influence on peak current. For a step potential equal to 1 mV the peak current was 70 nA, and

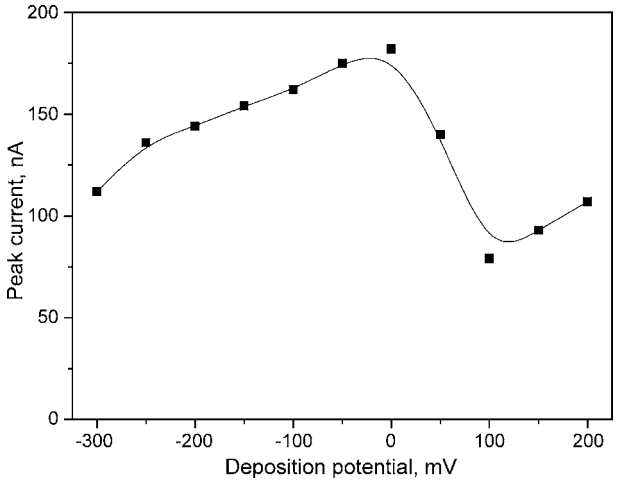

Fig. 4. Dependence of the peak current on preconcentration potential in the range from −300 mV to 200 mV for 25 nM molybdenum(VI) in 100 μM chloranilic acid and HNO_3 (pH of base electrolyte 2.5). All other conditions as in Fig. 2.

for a step potential of 6 mV the peak current was ~210 nA. The step potential of 4 mV was applied in further work.

The waiting time was changed in the range from 10 ms to 80 ms. The best result was obtained for waiting time of 10 ms, and this was the value chosen for further work.

3.3. Influence of preconcentration potential and time on molybdenum(VI) peak

Influence of preconcentration potential and time are always important factors on the sensitivity and detection limit of the method. Optimal preconcentration potential for molybdenum(VI) determination in 100 μM chloranlilic acid and HNO_3 (pH of base electrolyte 2.5) is in the range from −0.050 V to 0.0 V (Fig. 4). For preconcentration potentials lower than −50 mV and higher than 0 mV, the molybdenum peak decreased significantly. For further work, a 0 mV preconcentration potential was applied.

The changes in magnitude of the molybdenum peak current and its potential vs. preconcentration time are presented in Fig. 5. The peak current increased with the increase of the preconcentration time from 66 nA (t_{acc} = 10 s) to 582 nA (t_{acc} = 240 s). For a preconcentration time of 240 s and higher, practically no increase of the molybdenum peak current was observed, but there was an increase in halfway width and distortion of the peak. The molybdenum peak potential is dependent on either the preconcentration potential (ΔE_p = 6 mV) and the preconcentration time (from 632 mV (10 s) to 612 mV (240 s)).

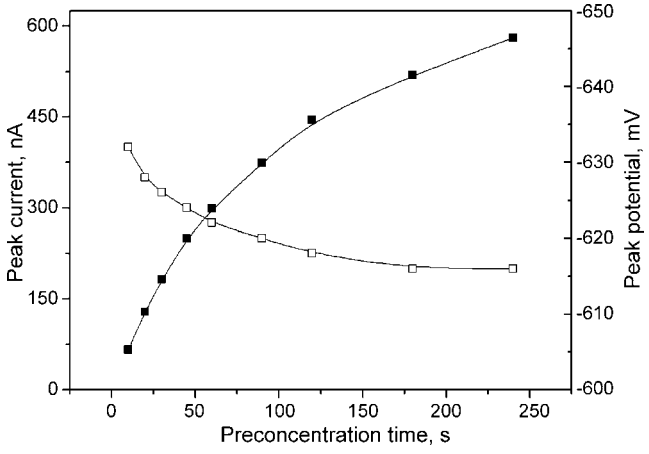

Fig. 5. Dependence of the peak current and its potential on preconcentration time in the range from 10 s to 240 s for 25 nM molybdenum(VI) in 100 μM chloranilic acid and HNO_3 (pH of base electrolyte 2.5). All other conditions as in Fig. 2.

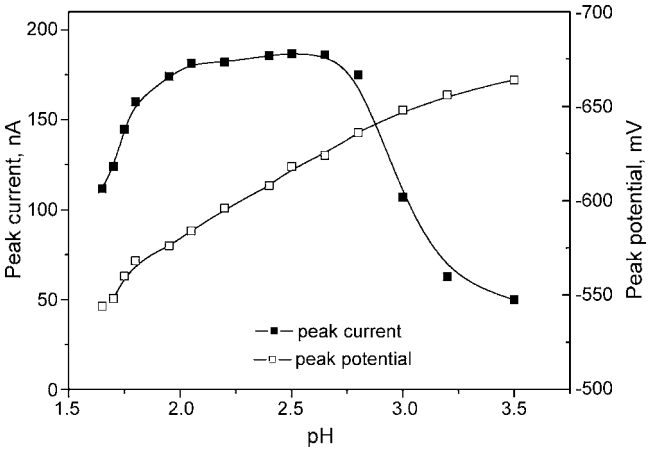

Fig. 6. Dependence of the peak current and its potential on pH in the range from 3.5 to 1.65 for 25 nM molybdenum(VI) in 100 μM chloranilic acid and HNO_3. All other conditions as in Fig. 2.

3.4. Influence of pH on molybdenum(VI) peak

Determination of molybdenum in presence of chloranilic acid requires a low pH in order to obtain a complex, which is adsorbed on the working electrode during the preconcentration. The peak current of Mo(VI)-complex depend on the pH. In Fig. 6, the dependence of peak current and its potential on pH is presented. For a pH of 3.5 the observed molybdenum peak current was 50 nA and increased with more acidic conditions. The optimal pH was in the range from 2 to 2.8 (with the peak current reaching values about 180 nA). More acidic conditions caused a decrease in the peak current, e.g. for a pH of 1.65 the peak current was 112 nA. The pH also had an influence on the peak potential, which changed significantly to positive values for lower pH values. For example, for a pH of 3.5 the peak potential was −664 mV and for a pH of 1.65 the peak potential was −554 mV. For further measurements, a pH of 2.5 was applied (the pH was adjusted with HNO_3 1:10).

3.5. Influence of chloranilic acid concentration on the peak of molybdenum(VI)

Chloranilic acid was used as a complexing agent for molybdenum determination. In general, there are two main mechanisms for the adsorptive accumulation of complexes. First, the adsorption of the complex, built in the solution and second, the adsorption of the ligand at the electrode and the complexation of the central atom with the adsorbed ligand. The last mechanism is preferred in the chloranlilic acid molybdenum system [40]. The molybdenum peak current and its potential depend on the concentration of chloranilic acid (Fig. 7). The addition of chloranilic acid to the base electrolyte is accompanied by increase of the Mo(VI) peak. The optimal concentration of chloranilic acid was in the range from 50 μM to 100 μM (with the peak current reaching values around 180 nA). Higher concentrations of chloranilic acid cause decrease in the peak current. e.g. for 400 μM of chloranilic acid the peak current decreased by 35%. The concentration of chloranilic acid also had an influence on the peak potential, which changed to more negative values for higher chloranilic acid concentrations, e.g. for 2.5 μM of

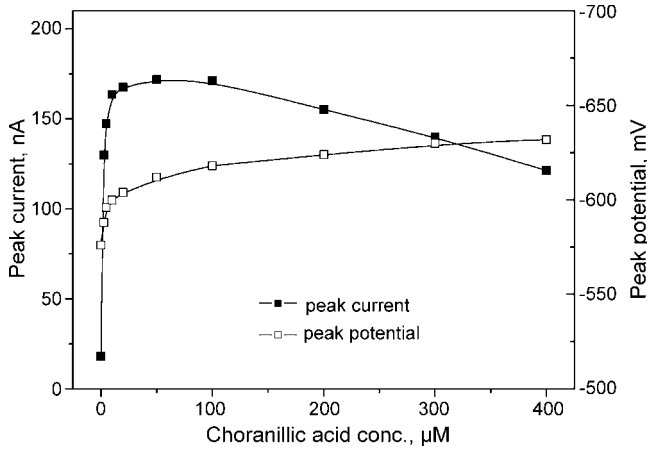

Fig. 7. Dependence of the peak current on chloranilic acid concentration in the range from 0 μM to 400 μM for 25 nM molybdenum(VI) in HNO_3 (pH of base electrolyte 2.5). All other conditions as in Fig. 2.

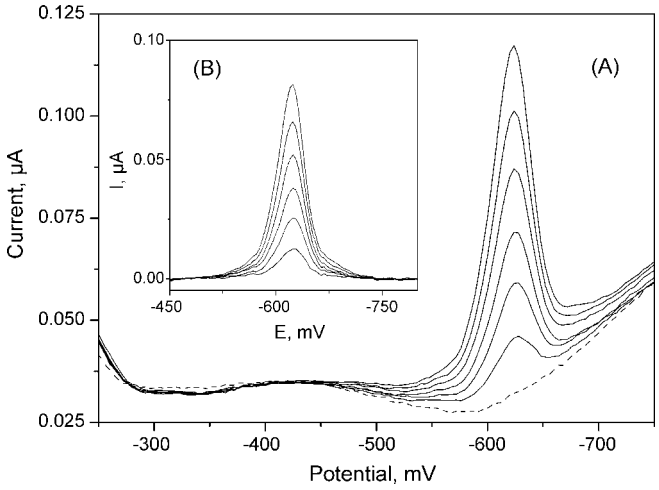

Fig. 8. DP AdSV molybdenum(VI) calibration voltammograms for 0 nM, 2 nM, 4 nM, 6 nM, 8 nM, 10 nM and 12 nM Mo(VI) obtained for preconcentration time 30 s in 100 μM chloranilic acid and HNO_3 (pH of base electrolyte 2.5) (A) before background current subtraction, (B) after background current subtraction. All other conditions as in Fig. 2.

Table 1
Recovery and precision of the determination of trace molybdenum(VI)

Added (nM)	Found (nM)	Recovery (%)	R.S.D. (%)
3.5	3.62	103	3.6
7.5	7.65	102	2.9
27	26.5	98	2.1

chloranilic acid the peak potential was −588 mV and for 400 μM of chloranilic acid the peak potential was −632 mV. For further work, a concentration of 100 μM was used.

3.6. Interferences

The examined ions, such as Fe(III) in a 1000-fold excess, and Pb(II), Cd(II), Zn(II), Sb(III), Bi(III), Cu(II), U(VI), As(III), V(V), Cr(III), Mn(II), Mn(VII) in a 100-fold excess did not interfere. However, it was observed that for Se(IV) ions in a concentration of 50 nM, the Mo(VI) peak current decreased by 21%, for a 10-fold excess by 65%, and for a 20-fold excess by 80%. Fortunately, Se(IV) concentrations in water samples are very low. For W(VI) ions in a concentration of 500 nM, the Mo(VI) peak current decreased by 39%, for a 50-fold excess peak current decreased completely. For Cr(VI) ions in a concentration of 250 nM, the Mo(VI) peak current decreased by 9%, for a 20-fold excess by 26%, for a 50-fold excess by 55%, and for a 100-fold excess by 80%.

The surface-active compounds are usually a source of strong interferences in voltammetric methods. A non-ionic surface-active compound (Triton X-100) and humic acid were investigated in this respect. For 1 mg L^{-1} of Triton X-100 concentration, no suppress of the signal was observed. Higher concentration of Triton X-100 caused suppress the signal e.g. for 2 mg L^{-1} of Triton X-100 by 33% and for 5 mg L^{-1} of Triton X-100 by 83%, and in the case of humic acid a concentration of 0.35 mg L^{-1} was enough to suppress the signal completely. Consequently, humic acid should be thoroughly destroyed by digestion prior to analysis.

3.7. Analytical performance

The DP AdSV voltammograms for the 0–12 nM concentration range of Mo(VI) are presented in Fig. 8. The width of the peak at half-height was 45 mV. For a short preconcentration time (15 s) the obtained detection limit [41], is 0.4 nM and the linearity is up to 200 nM. For example, for a preconcentration time of 30 s the detection limit is 0.2 nM, and for 60 s the detection limit is 0.08 nM. The slopes (nA nM^{-1}), intercepts (nA) and correlation coefficients for regression lines are: (3.39 ± 0.03, 3.74 ± 2.38, R = 0.9995); (7.13 ± 0.072, −1.79 ± 1.62, R = 9996) and (16.75 ± 0.19, 0.45 ± 1.12, R = 0.9986) for preconcentration times of 15 s, 30 s and 60 s, respectively. Precision and recovery (based on three repetitions of analysis and using the standard additions method) were determined using three different samples spiked by 3.5 nM, 7.5 nM and 27 nM of Mo(VI) (Table 1).

To validate the method the certified reference material rain water (TMRAIN-95 National Water Research Institute, Canada) was applied. 0.197 ± 0.012 ppb molybdenum(VI) was determined (based on three repetitions of analysis). This result is in good agreement with certified value of 0.17 ± 0.10 ppb.

The tap water samples from, spiked with molybdenum(VI), were analyzed according to the described procedure using the Hg(Ag)FE electrode. Determinations of Mo(VI) were performed using the standard addition method. Results from Mo(VI) determination are presented in Table 2. The recovery of Mo(VI) ranged from 92% to 102%. The analytical usefulness, of the presented method for the

Table 2
Results of molybdenum(VI) determination in the water samples and sediment

Mo(VI) added (nM)	Mo(VI) found $\bar{x} \pm s$ (recovery, %) (nM)		
	Tap water (nM)	Raba river (nM)	Dobczyce reservoir sediment (mg L^{-1})
0	4.13 ± 0.18	0.42 ± 0.05	1.89 ± 0.15
2.5	6.61 ± 0.11 (99)	2.80 ± 0.17 (96)	–
5.0	9.1 ± 0.12 (99)	–	–
10.0	14.33 ± 0.13 (102)	–	–
2.0 (mg L^{-1})	–	–	3.58 ± 0.24 (92)

determination of trace molybdenum(VI) in samples and sediment was confirmed.

For short-term reproducibility of the analytical response for the Hg(Ag)FE electrode is very good (for 25 nM Mo(VI) at 30 s electrodeposition time is 2–3%). The shape and the reproducibility of molybdenum stripping peaks remain unchanged. The long-term stability (three months) of the Hg(Ag)FE electrode is excellent. The sensitivity of the electrode over long periods of time and over a large amount of measurements may by about 5%.

4. Conclusions

The presented DP AdSV method for the electrochemical determination of molybdenum(VI) using a new cylindrical silver based mercury film electrode, refreshed before each measurement, allows to determine Mo(VI) at ultra-trace level, in concentrations as low as 0.08 nM (8 ng L^{-1}) for a short preconcentration time of 60 s. The reproducibility of the method is very good, i.e. when measured as R.S.D. is 1.3% (with each measurement performed at a fresh surface of the working electrode). Acceptable recovery (92–102%) shows that the proposed method can be used for the determination of Mo(VI) in water samples and sediments.

The simple, mechanical system of mercury film refreshing provides a good surface electrode repeatability and reproducibility that is not available for other mercury film electrodes. The miniature construction of the device and possibility of automation of the process indicate that the Hg(Ag)FE may be especially useful in flow measurements conditions. With the Hg(Ag)FE, the disadvantages of the HMDE (low surface area, poor mechanical resistance, susceptibility to damage and the application of mercury in measurements [42,43], etc.) may be eliminated to a large degree.

The Hg(Ag)FE refreshed before each measurement demonstrates many properties which are specific only to the hanging mercury electrode. The Hg(Ag)FE displays long-term stability for at least 2–3 months.

Acknowledgment

The study was financed as an R&D project by the Polish Ministry of Science and Education from research funds for the years 2007–2010. No. 15 020 02.

References

[1] E.I. Stiefel, Science 272 (1996) 1599.
[2] H. Schindelin, C. Kisker, J. Hilton, K.V. Rajagopalan, D.C. Rees, Science 272 (1996) 1615.
[3] D. Sellmann, Angew. Chem.-Int. Ed. 32 (1993) 64.
[4] J. Kim, D. Woo, D.C. Rees, Biochemistry 32 (1993) 7104.
[5] R.H. Burris, G.P. Roberts, Annu. Rev. Nutr. 13 (1993) 317.
[6] A. Petrosek, E. Steven, Ind. Water Eng. 10 (1971) 26.
[7] J.C. de Andrade, A.M. de Almeida, A.R. Coscione, L.M. Aleixo, Analyst 126 (2001) 892.
[8] T.A. Asmangulan, Gig. Sanit. 4 (1965) 6.
[9] J.P. Riley, D. Taylor, Anal. Chim. Acta 41 (1968) 175.
[10] M. Ponta, Modern Methods for Trace Elements Analysis, Ann Arbor Sci., Ann Arbor, MI (1978).
[11] P.B. Barrera, C.P. Calvo, J.A.C. de Juan, Anal. Chim. Acta 231 (1990) 321.
[12] A. Kimura, A. Yoneda, Y. Maeda, T. Azumi, Nippon Kaisui Gakkai-Shi. 40 (1986) 141.
[13] F. Capitán, G.S. Palencia, A. Navalon, L.F. C-Vallvey, J.L. Vilchez, Anal. Chim. Acta 259 (1992) 345.
[14] M.M.P.M. Neto, M.M.G.S. Rocha, C.M.A. Brett, Talanta 41 (1994) 1597.
[15] S.B. Adeloju, F. Pablo, Electroanalysis 7 (1995) 476.
[16] Z.Q. Gao, K.S. Siow, Talanta 43 (1996) 719.
[17] Y.C. Sun, J. Mierzwa, C.R. Lan, Talanta 52 (2000) 417.
[18] M. Karakaplan, G. Henze, Electroanalysis 5 (1993) 623.
[19] A. Safavi, E. Shams, Anal. Chim. Acta 396 (1999) 215.
[20] A.A. Ensafi, T. Khayamian, M. Atabati, Talanta 57 (2002) 785.
[21] K. Jiao, W. Jin, H. Metzner, Anal. Chim. Acta 260 (1992) 35.
[22] J.C. De Andrade, A.M. De Almeida, A.R. Coscione, L.M. Aleixo, Analyst 126 (2001) 892.
[23] Z.Q. Gao, K.S. Siow, A. Ng, Electroanalysis 8 (1996) 1183.
[24] J.C. de Andrade, A.M. de Almeida, L.M. Aleixo, A.R. Coscione, M.F. de Abreu, Anal. Chim. Acta 487 (2003) 243.
[25] F. Quentel, Electroanalysis 11 (1999) 1355.
[26] H. Li, R.B. Smart, J. Electroanal. Chem. 429 (1997) 169.
[27] I.C.S. Fraga, P.A.M. Farias, A.K. Ohara, Fresenius J. Anal. Chem. 366 (2000) 307.
[28] G.V. Prokhorova, V.M. Ivanov, G.A. Kochelaeva, J. Anal. Chem. 55 (2000) 669.
[29] M. Stadlober, K. Kalcher, G. Raber, Anal. Chim. Acta 350 (1997) 318.
[30] Z.L. Jiang, Q. Gong, M.D. Liu, Anal. Lett. 27 (1994) 1954.
[31] Z.Q. Gao, K.S. Siow, Mikrochim. Acta 124 (1996) 211.
[32] A.A. Ensafi, T. Khayamian, S.S. Khaloo, Anal. Chim. Acta 505 (2004) 201.
[33] K. Yokel, C.M.G. van den Berg, Anal. Chim. Acta 257 (1992) 293.
[34] J. Wang, S. Thongngamdee, D. Lu, Electroanalysis 18 (2006) 59.
[35] D. Lowinsohn, M. Bertotti, Electroanalysis 14 (2002) 619.
[36] K. Sugawara, T. Miyasita, S. Hoshi, K. Akatsuka, Anal. Chim. Acta 353 (1997) 301.
[37] B. Baś, Z. Kowalski, Electroanalysis 15 (2002) 14.
[38] Polish Patent No. P-319 984 (1997).
[39] S. Sander, Anal. Chim. Acta 394 (1999) 81.
[40] S. Sander, Fresenius J. Anal. Chem. 365 (1999) 435.
[41] J. Winefordner, G. Long, Anal. Chem. 55 (1983) 7.
[42] http://www.internat.environ.se/
[43] The Ordinance on Prohibition in Connection with Handling, Importation and Exportation of Chemical Products Etc. (Certain Cases), 9–11 (SFS 1998:944).

Talanta 76 (2008) 407–412

Contents lists available at ScienceDirect

Talanta

journal homepage: www.elsevier.com/locate/talanta

Semi-empirical topological index: Development of QSPR/QSRR and optimization for alkylbenzenes

Ledilege Cucco Porto[a], Érica Silva Souza[a], Berenice da Silva Junkes[b], Rosendo Augusto Yunes[a], Vilma Edite Fonseca Heinzen[a,*]

[a] Departamento de Química, Universidade Federal de Santa Catarina, Campus Universitário, Trindade, 88040-900 Florianópolis, SC, Brazil
[b] Departamento Acadêmico de Formação Geral, Centro Federal de Educação Tecnológica de Santa Catarina, Av. Mauro Ramos, 950, Centro, 88020-300 Florianópolis, SC, Brazil

ARTICLE INFO

Article history:
Received 13 November 2007
Received in revised form 14 March 2008
Accepted 15 March 2008
Available online 25 March 2008

Keywords:
Gas chromatographic retention indices
Topological indices
Alkylbenzenes
Quantitative structure–retention relationships
Semi-empirical topological index

ABSTRACT

The semi-empirical topological index, I_{ET}, was developed and optimized to describe the chromatographic retention of alkylbenzenes on the squalane stationary phase. The simple linear regression between the chromatographic retention and the proposed index, for 122 alkylbenzenes studied, is of good quality (determination coefficient, $r^2 = 0.9996$, standard deviation, S.D. = 5.5, and leave-one-out cross-validation correlation coefficient, $r^2_{CV} = 0.9996$). The predictive ability of I_{ET} was also verified for stationary phases with two different polarities (SE-30 and Carbowax 20 M), and good results were obtained, especially for the stationary phase with low polarity, showing that the specific molecular interactions occur on highly polar phases. The I_{ET} was applied to construct quantitative structure–property relationship (QSPR) models for representative properties such as boiling point, Bp(°C), octanol/water partition coefficient, log *P*, van der Waals volume (V_W) and molar refractivity (R_M). Satisfactory quality QSPR models were obtained with Bp, V_W and R_M showing that the molecular size and dispersive forces are dominating factors with respect to the chromatographic retention.

1. Introduction

Quantitative structure–retention relationships (QSRR) are unquestionably of great importance in modern chemistry and biochemistry; their study involves the prediction of chromatographic retention parameters based on molecular structure. The molecular descriptors that are created from the structure encode most of the interactions (solute–solute, solute–stationary phase) that are responsible for the distribution of solute on a GC column. A large number of topological descriptors have been derived from molecular graphs [1–7]. The relevance of QSRR studies can be seen in recently published reviews [8,9]. Although there are several articles reporting studies on the structure–retention relationship for alkylbenzenes using many descriptors through multiple correlations [10–23], the search for new and better indices that can elucidate the interactions between the solute–stationary phases in a simple way through a single specific descriptor is gaining importance. In this context, the alkylbenzenes were selected because of their wide use as solvents and artificial flavors, their importance in the petrochemical industry and their use as markers of environmental pollution by petroleum products. Thus, the study of their physicochemical properties serves in the optimization of the separation of industrial alkyl–benzene mixtures [24]. These are an attractive class of organic compounds for the application of QSPR/QSAR studies.

In recent years, our group has introduced a semi-empirical topological index for QSRR/QSPR studies of alkanes, alkenes, esters, ketones, aldehydes and alcohols [25–34]. This index is based on the hypothesis that the chromatographic retention of the compounds is a result of the number of each specific carbon atom and/or functional group and their interaction with the stationary phase. Consequently, this interaction is reduced by the steric effects of neighboring carbon atoms and/or functional groups. The interaction of each carbon atom and/or functional group with the stationary phase is determined by its contribution to the intermolecular forces of the solute, which in turn is determined by its electrostatic and steric properties. The values attributed to each carbon atom and functional group (the vertexes of the molecular graphs) are based on the experimental chromatographic behavior of the compounds interpreted according to the theoretical hypothesis cited above. For this reason our index was named the semi-empirical topological. The main advantage of this novel approach is the prediction of chromatographic retention with a single topological index differentiating the isomeric structures of the compounds.

* Corresponding author.
E-mail address: heinzen@qmc.ufsc.br (V.E.F. Heinzen).

0039-9140/$ – see front matter © 2008 Elsevier B.V. All rights reserved.
doi:10.1016/j.talanta.2008.03.023

The primary proposal of this paper is to extend the semi-empirical topological method in order to predict the chromatographic retention of alkylbenzene compounds and to test its predictive ability on stationary phases with different polarities. The second aim of this study is to demonstrate the applicability of I_{ET} to predict physicochemical properties that are dependent on the strength of intermolecular forces.

2. Methods

2.1. Calculation of the semi-empirical topological index

The same considerations employed in the generation of the semi-empirical topological index, I_{ET}, for linear and branched alkanes and alkenes described in previous papers [25,26] were applied to this group of compounds (alkylbenzenes).

Firstly, the molecules were represented by hydrogen-suppressed molecular graphs based on chemical graph theory [35] where the carbon atoms were considered as vertexes of the molecular graph of these compounds. The contribution of each carbon atom to the chromatographic retention is represented by a single symbol, C_i, as can be observed from Eq. (1). Thus, the semi-empirical topological index, I_{ET}, is expressed as:

$$I_{ET} = \Sigma(C_i + \delta_i)$$
$$\delta_i = \log C_1 + \log C_2 + \ldots.. \quad (1)$$

where C_i is the value attributed to (=C<) fragments and/or each carbon atom i in the molecule; and δ_i is the sum of the logarithm of the values for each adjacent carbon atom (C_1, C_2, C_3 and C_4).

The values to be attributed to the carbon atoms (C_i) for alkylbenzenes, were calculated by numerical approximation based on the experimental RI values and supported by theoretical considerations, as follows:

(i) The alkylbenzenes were subdivided into the following groups: linear; branched; substituted in *ortho*, *meta* and *para* positions; tri-substituted and tetra-substituted.
(ii) From the retention index values of benzene and alkylbenzenes, an approximate I_{ET} value was calculated through the equation previously obtained for linear alkanes containing 3–10 carbon atoms ($RI_{EXP} = 123.6871(\pm0.0007)I_{ET} - 47.3557(\pm0.0044)$; $N = 8$; S.D. = 0.004; $r^2 = 1.0$) [25].
(iii) The C_i value of the fragment (=CH—) of benzene was calculated through the approximate I_{ET} value.
(iv) The fragment values (=C<) for the linear alkylbenzenes were calculated through Eq. (1) using the values of C_i for primary (—CH_3) and secondary (—CH_2—) carbon atoms reported by Yunes and co-workers [25], the previously determined value of the fragment (=CH—) (item iii) and the approximate I_{ET}.
(v) For the other groups classified, the approximate I_{ET} was calculated through the equation obtained for linear alkylbenzenes [$RI_{EXP} = -47.01474 + 123.7663I_{ET}$ $r = 0.99997$, S.D. = 3.1, $n = 13$].
(vi) The fragment values (=C<) for the branched alkylbenzenes were obtained in the same way as those of the linear alkylbenzenes, i.e., the values of C_i tertiary (—CH<) and quaternary (>C<) carbon atoms previously reported by Yunes and co-workers [25] were considered.
(vii) The C_i values (=C<) for alkylbenzenes substituted in *ortho*, *meta* and *para* positions were estimated according to the chromatographic behavior observed, with the objective of differentiating between the I_{ET} values for the different isomers.
(viii) The C_i values (=C<) for tri-substituted and tetra-substituted alkylbenzenes were obtained by considering the position of one substituent in relation to another closer substituent, using the values previously calculated for alkylbenzenes substituted in *ortho*, *meta* and *para* positions (item vii).

2.2. Data set

The retention indices (RI) of 122 alkylbenzenes with 7–19 carbon atoms in the molecule, subdivided into linear, branched, *ortho*, *meta* and *para* substituted, tri-substituted and tetra-substituted alkylbenzenes, were taken from the literature (Table 1). The retention indices were measured on different stationary phases, non-polar or low polarity squalane [15–17], OV-101 [18], DB-1 [19] and SE-30 [36]. The retention indices were extrapolated to the squalane phase (SQ) at 100 °C according to Eqs. (2)–(6):

$$RI_{SQ\text{-}100\,^\circ C} = 3.9036 + 0.9980\,RI_{SQ\text{-}96\,^\circ C} \quad (2)$$

$$RI_{SQ\text{-}95.4\text{–}140\,^\circ C} = 42.6845 + 0.9675 RI_{SQ\text{-}100\,^\circ C} \quad (3)$$

$$RI_{OV\text{-}101} = 7.9969 + 0.9988\,RI_{SQ\text{-}100\,^\circ C} \quad (4)$$

$$RI_{SQ\text{-}100\,^\circ C} = 2.1909 + 0.9562\,RI_{DB\text{-}1} \quad (5)$$

$$RI_{SE\text{-}30} = 14.4789 + 0.9828\,RI_{SQ\text{-}100\,^\circ C} \quad (6)$$

2.3. Regression analysis

The Origin and Bilin [37–39] program packages were used in the regression analysis. To test the quality of the regression equation, the coefficient of determination (r^2), the coefficient of correlation (r) and the standard deviation (S.D.) were utilized as statistical parameters. To verify the validity and stability of the model obtained, the cross-validation test (r^2_{CV}) using the "leave-one-out" method [38] was performed, and a further examination of the external stability of the model was carried out by means of a procedure in which the entire data group is systematically divided into three subgroups and each subgroup is predicted using the other two as the training group.

3. Results and discussion

3.1. Prediction of retention indices

The values of C_i for primary, secondary, tertiary and quaternary carbon atoms and carbon atoms for linear, branched, *ortho*, *meta* and *para* substituted, tri-substituted and tetra-substituted alkylbenzenes used in the calculation of the semi-empirical topological index (I_{ET}) are listed in Table 2. These values were obtained by observing the general behavior of the experimental retention of compounds measured on low polarity stationary phases along with theoretical considerations.

In the chromatographic retention of compounds in the non-polar or low polarity stationary phases two important types of interactions contribute to the chromatographic retention of the compounds: the induction and dispersion forces. The dispersion forces are related to steric factors, molecular size and branching, while the induced forces are related to the dipolar moment, which should stimulate dipole-induced dipole interactions.

Observing the behavior of the chromatographic retention, different values were attributed to the substituted fragment (=C<) for a series of linear alkylbenzenes according to the small substituents, such as methyl and ethyl groups, and the number of carbon atoms in the alkyl chain (3–10 or 11–13) as seen in Table 2. It can be observed that the *ortho*-isomers comprised of small electron-rich substituents are retained to a greater extent than the *meta*- or *para*-isomers. This makes sense from a dipolar standpoint. When the substituents are in *ortho*-position the electrons are probably

Table 1
Values of experimental retention indices, RI_{EXP} (squalane 100 °C) and values of semi-empirical topological index, I_{ET} calculated for 122 alkyl benzenes

No.	Compounds	RI_{EXP}	I_{ET}	No.	Compounds	RI_{EXP}	I_{ET}
1	Benzene[a,b,c]	650.5	5.6421	62	1-Methyl-3-*n*-propylbenzene[a,b,c]	1034.6	8.7094
2	Methylbenzene[a,b,c]	760.1	6.5282	63	terc-Pentylbenzene	1071.2	9.0436
3	Ethylbenzene[a,b,c]	850.0	7.255	64	*iso*-Pentylbenzene	1100.1	9.1937
4	*iso*-Propylbenzene[b,c]	908.4	7.7251	65	1-Methyl-3-*tert*-butylbenzene	1057.9	8.9339
5	*n*-Propylbenzene[a,b,c]	938.0	7.9317	66	1-Methyl-4-*tert*-butylbenzene	1076.4	9.0555
6	*tert*-Butylbenzene[b]	971.7	8.2351	67	1-Methyl-2-*tert*-butylbenzene	1092.6	9.2142
7	*sec*-Butylbenzene	990.2	8.3853	68	1-Methyl-4-*sec*-butylbenzene	1092.7	9.1553
8	*iso*-Butylbenzene[b,c]	991.3	8.3853	69	1-Ethyl-3-*iso*-propylbenzene	1078.2	9.0629
9	*n*-Butylbenzene[a,b,c]	1036.8	8.7402	70	1-Ethyl-2-*iso*-propylbenzene	1081.5	9.1201
10	*n*-Pentylbenzene[a,b,c]	1133.0	9.5486	71	1-Ethyl-4-*iso*-propylbenzene	1099.0	9.2524
11	1,4-Dimethylbenzene[a,b,c]	864.6	7.3709	72	1-Ethyl-3-*n*-propylbenzene[a]	1112.7	9.3667
12	1,3-Dimethylbenzene[a,b,c]	864.8	7.3724	73	1-Ethyl-2-*n*-propylbenzene[a]	1120.8	9.3215
13	1,2-Dimethylbenzene[a,b,c]	886.0	7.5442	74	1,2-diiso-Propylbenzene	1121.9	9.4514
14	1-Methyl-3-ethylbenzene[a,b,c]	949.7	8.0298	75	1-Ethyl-4-*tert*-butylbenzene	1162.5	9.7666
15	1-Methyl-4-ethylbenzene[a,b,c]	954.3	8.0821	76	1-Methyl-3-*n*-butylbenzene[a]	1134.1	9.5178
16	1- Methyl -2-ethylbenzene[a,b,c]	966.0	8.1665	77	1-Butylhexylbenzene	1491.4	12.3713
17	1-Methyl-3-*iso*-propylbenzene[b,c]	1009.9	8.4055	78	1-Propylheptylbenzene	1499.1	12.4524
18	1,3-Diethylbenzene[a,b,c]	1027.4	8.6871	79	1-Ethyloctylbenzene	1517.2	12.6099
19	1-Methyl-4-*n*-propylbenzene[a,b,c]	1040.2	8.7541	80	1-Methylnonylbenzene	1550.7	12.8906
20	1,4-Diethylbenzene[b,c]	1040.5	8.7932	81	*n*-Decylbenzene[b]	1637.3	13.5911
21	1-Methyl-2-*n*-propylbenzene[a,b,c]	1045.6	8.6992	82	1-Pentylhexylbenzene	1581.3	13.1131
22	1-Ethyl-4-*n*-propylbenzene	1126.4	9.4652	83	1-Butylheptylbenzene	1587.0	13.1797
23	1-Methyl-4-*n*-butylbenzene[a]	1138.8	9.5626	84	1-Propyloctylbenzene	1596.6	13.2608
24	1,3-diiso-Propylbenzene	1120.5	9.4386	85	1-Ethylnonylbenzene	1615.4	13.4183
25	1,4-diiso-Propylbenzene	1154.1	9.7116	86	1-Methyldecylbenzene	1650.1	13.699
26	1,3,5-Trimethylbenzene[a,b,c]	969.0	8.2376	87	1-Pentylheptylbenzene	1676.0	13.9216
27	1,2,4-Trimethylbenzene[b,c]	987.0	8.4094	88	1-Butyloctylbenzene	1679.8	13.9882
28	1,2,3-Trimethylbenzene[a,b,c]	1012.9	8.4953	89	1-Propylnonylbenzene	1691.3	14.0693
29	1,4-Dimethyl-2-ethylbenzene[b,c]	1062.2	9.0317	90	1-Ethyldecylbenzene	1710.4	14.2268
30	1,2-Dimethyl-4-ethylbenzene[b,c]	1072.7	9.0668	91	1-Methylundecylbenzene	1744.8	14.5075
31	1,2,4,5-Tetramethylbenzene[b,c]	1107.1	9.3606	92	*n*-Dodecylbenzene	1820.4	15.116
32	1,2,3,5-Tetramethylbenzene[b,c]	1113.1	9.3606	93	1-Pentyloctylbenzene	1766.8	14.7301
33	1,2,3,4-Tetramethylbenzene[a,b,c]	1138.6	9.4465	94	1-Butylnonylbenzene	1773.5	14.7967
34	1,4-Dibutylbenzene[b]	1410.8	11.7542	95	1-Propyldecylbenzene	1785.0	14.8778
35	1,4-Dipropylbenzene	1212.5	10.1372	96	1-Ethylundecylbenzene	1807.0	15.0353
36	1,4-disec-Butylbenzene	1304.3	10.9396	97	1-Methyldodecylbenzene	1843.3	15.316
37	1,4-diiso-Butylbenzene	1307.7	10.9396	98	*n*-Tridecylbenzene	1923.6	15.9245
38	*n*-Hexylbenzene[a,b]	1231.0	10.3571	99	1,3-Dimethyl-5-ethylbenzene[b,c]	1046.1	8.9255
39	1-Propyl-4-butylbenzene	1311.0	10.9457	100	1,3-Dimethyl-2-ethylbenzene[b,c]	1073.5	9.1176
40	1-Propyl-4-pentylbenzene	1418.9	11.7542	101	1,2-Dimethyl-3-ethylbenzene[b]	1087.7	9.1176
41	*sec*-Pentylbenzene	1078.2	9.1937	102	1,3-Dimethyl-5-propylbenzene	1130.9	9.5746
42	1,3-Dipropylbenzene	1195.5	10.0463	103	1,4-Dimethyl-2-propylbenzene	1145.2	9.5644
43	1-Ethyl-4-*n*-butylbenzene	1227.1	10.2737	104	1,2-Dimethyl-4-propylbenzene	1154.8	9.7464
44	1-Methyl-4-*n*-pentylbenzene	1236.3	10.3711	105	1,3-Dimethyl-2-propylbenzene	1157.6	9.6503
45	1-Ethyl-4-*n*-penthylbenzene	1322.1	11.0822	106	1,2-Dipropylbenzene	1183.2	9.8542
46	1-Methyl-4-*n*-hexylbenzene	1333.4	11.1796	107	1-Ethyl-2-butylbenzene	1204.3	10.1299
47	1,4-Diterc-butylbenzene	1281.3	10.74	108	1-Propyl-2butylbenzene	1278.1	10.6626
48	1-Isobutyl-4-*tert*-butylbenzene	1290.6	10.8398	109	1,2-Dibutylbenzene	1371.9	11.4711
49	1-*sec*-Butyl-4-*tert*-butylbenzene	1290.7	10.8398	110	1-Propyl-2-pentylbenzene	1373.8	11.4711
50	1-Isobutyl-4-*sec*-butylbenzene	1305.8	10.9396	111	1-Ethyl-2-hexylbenzene	1400.5	11.7469
51	1-*n*-Butyl-4-*tert*-butylbenzene	1345.3	11.2471	112	1-Butyl-2-pentylbenzene	1465.5	12.2796
52	1-*n*-Butyl-4-*sec*-butyilbenzene	1358.4	11.3469	113	1-Propyl-2-hexylbenzene	1471.9	12.2796
53	1-*n*-Butyl-4-isobutylbenzene	1359.6	11.3469	114	1-Ethyl-2-heptylbenzene	1502.5	12.5554
54	1-Ethyl-4-*n*-hexylbenzene	1421.1	11.8907	115	1,2-Dipentylbenzene	1559.8	13.0881
55	1-Methyl-4-*n*-heptylbenzene	1433.9	11.988	116	1-Butyl-2-hexylbenzene	1563.2	13.0881
56	1-Isopropyl-4-*n*-propylbenzene	1181.9	9.9244	117	1-Propyl-2-heptylbenzene	1572.7	13.0881
57	1,3-Dimethyl-4-ethylbenzene[b,c]	1066.3	8.9458	118	1-Ethyl-2-octylbenzene	1604.4	13.3639
58	1,3-Dimethyl-5-*tert*-butylbenzene	1150.8	9.7791	119	*n*-Heptylbenzene	1328.1	11.1656
59	1-Methyl-4-isopropylbenzene[c]	1011.8	8.5413	120	*n*-Octylbenzene	1431.1	11.9741
60	1-Methyl-2-isopropylbenzene[b,c]	1017.6	8.4978	121	*n*-Nonylbenzene[b]	1534.3	12.7826
61	1,2-Diethylbenzene[a,b,c]	1039.9	8.7888	122	*n*-Undecylbenzene	1725.7	14.3075

[a,b,c] Compounds included in the models of Tables 3 and 4.
[a] Bp, V_W and R_M.
[b] log *P*.
[c] RI_{EXP}.

more able to induce a more significant dipole at the carbon surface. In the case of the *meta*- and *para*-positions, local dipoles also exist, but the electronic distribution around the molecule is more symmetric leading to a different set of induced dipoles at the carbon surface. These results suggest that the contribution of dipole-induced-dipole interactions is small in these stationary phases. Longer substituents have a different elution sequence *para*- > *meta*- > *ortho*- for low stationary phases.

The distinct C_i (=C<) values were considered for branching alkylbenzenes, the retentions of these compounds decrease due to steric effects, decreasing the intermolecular forces between solute and stationary phases, when compared with their linear isomers.

Table 2
Values of C_i for primary, secondary, tertiary and quaternary carbon atoms and carbon atoms for linear, branched, *ortho*, *meta* and *para* substituted, tri-substituted and tetra-substituted alkyl benzenes

Fragment	Fragment position	C_i
—CH_3	–	1.0
—CH_2—	–	0.9
—CH<	–	0.8
>C<	–	0.7
=CH—	–	0.9683
=C< [a]	monosubstituted	0.9263
	ortho	0.9535
	meta	0.9176
	para	0.9173
=C< [b]	monosubstituted	0.8927
	ortho	0.8767
	meta	0.8564
	para	0.8774
=C< [c]	monosubstituted	0.8401
	ortho	0.7700
	meta	0.8062
	para	0.8237
=C< [d]	monosubstituted	0.8045
=C< [e]	monosubstituted	0.7576
=C< [f]	2	0.6275
	3	0.5407
	4	0.4959
	5	0.4738
	6	0.4564
=C< [g]	monosubstituted	0.7788
	meta	0.7181
	para	0.7624
=C< [h]	monosubstituted	0.8019
	ortho	0.7357
	meta	0.7304
	para	0.7836

[a] Methyl.
[b] Ethyl.
[c] 3–10 carbon atoms in the carbon chain.
[d] 11–13 carbon atoms in the carbon chain.
[e] α, β and γ branching positions (up to 6 carbon atoms).
[f] α branching position (10–13 carbon atoms).
[g] Quaternary carbon atom.
[h] Isopropyl.

Distinct values were also obtained for the fragments (=C<) of the *ortho*, *meta* and *para* positions in the substituted alkylbenzenes to distinguish the isomers. The *meta* position shows a smaller contribution to the chromatographic retention than their *ortho* and *para* isomers. This may be due to the dipolar moment and the molecular surface characteristics of these compounds. The dipolar moments on the *ortho*, *meta* and *para* substituted compounds decrease, in this order, and thus, the *ortho* substituted compounds are retained in the chromatographic column to a greater extent than the others. However, when the surface area of the molecule interacts with the stationary phase, the chromatographic data show that this behavior begins to predominate in relation to dispersive interactions, the retention index values of the *para* isomers being the highest.

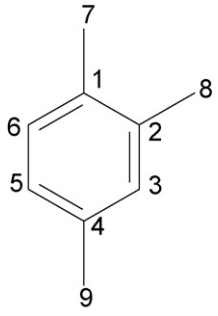

Fig. 1. The hydrogen-suppressed molecular graph of 1,2,4-trimethyl benzene.

For the tri-substituted and tetra-substituted alkylbenzenes the same values attributed to the di-substituted alkylbenzenes were used according to the position of one substituent with reference to another. In this calculation it is important to observe the position of the sustituents. In this case, the 1 and 2 carbon atom positions in the aromatic ring are in *ortho* position and the 4 carbon atom in *meta* position, in relation to the 2 carbon atom (nearest substituent).

The molecule 1,2,4-trimethyl benzene (Fig. 1) is taken as an example of the calculation of the semi-empirical topological index, through Eq. (1) using the C_i values listed in Table 2:

$$C_1 = (=C<) = C_1 + \log C_7 + \log C_2 + \log C_6$$
$$= 0.9535 + \log 1.0 + \log 0.9535 + \log 0.9683$$
$$C_2 = (=C<) = C_2 + \log C_1 + \log C_8 + \log C_3$$
$$= 0.9535 + \log 0.9535 + \log 1.0 + \log 0.9683$$
$$C_3 = (=CH—) = C_3 + \log C_2 + \log C_4$$
$$= 0.9683 + \log 0.9535 + \log 0.9176$$
$$C_4 = (=C<) = C_4 + \log C_9 + \log C_3 + \log C_5$$
$$= 0.9176 + \log 1.0 + 2(\log 0.9683)$$
$$C_5 = (=CH—) = C_5 + \log C_4 + \log C_6$$
$$= 0.9683 + \log 0.9176 + \log 0.9683$$
$$C_6 = (=CH—) = C_6 + \log C_1 + \log C_5$$
$$= 0.9683 + \log 0.9535 + \log 0.9683$$
$$C_7 = (=CH_3) = C_7 + \log C_1$$
$$= 1.0 + \log 0.9535$$
$$C_8 = (=CH_3) = C_8 + \log C_2$$
$$= 1.0 + \log 0.9535$$
$$C_9 = (=CH_3) = C_9 + \log C_4$$
$$= 1.0 + \log 0.9176$$
$$I_{ET} = 8.4094$$

Analyzing the behavior of the experimental retention of the monoalkyl benzene molecules, in relation to the position of the phenyl group in the alkyl chains constituted by 10–13 carbon atoms, it was observed that the retention index values decrease when the position of the phenyl group moves from the end (external isomers) toward the middle (internal isomers) of the alkyl chain showing a logarithm tendency. This behavior reflects the importance of the steric effects in the chromatographic retention process. When the position of the phenyl group is further inside the molecule, it interposes between the alkyl chain and the stationary phase and the molecule becomes more symmetrical and more compact, decreasing the interaction surface, and thus its chromatographic retention decreases owing to the steric and conformational effects.

The simple linear regression obtained between the values for the semi-empirical topological index (I_{ET}) and the experimental retention index (RI_{EXP}) for 122 alkylbenzenes is of good quality (Eq. (7)).

$$RI_{calc} = -39.7381 + 123.0824\, I_{ET}$$
$$N = 122;\ r = 0.9998;\ \text{S.D.} = 5.5;\ r^2_{cv} = 0.9996 \quad (7)$$

The corresponding graph of RI_{EXP} versus the retention index (RI_{calc}) calculated using I_{ET} (Table 1) is given in Fig. 2.

The internal stability of the model obtained is indicated by the cross-validated correlation coefficient, r^2_{cv} (0.9996), using the "leave-one-out" method in comparison with the determination coefficient, r^2 (0.9996). The elution order of the majority of the compounds is correct. The average difference between the experimental and the predicted values (average error) was 4.09 u.i., close to the average experimental value of 4.0 u.i. [40]. The compounds that have a residual error above ten units are compounds whose steric effects are probably predominant due to the molecular form; which plays an important role in the interactions between solute

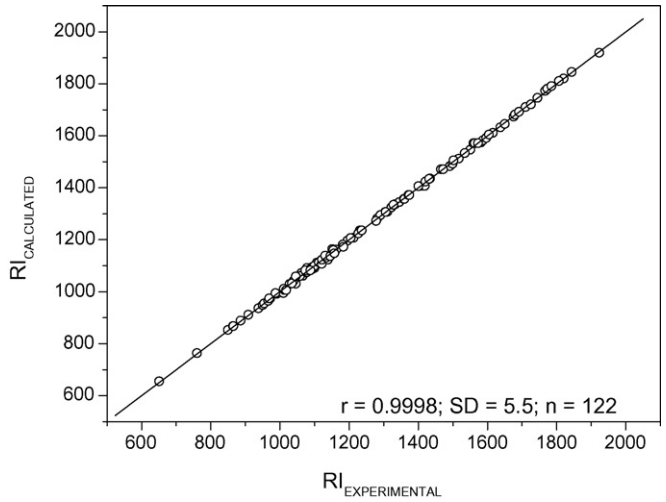

Fig. 2. Plot of the calculated vs. experimental retention indices for 122 alkylbenzenes.

and stationary phases (e.g., 1,3-dimethyl-5-*tert*-butylbenzene). A good model should have a high level of description ability both for internal and external samples. A QSRR model was thus obtained using 110 alkylbenzenes as a training set, which was chosen in a random way from the original group. This model was used to describe the chromatographic retention of 12 compounds of a subset, considered as an external group. The equation obtained for the 110 compounds was:

$$\mathrm{RI_{calc}} = -39.2508 + 123.0412\, I_{ET}$$
$$N = 110; r = 0.9998; \mathrm{S.D.} = 5.7 \quad (8)$$

To verify the ability of the model obtained, Eq. (8) was used to estimate the retention indices of the 12 alkylbenzenes. The statistical parameters obtained in the correlation between the experimental and calculated retention indices were of excellent quality $r = 0.9999$ and, according to Fig. 3, S.D. = 3.5, indicating that the proposed model has a high statistical stability and validity.

3.2. Retention indices on stationary phases with different polarity

The I_{ET} was developed on non-polar or low polarity stationary phases, where the dispersion and induction intermolecular interaction forces between the solute and the stationary phases predominate.

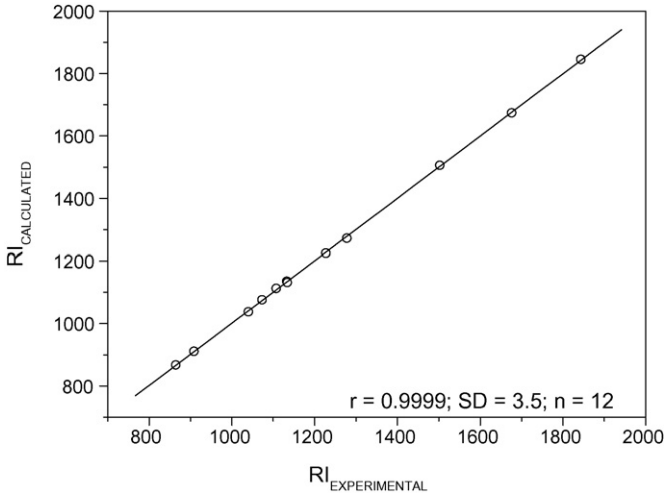

Fig. 3. Simple linear regression between experimental and calculated retention indices for the subset with 12 compounds in the external validation test.

Table 3
Summary of the coefficients and statistical parameters of simple linear regressions between $\mathrm{RI_{EXP}}$ and I_{ET} ($\mathrm{RI_{EXP}} = a + b\, I_{ET}$) using stationary phases of different polarity

Equation	Phase	P_R[a]	a[a]	b[a]	N[a]	r[a]	S.D.[a]
9	Squalane	Zero	−43.5459	123.4200	34	0.9983	6.7
10	SE-30	6.80	−43.6579	123.0632	34	0.9974	8.3
11	Carbowax 20 M	71.91	303.1924	303.1924	34	0.9731	25.1

Deviation; r^2_{cv} = cross-validated correlation coefficient; P_R = McReynolds polarity.

Table 4
Simple linear regression between I_{ET} and the properties studied (Bp, V_W, R_M and log P) and their respective statistical parameters

Property	Regression equation	N[a]	r[a]	r^2_{cv}[a]	S.D.[a]
Bp (°C)	$-94.2596 + 31.6307\, I_{ET}$	25	0.9980	0.995	2.1
V_W (mL/M)	$-29.6796 + 13.6713\, I_{ET}$	25	0.9889	0.974	2.2
R_M (mL/M)	$-9.7139 + 6.2385\, I_{ET}$	25	0.9774	0.948	1.5
log P	$-1.2579 + 0.6214\, I_{ET}$	39	0.9384	0.869	0.32

[a] N = number of alkylbenzenes; r = correlation coefficient; S.D. = standard deviation; r^2_{cv} = cross-validated correlation coefficient.

The contribution of the stationary phase to the chromatographic retention can be reflected in its polarity, which is its most representative property.

The QSRR models ($\mathrm{RI_{EXP}} = a + b\, I_{ET}$) with the statistical parameters for 34 alkylbenzenes on three stationary phases, squalane [15], SE-30 [36] and Carbowax 20 M [15], reported in the literature, with their polarities obtained according to the McReynolds scale [41], are summarized in Table 3.

It can be observed that in the polar stationary phase (Carbowax) other types of interactions besides dispersion and induction forces occur between the solute and stationary phase, such as dipole–dipole interactions. However, it can be concluded that dispersive and inductive effects have a greater influence on the retention of these compounds than polar effects.

3.3. Physicochemical properties

The application of the I_{ET} index was extended in a QSPR/QSAR study to some representative physicochemical properties, biological activities and toxicities of some aliphatic compounds [33,34] and most of the properties investigated were well modeled ($r > 0.98$).

The motivation for this study arose from the supposition that properties that are determined by intermolecular forces can be adequately modeled by the semi-empirical topological indices.

The representative properties of alkylbenzenes selected in this study were the boiling point, Bp(°C), van der Waals volume, V_W, molar refractivity, R_M [18] and octanol/water partition coefficient, log P [42].

Table 4 summarizes the QSPR models obtained to describe the physicochemical properties with a single index, I_{ET}, together with the statistical quality of the models. The temperature was the property that represented the best correlation model, this being one of the important physical properties used in the identification of compounds that are strongly dependent on intermolecular interactions.

4. Conclusion

The QSRR study produced a good model with high internal stability (determination coefficient, $r^2 = 0.9996$, standard deviation, S.D. = 5.5, and leave-one-out cross-validation correlation coefficient, $r^2_{CV} = 0.9996$), which is able to describe with very good

approximation the retention indices of the compounds studied (alkylbenzenes).

On stationary phases of different polarities, the correlations applying I_{ET} indicate that the dispersive and inductive interactions between the solute and stationary phases play a more important role than the polar effects in the retention of these compounds, the best correlations being obtained for stationary phases with low polarities.

This study indicates that theoretical models have a good capacity for describing the physicochemical properties of alkylbenzenes based on their molecular structure, using I_{ET}, and offer the advantage of simplicity, using only one parameter.

The quality of the results obtained in this study, in terms of describing the chromatographic retention and the physicochemical properties using I_{ET}, can be considered important in relation to deriving QSPR models for other compounds.

Acknowledgement

The authors acknowledge the financial support from CNPq (Brazil) for this research.

References

[1] L.B. Kier, L.H. Hall, Molecular Connectivity in Chemistry and Drug Research, Academic Press, New York, 1976.
[2] R. Kaliszan, Quantitative Structure–Chromatography Retention Relationships, Wiley-Interscience, New York, 1987.
[3] L.B. Kier, L.H. Hall, Molecular Connectivity in Structure–Activity Analysis, Wiley, New York, 1986.
[4] L.H. Hall, L.B. Kier, J. Mol. Graph. Mol. Model. 20 (2001) 4.
[5] M. Randic, J. Mol. Graph. Mol. Model. 20 (2001) 19.
[6] M. Randic, S.C. Basak, J. Chem. Inf. Comput. Sci. 41 (2001) 650.
[7] D. Bonchev, J. Mol. Graph. Mol. Model. 20 (2001) 65.
[8] R. Kaliszan, Chem. Rev. 107 (2007) 3212.
[9] K. Hebérger, J. Chromatogr. A 1158 (2007) 273.
[10] V.E.F. Heinzen, R.A. Yunes, J. Chromatogr. A 719 (1996) 462.
[11] K. Hebérger, T. Kowalska, Chromatographia 44 (1997) 179.
[12] K. Hebérger, Chromatographia 29 (1990) 375.
[13] A. Yan, Z. Hu, Anal. Chim. Acta 433 (2001) 145.
[14] A. Yan, G. Jiao, Z. Hu, B.T. Fan, Comput. Chem. 24 (2000) 171.
[15] J. Bermejo, J.S. Canga, O.M. Gayol, M.D. Guillen, J. Chromatogr. Sci. 22 (1984) 252.
[16] J. Macák, V. Nabivach, P. Buryan, S. Sindler, J. Chromatogr. A 234 (1982) 285.
[17] D. Bonchev, Ov. Mekenian, G. Protić, N. Trinajstić, J. Chromatogr. A 176 (1979) 149.
[18] V.A. Gerasimenko, V.M. Nabivach, J. Chromatogr. A 498 (1990) 357.
[19] C.T. Peng, R.L. Hua, D. Maltby, J. Chromatogr. A 589 (1992) 231.
[20] N. Dimov, A. Osman, Ov. Mekenyan, D. Papazova, Anal. Chim. Acta 298 (1994) 303.
[21] J.M. Sutter, T.A. Peterson, P.C. Jurs, Anal. Chim. Acta 342 (1997) 113.
[22] N. Dimov, Ov. Mekenyan, J. Chromatogr. A 471 (1989) 227.
[23] O. Ivanciuc, T. Ivanciuc, D.J. Klein, W.A. Seitz, A.T. Balaban, SAR QSAR Environ. Res. 11 (2001) 419.
[24] S.P. Verevkin, J. Chem. Thermodyn. 38 (2006) 1111.
[25] V.E.F. Heinzen, M.F. Soares, R.A. Yunes, J. Chromatogr. A 849 (1999) 495.
[26] B.S. Junkes, R.D.M.C. Amboni, R.A. Yunes, V.E.F. Heinzen, Chromatographia 55 (2002) 75.
[27] B.S. Junkes, R.D.M.C. Amboni, R.A. Yunes, V.E.F. Heinzen, Chromatographia 55 (2002) 707.
[28] R.D.M.C. Amboni, B.S. Junkes, R.A. Yunes, V.E.F. Heinzen, J. Mol. Struct. (Theochem.) 579 (2002) 53.
[29] R.D.M.C. Amboni, B.S. Junkes, R.A. Yunes, V.E.F. Heinzen, J. Mol. Struct. (Theochem.) 586 (2002) 71.
[30] B.S. Junkes, R.D.M.C. Amboni, R.A. Yunes, V.E.F. Heinzen, Internet Electron. J. Mol. Des. 2 (2003) 33, http://www.biochempress.com/.
[31] B.S. Junkes, R.D.M.C. Amboni, R.A. Yunes, V.E.F. Heinzen, Anal. Chim. Acta 477 (2003) 29.
[32] B.S. Junkes, R.D.M.C. Amboni, R.A. Yunes, V.E.F. Heinzen, J. Braz. Chem. Soc. 15 (2004) 183.
[33] R.D.M.C. Amboni, B.S. Junkes, R.A. Yunes, V.E.F. Heinzen, J. Agric. Food. Chem. 48 (2000) 3517.
[34] B.S. Junkes, A.C.S. Arruda, R.A. Yunes, L.C. Porto, V.E.F. Heinzen, J. Mol. Model. 11 (2005) 128.
[35] P.J. Hansen, P.C. Jurs, J. Chem. Educ. 65 (1988) 574.
[36] X. Zhang, P. Lu, J. Chromatogr. A 731 (1996) 187.
[37] Microcal Origin, version 5.0, serial number G43S5-9478-7055154, 1997.
[38] M.M.C. Ferreira, A.M. Antunes, M.S. Melgo, P.L.O. Volpe, Química Nova 22 (1999) 724.
[39] H. Kubinyi, in: R. Mannhold, P. Krogsgaard-Larsen, H. Timmerman (Eds.), QSAR: Hansch Analysis and Related Approaches, VCH, Weinheim, 1993.
[40] A.R. Katritizky, K. Chen, D.A. Carlson, Anal. Chem. 72 (2000) 101.
[41] G. Tarján, S. Nyiredy, M. Gyor, E.R. Lombosi, T.S. Lombosi, M.V. Budahegvi, S.Y. Mészáros, J.M. Takács, J. Chromatogr. 472 (1989) 1.
[42] C. Hansch, A. Leo, D. Hoekman, Exploring QSAR: Hydrophobic, Electronic and Steric Constants, ACS Professional Reference Book, Washington, DC, 1995.

Talanta 76 (2008) 254–258

Contents lists available at ScienceDirect

Talanta

journal homepage: www.elsevier.com/locate/talanta

Study of contamination sources in the process of cryogenic grinding

Miloslav Pouzar[a,*], Anna Krejčová[a], Tomáš Černohorský[a], Květa Pešková[b]

[a] Department of Environmental Protection, University of Pardubice, Čs. legií 565, Pardubice 532 10, Czech Republic
[b] Institute of Analytical Chemistry, Czech Academy of Sciences, Veveří 97, Brno 611 42, Czech Republic

ARTICLE INFO

Article history:
Received 21 November 2007
Received in revised form 18 February 2008
Accepted 20 February 2008
Available online 4 March 2008

Keywords:
Cryogenic grinding
Contamination
Cross-contamination
Cellulose
Electro-waste

ABSTRACT

The study of contamination effect during cryogenic grinding of pure cellulose was carried out. The optimisation of important parameters of the grinding process (pre-cooling time, grinding time, cooling time and number of cycles) was performed and the different sources of a possible contamination of samples (earlier processed sample, metal parts of grinding tool) were evaluated. The results of ICP-*oa*-TOF MS analysis after microwave digestion of cellulose samples were used in this study. Significant contamination of cellulose samples by Fe at the level 130 $\mu g\,kg^{-1}$ caused by wearing of steel stoppers and an impact bar was detected. Cross-contamination by Fe, Cr, Mn and Cu at the level 400, 200, 200 and 2100 $\mu g\,kg^{-1}$, respectively was caused by previous grinding of electro-waste sample. This cross-contamination was possible to be avoided by changing of a polycarbonate part of a grinding vessel.

1. Introduction

During the process of the cryogenic grinding, a material is deeply frozen in order to be more fragile and easier to grind. Chilling leads to an increase in hardness of a ground matter, an insertion of failures in its structure and consequently a reduction of time and energy vital to favourable sample pulverization. This technique is favourable and used when a sample with the highly homogeneous particle size distribution and a diameter below 100 μm is required [1]. Typical application area of that modern sample preparation method is elemental analysis of various biological materials or foods using the direct introduction of slurries into GF AAS. The cryogenic grinding solves problems with agglomeration of samples containing a high portion of fat [2]. It is beneficial for pulverization of fibrous specimens [3,4] as well as for powdering of soft, elastic and pasty matters [5,6], or tough and hard ones contrariwise [7]. This procedure is efficient for a fast and effective comminution and homogenisation of heavily heterogeneous and complex mixtures if a small portion sampled have to represent its' whole bulk [8]. Prevention of a thermo-labile species degradation and fixation of high volatile compounds in the sample matrix during the process of mechanical des-integration are another benefits of the cryogenic processing [9].

A hazard of sample contamination in the process of the cryogenic grinding strongly depends on a design of a mill used and conditions selected for its operation. A type of ground matter and desired limits of detection of applied analytical method are another very important parameters usually mentioned in this context. Potential sources of the sample contamination in the process of cryogenic grinding of plant materials were examined by Engelsen and Wibetoe [2]. Yoshinaga and Morita [4] assigned the material of a grinding vessels as the probable source of a hair sample contamination by Al, Fe and Mg. No significant contamination of cryogenically homogenised samples of breakfast cereals by Zn and Fe was detected by Gouveia at al. [8].

The aim of this work was to evaluate main sources of contamination in the process of the cryogenic grinding. The fibre cellulose was chosen as a convenient material for this study because of its physical character (elastic fibres) and chemical composition (poor organic matrix with minimum trace elements). Contamination caused by metal parts of grinding vessel was studied as well as cross-contamination by previously ground sample.

2. Experimental

2.1. Instrumentation

The cryogenic impact grinder with a self-contained liquid nitrogen bath (4-5l) Model 6750 Freezer Mill (Spex, Certiprep, USA) operated at the liquid nitrogen temperature was used in order to comminute samples. The pulverization of frozen samples was car-

* Corresponding author. Tel.: +420 46 6037196.
E-mail address: milan.pouzar@upce.cz (M. Pouzar).

0039-9140/$ – see front matter © 2008 Elsevier B.V. All rights reserved.
doi:10.1016/j.talanta.2008.02.035

Fig. 1. Clots of crude fibrous cellulose.

ried out by a magnetically shuttling steel impact bar back-and-forth against two stationary end plugs closing a cylindrical polycarbonate vial. Model 6751C20 grinding vials (volume 25 mL) were used for all performed experiments.

The evacuable KBr die set with an inner diameter 16 mm (ICL, Garfield, USA) and the hydraulic press with manual drive (Maassen, Germany) were used for the cellulose pellet preparation.

The measurement of the cellulose fibres length for the optimisation of grinding parameters was carried out using electron microscopy (SEM Jeol 5600 LV, Japan), the sputter tool (MED 010, Balzers union, Germany) and the software for image analysis (ACC Version 6.0, Sofo, Czech Republic).

The qualitative and semi-quantitative analysis of possible sources of contamination (pre-grinded sample of electro-waste, impact bar and stoppers of grinding set) was performed using energy-dispersive X-ray fluorescence spectrometer Elva-X (Elvatech, Kiev, Ukraine).

The elemental analysis of ground cellulose samples was carried out with the ICP-*oa*-TOF mass spectrometer Optimass 8000 (GBC Scientific Equipment Pty Ltd., Australia) equipped with the concentric nebulizer Micro Mist coupled to a 70-ml thermostated (15 °C) cyclonic spray chamber (all Glass expansion Pty Ltd., Australia). Microwave system Speedwave™ MWS-3$^+$ with high-pressure PFA vessels DAC 100 and the maximum total output of the microwave generator 1450 W (Berghof, Germany) was used for digestions of samples. The demineralised water was taken from the Milli-Q Plus water-purification system (Millipore, Bedford, USA). Other equipment used included calibrated volumetric glassware. The calculations and statistical evaluation were carried out using commercial software ADSTAT 1.25 (Trilobyte Statistical Software Ltd., Pardubice, Czech Republic).

2.2. Optimisation of parameters of cryogenic grinding

Trying to grind cellulose in the original form of fibrous clots (provided by Department of Wood, Pulp and Paper University of Pardubice, Fig. 1), an impact bar broke through the sample and kept moving only through the channel formed. The main part of the sample remained distributed along the walls of the polycarbonate vial and stayed untreated in this case. To solve the above-mentioned problem, we decided to insert the sample in the form of pellets. Cellulose was pressed in the evacuable die with inner diameter 16 mm by force 10 tons for 2 min. Two pellets were positioned on the each side of an impact bar in the space between its end and stopper. The total mass of four pellets ground in every grinding program was 2.5 g.

The operating program used for the grinding equipment included following parameters: the pre-cooling time (a period before grinding, when a vial was immersed in the liquid nitrogen for purpose of sample freezing), the grinding time (a period of an impact bar motion in each working cycle), the re-cooling time (a period between two working cycles, when the oscillation of an impact bar was interrupted to avoid heating due to an attrition of a magnetic bar with a sample and a sampling vial), the number of working cycles (one cycle consists of a period of grinding time followed by a period of cooling time), the impact bar frequency (the number of back-and-forth movements of an impact bar per second). Samples of fibrous cellulose were submitted to different grinding procedures to optimise working parameters. The pre-cooling time was set in the range 3–15 min. The grinding and re-cooling periods took always the same time and both were changed in the range of 2–6 min. The number of working cycles was set with respect to value of the total grinding time (the sum of all grinding times at particular grinding program) that was always 6 min. The impact bar frequency 10 Hz was applied at all tested grinding programs. The statistical characteristics of fibre length distribution in the cellulose sample after grinding process were adopted as the optimisation criterion.

2.3. Study of the contamination caused by the grinding set

A friction of an impact bar beating against an end stoppers in the process of cryogenic grinding was considered as a possible source of contamination. Working parts of the grinding tool were analysed by ED XRF spectrometry to find out probable contaminants derivable from that source. Levels of elements detected as components of the impact bar and the end stoppers were analysed in ground cellulose by ICP-*oa*-TOF MS after microwave digestion and they were compared with these obtained from samples of crude non-ground fibre cellulose. The grinding was in that case carried out under optimal conditions previously optimised. To avoid contamination from the process of pellets pressing, ungrounded pellets were also analysed by ICP-*oa*-TOF MS.

2.4. Study of a cross-contamination caused by previously ground sample

To simulate the worst possible case of the cross-contamination danger, electronic waste (parts of printed circuit board) was ground just before cellulose samples using the same grinding set. After processing of an electronic sample, the vial, stoppers and impact bar used were washed in distilled water, dried and then cellulose pellets were inserted. Three cellulose samples were ground subsequently and careful washing of the grinding set was performed at the end of each grinding program. Thereafter, the polycarbonate part of vial was replaced by a new un-used one and next three grindings of the cellulose were carried out. Elements found out at ED XRF spectrum of electro-waste were consequently analysed in all cryogenically ground samples of cellulose with using ICP-*oa*-TOF MS after microwave digestion.

2.5. Analysis of cellulose samples by ICP-oa-TOF MS

2.5.1. Standards preparation

The single component standards of Fe, Cr, Mn, Cu, Pb, Ag and Mo ($1000 \pm 2\ \mu g\ mL^{-1}$, Analytika Co. Ltd., Czech Republic) were used for the preparation of multi-element ones. Multi-element standards were prepared containing four levels of concentration: (i) Cr, Mn, Cu, Pb, Ag and Mo all $200\ \mu g\ L^{-1}$ and Fe $400\ \mu g\ L^{-1}$, (ii) the same elements 10-fold times, (iii) 20 times and (iv) 40 times diluted as (i). Calibration standards were prepared with 1 mL 65% (w/v) HNO_3/100 mL of solution which was used for the microwave decomposition in that volume. The water standard blank contained 1 mL 65% (w/v) HNO_3/100 mL of solution. The internal standard *Y* $50\ \mu g\ L^{-1}$ was used in both calibration standards and blank.

Table 1
The working parameters of ICP-*oa*-TOF MS

Parameter	Value
Ion optics	
Skimmer	−1 050 V
Extraction	−1 300 V
Z1	−700 V
Y mean	−455 V
Y deflection	4 V
Z lens mean	−1400 V
Z lens deflection	−40 V
Lens body	−180 V
Pulse shaping	
Fill	−40 V
Fill bias	0 V
Fill grid	−40 V
Pushout grid	−390 V
Pushout plate	492 V
Blanker	200 V
Spectral frequency	33 kHz
Reflectron	690 V
Detection	
Multiplier gain	2800 V
Ion threshold	8.4 mV
Integration window	Auto
Measurement	Pulse
Mode	counting/analog

2.5.2. Microwave decomposition of cellulose samples

Approximately 0.2 g of cryogenically ground cellulose sample was accurately weighed into an acid washed TFM-PTFE digestion tube and 5 mL of nitric acid of analytical grade (65% (w/v) HNO_3, Lach-Ner, Czech Republic) was added. The tube was heated in a microwave oven at the power setting of 80% and 180 °C for 5 min, at 90% and 220 °C for 5 min. The maximum total output of the microwave generator was 1450 W and maximum pressure in a digestion tube 100 bar. The digest was transferred into a 50-mL acid washed volumetric flask and the flask was filled up with demineralised water and stored in polypropylene container. Each sample was decomposed in four replicates. Two water blanks were run with each batch of samples. Before analysis, digests were diluted 10-fold with demineralised water and the internal standard *Y* was added in the final concentration 50 μg L^{-1}.

Table 2
The fibre length distribution of cellulose samples ground under different conditions

Sample	C_1	C_2	C_3	C_4	C_5	C_6
Number of cycles	3	3	3	3	2	1
Grinding time (min)	2	2	2	2	3	6
Re-cooling time (min)	2	2	2	2	3	–
Pre-cooling time (min)	3	5	10	15	15	15
Mean length of fibres (μm)	42.1	49.9	44.1	45.5	59.7	73.5
Median length of fibres (μm)	37.2	44.7	35.9	40.0	48.5	58.4
P_{99} (μm)	117	132	132	149	185	322

2.5.3. The ICP-oa-TOF MS method

The operating conditions of ICP-*oa*-TOF MS analysis were adjusted according to the manufacturer's recommendations: the sample aspiration rate 1 mL min^{-1}, power 1200 W, flows of plasma, auxiliary and nebulizer gas 11, 1.0 and 0.9 L min^{-1} and the other parameters are summarised in Table 1. The sensitivity of 440 000 counts s^{-1} per μg l^{-1} (mass integrated peak) and the resolution of 1600 was reached for ^{139}La. The same parameters for ^{238}U were 675 000 counts s^{-1} per μg l^{-1} and 1700. Mass calibration was achieved using responses from ^{7}Li, ^{114}In and ^{238}U. The aqueous calibration with internal standard *Y* was used for quantification. Peak area mode and 5-s data acquisition time and five replicates were used for measurement. Main analytical characteristics of ICP-*oa*-TOF MS method were described for example by Sturgeon at al. [10].

3. Results and discussion

3.1. The optimisation of parameters of the cryogenic grinding

With the respect to the fibrous character of the cellulose matrix we decided to monitor the fibres length distribution as the parameter, which could describe the quality of a sample des-integration in the best way. Three-electron microscopy shots (100× magnification) of each cellulose sample were treated by the software for the image analysis. The length of each visible fibre was measured as the main axis of a circumscribed ellipse. The minimum number of evaluated objects at each microscopy shot was 100 and the total number of evaluated objects for each particular sample always exceeded 400 units. The main statistical characteristics of the fibre length distribution (arithmetical mean, median and 99th percentile) for cellulose samples ground under different conditions

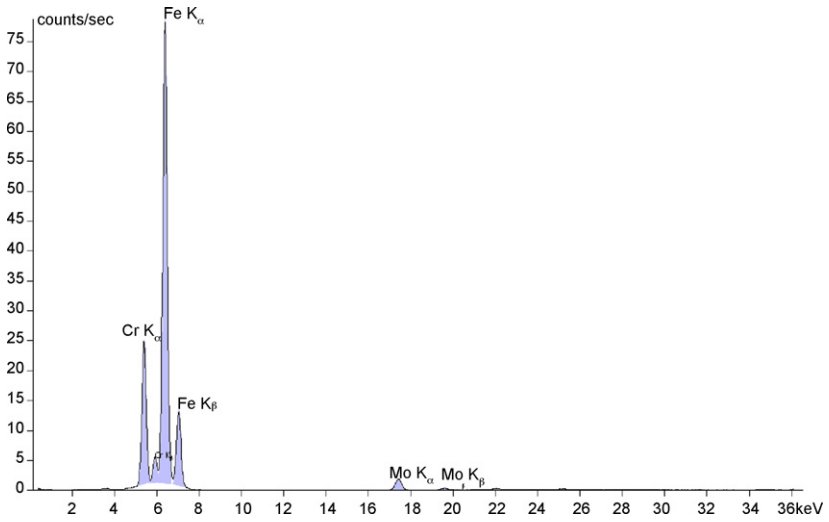

Fig. 2. The ED XRF spectrum of material of impact bar and end stoppers.

Table 3
Contamination caused by grinding set (samples C_1–C_3) and cross-contamination caused by previously ground sample (samples C_4–C_9)

	Fe ($\mu g\,kg^{-1}$)	Cr ($\mu g\,kg^{-1}$)	Mn ($\mu g\,kg^{-1}$)	Cu ($\mu g\,kg^{-1}$)	Pb ($\mu g\,kg^{-1}$)	Ag ($\mu g\,kg^{-1}$)
Ungrounded crude cellulose	74 ± 2.4	<LOD	<LOD	<LOD	<LOD	<LOD
Ungrounded cellulose pellet	71 ± 3.1	<LOD	<LOD	<LOD	<LOD	<LOD
C_1	195 ± 5.9	<LOD	<LOD	<LOD	<LOD	<LOD
C_2	187 ± 5.4	<LOD	<LOD	<LOD	<LOD	<LOD
C_3	209 ± 7.2	<LOD	<LOD	<LOD	<LOD	<LOD
C_4	397 ± 8.6	222 ± 6.3	241 ± 6.5	2146 ± 66	<LOD	<LOD
C_5	483 ± 12	197 ± 5.7	188 ± 5.9	2205 ± 63	<LOD	<LOD
C_6	451 ± 13	206 ± 6.7	224 ± 5.8	2035 ± 58	<LOD	<LOD
C_7	326 ± 11	<LOD	<LOD	<LOD	<LOD	<LOD
C_8	312 ± 11	<LOD	<LOD	<LOD	<LOD	<LOD
C_9	294 ± 9.9	<LOD	<LOD	<LOD	<LOD	<LOD
LOD (3σ[a])	5.6	7.6	7.5	10.4	7.9	6.6
LQ (10σ[a])	18.8	25.4	25.0	34.8	26.3	22.1

[a] σ: standard deviation of five replicate measurements of the lowest calibration standard solution by ICP-*oa*-TOF MS multiplied by dilution factor.

are summarised in Table 2. From the data presented it is obvious that the protraction of the pre-cooling time have no significant effect on quality of a ground cellulose sample. On the other hand, the number of grinding cycles is possible to consider as an important parameter. We can conclude that a division of the total grinding time on several shorter periods with an alternating re-cooling sentence gives better results than an uninterrupted processing.

3.2. Study of the contamination caused by the grinding set

The ED XRF spectrum of steel components of the cryogenic mill is depicted in Fig. 2. As can be seen, main constituents of the impact bar and the end stopper are Cr, Fe and Mo. Their contents at the analysed material assessed by the fundamental parameters method were 16.5, 83 and 0.5%, respectively. The material of KBr die set used for preparation of pellets before cryogenic grinding was analysed by the same way and its composition found out was very similar. The concentrations of above-mentioned possible contaminants measured in crude ungrounded cellulose, in ungrounded pellets and in grounded cellulose are summarised in Table 3. All detection and quantification limits (LOD, LQ) for ICP-*oa*-TOF MS method used were calculated as a concentration equivalent to 3 times (LOD) or 10 times (LQ) of the standard deviation of five replicate measurements of the lowest calibration standard multiplied by the dilution factor. The concentration of Fe at that standard was 1 $\mu g\,L^{-1}$ and concentrations of the other elements were 0.1 $\mu g\,L^{-1}$. A significant content of Fe on the level of quantification limit of ICP-*oa*-TOF method used was observed at all ground cellulose samples (C_1–C_3). Lower concentrations of Fe on the level of the detection limit were found in both ungrounded crude and pelletized cellulose samples. As can be seen from the same concentrations of Fe found out in the crude and the pelletized cellulose, no contamination by Fe can be connected with the process of the pellet preparation. In this case, the detected Fe is probably natural component of the cellulose matrix. On the other hand, significantly higher concentrations of Fe in the ground samples pointed out the serious contamination from the process of the cryogenic grinding. Next constituents of the grinding set Cr and Mo was not detected neither in crude and pelletized cellulose, neither in ground samples. The contamination by these elements in the process of cryogenic grinding was hence considered to be negligible. Our results are inconsistent with that obtained by Goueya et al. [8]. The same grinding tool (Model 6750 Freezer Mill from Spex Certiprep, USA) was used for homogenisation of breakfast cereals in that work. Real samples were ground with a consequently increasing time and the relation of Zn and Fe concentrations on the duration of grinding step was evaluated. No contamination caused by wearing of metal parts of the mill was detected. Incomparable results were obtained probably through the difference in the study

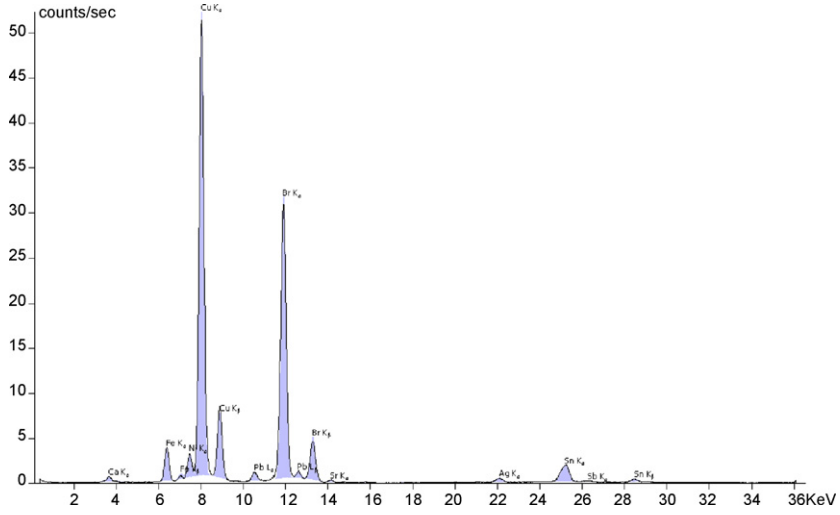

Fig. 3. The ED XRF spectrum of electro-waste sample.

designs. We analysed ultra-traces of contaminants in a poor matrix and the Fe content increase was about 130 $\mu g\,kg^{-1}$. Goueya et al. treated a real matrix with high natural contents of Fe and Zn (30 and 20 $mg\,kg^{-1}$ approximately). A such high background content of possible contaminants and corresponding standard deviations of measurements (units or tens of $mg\,kg^{-1}$) made impossible to detect elements content increasing in magnitude of hundreds $\mu g\,kg^{-1}$.

3.3. Study of the cross-contamination caused by previously ground sample

The possible contaminants Fe, Cr, Mn, Cu, Pb and Ag were chosen on the basis of ED XRF qualitative analysis of electro-waste sample. The corresponding ED XRF spectrum is depicted in Fig. 3. Three groups of samples were subsequently ground with using the same grinding set—first, three samples of pelletized pure fibre cellulose (C_1–C_3), next two samples of electro-waste and than again three cellulose samples (C_4–C_6). After that, the polycarbonate part of the grinding set was replaced by new one and next three samples were ground (C_7–C_9). The results of the analysis of above-mentioned cellulose samples are summarised in Table 3. As can be seen, Pb and Ag were not detected at any sample. The concentrations of Cr and Mn on the level of their quantification limits were found out at samples ground after electro-waste samples. When a polycarbonate part of a grinding vessel was replaced, concentration of these elements lowered to a level corresponding with limits of detection. The same behaviour was possible to observe in the case of Cu, when its concentration in the samples ground before polycarbonate part changing was 10 times higher than the corresponding quantification limit. The content of Fe at samples ground after electro-waste was two times higher than its' quantification limit and two times higher than the content of Fe at samples ground before electro-waste. After replacing of polycarbonate part, the level of Fe decreased but stayed still significantly higher, than in samples ground before electro-waste.

4. Conclusion

Two main sources of sample contamination in the process of cryogenic grinding were studied—the contamination caused by friction of a grinding set and cross-contamination caused by previously ground sample. In the first case, the significant contamination by Fe on the level of hundreds of microgram per gram was observed. Wearing of steel stoppers and an impact bar was not only one source of contamination by Fe. This element was an important part of cross-contamination by previous ground electro-waste sample as well. In contrast to other cross-contaminants (Cu, Cr and Mn), the replacing of a polycarbonate part of grinding set did not solve the cross-contamination by Fe.

Acknowledgements

Financial support from the projects GAČR203/06/0134 and MSM 0021627502 used in this work is greatly appreciated.

References

[1] D. Santos Jr., F. Barbosa Jr., A.C. Tomazelli, F.J. Krug, J.A. Nobrega, M.A.Z. Arruda, Anal. Bioanal. Chem. 373 (2002) 183–189.
[2] Ch. Engelsen, G. Wibetoe, Fressen. J. Anal. Chem. 366 (2000) 494–503.
[3] K.G. Fernandes, A.R.A. Nogueira, J.A.G. Neto, J.A. Nobrega, Talanta 71 (2007) 1118–1123.
[4] J. Yoshinaga, M. Morita, K. Okamoto, Fressen. J. Anal. Chem. 357 (1997) 279–283.
[5] C.S. Nomura, C.S. Silva, A.R.A. Nogueira, P.V. Oliveira, Spectrochim. Acta B 60 (2005) 673–680.
[6] F.A. Silva, C.C.F. Padilha, L.E. Pezzato, M.M. Barros, P.M. Padilha, Talanta 69 (2006) 1025–1030.
[7] D. Santos Jr., F. Barbosa Jr., S.S. de Souza, F.J. Krug, J. Anal. Atom. Spectrom. 18 (2003) 939–945.
[8] S.T. Gouveia, G.S. Lopes, O. Fattibello-Filho, A.R.A. Nogueira, J.A. Nobrega, J. Food Eng. 51 (2002) 59–63.
[9] D. Point, W.C. Davis, S.J. Christopher, M.B. Ellisor, R.S. Pugh, P.R. Becker, O.F.X. Donard, B.J. Porter, S.A. Wise, Anal. Bioanal. Chem. 387 (2007) 2343–2355.
[10] R.E. Sturgeon, W.H. Lam, A. Saint, J. Anal. Atom. Spectrom. 15 (2000) 607–616.

Talanta 76 (2008) 424–431

Contents lists available at ScienceDirect

Talanta

journal homepage: www.elsevier.com/locate/talanta

Investigation of the enzyme hydrolysis products of the substrates of alkaline phosphatase in electrochemical immunosensing

Anchana Preechaworapun[a,b], Zong Dai[a], Yun Xiang[a], Orawon Chailapakul[b,*], Joseph Wang[a,*]

[a] Department of Chemical and Material Engineering, Chemistry and Biochemistry, Biodesign Institute, Arizona State University, Tempe, AZ 85287-5801, United States
[b] Sensor Research Unit, Department of Chemistry, Faculty of Science, Chulalongkorn University, Patumwan, Bangkok 10330, Thailand

ARTICLE INFO

Article history:
Received 2 January 2008
Received in revised form 17 March 2008
Accepted 18 March 2008
Available online 25 March 2008

Keywords:
Amperometric immunosensor
Alkaline phosphatase
Immunoglobulin G
2-Phospho-L-ascorbic acid
Au electrode
Glassy carbon electrode
Screen-printed carbon electrode

ABSTRACT

In this paper, we have critically evaluated the electrochemical behavior of the products of seven substrates of the enzyme label, alkaline phosphate, commonly used in electrochemical immunosensors. These products (and the corresponding substrates) include indigo carmine (3-indoyl phosphate), hydroquinone (hydroquinone diphosphate), 4-nitrophenol (4-nitrophenol phosphate), 4-aminophenol (*p*-aminophenyl phosphate), 1-naphthol (1-naphthyl phosphate), phenol (phenyl phosphate), and L-ascorbic acid (2-phospho-L-ascorbic acid). Cyclic voltammetry and amperometry of these products were carried out at glassy carbon (GC), screen-printed carbon (SPC) and gold (Au) electrodes, respectively. Among the products, L-ascorbic acid showed the most sensitive (24.8 $\mu A\,cm^{-2}$, 12.0 $\mu A\,cm^{-2}$, and 48.0 $\mu A\,cm^{-2}$ of 100 μM ascorbic acid at GC, SPC, and Au electrodes, respectively) and well-defined amperometric response at all electrodes used, making 2-phospho-L-ascorbic acid the best substrate in electrochemical detection involving an alkaline phosphatase (ALP) enzyme label. The 2-phospho-L-ascorbic acid is also commercially available and inexpensive. Therefore, it was the best choice for electrochemical detection using ALP as label. Using mouse IgG as a model, an ALP enzyme-amplified sandwich-type amperometric immunosensor was constructed. The immunosensor was designed by electropolymerization of *o*-aminobenzoic acid (*o*-ABA) conductive polymer on the surface of GC, SPC, and Au electrodes. The anti-mouse IgG was subsequently attached on the electrode surface through covalent bonding between IgG antibody and the carboxyl groups from poly(*o*-ABA). Using 2-phospho-L-ascorbic acid as a substrate, the poly(*o*-ABA)/Au immunosensor produced the best signal (about 297 times of current density response ratio between 1000 $ng\,mL^{-1}$ and 0 $ng\,mL^{-1}$ of mouse IgG), demonstrating that amperometric immunosensors based on a conducting polymer electrode system were sensitive to concentrations of the mouse IgG down to 1 $ng\,mL^{-1}$, with a linear range of 3–200 $ng\,mL^{-1}$ (S.D. < 2; $n = 3$), and very low non-specific adsorption.

1. Introduction

In recent years, immunoassay has become an important analytical technique. Enzyme immunoassay is an analytical technique that relies on a specific immuno-interaction to quantitatively determine antibody or antigen present in an analyte by measuring the activity of an enzyme label conjugated to either the antibody or antigen. The main advantage of using enzyme labels is the remarkable signal amplification that may be gained by the high turnover of enzyme product molecules for each enzyme label [1]. Alkaline phosphatase (*o*-phosphoric monoester phosphohydrolase; ALP) [2] is a common enzyme label used in immunoassays. It has been investigated for more than 70 years and it is easily conjugated to haptens, antibodies, and other proteins. Moreover, ALP has a high turnover number and broad substrate specificity.

Different substrates for ALP have been investigated in different detection systems such as spectrophotometry using fosfestrol [3], fluorescence using 8-quinolyl phosphate [4] and 2-carboxy-1-naphthyl phosphate [5], chemiluminescence using lumiphos [6], bioluminescence using adenosine-3′-phosphate-5′-phosphosulfate [7], and electrochemistry using phenyl phosphate [8].

In electrochemical immunosensors, an ALP enzyme is used to generate organic electroactive products most of which can be detected and quantified. This detector is generally sensitive and rapid for the redox reaction of the product of the enzyme hydrolysis of an ALP substrate. Several substrates for electroanalysis have been studied in immunoassays involving the substrates of ALP such as catechol monophosphate [9], 3-indoyl phosphate (IP) [10–13], hydroquinone diphosphate (HQDP) [14], 4-nitrophenol phosphate (NPP) [15–17], *p*-aminophenyl phosphate (APP) [17–23],

* Corresponding authors.
E-mail addresses: corawon@chula.ac.th (O. Chailapakul), Joseph.Wang@asu.edu (J. Wang).

0039-9140/$ – see front matter © 2008 Elsevier B.V. All rights reserved.
doi:10.1016/j.talanta.2008.03.025

1-naphthyl phosphate (NTP) [23–25], phenyl phosphate (PheP) [14,17,20,26], and 2-phospho-L-ascorbic acid (AAP) [19,22,27]. During the enzymatic process, these substrates are converted to the electroactive species catechol, indigo carmine (IC), hydroquinone (HQ), 4-nitrophenol (NP), 4-aminophenol (AP), 1-naphthol (NT), phenol (Phe), and L-ascorbic acid (AA), respectively.

Electrochemical immunosensors, which combine specific immunoreactions with electrochemical transduction, have attracted growing attention in recent years. Different electrode materials have been used for electrochemical immunosensors, including GC [17,22], graphite [19], platinum (Pt) [8,22], SPC [11,15,20,22–25], iridium oxide [14], and Au [21,22,25,28]. The modified electrode surface allows highly dense immobilization of biomolecules, long-term stability of attached biomolecules, low non-specific binding, and proper biomolecular orientation to permit simple and rapid specific interactions. Basically Au material is very good for self-assembled monolayers (SAM) as the basis of the covalent bonding immunosensor, because strong bonding between the Au surface with SAM and the ease to modify the Au surface to cover with a COOH group. Therefore, SAMs of thiol are widely used as a scaffold to immobilize the primary antibody on Au surface. For example, a mixed SAM monolayer of 11-mercaptoundecanoic acid and 6-mercaptoethanol was applied to modify as the base at Au plate for sandwich immunoassay [29]. In our paper also used this mix SAM monolayer modified on Au surface to obtain the carboxyl functional group binding with antibody by covalent bonding. In this work SAM/Au was prepared for comparison with our system. Alternately, conducting polymers [30] based on electrodes have gained increasing applications in the development of immunosensors, such as poly(pyrrole) [31,32], polyaniline [33], poly(3-hexylthiophene) [34], poly 5,2′:5′2″-terthiophene-3′-carboxylic acid [35], polyanionic perfluorosulfonated Nafion polymer [36].

Previous works, the electropolymerized *o*-ABA synthesis at Au [37], Pt [38], and GC [39,40] were reported. Wang and Knoll [37] fabricated the self-doped conducting polyaniline by electrochemical polymerization of aniline and *o*-ABA, and investigated the carboxyl groups by in situ electrochemistry and surface plasmon resonance spectroscopy (SPR). Benyoucef et al. [38] synthesized the homo-polymer of *o*-ABA on Pt electrode by electrochemical cyclic scanning of the potential and characterized this polymer with in situ FTIR. The FTIR result showed carboxyl groups on the electrode surface. This functional group is connected to the antibody by covalent bond. Therefore, poly(*o*-ABA) as a derivative polyaniline was used as the base of covalent bonding for orientation of the immobilized primary antibody by electropolymerization at electrode surface. The five main factors involved in the design of a sensitive immunoassay are optimized orientation of the immobilized primary antibody, the format of the assay, the type of label used, the method of detection, and the minimization of non-specific binding.

The goal of this paper is to critically compare different substrates and products of the ALP enzymatic reaction towards the development of a sensitive electrochemical immunosensor. The seven products of substrates (Scheme 1) for the ALP reaction have been investigated by cyclic voltammetry and amperometry with three electrode materials as GC, SPC, and Au in the same condition. The highest amperometric response was obtained from AA, which is the product of AAP substrate of ALP enzyme. Therefore, this substrate was applied to amperometric immunosensors based on an electropolymerized poly(*o*-ABA) as their electrode materials. Electrode modified with poly(*o*-ABA) provides the abundant carboxyl groups on the polymer surfaces, leading to fast and reliable amperometric responses. In our studies, mouse IgG is selected as a model analyte and its detection is conducted using the sandwich mode with anti-mouse IgG and anti-mouse IgG conjugated to ALP as the primary and second antibodies, respectively. Also, a mix SAM of 11-mercaptoundecanoic acid and 6-mercaptoethanol modified Au electrode surface was compared with poly(*o*-ABA)-modified Au electrode surface using the same sandwich immunoassay system. The performance of the immunosensor with respect to detection sensitivity and reliability is presented and discussed in detail.

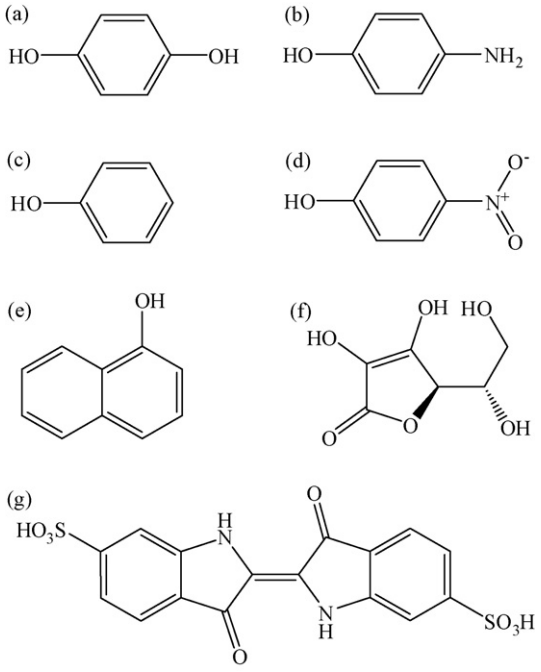

Scheme 1. Structures of the seven substances: (a) hydroquinone; (b) 4-aminophenol; (c) phenol; (d) 4-nitrophenol; (e) 1-naphthol; (f) L-ascorbic acid and (g) indigo carmine.

2. Experimental

2.1. Reagents

NT, AA, Phe, IC, Tris–hydrochloride (Tris), sodium chloride (NaCl), Tween 20, 1-ethyl-3-(3-dimethyl aminopropyl) carbodiimide (EDAC), *N*-hydroxysulfosuccinimide (NHS), ethanolamine–HCl, *o*-ABA, sulfuric acid, bovine serum albumin fraction V (BSA), anti-mouse IgG antibody (produced in goat), mouse IgG (from serum), and ALP conjugated anti-mouse IgG antibody (from goat) were purchased from Sigma. HQ, NP, acetic acid, sodium acetate, and 11-mercaptoundecanoic acid were purchased from Aldrich. AP, AAP, and 6-mercapto-1-hexanol were obtained from Fluka. All stock and buffer solutions were prepared using autoclaved double-deionized water (18.2 MΩ cm).

2.2. Apparatus

Electrochemical measurements were conducted using a μAutolab III analysis system with GPES 4.9 software (Eco Chemie) at room temperature in a conventional three-electrode electrochemical cell (1.5 mL), which was used for cyclic voltammetric and amperometric experiments. An Ag/AgCl reference electrode (CH Instruments), and a platinum wire counter electrode were used. A Au disk electrode (2-mm diameter, CH Instruments), a GC disk electrode (3-mm diameter, CH Instruments) and a SPC electrode were used as working electrodes, respectively. Magnetic stirring was employed during the amperometric experiment.

The SPCEs were manufactured using a semi-automatic screen printer (Model SPM/B, MPM, Franklin, MA), using a carbon ink (Ercon, G-449(I), Wareham, MA) and alumina ceramic plates. The electrodes were cured for 1 h at 200 °C. A layer of insulator (Ercon, E6165-116 Blue Insulayer, Wareham, MA) was then printed on a portion of the conducting lines, exposing a rectangular (1.5 mm × 6.0 mm) working electrode area.

2.3. Electrochemical measurement products of substrates of ALP

The Au and the GC electrodes were polished to a mirror-like surface with 0.05 μm alumina slurries and then rinsed with deionized water prior to use.

Electrochemical measurements were performed at room temperature. A 0.5 M Tris buffer solution (pH 8.5) was used as a supporting electrolyte for IC, HQ, AP, Phe, NT and AA, and a 0.1 M acetate buffer solution (pH 4.6) for NP. The responses of different products on different electrode materials were detected by cyclic voltammetry with a scan rate of 100 mV s^{-1} and the corresponding voltammograms were recorded.

Hydrodynamic amperometric measurements were performed under stirring in 1.0 mL of the same electrolyte as used in cyclic voltammetric measurements. The anodic potentials (+0.50 V, +0.30 V, +1.10 V, +0.15 V, +0.35 V, +0.70 V and +0.50 V for IC, HQ, NP, AP, NT, Phe and AA, respectively) and cathodic potentials (−0.40 V, −0.20 V and −0.70 V for IC, HQ and NP, respectively) were applied to the SPC working electrode. The Au and GC working electrodes were applied anodic potentials at +0.50 V, +0.10 V, +1.10 V, +0.20 V, +0.35 V, +0.65 V and +0.40 V for IC, HQ, NP, AP, NT, Phe and AA, respectively, and cathodic potentials of −0.40 V, −0.10 V and −0.70 V for IC, HQ and NP, respectively. After the background current reached steady state, the aliquots of each ALP substrate were added, and the corresponding current responses were recorded as a function of time.

2.4. Mouse IgG detected at poly(o-ABA)-modified electrode immunosensors

2.4.1. The poly(o-ABA)-modified electrode immobilization

The GCEs were polished with alumina (0.05 μm) prior to use. The SPCEs were pretreated with 0.1 M H_2SO_4 applying an anodic current of 25 μA for 300 s. Then, the electrodes were washed using a 0.1 M Tris buffer solution (pH 7.4). The Au electrodes were first polished with alumina (0.05 μm) prior to use. The electrodes were soaked in freshly prepared *piranha solution* (H_2SO_4:H_2O_2 (30%, v/v) 3:1) for an hour (*safety note*: the *piranha solution* should be handled with extreme caution) and rinsed with double-distilled water. The cleaned Au electrodes were scanned with a cyclic potential between 0.0 V and 1.6 V in 0.2 M H_2SO_4 continuously until the characteristic Au peak was observed [41].

All electrodes were electropolymerized in the potential range 0–1.0 V in the presence of 50 mM *o*-ABA in 1 M H_2SO_4 by cyclic voltammetry at a scan rate of 40 mV s^{-1}. Poly(*o*-ABA)-modified electrodes were then immersed in 40 μL of NHS/EDAC solution (1/1 mg in 100 μL of 100 mM MES buffer, pH 6.0) for 30 min, and then the solution was removed. A drop of 40 μL of 40 ppm anti-mouse IgG (in 20 mM PBS buffer pH 8.6) was applied to every poly(*o*-ABA)-modified electrode. After 120 min of incubation, the solution was removed, and 40 μL of 1 M ethanolamine solution was applied on every poly(*o*-ABA)-modified electrode and incubated for 30 min. After removal of the excess of the ethanolamine solution, the poly(*o*-ABA)-modified electrodes were washed three times using 40 μL of a washing solution of 0.1% (w/v) Tween 20 in 50 mM Tris buffer solution (containing 0.1 M NaCl, pH 7.4).

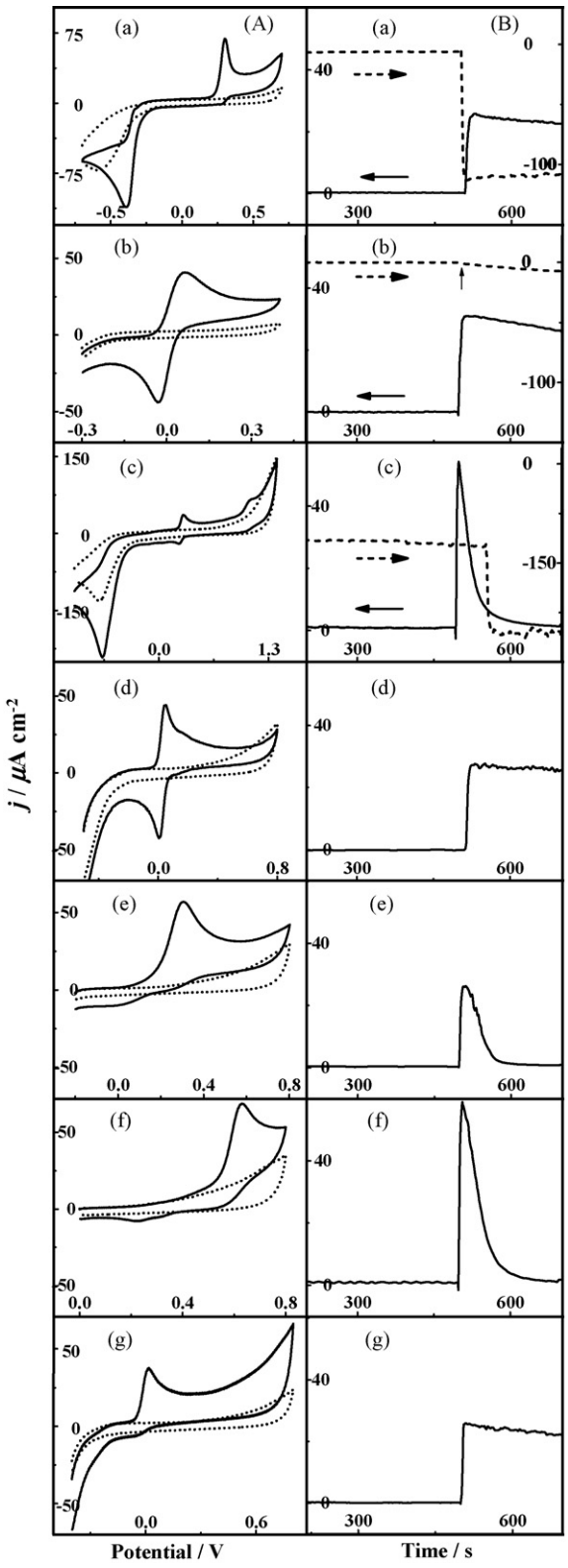

Fig. 1. (A) Cyclic voltammograms (dotted lines: background; solid lines: 100 μM substances) and (B) amperograms (solid lines: anodic current; dashed lines: cathodic current) of different substances at GCE. (a) IC; (b) HQ; (c) NP; (d) AP; (e) NT; (f) Phe and (g) AA. The electrolyte for (a), (b), and (d)–(g) were 0.5 M Tris buffer solution (pH 8.5); and for (c) was 0.1 M acetate buffer solution (pH 4.6). The scan rate for cyclic voltammetry was 100 mV/s. The potentials applied for anodic amperometry (solid lines) were (a) +0.50 V; (b) +0.10 V; (c) +1.10 V; (d) +0.20 V; (e) +0.35 V; (f) +0.65 V and (g) +0.40 V; and for cathodic amperometry (dashed lines) were (a) −0.40 V; (b) −0.10 V and (c) −0.70 V.

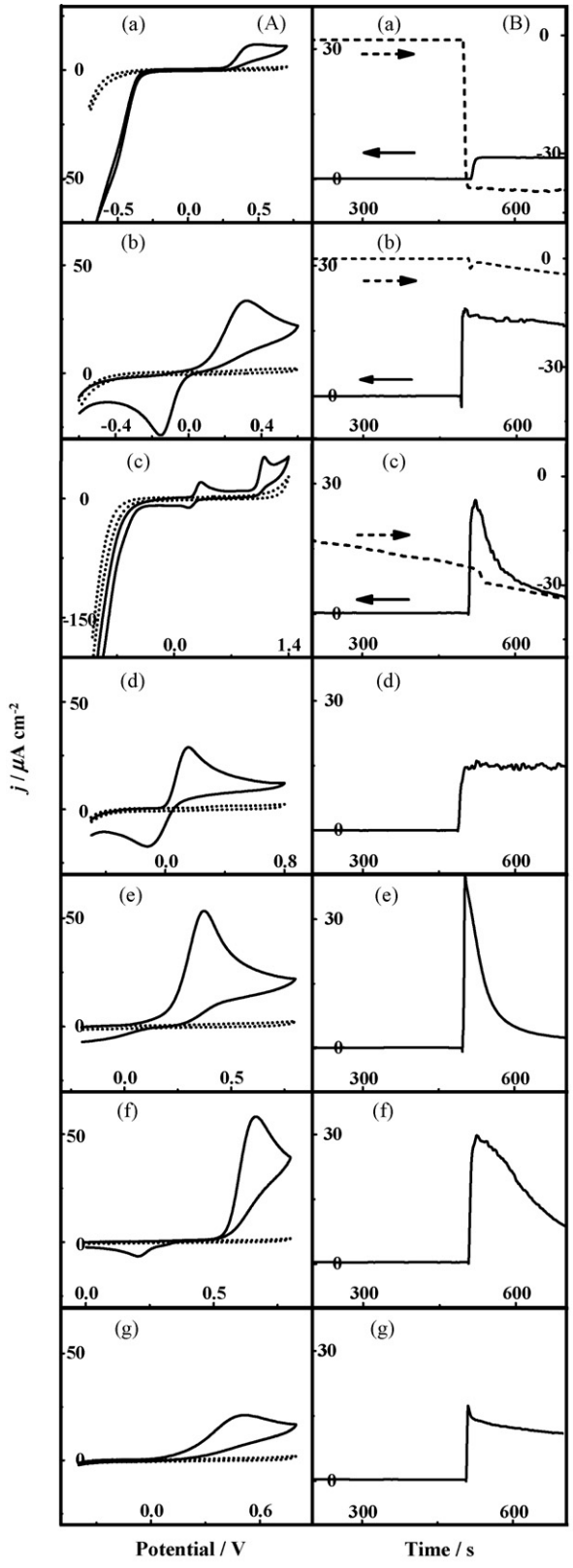

Fig. 2. (A) Cyclic voltammograms (dotted lines: background; solid lines: 100 μM substances) and (B) amperograms (solid lines: anodic current; dashed lines: cathodic current) of different substances at SPCE. (a) IC; (b) HQ; (c) NP; (d) AP; (e) NT; (f) Phe and (g) AA. The potentials applied for anodic amperometry (solid lines) were (a) +0.50 V; (b) +0.30 V; (c) +1.10 V; (d) +0.15 V; (e) +0.35 V; (f) +0.70 V and (g) +0.50 V; and for cathodic amperometry (dashed lines) were (a) −0.40 V; (b) −0.20 V and (c) −0.70 V. The other conditions were the same as Fig. 1.

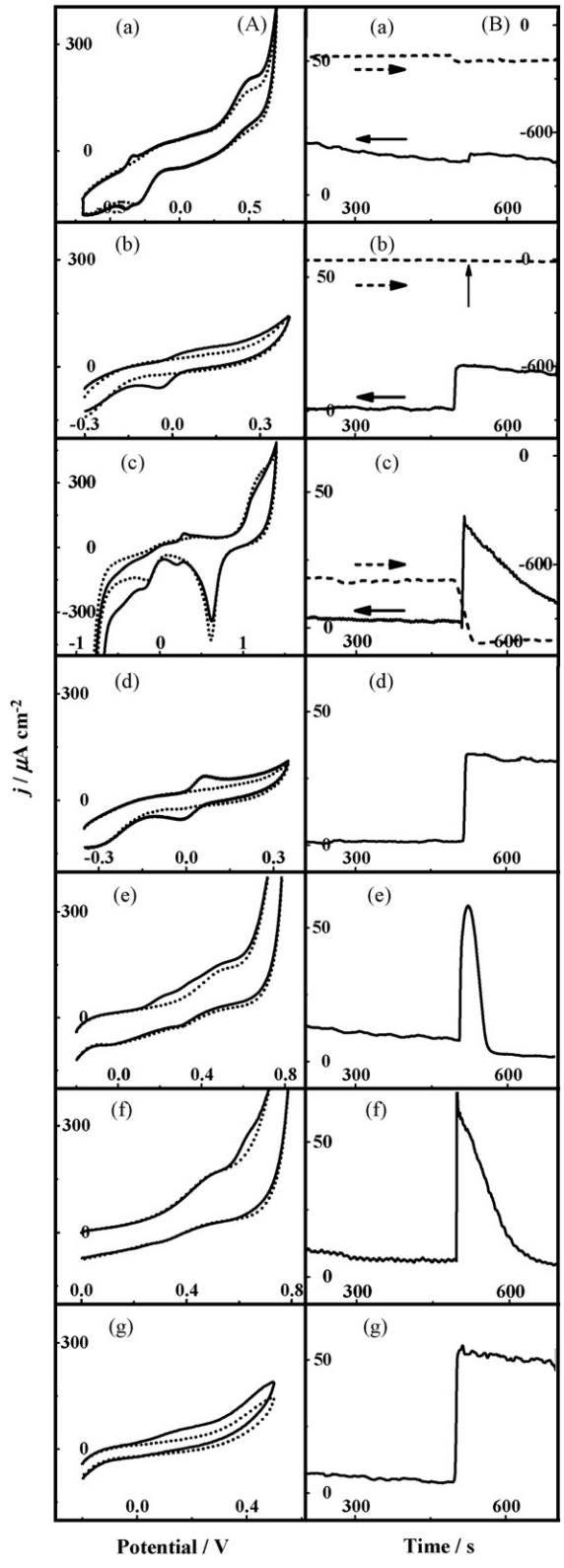

Fig. 3. (A) Cyclic voltammograms (dotted lines: background; solid lines: 100 μM substances) and (B) amperograms (solid lines: anodic current; dashed lines: cathodic current) of different substances at Au electrode. (a) IC; (b) HQ; (c) NP; (d) AP; (e) NT; (f) Phe and (g) AA. The other conditions were the same as Fig. 1.

2.4.2. Sandwich assay using poly(o-ABA)-modified electrode immunosensors

The immunosensors were first coated with the desired amount of the target mouse IgG (in 0.1 M Tris buffer solution containing 1% (w/v) BSA and 0.1% (w/v) Tween 20, pH 7.4) at room temperature for 60 min. After washing with the washing solution, the immunosensor was finally incubated with ALP-conjugated anti-mouse IgG for 60 min and afterwards washed three times as described above.

2.4.3. The poly(o-ABA)-based immunosensor detection

Amperometric measurements were performed in 1.2 mL of a 0.5 M Tris buffer solution (pH 8.5) by applying a potential of +0.4 V (for GC and Au) and +0.5 V (for SPC) on the poly(*o*-ABA)-modified electrode immunosensors at room temperature. A 100 μL aliquot of 50 mM substrate (AAP) was added to the stirred solution once the background current reached a steady state, and the corresponding current vs. time curve was recorded.

2.5. Mouse IgG detected at SAM/Au immunosensor

The Au electrodes were cleaned by the above method. After cleaning, a mixture of 11-mercaptoundecanoic acid and 6-mercapto-1-hexanol (1 mM each in ethanol, respectively) with volume ratio of 1:9 was applied on the clean, dried Au surface and kept overnight for the co-assembly process. After washing twice with ethanol, the Au electrodes were subsequently coated with 40 μL of NHS/EDAC solution (1/1 mg in 100 μL of 100 mM MES buffer, pH 6.0) for 30 min, and then processed in the same manner as the poly(*o*-ABA)-modified electrode for immobilization, sandwich assay and detection.

3. Results and discussion

3.1. Electroanalysis of products of substrates of ALP

Under alkaline conditions, ALP hydrolyses the phosphate ester ($RHPO_4^-$) functional group of its substrates (IP, HQDP, NPP, APP, NTP, PheP, and AAP) to the respective alcoholic (ROH) products (IC, HQ, NP, AP, NT, Phe, and AA), as shown in reaction (1). These products can then be electrochemically detection via reaction (2).

Enzyme reaction:

$$RHPO_4^- + H_2O \xrightarrow{ALP} RHO + H_2PO_4^- \quad (1)$$

Electrochemical reaction:

$$ROH \rightarrow R{=}O + ne^- + nH^+ \quad (2)$$

A substrate of ALP should not produce any electrochemical signal at the same potential as its of dephosphorylated form (product; ROH). The electrochemical behaviors of seven most commonly used products named, IC, HQ, NP, AP, NT, Phe, and AA (the structures shown in Scheme 1), were examined by cyclic voltammetry and amperometry at unmodified GC, SPC and Au electrodes. Figs. 1–3 display the corresponding cyclic voltammograms (Figs. 1–3A) and amperograms (Figs. 1–3B) that indicated the different products have different electrochemical behaviors on the same electrode material, and the same products also show different behaviors on different electrode materials. Figs. 1–3A show the voltammograms at GC and SPC and Au electrodes. It can be observed that the background signals at GC and SPC background CV signals are lower than at Au electrode. This can be explained that GC and SPC are less conductive than Au electrode, resulting in less electrical double layer at GC and SPC electrodes. Therefore, the large background current is obtained at Au electrode. The cyclic voltammogram in Figs. 1–3A, Phe provided the highest anodic current density of 58.10 μA cm^{-2} and 66.00 μA cm^{-2} at anodic potential peak at 0.66 V, and 0.64 V at SPC, and Au electrodes, respectively. Using GC electrode, the highest anodic current density of IC 62.5 μA cm^{-2} was obtained at 0.30 V. The lowest anodic potentials of AA were obtained at 0.01 V for GC, and AP at 0.15 V and 0.07 V for SPC and Au electrodes, respectively.

Basically, the IC (Figs. 1–3a), HQ (Figs. 1–3b), NP (Figs. 1–3c), and AP (Figs. 1–3d) show both oxidation and reduction peaks in their cyclic voltammograms. The reduction peaks of IC (Figs. 1–3A(a)) and NP (Figs. 1–3A(c)) at the potential −0.39 V and −0.68 V (for GC), −0.50 V and −0.70 V (for SPC), and −0.38 V and −0.60 V (for Au) provided very high current in solid lines. The electrolyte also gave a hydrogen evolution at about −0.7 V. HQ provided quasi-reversible shapes of cyclic voltammogram at all of three electrodes. Using AP at SPC and Au electrodes, quasi-reversible behavior was obtained. Only, at GC, AP exhibited reversible behavior (the ratio of i_{pc}/i_{pa} is 0.95 and peak separation is 0.6/n V).

Normally in an ALP reaction, IP substrate can generate indigo blue (IB) by the enzymatic hydrolysis as shown in reaction (3). IB is less soluble in aqueous solution. Therefore, fuming sulphuric acid was added in the solution to form soluble IC. IC is redox couples, which can be investigated by electrochemical detection [17]. It is complicated, therefore; IP is not good choice as a substrate:

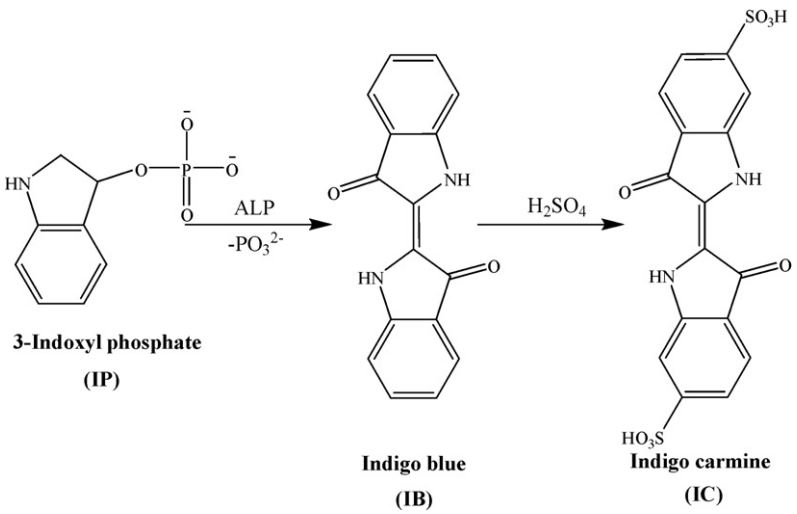

3-Indoxyl phosphate (IP) **Indigo blue (IB)** **Indigo carmine (IC)**

(3)

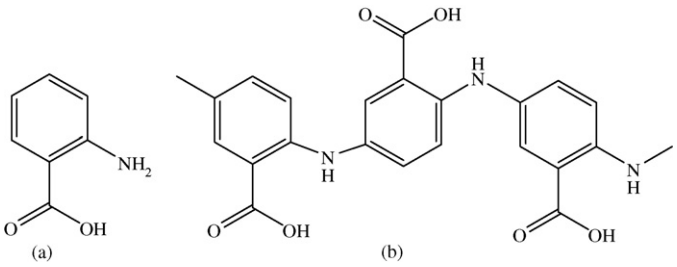

Scheme 2. Structures of (a) *o*-aminobenzoic acid (*o*-ABA) and (b) poly(*o*-aminobenzoic acid) (poly(*o*-ABA)).

In contrast, NT (Figs. 1–3e), Phe (Figs. 1–3f) and AA (Figs. 1–3g) display only an oxidation peak due to their irreversible chemical reaction corresponding to the previous works in the literatures [15,17,19,20,22,23,25]. Phe, NP, and NT cyclic voltammograms display a poor redox reversibility in all oxidation studies [15,17,25]. The NP, and NT electrochemical reactions were similar to Phe reaction. Their amperometric responses quickly decayed to zero (or base line current density) as electrode fouling occurred as shown in solid lines of Figs. 1–3B(c), (e), and (f) for NP, NT, and Phe, respectively. The NP, NT, and Phe electrooxidation reactions caused the accumulation of electroinactive species at the electrode surface, polymer formation on the electrode leads to passivation of the electrode. Electrode passivation or fouling can pose problems for the development and application of electrochemical immunosensors. For AA in Figs. 1–3A(g), cyclic voltammograms showed the oxidation peaks at 20 mV, 500 mV, and 200 mV for GC, SPC, and Au, respectively. These irreversible reactions were consistent with the previous studies [19,22]. Figs. 1–3B(g) demonstrated the amperometric response of AA, after added AA in electrolyte solution. The current was nearly constant indicating that less passivation occurring at all of electrodes.

Most electrochemical immunoassay methods are based on the application of a constant potential to an electrode transducer and measurement of the current generated by oxidation of enzyme hydrolysis products. Thus amperometric detection was performed to evaluate the behavior of these products. When NP, NT and Phe solutions were added, the responds rapidly decayed due to electrode fouling. These results were similar to the results reported in the literatures [19,22]. Then contrast, HQ, AP, and AA amperograms in Figs. 1–3B(b), (d), and (g) displayed nearly constant anodic current signals after standard of HQ, AP, and AA solution were added in electrolyte. The electrode was reused to repeat experiments for three times. The sensitivity (±S.D.) of the detection of HQ, AP, and AA were $0.29 \pm 0.02\ \mu A\ cm^{-2}\ \mu M^{-1}$, $0.17 \pm 0.01\ \mu A\ cm^{-2}\ \mu M^{-1}$, and $0.15 \pm 0.01\ \mu A\ cm^{-2}\ \mu M^{-1}$ for HQ; $0.25 \pm 0.00\ \mu A\ cm^{-2}\ \mu M^{-1}$, $0.14 \pm 0.02\ \mu A\ cm^{-2}\ \mu M^{-1}$, and $0.32 \pm 0.01\ \mu A\ cm^{-2}\ \mu M^{-1}$ for AP; and $0.24 \pm 0.02\ \mu A\ cm^{-2}\ \mu M^{-1}$, $0.12 \pm 0.02\ \mu A\ cm^{-2}\ \mu M^{-1}$, and $0.47 \pm 0.01\ \mu A\ cm^{-2}\ \mu M^{-1}$ for AA at GC, SPC, and Au electrodes, respectively. For ALP enzyme reaction HQ, AP, and AA are generated from HQP, APP, and AAP substrates, respectively. The AAP substrate was commercially available, less expensive, non-fouling, non-toxic nature of AA product, good chemical stability, and very sensitive response at electrodes [19,22,27]. It was compared with the no-commercially available HQDP, and to the high price of APP. Thus, AAP was chosen as the enzyme substrate for the immunoassay experiments.

3.2. The o-ABA electropolymerization

Poly(*o*-ABA), conducting polymer [30], has π electron backbone in the structure as shown in Scheme 2. In previous works [37,38],

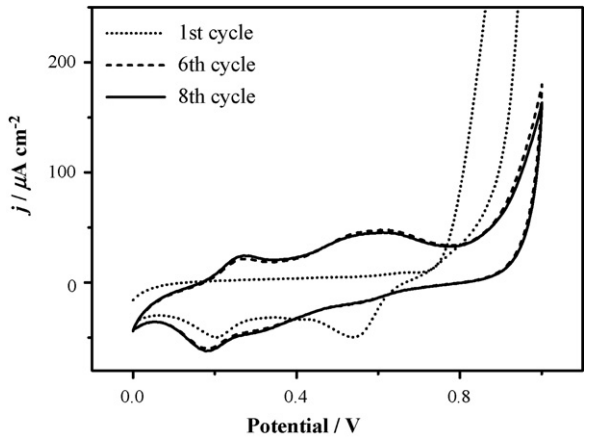

Fig. 4. Cyclic voltammogram of *o*-ABA electropolymerization at Au electrode: 1st cycle (dotted line); 6th cycle (dashed line); and 8th cycle (solid line). Scan rate is $40\ mV\ s^{-1}$.

this polymer was characterized by in situ FTIR. The FTIR results displayed that there was the carboxyl group on the surface after electropolymerization. The *o*-ABA solution was electropolymerized in the potential range of 0–1 V at GC, SPC, and Au electrodes with $40\ mV\ s^{-1}$ by cyclic voltammetry. The cyclic voltammograms of poly(*o*-ABA) at Au electrode was shown in Fig. 4. The polymerization of *o*-ABA at SPC and GC were also analogous to Au electrode. Fig. 4 showed 1st, 6th, and 8th cycle of *o*-ABA cyclic voltammetric electropolymerization indicating that voltammogram grew very fast in the first of six cycles. Thus we selected eight cycles for electropolymerization of these sandwich immunoassay system.

3.3. Mouse IgG poly(o-ABA)-modified electrode immunosensors

In this paper, an enzyme-amplified electrochemical immunosensor based on poly(*o*-ABA) conducting polymer for sensing antibody–antigen interaction was developed. The immunosensing system is illustrated in Scheme 3, where a poly(*o*-ABA)-modified electrode serves as the scaffold of the sandwich immunoassay for mouse IgG, and uses ALP as the enzyme label and AAP as the enzyme

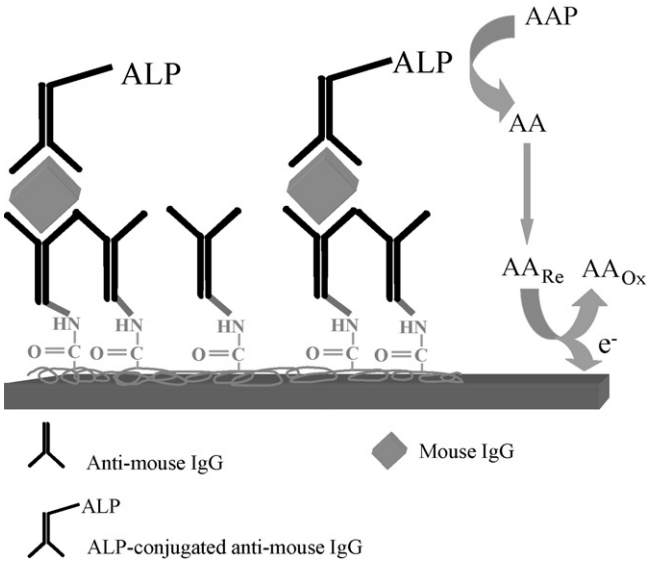

Scheme 3. Schematic illustration of an enzyme-amplified immunosensor using poly(*o*-ABA)-based electrode.

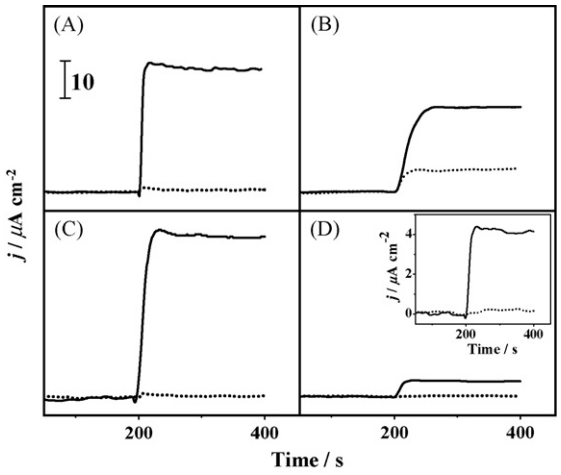

Fig. 5. Amperometric responses of 1000 ng mL^{-1} (solid lines) and 0 ng mL^{-1} mouse IgG (dotted lines) at poly(*o*-ABA)/GC (A), poly(*o*-ABA)/SPC (B), poly(*o*-ABA)/Au (C), and SAM/Au (D) immunosensors in 0.5 M Tris buffer solution (pH 8.5) at +0.40 V (A, C, and D) and +0.50 V (B) vs. Ag/AgCl. Inset of (D) shows the amperogram responses zooming from SAM/Au immunosensors.

substrate. Once the poly(*o*-ABA) is deposited on electrodes, the carboxyl group on the surface can react, via the reactions involving EDAC/NHS, to form a covalent bonding with the amine group of an anti-mouse IgG. In this way, the capture mouse IgG can be immobilised on the electrode surface. Anti-mouse IgG-conjugated ALP was bound to mouse IgG to catalyze the conversion of AAP to AA, as shown in reaction (4). The AA product can be detected electrochemically, giving an anodic current response proportional to the mouse IgG quantity:

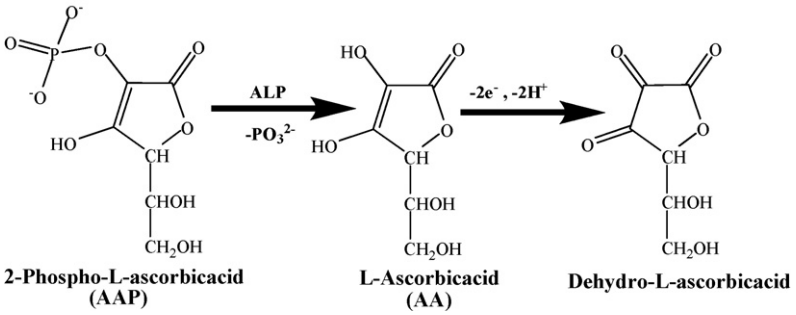

(4)

The incubation times were varied by soaking of anti-mouse IgG, mouse IgG, and anti-mouse IgG conjugated with ALP solutions for 60 min, 120 min, and 180 min. The current signal of target and control of mouse IgG were measured. The ratio of target signal and control signal were calculated to obtain the optimum incubation time. It was found that the incubation times of anti-mouse IgG, mouse IgG, and anti-mouse IgG conjugated with ALP as 120 min, 60 min, and 60 min, respectively.

The preparation of mouse IgG immunosensor on poly(*o*-ABA)/SPC electrode was optimized by non pre-treatment and pre-treatment with an applied current of 25 μA for 300 s, and curing temperatures of 200 °C, 250 °C, and 300 °C for SPC electrode preparation before poly(*o*-ABA) electropolymerization. The best curing temperatures were selected from the highest current response of 1 mM $K_4Fe(CN)_6$. The maximum response was found on SPC electrodes with a curing temperature of 200 °C after pre-treatment with an anodic current of 25 μA for 300 s. The optimum pre-treatment of SPC electrode was measured by immunoassay process at the highest ratio of target as 1000 ng mL^{-1} mouse IgG to control as 0 ng mL^{-1} mouse IgG. After pre-treatment, the SPC electrode surface has hydrophilic property, so it can be electropolymerized better than a non pre-treated SPC electrode.

Fig. 5A–C shows the amperometric responses of AA generated from AAP by ALP enzyme on mouse IgG immunosensors based on poly(*o*-ABA)/GC, poly(*o*-ABA)/SPC, and poly(*o*-ABA)/Au electrodes (immunosensor showed in Scheme 3) at the potentials of 0.40 V, 0.50 V, and 0.40 V, respectively. The suitable potentials of their electrode immunosensors were obtained from hydrodynamic voltammetric measurement at each immunosensors. The current density of target, solid lines (1000 ng mL^{-1} mouse IgG) at the poly(*o*-ABA)/GC (Fig. 5A), poly(*o*-ABA)/SPC (Fig. 5B), and poly(*o*-ABA)/Au (Fig. 5C) immunosensors was 33.10 μA cm^{-2}, 22.49 μA cm^{-2}, and 43.50 μA cm^{-2}. The current density of control, dotted lines (zero concentration of mouse IgG) was 0.33 μA cm^{-2}, 5.88 μA cm^{-2}, and 0.15 μA cm^{-2}, respectively. We found that mouse IgG immunosensor on poly(*o*-ABA)/Au gave the highest current density response ratio between target and control of approximately 297, which implied that the poly(*o*-ABA) on the Au surface would produce a surface with the least non-specific adsorption. Thus, we used this immunosensor for mouse IgG sensor in the subsequent experiments. For the behavior of larger molecule of substrate may exhibit slower turnover in the enzymatic reaction and may also exhibit slower diffusion though the biolayer towards the electrode surface. In this case, using small molecules of AAP, after the AAP substrate is added in the Tris buffer solution, it can be generated to AA very fast, becoming a stable current within 30 s at all of three immunosensors.

3.4. Comparison of SAM/Au and poly(*o*-ABA)/Au immunosensors

The preparation of mouse IgG SAM/Au immunosensors was optimized by changing the 11-mercaptoundecanoic acid to 6-mercapto-1-hexanol at ratios of 1:9, 1:4, 1:3, 1:1 and 4:1. The highest ratio for target (1000 ng mL^{-1} mouse IgG) to control was obtained when using 1:9 as mixed-monolayer. This could be because the high ratio of 6-mercapto-1-hexanol could efficiently minimize non-specific adsorption, and the 11-mercaptoundecanoic acid could also provide enough binding for anti-mouse IgG at the same time. This is shown in Fig. 5D.

The current densities of 1000 ng mL^{-1} of target and 0 ng mL^{-1} of control were 4.19 μA cm^{-2} and 0.13 μA cm^{-2}, respectively. SAM/Au (Fig. 5D) and poly(*o*-ABA)/Au (Fig. 5C) were compared at the same condition of sandwich immobilization, detection, and target concentration (1000 ng mL^{-1} mouse IgG). The results showed target/control ratios between SAM/Au and poly(*o*-ABA)/Au as 33 and 297, respectively.

Therefore, using poly(*o*-ABA) conductive polymer has more sensitivity than using SAM for base Au immunosensor, because electron transfer on conductive polymer is very good. In comparison, layers of SAM and biomolecules lead to blocking of the direct electron transfer between electroactive species and an electrode.

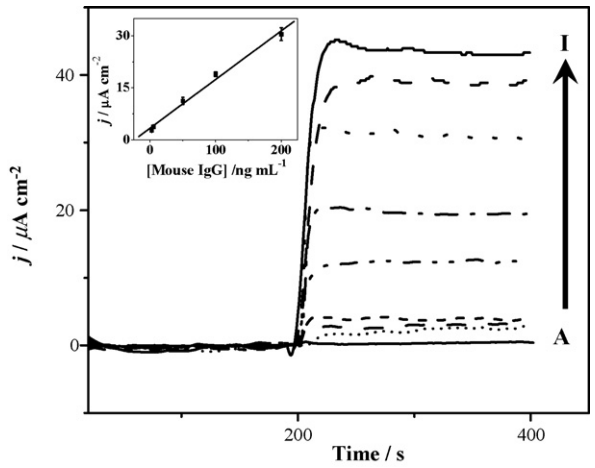

Fig. 6. Amperograms of 0 ng mL^{-1}, 1 ng mL^{-1}, 3 ng mL^{-1}, 5 ng mL^{-1}, 50 ng mL^{-1}, 100 ng mL^{-1}, 200 ng mL^{-1}, 500 ng mL^{-1}, and 1000 ng mL^{-1} mouse IgG (A to I) at poly(*o*-ABA)/Au immunosensor in 0.5 M Tris buffer solution (pH8.5) at +0.40 V vs. Ag/AgCl. Inset shows the linear range 3–200 ng mL^{-1} of mouse IgG (R^2 = 0.9905 and y = 0.1401x + 3.3893).

3.5. Calibration curve of immunosensor

The poly(*o*-ABA)/Au immunosensing system display the most sensitive response to the mouse IgG detection. Fig. 6 represents amperograms of various mouse IgG concentrations on the relationship between current density response and time. Measurements were performed in triplicate using three different immunosensors. The inset shows the dynamic range of the relationship between the average of current density responses (n = 3) and mouse IgG concentration. It can be seen that the dynamic range is from 3 ng mL^{-1} to 200 ng mL^{-1} (R^2 = 0.9905), the sensitivity is 0.1401 μA cm^{-2} (ng mL^{-1})$^{-1}$, S.D. < 2 (n = 3), and the detection limit is 1 ng mL^{-1}. Poly-*o*-ABA-modified Au electrode is comparable to electrochemical immunosensor studied by Wilson [42,43]. That found our immunosensor is wider dynamic range and lower detection limit than Wilson's electrochemical immunosensor system using HQDP as substrate of ALP. For our sensitivity is higher than the microelectrochemical immunoassay using SAM modified Au and APP as substrate of ALP report [44].

4. Conclusions

Alkaline phosphatase can be used as an effective label for sensitive immunoelectrochemical assays, which has many substrates for use. Seven products of ALP substrates were examined and compared by cyclic voltammetry and amperometry. The AA product of the AAP substrate gave a large and stable signal, along with an inexpensive substrate. It was selected for immunosensors at GC, SPC, and Au electrodes, using mouse IgG as a model analyte. Immunosensors using the conductive polymer of *o*-ABA were based on all electrodes and coupled with sandwich-type immunoassay technique. We found that not only did poly(*o*-ABA)/Au immunosensor gave the most favorable response (linear range 3–200 ng mL^{-1}), with good sensitivity, reproducibility (S.D. < 2; n = 3) for mouse IgG sensor, but also had very low non-specific adsorption.

Acknowledgements

Financial from the NIH (Award Numbers EB002189 and R01A 1056047-04) is gratefully acknowledged. A.P. and O.C. acknowledge Thai government fellowship, and the Thailand research fund (Basic Research Grant).

References

[1] A. Brajter-Toth, J.Q. Chambers, Electroanalytical Methods for Biological Materials, Marcel Dekker, Inc., New York, 2002.
[2] W.W. Cleland, A.C. Hengge, Chem. Rev. 106 (2006) 3252.
[3] P.D. Tzanavaras, D.G. Themelis, B. Karlberg, Anal. Chim. Acta 462 (2002) 119.
[4] X.J. Zhu, C.Q. Jiang, Clin. Chim. Acta 377 (2007) 150.
[5] X.J. Zhu, Q.K. Liu, C.Q. Jiang, Anal. Chim. Acta 570 (2006) 29.
[6] B.A. Tannous, M. Verhaegen, T.K. Christopoulos, A. Kourakli, Anal. Biochem. 320 (2003) 266.
[7] H. Arakawa, M. Shiokawa, O. Imamura, M. Maeda, Anal. Biochem. 314 (2003) 206.
[8] M.P. Kreuzer, C.K. O'Sullivan, G.G. Guilbault, Anal. Chim. Acta 393 (1999) 95.
[9] D. Szydlowska, M. Campas, J.L. Marty, M. Trojanowicz, Sens. Actuators B 113 (2006) 787.
[10] M. Diaz-Gonzalez, C. Fernandez-Sanchez, A. Costa-Garcia, Anal. Sci. 18 (2002) 1209.
[11] M. Diaz-Gonzalez, M.B. Gonzalez-Garcia, A. Costa-Garcia, Biosens. Bioelectron. 20 (2005) 2035.
[12] P. Fanjul-Bolado, M.B. Gonzalez-Garcia, A. Costa-Garcia, Talanta 64 (2004) 452.
[13] S. Martinez-Montequin, C. Fernandez-Sanchez, A. Costa-Garcia, Anal. Chim. Acta 417 (2000) 57.
[14] M.S. Wilson, R.D. Rauh, Biosens. Bioelectron. 20 (2004) 276.
[15] P. Fanjul-Bolado, M.B. Gonzalez-Garcia, A. Costa-Garcia, Anal. Bioanal. Chem. 385 (2006) 1202.
[16] H.J. Kim, J. Kwak, J. Electroanal. Chem. 577 (2005) 243.
[17] I. Rosen, J. Rishpon, J. Electroanal. Chem. 258 (1989) 27.
[18] H. Dong, C.M. Li, W. Chen, Q. Zhou, Z.X. Zeng, J.H.T. Luong, Anal. Chem. 78 (2006) 7424.
[19] R.E. Gyurcsanyi, A. Bereczki, G. Nagy, M.R. Neuman, E. Lindner, Analyst 127 (2002) 235.
[20] J.P. Hart, R.M. Pemberton, R. Luxton, R. Wedge, Biosens. Bioelectron. 12 (1997) 1113.
[21] S.J. Kwon, E. Kim, H. Yang, J. Kwak, Analyst 131 (2006) 402.
[22] E.J. Moore, M. Pravda, M.P. Kreuzer, G.G. Guilbault, Anal. Lett. 36 (2003) 303.
[23] R.M. Pemberton, J.P. Hart, P. Stoddard, J.A. Foulkes, Biosens. Bioelectron. 14 (1999) 495.
[24] M. Chikae, K. Kerman, N. Nagatani, Y. Takamura, E. Tamiya, Anal. Chim. Acta 581 (2007) 364.
[25] V.K. Rao, M.K. Sharma, P. Pandey, K. Sekhar, World J. Microbiol. Biotechnol. 22 (2006) 1135.
[26] X.M. Sun, N. Gao, W.R. Jin, Anal. Chim. Acta 571 (2006) 30.
[27] A. Kokado, H. Arakawa, M. Maeda, Anal. Chim. Acta 407 (2000) 119.
[28] Z.H. Wang, A.S. Viana, G. Jin, L.M. Abrantes, Bioelectrochemistry 69 (2006) 180.
[29] Z. Dai, A.-N. Kawde, Y. Xiang, J.T.L. Belle, J. Gerlach, V.P. Bhavanandan, L. Joshi, J. Wang, J. Am. Chem. Soc. 128 (2006) 10018.
[30] M. Gerard, A. Chaubey, B.D. Malhotra, Biosens. Bioelectron 17 (2002) 345.
[31] G. Lillie, P. Payne, P. Vadgama, Sens. Actuators B 78 (2001) 249.
[32] M.A. Rahman, M.J.A. Shiddiky, J.-S. Park, Y.-B. Shim, Biosens. Bioelectron. 22 (2007) 2464.
[33] J.-H. Kim, J.-H. Cho, G.S. Cha, C.-W. Lee, H.-B. Kim, S.-H. Paek, Biosens. Bioelectron. 14 (2000) 907.
[34] T.L. Fare, M.D. Cabelli, S.M. Dallas, D.P. Herzog, Biosens. Bioelectron. 13 (1998) 459.
[35] F. Darain, S.-U. Park, Y.-B. Shim, Biosens. Bioelectron. 18 (2003) 773.
[36] Y.-M. Zhou, Z.-Y. Wu, G.-L. Shen, R.-Q. Yu, Sens. Actuators B 89 (2003) 292.
[37] Y.J. Wang, W. Knoll, Anal. Chim. Acta 558 (2006) 150.
[38] A. Benyoucef, F. Huerta, J.L. Vazquez, E. Morallon, Eur. Polym. J. 41 (2005) 843.
[39] W. Cheng, G. Jin, Y. Zhang, Russian J. Electrochem. 41 (2005) 940.
[40] Y.Z. Zhang, G.Y. Jin, W.X. Cheng, S.P. Li, Front. Biosci. 10 (2005) 23.
[41] C. Berggren, P. Stalhandske, J. Brundell, G. Johansson, Electroanalysis 11 (1999) 156.
[42] M.S. Wilson, Anal. Chem. 77 (2005) 1496.
[43] M.S. Wilson, W. Nie, Anal. Chem. 78 (2006) 2507.
[44] Z.P. Aguilar, W.R. Vandaveer IV, I. Fritsch, Anal. Chem. 74 (2002) 3321.

Talanta 76 (2008) 448–453

Contents lists available at ScienceDirect

Talanta

journal homepage: www.elsevier.com/locate/talanta

Assessment of a modified and optimised method for determining chemical oxygen demand of solid substrates and solutions with high suspended solid content

F. Raposo*, M.A. de la Rubia, R. Borja, M. Alaiz

Instituto de la Grasa (CSIC), Avda. Padre García Tejero 4, 41012 Seville, Spain

ARTICLE INFO

Article history:
Received 7 November 2007
Received in revised form 11 March 2008
Accepted 21 March 2008
Available online 28 March 2008

Keywords:
Chemical oxygen demand (COD)
Solid substrates
Suspended solids
Elemental analysis
Dichromate oxidation
Anaerobic digestate

ABSTRACT

A modified approach to determine the chemical oxygen demand (COD) of solid substrates based on the DIN 38414-S9 standard method is proposed. The adapted procedure is assessed and compared with standard methods widely used for water and wastewater such as the American Public Health Association–American Water Works Association–Water Pollution Control Federation (APHA–AWWA–WPCF) standard methods 5220 B-open reflux (SM-OR) and 5220 D-closed reflux colorimetric (SM-CR). Solutions with high suspended concentration of solids, as well as digestates from an anaerobic reactor, were used during the comparative test. For solid substrates, the COD recovery was about 100% when the proposed method was used. For solutions with solid content higher than 20 g TS L^{-1}, the recovery was only completed when the proposed method was used, showing that the methods traditionally employed are not very appropriate for samples with the described characteristics. For instance, percentages of COD recovery in the ranges of 77.3–87.1% and 89.4–94.1% were achieved when the SM-OR and SM-CR methods were used, respectively.

1. Introduction

One of the most important water quality parameters controlled by environmental regulatory agencies is the so-called "oxygen demanding" substances. Oxygen demand is an important delimiter for the effect of organic pollutants in aqueous environmental systems. The biodegradation of oxygen-demanding compounds in the environment is linked to aerobic degradation by microorganisms which results in the consumption of oxygen with the adverse effect that this can cause on the natural balance of the aquatic ecosystem. There are three main methods for assessing organic pollutants in water: total organic carbon (TOC), biochemical oxygen demand (BOD) and chemical oxygen demand (COD). TOC is a generic measurement which relies on specific instrumentation; BOD is related to carbon oxidation carried out biochemically but has the disadvantage of time consumption and often lacks reproducible results; COD is defined as a measure of the oxygen equivalent of the organic matter content of a sample susceptible to oxidation by a strong chemical oxidant, and it is used as the principal water quality parameter at many wastewater treatment facilities.

For COD determination, a wide range of chemicals has been used as oxidizing agents, including dichromate, permanganate, ceric acid, iodate and persulphate. The dichromate reflux method is preferable to the other methods using other oxidants because of its superior oxidizing ability, its applicability on a wide variety of samples and its easy manipulation. The reference method for COD determination consists of oxidizing the organic matter of the sample by adding a known amount of oxidant in an acid sulphuric medium, refluxing at high temperature on open containers and titrating the excess oxidant. The historical development of the open reflux standard method will be summarized as follows. Adeney and Dawson [1] were among the first to use dichromate in the presence of sulphuric acid to determine the organic matter in water. The mixture was heated at 100–110 °C for 2 h and the excess dichromate titrated with ferrous ammonia sulphate (Mohr's salt) using an outside indicator. Moore et al. [2] demonstrated the effectiveness of some organic compounds in oxidation by the dichromate open reflux method. Later, Moore et al. [3] proposed the use of silver sulphate as a catalyst to improve the oxidation of some recalcitrant compounds. Dobbs and Williams [4] described the method for removing the chloride interference by using mercuric sulphate to prevent it, and Baumann [5] proposed a weight ratio $HgSO_4$:Cl^- equal to 10:1 to avoid this interference.

One of the drawbacks of this methodology is the high consumption of expensive chemicals, such as catalyst and toxic metal to prevent the interference of halide anions. Several modifications were proposed to circumvent this disadvantage. Jirka and Carter [6] introduced a micro semi-automated method in which diges-

* Corresponding author. Tel.: +34 95 4689654; fax: +34 95 4691262.
E-mail address: fraposo@cica.es (F. Raposo).

0039-9140/$ – see front matter © 2008 Elsevier B.V. All rights reserved.
doi:10.1016/j.talanta.2008.03.030

tion is carried out in sealed glass tubes. They determined the COD of wastewater samples spectrophotometrically by measuring the increase in Cr^{3+} at 600 nm. They reduced the volume of chemical consumption by 95%, using the same sample of reagent ratio, temperature and time digestion that was used in the open reflux method. Himebaugh and Smith [7] introduced a closed reflux method with titration determination to maintain the advantages of the colorimetric method where no spectrophotometer was available.

In the past few years the colorimetric measurement of COD has been most commonly used because of its simplicity, how easy it is to use, and the fact that the tubes can be purchased already prepared just for adding the sample. Even Lapara et al. [8] assayed a miniaturized closed reflux method to minimize the use of toxic substances and the production of hazardous waste in the laboratory, reducing the volume of the standard methods 5220 B-open reflux (SM-OR) and 5220 D-closed reflux colorimetric (SM-CR) by 84% and 99.2%, respectively.

Taking recent interest in improving agriculture by-products as source of energy trough anaerobic digestion, and the use of the COD as a widely balanced unit in anaerobic reactors into account, the reliable measure of COD in solids substrate is a very important parameter for consideration. Only a few references detailed the analytical procedure for measuring the organic content of solid substrates. Walkley and Black [9] proposed potassium dichromate in a sulphuric acid medium to determine the soil organic matter. In Italy the UNI 10665-Spinger-Klee volumetric method [10] also used potassium dichromate in a sulphuric acid medium to evaluate the organic carbon content of fertilizers. The German DIN 38414-S9 standard method [11] is applicable for estimating the COD of sludges and sediments, although any reference of use appeared in the literature. The sample is heated with potassium dichromate and silver sulphate in a strong sulphuric acid solution, using a potentiometric back titration method to measure the end-point reaction. On the other hand, the literature contains many recent research works where the American Public Health Association–American Water Works Association–Water Pollution Control Federation (APHA–AWWA–WPCF) [12] methods for COD determination have been used in solid samples [13,14] or high suspended solid content samples, such as broiler manure and cattle dung [15], pig manure [16], olive mill wastewater [17] and municipal waste sludge [18] among other reported works. As the APHA–AWWA–WPCF methods are standardized to COD values below 1000 mg O_2 L^{-1}, the way to resolve this problem was to use several dilutions of the original sample, with the corresponding decrease in accuracy, as reported by Liao and Lo [19]. Yadvika et al. [20] demonstrated that the open reflux standard method failed to produce consistent and representative results due to the high solid contents in the sample. Their new methodology suffers from a series of drawbacks: (i) the low amount of sample used (25 mg), (ii) the extra analytical time for drying the slurry, and (iii) the lack of studies into the recovery of spiked samples.

The purpose of this research work was to assess an adapted method for COD determination of solid samples and report the comparative study of samples with high suspended solid concentrations, using the COD standard methods for water and wastewater (APHA–AWWA–WPCF, 1998) [12] and the modified proposed COD method based on the DIN 38414-S9 standard method. The most important novelties of the research work undertaken were: (i) no COD method for solid samples was previously validated using solid substrates, including a solid certified reference material (CRM). For example, the DIN 38414-S9 standard method used a solution of potassium hydrogen phthalate to check the reliability of the procedure. Moreover, FAPAS (the world leader company organising proficiency testing) has not any program to test the COD of solid material, (ii) the results obtained by the modified COD solid method were compared with the theoretical oxygen demand values proportioned by the solid substrates elemental analysis.

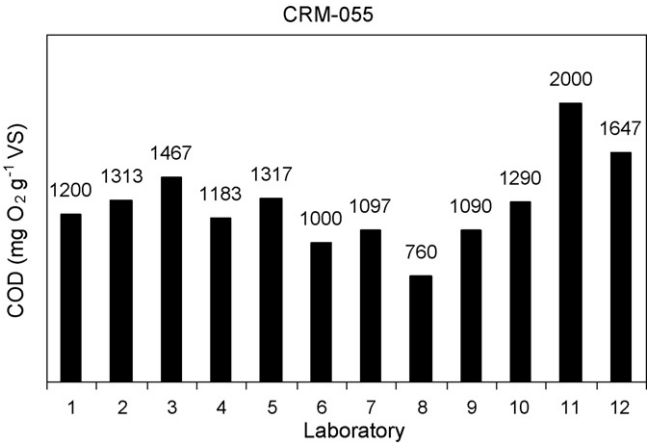

Fig. 1. COD values of CRM-055 obtained in the certification study.

2. Materials and methods

2.1. Materials

The reference method used to determine the COD parameter is based on the APHA–AWWA–WPCF standard method [12] for the analysis of water and wastewater. In order to evaluate the efficiency of the COD method for solid samples and solutions with solid content higher than 20 g TS L^{-1}, five substrates were selected:

- Potassium hydrogen phthalate (KHP): primary standard grade Panreac brand. It is used internationally as the accepted standard for this determination [11,12].
- Cellulose powder (CP): analytical grade Avicel PH-101-Fluka, 50 μm in size. It is a pure and homogeneous organic compound with a high prevalence in agro-wastes.
- Sunflower oil cake (SuOC): the part of whole sunflower seed which remains after the oil extraction processes. This heterogeneous by-product can be broken down into three main components: a proteinaceous fraction, a lignocellulosic fraction and a soluble fraction. The SuOC sample used in this study was taken from a sunflower oil factory located near Seville (Spain). Prior to using the substrate, it was grinded and sieved to give a fraction with a particle size lower than 0.5 mm.
- Anaerobic sludge (An-S): from a full-scale anaerobic digester treating brewery wastewater, with a composition of total solids (TS) of 70 g L^{-1} and volatile solids (VS) of 46 g L^{-1}. The substrate was dried at 105 °C until it reached a constant weight and then grinded and sieved to give a fraction with a particle size lower than 0.5 mm.
- Certified reference material sludge (CRM-S): sewage sludge LGC Promochem reference 055-050 (19 metals plus COD, Kjeldahl nitrogen and total phosphorus). This sewage sludge is produced and certified by Resource Technology Corporation (USA). Unfortunately, no analytical method was provided by the company organising the certification study (interlaboratory test used for establishing the true value of an analyte concentration in a reference material). Fig. 1 shows the reference values reported by the participant laboratories, which ranged from 760 to 2000 mg O_2 g^{-1} VS. Therefore, the CRM used had low accuracy and high uncertainty. The value of COD certified was 1280 ± 320 mg O_2 g^{-1} VS.

Four different SuOC solutions with high suspended solid contents, ranging from 20 to 80 g TS L^{-1}, were prepared and the influence of the concentration in the COD measurement was also evaluated. In addition, an An-S with high solid content (70 g TS L^{-1}) was used directly, without previously drying it so as to check the influence of microorganism concentration in the COD parameter.

2.2. Analytical methods

For each analytical method, solid substrate and concentration of solution spiked, five replicates were done.

2.2.1. Theoretical oxygen demand (ThOD)

Initially, the calculation of the ThOD was determined. This parameter is defined as the stoichiometric amount of oxygen required to oxidize a compound to end products, mainly CO_2 and H_2O, although other additional products should be produced (P_2O_5, Na_2O, HCl, NH_3) when the organic compound contains P, Na, Cl or N atoms in the molecule. For this purpose a complementary elemental analysis was carried out. The chemical compositions of the selected substrates were determined using a Leco CHNS-932 elemental analyzer, following the manufacturer's standard procedures. With the data of chemical compositions proportioned by five replicates samples of each substrate and using an empirical equation it is possible to calculate the theoretical oxygen demand. The equation used is detailed in the ISO 10707 [21].

2.2.2. COD experimental methods

2.2.2.1. Solid substrates open reflux method (SS-OR). The DIN 38414-S9 standard method [11] was originally developed and reported in the literature to determine the organic content of fine ground dry matter obtained from sludge and sediments. Given the widespread use and importance of COD measurements, the method described here has been re-designed in an effort to simplify the initial protocol. Basically, the proposed method consisted of a wet oxidation with potassium dichromate as the oxidant and silver sulphate as the catalyst in a strong sulphuric acid solution. The following apparatus and reagents were used.

2.2.2.1.1. Apparatus.

- 40 mm × 300 mm glass digestion vessels with ground-glass joint.
- 300 mm jacket condensers with ground-glass joint.
- Heating block to operate at 150 ± 2 °C from J.P. Selecta (Barcelona-Spain).
- Big mouth Erlenmeyer flasks of 500 mL nominal capacity.
- Burette of 25 mL nominal capacity.
- Magnetic stirrer.

2.2.2.1.2. Reagents.

- Sulphuric acid 96%.
- Digestion reagent: dissolve 33.3 g of mercuric sulphate ($HgSO_4$), 167 mL of sulphuric acid 96% and 600 mL of water. Then dissolve 58.844 g of potassium dichromate ($K_2Cr_2O_7$) primary standard grade, previously dried at 105 °C for 2 h, and finally top up the solution with distilled water to 1000 mL.
- Sulphuric acid reagent: dissolve 10 g of silver sulphate ($AgSO_4$) in 1000 mL of sulphuric acid 96%. This reagent may be purchased already prepared.
- Potassium dichromate solution 1N: dissolve 49.13 g $K_2Cr_2O_7$ primary standard grade, previously dried at 105 °C for 2 h in 500 mL distilled water and 167 mL sulphuric acid 96%. Dissolve, cool to room temperature and dilute to 1000 mL. This reagent may be purchased already prepared.
- Ferroin indicator solution: dissolve 1.485 g 1,10-phenantroline monohydrate and 695 mg $FeSO_4{\cdot}7H_2O$ in distilled water and dilute to 100 mL. This reagent may be purchased already prepared.
- Ferrous ammonium sulphate (FAS) solution, approximately 0.5N: dissolve 200 g $(NH_4)_2Fe(SO_4){\cdot}6H_2O$ in 500 mL of distilled water and mix with 40 mL of sulphuric acid 96%. Cool and dilute to 1000 mL. This solution shall be standardized before use against dichromate as follows: dilute 10 mL $K_2Cr_2O_7$ 1N to about 70 mL of distilled water, add 30 mL sulphuric acid 96% and cool. Titrate with FAS 0.5N using 3 drops of ferroin indicator solution. The concentration of the reducing reagent is calculated using the following equation:

$$N_{FAS} = \frac{10\,\text{mL} \times 1\text{N}}{V_{FAS}\,(\text{mL})} \quad (1)$$

where N_{FAS} and V_{FAS} are the concentration (N) and volume (mL) of the reducing agent used.

2.2.2.1.3. Procedure. For solid samples, use weighing boats to transfer the raw sample (100–150 mg) inside the glass digestion vessels and add 10 mL of distilled water. Use a further raw sample to determine the substrate moisture and the dry sample weight. For liquid samples, use a magnetic stirrer to mix the solution for 30 min and a micropipeter to withdraw the volume necessary for analysis. Taking into account that the total volume always will be 10 mL, distilled water must be added when the maximum volume of liquid sample is not used. Add 20 mL of the digestion reagent, 30 mL of sulphuric acid reagent slowly and carefully to the mixture while mixing thoroughly. After joining the condenser in the digestion vessels and placing the vessels in the block heater fixed at 150 °C for 2 h, remove the tubes and cool them down to room temperature. Finally, transfer the content of the digestion vessel to big mouth 500 mL Erlenmeyer flask and rinse the tube with distilled water. Add three drops of ferroin indicator solution and titrate the excess potassium dichromate with FAS 0.5N until the colour changes from light to dark green. To facilitate the end-point reaction, a magnetic bar and a magnetic stirrer were used in each titration. A blank containing 10 mL of distilled water was run simultaneously for each group of samples.

2.2.2.1.4. Calculation. The chemical oxygen demand of a dry solid sample shall be calculated using the following equation:

$$\text{COD}\,(\text{mg O}_2\,\text{g}^{-1}\,\text{VS}) = \frac{(\text{FAS}_{\text{Bl}} - \text{FAS}_{\text{Solid sample}}) \times N_{FAS} \times 8}{W_{\text{Solid sample}}} \quad (2)$$

The chemical oxygen demand of a liquid sample shall be calculated using the following equation:

$$\text{COD}\,(\text{mg O}_2\,\text{L}^{-1}) = \frac{(\text{FAS}_{\text{Bl}} - \text{FAS}_{\text{Liquid sample}}) \times N_{FAS} \times 8000}{V_{\text{Liquid sample}}} \quad (3)$$

where FAS_{Bl}: volume of FAS used in the titration of the blank sample (mL). $\text{FAS}_{\text{Solid sample}}$: volume of FAS used in the titration of the solid sample (mL). $\text{FAS}_{\text{Liquid sample}}$: volume of FAS used in the titration of the liquid sample (mL). N_{FAS}: concentration of reducing reagent (N). $W_{\text{Solid sample}}$: weight of dry solid sample (g VS). $V_{\text{Liquid sample}}$: volume of liquid sample (mL).

2.2.2.2. APHA–AWWA–WPCF standard method 5220 B-open reflux method (SM-OR). The digestion solution was prepared by mixing 33.3 g of $HgSO_4$, 10.216 g of $K_2Cr_2O_7$, primary standard grade, previously dried at 105 °C for 2 h, 167 mL of sulphuric acid and 600 mL of distilled water. After cooling down, the solution was diluted to 1000 mL with distilled water.

The catalyst solution was prepared by adding 10 g L^{-1} of $AgSO_4$. This reagent may be purchased already prepared.

For COD analysis, 50 mL of sample were mixed with 25 mL of digestion solution and 75 mL of catalyst solution in a glass diges-

Table 1
VS and elemental composition of the different substrates used

Substrate	VS (%)	Elemental composition (%)					Formula
		C	H	N	S	O	
KHP_{Th}	80.86	47.1	2.5	–	–	31.3	$C_8O_4H_5K$
KHP_{Exp}	80.86	46.9	2.5	–	–	31.5	$C_{392}O_{196}H_{245}$
CP_{Th}	100	44.4	6.2	–	–	49.2	$C_6H_{10}O_5$
CP_{Exp}	100	44.4	6.2	–	–	49.2	$C_{367}H_{625}O_{310}$
SuOC	93	46.7	5.8	5.5	0.24	34.8	$C_{389}H_{575}O_{218}N_{39}S_1$
An-S	66	35.3	4.7	7.4	0.6	18.0	$C_{294}H_{466}O_{110}N_{53}S_2$
CRM-S	60	33.3	4.4	4.6	0.8	16.9	$C_{277}H_{437}O_{105}N_{33}S_3$

Subscripts: Th, theoretical; Exp, experimental.

tion vessel with reflux adapter and heated at 150 °C for 2 h. The routine is similar to the SS-OR method, except for a 0.24N solution of potassium dichromate that is used to standardize the 0.25N FAS.

2.2.2.3. APHA–AWWA–WPCF standard method 5220 D-closed reflux, colorimetric method (SM-CR). The digestion and the catalyst solutions were prepared as previously described in Section 2.2.2.2.

For COD analysis, 2.5 mL of sample were mixed with 1.5 mL of digestion solution and 3.5 mL of catalyst solution in screw-cap test tubes and heated at 150 °C for 2 h in a block heater. After allowing the tubes to cool to room temperature, COD levels were determined by measuring the absorbance of the digested assay solution at λ = 600 nm on a Genesis TM 10 Series Visible recording spectrophotometer with a tube adapter, to avoid transferring the sample. COD level was determined using a standard curve (50–1000 mg O_2 L^{-1}) with KHP as the chemical standard reference and correlated to the COD level taking into account that the theoretical oxygen demand of substrate is 1175 mg O_2 TS g^{-1} (1453 mg O_2 VS g^{-1}).

2.2.3. Total solids and volatile solids

TS and VS were determined according to the standard methods 2540 B and 2540 E, respectively [12].

2.2.4. Statistical analysis

COD recovery was used to carry out the comparative study of the accuracy and precision of the different methods assayed. The differences between theoretical (100%) and experimental COD measurements were calculated for each method, level of concentration of solutions and substrate assayed. They were also used to calculate the experimental Student's *t*-values (t_{exp}), and these data were compared with the critical Student's *t*-value of 2.78, based on five replicates at a confidence level of 95%, proposed by Miller and Miller [22]. The paired *t*-tests were used to take a decision about the presence of the significant statistical difference in the results obtained, and therefore, about the traceability of the methods compared.

3. Results and discussion

3.1. COD of solid substrates

Firstly, a complementary elemental analysis was carried out to obtain the elemental composition of the substrates analysed. These data were used to calculate the molecular formula. Table 1 summarizes the results obtained. For standard pure solid substrates, such as KHP and cellulose, the percentage obtained for the C, H and O elementals from combustion analysis were the same as the theoretical values, although obviously the molecular formulae were different. The good correlations in the results indicate that obtaining molecular formulae by the combustion analysis can be considered as an adequate alternative for much more complex substrates. After setting up the general molecular formulae of substrates used, the ThOD values were calculated. Table 2 shows the results obtained for ThOD and also the experimental values of COD obtained by wet oxidation with the modified proposed method. The recovery studies for the two pure standard substrates assayed showed very high values, for instance 98% for KHP and 101% for CP. The results obtained demonstrated that the incomplete oxidation of substrate with the proposed method is totally rejected. For heterogeneous substrates such as SuOC and An-S, the theoretical and experimental values gave very similar results, with a recovery of around 100% in both cases. The proposed method was also checked with the CRM-S. It had a reference value of 1280 ± 320 mg O_2 g VS^{-1}, with a confidence interval of 1031–1537 mg O_2 g^{-1} VS and a prediction interval of 503–2065 mg O_2 g^{-1} VS. The reference value certified had a relative standard deviation (R.S.D.) of 25%, which is very high for a reference material. The experimental average COD value and standard deviation (S.D.) obtained were 1498 ± 4 mg O_2 g^{-1} VS, a value within the confidence interval limits, but far from the reference value. The positive interference of CRM-S inorganic constituents on COD was checked with samples previously incinerated at 550 °C, therefore in the absence of any oxidizable organic compound. It was observed that the results were not different than that obtained in a blank, and as consequence the interference of inorganic constituents was rejected. Nevertheless, the results obtained for chemical composition and experimental COD were the same, and in this way the validity of the modified SS-OR method used was again confirmed.

Table 2
ThOD and COD values of the different solid substrates tested

Substrate	ThOD	$COD_{Experimental}$			
	Average (mg O_2 g^{-1} VS)	Average (mg O_2 g^{-1} VS)	S.D. (mg O_2 g^{-1} VS)	R.S.D. (%)	Recovery (%)
KHP	1453[a]	1425	2	0.2	98
CP	1184[a]	1193	5	0.4	101
SuOC	1340[b]	1291	3	0.2	96
An-S	1442[b]	1486	7	0.5	103
CRM-S	1493[b]	1498	4	0.3	100

S.D.: standard deviation; R.S.D.: relative standard deviation.
[a] Value obtained using the theoretical elemental composition.
[b] Value obtained using the experimental elemental composition.

In a previous work, Baker et al. [23] examined the relationship between ThOD and COD for 565 organic chemicals, with reliable results only for easily oxidizable compounds.

The other statistic parameter of interest studied was precision. The DIN 38414-S9 standard method [11] protocol included an interlaboratory test for two solid samples not described, that reported R.S.D. values of 2.0% and 2.7%. The proposed method yielded a very low R.S.D. for each substrate assayed, which ranged between 0.2% and 0.5%. The improvement in the repeatability values of the method assayed was demonstrated.

Table 3
Summary of COD determination conditions for different solutions of SuOC and An-S for the three methods compared

Substrate	SS-OR method		SM-OR method		SM-CR method	
	Dilution	Volume[a] (mL)	Dilution	Volume (mL)	Dilution	Volume (mL)
I. SuOC	No		Yes		Yes	
I.1. 20 g TS L^{-1}		5	10/500	50	10/500	2.5
I.2. 40 g TS L^{-1}		3	5/500	50	5/500	2.5
I.3. 60 g TS L^{-1}		2	3/500	50	3/500	2.5
I.4. 80 g TS L^{-1}		1	5/1000	50	5/1000	2.5
II. An-S	No		Yes		Yes	
II.1. 70 g TS L^{-1}		2	3/500	50	3/500	2.5

[a] The total volume of liquid used is always 10 mL. Distilled water must be added when the maximum volume of liquid sample is not used.

Table 4
Comparison between theoretical and experimental solid content values and significance *t*-tests in spiked SuOC solutions

Total solids					Volatile solids				
Th ($g\,TS\,L^{-1}$)	Exp ($g\,TS\,L^{-1}$)	S.D. ($g\,TS\,L^{-1}$)	Recovery (%)	t_{exp}	Th ($g\,VS\,L^{-1}$)	Exp ($g\,VS\,L^{-1}$)	S.D. ($g\,VS\,L^{-1}$)	Recovery (%)	t_{exp}
20	19.92	0.78	99.6	0.23	18.6	18.69	0.74	100.5	0.28
40	39.82	1.77	99.6	0.20	37.2	36.91	1.72	99.2	0.39
60	59.27	0.84	98.8	1.92	55.8	55.09	0.94	98.7	1.73
80	77.60	2.02	97.0	2.68	74.4	72.03	1.94	96.8	2.76

Th, theoretical; Exp, experimental.

3.2. COD of solutions with high suspended solids content

Once the solid substrate COD values were confirmed, the second stage of the research work was to make a comparative study of COD values from solutions with a high concentration of suspended solids. For this purpose, several solutions were made by incorporating known amounts of solid substrates into distilled water, covering a broad range of COD values. The two standard methods for water and wastewater COD determination were compared with the SS-OR method using different solutions of SuOC and An-S. Table 3 shows a summary of the different analyses carried out, focusing on whether dilution is needed or not and on the volume of sample used. Considering the nature of the solutions prepared, one very important factor was the sampling. To study its influence on the results, the same amount of volume was used 5 times to check TS and VS concentrations of the different solutions evaluated. Table 4 summarized these gravimetric determination and the paired *t*-test studies based on the corresponding recoveries. The performances decreased slightly with the increase in organic matter, but no statistical differences were found because the Student's *t*-values obtained were lower than 2.78 in all cases. On the basis of results obtained, the influence of the sampling in the possible lack of COD recovery is totally discarded.

Table 5
Comparison between theoretical and experimental COD values and significance *t*-tests for different spiked solutions of SuOC and An-S using the three analytical methods tested

Substrate	COD method				
COD_{Th} ($mg\,O_2\,L^{-1}$)	COD_{Exp} ($mg\,O_2\,L^{-1}$)	S.D. ($mg\,O_2\,L^{-1}$)	R.S.D. (%)	Recovery (%)	t_{exp}
		SS-OR method			
I. SuOC					
I.1. 24000	23,462	491	2.1	97.8	2.45
I.2. 48000	49,020	1046	2.1	102.1	2.18
I.3. 72000	70,621	1120	1.6	98.1	2.75
I.4. 96000	92,428	2898	3.1	96.3	2.76
II. An-S					
II.I. 68300	67,582	684	1.0	98.9	2.35
		SM-OR method			
I. SuOC					
I.1. 24000	18,552	769	4.1	77.3	15.84
I.2. 48000	39,776	2328	5.9	82.9	5.53
I.3. 72000	63,301	1643	6.0	82.6	7.84
I.4. 96000	81,366	3117	3.8	84.8	10.50
II. An-S					
II.I. 68300	59,476	792	1.3	87.1	24.91
		SM-CR method			
I. SuOC					
I.1. 24000	21,459	1130	5.3	89.4	5.03
I.2. 48000	43,024	2429	5.6	89.6	4.58
I.3. 72000	64,840	4900	6.7	90.0	2.95
I.4. 96000	88,889	9405	10.6	92.6	1.69
II. An-S					
II.I. 68300	64,250	2410	3.8	94.1	3.76

3.2.1. Solutions of SuOC

In order to cover a broad range of COD, four spiked solutions of SuOC were prepared using the experimental COD value of 1291 $mg\,O_2\,g\,VS^{-1}$ as reference. Each solution was evaluated for the three analytical methods, the two APHA–AWWA–WPCF standard methods for water and wastewater [12] and the adapted proposed one for COD determination of solid substrates. Table 5 shows theoretical COD, experimental COD, S.D. and R.S.D. for each spiked solution used. The recovery and the statistical evaluation using significance *t*-test of the three analytical methods also were obtained. The data of accuracy and precision were compared as follows:

- SS-OR: The recovery yields ranged from 96.3% to 102.1%, and no differences in statistical significance *t*-test were showed. The R.S.D. values were the lowest of the three methods compared. They ranged between 1.6% and 3.1% and no concentration dependence on the repeatability studies was observed.
- SM-OR: The recovery yields ranged from 77.3% to 84.8%, and a clear difference in statistical significance *t*-test was shown. The R.S.D. values were less constant than those obtained in the earlier method, but the values were of the same order or lower than 6.5%, a percentage reported by the APHA–AWWA–WPCF method [12] for standard reference KHP low concentration solutions.
- SM-CR: The recovery yields were higher than those obtained in the other standard method. They ranged between 89.4% and 92.6% but again differences in statistical significance *t*-test were shown. The R.S.D. values were proportional to the concentration of organic matter, but only the most concentrated solution showed a value higher than 8.6%, a percentage reported by the APHA–AWWA–WPCF method [12] for standard reference KHP low concentration solutions.

3.2.2. Solution of An-S

An anaerobic sludge with a theoretical COD value of 68,300 $mg\,O_2\,L^{-1}$, obtained from the experimental sludge values of COD (1486 $mg\,O_2\,g^{-1}$ VS) and organic content (46 $g\,VS\,L^{-1}$), was analysed. The results obtained followed the trend of the earlier substrate as regards recoveries, with a general increase in the results of the three methods compared, but only the SS-OR method showed no differences in statistical significance *t*-test. The precision of the results was also better, with a reduction in the R.S.D. on the three methods compared, probably due to the different consistency in the solution used, with a better homogenisation of the sample.

4. Conclusions

The results obtained in this study allow the following conclusions to be drawn:

(1) It was demonstrated that the modified SS-OR method described in this paper is useful and very appropriate to measure the organic content of solid substrates.
(2) In the comparative study of the three COD methods tested, the proposed SS-OR gave the lowest R.S.D. values and the highest

recovery percentages, being the only method with no differences in statistical significance *t*-test.

(3) While the SS-OR method allowed COD recovery values around 100%, COD recoveries in the ranges of 77.3–87.1% and 89.4–94.1% were achieved with the standard methods SM-OR and SM-CR, respectively.

(4) Therefore, based on the experimental results obtained, the only way to work with a reliable accuracy in COD determination with samples containing high suspended solid content is the use of the modified proposed method.

Acknowledgements

The authors wish to express their gratitude to the European Union (Cropgen project, reference: SES-CT-2004-502824, 6th Frame work programme, Sustainable Energy Systems) and to the "Comisión Interministerial de Ciencia y Tecnología, CICYT" of the Ministry of "Educación y Ciencia" of the Spanish Government (Project CTM 2005-01260/TECNO) and the "Junta de Andalucía" for providing financial support.

References

[1] W.E. Adeney, B.B. Dawson, Sci. Proc. R. Dublin Soc. 19 (1926) 199.
[2] W.A. Moore, R.C. Kroner, C.C. Ruchhoft, Anal. Chem. 21 (1949) 953.
[3] W.A. Moore, F.J. Ludzack, C.C. Ruchhoft, Anal. Chem. 23 (1951) 1297.
[4] R.A. Dobbs, R.T. Williams, Anal. Chem. 35 (1963) 1064.
[5] F.J. Baumann, Anal. Chem. 46 (1974) 1336.
[6] A.M. Jirka, M.J. Carter, Anal. Chem. 47 (1975) 1397.
[7] R.R. Himebaugh, M.J. Smith, Anal. Chem. 51 (1979) 1085.
[8] T.M. Lapara, J.E. Alleman, P.G. Pope, Waste Manage. 20 (2000) 295.
[9] A. Walkley, A. Black, Soil Sci. 37 (1934) 29.
[10] UNI 10665, Determinazione del carbono organico secondo Springer-Klee, Metodo volumetrico, 1998.
[11] DIN 38414-S9, German standard methods for the examination of water, wastewater and sludge, Determination of chemical oxygen demand of sludge and sediment, 1986.
[12] APHA–AWWA–WPCF, Standard Methods for the Examination of Water and Wastewater, twentieth edition, Washington, DC, 1998.
[13] A. Veeken, B. Hamelers, Bioresour. Technol. 69 (1999) 249.
[14] L. Neves, R. Oliveira, M.M. Alves, Process Biochem. 39 (2004) 2019.
[15] G. Güngör-Demirci, G.N. Demirer, Bioresour. Technol. 93 (2004) 109.
[16] S. Montalvo, F. Díaz, L. Guerrero, E. Sánchez, R. Borja, Process Biochem. 40 (2005) 1475.
[17] F. Raposo, R. Borja, E. Sánchez, M.A. Martín, A. Martín, Water Res. 38 (2004) 2017.
[18] M.A. de la Rubia, M. Pérez, L.I. Romero, D. Sales, Process Biochem. 41 (2006) 79.
[19] P.H. Liao, K.V. Lo, Biotechnol. Bioeng. 27 (1985) 266.
[20] Yadvika, A.K. Yadav, T.R. Sreekrishnan, S. Satyaa, S. Kohli, Bioresour. Technol. 97 (2006) 721.
[21] ISO 10707, Evaluación en medio acuoso de la biodegradabilidad aerobia "final" de compuestos orgánicos. Método por análisis de la demanda bioquímica de oxígeno (ensayo en recipientes cerrados), 1994.
[22] J.C. Miller, J.N. Miller, Statistics for Analytical Chemistry, second edition, Wiley, London, 1988.
[23] J.R. Baker, M.W. Milke, J.R. Mihelcic, Water Res. 33 (1999) 327.

Talanta 76 (2008) 271–275

Contents lists available at ScienceDirect

Talanta

journal homepage: www.elsevier.com/locate/talanta

Environmental formaldehyde analysis by active diffusive sampling with a bundle of polypropylene porous capillaries followed by capillary zone electrophoretic separation and contactless conductivity detection

Flávio R. Rocha[a], Lúcia H.G. Coelho[a], Marcelo L.A. Lopes[a], Lilian R.F. Carvalho[a], José A. Fracassi da Silva[b], Claudimir L. do Lago[a], Ivano G.R. Gutz[a,*]

[a] Instituto de Química, Universidade de São Paulo, Av. Prof. Lineu Prestes, 748, 05508-000 São Paulo, SP, Brazil
[b] Instituto de Química, Universidade Estadual de Campinas, CP 6154, 13083-090 Campinas, SP, Brazil

ARTICLE INFO

Article history:
Received 13 December 2007
Received in revised form 22 February 2008
Accepted 25 February 2008
Available online 4 March 2008

Keywords:
Air pollution
Formaldehyde
Hydroxymethanesulfonate
Microporous polypropylene membrane
Diffusion scrubber
Capillary electrophoresis
Contactless conductivity detection

ABSTRACT

Compared to other volatile carbonylic compounds present in outdoor air, formaldehyde (CH_2O) is the most toxic, deserving more attention in terms of indoor and outdoor air quality legislation and control. The analytical determination of CH_2O in air still presents challenges due to the low-level concentration (in the sub-ppb range) and its variation with sampling site and time. Of the many available analytical methods for carbonylic compounds, the most widespread one is the time consuming collection in cartridges impregnated with 2,4-dinitrophenylhydrazine followed by the analysis of the formed hydrazones by HPLC. The present work proposes the use of polypropylene hollow porous capillary fibers to achieve efficient CH_2O collection. The Oxyphan® fiber (designed for blood oxygenation) was chosen for this purpose because it presents good mechanical resistance, high density of very fine pores and high ratio of collection area to volume of the acceptor fluid in the tube, all favorable for the development of air sampling apparatus. The collector device consists of a Teflon pipe inside of which a bundle of polypropylene microporous capillary membranes was introduced. While the acceptor passes at a low flow rate through the capillaries, the sampled air circulates around the fibers, impelled by a low flow membrane pump (of the type used for aquariums ventilation). The coupling of this sampling technique with the selective and quantitative determination of CH_2O, in the form of hydroxymethanesulfonate (HMS) after derivatization with HSO_3^-, by capillary electrophoresis with capacitively coupled contactless conductivity detection ($CE–C^4D$) enabled the development of a complete analytical protocol for the CH_2O evaluation in air.

1. Introduction

The atmosphere contains traces of thousands of organic and inorganic compounds in gaseous state or as aerosols. They are classified as pollutants when their concentrations are considered hazardous for human health, for animal and vegetal life or when they may cause damage to various materials [1,2].

The commonest carbonyl compounds in the atmosphere are formaldehyde, acetaldehyde and acetone, which participate in several chemical and photochemical reactions [1,3]. Formaldehyde (CH_2O) is emitted during the production and use of household goods (such as cleaning products and manufactured wood products) and combustion processes (cigarette smoke, gas cookers, fireplaces and automobile exhaust). Atmospheric CH_2O concentrations are affected by direct emissions, photochemical activity and availability of other pollutants (e.g. hydrocarbons) and of liquid phase [4]. Formaldehyde presents lifetimes of hours or even days in the air; it can be oxidized to formic acid [5] or accumulated in the liquid phase, due to its high Henry constant ($\sim 6.0 \times 10^3$ mol L^{-1} atm^{-1} [6]), and be removed by precipitation events. When CH_2O and SO_2 are absorbed by clouds, their reaction in aqueous phase produces hydroxymethanesulfonate (HMS), a stable, oxidation resistant S(IV) species. In the present work, this reaction was exploited to convert the collected CH_2O into the charged HMS anion suitable for electrophoretic separation and conductometric detection.

Due to its toxicity and carcinogenic potential, many methods are available for the collection and determination of CH_2O in the gaseous phase of the atmosphere [7,8]. The concentration of formaldehyde is very low, typically a few $\mu g\,m^{-3}$, and only a few analytical techniques are capable of sensitive and selective *in situ* measurements, such as tunable diode laser spectroscopy [9] and laser induced fluorescence spectroscopy [10]. However, they

* Corresponding author. Tel.: +55 11 3091 2150; fax: +55 11 3091 2150.
E-mail address: gutz@iq.usp.br (I.G.R. Gutz).

0039-9140/$ – see front matter © 2008 Published by Elsevier B.V.
doi:10.1016/j.talanta.2008.02.037

require long optical pathways and the instrumentation is expensive, restricting their field usage.

Many spectroscopic and electrochemical techniques require a preconcentration step of the gaseous CH_2O before the analysis. In general, carbonylic compounds are sampled in aqueous solution (impingers), solid sorbents impregnated with a derivatizing agent (denuders) or diffusion scrubbers (with a porous membrane).

Impingers are easy to implement and do not require continuous maintenance. However, the acceptor solution might evaporate in high flow-rates of sampled air or when long-period sampling is required. That disadvantage can be suppressed by the use of denuders, commercially available as glass fiber filters, silica or C_{18} impregnated with 2,4-dinitrophenylhydrazine, DNPH [8,11]. However, in the presence of ozone there is a possibility of direct DNPH oxidation, with the generation of interfering species and the loss of performance of the sampling device, so that ozone removal is necessary and has been done with potassium iodide impregnated filters [12]. Moreover, sampling efficiency declines at high relative humidity of the air, as during wet precipitation events.

Diffusion scrubbers are also employed for carbonylic compounds sampling. Dasgupta et al. [7,13] utilized a flow system with microporous hydrophobic membrane (Nylon®) for CH_2O collection and determination by fluorimetry with the Hantsch reaction. Bao and Dasgupta [14] developed similar devices with polypropylene, silicone and cellulose acetate membranes for collection of HNO_2, HNO_3, HCl and HCOOH in the atmosphere and determination by capillary electrophoresis (CE) with UV detector. Many works in the literature deals with the use of PTFE [15] and polypropylene [16] membranes for gaseous CH_2O collection with preconcentration.

Alternative diffusion scrubbers without membranes were also employed for formaldehyde sampling. Larsen et al. [4] developed a sampling system based on the high solubility of CH_2O in water in a diffusion scrubber coil made of a spiraled glass pipe.

Classical methodologies are largely employed for CH_2O analysis after the preconcentration step. Colorimetric methods using chromotropic acid [17] and pararosaniline [18] are widely used for carbonylic detection due to the use of simple equipment. However, they are laborious, suffer interferences and a relatively long sampling period is required to achieve the sensitivity. Conventional fluorescence methods based on specific reactions with the Hantsch reagent [19] or 1,3-cyclohexadione [20] are capable of intermittent measurements with the necessary sensitivity and selectivity.

Chromatographic methods are also available for carbonyls, including CH_2O, always preceded by a sampling step with preconcentration. The most widely used sampling procedure consists in aspirating air through silica gel or C_{18} cartridges impregnated with DNPH during a relatively long period (1–2 h) [8,21]. The carbonylhydrazones thus formed are extracted with acetonitrile and the analysis is usually performed by HPLC.

Capillary electrophoresis appears as an alternative technique for the analysis of air pollutants and environmental species [22]. The most common detector for CE is based on UV–vis absorption, unsuitable for the non-absorbing CH_2O. Derivatization with DNPH has been employed to overcome this limitation, but the hydrazones (like formaldehyde itself) are not prone to ionization in a wide range of pH values, so that separation is possible only by micellar electrokinetic chromatography (MEKC) [23] or capillary electrochromatography (CEC) [24]. Derivatization with 5-(dimethylamine)-naphtalene-1-sulfo-hydrazine (DNSH), or dansylhydrazine, produces hydrazones with ionizable groups, as required for conventional capillary zone electrophoresis [25,26].

Conductivity detection (CD) is an attractive alternative for CE of ionic compounds and its performance has been demonstrated for many environmental matrices [27,28]. Capacitively coupled contactless conductivity detection (C^4D) [29,30] has gained acceptance, relative to the conventional CD, due to its ease of implementation and operation. No capillary modification or micropositioning of electrodes is required and there is no fouling of the electrodes because they are fixed externally, around the fused silica or polymeric capillary (two or four electrodes depending on the circuit), an arrangement that also decouples the high electric field used for the separation. The limits of detection are comparable to those obtained by UV–vis absorption detection [29,31]. Assuming the two electrodes configuration, a high-frequency signal is applied to one of the electrodes, and this signal is transmitted to the second electrode through multiple paths, such as the capillary wall, external transmission, and the solution inside the capillary in the region between the electrodes, corresponding to the conductance of the solution [32–34].

This work presents an alternative method for the collection and analysis of gaseous formaldehyde; the use of a new sampling device constructed with polypropylene porous tubes (PPT) for CH_2O collection and preconcentration. A bundle of PPT was fixed inside a Teflon® tube guide. The bundle was filled with de-ionized water, while air samples were externally passed over them. Formaldehyde diffuses through the pores and dissolves in the aqueous phase. An effective preconcentration is obtained by using a low flow rate of the liquid phase and a relatively high one for the gaseous phase.

After the preconcentration step, formaldehyde was derivatized with bisulfite to form hydroxymethanesulfonate (HMS) ions, according to the following reaction:

$$CH_2O + HSO_3^- \rightarrow H_2C(OH)SO_3^-$$

The HMS thus formed could be promptly separated from other anions and detected by CE–C^4D. Differently from DNPH, a HSO_3^- solution can be easily obtained, does not require exhaustive purification and presents no toxicity.

The conditions were optimized for the complete separation between HMS and the excess of sulfite, as well as other ions present in the sample. The results achieved for CH_2O in air by sampling and determination as HMS using CE–C^4D were compared with the HPLC methodology with collection in cartridges derivatized with DNPH [35].

2. Experimental

2.1. Sampler construction

The air sampler was constructed by inserting 12 polypropylene microporous capillaries (Oxyphan® from MEMBRANA, Wuppertal, Germany) into a 1.5-m long, 5 mm in diameter PTFE tube. The external and pore mean diameters for these capillaries were of 387 and 0.2 μm, respectively. The 12 capillaries were glued together at their ends (without clogging them) with silicone rubber adhesive in order to form a bundle (Fig. 1). The internal volume of the bundle was about 1.0 mL. The bundle inlet was connected to a peristaltic pump Ismatec Reglo® (Glattbrugg, Switzerland) and de-ionized water was passed inside the capillaries at a flow rate of 10 μL min^{-1},

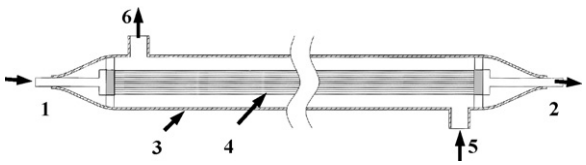

Fig. 1. Diffusion collector: 1, inlet of the acceptor liquid (de-ionized water); 2, collected sample outlet; 3, Teflon® tube (150 cm, 5-mm diameter); 4, bundle of polypropylene hollow porous tubes (Oxyphan®) with 387 μm external diameter and 0.2 μm pores; 5, air inlet; and 6, air outlet.

in order to renew the acceptor phase. Air samples were aspirated through the sampler with an inexpensive membrane pump (of the type used for aquarium aeration). The flow rate of 350 mL min^{-1} was adjusted with a needle valve and read on a rotameter using the calibration table provided by the manufacturer (Cole-Palmer Model N112-02, Illinois, USA), occasionally checked by water displacement from an inverted graduated cylinder. Aliquots of the sample in the acceptor solution were kept in 2 mL polypropylene vials (sold by Agilent, Brazil) for further treatment.

The volumes of the collected acceptor phase were determined by weighing the vials before and after sampling by the diffusion collector.

Although it is known that exposure of polypropylene to ozone cause deleterious effects on the polymer such as formation of hydroperoxide groups on the surface morphology, with loss in tensile strength [36], the bundle of capillaries protected in the PTFE tube could be used for many months without maintenance.

2.2. Standard atmosphere

The efficiency of the sampling system was determined using a standard CH_2O atmosphere generator based on paraformaldehyde sublimation in a permeation device. A mass of 0.5 g of paraformaldehyde was introduced in a 1.5-mL glass vial, covered by a silicone septum hold in place by a perforated plastic screw cap. This vial was introduced in a 100-mL borosilicate glass bottle (Schott Duran), with a large and very tight cap that was perforated and provided with inlet and outlet gas lines made from thick walled PTFE tubing. The flask was maintained at 30 °C in a water bath. Nitrogen was fed to the standard atmosphere generator at flow rate of 350 mL min^{-1}. The flask was weighted at 24 h intervals and the loss of mass, corresponding to flux of sublimated formaldehyde released to the gas stream was determined as 2.0 μg min^{-1}. The diffusion collector with the Oxyphan® capillaries was connected to the output of the generator directly or after extra dilution with N_2 and release of the excess flow. Two diffusion collectors were connected in series to evaluate the sampling efficiency for CH_2O.

2.3. Capillary electrophoresis

The CE equipment was built in our laboratory [29] and consists of two platinum electrodes connected to a high voltage source (AR-30, Bertan High Voltage Co., New York, USA) and immersed in reservoirs containing running buffer solution. The system was assembled inside an acrylic box with a fan, a heating element and temperature control circuit, which maintains the inside temperature between 28 and 30 °C. A power-off switch at the door of the box protects the operator from accidental exposure to high voltage. A microcomputer controls the equipment and the data acquisition from the C^4D. The C^4D cell consists of two 2 mm wide ring electrodes, 1 mm apart, and fitted around the capillary. One ring was connected to a Goldstar FG-2002 C Function Generator set to deliver a sine wave of 600 kHz with 2 V_{pp} of amplitude. The other electrode was connected to an operational amplifier circuit comprising a current to voltage converter, a rectifier and an amplifier. The output signal, proportional to the conductivity of the solution inside the capillary, was fed to the analog to digital converter of a PCL711 card (Advantech Co., Taiwan), placed in a free slot of the PC. The control software was developed in the laboratory. The samples were injected into the capillary from the cathodic reservoir by gravity at 100 mm water column for 40 s. The separation potential of −25 kV was applied to a 50-cm long fused silica capillary of 75-μm i.d., 360-μm o.d.

All reagents used were of analytical grade. Sodium sulfite, paraformaldehyde, lactic acid, formic acid, acetic acid, *N*-cetyl-*N*,*N*,*N*-trimethylammonium bromide (CTAB) and 2-[*N*-morpholino]ethanesulfonic acid were from Merck (Darmstadt, Germany). L-Histidine (His) and formaldehyde (37%) were from Sigma Chemical Co. (St. Louis, MO, USA). Lactic acid (50 μmol L^{-1}) was added as internal standard.

Running buffers and standards were prepared daily from 0.1 mol L^{-1} stock solutions by dilution with de-ionized water (NANOpure UV, Barnstead/Thermolyne Co., Iowa, USA). The HMS was prepared immediately before analysis. The running buffer optimized for the analysis was MES/His 20 mmol L^{-1} and CTAB 0.2 mmol L^{-1} for electroosmotic flow inversion.

2.4. Derivatization

To a known sample volume, HSO_3^- was added to reach a final concentration around 0.5 mmol L^{-1} in the resulting aqueous phase. After HSO_3^- addition, the pH of the solution was kept around 5.5 by adding HCl to promote a quantitative formation of the HMS adduct. Subsequently the sample was injected in the CE–C^4D equipment and the HMS adduct concentration, proportional to the formaldehyde one, was determined by integration of the peak areas with a graphics program (Origin® from Microcal).

2.5. HPLC

Carbonyls were collected at an airflow rate of 2.0 mL min^{-1} on a silica gel cartridge (Sep-Pak, Waters) previously cleaned with methanol and acetonitrile and coated with DNPH. Gaseous aldehydes retained in the silica–DNPH cartridges were eluted with 5 mL of acetonitrile, and the extracts stored in amber glass flasks in a freezer until analysis by HPLC (Shimadzu, model LC-9A), with UV-detection at 360 nm [33]. The concentration of formaldehyde in air samples was calculated using the external calibration data for formaldehyde–DNPH standards.

2.6. Sampling site

The University campus, located 9 km southwestern from São Paulo city center and half way from the metropolis perimeter, can be considered potentially impacted by many different types of sources. The sampling site is about 1.5 km from a major highway with heavy vehicle traffic fueled by gasohol, diesel and ethanol. Samplers were placed in an area of the Chemistry Institute building, about 6 m above ground level.

3. Results and discussion

The formaldehyde sampling efficiency in air was determined using the standard atmosphere generator device, which was connected to the diffusion collector, with a yield better than 90% at the given flow-rates. During tests with two samplers connected in series, the CH_2O concentration in the second device was below the detection limit (1.0 μmol L^{-1}).

After collection and weighting, aliquots were injected into the CE–C^4D. Fig. 2a shows the electropherogram of one of the samples collected on August 27 without derivatization. The presence of formiate and acetate anions is noticeable, but no peak associated with formaldehyde is observed because it neither presents electrophoretic mobility nor conductivity.

Fig. 2b shows an electropherogram of the same sample after derivatization with HSO_3^-. A peak for hydroxymethanesulfonate is now observed (peak 8), between the formiate and acetate anions. The addition of HCl and Na_2SO_3 to provide HSO_3^- in large excess causes not only the appearance of peak 7 but also the growth of peak 1, while the oxidation of part of the bisulfite by dissolved oxygen

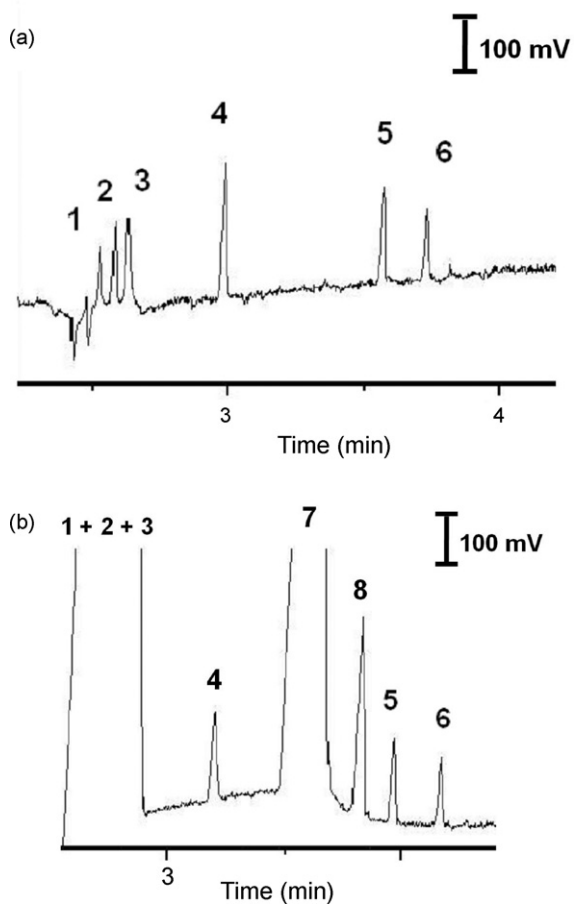

Fig. 2. Electropherograms of a typical sample collected with the diffusion collector of Fig. 1. Running buffer 20 mmol L^{-1} MES/histidine (pH 6.2) + 0.2 mmol L^{-1} CTAB; −25 kV, hydrodynamic injection (40 s, 10 cm); (a) without HSO_3^- addition; (b) after addition of 0.50 mmol L^{-1} HSO_3^-. Peak identification: (1) Cl^-, (2) NO_3^-, (3) SO_4^{2-}, (4) formiate, (5) acetate, (6) lactate (internal standard), (7) HSO_3^- and (8) HMS.

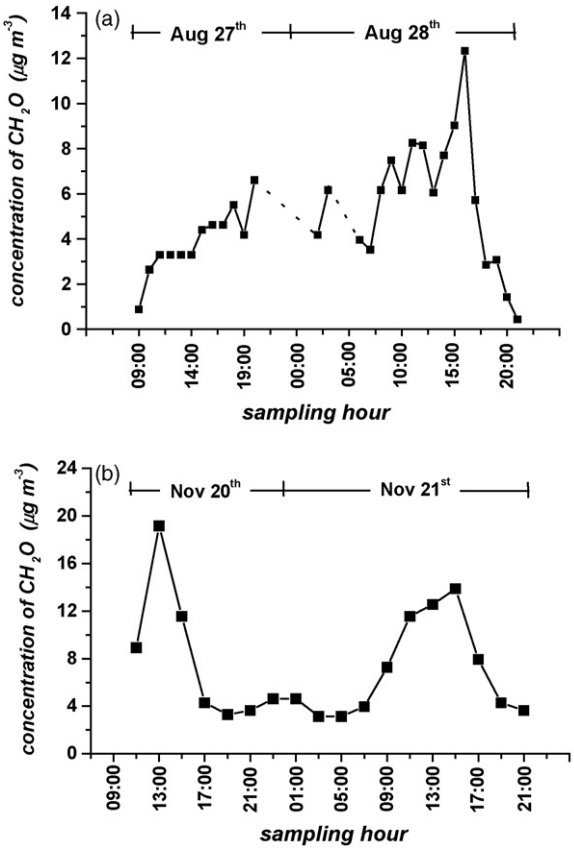

Fig. 3. Variation of formaldehyde concentration in the gaseous phase of the atmosphere during 36 h consecutive sampling periods at the São Paulo University Campus, São Paulo, Brazil. (a) 27/28 August 2002. Dotted lines connect measurements with one missing sample in between; (b) 20/21 November 2000. Concentrations in μg m^{-3}.

reinforces the sulfate peak, so that peaks 1, 2 and 3 merge together. The electromigration time of the ions in Fig. 2b is somewhat longer than in Fig. 2a due to the increased conductance of the sample plug, reducing the electric field in this region at the initial stages of the run. The presence of formiate and acetate peaks opened the possibility to develop a method for the joint determination of the three analytes, not explored in this work.

The formaldehyde concentrations in the collected samples were determined by using a calibration curve covering the range from 3 to 30 μmol L^{-1} of CH_2O. Afterwards, the number of moles of the species in the solutions collected was calculated, and knowing the air volume aspirated through the diffusion collector (measured with the calibrated flow-meter), their concentrations in the atmosphere were estimated.

To determine the performance of the methodology developed for CH_2O analysis, air samples were collected with the bundle of porous polypropylene tubes during 36 consecutive hours on 20 November 2000 and on 27 August 2002 and during 10 h on 23 February 2007 at the Chemistry Institute—USP.

Fig. 3a presents the variation of the formaldehyde concentrations in the gaseous phase during the sampling campaign in 2002, with a minimum of 1.0 μg m^{-3} and a maximum of 12.2 μg m^{-3}.

In the sampling cycle started on 20 November, precipitation of moderate intensity begun around 3:00 p.m. at 21 November, and persisted until around 6:00 p.m., removing a great part of the atmospheric pollutants, as verified by the abrupt decrease in CH_2O concentration. Nevertheless, the concentration of this species has increased again at around 23:00 h and then diminished at 3:00 h, reaching a minimum at 5:00 h of the next day, as can be seen in Fig. 3b.

It is very important to note that even under atmospheric precipitation, when sampling by diffusion tubes impregnated with DNPH is notoriously inefficient, the sampling by polypropylene porous

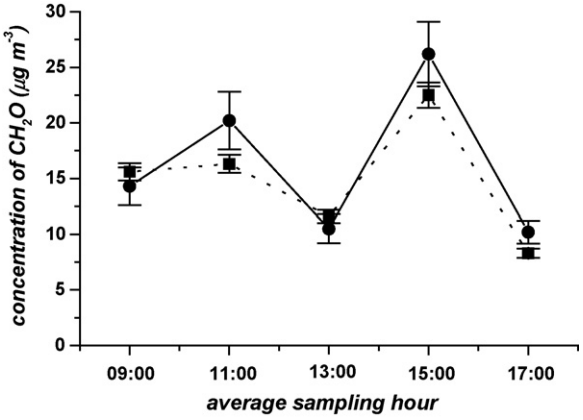

Fig. 4. Intercomparison of two techniques for the determination of CH_2O in air. Full line, collection with the diffusive sampler and determination by CE–C^4D; dotted line, collection in silica–DNPH cartridges and determination by HPLC with UV-detection. Error bars correspond to standard deviation of triplicate determinations.

tubes has shown itself satisfactory. Anyway, being the collection in silica–DNPH cartridges and determination by HPLC the most widely used method for the determination of carbonylic compounds in the atmosphere, an intercomparison study was performed under dry weather conditions. Samples were collected with 1-h interval in the diffusive sampler and afterwards analyzed by CE–C^4D. At the same time, samples were collected in silica–DNPH cartridges with 2 h of interval and consequently analyzed by HPLC after elution with acetonitrile. Fig. 4 illustrates the correlation between the formaldehyde concentrations determined by the two methods for samples collected on 23 February 2007. To facilitate the comparison, the more frequent CE–C^4D results were plotted every 2 h as averages of the two respective 1-h measurements.

The concentration profile is the same for both methodologies. The average relative deviation of the results by the two techniques was estimated in 15%. No significant difference was observed between the replicates of the two methodologies, considering a 95% confidence level. Taking in account the preconcentration of CH_2O during diffusion sampling, the detection limit reached by CE–C^4D, of 1.0 $\mu mol\,L^{-1}$, corresponds to approximately 0.9 $\mu g\,m^{-3}$ of CH_2O in the atmosphere, not as low as by HPLC ($\sim$0.01 $\mu mol\,L^{-1}$ [33]), but still adequate for urban atmospheres.

4. Conclusions

The proposed sampling system by diffusion enables the use of de-ionized water as collecting medium for environmental chemical species with high Henry constant, as is the case for formaldehyde, being versatile for fieldwork, avoiding additional sample extraction procedures in the laboratory (with mechanical stirrer or ultrasound). An inexpensive aquarium pump suffices to push the air through the collector. Moreover, the sampling system is easy to assemble and operate. The external Teflon® tube protects the bundle of capillaries from direct contact and strain. Additionally, the system allows formaldehyde sampling during precipitation events or at high relative humidity, a definite advantage in comparison with DNPH treated denuders or impregnated cartridges.

The combination of sampling and determination methods here described has shown enough sensitivity for the analysis of formaldehyde found in the urban atmosphere, potentially applicable to indoor monitoring, where the prescribed NIOSH limit is 25 $\mu g\,m^{-3}$. Sampling is nearly quantitative, as is the conversion of the analyte into HMS, a key step to allow separation by capillary electrophoresis and detection by contactless conductivity with quickness, versatility, low consumption of sample and reagents and minimum operational cost. The method represents also an advance in the goal of "green analytical chemistry", in comparison with the DNPH/HPLC methodology, once few microliters of residues are generated and the HSO_3^- solution does not require exhaustive purification and presents no toxicity. Perspectives include evaluation of the feasibility of simultaneous quantitative determinations by CE of other gaseous analytes collected together with CH_2O and the scale-down of the sampling device (possibly to a single capillary version), since less than a microliter of sample volume is consumed in CE with triplicate injections.

Acknowledgements

The authors wish to thank CNPq (Conselho Nacional do Desenvolvimento Científico e Tecnológico, Brazil) and FAPESP (Fundação de Amparo à Pesquisa do Estado de São Paulo) for a grant and fellowships.

References

[1] J.H. Seinfeld, Atmospheric Chemistry Physics of Air Pollution, Wiley, New York, 1986, p. 303.
[2] D.F. Gatz, Atmos. Environ. 25B (1991) 1.
[3] A.P. Altshuller, Atmos. Environ. 27A (1993) 21.
[4] B.R. Larsen, C. Brussol, D. Kotzias, T. Veltkamp, O. Zwaagstra, J. Slanina, Atmos. Environ. 32 (1998) 1485.
[5] R.J. Kieber, M.F. Rhines, J.D. Willey, G.B. Avery, Atmos. Environ. 33 (1999) 3659.
[6] J.A. Dean, Langeïs Handbook of Chemistry, 19th ed., MacGraw Hill Inc., New York, 1999, p. 645.
[7] J.Z. Li, P.K. Dasgupta, W. Luke, Anal. Chim. Acta 531 (2005) 51.
[8] A. Vairavamurthy, J.M. Roberts, L. Newman, Atmos. Environ. 26A (1992) 1965.
[9] A. Fried, S. Sewell, B. Henry, B.P. Wert, T. Gilpin, J.R. Drummond, J. Geophys. Res. 102 (1997) 6253.
[10] G.R. Mohlmann, Appl. Spectros. 39 (1985) 98.
[11] H. Schlitt, J. Chromatogr. A 762 (1997) 187.
[12] S. Garcia-Alonso, R.M. Perez-Pastor, Anal. Chim. Acta 367 (1998) 93.
[13] P.K. Dasgupta, G.F. Zhang, J.Z. Li, C.B. Boring, S. Jambunathan, R. Al-Horr, Anal. Chem. 71 (1999) 1400.
[14] L. Bao, P.K. Dasgupta, Anal. Chem. 64 (1992) 991.
[15] Y. Komazaki, M. Hiratsuka, Y. Narita, S. Tanaka, T. Fujita, Fresenius J. Anal. Chem. 363 (1999) 686.
[16] S. Uchiyama, S. Hasegawa, Atmos. Environ. 33 (1999) 1999.
[17] A. Altshuller, D.L. Miller, S.F. Sleva, Anal. Chem. 33 (1961) 621.
[18] N. Johns, G.W. Kirby, J.D. Bulock, A.P. Ryles, J. Chem. Soc., Perkin Trans. 1 (1975) 383.
[19] F. Reche, M.C. Garrigos, A. Sanchez, A. Jimenez, J. Chromatogr. A 896 (2000) 51.
[20] Q. Fan, P.K. Dasgupta, Anal. Chem. 66 (1994) 551.
[21] M. Pires, L.R.F. Carvalho, Anal. Chim. Acta 367 (1998) 223.
[22] E. Dabek-Zlotorzynska, V. Celo, Electrophoresis 27 (2006) 304.
[23] E.A. Pereira, A.A. Cardoso, M.F.M. Tavares, Electrophoresis 24 (2003) 700.
[24] E. Dabek-Zlotorzynska, E.P.C. Lai, J. Chromatogr. A 853 (1999) 487.
[25] K. Bachmann, I. Haag, K.Y. Han, R.Q. Schmitzer, Fresenius J. Anal. Chem. 346 (1993) 786.
[26] E.A. Pereira, M.O.O. Rezende, M.F.M. Tavares, J. Sep. Sci. 27 (2004) 28.
[27] A.E.F. Nassar, S.V. Lucas, W.R. Jones, L.D. Hoffland, Anal. Chem. 70 (1998) 1085.
[28] C. Haber, W.R. Jones, J. Soglia, M.A. Surve, M. McGlynn, A. Caplan, J.R. Reineck, C. Krstanovic, J. Capillary Electrophor. 3 (1996) 1.
[29] J.A.F. da Silva, C.L. do Lago, Anal. Chem. 70 (1998) 4339.
[30] A.J. Zemann, E. Schnell, D. Volgger, G.K. Bonn, Anal. Chem. 70 (1998) 563.
[31] D. Kaniansky, M. Masar, J. Marak, R. Bodor, J. Chromatogr. A 834 (1999) 133.
[32] J.G.A. Brito-Neto, J.A.F. da Silva, L. Blanes, C.L. do Lago, Electroanalysis 17 (2005) 1198.
[33] S.E. Johnston, K.E. Fadgen, L.T. Tolley, J.W. Jorgenson, J. Chromatogr. A 1094 (2005) 148.
[34] P. Kubán, P.C. Hauser, Anal. Chim. Acta 21 (2008) 15.
[35] L. Montero, P.C. Vasconcellos, S.R. Souza, M.A.F. Pires, O.R. Sanchez-Ccoyllo, M.F. Andrade, L.R.F. Carvalho, Environ. Sci. Technol. 35 (2001) 3071.
[36] O.V. Alexeeva, M.L. Konstantinova, S.D. Razumovskij, G.E. Zaikov, Oxid. Commun. 30 (2007) 427.

Talanta 76 (2008) 395–399

Contents lists available at ScienceDirect

Talanta

journal homepage: www.elsevier.com/locate/talanta

Comparison of a gas chromatography-optical fibre (GC-OF) detector with a gas chromatography-flame ionization detector (GC-FID) for determination of alcoholic compounds in industrial atmospheres

Lurdes I.B. Silva [a,b,*], Teresa A.P. Rocha-Santos [a], A.C. Duarte [b]

[a] ISEIT/VISEU-Instituto Piaget, Estrada do Alto do Gaio, Galifonge, 3515-776 Lordosa, Viseu, Portugal
[b] CESAM & Department of Chemistry, University of Aveiro, 3810-193 Aveiro, Portugal

ARTICLE INFO

Article history:
Received 22 November 2007
Received in revised form 4 March 2008
Accepted 12 March 2008
Available online 21 March 2008

Keywords:
Alcoholic compounds monitoring
Optical fibre detector
Optical fibre monitoring

ABSTRACT

An analytical methodology based on an optical fibre detector coupled to gas chromatograph has been developed for the speciation of some volatile alcoholic compounds. This methodology combines the separation capability of gas chromatography with an optical fibre detector made of an optical fibre sensitized with a thin polymeric film of poly[methyl(3,3,3-trifluoropropyl)siloxane] (PMTFPS). The response of the detector has been characterized at 650 nm for nine different alcohols (allyl alcohol, *n*-propyl alcohol, *sec*-butyl alcohol, isobutyl alcohol, *n*-butyl alcohol, isoamyl alcohol, methyl isobutyl carbinol, cyclohexanol and diacetone alcohol). An alternative method based on gas chromatography-flame ionization detector (GC-FID) was also used in order to evaluated the performance and compare the analytical results with the proposed method. The time of analysis, the analytical error and the analytical performance were similar for both methods. However, the analytical apparatus based on the GC-OF detector is much less expensive than the GC-FID and show high accuracy and suitability for actual monitoring on indoor atmospheres.

1. Introduction

Volatile organic compounds (VOCs), including alcohols, can reach high concentrations in some confined industrial environments. Human exposure to alcohols such as *sec*-butyl alcohol, isobutyl alcohol, *n*-butyl alcohol, isoamyl alcohol, methyl isobutyl carbinol, cyclohexanol and diacetone alcohol could occur through inhalation, ingestion and skin contact/absorption and acute effects resulting from overexposure include: headache, irritation/inflammation of eyes and mucous membranes, lacrimation, nausea, dizziness and central nervous system depression [1,2]. These compounds are widely used as solvents in resins and oils, synthesis of flavours, perfumes and also for industrial cleansing and paint removal [1].

The development and application of fibre optic-based chemical analyzers for environmental monitoring constitute a very interesting subject in analytical sciences since they show advantages such as safe detection, durability, remote operation and immunity to electromagnetic interferences [3]. In the last few years various optical fibre sensors have been reported on organic vapour detection based on the reflection of light on polymeric films [4–6], the surface plasmon resonance [7–9], the use of a fluorescence dye [10], on colorimetric compounds which change colour in the presence of organic vapours [11–14], mode-filtered light chemical sensor [15], tapered optical fibres [16] and surface acoustic waves [17]. Some optical fibre sensors have already been developed specifically for alcoholic compounds monitoring. For example, Elosúa et al. [14] developed a fibre optic nanosensor for volatile alcoholic compounds, based on a vapochromic material and Mitsushio et al. [18] have constructed a gold-deposited optical fibre sensor using surface plasmon resonance for quantitative analysis of different alcohols. NIOSH recommends the Method 1405, a GC-FID-based analytical methodology, for the determination of combined alcohols [19]. Bruckner and Synovec [20] have reported a GC coupled to optical fibres for separation and detection of methane, benzene, betanone and chlorobenzene.

In optical fibre detectors based on polymeric films as the sensitive component, the analytical signal generation and characteristics must be understood as an interaction between several physical and chemical factors. Firstly, the analytical signal depends on the wave guide, the polymeric cladding and the analyte proprieties. Secondly, it is important to take into account the molecular interactions that occur between the analyte molecules and the polymeric film with consequent changes in the intensity of the light power transmit-

* Corresponding author at: ISEIT/VISEU-Instituto Piaget, Estrada do Alto do Gaio, Galifonge, 3515-776 Lordosa, Viseu, Portugal. Tel.: +351 232 910 100; fax: +351 232 910 183.
E-mail address: lisilva@ua.pt (L.I.B. Silva).

0039-9140/$ – see front matter © 2008 Elsevier B.V. All rights reserved.
doi:10.1016/j.talanta.2008.03.012

ted. When the analyte molecules contact with the polymeric film, the intensity of the optical power transmitted will vary [9,20] and the optical power changes are proportional to the amount of the analyte present.

In this paper, a GC-OF detector operating in the visible region (650 nm) is developed as an analytical methodology for analysis of some alcohols as an alternative to the NIOSH recommended method (Method 1405) for organic vapours detection.

2. Experimental

2.1. Analytical details and experimental apparatus

Fig. 1 shows the experimental apparatus used for the newly proposed method, highlighting a detailed view of the analytical tube (T). The detection system is constituted by an optical fibre pigtail, core and cladding diameters of 4 and 125 μm, respectively, sensitized on a length of 26 mm by a thin polymeric film of PMTFPS, Aldrich (481645) deposited by a spray technique. The optical fibre is introduced through a teflon plug inside the 7.7 cm long glass tube. On the other side of the tube, the capillary column from the GC was aligned with the OF through a ferrule and a teflon plug. The detection apparatus is complete with a laser diode from Oz Optics to create the optical signal and a silicone photodetector also from Oz Optics to measure the changes in intensity of the optical signal. The analytical apparatus response was measured in the visible spectral region, namely at 650 nm.

The capillary column (fused silica-Supelcowax 10, 30 m × 0.32 mm I.D. × 0.5 μm, Cat no. 24084, Supelco, Spain) was connected to the injection unit of the GC and to the analytical tube. Column temperature started at 35.0 °C (kept for 7 min) with a program rate of 5.0 °C min^{-1} until 60.0 °C (kept for 5 min) and 10.0 °C min^{-1} until 120.0 °C (kept for 3 min). The temperature of the injector and analytical tube were maintained at 220 and 25 °C, respectively, during the analysis. Helium was used as carrier gas with a constant flow of 4.0 mL min^{-1}. Data acquisition was performed by a PC with homemade software.

The GC-FID methodology was performed according to NIOSH methodology [19] in a Gow-Mac Series 600 with a capillary column (fused silica–Supelcowax 10, 30 m × 0.32 mm I.D. × 0.5 μm, Cat no. 24084, Supelco, Spain) with the same temperature program as for the GC-OF method and the FID temperature was set at 270 °C.

2.2. Sampling in industrial environment

Sampling took place at a confined environment in a Portuguese solvent industry and it was performed according to NIOSH Method 1405 [19] using coconut shell charcoal, 100 mg/50 mg (Supelco Cat no. 20267-U). The sampling flow rate was 0.2 L/min, with a total sampling time and volume of 25 min and 5 L, respectively. Sample desorption was performed with 1 mL of 2-propanol 5% in carbon disulfide (CS_2).

2.3. Preparation of standard solutions

Standard solutions of allyl alcohol, *n*-propyl alcohol, *sec*-butyl alcohol, isobutyl alcohol, *n*-butyl alcohol, isoamyl alcohol, methyl isobutyl carbinol, cyclohexanol and diacetone alcohol, have been prepared by mixing in a syringe appropriate amounts of each alcoholic compound. All reagents used were analytical grade from Sigma–Aldrich (Cat. no. 05788; 82090; 19440; 58450; 19420; M3, 265-8; 68440; 29100 and 31450, respectively).

3. Results and discussion

The performance of the optical fibre detector was evaluated for different amounts of nine volatile alcoholic compounds and compared to the GC-FID. The calibration curves for both methods were obtained for five standard solutions prepared by mixing in a syringe, appropriate amounts of alcohols accordingly to Table 1. Fig. 2 shows the optical power decrease obtained with GC-OF for allyl alcohol, *n*-propyl alcohol, *sec*-butyl alcohol, isobutyl alcohol, *n*-butyl alcohol, isoamyl alcohol, methyl isobutyl carbinol, cyclohexanol and diacetone alcohol.

The alcoholic compounds show the following retention times in the newly developed analytical apparatus: 1102 s for allyl alcohol; 1114 s for *n*-propyl alcohol; 1142 s for *sec*-butyl alcohol; 1180 s for isobutyl alcohol; 1214 s for *n*-butyl alcohol; 1268 s for isoamyl alcohol; 1306 s for methyl isobutyl carbinol; 1393 s for cyclohexanol; and 1432 s for diacetone alcohol.

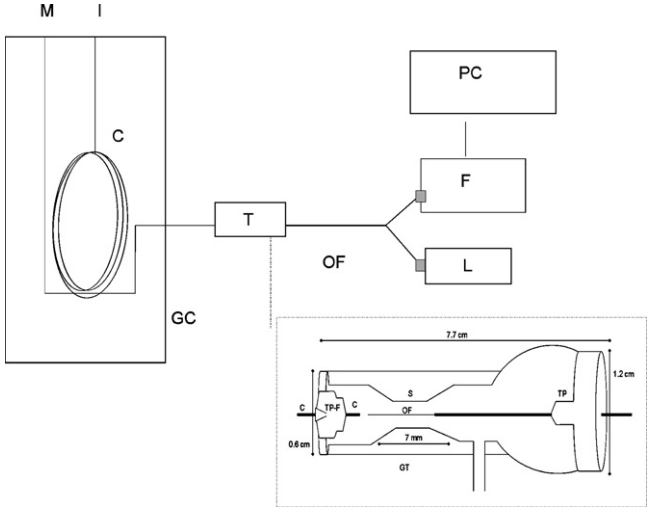

Fig. 1. Experimental apparatus for the analytical method based on the GC-OF (I, injector; C, capillary column; M, make up gas; GC, gas chromatograph; T, analytical tube; OF, optical fibre; L, laser; F, photodetector; PC, computer; TP-F, teflon plug with ferrule; S, narrowed region, GT, glass tube; TP, teflon plug.

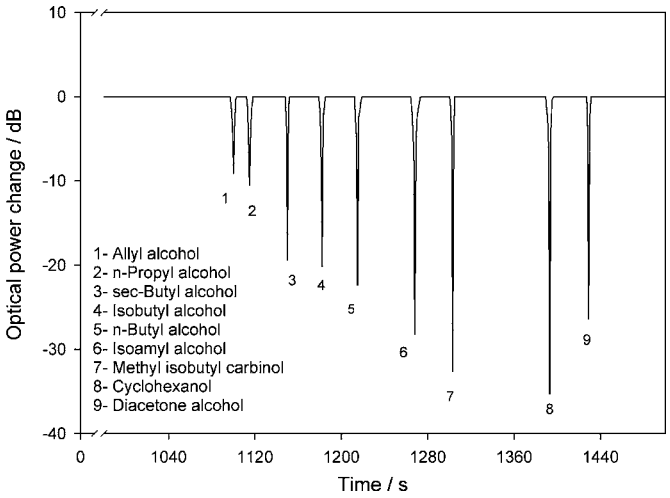

Fig. 2. Analytical signals obtained with the GC-OF detector for the standard mixture of allyl alcohol, *n*-propyl alcohol, *sec*-butyl alcohol, isobutyl alcohol, *n*-butyl alcohol, isoamyl alcohol, methyl isobutyl carbinol, cyclohexanol and diacetone alcohol.

Table 1
Composition of the standard solutions used for calibration of both GC-OF and GC-FID methods

Standard solution	Alcoholic compound (μg)								
	Allyl alcohol	*n*-Propyl alcohol	*sec*-Butyl alcohol	Isobutyl alcohol	*n*-Butyl alcohol	Isoamyl alcohol	Methyl isobutyl carbinol	Cyclohexanol	Diacetone alcohol
1	8.48	8.00	8.03	7.97	8.06	7.93	7.88	9.48	9.19
2	16.95	16.00	16.06	15.94	16.12	15.86	15.76	18.97	18.38
3	25.43	24.00	24.09	23.91	24.18	23.78	23.63	28.45	27.58
4	33.91	32.00	32.12	31.88	32.24	31.71	31.51	37.94	36.77
5	42.39	40.00	40.15	39.85	40.3	39.64	39.39	47.42	45.96

The intensity and hence the sensitivity (slope of the calibration curves) of the analytical signal (optical power change) obtained for the alcoholic compounds, increases in the following order: allyl alcohol < *n*-propyl alcohol < *sec*-butyl alcohol < isobutyl alcohol < *n*-butyl alcohol < diacetone alcohol < isoamyl alcohol < methyl isobutyl carbinol < cyclohexanol. It could be observed that the sensitivity of the newly method increases as the boiling temperatures of the analytes increases (97–98 °C ≈ 97–98 °C < 99–100 °C < 107–108 °C < 116–118 °C < ?158–162 °C < 130 °C < 130–133 °C < 160–161 °C for allyl alcohol < n-propyl alcohol < *sec*-butyl alcohol < isobutyl alcohol < *n*-butyl alcohol < ? diacetone alcohol < isoamyl alcohol < methyl isobutyl carbinol < cyclohexanol), respectively, which is in agreement with the results obtained with porous silica films [6]. However, diacetone alcohol, with a higher boiling temperature (158.0–162 °C) shows an analytical sensitivity lower than expected, which could be due to the fact of this compound has a ketone functional group besides a group alcohol in the molecular structure. Allyl alcohol and *n*-propyl alcohol have boiling temperature similar and different sensitivities which could be explained by the fact that the sensitivity also increases with the decrease of vapour pressure (allyl alcohol > *n*-propyl alcohol): at 20 °C the vapour pressure of allyl alcohol and *n*-propyl alcohol are 17 and 15 mmHg, respectively. The same comment, that is, the increase in sensitivity with the decrease in analyte pressure vapour is also valid for the remaining alcoholic compounds with a vapour pressure value in mmHg at 20 °C of 13, 9, 4.2, 28, 3, 1 and 0.8 for *sec*-butyl alcohol, isobutyl alcohol, *n*-butyl alcohol, isoamyl alcohol, methyl isobutyl carbinol, cyclohexanol and diacetone alcohol, respectively.

Fig. 3 shows the calibration curves obtained with GC-OF method for nine alcoholic compounds.

Assuming a linear model for calibration, the statistical parameters for the linear regression (estimates of slope with associated standard deviation, interception with associated standard deviation, r^2 and p) were calculated and they are shown in Table 2.

The detection limits based on 3 times the residual standard deviation [21], obtained for the nine alcoholic compounds analysed by GC-OF and GC-FID were, respectively, 0.67 and 0.90 μg for allyl alcohol, 0.73 and 0.82 μg for *n*-propyl alcohol, 0.88 and 0.93 μg for *sec*-butyl alcohol, 0.89 and 0.96 μg for isobutyl alcohol, 0.72 and 0.98 μg for *n*-butyl alcohol, 0.81 and 0.95 μg for isoamyl alcohol, 0.84 and 0.96 μg for methyl isobutyl carbinol, 0.76 and 0.86 μg for cyclohexanol and 0.73 and 0.99 μg for diacetone alcohol. These values show that the detection limits for both methods are in the same order of magnitude suggesting that these methods cannot be differentiated in terms of this figure of merit.

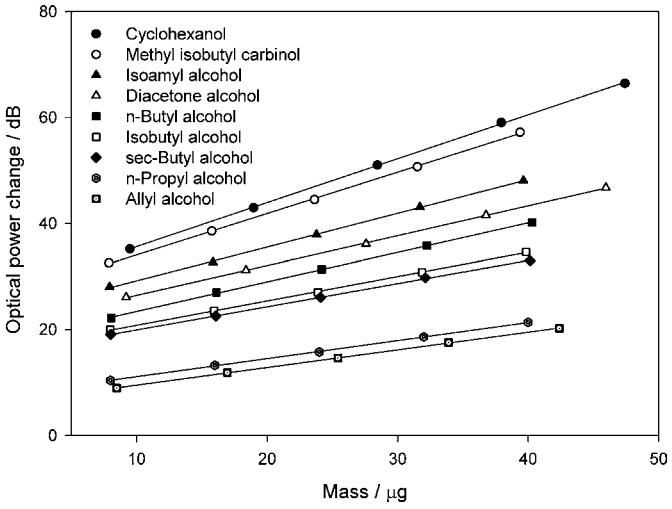

Fig. 3. Calibration curves obtained with GC-OF method for several alcohols.

In order to test and compare the performance of the proposed method (GC-OF) with GC-FID ten different concentration of a standard mixture of the alcohols under study were processed with both methods.

The comparison between the performances of the two methods can be discussed on the basis of Fig. 4 showing the results obtained for both methods. The *y*-axis represents the results obtained by the proposed method and the *x*-axis represents the results obtained by the GC-FID method. Each point on the graph thus represents a single sample (mean of five experiments) analysed by each of the methods.

Table 2
Calibration parameters obtained for both GC-OF and GC-FID methods

Alcohols	GC-OF method				GC-FID method			
	Slope (dB/μg)	Interception (dB)	r^2	p	Slope (area/μg)	Interception (area)	r^2	p
Allyl alcohol	0.333 ± 0.003	6.19 ± 0.08	0.9998	$<1.28 \times 10^{-6}$	0.311 ± 0.003	18.33 ± 0.10	0.9996	$<3.10 \times 10^{-6}$
n-Propyl alcohol	0.341 ± 0.003	7.71 ± 0.09	0.9997	$<1.94 \times 10^{-6}$	0.251 ± 0.003	24.52 ± 0.07	0.9996	$<2.83 \times 10^{-6}$
sec-Butyl alcohol	0.436 ± 0.005	15.59 ± 0.13	0.9996	$<3.38 \times 10^{-6}$	0.313 ± 0.004	34.45 ± 0.10	0.9996	$<3.95 \times 10^{-6}$
Isobutyl alcohol	0.459 ± 0.005	16.23 ± 0.14	0.9996	$<3.57 \times 10^{-6}$	0.311 ± 0.004	39.73 ± 0.10	0.9995	$<4.44 \times 10^{-6}$
n-Butyl alcohol	0.556 ± 0.006	17.87 ± 0.16	0.9997	$<2.54 \times 10^{-6}$	0.320 ± 0.004	41.56 ± 0.11	0.9995	$<4.66 \times 10^{-6}$
Isoamyl alcohol	0.637 ± 0.007	22.81 ± 0.18	0.9997	$<2.70 \times 10^{-6}$	0.328 ± 0.004	45.08 ± 0.11	0.9995	$<4.51 \times 10^{-6}$
Methyl isobutyl carbinol	0.780 ± 0.009	26.27 ± 0.23	0.9996	$<3.14 \times 10^{-6}$	0.359 ± 0.005	51.09 ± 0.12	0.9995	$<4.62 \times 10^{-6}$
Cyclohexanol	0.828 ± 0.007	27.37 ± 0.22	0.9998	$<1.31 \times 10^{-6}$	0.288 ± 0.003	54.99 ± 0.09	0.9997	$<1.91 \times 10^{-6}$
Diacetone alcohol	0.562 ± 0.005	20.85 ± 0.14	0.9998	$<1.28 \times 10^{-6}$	0.272 ± 0.003	48.27 ± 0.09	0.9996	$<3.20 \times 10^{-6}$

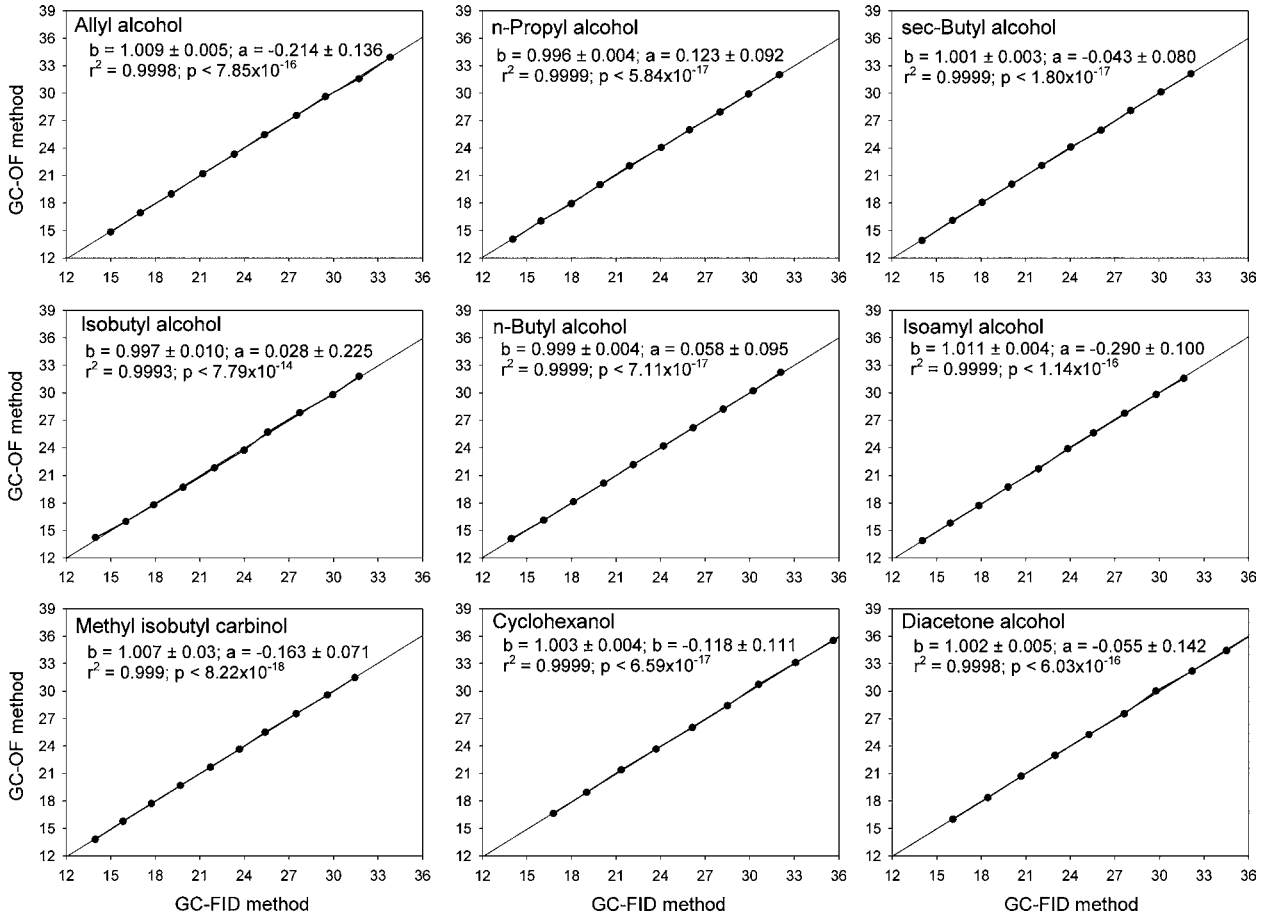

Fig. 4. Comparison of the results obtained with the CG-FID and CG-OF methods for alcoholic compounds.

Assuming the null hypothesis (same sensitivity, i.e. slope equals 1 and no systematic errors, i.e. intercept equals to 0) for the results obtained with both methods the slope (b), the intercept (a), r^2 and p of the regression line, of each of the data sets were calculated and included in Fig. 4. For all the alcohols analysed the regression line has approximately zero intercept, and a slope and a correlation coefficient of approximately 1, allowing to conclude that the results obtained with the two analytical methods can not be statistically differentiated. This fact it was also corroborated by the results of an ANOVA (using SIGMASTAT 3.0 [22]) applied to all data obtained on alcohols analysis by GC-OF and GC-FID method. The ANOVA of the results shows that there is no statistically significant difference (p = 0.138, 0.115, 0.345, 0.324, 0.144, 0.069, 0.858, 0.190 and 0.884, for allyl alcohol, *n*-propyl alcohol, *sec*-butyl alcohol, isobutyl

Table 3
GC-OF and GC-FID results for five actual samples of confined atmosphere from a Portuguese solvent industry

Alcoholic compound	GC-FID method				
	Sample 1	Sample 2	Sample 3	Sample 4	Sample 5
Allyl alcohol	2.982 ± 0.027	3.039 ± 0.009	3.019 ± 0.010	3.088 ± 0.015	2.874 ± 0.024
n-Propyl alcohol	3.979 ± 0.026	4.041 ± 0.021	4.093 ± 0.006	3.980 ± 0.011	4.179 ± 0.020
sec-Butyl alcohol	6.440 ± 0.019	6.400 ± 0.016	6.519 ± 0.012	6.513 ± 0.023	6.568 ± 0.026
Isobutyl alcohol	4.403 ± 0.038	4.456 ± 0.018	4.569 ± 0.025	4.539 ± 0.015	4.192 ± 0.034
n-Butyl alcohol	8.035 ± 0.018	8.104 ± 0.016	7.996 ± 0.014	7.918 ± 0.021	7.836 ± 0.022
Isoamyl alcohol	3.160 ± 0.019	3.135 ± 0.011	3.273 ± 0.009	3.099 ± 0.014	3.134 ± 0.027
Methyl isobutyl carbinol	4.610 ± 0.019	4.586 ± 0.011	4.720 ± 0.008	4.551 ± 0.014	4.585 ± 0.026
Ciclohexanol	5.677 ± 0.021	5.651 ± 0.012	5.798 ± 0.009	5.612 ± 0.015	5.649 ± 0.029
Diacetone alcohol	6.877 ± 0.019	6.854 ± 0.011	6.987 ± 0.008	6.819 ± 0.014	6.852 ± 0.026
GC-OF method					
Allyl alcohol	2.987 ± 0.025	3.041 ± 0.008	3.022 ± 0.009	3.086 ± 0.014	2.887 ± 0.022
n-Propyl alcohol	3.990 ± 0.019	4.036 ± 0.016	4.075 ± 0.004	3.991 ± 0.008	4.138 ± 0.015
sec-Butyl alcohol	6.432 ± 0.014	6.402 ± 0.012	6.490 ± 0.009	6.486 ± 0.017	6.527 ± 0.019
Isobutyl alcohol	4.385 ± 0.017	4.409 ± 0.008	4.461 ± 0.011	4.447 ± 0.007	4.289 ± 0.016
n-Butyl alcohol	8.011 ± 0.010	8.050 ± 0.009	7.990 ± 0.008	7.946 ± 0.011	7.900 ± 0.012
Isoamyl alcohol	3.166 ± 0.010	3.154 ± 0.005	3.222 ± 0.004	3.135 ± 0.007	3.153 ± 0.013
Methyl isobutyl carbinol	4.721 ± 0.008	4.711 ± 0.004	4.767 ± 0.004	4.696 ± 0.006	4.711 ± 0.011
Ciclohexanol	5.500 ± 0.007	5.491 ± 0.004	5.544 ± 0.003	5.477 ± 0.005	5.490 ± 0.010
Diacetone alcohol	6.887 ± 0.011	6.874 ± 0.006	6.951 ± 0.005	6.853 ± 0.008	6.873 ± 0.015

alcohol, *n*-butyl alcohol, isoamyl alcohol, methyl isobutyl carbinol, cyclohexanol and diacetone alcohol, respectively) for the effects of differences in the two methods. However, as expected there is a significant statistic difference ($p < 0.001$) between the different levels of the concentrations.

The analytical error, measured as the residual standard deviation of both methods, varied between 1.3×10^{-2} and 1.3×10^{-1} μg.

The effects of possible interferents, namely CS_2 and 2-propanol, used as eluent desorption of alcohols from solid sorbent tubes used for sampling, were evaluated in separate experiments. In CS_2 cases no analytical signal was obtained, suggesting that there are not interactions between this inorganic carbon compound and the sensitive cladding and 2-propanol does not exhibit interference on the signal due to the fact that this compound produces a peak in a different analytical time (1105 s).

Table 3 shows the results obtained by the GC-FID and the newly proposed GC-OF method when applied to five actual samples collected in a Portuguese solvent industry.

The obtained results for the nine alcoholic compounds analysed (allyl alcohol, *n*-propyl alcohol, *sec*-butyl alcohol, isobutyl alcohol, *n*-butyl alcohol, isoamyl alcohol, methyl isobutyl carbinol, cyclohexanol and diacetone alcohol) are much lower than the occupational exposure limits recommend by NIOSH: 5 mg/m^3 for allyl alcohol [23], 500 mg/m^3 for *n*-propyl alcohol [24], 305 mg/m^3 for *sec*-butyl alcohol [25], 150 mg/m^3 for isobutyl alcohol [26], 150 mg/m^3 for *n*-butyl alcohol [2], 360 mg/m^3 for isoamyl alcohol [27], 100 mg/m^3 for methyl isobutyl carbinol [28], 200 mg/m^3 for cyclohexanol [29] and 240 mg/m^3 for diacetone alcohol [30].

4. Conclusions

The developed analytical system based on GC-OF showed high linearity and stability of the analytical signal, allowing alcohols measurements with both high sensitivity and accuracy. The GC-OF method showed also high suitability for analysis of alcohols in actual samples from industrial environments.

The analytical performance obtained for the GC-FID and GC-OF methods for determination of alcohols in confined environments were similar and the analysis time was around 24 min for both methods. However, the GC-OF constitutes an excellent alternative to GC-FID for speciation of alcoholic compounds in confined areas due to its easiness of operation and cost of equipment. Furthermore the developed analytical system shows high miniaturization potential, allowing the possibility for VOCs monitoring *in situ* and in real time without any special safety precaution.

Acknowledgments

This work has been developed under the scope of the FCT (Portugal) funded research project POCTI/CTA/44899/02: "Development of a new Optical Fiber Chemical Sensor for in situ monitoring of VOCs (VOCSENSOR)" and a Ph.D. grant (SFRH/BD/17288/2004) awarded to Lurdes I. B. Silva is also gratefully acknowledged.

References

[1] The Merck Index, Merck Laboratories Division of Merck & CO., 12th ed., 1996.
[2] NIOSH Pocket Guide to Chemical Hazards, http://www.cdc.gov/niosh/npg/npgd0076.html.
[3] M. Campbell, Sensor Systems for Environmental Monitoring, 1, Blackie Academic & Professional, Cap. 1 London, 1997, pp. 3–4.
[4] B. Zimmermann, J. Bürck, H.-J. Ache, Sens. Actuator B 41 (1997) 45–54.
[5] B. Kondratowicz, R. Narayanaswamy, K.C. Persuad, Sens. Actuator B 74 (2001) 138–144.
[6] F. Addelmalek, J.M. Chovelon, M. Lacroix, N. Jaffrezic-Renault, V. Matejec, Sens. Actuator B 56 (1999) 234–242.
[7] A. Abdelghani, J.M. Chovelon, N. Jaffrezic-Renault, C. Veilla, H. Gagnaire, Anal. Chim. Acta 337 (1997) 225–232.
[8] A. Abdelghani, N. Jaffrezic-Renault, Sens. Actuator B 74 (2001) 117–123.
[9] A. Abdelghani, J.M. Chovelon, N. Jaffrezic-Renault, M. Lacroix, H. Gagnaire, C. Veillas, B. Berkova, M. Chomat, V. Matejec, Sens. Actuator B 44 (1997) 495–498.
[10] X. Wang, H. Zeng, L. Zhao, J.-M. Lin, Talanta 70 (2006) 160–168.
[11] C. Bariáin, I. Matías, I. Romeo, J. Garrido, M. Laguna, Sens. Actuator B 76 (2001) 25–31.
[12] C. Bariáin, I.R. Matías, C. Fernández-Valdivielso, F.I. Arregui, M.L. Rodrígues-Méndez, J.A. Saja, Sens. Actuator B 93 (2003) 153–158.
[13] C. Bariáin, I.R. Matías, C. Fdez-Valdivielso, C. Elosúa, A. Luquin, J. Garrido, M. Laguna, Sens. Actuator B 108 (2005) 535–541.
[14] C. Elosúa, C. Bariáin, I.R. Matías, F.J. Arregui, A. Luquin, M. Laguna, Sens. Actuator B 115 (2006) 444–449.
[15] K. Wang, L. Zhou, D. Mao, X. Yang, K. Luo, Sens. Actuator B 66 (2000) 4–5.
[16] C. Bariáin, I.R. Matías, F.J. Arregui, M. López-Amo, Sens. Actuator B 69 (2000) 127–131.
[17] M.C. Horrillo, M.J. Fernández, J.L. Fontecha, I. Sayago, M. García, M. Aleixandre, J.P. Santos, L. Arés, J. Gutiérrez, L. Gràcia, C. Cané, Thin Solid Films 467 (2004) 234–238.
[18] M. Mitsushio, S. Higashi, M. Higo, Sens. Actuator A 111 (2004) 252–259.
[19] Alcohols Combined: Method 1405, NIOSH Manual of Analytical Methods (NMAM), 4th ed. DHHS (NIOSH) Publication, 2003.
[20] C.A. Bruckner, R.E. Synovec, Talanta 43 (1996) 901–907.
[21] J.C. Miller, J.N. Miller, Statistics for Analytical Chemistry, 3rd ed., Ellis Horwood and Prentice Hall, New York, 1993.
[22] Sigma Stat (Statistic Software for Windows), 1994, Jandel Scientific, Erkrath, Germany.
[23] NIOSH Pocket Guide to Chemical Hazards, http://www.cdc.gov/Niosh/npg/npgd0017.html.
[24] NIOSH Pocket Guide to Chemical Hazards, http://siso.org.sg/web/NIOSH/npgd0533.html.
[25] NIOSH Pocket Guide to Chemical Hazards, http://0-www.cdc.gov.mill1.sjlibrary.org/niosh/npg/npgd0077.html.
[26] NIOSH Pocket Guide to Chemical Hazards, http://0-www.cdc.gov.mill1.sjlibrary.org/niosh/npg/npgd0352.html.
[27] NIOSH Pocket Guide to Chemical Hazards, http://www.siso.org.sg/web/NIOSH/npgd0348.html.
[28] NIOSH Pocket Guide to Chemical Hazards, http://siso.org.sg/web/NIOSH/npgd0422.html.
[29] NIOSH Pocket Guide to Chemical Hazards, http://www.siso.org.sg/web/NIOSH/npgd0165.html.
[30] NIOSH Pocket Guide to Chemical Hazards, http://siso.org.sg/web/NIOSH/npgd0178.html.

Talanta 76 (2008) 347–352

Contents lists available at ScienceDirect

Talanta

journal homepage: www.elsevier.com/locate/talanta

Sodium hydroxide as pretreatment and fluorosurfactant-capped gold nanoparticles as sensor for the highly selective detection of cysteine

Hsin-Pin Wu[a], Chia-Chi Huang[a], Tian-Lu Cheng[b,c], Wei-Lung Tseng[a,c,*]

[a] Department of Chemistry, National Sun Yat-sen University, Taiwan
[b] Faculty of Biomedical Science and Environmental Biology, Kaohsiung Medical University, Kaohsiung, Taiwan
[c] National Sun Yat-sen University-Kaohsiung Medical University Joint Research Center, Kaohsiung, Taiwan

ARTICLE INFO

Article history:
Received 21 January 2008
Received in revised form 3 March 2008
Accepted 4 March 2008
Available online 15 March 2008

Keywords:
Homocysteine
Cysteine
Gold nanoparticles
Fluorosurfactant

ABSTRACT

A sensor for detecting cysteine (Cys) in a solution of fluorosurfactant (FSN)-capped gold nanoparticles (AuNPs) has been developed. Under acidic conditions, FSN-capped AuNPs are aggregated in the presence of homocysteine (HCys) and Cys but not in the presence of cysteinylglycine, glutathione, and γ-glutamycysteine. When adding NaOH to a solution of HCys, the five-membered ring transition state is formed through intramolecular hydrogen abstraction. By contrast, it is difficult for Cys to form a four-membered ring transition state after Cys has been pretreated with NaOH. As a result, the HCys-induced aggregation of the FSN-capped AuNPs is suppressed because the five-membered ring transition state exhibits relatively larger steric hindrance and has stronger interaction with the FSN molecules. Thus, we can discriminate between Cys and HCys on the basis of different aggregation kinetics. Under the optimum condition, the selectivity of the probe for Cys in aqueous solutions is remarkably high over the other aminthiols. Note that HCys and Cys have very similar structure and pK_a value. We have validated the applicability of our method through the analyses of Cys in urine samples. It is believed that this approach has great potential for the detection of Cys in biological samples.

1. Introduction

Low-molecular-weight aminothiols, including cysteine (Cys), homocysteine (HCys), cysteinylglycine (Cys–gly), glutathione (GSH), and γ-glutamycysteine (Glu–cys), play important roles in many biological processes such as metabolism [1] and detoxification [2]. Compared with GSH found in a large amount (0.5–10 mM) inside the cell [3], Cys is a very abundant extracellular aminothiol [4]. The concentrations of Cys in plasma and urine provide biomedical scientists an avenue to evaluate a number of clinical disorders [5–11]. Elevated level of Cys in plasma is a vascular disease risk factor [5] and is associated with neurotoxicity [6]. On the contrary, deficiency of Cys may result in some serious diseases such as hematopoiesis decrease, leucocyte loss, and psoriasis [7]. Additionally, altered level of Cys has been implicated in hyperhomocysteinemia [8], which has been linked to the increased risks of Alzheimer's disease [9], neural tube defect [10], and osteoporosis [11]. Thus, the detection of Cys continues to be of interest.

Since aminothiols possess a very low molar extinction coefficient, many fluorescent dyes such as *o*-phthaladehyde [12], monobromobimane [13], fluorescein-5-maleimide [14], and 5-iodoacetamido-fluorescein [15], have been developed and demonstrated to be useful as thiol-selective probes. However, these reagents are nonselective for specific aminothiols. To overcome this limitation, Strongin's group reported that xanthene dye in the efficient detection of Cys and HCys [16]. They also demonstrated that the direction detection of HCys has been accomplished upon the addition of heating a colorless solution of methyl viologen, which served as an oxidant [17]. The recognition of Cys and Hcys with 8-oxo-8H-acenaphtho[1,2-*b*]pyrrole-9-carbonitrile has been achieved in the presence of 30% methanol [18]. On the other hand, an electrochemical sensor for the detection of aminothiols is generally on the basis of the oxidation of thiols to form disulfide bonds. Because the direct oxidation of aminothiols using bare metal electrode shows very poor activity, analyses of aminothiols have focused on the use of chemically modified electrodes [19]. Recently, laccase-based biosensor has been utilized for the detection of Cys through the reaction between *p*-benzoquinone and Cys; nevertheless, its selectivity toward the other aminothiols has not been investigated [20].

Recently, gold nanoparticles (AuNPs) have also been considered as an aminothiol sensor because they provide strong affinity toward thiols [21]. Upon the addition of aminothiols, the aggregation of AuNPs is driven; this phenomenon leads to a decrease in the plasmon band at around 520 nm and the formation of a new red shifted

* Corresponding author at: Department of Chemistry, National Sun Yat-sen University, 70, Lien-hai Road, Kaohsiung 804, Taiwan. Fax: +886 7 3684046.
E-mail address: tsengwl@mail.nsysu.edu.tw (W.-L. Tseng).

0039-9140/$ – see front matter © 2008 Elsevier B.V. All rights reserved.
doi:10.1016/j.talanta.2008.03.004

band [22]. Thus, the absorption ratio of separated to aggregated nanoparticles can be used to assess the degree of aggregation. The resonance light scattering of AuNPs can be greatly enhanced while they are aggregated [23]. By applying this detection technique, the limits of detection for Cys is down to 16.5 nM. On the other hand, AuNPs possess a high extinction coefficient ($\sim 10^8\ cm^{-1}\ mol^{-1}\ L$ for 13-nm AuNPs at 520 nm) in the ultraviolet and visible regions [24]. Therefore, when fluorophores are adsorbed on the surface of AuNPs, their fluorescence will be quenched through fluorescence resonance energy transfer [25]. Upon the addition of aminothiols, fluorophores are released from the surface of AuNPs, resulting in an increase in fluorescence intensity. Although these abovementioned approaches all provide a highly sensitive detection for aminothiols, they are not selective with respect to specific aminothiols. To achieve better selectivity, AuNPs stabilized with nonionic fluorosurfactant (Zonyl FSN) have been developed for highly selective and sensitive detection of Cys and HCys [26]. Moreover, the selective detection of Cys and GSH has been accomplished by means of cationic surfactant-capped gold nanorods [27].

In this work, we proposed a simple approach for sensing Cys by means of the FSN-capped AuNPs after aminothiols have been pretreated with NaOH. Under acidic conditions, the FSN-capped AuNPs were aggregated upon the addition of both HCys and Cys. After HCys was treated with 1 M NaOH, the aggregation of AuNPs was suppressed. Under identical condition, AuNPs were aggregated upon the addition of Cys. As a result, we could discriminate between Cys and HCys based on their different aggregation kinetics. Moreover, in order to demonstrate practicability, the present approach was applied to determinate Cys in urine samples.

2. Experimental

2.1. Reagents

Cys, HCys, Cys–gly, GSH, and Glu–cys were obtained from Sigma (St. Louis, MO, USA). Sodium borohydride, hydrogen tetrachloroaurate (III) dehydrate, trisodium citrate, sodium hydroxide, glucose, Zonyl FSN, NaH_2PO_4, and Na_2HPO_4 were purchased from Aldrich (Milwaukee, WI, USA). The molecular formula of Zonyl FSN is $F(CF_2CF_2)_{3-8}CH_2CH_2O(CH_2CH_2O)_xH$. Buffer solutions were 20 mM NaH_2PO_4 and Na_2HPO_4 (NaOH was used to adjust the solution pH ranged from 4.0 to 13.0). Milli-Q ultrapure water was used in all of the experiments.

2.2. Characterization of AuNPs

A double-beam UV–visible spectrophotometer (Cintra 10e, GBC Scientific Equipment Pty Ltd., Dandenong, Victoria, Australia) was used to examine the absorption spectra of the AuNPs. A H7100 transmission electron microscopy (TEM) (Hitachi High-Technologies Corp., Tokyo, Japan) operating at 75 keV was used to collect TEM images of as-prepared AuNPs.

2.3. Nanoparticle synthesis

The citrate-capped AuNPs have been prepared by the chemical reduction of metal salt precursor (hydrogen tetrachloroaurate, $HAuCl_4$) in a liquid phase [28]. Briefly, 10% $HAuCl_4$ (54 μL) was added rapidly to a solution of 0.075% sodium citrate (60 mL) that was heated under reflux. Heating under reflux was continued for an additional 15 min, during which time the color changed to deep red. The TEM images confirmed that the size of the AuNPs is 13.1 nm with standard deviation of 0.3 nm. The maximum absorption wavelength of the AuNPs, which was measured by UV–visible spectrophotometer, was 520 nm. The particle concentration of the AuNP solution was 4.82 nM, which was determined by Beer's law; the extinction coefficient of 13.1 nm AuNPs at 520 nm was approximately $10^8\ M^{-1}\ cm^{-1}$ [24]. The FSN-capped AuNPs were obtained when 240 μL of 10% FSN was added to a solution of 4.82 nM citrate-capped AuNPs. The resulting mixture was stored at 4 °C until further use. Note that the FSN-capped AuNPs remain dispersed in the solution containing high concentration of salts.

2.4. Sample preparation

A stock solution of aminothiol (1 mM) was prepared in deionized water and diluted with phosphate buffer if necessary. Two sample preparation methods for analysis of aminothiols were tested before colorimetric detection. (a) The aminothiols (5–500 μM; 450 μL) were added to a solution of 4.82 nM FSN-capped AuNPs (500 μL), which was prepared in 20 mM phosphate buffer at different values of pH. The pH values of solution were adjusted by adding different amount of NaOH (0.1–5 M; 50 μL). (b) The aminothiols (5–500 μM; 450 μL) reacted with different concentrations of NaOH (0.1–5 M; 50 μL). After 5 min, the resulting mixture was added to a solution of 4.82 nM FSN-capped AuNPs (500 μL), which was prepared in 20 mM phosphate buffer (pH 4.0). Two sample preparation methods were equilibrated for the optimum incubation time (<15 min). Subsequently, UV–vis absorption spectra of the solution were recorded. In the case of analysis of Cys (collected from healthy female) in urine, the sample was filtered using a membrance filter with 3 kDa. Then, a 450 μL of urine sample reacted with a solution (50 μL) of 1 M NaOH and 1 M sodium borohydride. For total thiol quantification, sodium borohydride was utilized as a reducing agent to convert disulfides into thiols [29]. After 5 min, the resulting mixture was added to a solution (500 μL) of 20 mM phosphate solution (pH 4.0) and 4.82 nM FSN-capped AuNPs. Finally, they were equilibrated for 2 min at room temperature.

3. Results and discussion

3.1. Effect of pH and NaOH on the selectivity of the FSN-capped AuNPs

Previous studies have shown that the pH of the solution has a strong effect on the degree of aggregation of HCys-capped AuNPs, which were disassembled when the solution pH went above 11.0 [30]. The main reason is due to that hydroxide ions play an important role in disrupting the electrostatic interaction between amino acid groups. To compare the selectivity of the citrate- and FSN-capped AuNPs as well as understand the effect of pH on the selectivity of the FSN-capped AuNPs, we investigated the changes in their absorption spectra that occurred within 15 min of separately adding the following aminothiols (10 μM): Cys, HCys, GSH, Cys–gly, and Glu–cys. At pH 4.0, it is not surprised that the addition of Cys and HCys to a solution of the citrate-capped AuNPs resulted in a high ratio of absorption, from 600 to 520 nm, while the remaining aminothiols exhibited low absorption ratio (Fig. 1A). When the citrate-capped AuNPs were modified by the FSN, the AuNP aggregation took place in the only presence of Cys and HCys (Fig. 1B). Li and Zu reported that the FSN molecules are adsorbed with their hydrophilic heads on the gold surface while the hydrophobic chains intrude into the solution [31]. According to this observation, it is suggested that both Cys and HCys diffuse smoothly into the FSN layers, which are deposited on the nanoparticle surface. In contrast, GSH, Cys–gly, and Glu–cys cannot penetrate the FSN layer because they have stronger interaction with the FSN molecules. As a result, the relatively large aminothiols cannot penetrate the FSN layers and further displace the FSN molecules from the gold surface. Another reason may be due to the steric effect.

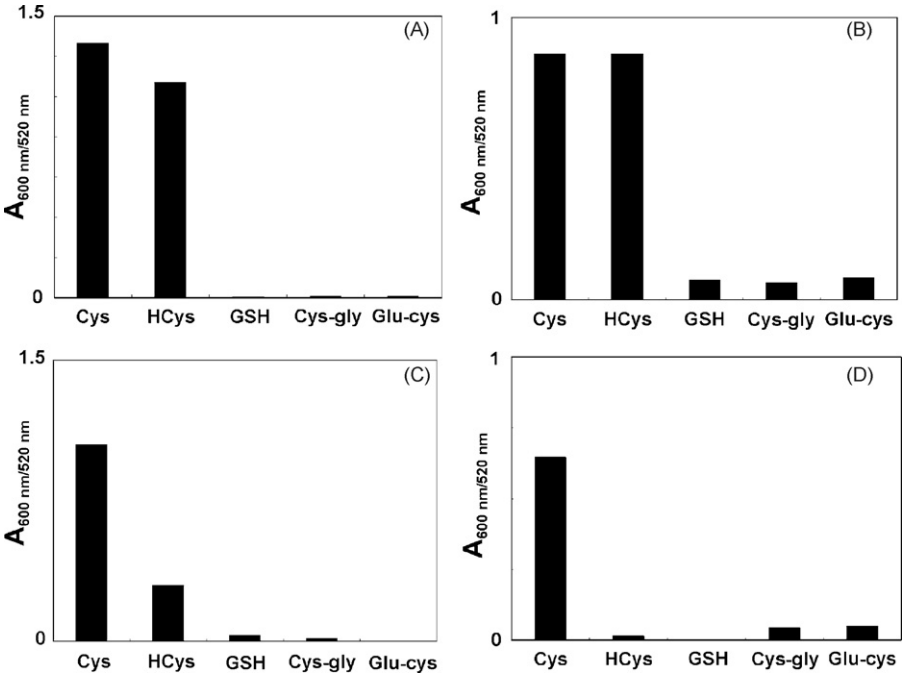

Fig. 1. Values of $A_{600nm/520nm}$ ratios for (A) the citrate- and (B–D) the FSN-capped AuNPs obtained (A and B) at pH 4.0 upon the addition of aminothiols, (C) at pH 12.0 upon the addition of aminothiols, and (D) upon the addition of aminothiols, which have been incubated with 1 M NaOH (50 μL) for 5 min. Note that the pH of the solution in part D is 12.0 and the final concentration of NaOH is 50 mM. The aminothiols are incubated with the FSN-capped AuNPs for 15 min. Buffer: (A, B, and D) 20 mM phosphate solution, pH 4.0 and (C) 20 mM phosphate solution, pH 12.0.

When Cys- or HCys-capped AuNPs are formed, the hydrogen bonding and electrostatic interactions between the two amino acid groups drive the assembly of AuNPs. Another reason is that the stabilized molecules (i.e. FSN), desorbed from the particle surface, result in an unstable colloidal solution. The aggregation could be also driven by the London-van der Waals attractive force between the nanoparticles [26]. This type of AuNP aggregation has been reported by Sato et al. [32]. Furthermore, when the solution pH was adjusted to 12.0, the HCys-induced aggregation of the FSN-capped AuNPs was suppressed (Fig. 1C).

To further improve the selectivity of the AuNP probe toward Cys, five aminothiols were pretreated with 1 M NaOH for 5 min. Then, the absorption spectra of the FSN-capped AuNPs were measured upon the addition of NaOH-treated aminothiols. As a result, the FSN-capped AuNPs exhibited a high selectivity toward Cys with respect to the other aminothiols (Fig. 1D). It is noted that the final pH of the solution used in Fig. 1D is identical to the one used in Fig. 1C. The HCys-induced aggregation of the FSN-capped AuNPs could be slowed down after the pretreatment of HCys with NaOH. We attributed this result to the formation of the five-membered (i.e. HCys) ring transition state through intramolecular hydrogen abstraction (Scheme 1A) [33]. By contrast, it is difficult for Cys to form a four-membered ring transition state after pretreatment of Cys with NaOH (Scheme 1B). Because the five-membered ring pos-

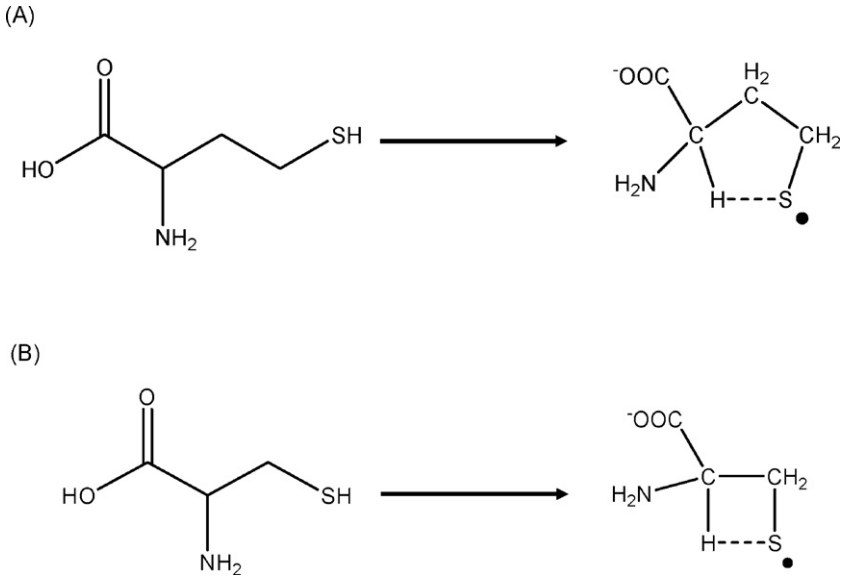

Scheme 1. The possible structures for (A) HCys and (B) Cys involved in the intramolecular hydrogen abstraction.

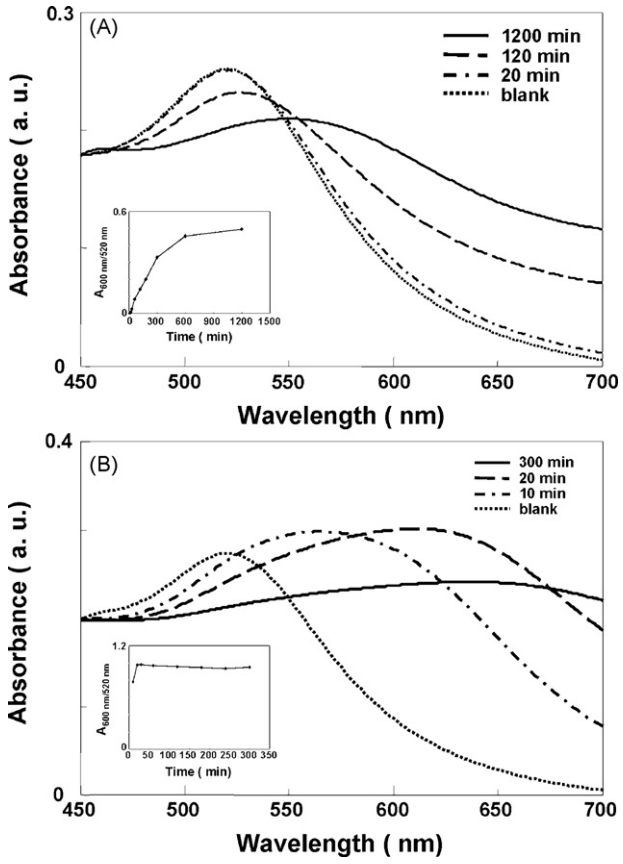

Fig. 2. Time course measurement of UV–vis absorption spectra of the FSN-capped AuNPs upon the addition of (A) HCys and (B) Cys, which has been incubated with 1 M NaOH 5 min. Inset in (A) and (B): the absorption ratios ($A_{600nm/520nm}$) of the FSN-capped AuNPs as a function of incubation time. The other conditions are the same as those in Fig. 1D.

sesses stronger hydrophobic interaction with the FSN layer, we can reasonably suppose that the penetration of HCys molecules into the FSN layer should become slow. To support our hypothesis, HCys-induced aggregation kinetics of the FSN-capped AuNPs was monitored by UV–vis absorption spectra; it is noted that HCys has been pretreated with 1 M NaOH for 5 min. After 20 min, a slight increase in absorbance at 600 nm for the FSN-capped AuNPs was observed in the presence of 10 μM HCys (Fig. 2A). The inset showed the absorption ratio ($A_{600nm/520nm}$) of the FSN-capped AuNPs as a function of incubation time. The aggregation of the FSN-capped AuNPs reached completion after 600 min when adding NaOH-treated HCys. When the FSN-capped AuNPs were employed for the detection of 10 μM Cys, the aggregation was close to completion after 20 min (Fig. 2B). The results provided clear evidence that the HCys-induced aggregation of the FSN-capped AuNPs could be effectively suppressed owing to the formation of the five-membered ring transition state, which exhibited relatively larger steric hindrance.

3.2. Effect of NaOH concentration on the sensitivity of the FSN-capped AuNPs

The addition of NaOH concentration to sample solution was further optimized by comparing the absorption ratio ($A_{600nm/520nm}$) of the FSN-capped AuNPs (Fig. 3). The aminothiols were incubated with NaOH for 5 min. The absorption ratio of the FSN-capped AuNPs sharply decreased when 0.4 M NaOH was added to a solution of HCys. Under identical condition, the FSN-capped AuNPs remained aggregated in the presence of Cys. In the range of 1–5 M NaOH,

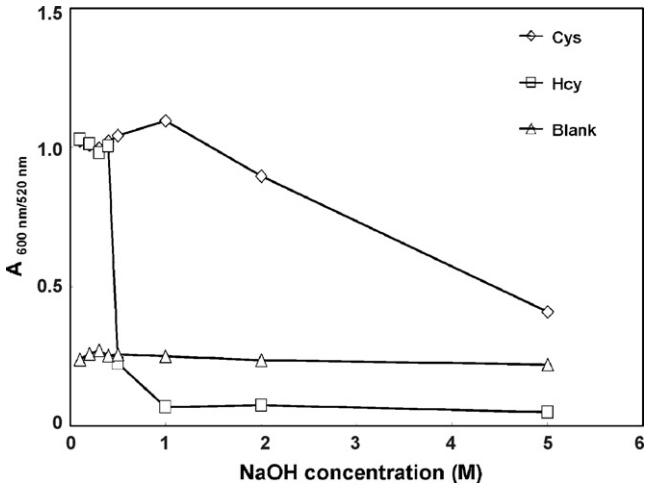

Fig. 3. Effect of NaOH concentrations on UV–vis absorption spectra of solutions of the FSN-capped AuNPs upon the addition of 10 μM aminothiols. The 450 μL aminothiols were incubated with different concentration of NaOH (50 μL) for 5 min. Then, the resulting solution was added to the FSN-capped AuNPs, which were prepared in 20 mM phosphate solution at pH 4.0. The other conditions are the same as those in Fig. 1D.

very low absorption ratios of the FSN-capped AuNPs indicated that HCys did not induce the aggregation. In the case of NaOH-treated Cys, the absorption ratio of the FSN-capped AuNPs gradually diminished when NaOH concentrations were larger than 1 M. From these results, we suggested that the pretreatment of aminothiols with NaOH is necessary for improving the selectivity of the FSN-capped AuNPs toward Cys, and the optimum concentration of NaOH is 1 M.

3.3. Sensitivity and application

With the assistance of the NaOH, the aggregation kinetics of the FSN-capped AuNPs with different concentrations of Cys were monitored by UV–vis absorption spectra. After the addition of different amounts of Cys (50–500 μM) to a solution of the FSN-capped AuNPs, the aggregation was close to completion after 10 min. When plotting absorption ratios ($A_{600nm/520nm}$) against the concentrations of Cys, it was discovered that the optimum incubation time for quantification was 1 min (Fig. 4A). At a low concentration of Cys (<10 μM), a slow rate of aggregation would make a difference in the optimal incubation time. The optimal incubation time for quantification was 10 min in the concentration range of 5–10 μM (Fig. 4B). When the concentration of Cys was lower than 1 μM, the absorption ratio of the FSN-capped AuNPs retained constant. Thus, it is suggested that the lowest detectable concentration of Cys using this proposed method is 1 μM. Table 1 shows that the correlation coefficients were 0.9909 and 0.9971 for the determination of Cys in the ranges of 5–10 and 50–500 μM, respectively. This new sensor exhibits great potential for sensing Cys in human fluids. Note that, in general, the total concentration of Cys contained in human fluids is approximately 10–20-fold larger than that of HCys [26].

Having high sensitivity and selectivity, we tested the application of our methods in the practical analyses of Cys in urine samples. The

Table 1
Sodium hydroxide as pretreatment and the FSN-capped AuNPs as sensor for quantitative analysis of Cys in the different sample matrix

Sample matrix	Concentration range (M)	Linear regression equation	R^2
Water	5×10^{-5} to 5×10^{-4}	$y = 0.0050x + 0.0334$	0.9971
Water	5×10^{-6} to 1×10^{-5}	$y = 0.0017x + 0.3761$	0.9909
Urine	2.5×10^{-5} to 2×10^{-4}	$y = 0.1777x - 0.5396$	0.9879

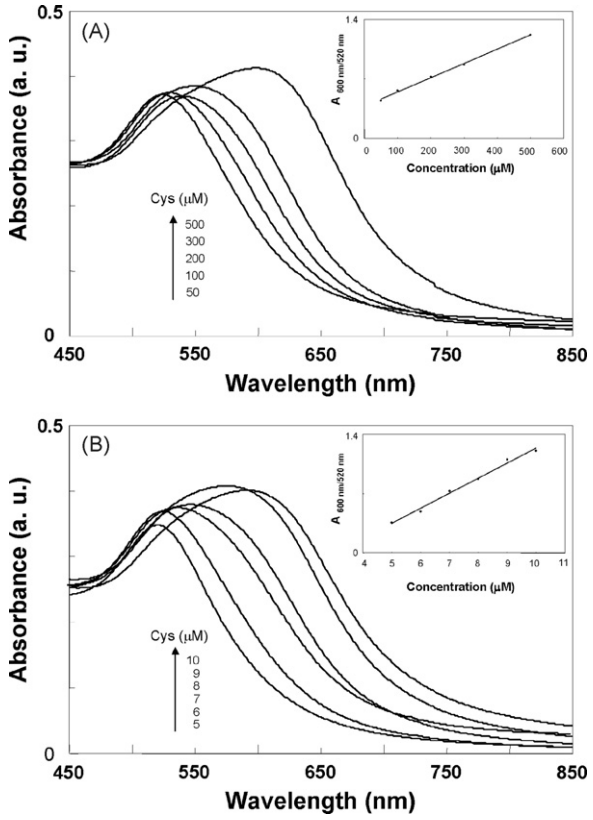

Fig. 4. Absorption spectral changes of the FSN-capped AuNPs upon addition of Cys concentrations within the range of (A) 50–500 μM and (B) 5–10 μM. The Cys was incubated with 1 M NaOH for 5 min before colorimetric detection. The resulting mixture was incubated with the FSN-capped AuNPs for (A) 1 min and (B) 10 min. Inset: plot of $A_{600nm/520nm}$ ratios of the FSN-capped AuNPs as a function of the Cys concentration. The other conditions are the same as those in Fig. 3.

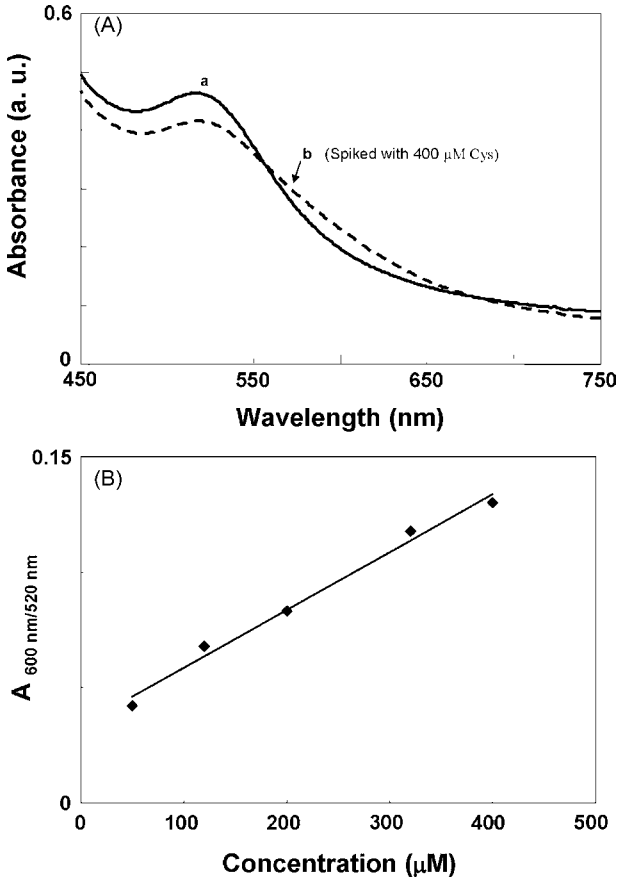

Fig. 5. Detection of Cys in urine samples. (A) The urine samples were spiked (a) without and (b) with 400 μM of Cys. (B) Calibration curve for the detection of Cys in urine samples. The urine samples were incubated with 1 M NaOH for 5 min before colorimetric detection. The resulting mixture was incubated with the FSN-capped AuNPs for 1 min. The other conditions are the same as those in Fig. 3.

normal concentrations of Cys in urine range from 20 to 80 μM [34]. Although other aminothiols such as GSH and HCys also appear in urine samples, their interference is not significant because their concentrations are considerably lower in urine samples and they had no reaction with the FSN-capped AuNPs. To minimize the detrimental effect of proteins, we subjected the urine to deproteination using a membrance filter with 3 kDa. An apparent increase in the absorption ratio ($A_{600nm/520nm}$) of the FSN-capped AuNPs was obtained after 400 μM Cys was spiked into the urine samples (Fig. 5A). Using a standard addition method as shown in Fig. 5B, the concentration of Cys in urine samples was estimated to be 66.7 μM with standard deviation of 1.42 μM ($n = 3$); the correlation coefficient was 0.9879 (Table 1). The result is in good agreement with the normal values between 20 and 80 μM.

4. Conclusions

We have demonstrated a highly selective method for detecting Cys using the FSN-capped AuNPs as sensor and NaOH as pretreatment. After aminothiols were incubated with 1 M NaOH, the

Table 2
A comparison of the FSN-capped AuNPs and other sensors for the detection of Cys

Sensor	Detection	Selectivity	Linear range (μM)	Analysis time (min)	Cost efficiency	Ref.
Xanthene dye	Fluorescence	HCys and Cys	0.01–0.06[a]	5	Moderate	[16]
Methyl viologen	Absorption	HCys	0.5–70	5	Moderate	[17]
Fluorescent dye[b]	Fluorescence	HCys and Cys	0.01–0.06[a]	10	Moderate	[18]
Laccase-modified electrode	Cyclic voltammetry	Thiols	197–324[a]	N/A[c]	Low	[20]
Citrate-capped AuNPs	Absorption	Thiols	N/A[c]	3	Low	[22]
Citrate-capped AuNPs	Scattering	Thiols	0.08–2[a]	60	Low	[23]
Nile red-modified AuNPs	Fluorescence	Thiols	0.05–5[a]	10	Low	[25]
FSN-capped AuNPs	Absorption	HCys and Cys	N/A[c]	30	Low	[26]
Surfactant-capped gold nanorods	Absorption	GSH and Cys	N/A[c]	N/A[c]	Low	[27]
FSN-capped AuNPs[d]	Absorption	Cys	50–500	1	Low	This study
FSN-capped AuNPs[d]	Absorption	Cys	5–10	10	Low	This study

[a] For Cys only.
[b] 8-Oxo-8H-acenaphtho[1,2-*b*]pyrrole-9-carbonitrile.
[c] Not avaliable.
[d] The aminothiols were pretreated with 1 M NaOH.

selectivity of this system for Cys over other aminothiols (HCys, GSH, Cys–gly, Glu–cys) became remarkably high. The present approach offers the advantages of rapidity (<10 min), simplicity, and low cost over the conventional methods (Table 2). We believe that this approach may be efficiently applied for the rapid determination of Cys concentrations in aqueous biological samples.

Acknowledgments

We would like to thank National Science Council (NSC 96-2113-M-110-008-) and National Sun Yat-sen University-Kaohsiung Medical University Joint Research Center for the financial support of this study.

References

[1] E. Camera, P. Mauro, J. Chromatogr. B 781 (2002) 181.
[2] A. Pastore, G. Federici, E. Bertini, F. Piemonte, Clin. Chim. Acta 333 (2003) 19.
[3] N.S. Kosower, E.M. Kosower, Int. Rev. Cytol. 54 (1978) 109.
[4] A. Pastore, R. Massoud, C. Motti, A.L. Russo, G. Fucci, C. Cortese, G. Federici, Clin. Chem. 44 (1998) 825.
[5] Q. Han, M. Xu, L. Tang, X. Sun, N. Zhang, X. Tan, X. Tan, Y. Tan, R.M. Hoffman, Clin. Chem. 50 (2004) 1229.
[6] R. Janaky, V. Varga, A. Hermaan, P. Saransaari, S.S. Oja, Neurochem. Res. 25 (2000) 1397.
[7] S. Shahrokhian, Anal. Chem. 73 (2001) 5972.
[8] G.L. Hortin, P. Sullivan, G. Csako, Clin. Chem. 47 (2001) 1121.
[9] S. Seshadri, A. Beiser, J. Selhub, P.F. Jacques, I.H. Rosenberg, R.B. D'Agostino, P.W.F. Wilson, N. Engl. J. Med. 346 (2002) 476.
[10] R.P. Steegers-Theunissen, G.H. Boers, F.J. Trijbels, T.K. Eskes, N. Engl. J. Med. 324 (1991) 199.
[11] J.B.J. van Meurs, R.A.M. Dhonukshe-Rutten, S.M.F. Pluijm, M. van der Klift, R. de Jonge, J. Lindemans, L.C.P.G.M. de Groot, A. Hofman, J.C.M. Witteman, J.P.T.M. van Leeuwen, M.M.B. Breteler, P. Lips, H.A.P. Pols, A.G. Uitterlinden, N. Engl. J. Med. 20 (2004) 2033.
[12] R.N. Puri, R. Roskoski, Anal. Biochem. 173 (1988) 26.
[13] B.L. Hogan, E.S. Yeung, Anal. Chem. 64 (1992) 2841.
[14] C. Chassaing, J. Gonin, C.S. Wilcox, I.W. Wainer, J. Chromatogr. B 735 (1999) 219.
[15] A. Zinellu, S. Sotgia, A.M. Posadino, V. Pasciu, M.G. Perino, B. Tadolini, L. Deiana, C. Carru, Electrophoresis 26 (2005) 1063.
[16] O. St. Rusin, N.N. Luce, R.A. Agbaria, J.O. Escobedo, S. Jiang, I.M. Warner, F.B. Dawan, K. Lian, R.M. Strongin, J. Am. Chem. Soc. 126 (2004) 438.
[17] W. Wang, J.O. Escobedo, C.M. Lawrence, R.M. Strongin, J. Am. Chem. Soc. 126 (2004) 3400.
[18] M. Zhang, M. Yu, F. Li, M. Zhu, M. Li, Y. Gao, L. Li, Z. Liu, J. Zhang, D. Zhang, T. Yi, C. Huang, J. Am. Chem. Soc. 129 (2007) 10322.
[19] P.C. White, N.S. Lawrence, J. Davis, R.G. Compton, Electroanalysis 14 (2002) 89.
[20] M. Santhiago, I.C. Vieir, Sens. Actuators B 128 (2007) 279.
[21] M.-C. Daniel, D. Astruc, Chem. Rev. 104 (2004) 293.
[22] F.X. Zhang, L. Han, L.B. Israel, J.G. Daras, M.M. Maye, N.K. Ly, C.J. Zhong, Analyst 127 (2002) 462.
[23] Z.P. Li, X.R. Duan, C.H. Liu, B.A. Du, Anal. Biochem. 351 (2006) 18.
[24] R.C. Mucic, J.J. Storhoff, C.A. Mirkin, R.L. Letsinger, J. Am. Chem. Soc. 120 (1998) 12674.
[25] S.-J. Chen, H.-T. Chang, Anal. Chem. 76 (2004) 3727.
[26] C. Lu, Y. Zu, V.W.-W. Yam, Anal. Chem. 79 (2007) 666.
[27] P.K. Sudeep, S.T.S. Joseph, K.G. Thomas, J. Am. Chem. Soc. 127 (2005) 6516.
[28] P.C. Lee, D. Meisel, J. Phys. Chem. 86 (1982) 3391.
[29] K. Kus'mierek, E. Bald, Food Chem. 106 (2008) 340.
[30] I.S. Lim, W.I.E. Crew, P.N. Njoki, D. Mott, C.-J. Zhong, Y. Pan, S. Zhou, Langmuir 23 (2007) 826.
[31] F. Li, Y. Zu, Anal. Chem. 76 (2004) 1768.
[32] K. Sato, K. Hosokawa, M. Maeda, J. Am. Chem. Soc. 125 (2003) 8102.
[33] W. Wang, O. Rusin, X. Xu, K.K. Kim, J.O. Escobedo, S.O. Fakayode, K.A. Fletcher, M. Lowry, C.M. Schowalter, C.M. Lawrence, F.R. Fronczek, I.M. Warner, R.M. Strongin, J. Am. Chem. Soc. 127 (2005) 15949.
[34] T. Inoue, J.R. Kirchhoff, Anal. Chem. 74 (2002) 1349.

Talanta 76 (2008) 369–372

Contents lists available at ScienceDirect

Talanta

journal homepage: www.elsevier.com/locate/talanta

A lamp light-emitting diode-induced fluorescence detector for capillary electrophoresis

Jing Xu, Yan Xiong, Shiheng Chen, Yafeng Guan*

Department of Analytical Chemistry and Micro-Instrumentation, Dalian Institute of Chemical Physics, Chinese Academy of Sciences, Dalian 116023, China

ARTICLE INFO

Article history:
Received 19 December 2007
Received in revised form 10 March 2008
Accepted 11 March 2008
Available online 26 March 2008

Keywords:
Light-emitting diode
Fluorescence detector
Filter
Electrophoresis

ABSTRACT

A light-emitting diode-induced fluorescence detector (LED-FD) for capillary electrophoresis was constructed and evaluated. A lamp LED with an enhanced emission spectrum and a band pass filter was used as the excitation light source. Refractive index matching fluid (RIMF) was used in the detection cell to reduce scattering light and the noise level. The limit of detection (LOD) for fluorescein was 1.5 nM (SNR = 3). The system exhibited linear responses in the range of 1×10^{-8} to 5×10^{-6} M ($R = 0.999$). Application of the lamp LED-FD for the analysis of FITC-labeled *ephedra herb* extract by capillary electrophoresis was demonstrated.

1. Introduction

Fluorescence detection has been one of the most sensitive and selective detection schemes available for capillary flow systems [1–6]. Light-emitting diode (LED) has the advantages including long lifetime, high stability, small in size, low cost, and commercially available at wavelengths ranging from near-UV to near-IR regions, and has been used in fluorescence detections. Bruno et al. [7] presented a LED induced fluorescence detector (LED-FD) with pigtailing approach using a green LED as excitation source. Hillebrand et al. [8] reported a LED-FD in CE using a pulsed mode-operating ultraviolet LED. Our group has developed a series of LED-FD with different structures using a high-bright blue LED [9–11]. However, the sensitivity of the detector was limited mainly by the low power dissipations of the LED, viz. low excitation light intensity.

In the present work, a miniaturized LED-FD was built using a lamp LED instead of a high-bright LED (HB LED). The lamp LED had 10-fold power dissipations than that of HB LED, and showed enhanced emission spectrum and better transmittance through the excitation filter, resulting in higher excitation light intensity. Refractive index matching fluid (RIMF) was utilized in the detection cell to reduce scattering light and the noise level. The size of the whole detector body was 6 cm × 15 cm × 7 cm ($W \times L \times H$), which was about 4% of the volume of conventional fluorometer or laser induced fluorescence (LIF) system. The performance of the detector was evaluated by both flow injection analysis of standards and CE analysis of *ephedra herb* extract.

2. Experimental

2.1. Apparatus and reagents

A thermometer, consisting of a Pt-100 element (Juchheim, Germany) and a Model REX-C100 temperature controller (RKC Instrument, Japan) was used for the temperature measurement of the lamp LED.

A spectrometer (USB4000, Ocean Optics, USA) was used for the spectral measurement of the LEDs.

A P230 HPLC pump (Elite Co. Ltd., China) was used to carry out flow injection analysis. Injection was performed using a six-port injection valve (Valco Instruments, USA) with a 2-μL loop.

A homemade CE system, consisting of a fused silica capillary (45 cm × 100 μm i.d., 35 cm to the detector) and a high-voltage power supply (0–30 kV, Dongwen, China), was used to evaluate the detector. The working electrolyte for CE separation was $Na_2B_4O_7$ buffer (10 mM or 100 mM, pH 9.5). Sample injection was carried out by hydrodynamic technique.

Ephedra herb (purchased from a local Chinese medicine store) was extracted and labeled by fluorescein isothiocyanate (FITC) (Molecular probes, USA) according to Ref. [8]; fluorescein was obtained from Sigma, USA. All the reagents used were of reagent grade, and deionized (DI) water was used throughout.

* Corresponding author. Tel.: +86 411 84379570; fax: +86 411 84379590.
E-mail address: guan_yafeng@yahoo.com.cn (Y. Guan).

0039-9140/$ – see front matter © 2008 Elsevier B.V. All rights reserved.
doi:10.1016/j.talanta.2008.03.027

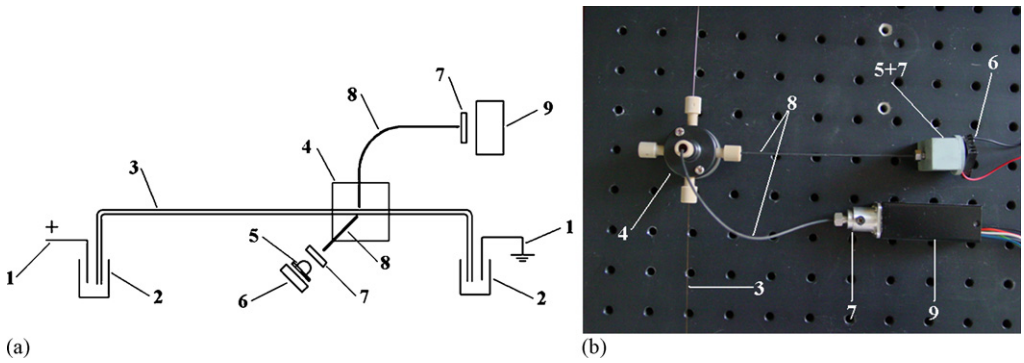

Fig. 1. Schematic diagram of lamp LED-FD system (a) and the picture of the optical system (b). 1, platinum electrode; 2, reservoir; 3, fused-silica capillary; 4, manifold; 5, lamp LED; 6, cooling fin; 7, filter; 8, optical fiber; and 9, photomultiplier tube.

2.2. Optical systems

The optical arrangement of LED-FD for CE is shown in Fig. 1. A lamp LED (volume, Ø5.5 mm × 5 mm; power dissipation, 150 mA × 3.05 V; Shifeng Corp., China) was used as the excitation source. A previously reported HB LED (volume, Ø5 mm × 9 mm; power dissipation, 15 mA × 3.05 V; Shifeng Corp., China) was used as comparison light source. An optical fiber (OF) (core 0.5 mm, cladding 0.6 mm, Chunhui Inc., China) was used to carry the excitation light to the detection window. Interference filter (BP 470 nm; FWHM 30 nm; Huibo Optical Corp. Ltd., China) was inserted between the LED and the OF to eliminate the interference of long wavelength light from LED. A commercial 5-port manifold (Upchurch Scientific, USA) was used to fix the OFs and the capillary. Part of the polyimide coating (4 mm in length) on the capillary was burned off with an electrical coiled resistance to form a detection window. Fluorescence was collected with a right-angle geometry by another OF, passed through an interference filter (BP 530 nm; FWHM 30 nm; Huibo Optical Corp. Ltd., China), then detected by a metal packaged mini PMT (H5784, Hamamatsu, Japan). Both ends of the OFs were polished by the vendor. Teflon tubings were used to seal the OFs and capillaries. The precision of the manifold ensured the optical alignment among the capillaries and OFs. The size of the whole detector body was 6 cm × 15 cm × 7 cm ($W \times L \times H$).

3. Results and discussion

3.1. Heat-dissipation of the lamp LED

The excess heat of LED can deteriorate the light stability and the lifetime of LED. The surface temperature of the metal disk on the back of the lamp LED raised rapidly as power turned on, and reached 75 °C in 5 min. A cooling fin (25 mm × 15 mm × 7 mm) was attached to the base of the lamp LED with addition of thermal conductive silicon grease. Thermal equilibrium was reached in 15 min, and the temperature of the LED stayed at 42 °C.

3.2. Comparison between the HB LED and the lamp LED

Spectrometer was used to measure the emission spectrum of the LEDs, as shown in Fig. 2 (curve 1). The emission spectrum of the HB LED yielded the typical curve of Gaussian distribution at λ_{max} = 465 nm. The emission spectrum of the lamp LED was much more complex, with a peak wavelength of λ_{max} = 469 nm as well as enhanced peaks at 461, 479 and 485 nm. The emission light intensity from lamp LED was much higher than that of HB LED.

The two LEDs were used as excitation source and coupled to OF without excitation filter, while keeping other structures the same. The two systems were evaluated by flow injection analysis of 0.5 μM fluorescein, and the chromatograms were shown in Fig. 3. Compared with the HB LED, the lamp LED-FD gave an enhancement of 1.6-fold on signals and 1.1-fold on noise levels, resulting 1.4-fold enhancement on signal-to-noise ratio (SNR). The detailed data was listed in Table 1.

3.3. Effect of the excitation filter

Compared with lasers, LED is a polychromatic source. The relative broad emission spectrum of LED often overlaps with fluorescence spectrum, especially for fluorophores that possessed smaller Stokes' shift. Scattering light from the LED which coincides with the detection wavelength will produce high background sig-

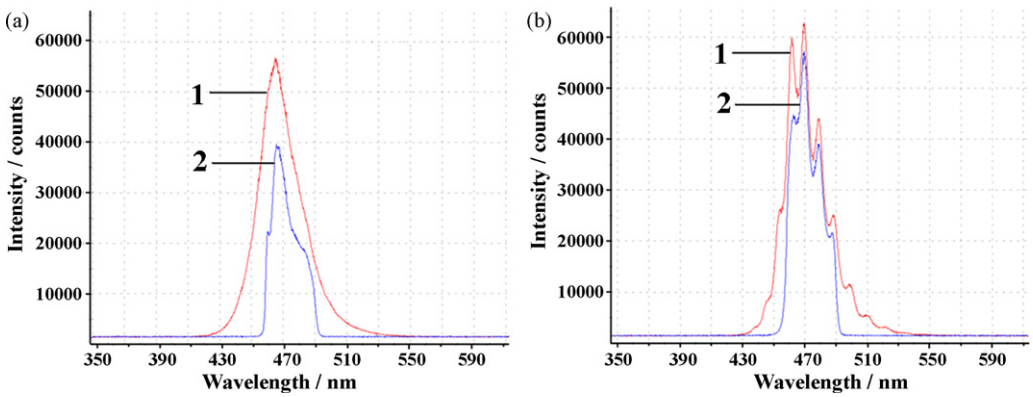

Fig. 2. Emission spectrum of LEDs and the effect of the filter on HB LED (a) and lamp LED (b). 1, without filter and 2, with filter.

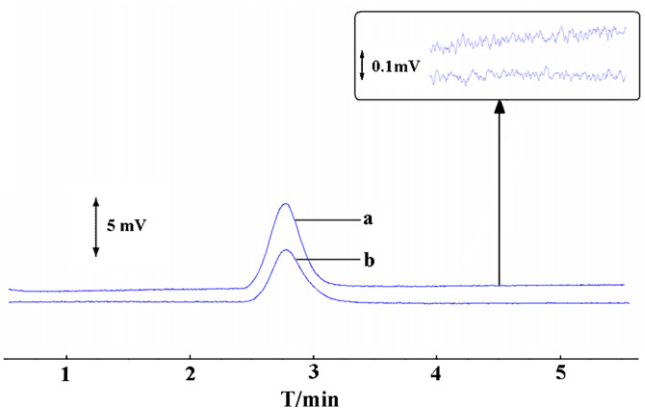

Fig. 3. Comparison between the HB LED and the lamp LED as light sources. a, lamp LED and b, HB LED. Flow injection analysis: sample, 0.5 μM fluorescein solution; flow rate, 10 μL/min; and the PMT voltage, 320 V.

nals and noise [12]. It is essential to use filter at the excitation axis to exclude longer-wavelength LED light. However, the use of excitation filter also reduces the flux of excitation light that reaches the sample; the reduction is determined by the transmittance of light source through the filter. Fig. 2 showed the emission spectrum of LEDs with/without filter. The emission spectrums of the two LEDs spreaded from 420 to 560 nm, and were limited in the range of 450–495 nm when the bandpass filter was applied. We also found that the two LEDs showed different transmittance at the maximum wavelength through the same filter, due to the different spectral characteristics of the two LEDs'. Compared with the Gaussian emission spectrum of HB LED, the emission spectrum of lamp LED had steeper edges, which was more compatible with the rectangular profile of cut-off edges of the bandpass filter. This is beneficial to the integration transmittance (corresponding to the area ratio of curve 2 to curve 1 in Fig. 2) because more flux of the excitation light can be transmitted in the restricted wavelength window. The enhanced peaks (461, 479 and 485 nm) of the lamp LED also contributed to the enhancement of the integration transmittance. The integration transmittance of the lamp LED and the HB LED was ~60% and ~40%, respectively (data acquired by the spectrometer).

Table 1
The performance of the different optical setup

Arrangement of the detector	Signal (mV)	Noise level (mV)	SNR
LED	4.5	0.07	64
Lamp LED	7.2	0.08	90
LED + filter	15.7	0.07	225
Lamp LED + filter	42.3	0.09	470
LED + filter + RIMF	14.1	0.03	469
Lamp LED + filter + RIMF	29.3	0.03	977

Data acquired by flow injection of 0.5 μM fluorescein. The PMT voltage was set at 320 V for the without filter arrangement and 415 V for the filter-used arrangement.

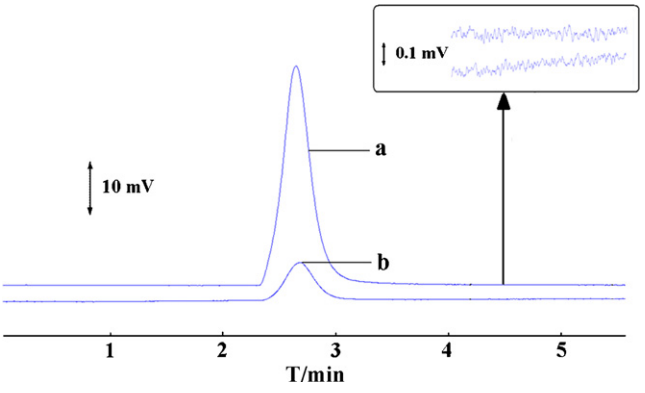

Fig. 4. Chromatogram of the lamp LED-FD with filter (a) and without filter (b) at the excitation axis. PMT voltage was set at 415 V; other conditions were the same as in Fig. 3.

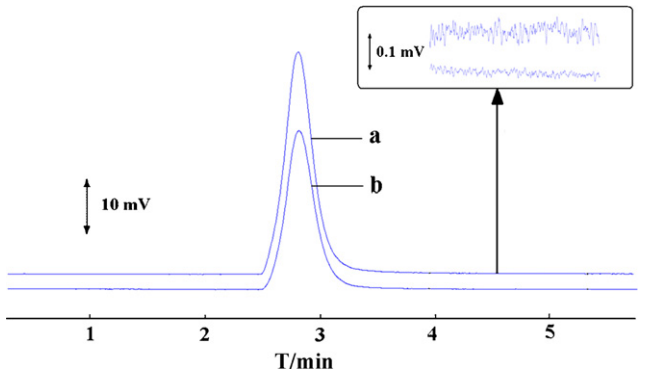

Fig. 5. Chromatogram of the lamp LED-FD without RIMF (a) and with RIMF (b). The conditions were the same as in Fig. 4.

The effect of the excitation filter on signal, noise and SNR was shown in Table 1. The SNR was improved by 3.5-fold for HB LED and 5.2-fold for lamp LED, respectively. The excitation filter played more important role on lamp LED than on HB LED, due to the transmittance discrepancy. Chromatogram of the lamp LED-FD with/without filter at the excitation axis was shown in Fig. 4.

3.4. Effect of the RIMF

In on-column detections, both excitation light and fluorescence travel through three propagating medias, i.e. fused silica OF (RI = 1.467), air (RI = 1.000) and fused silica capillary wall (RI = 1.467). The RI changes abruptly in air and results in optical interfaces. Scattering by total and multiple reflections on the capillary wall leads to high background noise and poor sensitivity [11].

To eliminate the optical interfaces, RIMF was used to fill the gap between the end of OFs and the detection window on the capillary. Cyclohexane was chosen as the RIMF considering its RI (1.426 at 20 °C) and viscosity (0.97 mPa s at 20 °C). The effect of RIMF was shown in Table 1. The signal was reduced to 2/3 while the noise level was reduced to 1/3, compared with non-RIMF mode for both HB LED and lamp LED. The SNR was then enhanced twofold. Chromatogram of the lamp LED-FD with/without RIMF in the detection cell was shown in Fig. 5.

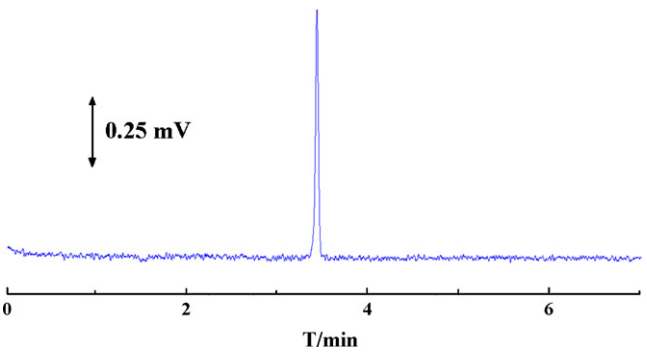

Fig. 6. Electropherogram of fluorescein solution. Siphon injection, 10 cm × 10 s; separation voltage, 20 kV; buffer solution, $Na_2B_4O_7$ buffer (20 mM)/acetonitrile (15/4); and sample concentration, 15 nM.

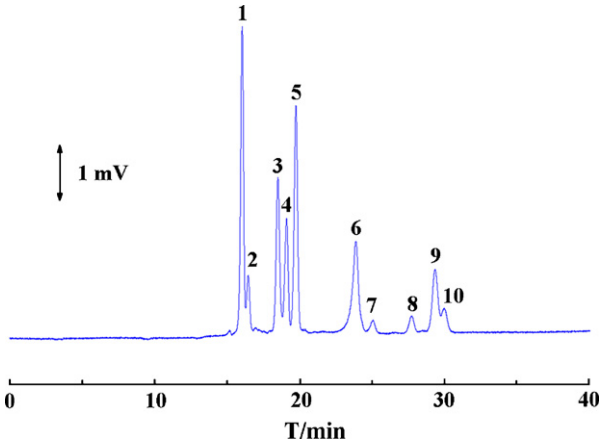

Fig. 7. Electropherogram of FITC-labeled *ephedra herb* extract. Siphon injection, 10 cm × 10 s; separation voltage, 5 kV; buffer solution, $Na_2B_4O_7$ buffer (100 mM); sample concentration, 0.3 μM; peak identification: 1–4 and 6–10, FITC-labeled *ephedra herb* extract; and 5, excess FITC.

3.5. System characteristics

The performance of the lamp LED-FD was evaluated in terms of the reproducibility of peak heights, response linearity and the limit of detection (LOD) by flow injection method. The error of reproducibility was within 2.0% R.S.D. on peak height in a six-repeated injection of fluorescein solution. The system exhibited linear response in the concentration range of 1.0×10^{-8} to 500×10^{-8} M ($R = 0.999$). Fig. 6 showed the electropherogram obtained from an analysis of 15 nM fluorescein solution. From this electropherogram, the LOD of fluorescein (SNR = 3) was estimated to be 1.5 nM, which was better than our previous report (4 nM) [11]. Though the LOD value was much higher than those achieved by LIF detection, this detector has the advantages including simple in structure, easy to use and maintenance, no moving parts or adjustments, reasonable sensitivity and low cost for ordinary application in CE and μLC.

To show the utility of this detector in CE, a representative application was demonstrated. Fig. 7 showed the analysis of FITC-labeled *ephedra herb* extract. To improve the separation resolution, running buffer with higher concentration was used. We did not make identification of the peaks in the electropherogram due to lack of standard ephedrine and pseudoephedrine sample. Other applications such as peptides and amino acids analysis were demonstrated in our previous work. These results showed that this lamp LED-FD is suitable for routine analysis of some drugs and biomolecules.

4. Conclusions

We have developed a miniaturized LED-FD for capillary flow systems. A lamp LED with enhanced emission spectrum and better transmittance though the excitation filter was used as the light source. The sensitivity was 2.7-fold better than that of our previous report. The detector contains no moving parts and needs no adjustments during operation, and was readily applied to flow injection analysis, capillary electrophoresis and capillary liquid chromatography.

Acknowledgements

This work was supported by the National Natural Science Foundation of China (Grant no.: 20227501), the Ministry of Science and Technology of China (Grant no.: 2007AA09Z134007), and Knowledge Innovation Program on Scientific Instrumentation (Chinese Academy of Sciences, Grant no.: YZ0605).

References

[1] K. Tsunoda, T. Yagasaki, S. Aizawa, H. Akaiwa, K. Satake, Anal. Sci. 13 (1997) 757.
[2] S.L. Wang, X.J. Huang, Z.L. Fang, P.K. Dasgupta, Anal. Chem. 73 (2001) 4545.
[3] X.W. Chen, J.H. Wang, Talanta 69 (2006) 681.
[4] X.W. Chen, Z.R. Xu, B.Y. Qu, Y.F. Wu, J. Zhou, H.D. Zhang, J. Fang, J.H. Wang, Anal. Bioanal. Chem. 388 (2007) 157.
[5] N. Vachirapatama, M. Macka, P.R. Haddad, Anal. Bioanal. Chem. 374 (2002) 1082.
[6] X.W. Chen, W.X. Wang, J.H. Wang, Analyst 130 (2005) 1240.
[7] A.E. Bruno, F. Maystre, B. Krattiger, P. Nussbaum, E. Gassmann, Trends Anal. Chem. 13 (1994) 190.
[8] S. Hillebrand, J.R. Schoffen, M. Mandaji, C. Termignoni, H.P.H. Grieneisen, T.B.L. Kist, Electrophoresis 23 (2002) 2445.
[9] B.C. Yang, H.Z. Tian, J. Xu, Y.F. Guan, Talanta 69 (2006) 996.
[10] J. Xu, B.C. Yang, H.Z. Tian, Y.F. Guan, Anal. Bioanal. Chem. 384 (2006) 1590.
[11] J. Xu, S.H. Chen, Y. Xiong, B.C. Yang, Y.F. Guan, Talanta 75 (2008) 885.
[12] E.P. de Jong, C.A. Lucy, Anal. Chim. Acta 546 (2005) 37.

Available online at www.sciencedirect.com
ScienceDirect
Talanta 76 (2008) 235–240
Talanta
www.elsevier.com/locate/talanta

Spectral study on the interaction of cryptophane-A and neutral molecules CH_nCl_{4-n} ($n = 0, 1, 2$)

Caihong Zhang [a], Weili Shen [a], Guangming Wen [a], Jianbin Chao [a], Liping Qin [a], Shaomin Shuang [a], Chuan Dong [a,*], Martin M.F. Choi [b,**]

[a] *Center of Environmental Science and Engineering Research, Shanxi University, Taiyuan 030006, PR China*
[b] *Department of Chemistry, Hong Kong Baptist University, Kowloon Tong, Hong Kong SAR, PR China*

Received 11 August 2007; received in revised form 13 November 2007; accepted 16 November 2007
Available online 24 November 2007

Abstract

Cryptophane-A was synthesized from vanillin by a three-step method and its spectroscopic properties in different organic solvents were determined. Two absorption bands at about 240–250 and 280–290 nm were observed for cryptophane-A. A fluorescence emission peak was obtained at 320–330 nm using a solution of $\sim 10^{-5}$ M cryptophane-A. The interaction of cryptophane-A with chlorinated compounds CH_nCl_{4-n} ($n = 0, 1, 2$) in dioxane and ethyl acetate solvents were studied in detail by fluorescence spectroscopy, respectively. The results show that cryptophane-A is well suited for inclusion of CH_2Cl_2 to form a stable 1:1 complex and the binding constant was estimated to be $19 \pm 2\,M^{-1}$. These results were also confirmed by ^1H NMR and CPK models. Larger similar molecules such as $CHCl_3$ and CCl_4 are unable to enter the cavity of cryptophane-A because of their bigger sizes. However, the fluorescence emission of cryptophane-A can be efficiently quenched by $CHCl_3$ and CCl_4, following the Stern–Volmer relationship.

Keywords: Cryptophane-A; Fluorescence; Inclusion complex; Interaction

1. Introduction

A variety of natural and synthetic molecules can reversibly bind with small neutral species to form inclusion complexes. Such complexes are generally characterized by weak but specific non-covalent interactions between host and guest and have been the subject of considerable work covering a wide range of possible and realized applications, including drug formulation and delivery, molecular recognition, separation and storage, and catalysis [1–9]. Up till now, the design of hosts capable of binding neutral substrates, especially the smaller aliphatic molecules, is still a challenge for researchers [10].

Cryptophanes consist of two rigid cone-shaped units (cyclotriveratrylene) linked by three O–Z–O bridges as shown in Scheme 1. The specific molecular recognition is mainly determined by the internal volume of the cavity which in turn is controlled by the Z function, and external properties such as binding and tensioactivity related to the X and Y groups. The cryptophane family can complex with neutral molecules like halogenomethanes in organic solvents and water. Cryptophanes are molecular hosts of primary importance for the transport of apolar guests as well as for understanding the interactions between a host and a neutral guest in solution [10a]. The most commonly studied hosts are cryptophane-A, cryptophane-C, cryptophane-E, and their derivatives. Collet and co-workers have shown by NMR that gases such as methane (CH_4) and xenon can be trapped by cryptophane-A to form complexes in organic solvents [11–13]. Similar inclusion complexes of other cryptophanes, such as cryptophane-C–CHFClBr, cryptophane-E–$CHCl_3$, cryptophane-E–butane and cryptophane-E–N^+Me_4, have also been determined in organic solvents by NMR [14–31]. Previous NMR studies of cryptophane/halohydrocarbon complexes in organic solutions have provided detailed characterization. Generally speaking, cryptophane complexes are reversibly formed and their stabilities (i.e., the magnitudes of their binding constants) depend on a variety of factors. Other parameters, which do not directly

* Corresponding author. Tel.: +86 351 7018613; fax: +86 351 7018613.
** Corresponding author. Tel.: +86 852 3411 7839; fax: +86 852 3411 7348.
E-mail addresses: dc@sxu.edu.cn (C. Dong), mfchoi@hkbu.edu.hk (M.M.F. Choi).

0039-9140/$ – see front matter © 2007 Elsevier B.V. All rights reserved.
doi:10.1016/j.talanta.2007.11.047

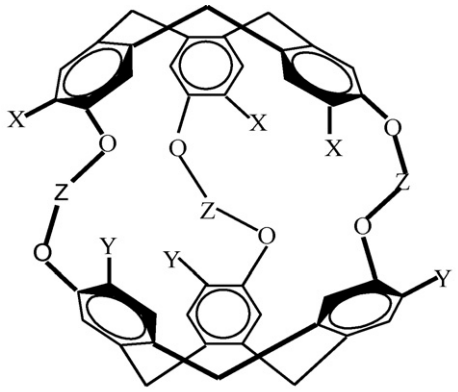

Cryptophane-A x,y=OCH_3 Z=$(CH_2)_2$
Cryptophane-C x=H, y=OCH_3 Z=$(CH_2)_2$
Cryptophane-E x,y=OCH_3 Z=$(CH_2)_3$

Scheme 1. The chemical structure of cryptophanes.

involve cryptophane such as solvent–guest interaction, may be significant in the formation of cryptophane host–guest complexes. Even so, experimental data support the idea that host–guest and host–solvent interactions are dominant. For instance, it is likely that the host–solvent interactions will play a major role in aqueous solvents. Moreover, experiments indicate that the complexation and release of guest molecules is comparatively slow (barriers in the range of 10–17 kcal/mol). For some guests, their static structures sterically hinder their passage through a cryptophane pore. This implies that the pore size of the host molecules is crucial to the binding kinetics of guest molecules. Recently, Cavagnat et al. have used Raman microspectrometry in conjunction with X-ray diffraction to study the inclusion complexes of chloroform and several cryptophanes (A, E, and bis-) in order to investigate the feasibility of that technique for studying host–guest systems [29]. In addition, inclusion complexes of methane and cryptophanes (A and E) were recently studied via evanescent wave optical fiber as well as to detect methane [32]. Related optical activity of cryptophanes has been investigated by circular dichroism spectra [33]. To our knowledge, there are very few reports on the interactions of crytophanes and halogenated compounds based on fluorescence and absorption spectroscopies.

In this article, we report the fluorescence and UV spectral studies of cryptophane-A and its complexes in organic solvents. The fundamental spectroscopic characteristics of cryptophane-A in different organic solvents, the inclusion complex of cryptophane-A and CH_2Cl_2, association constants and interaction of cryptophane-A with $CHCl_3$ and CCl_4 have been investigated in detail. Our results are consistent with the NMR spectroscopic data. These fundamental data and the spectral method should provide valuable information for understanding the structure, dynamics, and ordering behavior of host–guest inclusion complexes.

2. Experimental

2.1. Materials

The chemicals and reagents for preparation of cryptophane-A were used as received unless otherwise stated. Acetonitrile, cyclohexane, dibromoethane, dichloromethane (CH_2Cl_2), diethyl ether, dioxane, ethanol, ethyl acetate, formic acid, methanol, sodium borohydride ($NaBH_4$), tetrachloromethane (CCl_4), trichloromethane ($CHCl_3$), and vanillin were purchased from Beijing Chemical Plant (Beijing, China).

2.2. Synthesis of cryptophane-A

Cryptophane-A was synthesized from vanillin by a three-step method according to a previous report [32]. The ^{1}HNMR ($CDCl_3$) data of cryptophane-A were obtained and they are consistent with the literature values [32]. The compound was pretreated according to the standard methods used.

2.3. Instrument

UV absorption spectra were recorded on a Shimadzu UV-265 spectrophotometer (Tokyo, Japan). Fluorescence spectra were taken on a Hitachi F4500 spectrofluorometer (Tokyo, Japan). Both excitation and emission slits were set at 5 nm. All the experiments are carried out at 20 ± 1 °C. ^{1}H NMR spectra were done on a Bruker Avance DRX 300 MHz nuclear magnetic resonance spectrometer (Fällanden, Switzerland).

Table 1
The absorption and fluorescence maxima of cryptophane-A in various organic solvents

Solvent	Cyclohexane	Dioxane	Diethyl ether	Ethyl acetate	Acetonitrile
λ_{abs} (nm)	245, 283	293	245, 282	255, 286	246, 286
λ_{ex} (nm)	292	300	291	292	294
λ_{em} (nm)	323	331	324	322	320
Solvent	CH_2Cl_2	$CHCl_3$	CCl_4	Methanol	Ethanol
λ_{abs} (nm)	248, 285	250, 285	288	245, 282	247, 285
λ_{ex} (nm)	292	–	–	292	292
λ_{em} (nm)	322	–	–	320	322

λ_{abs} (nm): absorption peak maximum, λ_{ex} (nm): excitation maximum, λ_{em} (nm): emission maximum.

3. Results and discussion

3.1. Absorption and fluorescence excitation and emission spectral characteristics

The UV–vis absorption and fluorescence emission spectral maxima of cryptophane-A in different solvents including cyclohexane, dioxane, ethyl acetate, diethyl ether, CH_2Cl_2, $CHCl_3$, CCl_4, methanol, ethanol and acetonitrile were taken and shown in Table 1. Cryptophane-A has two absorption peaks at ~240–250 and 280–290 nm. The excitation and emission maxima are at ~290–295 and 320–330 nm when the concentration range is $\sim 10^{-5}$ M. The absorption, excitation and emission maxima of cryptophane-A in the solvents did not vary much with the change in the solvent polarity (except in dioxane). Cryptophane-A has a rigid framework with three "–OCH_2CH_2O–" bridges and its structure shows similarity with dioxane. The obvious shift of cryptophane-A in dioxane is possibly attributed to the dipole–dipole interaction of its excited state with dioxane. However, cryptophane-A does not show fluorescence in $CHCl_3$ and CCl_4 and this will be discussed in the later section.

3.2. Inclusion complex of cryptophane-A and CH_2Cl_2

Since cryptophane-A can form inclusion complexes with various halogenomethanes, the interaction of cryptophane-A with CH_2Cl_2, $CHCl_3$, and CCl_4 in solvents such as dioxane and ethyl acetate was investigated. Diethyl ether, methanol and acetonitrile were not chosen as the solvent media due to their strong competition with the guests, halogenomethanes. The fluorescence quenching effect of CH_2Cl_2 on cryptophane-A (2.013×10^{-5} M) in dioxane is depicted in Fig. 1. Cryptophane-A displayed strong fluorescence with an emission maximum at 330 nm when was excited at 295 nm. The fluorescence was efficiently quenched and the emission spectrum was also slightly hypsochromic shifted on the addition of CH_2Cl_2. Similar results were obtained in ethyl acetate solvent (not shown). This can be explained by the reason that an inclusion complex between cryptophane-A and CH_2Cl_2 has been formed which can affect the fluorescence yield and spectral characteristics of cryptophane-A.

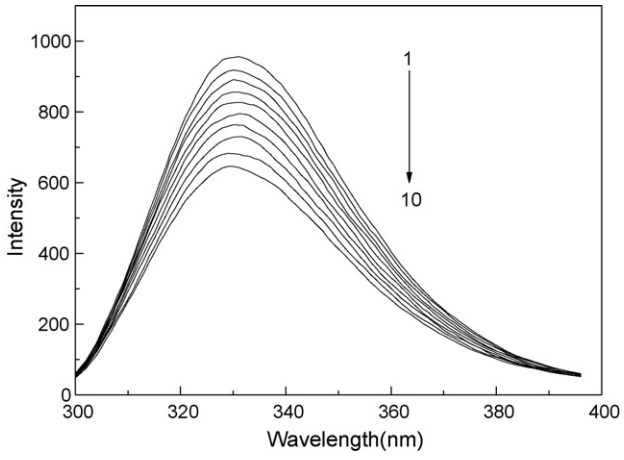

Fig. 1. Fluorescence quenching effect of CH_2Cl_2 on the emission of 2.013×10^{-5} M of cryptophane-A in dioxane. 1: 0; 2: 0.007130; 3: 0.01425; 4: 0.02557; 5: 0.04384; 6: 0.08037; 7: 0.1534; 8: 0.2630; 9: 0.4091; and 10: 0.5918 M of CH_2Cl_2. Excitation wavelength is 295 nm.

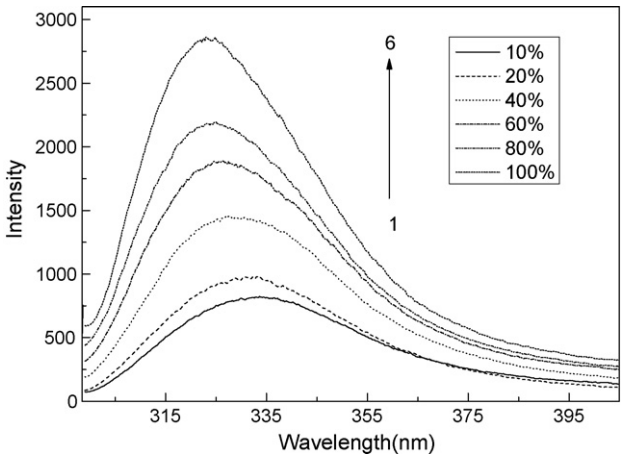

Fig. 2. Fluorescence spectra of 6.04×10^{-6} M cryptophane-A in solvent mixtures of CH_2Cl_2/dioxane. 1: 10; 2: 20; 3: 40; 4: 60; 5: 80; and 6: 100 (%, v/v) of CH_2Cl_2 when excited at 295 nm.

In order to study the CH_2Cl_2 solvent effect, the behavior of cryptophane-A in dioxane/CH_2Cl_2 mixtures was determined. Same concentrations of cryptophane-A were prepared in various CH_2Cl_2 contents of dioxane/CH_2Cl_2 mixtures. The emission spectra of cryptophane-A in these different binary solvent mixtures are displayed in Fig. 2. The fluorescence emission band is hypsochromically shifted from 331 to 322 nm with the increase of CH_2Cl_2 in the solvent mixtures. Cryptophane-A initially forms complex with CH_2Cl_2; afterwards, the excess CH_2Cl_2 and dioxane solvent molecules then solvate the cryptophane-A–CH_2Cl_2 complex. The fluorescence intensity and emissive shift of the cryptophane-A–CH_2Cl_2 complex is sensitive to the excess CH_2Cl_2 content in the binary solvent mixture. The emission intensity increases and the emission band blue-shifts when the solvent effect of CH_2Cl_2 increases.

3.3. Binding constants

The binding constant (K) is an important parameter, indicating the inclusion capacity of the host–guest complex. The binding constants can be estimated by the least-squares fit to the experimental data obtained from the fluorescence titrations [34] as

$$\Delta F = \frac{1}{2}\left\{\alpha\left([H]_0 + [G]_0 + \frac{1}{K}\right) - \sqrt{\partial^2\left([H]_0 + [G]_0 + \frac{1}{K}\right)^2 - 4[H]_0[G]_0\alpha^2}\right\}$$

where $[H]_0$ and $[G]_0$ are the initial concentrations of host cryptophane-A and guest CH_2Cl_2, respectively. ΔF denotes the change of the fluorescence intensity of cyptophane-A with

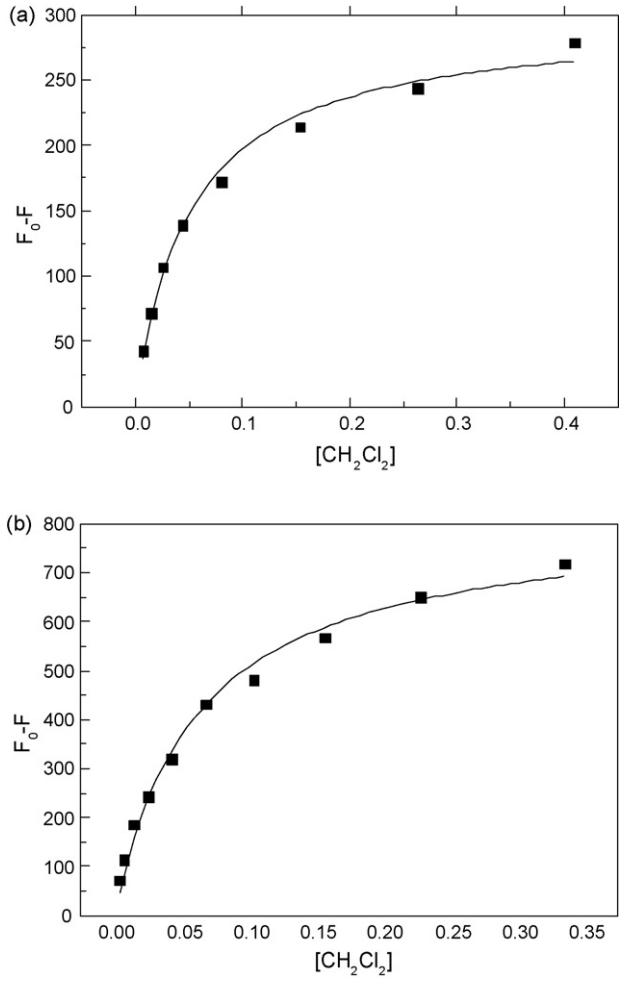

Fig. 3. Nonlinear curve fits for the cryptophane-A–CH_2Cl_2 complex in (a) dioxane and (b) ethyl acetate.

the addition of CH_2Cl_2. α is a sensitive factor of the structure change of the complex cyptophane-A–CH_2Cl_2 at the interactive course. Fig. 3 shows the nonlinear curve fit of cryptophane-A–CH_2Cl_2 in (a) dioxane and (b) ethyl acetate solvents, respectively. The binding constants were estimated to be 19 ± 2 and $16 \pm 2\,M^{-1}$ in dioxane and ethyl acetate solvents, respectively. The linear correlation coefficients, r were 0.9941 and 0.9944, respectively, inferring the formation of 1:1 host–guest inclusion complex. Comparatively, the binding constants of the complexes of chlorofluorocarbons (CHF_2Cl and CF_2Cl_2) and cyptophane-A by ^{1}HNMR in $(CDCl_2)_2$ were 12 ± 3 and $13 \pm 4\,M^{-1}$, respectively [11]. CPK model and X-ray confirmed that cryptophane-A–CH_4 and cryptophane-C–$CHCl_3$ were 1:1 host–guest systems [11,14]. Our result of 1:1 host–guest inclusion complex of cyptophane-A–CH_2Cl_2 shows similarity with CHF_2Cl and CF_2Cl_2.

3.4. ^{1}H NMR

The lipophilicity of the cryptophane family favors the inclusion of neutral molecules with complementary size and shape to form stable 1:1 complexes. The cryptophane-A–CH_2Cl_2 inclusion complex by the ^{1}H NMR spectroscopy is displayed in Fig. 4. On addition of one equivalent CH_2Cl_2 to cryptophane-A in $CDCl_3$ solution at 298 K, a peak was detected at the expected position of 5.30 ppm, corresponding to free CH_2Cl_2. When more than five equivalents of guest (CH_2Cl_2) were added, a new peak at 0.91 ppm was obtained. The large upfield shift and broadening effect of the CH_2Cl_2 complex peak indicated that CH_2Cl_2 was reversibly bound and there was a fast exchange between the free and complex molecules [11,14]. Our result is consistent with the reported values for halogenomethanes of free and complex peaks: cryptophane-A–CH_4 (free: 0.2 ppm and complex: −4.0 ppm in $(CDCl_2)_2$ at 300 K), cryptophane-C–CH_2Cl_2 (free: 5.25 ppm and complex: 0.74 ppm in $CDCl_3$ at 300 K), and cryptophane-E–$CHCl_3$ (free: 7.23 ppm and complex: 2.38 ppm in $(CDCl_2)_2$ at 300 K) [3,11,14]. Our work indicates that the host cryptophane-A can reversibly bind with the guest CH_2Cl_2.

3.5. Fluorescence quenching of $CHCl_3$ and CCl_4 on cryptophane-A

The fluorescence quenching of $CHCl_3$ and CCl_4 on cryptophane-A was studied in dioxane and ethyl acetate solvents, respectively. It is found that the interactions of $CHCl_3$ or CCl_4 with cryptophane-A do not fit in the nonlinear equation (*vide supra*), indicating that the interactions of cryptophane-

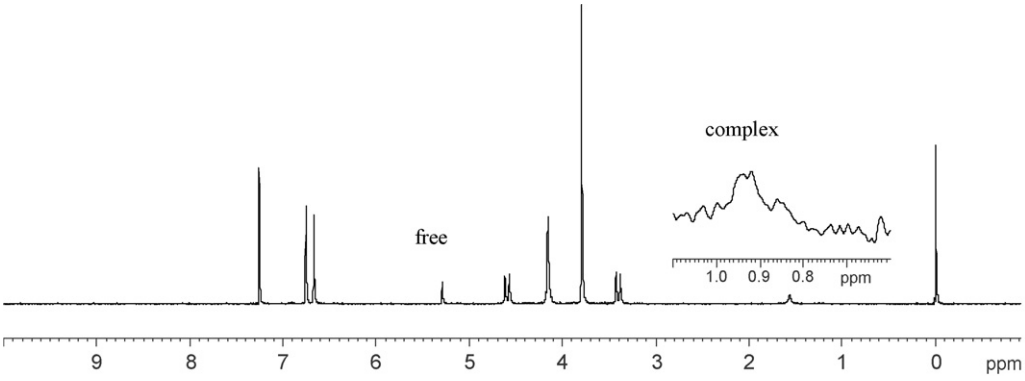

Fig. 4. H^1 NMR spectrum of a 10^{-3} M solution of cryptophane-A with five equivalents CH_2Cl_2 in $CDCl_3$ at room temperature.

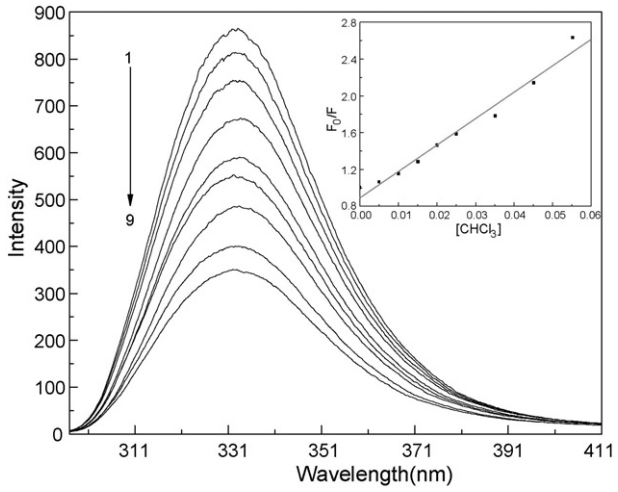

Fig. 5. Fluorescence quenching effect of $CHCl_3$ on the emission of 2.013×10^{-5} M of cryptophane-A in dioxane. 1: 0; 2: 0.005030; 3: 0.01005; 4: 0.01508; 5: 0.02010; 6: 0.02510; 7: 0.03518; 8: 0.04520; and 9: 0.05530 M of $CHCl_3$. Excitation wavelength is 295 nm.

A with $CHCl_3$ or CCl_4 are different from that with CH_2Cl_2. The fluorescence emission spectra of cryptophane-A at various $CHCl_3$ concentrations are shown in Fig. 5. The fluorescence intensity decreases with the increase in $CHCl_3$. Instead, the fluorescence quenching behavior fits well with the Stern–Volmer equation: $F_0/F = 1 + K_{SV}[Q]$, where F_0 and F are the fluorescence intensities in the absence and presence of $CHCl_3$ or CCl_4, respectively, K_{SV} is the Stern–Volmer constant, and $[Q]$ is the molar concentration of $CHCl_3$ or CCl_4. The Stern–Volmer plots are found to be linear and the K_{SV} and r values are displayed in Table 2. It is possible that the formation of a nonfluorescent ground state complex between cryptophane-A and $CHCl_3$ or CCl_4 molecules leads to the static quenching process [35,36]. This is supported by an experiment that no fluorescence emission was detected for cryptophane-A when it was dissolved in $CHCl_3$ or CCl_4 solution.

3.6. Effect of guest volume

The formation of cryptophane-A and guest complex is governed by many factors: effective complement of guest to host, host–guest interaction, and solvent–guest and solvent–host interactions. The latter is probably unimportant here since cryptophane-A behaves similarly in dioxane and ethyl acetate solvents. These solvents are favorable for the formation of cryptophane-A–CH_2Cl_2 complex where the guest is transferred from the solvent to the host interior, depending on the guest volume. The guest volume and the occupancy factor [11] of halogenomethanes in cryptophane-A are listed in Table 3.

Table 3
The guest volume and the occupancy factor of guest in cryptophane-A

	CH_2Cl_2	$CHCl_3$	CCl_4
V_{vdw} (Å^3)	55.6	72.2	86.8
Occupancy factor	0.68	0.89	–

The van der Waals volume of the cavity for cryptophane-A is 81.5 Å^3.

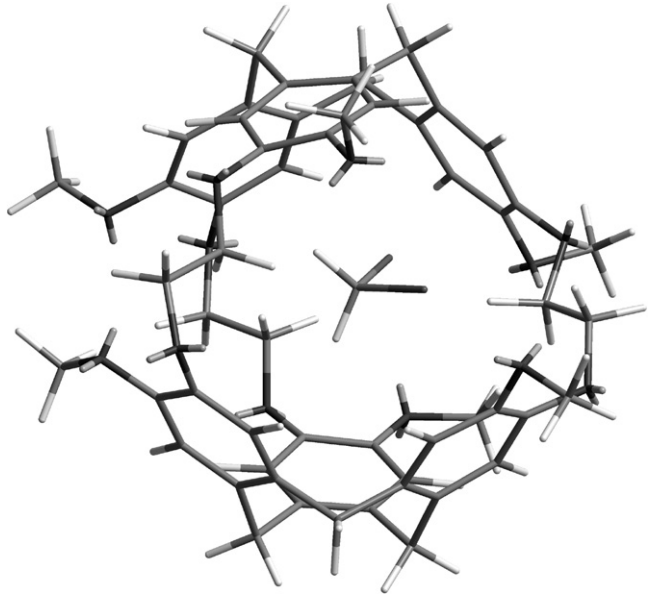

Scheme 2. The optimal structure of the cryptophane-A-CH_2Cl_2 complex simulated by computer modeling.

The occupancy factor is 0.68 for one molecule of CH_2Cl_2 in one cryptophane-A, which is quite a reasonable number for such a complex, signifying that it is neither too tight nor too loose.

In addition, the cryptophane-A–CH_2Cl_2 complex was simulated by molecular dynamic calculation (Computer Molecular Modeling System CS Chem 3D Pro 7.0, Cambridge Soft Corporation). The optimal configuration of the cryptophane-A–CH_2Cl_2 complex that has the lowest total energy is displayed in Scheme 2. This confirms that CH_2Cl_2 penetrated into the cavity of cryptophane-A to form the 1:1 host–guest system. When CH_2Cl_2 is replaced by $CHCl_3$ or CCl_4, the formation of inclusion complexes is difficult as shown by the fluorescence and ^{1}H NMR data because these molecules have larger guest volumes. These findings are also supported by the CPK model which shows that the six –OCH_3 groups of the host obstruct the windows so that the $CHCl_3$ or CCl_4 molecules cannot enter the cavity of cryptophane-A [3].

Table 2
The K_{SV} and the correlation coefficient r of cryptophane-A with $CHCl_3$ and CCl_4

Quencher (solvent)	$CHCl_3$ (dioxane)	$CHCl_3$ (ethyl acetate)	CCl_4 (dioxane)	CCl_4 (ethyl acetate)
K_{SV}	26.61	41.15	25.33	72.16
r	0.996	0.998	0.998	0.999

4. Conclusion

In summary, cryptophane-A is an aliphatic fluorescence host molecule. The properties of host and its complexes can be studied using molecular spectral methods. Our experimental results demonstrate that the formation of cryptophane-A–CH_2Cl_2 inclusion complex is governed by the good size matching of the guest with the cryptophane-A cavity. Solvents including dioxane and ethyl acetate are favorable for CH_2Cl_2 to enter the cavity of cryptophane-A. In addition, the reactions between cryptophane-A and $CHCl_3$ or CCl_4 are possibly attributed to the formation of a nonfluorescent ground state complex between cryptophane-A and $CHCl_3$ or CCl_4 molecules.

Acknowledgements

The work described in this paper was supported by the National Nature Science Foundation Key Project (No. 50534100), the Youth Science Foundation of Shanxi Province (No. 2007021007) and the Undergraduate Foundation of Taiyuan City.

References

[1] D.J. Cram, J.M. Cram, in: J.F. Stoddart (Ed.), Container Molecules and Their Guests, RSC, Cambridge, UK, 1994.
[2] J.M. Lehn, Supramolecular Chemistry: Concepts and Perspectives, SCH, Weinheim, 1995.
[3] A. Collet, Tetrahedron 24 (1987) 5725.
[4] A. Collet, in: J.L. Atwood, J.E.D. Davies, D.D. MacNicol, F. Vogtle (Eds.), Comprehensive Supramolecular Chemistry, Pergamon Press, New York, 1996, p. 325.
[5] J. Kang, J.J. Rebek, Nature 385 (1997) 50.
[6] J.L. Atwood, L.J. Barbour, A. Jerga, B.L. Schottel, Science 298 (2002) 1000.
[7] D.M. Rudkevich, A.V. Leontiev, Aust. J. Chem. 57 (2004) 713.
[8] M.E. Davis, M.E. Brewster, Nat. Rev. Drug Discov. 3 (2004) 1023.
[9] Y.K. Agrawal, C.R. Sharma, Rev. Anal. Chem. 24 (2005) 35.
[10] R.M. Izatt, J.S. Bradshaw, Chem. Rev. 92 (1992) 1261;
(a) H.A. Fogarty, P. Berthault, T. Brotin, G. Huber, H. Desvaux, J.-P. Dutasat, J. Am. Chem. Soc. 129 (2007) 10332.
[11] L. Garel, J.P. Dutasta, A. Collet, Angew. Chem. Int. Ed. Engl. 32 (1993) 1169.
[12] T. Brotin, A. Lesage, L. Emsley, A. Collet, J. Am. Chem. Soc. 122 (2000) 1171.
[13] K. Bartik, M. Luhmer, J.P. Dutasta, A. Collet, J. Reisse, J. Am. Chem. Soc. 120 (1998) 784.
[14] J. Canceill, L. Lacombe, A. Collet, J. Chem. Soc. Chem. Commun. 3 (1987) 219.
[15] P.D. Kirchhoff, M.B. Bass, B.A. Hanks, J.M. Briggs, A. Collet, J.A. McCammon, J. Am. Chem. Soc. 118 (1996) 3237.
[16] M. Luhmer, B.M. Goodson, Y.-Q. Song, D.D. Laws, L. Kaiser, M.C. Cyrier, A. Pines, J. Am. Chem. Soc. 121 (1999) 3502.
[17] P.D. Kirchhoff, J.P. Dutasta, A. Collet, J.A. McCammon, J. Am. Chem. Soc. 121 (1999) 381.
[18] T. Brotin, T. Devic, A. Lesage, L. Emsley, J.P. Dutasta, Chem. Eur. J. 7 (2001) 1561.
[19] J. Lang, J.J. Dechter, M. Effemey, J. Kowalewski, J. Am. Chem. Soc. 123 (2001) 7852.
[20] Z. Tosner, J. Lang, D. Sandstrom, O. Petrov, J. Kowalewski, J. Phys. Chem. A 106 (2002) 8870.
[21] M. Darzac, T. Brotin, D. Bouchu, J.P. Dutasta, Chem. Commun. (2002) 48.
[22] T. Brotin, J.P. Dutasta, Eur. J. Org. Chem. (2003) 973.
[23] H. Desvaux, J.G. Huber, T. Brotin, J.P. Dutasta, P. Berthault, ChemPhysChem 4 (2003) 384.
[24] M. Marjanska, B.M. Goodson, F. Castiglione, A. Pines, J. Phys. Chem. B 107 (2003) 12558.
[25] D.N. Sears, C.J. Jameson, J. Chem. Phys. 119 (2003) 15.
[26] J.G. Huber, L. Dubois, H. Desvaux, J.P. Dutasta, T. Brotin, P. Berthault, J. Phys. Chem. A 108 (2004) 9608.
[27] L. Dubois, P. Berthault, J.G. Huber, H. Desvaux, C.R. Phys. 5 (2004) 305.
[28] M. Darzac, T. Brotin, L. Rousset-Arzel, D. Bouchu, J.P. Dutasta, New J. Chem. 28 (2004) 502.
[29] D. Cavagnat, T. Brotin, J.L. Bruneel, J.P. Dutasta, A. Thozet, M. Perrin, F. Guillaume, J. Phys. Chem. B 108 (2004) 5572.
[30] Z. Tosner, O. Petrov, S.V. Dvinskikh, J. Kowalewski, D. Sandstrom, Chem. Phys. Lett. 388 (2004) 208.
[31] O. Petrov, Z. Tosner, I. Csoregh, J. Kowalewski, D. Sandstrom, J. Phys. Chem. A 109 (2005) 4442.
[32] M. Benounis, N. Jaffrezic-Renault, J.-P. Dutasta, K. Cherif, A. Abdelghani, Sens. Actuators B 107 (2005) 32–39.
[33] J. Canceill, A. Collet, G. Gottarelli, P. Palmieri, J. Am. Chem. Soc. Chem. 109 (1987) 6454–6464.
[34] Y. Wei, X. Guo, S. Shuang, C. Dong, X. Sun, M. Wong, J. Photochem. Photobiol. B 81 (2005) 190.
[35] D.S. Biradara, J. Thipperudrappab, S.M. Hanagodimatha, J. Lumin. 126 (2007) 339.
[36] N. Celebi, M. Arık, Y. Onganer, J. Lumin. 126 (2007) 103.

Talanta 76 (2008) 246–253

Contents lists available at ScienceDirect

Talanta

journal homepage: www.elsevier.com/locate/talanta

Studies on the interaction of gallic acid with human serum albumin in membrane mimetic environments

Yaheng Zhang [b], Lijun Dong [b], Jiazhong Li [b], Xingguo Chen [a,b,*]

[a] State Key Laboratory of Applied Organic Chemistry, Lanzhou University, Lanzhou 730000, China
[b] Department of Chemistry, Lanzhou University, Lanzhou 730000, China

ARTICLE INFO

Article history:
Received 17 November 2007
Received in revised form 20 February 2008
Accepted 22 February 2008
Available online 4 March 2008

Keywords:
Microemulsion
Gallic acid
Human serum albumin
Spectrum
Binding
Molecular modeling

ABSTRACT

In this study the interaction between gallic acid and human serum albumin (HSA) in AOT/isooctane/water microemulsions was characterized for the first time using fluorescence quenching technique in combination with UV absorption spectroscopy, Fourier transform infrared (FT-IR) spectroscopy, circular dichroism (CD) spectroscopy and dynamic light scattering (DLS) technique. In water–surfactant molar ratio (ω_o) = 20 microemulsions fluorescence data revealed the presence of one binding site of gallic acid on HSA and its binding constants (K) were $(1.18 \pm 0.02) \times 10^4$, $(1.13 \pm 0.02) \times 10^4$, $(1.03 \pm 0.02) \times 10^4$, $(0.95 \pm 0.02) \times 10^4$, $(0.87 \pm 0.02) \times 10^4$ and $(0.82 \pm 0.03) \times 10^4$ M^{-1} at 282, 289, 296, 303, 310 and 317 K, respectively. The affinities in microemulsions were much higher than that in buffer solution. FT-IR and CD data suggested that the protein conformations were altered with the reductions of α-helices from 54–56% for free HSA in buffer to 40–41% for free HSA in microemulsion. After binding with gallic acid, the α-helices of HSA in microemulsion increased 2–7% for different drug–protein molar ratio. The thermodynamic functions standard enthalpy (ΔH^0) and standard entropy (ΔS^0) for the reaction were calculated to be −8.10 kJ mol^{-1} and 49.42 J mol^{-1} K^{-1}. These results indicated that gallic acid bound to HSA mainly by hydrophobic interaction and electrostatic interaction in microemulsions. In addition, the displacement experiments confirmed that gallic acid could bind to the site I of HSA, which was approved by the molecular modeling study. Furthermore, the DLS data suggested that HSA may locate at the interface of the microemulsion and gallic acid could interact with them.

1. Introduction

Microemulsions formed by surfactant molecules in hydrocarbon solvents with their polar headgroups pointing inward are simple yet interesting models of biological membranes [1,2]. The water solubilisation capacity is conventionally described in terms of the water–surfactant molar ratio ω_o ($\omega_o = [H_2O]/[S]$). The aggregates containing a large amount of water molecules (above $\omega_o = 15$) are usually called microemulsions whereas reverse micelles correspond to droplets containing a small amount of water (below $\omega_o = 15$) [3]. These systems are suitable media for processes that involve hydrophobic and hydrophilic reactants providing "microreactors" for a variety of chemical and biological reactions. These microheterogeneous systems can act as hosts for molecules such as proteins and drugs by providing them with unique microvicinity. In fact, under certain conditions, pharmaceuticals in these systems have shown enhanced structural and conformational stability and slow diffusivity [4]. Among the surfactants capable of forming microemulsions, the most widely used is sodium bis(2-ethylhexyl)sulfosuccinate (AOT). AOT microemulsion is optically transparent and the change in the system could be studied by different spectrophotometric techniques [5].

Human serum albumin (HSA) is the main protein component in blood serum with a concentration of ca. 0.63 mM. Its primary function is to maintain colloid osmotic pressure. It is a globular protein composed of a single polypeptide chain of 585 amino acid residues with a large α-helix. Its amino acid sequence contains a total of 17 disulfide bridges, one free thiol (Cys-34) and a single tryptophan (Trp-214). HSA binds strongly to many kinds of endogenous and exogenous substance and is thus the most important carrier for drugs and endogenous substances in the blood [6]. Binding of drugs to plasma proteins is an important pharmacological parameter, since very strong albumin binding diminishes the active concentration of a drug in plasma and leads to a competitive release of other drugs bound to albumin that are administered in the same time frame [7]. The subsequent increase of the concentration of the released drug may lead serious drug–drug interactions; therefore, a very high affinity to HSA is usually undesirable in potential drugs

* Corresponding author at: State Key Laboratory of Applied Organic Chemistry, Lanzhou University, Lanzhou 730000, China. Tel.: +86 931 8912763; fax: +86 931 8912582.
E-mail address: chenxg@lzu.edu.cn (X. Chen).

0039-9140/$ – see front matter © 2008 Elsevier B.V. All rights reserved.
doi:10.1016/j.talanta.2008.02.033

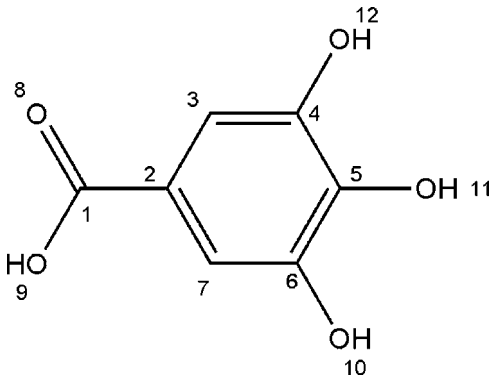

Fig. 1. The chemical structure of gallic acid.

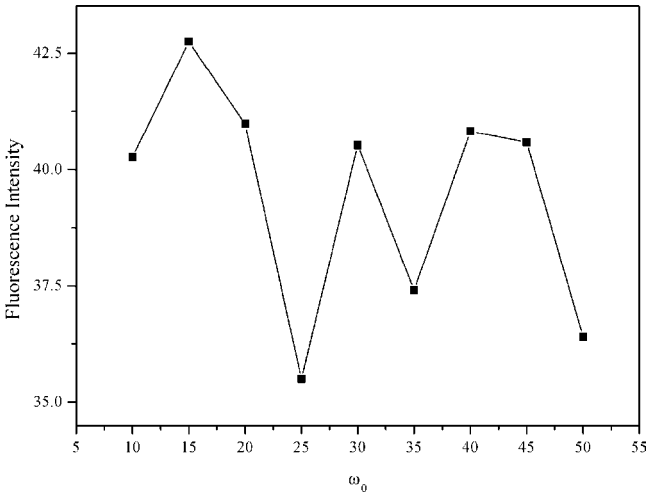

Fig. 2. The fluorescence intensity of HSA (3.0 μM) in microemulsions with different ω_o.

[8]. The studies on protein–drug interactions may provide information of the structural features that determine the therapeutic effectiveness of drugs, and become an important research field in life sciences, chemistry, and clinical medicine. Gallic acid (3,4,5-trihydroxybenzoic acid, structure shown in Fig. 1) is a naturally occurring plant phenol and is known by its antioxidant, anticarcinogenic and antifungal properties [9,10]. It possesses a scavenging activity against several types of free radicals, which could cause aberrance of normal tissue, and protects cells from damage induced by UV-B or ionizing irradiation [11]. However, higher concentration of gallic acid acts as a prooxidant [12]. Due to its pharmacological activity, it is necessary to study the interaction between gallic acid and protein for understanding the mechanism of drug action at a molecular level.

In previous studies, the molecular binding between protein and many drugs in aqueous solution under physiological conditions has been investigated successfully [13,14]. Liu et al. [15] researched the interaction of HSA with three organic acids in buffer solution including gallic acid by fluorescence and FT-IR spectrometry; Desfosses et al. [16] compared the behavior of HSA in the presence of three chemically distinct ligands: oxyphenylbutazone, dansylsarcosine, hemin in buffer and reverse micelles; Andrade and Costa probed the interaction of two water-soluble freebase porphyrins with two drug-carrier proteins (human serum albumin and β-lactoglobulin) in AOT/isooctane/water reverse micelles by means of steady-state and transient-state fluorescence spectroscopy [17]. Although some data can be found in literatures, less attention has been paid on the confined reaction of gallic acid and HSA in membrane mimetic environments monitored by diversiform analytical methods [6,18,19].

The aim of this study is to extend the earlier work on protein–drug complexation in aqueous solution to microemulsion, which is a unique microenvironment for multifarious chemical and biochemical reactions. Gallic acid entering the "water pool" of AOT/water/isooctane microemulsions and interacting with the encapsulated HSA could provide a useful model to mimic drugs transferring from outsides of cells to inside and reacting with proteins. The interaction of HSA with gallic acid in membrane mimetic environments was clearly demonstrated via fluorescence spectroscopy, FT-IR (both qualitative and quantitative analysis), circular dichroism (CD) and dynamic light scattering (DLS) approaches. Information regarding the binding constants (K), the number of binding sites (n), the location of the binding site, thermodynamic parameters of the reaction and the effect of gallic acid on the protein secondary structure was provided. In addition, the partial binding parameters of the reaction were calculated through SGI FUEL workstations. The nature of the gallic acid–HSA complications in vitro and in vivo was illustrated based on the results. This preliminary research has attempted to explore an extensive future application of microemulsions as membrane mimetic environments for studying the interactions of protein with drug.

2. Materials and methods

2.1. Materials

Sodium bis(2-ethylhexyl) sulfosuccinate (AOT) (Fluka, USA, ≥96% purity) was used without further purification. Human serum albumin (HSA), purchased from Sigma Chemical Company (USA), was used as received and its molecular weight was assumed to be 66,500. All HSA stock solutions were prepared in the pH 7.40 buffer solutions and were kept in the dark at 4 °C. Gallic acid, phenylbutazon (PB), fluofenamic acid (FA) and digitoxin (Dig) were of analytical grade, and obtained from the National Institute for Control of Pharmaceutical and Bioproducts (Beijing, China). Gallic acid solution was prepared in deionized water. Phenylbutazon, fluofenamic acid and digitoxin solutions were prepared in absolute ethanol. Buffer solution (pH 7.40) consisted of Tris (0.2 M, Tianjin Chemical Reagent, China) and HCl (0.1 M, Tianjin Chemical Reagent, China). Isooctane (Tianjin Chemical Reagent, China) and other reagents were of analytical grade and deionized water was used throughout all the experiments. All pH were checked with a PHS-10A acidity meter (Xiaoshan Science Instrumentation Factory, Zhejiang, China).

2.2. AOT reverse micelle preparation

Microemulsion solutions of desired ω_o were obtained by adding concentrated protein solutions, drug solutions or plain buffer (pH 7.40) to a 0.1 M AOT solution in isooctane. Volume of additivity was assumed in calculating AOT concentration and ω_o values. The samples were gently shaken until complete clarification. The final sample concentration was calculated according to the total volume of the microemulsion.

2.3. Apparatus and methods

The absorption and steady state fluorescence measurements were performed using a CARY-100 UV–vis spectrophotometer (Varian, CA, USA) and a RF-5301PC spetrofluorophotometer (Shimadzu, Kyoto, Japan), respectively. The fluorescence emission spectra were read at 280–500 nm (excitation wavelength 280 nm) using

5 nm/5 nm slit widths. Synchronous fluorescence spectra of HSA microemulsions in the absence and presence of increasing amount of gallic acid (0–9.33×10^{-5} M) were recorded from 280 to 500 nm.

Fluorometric titration experiments: 2.0 ml microemulsions containing appropriate concentration of HSA were titrated by successive additions of a 3.60×10^{-4} M of corresponding microemulsions of gallic acid (to give a final concentration of 8.78×10^{-6} to 7.76×10^{-5} M) with trace syringes. The fluorescence intensities were measured at excitation and emission wavelength of 280 and 310 nm. All fluorescence intensities were measured at six different temperatures (282, 289, 296, 303, 310 and 317 K). An electronic thermo regulating water-bath (NTT-2100, EYELA, Tokyo, Japan) was used for controlling the temperature. The data obtained were analyzed by the Scatchard equation [20] to calculate the binding parameters

$$\frac{r}{D_f} = nK - rK \quad (1)$$

where r represents the number of moles of bound drug per mole of protein, D_f represents the molar concentration of free drug, n and K are the number of binding sites and binding constant, respectively.

For the anisotropy measurements the excitation and emission bandwidths were both 5 nm. Steady state anisotropy (r) is defined by

$$r = \frac{I_{VV} - GI_{VH}}{I_{VV} + 2GI_{VH}} \quad (2)$$

where I_{VV} and I_{VH} are the intensities obtained with the excitation polarizer oriented vertically and the emission polarizer oriented in vertical and horizontal orientation, respectively. The G factor is defined as: $G = I_{HV}/I_{HH}$, similarly, I_{HV} and I_{HH} are the intensities obtained with the excitation polarizer oriented horizontally and the emission polarizer oriented in vertical and horizontal orientation.

Thermodynamic parameters were calculated based on the temperature dependence of the binding constant in ω_o 20 microemulsion for gallic acid–HSA binding. The temperatures were used 282, 289, 296, 303, 310 and 317 K. The enthalpy change (ΔH^0) was calculated from the slope of the Van't Hoff relationship:

$$\ln K = -\frac{\Delta H^0}{RT} + \frac{\Delta S^0}{R} \quad (3)$$

K is the binding constant at temperature T and R is gas constant. The value of ΔS^0 was obtained from linear Van't Hoff plot. The value of ΔG^0 was calculated from the equation:

$$\Delta G^0 = \Delta H^0 - T\,\Delta S^0 \quad (4)$$

FT-IR measurements were recorded at room temperature on a Nicolet Nexus 670 FT-IR spectrometer (WI, USA) equipped with a Germanium attenuated total reflection (ATR) accessory, a deuterated triglycine sulphate (DTGS) detector and a KBr beam splitter. All spectra were taken via the attenuated total reflection (ATR) method with a resolution of 4 cm^{-1} and using 60 scans. The background (containing all system components except protein) was recorded at the same condition and subtracted from the measured spectra. The subtraction criterion was that the original spectrum of protein solution between 2200 and 1800 cm^{-1} was featureless [21]. In this study Fourier self-deconvolution and secondary derivative were applied to the range of 1700–1600 cm^{-1} to estimate the number, position, and width of component bands. Based on these parameters a curve-fitting process was carried out by Galactic PeakSolve software (version 1.0) to get the best Gaussian-shaped curves that fit the original protein spectrum. After the identification of the individual bands, the representative structure of HSA was calculated using the area of their respective component bands.

Circular dichroism (CD) spectra were measured with an Olis DSM 1000 Circular Dichroism (GA, USA), using a 1 mm cell at 296 K. CD spectra (200–300 nm) were taken at a HSA microemulsion ($\omega_o = 20$) concentration of 3.0 μM, and the results were taken as millidegrees. The α-helical content of HSA was calculated from the molar ellipticity ($[\theta]$) at 208 nm according the equation $\%\text{helix} = \{(-[\theta]_{208} - 4000)/(33{,}000 - 4000)\} \times 100$ [22].

The crystal structure of HSA was taken from the Brookhaven Protein Data Bank (entry codes 1h9z) [23]. The potential of the 3D structure of HSA was assigned according to the Amber 4.0 force field with Kollman-all-atom charges. The initial structure of all the molecules was generated by molecular modeling software Sybyl 6.9 [24]. The geometry of the molecule was subsequently optimized to minimal energy using the Tripos force field with Gasteiger–Marsili charges. The FlexX program was used to build the interaction modes between the gallic acid and HSA.

Dynamic light scattering experiments were performed to determine hydrodynamic diameter of AOT microemulsions at room temperature. The measurements were done using a BI-200SM Static and Dynamic laser light scattering system (Brookhaven, NY, USA) coupled with a 4 W laser.

3. Results and discussion

3.1. Determination of ω_o value for HSA microemulsion

A series of different microemulsions with ω_o from 10 to 50 were prepared to determine an appropriate ω_o value for HSA microemulsion, in which microemulsion HSA has a better stability. The clear microemulsions tended toward turbid when the ω_o changed from 35 to 50. When the ω_o amounted to 10–25, the microemulsions maintained pellucid which were more stable than ω_o 30. According to the research result of Andrade et al. [25], HSA is a spherical protein, the radius of its sphericity r_p (Å) = $0.7 \times Mr^{1/3}$, and the radius of AOT micelle inner core is given by r_m (Å) = $4 + 1.5 \times \omega_o$ from an empirical equation, when $r_p = r_m$, the optimal ω_o value for HSA is expected to approximate to 16. So 20 was chosen as the optimized ω_o of the microemulsion for the spectroscopic measurements and the main fluorometric titration experiments. And in ω_o 20 microemulsion HSA had the higher fluorescence intensity (Fig. 2). Furthermore, 20 approached the calculated value 16 and literature values 21 [26], 22.4 [16] for HSA microemulsion, respectively.

3.2. Fluorescence data of HSA in microemulsions of different ω_o

The fluorescence spectra of HSA in various ω_o microemulsions were recorded. There was no distinct shift in the fluorescence emission maximum (λ_{max}) along with the change of ω_o. The λ_{max} was all about 309 nm when ω_o increased from 10 to 50. There could be two possible reasons for the result: (a) the microenvironment of HSA remains essentially invariant with ω_o, or (b) change of microenvironment does occur, but is not reflected through λ_{max} values. And the change of the relative fluorescence intensity was not evident in different ω_o microemulsions (Fig. 2). It is noticed that the properties of reverse micelle solubilized water are differ from those of bulk water, even at higher ω_o values, and its apparent microviscosity is 6–9 times greater than that of free aqueous solution [27]. Compared 309 nm with λ_{max} 332 nm of HSA in buffer solution, it may indicate a less polar environment of amino acid residues provided by microemulsion.

3.3. Fluorescence anisotropy of HSA in various microemulsions

The fluorescence anisotropy measurements of HSA in microemulsions against ω_o were carried out (λ_{ex}: 280 nm) and the result is shown in Table 1. It is evident that with the water

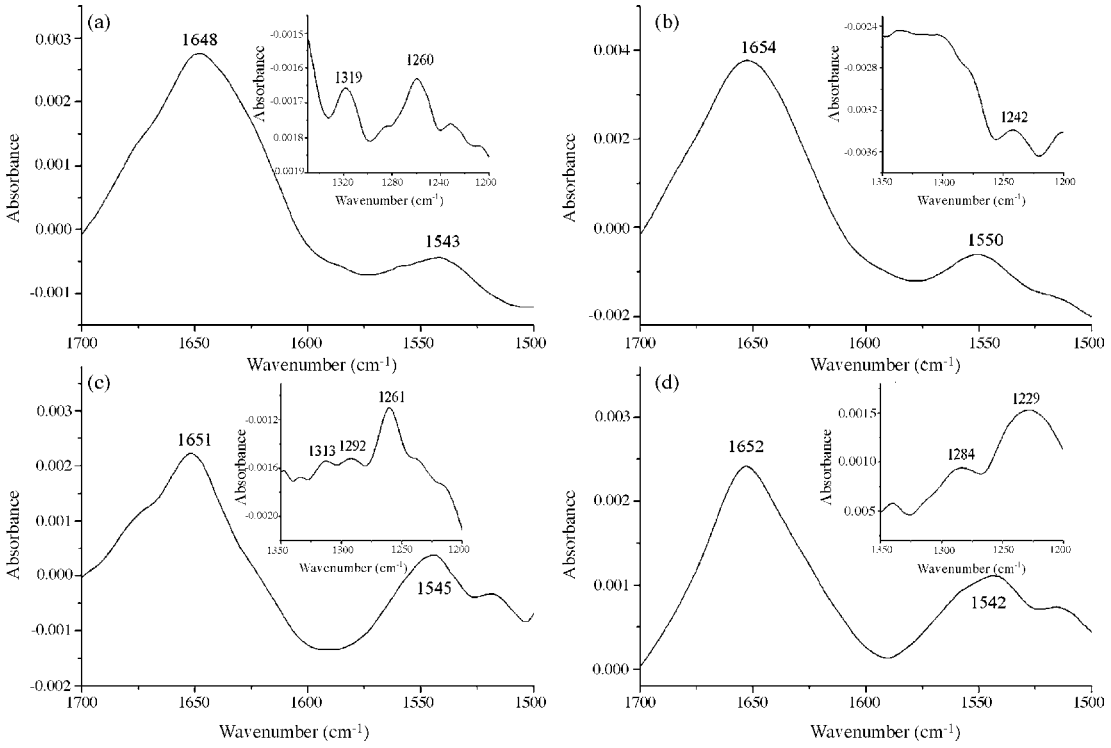

Fig. 3. FT-IR spectra and different spectra of HSA: (a) FT-IR spectrum of HSA in Tris buffer (pH 7.40); (b) FT-IR spectrum of ω_o 20 HSA microemulsion; (c) FT-IR difference spectrum of HSA obtained by subtracting the spectrum of the gallic acid-free form from that of the gallic acid-bound form in the region of 1800–1200 cm^{-1} in ω_o 20 microemulsion at 296 K ([HSA] = 7.5 × 10^{-6} M; [gallic acid] = 15 × 10^{-6} M). (d) FT-IR difference spectrum of HSA in ω_o 20 microemulsion at 296 K ([HSA] = 7.5 × 10^{-6} M; [gallic acid] = 112.5 × 10^{-6} M).

pool increase, very little change in the anisotropy (r) was observed, suggesting that there was no appreciable additional change in the average mobility of HSA molecules. It is noteworthy that all the r values were higher than that obtained from buffer solution of HSA, which showed that the mobility of the chromophores inside microemulsion droplets was more confined than in aqueous solution. This effect may be explained by interactions between amino acid side-chains and AOT sulphonate groups or the structured interfacial water layer in which these were hosted. Another simple and possible reason is that microviscosity increases when water serves as a component of the microemulsion.

3.4. UV spectra of HSA in different ω_o microemulsions

The UV absorption spectra variation of HSA was discussed upon changing ω_o value of microemulsions. In aqueous solutions there was an absorbance intensity band of HSA with a maximum at around 210 nm. But in AOT microemulsions the absorbance band tended towards a bathochromic shift from 210 to 239 nm for UV absorption spectra which suggested that the microenvironment polarity of chromophore decreased. The relative absorption intensities of peaks at 277 nm which character the conjugated double bond of tryptophan, tyrosine and phenylalanine residue to peaks at 239 nm were stronger than that in buffer solution. It means that microemulsions and water solutions provide different microenvironments for HSA. Variations of water quantity in microemulsions could affect the absorbance of HSA but not influence the peak positions.

Table 1
Fluorescence anisotropy (r) of HSA in different ω_o microemulsions and buffer solution at 296 K

	ω_o									Buffer
	10	15	20	25	30	35	40	45	50	
r	0.1035	0.1074	0.1025	0.1024	0.0980	0.1054	0.1024	0.0970	0.1034	0.0783

3.5. Binding studies between gallic acid and HSA in microemulsions using FT-IR and CD spectrum

The evidence coming from FT-IR spectroscopic results regarded the nature of structural changes induced in the HSA upon its confinement in the water pool and interaction with gallic acid. Since infrared spectra of proteins exhibit a number of so-called amide bands, which represent different vibrations of the peptide moieties. Protein amide I peak position occurred in the region between approximately 1600 and 1700 cm^{-1} (principally C=O stretch), the amide II band ≈1548 cm^{-1} (C—N stretch with N—H bending mode) [28] and the amide III peak position occurred in the region 1200–1350 cm^{-1} (mainly in-phase combination of C—N stretching vibrations and N—H in-plane-bending) [15,29], there was no major spectral shifting. They both have a relationship with the secondary structure of the protein. Amide III band is not disturbed by the absorbance of water vapor and it has the special characteristic reflecting the changes of protein secondary structure in its original spectra. Amide I band is more sensitive to the change of protein secondary structure than amide II and amide III [29]. Fig. 3 shows the FT-IR spectra of the HSA in buffer solution, gallic acid-free and gallic acid-bound form of HSA in microemulsions (ω_o = 20) with its difference absorption spectrum. The difference spectra [(protein microemulsion + gallic acid microemulsion) – (gallic acid microemulsion)] were obtained in order to monitor the intensity variations of these vibrations. Similarly, the quantitative analyses of each secondary structure of HSA were gathered by the IR self-

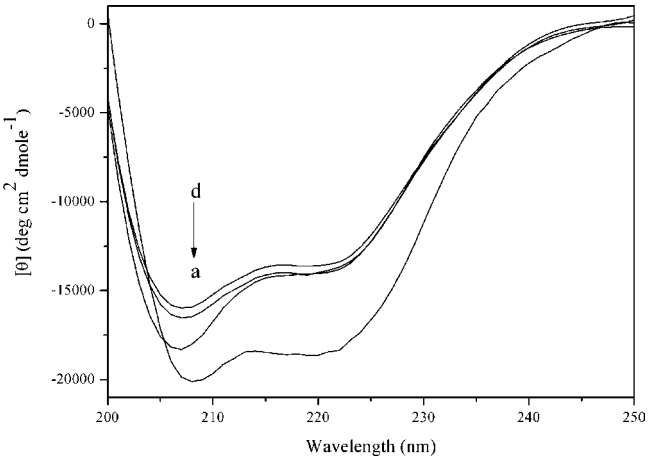

Fig. 4. CD spectra of the HSA–gallic acid system. (a) 3.0 μM HSA in Tris buffer; (b) 3.0 μM HSA in the presence of 45.0 μM gallic acid in ω_0 20 microemulsion; (c) 3.0 μM HSA in the presence of 6.0 μM gallic acid in ω_0 20 microemulsion; (d) 3.0 μM HSA in ω_0 20 microemulsion.

deconvolution with second-derivative resolution enhancement and curve-fitting procedure. The CD spectra were also examined to ascertain the changes of HSA secondary structure before and after addition of gallic acid in microemulsions and compared them with spectrum in buffer; the results are presented in Fig. 4.

From Fig. 3, it can be concluded that when HSA was introduced in the microemulsion, the secondary structure of HSA was changed because the shapes and positions of peaks for amide I band, amide II band and amide III band have evidently changed. Adding 15 μM gallic acid into HSA microemulsion, the intensities of the amide I weakened in the spectra of free HSA in microemulsion and the peak positions of amide I band (1654 cm^{-1}), amide II band (1550 cm^{-1}) and amide III band (1242 cm^{-1}) in the HSA infrared spectrum shifted to 1651, 1545 and 1261 cm^{-1}, respectively. The spectra suggested that when gallic acid entered the hydrophobic binding cavities (subdomain IIA or IIIA) by the hydrophobic interactions, the phenolic hydroxyl group can form hydrogen bonding with the C=O and C—N groups of main polypeptide in HSA, resulting in the rearrangement of polypeptide carbonyl hydrogen bonding network. The effect of gallic acid on HSA in microemulsion caused considerable changes in the protein secondary structure, and it may be the result of the formation of gallic acid–HSA complex. The rigidity of the protein molecule would be somewhat affected.

The CD data directly relate to the conformation of the protein. The negative ellipticity bands at 208 and 222 nm of CD spectra of HSA are characteristic of the amount of α-helix in the protein, and changes in the spectra at these wavelengths may reflect the shifts in the α-helical content of the protein. In Fig. 4, the CD spectrum of free HSA in buffer solution had a characteristic of the typical α-helix structure with negative bands at 208 and 220 nm. After encapsulating protein in microemulsion, the band intensity of negative Cotton effect of HSA at 208 and 220 nm is reduced, indicating the considerable changes in the protein secondary structure with the decrease of the α-helical content in HSA. This could mean that AOT microemulsion provided different chiral environments for HSA. Upon gallic acid complexation, the CD spectra of bound HSA were observed to be similar in shape with that in the absence of gallic acid in microemulsion and free HSA in buffer, indicating that the structure of HSA was predominantly α-helical in microemulsion. After interacting with gallic acid, the α-helical content in protein was increased. When the drug concentration in HSA microemulsion increased, the spectrum showed a significant augment in the α-helical content. From the above results, it may be the result of the formation of complex between gallic acid and HSA in microemulsion. At the same time, the intramolecular forces responsible for maintaining the secondary and tertiary structures can be altered, resulting in a conformational change of the protein when gallic acid binds to HSA.

Before the estimation of percentage content of each secondary structure, the component bands should be assigned. According to the well-established assignment criterion [28]: the bands range 1610–1640 cm^{-1} are generally assigned to β-sheet, 1640–1650 cm^{-1} to random coil, 1650–1658 cm^{-1} to α-helix, and 1660–1700 cm^{-1} to β-turn structure. Based on the integrated areas of the component bands in amide I the percentages of each secondary structure of HSA can be calculated. The quantitative analysis for the protein secondary structure of the free HSA and HSA–gallic acid complex (drug:HSA = 2:1, 15:1) in ω_0 20 microemulsion in comparison with the data of HSA in buffer are presented in Table 2. From Table 2, it can be seen that the native HSA contained major amounts of α-helix (54%), β-turn (18%) and β-sheet (26%), while in microemulsion the percentages of protein α-helix structure decreased about 14% and β-turn structure showed an augment about 8%, while β-sheet structure increased about 3% compared with the buffer solution. Some co-effect factors may contribute to these findings: in the process of protein solubilization, the contact of HSA molecules with isooctane could change the structure of HSA; the unusual properties of water localized in the interior of microemulsions can bring about a different environment for HSA; the interaction of HSA and AOT could also change the structure of protein. The binding of gallic acid to HSA led to the α-helix structure increased from 40 to 43%, β-turn structure increased from 26 to 28%, and β-sheet structure decreased from 29 to 26% when drug–protein molar ratio was 2. The obvious change occurred in the α-helical region in amide I band after binding with gallic acid. This indicated that the α-helix conformation of HSA was perturbed due to the interaction of gallic acid with HSA. The drug–protein interaction induced the HSA conformation to transform from β-sheet, β-turn structure to α-helix structure when gallic acid came into HSA microemulsion with a higher concentration; it was the evidence for some degree of stabilization of protein structure in the existence of gallic acid. The CD spectra of the free HSA in buffer, in microemulsion and its complexes with gallic acid (gallic acid:HSA = 2:1) in microemulsion also exhibited a reduction of α-helices from 56% (free HSA in buffer) to 41% (free HSA in microemulsion), an augment from 41 to 43% (bound HSA in microemulsions), which had the similarities with IR data. This suggested that, in spite of the conformation of HSA was influenced by the microemulsion environment, gallic acid could interact with the protein in microemulsion. Also, the binding constants obtained from fluorescence measurement as followed strongly supported the conformational changes induced by the drug–protein interaction observed in FT-IR and CD results. From CD measurements, Desfosses et al. [16] showed that upon hosted into AOT microemulsions of ω_0 = 22.4, the α-helical content of HSA decreased by approximately 15%.

3.6. Analysis of fluorescence quenching of HSA by gallic acid in microemulsion

The fluorescence spectra of HSA in microemulsion in the absence and presence of gallic acid compared with the native HSA in the pH 7.40 Tris buffer were measured with the excitation wavelength at 280 nm and their representative spectra are given in Fig. 5. In ω_0 20 microemulsion, HSA had a strong fluorescence emission peak at 310 nm, a large shift of emission to a shorter wavelength from 332 nm of HSA in aqua. It indicated perturbations of the amino acid residue microenvironment. The intensity of HSA fluorescence

Table 2
Secondary structure determination for the free HSA in Tris buffer (pH 7.40), ω_o 20 microemulsion and its coordination compounds in microemulsion at the molar concentration ratio: C_{drug}/C_{HSA} = 2:1, 15:1; T = 296 K

Amide I components (cm^{-1})	HSA-free in buffer	In microemulsion		
		HSA -free	HSA + gallic acid (1:2)	HSA + gallic acid (1:15)
The FT-IR results				
α-Helix (%)	54	40	43	47
β-Turn (%)	18	26	28	23
β-Sheet (%)	26	29	26	20
The CD results				
α-Helix (%)	56	41	43	48

emission in microemulsion was much higher than in aqueous solutions. It can be seen that the fluorescence intensity of HSA was weakened regularly with increasing concentrations of the gallic acid, indicating that the binding of HSA to gallic acid in microemulsion quenched the intrinsic fluorescence of the HSA.

The synchronous fluorescence spectra supply information about the molecular environment in the vicinity of the chromophores molecules. In the synchronous spectra, the sensitivity associated with fluorescence is maintained while offering several advantages: spectral simplification, spectral bandwidth reduction and avoiding different perturbing effect. According to Miller [30], the $\Delta\lambda$ values between excitation wavelength and emission wavelength were stabilized at 60 nm, the synchronous fluorescence of HSA shows the characteristic information of tryptophan residue. Fig. 6 displays the effect of the addition of gallic acid on synchronous fluorescence spectrum of HSA in ω_o 20 microemulsion when $\Delta\lambda$ = 60 nm. Compared with HSA in the Tris buffer, HSA encapsulation immediately resulted in a hypsochromic shift to 340–335 nm of λ_{max}. Increasing concentration of the drug led to a dramatic decrease in the fluorescence intensity. It is considered that the λ_{max} of the tryptophan residues is relative to the polarity of microenvironment. As reported that the λ_{max} at 330–332 nm indicates that tryptophan resides are located in the nonpolar region, namely, they are buried in a hydrophobic cavity in HSA; λ_{max} at 350–352 nm shows that tryptophan residues are exposed to water, namely, the hydrophobic cavity in HSA is disagglomerated and the structure of HSA is looser. Accordingly, Fig. 6 shows that after embedding HSA into microemulsion, the microenvironment of tryptophan residues became polar less. And gallic acid mainly bound to the hydrophobic cavity of HSA, which was in agreement with the latter results from the binding mode and molecular modeling.

The quantitative analysis for HSA–gallic acid at six different temperatures in ω_o 20 microemulsions was carried out using the Scatchard equation Eq. (1). The binding constants and the number of binding sites are summarized in Table 3. The linearity of Scatchard plots indicated that gallic acid bound to one class of site on HSA. The binding constants decreased with the increasing temperature in microemulsions and the temperature had an effect on the binding between gallic acid and HSA. Thus, gallic acid can be stored and removed by protein in body. The binding constants K for the gallic acid–HSA in ω_o 10, 15, 20, and 25 microemulsions were $(0.96 \pm 0.05) \times 10^4$, $(1.07 \pm 0.07) \times 10^4$, $(1.03 \pm 0.02) \times 10^4$ and $(0.82 \pm 0.02) \times 10^4\ M^{-1}$ at 296 K, respectively. There were no large differences in the binding constants K of each microemulsion with the diverse water capacity. The binding of gallic acid and HSA was relatively stronger in microemulsions with ω_o 15 and ω_o 20. It was possible that the activity of HSA in ω_o 15 and ω_o 20 microemulsions was higher because 15 and 20 were close to the calculated value 16. In buffer solution, the binding constant K ($(0.54 \pm 0.02) \times 10^4\ M^{-1}$) was lower to some degree than the microemulsions's, which could indicate greater accessibility of gallic acid toward HSA when HSA was encapsulated in microemulsion. It may imply that HSA associates with the interface of microemulsion, and an interesting conformational change is induced in the protein's structure.

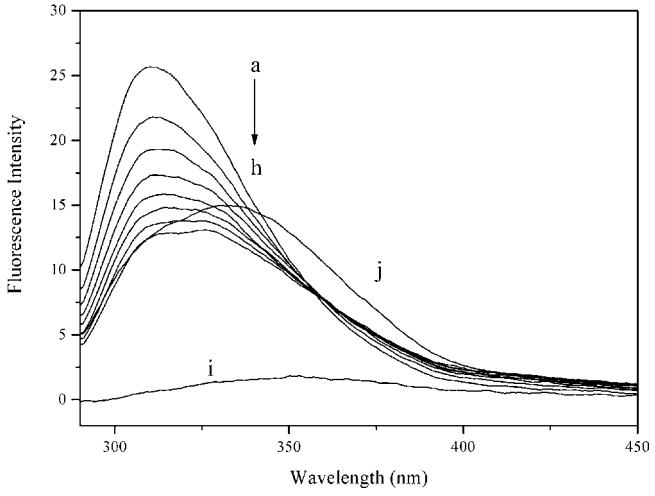

Fig. 5. The fluorescence spectra of gallic acid–HSA system in ω_o 20 microemulsion. The concentration of HSA was 3.0×10^{-6} M while the gallic acid concentration corresponding to 0, 1.71, 3.27, 4.70, 6.00, 7.20, 8.32, and 9.33×10^{-5} M from a to h; (i) [gallic acid] = 8.78×10^{-6} M in ω_o 20 microemulsion; T = 296 K; λ_{ex} = 280 nm, λ_{em} = 310 nm; (j) 3.0×10^{-6} M HSA in Tris buffer, pH 7.40; λ_{ex} = 280 nm, λ_{em} = 332 nm.

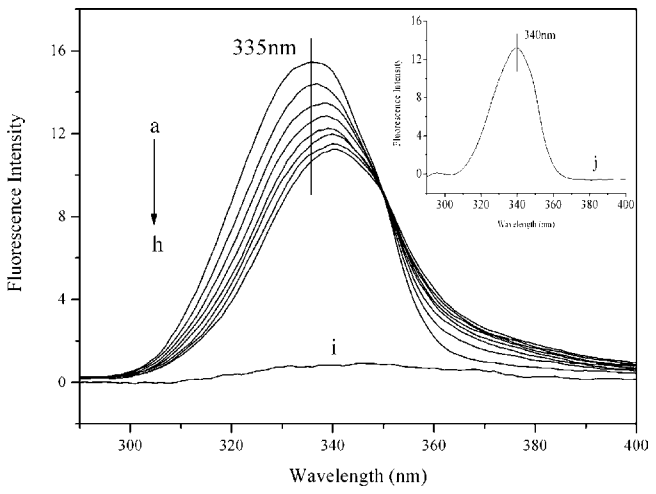

Fig. 6. Synchronous fluorescence spectra of HSA (3.0×10^{-6} M) in ω_o 20 microemulsion with $\Delta\lambda$ = 60 nm in the absence and presence of increasing amount of gallic acid (10^{-5} M): (a) 0; (b) 1.71; (c) 3.27; (d) 4.70; (e) 6.00; (f) 7.20; (g) 8.32; (h) 9.33; (i) [gallic acid] = 8.78×10^{-6} M in ω_o 20 microemulsion; T = 296 K; (j) 3.0×10^{-6} M HSA in Tris buffer, pH 7.40.

Table 3
Binding parameters and thermodynamic parameters of gallic acid–HSA in ω_o 20 microemulsions

T (K)	K ($\times 10^4$ M^{-1})	n	Regression coefficient	ΔG^0 (kJ mol^{-1})	ΔH^0 (kJ mol^{-1})	ΔS^0 (J mol^{-1} K^{-1})
282	1.18 ± 0.02	1.05	0.9991	−22.03		
289	1.13 ± 0.02	1.06	0.9999	−22.38		
296	1.03 ± 0.02	1.08	0.9996	−22.72	−8.10	49.42
303	0.95 ± 0.02	1.12	0.9993	−23.07		
310	0.87 ± 0.02	1.19	0.9996	−23.41		
317	0.82 ± 0.03	1.25	0.9993	−23.76		

3.7. Thermodynamic analysis

The acting forces between a small molecular substance and macromolecule mainly include hydrogen bond, van der Waals force, electrostatic force, hydrophobic interaction force, etc. The signs and magnitudes of thermodynamic parameters for protein reactions can account for the main forces contributing to protein stability. To obtain such information, the implications of the present results have been discussed in conjunction with thermodynamic characteristics obtained for gallic acid binding in ω_o 20 microemulsion, and the thermodynamic parameters were calculated from the Van't Hoff equation ($r = 0.9954$). From Table 3 it was clear that gallic acid–HSA complexes were accompanied by negative enthalpy change (ΔH^0) and positive entropy change (ΔS^0), which indicated that the binding processes were exothermic and entropy driven. The binding of gallic acid with HSA was spontaneous process as indicated by the negative ΔG^0. Positive ΔH^0 and ΔS^0 are generally considered as the evidence for typical hydrophobic interactions; In addition, van der Waals force and hydrogen bonding formation in low dielectric media are characterized by negative ΔH^0 and ΔS^0. Moreover, negative ΔH^0 might play a role in electrostatic interactions [14]. Therefore, the binding of gallic acid to HSA in microemulsion might involve hydrophobic interaction strongly as evidenced by the positive value of ΔS^0 and the electrostatic interaction can also not be excluded.

3.8. Identification of binding sites on HSA and molecule modeling

Descriptions of the 3D structure of crystalline albumin showed that HSA comprises three homologous domains (I–III): I (residues 1–195), II (196–383), III (384–585), and each of which can be divided into two sub-domains (A and B). HSA has a limited number of binding sites for endogenous and exogenous ligands that are typically bound reversibly and have binding constants in the range 10^4 to 10^8 M^{-1} [31]. Sudlow et al. [32] have suggested two main distinct binding sites on HSA, site I and site II, which locate in the hydrophobic cavities of sub-domains IIA and IIIA, respectively, and one tryptophan residue (Trp-214) of HSA is in sub-domain IIA [31]. There is a large hydrophobic cavity present in subdomain IIA that many drugs can bind to.

Many ligands, such as Warfarin and PB, were found to bind preferentially to site I of HSA, while ibuprofen, FA showed affinity for site II. Later studies suggested that Dig bound on the site III which is independent of site I and site II [33]. In order to classify gallic acid binding sites on the HSA molecule, competitive binding experiments were carried out, using drugs that specifically bind to a known site or region on HSA. Ternary mixture of PB, FA, or Dig, and gallic acid with HSA in ω_o 20 microemulsions were studied. According to the Scatchard equation Eq. (1), the fluorescence data were used to obtain the values of binding constant K $(0.91 \pm 0.02) \times 10^4$ M^{-1} ($r = 0.9991$), $(1.03 \pm 0.02) \times 10^4$ M^{-1} ($r = 0.9992$), $(1.01 \pm 0.03) \times 10^4$ M^{-1} ($r = 0.9989$) in the presence of PB, FA, and Dig at 296 K, respectively. The results indicated that the bound-gallic acid to HSA was affected by adding PB, and was not significantly displaced by FA or Dig. The linear Scatchard plots indicated the existence of a binding site for gallic acid in proximity of the tryptophan. Therefore, this evidence suggested that the primary binding site of gallic acid was at least the same as that of PB to HSA.

In order to further study the binding site, SGI FUEL workstation was used to calculate the partial binding parameters of the HSA–gallic acid system, and the best energy ranked result is shown in Fig. 7. It can be seen that gallic acid was situated within subdomain IIA in Sudlow's site I formed by helices. The gallic acid molecule was located within the binding pocket and it was important to note that the residue (Tyr-150), the residue (Arg-222) and the residue (Ser-287) of HSA were in close proximity to gallic acid molecule, suggesting the existence of hydrophobic interaction between them. Furthermore there were also a number of specific electrostatic interactions and hydrogen bonds, because several ionic and polar residues in the proximity of the ligand play an important role in stabilizing the gallic acid molecule via H-bonds and electrostatic interaction. There were hydrogen interactions between 8-O, 9-O of gallic acid and the residues Arg-257 of HSA; 10-OH and Glu-292, His-288; 11-OH and Glu-292; 12-OH and Ala-291. The results suggested that the formation of hydrogen bond decreased the hydrophilicity and increased the hydrophobicity to stability in the gallic acid–HSA system. The calculated binding Gibbs free energy (ΔG^0) was −17.94 kJ mol^{-1}, which was not very close to the experimental data (−22.72 kJ mol^{-1}) to some degree. A possible explanation may be that the X-ray structure of the protein from crystals differs from that of the microemulsion system used in this study. Therefore, the results of modeling indicated that the interaction between gallic acid and HSA was dominated by hydrophobic force, which was in accord with the binding mode study. It was

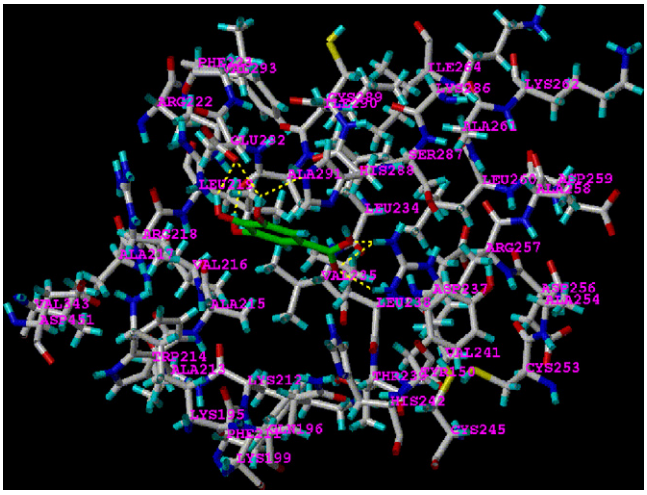

Fig. 7. The binding mode between gallic acid and HSA, only residues around 8 Å of gallic acid are displayed. The residues of HSA are represented using gray ball and stick model and the drug structure is represented by a green one. The hydrogen bond between gallic acid and HSA is represented using yellow dashed line. (For interpretation of the references to color in this figure legend, the reader is referred to the web version of the article.)

important to note that the Trp-214 residue of HSA was in close proximity to the drug molecule, this finding provided a good structural basis to explain the efficient fluorescence quenching of HSA emission in the presence of gallic acid. All the proofs coming from molecular modeling illuminated that gallic acid could interact with HSA at site I in subdomain IIA.

3.9. DLS data

Dynamic light scattering data gathered additional evidence to have insight on the localization of HSA and the binding of HSA with gallic acid which occurred after encapsulating them in AOT microemulsions. Hydrodynamic diameters (D_H) of ω_o 20 AOT microemulsions with and without 8.1 μM HSA, HSA–gallic acid (gallic acid:HSA = 11:1) were determined at 296 K. The D_H of ω_o 20 microemulsion was 10.3 nm, which was comparatively close to the literature's value [34]. When immersing HSA in microemulsion, the D_H value decreased to 6.3 nm. In terms of Pileni [3], HSA may locate at the interface leading to a decrease in the water pool, which may involve the conformational changes in HSA. Adding 89.1 μM gallic acid into ω_o 20 HSA microemulsion, the D_H value changed to 5.7 nm. It could be caused by the binding of HSA with gallic acid in microemulsion.

4. Conclusions

In the present work, AOT/isooctane/water microemulsions were chosen as membrane mimetic environments to investigate the interaction of gallic acid and HSA. The binding parameters were obtained from the fluorescence data in microemulsions. The qualitative and quantitative FT-IR and CD analytical data implied that the conformation of HSA was influenced after encapsulating the protein into microemulsions. And the interaction of gallic acid with HSA in microemulsions kept on changing the secondary structure of HSA. Displacement experiments and molecular modeling showed that gallic acid has one reactive site in HSA, that is, site I in subdomain IIA. Gallic acid could mainly bind HSA through the hydrophobic force and electrostatic interaction which was suggested by thermodynamic analysis. According to the DLS data HSA may locate at the interface of the microemulsion and has interaction with gallic acid. The studies presented here have also clearly indicated that gallic acid is a relatively weak quencher for HSA and binds to HSA with much higher affinities in microemulsions than in buffer solution.

This study is expected to provide important insight into the interaction of the physiologically important protein HSA with broad-spectrum pharmacological drug in microemulsion. It is noteworthy that the spectroscopic research described herein signifies a promising approach, exploiting the new application of microemulsion as the microenvironment for the interaction between protein and drug, which greatly broadens the study range of binding between proteins and drugs. The experiment could also supply some important information to clinical research and provide the theoretical basis for the new drug designing.

References

[1] S.M. Andrade, S.M.B. Costa, R. Pansu, J. Colloid Interface Sci. 226 (2000) 260.
[2] A.D. Jesus, M.M. Silva, M.G.R. Vale, Talanta 74 (2008) 1378.
[3] M.P. Pileni, J. Phys. Chem. 97 (1993) 6961.
[4] M. Maestro, J. Mol. Liq. 42 (1989) 71.
[5] K.D. Tapas, M. Amarnath, Adv. Colloid Interface Sci. 59 (1995) 95.
[6] J.H. Tang, S.D. Qi, X.G. Chen, J. Mol. Struct. 779 (2005) 87.
[7] D.C. Carter, J.X. Ho, Adv. Protein Chem. 45 (1994) 153.
[8] U. Mathias, M. Jung, Anal. Bioanal. Chem. 388 (2007) 1147.
[9] D.J. Yang, L.S. Hwang, J.T. Lin, J. Chromatogr. A 1156 (2007) 312.
[10] F.Z. Xie, X.C. Lin, X.P. Wu, Z.H. Xie, Talanta 74 (2008) 836.
[11] H.U. Gali-Muhtasib, S.Z. Yamout, M.M. Sidani, Nutr. Cancer 37 (2000) 73.
[12] G.Ch. Yen, P.D. Duh, H.L. Tsai, Food Chem. 79 (2002) 307.
[13] E. Karnaukhova, Biochem. Pharmacol. 73 (2007) 901.
[14] Y. Li, W.Y. He, J.N. Tian, J.H. Tang, Z.D. Hu, X.G. Chen, J. Mol. Struct. 743 (2005) 79.
[15] Y. Liu, M.X. Xie, M. Jiang, Y.D. Wang, Spectrochim. Acta Part A Molec. Biomolec. Spectr. 61 (2005) 2245.
[16] B. Desfosses, N. Cittanova, W. Urbach, M. Waks, Eur. J. Biochem. 199 (1991) 79.
[17] S.M. Andrade, S.M.B. Costa, Chem. Eur. J. 12 (2006) 1046.
[18] L.J. Dong, X.G. Chen, Z.D. Hu, Talanta 71 (2007) 555.
[19] P. Stratil, B. Klejdus, V. Kubáň, Talanta 71 (2007) 1741.
[20] G. Scatchard, Ann. N. Y. Acad. Sci. 51 (1949) 660.
[21] A.C. Dong, P. Huang, W.S. Caughey, Biochemistry 29 (1990) 3303.
[22] Z.X. Lu, T. Cui, Q.L. Shi, Applications of Circular Dichroism and Optical Rotatory Dispersion in Molecular Biology, first ed., Science Press, Beijing, 1987, pp. 79–82.
[23] I. Petitpas, A.A. Bhattacharya, S. Twine, M. East, S. Curry, J. Biol. Chem. 276 (2001) 22804.
[24] G. Morris, SYBYL Software, Version 6. 9, Tripos Associates, St. Louis, 2002.
[25] S. Andrade, E.O. Kamenskaya, A.V. Levashov, J.J.G. Moura, Biochem. Biophys. Res. Commun. 234 (1997) 651.
[26] D.M. Davis, D. McLoskey, D.J.S. Birch, P.R. Gellert, R.S. Kittlety, R.M. Swart, Biophys. Chem. 60 (1996) 63.
[27] R. Bermejo, D.J. Tobaruela, E.M. Talavera, A. Orte, J.M. Alvarez-Pez, J. Colloid Interface Sci. 263 (2003) 616.
[28] Y. Liu, M.X. Xie, J. Kang, D. Zheng, Spectrochim. Acta Part A Molec. Biomolec. Spectr. 59 (2003) 2747.
[29] L.J. Dong, X.G. Chen, Z.D. Hu, Biochim. Biophys. Acta 1764 (2006) 257.
[30] J.N. Miller, Proc. Anal. Div. Chem. Soc. 16 (1979) 203.
[31] T. Peters, All About Albumin. Biochemistry, Genetics and Medical Application, Academic Press, San Diego, 1996.
[32] G. Sudlow, D.J. Birkett, D.N. Wade, Mol. Pharmacol. 12 (1976) 1052.
[33] I. Sjoholm, B. Ekman, A. Kober, I. Ljungstedt-Pahlman, B. Seiving, T. Sjodin, Mol. Pharmacol. 16 (1979) 767.
[34] E.P. Melo, P. Fojan, J.M.S. Cabral, S.B. Petersen, Chem. Phys. Lipids 106 (2000) 181.

Talanta 76 (2008) 265–270

Contents lists available at ScienceDirect

Talanta

journal homepage: www.elsevier.com/locate/talanta

Determination of pyruvic acid by using enzymic fluorescence capillary analysis

Yuan-Yuan Zhao [a], Xiu-Feng Gao [b], Yong-Sheng Li [a,*], Xiang Ju [a], Jia Zhang [a], Jia Zheng [a]

[a] School of Chemical Engineering, Sichuan University, Chengdu 610065, China
[b] West China School of Preclinical and Forensic Medicine, Sichuan University, Chengdu 610041, China

ARTICLE INFO

Article history:
Received 14 October 2007
Received in revised form 24 February 2008
Accepted 25 February 2008
Available online 4 March 2008

Keywords:
Pyruvic acid
Fluorescence capillary analysis
Liquid enzyme
NADH
L-LDH

ABSTRACT

A new method (P-LE–FCA) for the determination of pyruvic acid was proposed based on liquid enzyme method (LE) and fluorescence capillary analysis (FCA). The optimum experimental conditions were as follows: the excitation and emission wavelengths were 350 and 460 nm, respectively; the reaction time and temperature were 20 min and 38 °C, respectively; the pH of phosphate buffer solution was 7.5; the concentrations of nicotinamide adenine dinucleotide and lactate dehydrogenase were 1.0 mmol L^{-1} and 5.0 kU L^{-1}, respectively. The linear range of this method was 0.2–1.2 mmol L^{-1} ($\Delta F = 327.13C - 10.018$, $r = 0.9942$). Its detection limit was 0.012 mmol L^{-1}. And its relative standard deviation was 0.86%. Only 18 μL of total reaction solution is enough for the detection. P-LE–FCA has some merits such as lower cost, simple operation procedure and micro determination. It has been used for the determination of pyruvic acid content in human urine samples.

1. Introduction

Pyruvic acid is a biologically important molecule involved in a variety of biochemical reactions in plants and animals, either as a substrate, product or intermediate. Recently, because pyruvic acid has excellent results in losing weight, it has become a dietary supplement [1]. Pyruvic acid can improve exercise endurance capacity [2], effectively reduce cholesterol [3] and serve as a potent antioxidant [4]. Therefore, the measurement of its concentration can give valuable information to the progress of specific biochemical reactions. In medical field, pyruvic acid serves as an aid for diagnosing ischemia [5], diabetic acidosis [6], alcoholism and hypovitaminosis and can also be used to optimize respiratory monitoring. In food industry, assaying this compound provides an indication of bacterial contamination of various media, such as dairy products.

Several techniques for the determination of pyruvic acid in various samples have been reported over the past few years, such as fluorescence spectra [8–10], chemiluminescence (CL) [11], ultraviolet spectrophotometry [12,13], enzyme electrode [14–16], voltamperometric analysis [17], colorimetric method [18], flow injection analysis (FIA) [19,20], high performance liquid chromatography (HPLC) [21–25], gas chromatography (GC) [26] and ion chromatography [7].

In the history of routine fluorometry for determining pyruvic acid, Olsen [8] first used it for the determination of 0.2 mL blood sample. Their procedure was based on an enzyme-catalyzed reaction system involving concentration changes of reduced nicotinamide adenine dinucleotide (NADH) which was a fluorescence substance. Linear correlation between pyruvic acid concentration and fluorescence intensity was established. Later, Ozand et al. [9] has developed a micro-autoanalytic system for the enzymic fluorometric determination of pyruvate. As many as 60–80 duplicate samples can be analyzed simultaneously in 8 h. The reproducibility, efficiency and versatility of this autoanalytic system will warrant its wide application in metabolic studies. Compared with the manual method developed by Olsen, this method has realized automation and quickened analytical speed. Xue and Yeung [10] used fluorescein as the fluorophore for indirect detection of pyruvate and other anions, and researched on the concentration variety of pyruvate in the intracellular fluid of erythrocytes.

Yoo et al. [18] has conducted many research on the determination of pyruvic acid. First they utilized colorimetric method to determine pyruvic acid in onions. Dinitrophenylhydrazine (DNPH) was added into onion sample solutions as color reagent, and the reaction mixture was heated for 10 min at 40 °C. Then, NaOH was added into the mixture and its absorbance was detected at 420 nm. Subsequently, they developed an automated system [19] based on FIA for pyruvic acid analysis. The system included two plunger pumps, an autosampler, a column heater, a spectrophotometric detector and an integrator. Onion juice sample was filtered through a nylon filter (microfilter) and injected into DNPH solution with an autosampler. Detection was made by an UV–vis detector and peak area was recorded by the integrator. This automated system showed highly significant correlations with the colorimetric

* Corresponding author. Tel.: +86 28 85417299.
E-mail address: lysgxf2005@yahoo.com.cn (Y.-S. Li).

0039-9140/$ – see front matter © 2008 Elsevier B.V. All rights reserved.
doi:10.1016/j.talanta.2008.02.031

method. In 2001, they used HPLC [21] to determine the pyruvic acid. It took only 30 min to run a sample. This HPLC method was employed instead of DNPH method, the possible interference from the related compounds could be eliminated.

In a word, each method as mentioned above has its advantages and disadvantages. GC and CL are not suitable for field determination. HPLC is applied increasingly, but eluting of sample residue in separation column still remains a problem in many instances. Whereas, the enzyme method has been proved that it has good selectivity and specificity and is a promising approach if enzyme price can changed to be cheap.

Fluorescence capillary analysis (FCA) [27] is a new method developed by the authors, based on common spectrofluorimetry and medical capillary (ID: 0.50–0.90 mm, length: 3–5 cm). The FCA can realize micro-dosage of expensive enzymes and chemical reagents, and promote the micromation of traditional fluorescence analysis instruments [28]. The FCA replaces the routine fluorescence cell (1 mL) with the capillary ($\leq$18 μL) and can save about 99% enzymes or reagents. Based on FCA, we have successfully developed an immobilized enzyme capillary bioreactor for the determination of alcohol in distilled spirit [29–31], and an immobilized probe biosensor marked by using Cy-5 reagent [32] for the determination of DNA, etc. [28]. Subsequently, Ho et al. [33] also have made an immobilized enzyme capillary bioreactor with a longer capillary (ID: 0.53 mm, length: 85 cm) and used for a FIA amperometric analysis system to determine blood glucose.

In this research, further combining FCA with liquid enzyme catalysis together, we have proposed a new method called pyruvic acid liquid enzymatic fluorescence capillary analysis (P-LE–FCA) for determination of pyruvic acid.

2. Experimental

2.1. Assay principle

Reaction principle used for the determination of pyruvic acid is shown in Eq. (1). In the presence of lactate dehydrogenase (L-LDH), pyruvic acid reacts with NADH. This reaction produces lactic acid and NAD^+ without fluorescence property. When NADH is excited at 350 nm, it will emit 460 nm of fluorescence. Based on fluorescence quenching the content of the pyruvic acid can be quantified.

$$\text{pyruvic acid} + \text{NADH} + \text{H}^+ \xrightarrow{\text{L-LDH(pH 7.5)}} \text{lactic acid} + \text{NAD}^+ \quad (1)$$

2.2. Chemicals and apparatus

All reagents used were of analytical-reagent grade with no further purification. Ultra-purified water (conductivity: 0.065 μS cm^{-1}) was used throughout all experiments. Sodium pyruvate was purchased from Huali Scientific Company (Chengdu, China). 2,4-Dinitrophenylhydrazine (DNPH), H_2SO_4, Na_2HPO_4 and KH_2PO_4 were obtained from Kelong Chemical Reagent Factory (Chengdu, China). NADH and L-LDH (EC 1.1.1.27, 53 units/mg) were bought from Sigma–Aldrich Japan K.K. (Tokyo, Japan).

F-4500 spectrofluorimeter used in this experiment was from Hitachi Co. (Tokyo, Japan). An AUW120D type electric balance (measuring precision: 0.01 mg) made by Simadzi Co. (Kyoto, Japan). A capillary holder was self-made and the capillaries (ID: 0.90 mm, 18 μL) were from Huaxi Scientific Company (Chengdu, China). pH meter was purchased from Leici Instrument Factory (Shanghai, China). A 721-A type spectrophotometer was product of Shanghai Third Analyzer Co. (Shanghai, China).

2.3. Preparations of reagent solutions

2.3.1. Phosphate buffer solutions (PBS, 0.10 mol L^{-1})

0.10 mol L^{-1} of Na_2HPO_4 solution was prepared by weighing 35.81 g of Na_2HPO_4, dissolving and diluting to 1000 mL with water. 0.10 mol L^{-1} of KH_2PO_4 solution was prepared by weighing 3.40 g of KH_2PO_4, dissolving and diluting to 250 mL with water. Preparations of buffer solutions with pH 4.42, 6.18, 7.50, 8.15 and 9.33 were completed by mixing Na_2HPO_4 solution and KH_2PO_4 solution together. The pH measurements were carried out on the pH meter.

2.3.2. NADH solution (2.0 mmol L^{-1})

1.5 mg of NADH was dissolved in water and diluted to 1.0 mL with PBS (pH 7.50).

2.3.3. Sodium pyruvate solution (50.0 mmol L^{-1})

The solution was prepared by weighing 0.1375 g of sodium pyruvate in 25 mL of calibrated flask, dissolving and diluting to the mark with PBS (pH 7.50).

2.3.4. L-LDH solution (50 kU L^{-1})

One milligram of L-LDH was exactly weighed and dissolved in 1.0 mL of PBS (pH 7.50). 5 kU L^{-1} of L-LDH solution used in the research was prepared by diluting 50 kU L^{-1} of L-LDH solution with PBS (pH 7.50).

2.3.5. H_2SO_4 solution (4.5 mol L^{-1})

Fifty milliliters of concentrated sulphuric acid was slowly added into ultra-purified water. The mixture was diluted to 200 mL with water.

2.3.6. DNPH solution (4%, w/v)

Four grams of DNPH was weighed, dissolved and diluted to 100 mL with H_2SO_4 solution (4.5 mol L^{-1}).

2.3.7. Fluorescent reaction solutions

No. 1 of fluorescent reaction solution was prepared by mixing 200 μL L-LDH (50 kU L^{-1}), 100 μL NADH (20 mmol L^{-1}) and 700 μL PBS.

No. 2 of fluorescent reaction solution was prepared by mixing 100 μL NADH (20 mmol L^{-1}) and 900 μL PBS.

2.4. Pretreatment of capillary

First the inner and outer surfaces of the capillaries were washed with ethanol-water solution containing 2 mol L^{-1} of NaOH, and then flushed with ultra-purified water. At last, these capillaries were put in a thermostat for drying at 40 °C.

2.5. Determination procedure

The FCA method has two important parts: a medical capillary and a self-made capillary holder [34]. When analyzing, the holder is inserted into the light path of F-4500. After reacting for 20 min, the mixture of reactant and product are sucked into the capillary. Then, the capillary is vertically inserted into the holder. When excitation beam (λ_{ex}: 350 nm) passes through the capillary, NADH in the mixture is excited and emits fluorescence (λ_{em}: 460 nm). The fluorescence with vertical direction of excitation beam enters into monochromatic filter and reaches the detector. At the same time, the fluorescence intensity is detected. In the research, the fluorescence intensity is proportional to the content of pyruvic acid.

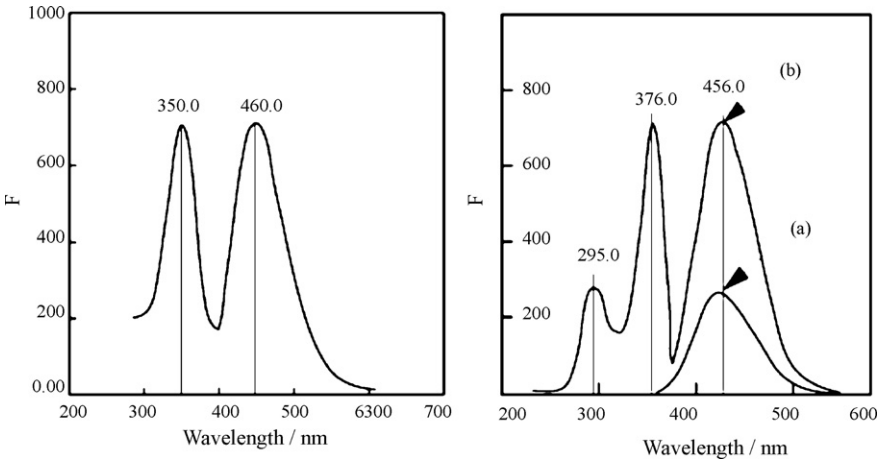

Fig. 1. Wavelength curves obtained by scanning NADH. The left part is the result of scanning of NADH in a capillary; the right part is the result of scanning of NADH in a common fluorescence cell. The curve (a) in the right part is the wavelength scanning at 295 nm of excitation light; the curve (b) is the wavelength scanning at 376 nm of excitation light.

3. Results and discussion

3.1. Scanning of excitation and emission wavelengths

To investigate whether the wavelength of NADH in capillary and in fluorescence cell is similar, the fluorescence intensity of NADH was scanned under different excitation and emission wavelengths. The results obtained were shown in Fig. 1. It was found that the intensities of NADH in capillary at $\lambda_{ex}/\lambda_{em}$ = 350/460 nm (slit 10 nm) and in fluorescence cell at $\lambda_{ex}/\lambda_{em}$ = 376/456 nm all reached to the maximum, respectively.

The wavelength differences of NADH in capillary and fluorescence cell were due to the differences of refractive index of glass and quartz. Therefore, $\lambda_{ex}/\lambda_{em}$ = 350/460 nm was used during next experiment.

3.2. Effect of NADH concentration

Under catalysis of L-LDH, NADH reacts with pyruvic acid and forms NAD^+ without fluorescence. The content of pyruvic acid can be quantified indirectly by detecting fluorescent quenching of NADH. Consequently, the content of NADH in the reaction system will affect the quantification of pyruvic acid.

In this experiment, the fluorescence intensity was detected under different concentrations of NADH (0, 0.50, 0.75, 1.00, 2.00 and 3.00 mmol L^{-1}, respectively). The concentrations of pyruvic acid used as testing samples were 5.0 and 1.0 mmol L^{-1}, respectively. The results obtained were shown in Fig. 2. When the concentration of pyruvic acid was 1.0 mmol L^{-1}, the fluorescent quenching ratio $[(F_2 - F_1)/F_2]$ reached the maximum at 0.8 mmol L^{-1} of NADH. And when the pyruvic acid concentration was 5.0 mmol L^{-1}, the fluorescent quenching ratio reached the maximum at 1.0 mmol L^{-1} of NADH.

Quenching ratio of NADH fluorescence and transforming ratio of chemical reaction (NADH → NAD^+) should has a maximum value in the raction system. From Fig. 2, it can be seen that under catalysis of L-LDH, first in the range 0–1.0 mmol L^{-1}, the quenching ratio of NADH fluorescence rises with the increase of its concentration, but when the concentration exceeds 1.0 mmol L^{-1}, reversibly the quenching ratio of NADH fluorescence falls with the increase of its concentration. The reason should be that in 0–1.0 mmol L^{-1}, with the increase of NADH concentration, NAD^+ without fluorescence and lactic acid produced by chemical reaction between NADH and pyruvic acid will gradually manifold and result in the rise of the

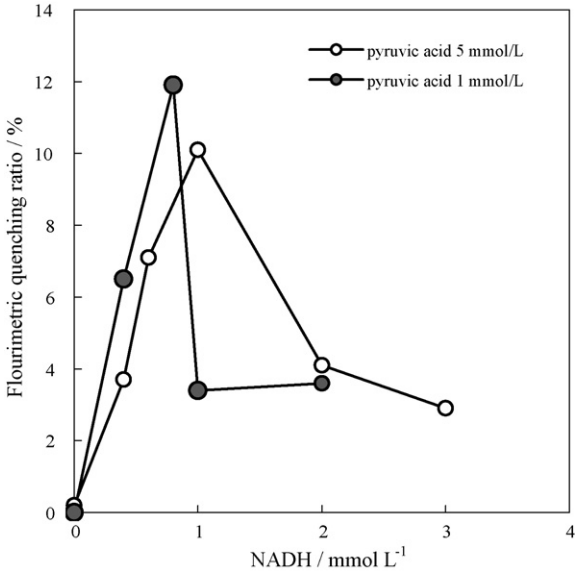

Fig. 2. Effect of NADH concentration on fluorescence intensity.

quenching ratio and the augmentation of the transforming ratio. Quenching and transforming ratios reach maximum value when NADH concentration is at 1.0 mmol L^{-1}. If the concentration of NADH is excessive (>1.0 mmol L^{-1}) in the reaction mixture solution, its self-fluorescence (blank fluorescence) is too intensive, this will cover up fluorescent portion quenched by the reaction and result un-conspicuousness in total fluorescent quenching in the reaction system, and result in the decrease of fluorescent quenching ratio. So, 1.0 mmol L^{-1} of NADH concentration was selected for use.

3.3. Effect of liquid L-LDH concentration

In this experiment, the concentration of NADH was fixed at l.0 mmol L^{-1} (pH 7.50). The effect of the liquid L-LDH concentration on the fluorescence intensity was investigated under different concentrations of pyruvic acid (1.0, 4.0 and 0.25 mmol L^{-1}). It could be seen that the fluorescence intensity decreased with increasing the L-LDH concentration and reached platform when the concentration was 2.5 kU L^{-1}. It proved that excessive L-LDH might not affect the reaction. Therefore, any concentration point on the plat-

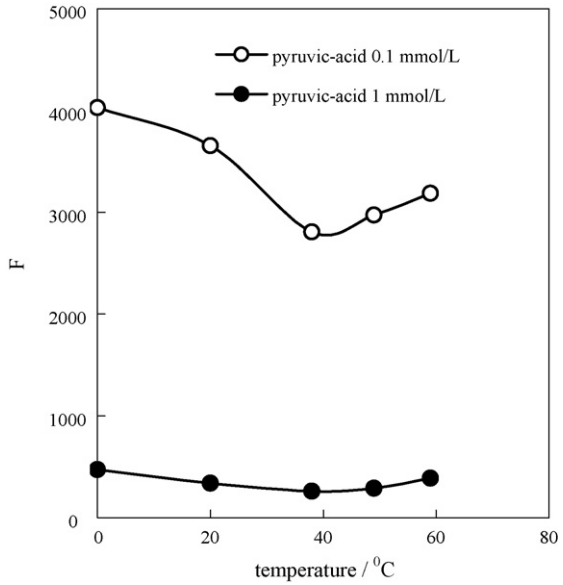

Fig. 3. Effect of reaction temperature on fluorescence intensity.

form could be selected. The later work used 5.0 kU L^{-1} as suitable concentration.

3.4. Effect of temperature

The effect of temperature on the fluorescence intensity was investigated under different pyruvic acid concentrations (1.0 and 0.1 mmol L^{-1}, respectively). The other experimental conditions were the same as Section 3.3, except that the concentration of L-LDH was 5.0 kU L^{-1}. The same reaction mixture solutions were put into a water bath at different temperatures to react for 25 min, respectively. After sucking the mixture, the capillary was inserted in the capillary holder at light path of F-4500 and its fluorescence intensity was detected. The results were shown in Fig. 3. The fluorescence intensity of the mixture solution decreased when the temperature was below 38 °C and increased when the temperature was above 38 °C. The reason for the increase of fluorescence intensity over 38 °C may be enzyme deactivation. Consequently, the reaction temperature used for the enzyme catalysis was selected to be 38 °C in the experiment.

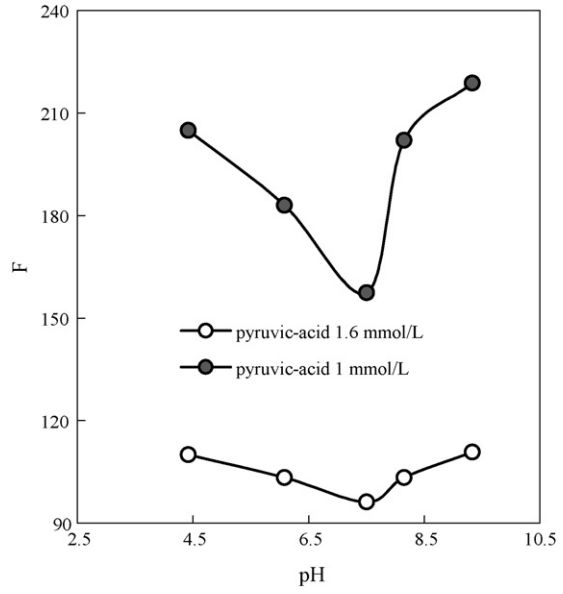

Fig. 4. Effect of P-LE–FCA system's pH on fluorescence intensity.

3.5. Effect of pH

The experimental conditions were the same as Section 3.4, except that the reaction temperature used was 38 °C. Different mixture solutions with different pH values (4.42, 6.18, 7.50, 8.15 and 9.33, respectively) were prepared with PBS buffer solutions. And then the effect of pH on fluorescence intensity was examined. Obtained results were shown in Fig. 4. It could be seen that the fluorescence intensity reached the minimum when pH value was 7.5. So, this pH value was selected by us.

3.6. Effect of reaction time

The effect of the reaction time on fluorescence intensity was investigated by respectively using 0.50 and 0.75 mmol L^{-1} of pyruvic acid used as test samples at 38 °C. The NADH concentration was fixed at 1.0 mmol L^{-1}. It could be seen that the fluorescence intensity of the reaction mixture solution decreases with the increase of the reaction time up to 6 min by using 0.50 mmol L^{-1} of pyruvic acid as the test sample, and up to 10 min by using 0.75 mmol L^{-1}. Namely, the different concentrations of pyruvic acid needed different reaction time. Therefore, considering high concentration of pyruvic acid can enough reacts with 1.0 mmol L^{-1} of NADH in the reaction system, the reaction time was selected to be 20 min.

4. Determination of the sample

4.1. Calibration of pyruvic acid

The optimum conditions used in the method were as follows. The pH of the buffer was 7.5, reaction time was 20 min, and reaction temperature was 38 °C. The excitation and emission wavelengths of NADH were 350 and 460 nm, respectively. The concentrations of L-LDH and NADH were 5.0 kU L^{-1} and 1.0 mmol L^{-1}, respectively. Under these conditions, a series of pyruvic acid standard solutions were determined by P-LE–FCA method. The linear range for the determination of pyruvic acid was 0.2–1.2 mmol L^{-1}. The linear equation of the pyruvic acid concentration (C) and difference value of the fluorescence intensity (ΔF) was $\Delta F = 327.13C - 10.018$ ($r = 0.9942$).

4.2. Determination of the sample

Three urine samples were chosen in the research as testing samples. When urine samples are determined, there are two main interferences containing the intrinsic enzymes and other co-existing fluorescence substances. In order to remove these interferences, urine samples were heated for 10 min at 100 °C and centrifuged.

After adding 50 μL No. 1 of the fluorescent reaction solution into test tube 1 (F_1) containing 50 μL of the sample, and 50 μL No. 2 of the fluorescent reaction solution into test tube 2 (F_2) containing 50 μL of the sample, two tubes were heated for 20 min at 38 °C (water bath). The reaction mixture in tube 1 was sucked into the capillary, its fluorescence intensity (F_1) was detected. And then the reaction mixture in tube 2 was sucked into the same capillary, the fluorescence intensity (F_2) of the blank in the reaction mixture was detected. The difference in the values of the fluorescence intensity ($\Delta F = F_2 - F_1$) was used for quantifying the content of pyruvic acid in the sample. The obtained results were shown in Table 1.

Table 1
Determination results of pyruvic acid content in urine samples obtained by using P-LE–FCA ($n = 3$)

Samples no.	F_2	F_1	ΔF	R.S.D. (%)	Found concentration (mmol L^{-1})
1	624.7	572.4 ± 1.575	52.3	0.28	0.306 ($\Delta F = 429.88C - 13.368$)
2	495.4	467.2 ± 3.536	28.2	1.43	0.234 ($\Delta F = 327.13C - 10.018$)
3	425.2	398.3 ± 7.071	26.9	0.83	0.223 ($\Delta F = 327.13C - 10.018$)

Table 2
Recovery determination results of urine samples obtained by using P-LE–FCA

Sample no.	Dilution multiple	Sample concentration (mmol L^{-1})	Added concentration (mmol L^{-1})	Calculated concentration (mmol L^{-1})	Found concentration (mmol L^{-1})	Recovery (%)
1	2	0.306	0.2	0.253	0.261	103.2
			1.6	0.953	0.920	96.5
2	2	0.234	0.2	0.217	0.223	102.8
			1.6	0.917	0.938	102.3
3	2	0.223	0.2	0.212	0.213	100.5
			1.6	0.912	0.878	96.3

To examine the credibility of the method, the recoveries of these urine samples were determined. Different concentrations of pyruvic acid standard solutions were added into the urine samples and their fluorescence intensities were determined. Obtained results were shown in Table 2. The recoveries were in the range 96–104%, and they were very satisfactory.

4.3. Effect of other co-existing substances

The composition of urine is very complex. It contains many kinds of substances such as NaCl, glucose, ascorbate, uric acid and lactic acid, etc. To investigate the effect of these coexisting substances on the P-LE–FCA, different concentrations of NaCl (100–600 mmol L^{-1}), glucose (0.10–0.70 mmol L^{-1}), ascorbate (0.029–0.200 mmol L^{-1}), uric acid (0.10–0.70 mmol L^{-1}) and lactic acid (2.0–20 mmol L^{-1}) were added into the pyruvic acid standard solutions, respectively. The obtained recoveries were in the range of 96–103% and were satisfactory. It was proved that the added substances did not interfere with the P-LE–FCA method for determining pyruvic acid.

4.4. Comparison with the colorimetric method

In order to evaluate the credibility of P-LE–FCA, three urine samples were used as testing samples, and contrast experiment was conducted with a common colorimetric method [18,20,35]. In the colorimetric method 4% of DNPH was used as the color reagent. Detection was made by a 721-A type spectrophotometer at 500 nm. The results were shown in Table 3. It can be seen that the results obtained between both methods do not exist obvious differences.

Table 3
Contrasting results between the P-LE–FCA and colorimetric method [18,20,35]

Sample no.	P-LE–FCA (mmol L^{-1})	Colorimetric method (mmol L^{-1})	P-LE–FCA R.S.D. (%)	Colorimetric method R.S.D. (%)
1	0.293 ± 0.010 0.284, 0.291, 0.304	0.290 ± 0.003 0.287, 0.290, 0.292	3.4	0.9
2	0.265 ± 0.002 0.267, 0.262, 0.266	0.258 ± 0.003 0.258, 0.260, 0.255	0.9	1.0
3	0.276 ± 0.001 0.277, 0.275, 0.276	0.271 ± 0.002 0.268, 0.271, 0.271	0.5	0.6

4.5. Reproducibility and detection limit

In order to examine the accuracy of P-LE–FCA, its reproducibility was determined in the linear range. The lower (0.2 mmol L^{-1}) and the higher (1.2 mmol L^{-1}) concentrations of pyruvic acid were used as testing samples. Obtained relative standard deviation ($n = 11$) were 0.86% (fluorescence intensity of mean value: 759.6 ± 4.04) and 3.34% (the mean value: 121.3 ± 6.06), respectively. From examination results, it can be seen that the accuracy of this method was satisfactory. Besides, by calculation ($\Delta F = 969.68C - 40.35$), the detection limit ($C_L$) of the method was 0.012 mmol L^{-1} ($C_L = 3(S/K) = 3(4.04/969.68) = 0.012$ mmol L^{-1}).

5. Conclusions

In this study, a new method for the determination of pyruvic acid has been established by leading the liquid enzyme method to FCA. Its determination range is 0.2–1.2 mmol L^{-1} for pyruvic acid, and detection limit is 0.012 mmol L^{-1}, as well as relative standard deviation is 0.86%. The optimized experimental conditions are that the reaction time is 20 min, reaction temperature is 38 °C, pH of PBS is 7.5, and the concentrations of NADH and L-LDH are 1.0 mmol L^{-1} and 5.0 kU L^{-1}, respectively. Because the capillary volume used as reaction container is only 18 μL, the P-LE–FCA can save many enzymes and reagents used in the experiment, and can realize trace analysis to a micro-volume sample. The operation procedure of the method and the apparatus adopted are simple, so it can be easily popularized. The method can be applicable for the determination of pyruvic acid samples in clinic medicine or industrial field. In further research, we will pay attention to the method of immobilized enzyme on the inner surface of the capillary and develop a new immobilized enzyme capillary bioreactor which can be recycled for the determination of pyruvic acid to save more enzymes and reagents.

Acknowledgements

The authors are grateful to the Promotion Program Foundation of the Sichuan University of China for the financial support of the project (No. 0082204127067), and to the laboratory center of state teaching base for engineering chemistry course for the supplying of F-4500 spectrofluorimeter.

References

[1] R.T. Stanko, D.L. Tietze, T.E. Areh, Am. J. Clin. Nutr. 56 (1992) 630.
[2] R.T. Stanko, R.W. Robertson, J. Reilly, J. Appl. Physiol. 69 (1990) 1651.
[3] R.T. Stank, H.R. Reynolds, R. Reynolds, Am. J. Clin. Nutr. 56 (1994) 423.
[4] A. Borle, P. Heely, Chin. Sports Nutr. (1994) 227.
[5] L. Persson, L. Hillered, J. Neurosurg. 76 (1992) 72.
[6] K.T. Kwon, V.W. Tsai, Emerg. Med. Clin. North Am. 25 (2007) 1041.
[7] P. Chen, L.-H. Nie, S.-Z. Yao, J. Chromatogr. B 673 (1995) 153.
[8] C. Olsen, Clin. Chim. Acta 33 (1971) 293.
[9] P.T. Ozand, R.L. Hawkins, R.M. Collins, J.T. Tildon, M. Cornblath, Biochem. Med. 14 (1975) 170.
[10] Q.F. Xue, E.S. Yeung, J. Chromatogr. A 661 (1994) 287.
[11] P.R. Tomas, M.L. Carmen, V. Tomas, J. Fenoll, Anal. Chim. Acta 485 (2003) 63.
[12] A. Horowitz, R. Meller, G.K. Moortgat, J. Photochem. Photobiol. A 146 (2001) 19.
[13] M. Abdelwahid, Y.J. Mu, J. Photochem. Photobiol. A 157 (2003) 295.
[14] J. Kulys, L.-Z. Wang, N. Anal. Chim. Acta 265 (1992) 15.
[15] F. Mizutani, S. Yabuki, Y. Sato, T. Sawaguchi, S. Iijima, Electrochim. Acta 45 (2000) 2945.
[16] L.A. Abayomi, L.A. Terry, S.F. White, P.J. Warner, Biosens. Bioelectron. 21 (2006) 2176.
[17] J. Kim, T.D. Chung, H. Kim, J. Electroanal. Chem. 49 (2001) 78.
[18] K.S. Yoo, L.M. Pike, B.K. Hamilton, Hort. Sci. 30 (1995) 1306.
[19] K.S. Yoo, L.M. Pike, Scientia Horticulturae 82 (1999) 193.
[20] P. Marcos, P.L.-M. Marco, R. Ricardo, G. Maximo, V. Maribel, B.J. Luis, B. Marcela, Talanta 64 (2004) 1299.
[21] K.S. Yoo, L.M. Pike, Scientia Horticulturae 89 (2001) 249.
[22] A. Hallstrom, A. Carlsson, L. Hillered, U. Uncerstedt, J. Pharmacol. Methods 22 (1989) 113.
[23] G.J. Stijntjes, J.M. Koppele, N.P.E. Vermeulen, Anal. Biochem. 2006 (1992) 334.
[24] Y.-S. Wu, T.-H. Tsai, T.-F. Wu, F.-C. Chengc, J. Chromatogr., A 913 (2001) 341.
[25] J.B. Ewaschuk, J.M. Naylor, W.A. Barabash, G.A. Zello, J. Chromatogr. B 805 (2004) 347.
[26] E. Hautala, M.L. Weaver, Anal. Biochem. 30 (1969) 32.
[27] Y.-S. Li, X.-F. Gao, Chin. Pat. No. 200510021832.2. (2005).
[28] Y.-S. Li, X.-F. Gao, Spectrosc. Spectral Anal. 127 (2007) 1565.
[29] Y.-S. Li, X.-F. Gao, J. Sichuan Univ. (Eng. Sci. ed.) 39 (2007) 74.
[30] Y.-S. Li, X.-F. Gao, Anal. Chim. Acta 588 (2007) 140.
[31] Y.-S. Li, X.-F. Gao, Chin. Pat. No. 200510022413.0. (2005).
[32] X.-F. Gao, Y.-S. Li, Y.-X. Jiang, Chin. J. Anal. Chem. 34 (2006) S220.
[33] J.-A. Ho, L.-C. Wu, N.-C. Fan, M.-S. Lee, H.-Y. Kuo, C.-S. Yang, Talanta 71 (2007) 391.
[34] Y.-S. Li, X.-F. Gao, Chin. Pat. No. 200510021542.8. (2005).
[35] Y.-G. Chi, Y.-L. Feng, S. Wen, H.-X. Lu, Z.-Q. Yu, W.-B. Zhang, G.-Y. Sheng, J.-M. Fu, Talanta 72 (2007) 539.

Talanta 76 (2008) 419–423

Contents lists available at ScienceDirect

Talanta

journal homepage: www.elsevier.com/locate/talanta

Direct electrochemistry and reagentless biosensing of glucose oxidase immobilized on chitosan wrapped single-walled carbon nanotubes

Yi Zhou [a], Hui Yang [b], Hong-Yuan Chen [a,*]

[a] The Key Lab of Analytical Chemistry for Life Science, MOE, School of Chemistry and Chemical Engineering, Nanjing University, Nanjing 210093, China
[b] Shanghai Institute of Microsystem and Information Technology, Chinese Academy of Sciences, Shanghai 200050, China

ARTICLE INFO

Article history:
Received 21 January 2008
Received in revised form 15 March 2008
Accepted 17 March 2008
Available online 27 March 2008

Keywords:
Glucose oxidase
Single-walled carbon nanotubes
Chitosan
Direct electron transfer
Biosensor

ABSTRACT

Single-walled carbon nanotubes (SWCNTs) selectively wrapped by a water-soluble, environmentally friendly, biocompatible polymer chitosan (CHI) were employed for the construction of a bioelectrochemical platform for the direct electron transfer (DET) of glucose oxidase (GOD) and biosensing purposes. Scanning electron microscopy and Raman spectroscopy were used to investigate the properties of the SWCNT–CHI film. The results show that the preferentially wrapped small-diameter SWCNTs are dispersed within the CHI film and exist on the surface of the electrode as small bundles. The DET between GOD and the electrode surface was observed with a formal potential of about ca. −460 mV vs. SCE in phosphate buffer solution. The heterogeneous electron transfer rate constant and the surface coverage of GOD are estimated to be 3.0 s^{-1} and 1.3×10^{-10} mol/cm^2, respectively. The experimental results demonstrate that the immobilized GOD retains its catalytic activity towards the oxidation of glucose. Such a GOD/SWCNT–CHI film-based biosensor not only exhibits a rapid response time, a wide linear rang and a low detection limits at a detection potential of −400 mV but also shows the effective anti-interference capability. Significantly improved analytical capabilities of the GOD/SWCNT–CHI/GC electrode could be ascribed to the unique properties of the individual SWCNTs and to the biocompatibility of CHI.

1. Introduction

Glucose oxidase (GOD), from Aspergillus or Penicillium, is a homodimer with a molecular weight of about 150–180 kDa containing two tightly bound Flavine adenine dinucleotide (FAD) cofactors [1], and can catalyze the electron transfer from glucose to oxygen accompanying the production of gluconic acid and hydrogen peroxide. The most important application of GOD is in biosensor for the quantitative determination of glucose in food analysis and bioprocess monitoring. In order to investigate the electrochemical properties of GOD and to fabricate glucose enzyme electrode, GOD has been usually immobilized on the surface of the electrode. As an important enzyme molecule, it is of great importance to study the direct electron transfer because it could help us not only to understand the intrinsic redox behavior of GOD, but also to exploit application of biosensor [2]. Unfortunately, it is difficult for GOD to carry out a direct electrochemical reaction at the electrode surface because a thick protein layer surrounds its flavin redox center [3]. Efforts to this end have involved the chemical modification of GOD with electron-relay groups [4], the immobilization of the enzyme into biopolymer matrix [5] or silicon material [6] and the adsorption of GOD onto different nanomaterials, such as Au nanoparticles [7] and carbon nanotubes (CNTs) [8]. Such surface modifications promote the direct electrochemistry of GOD and facilitate the biosensing application for glucose detection.

The first glucose enzyme electrode was proposed in 1962 by Clark and Lyons [9]. In the past 40 years, major achievements have been made for enhancing the capabilities and improving the reliability of measuring devices [2]. Research efforts have aimed at an increase in a wide linear range with a high sensitivity. The discovery of various novel nanomaterials, such as CNTs, has been the focus for the development of glucose enzyme electrode [10], because these nanomaterials could provide a desirable microenvironment between the redox sites of an enzyme and the electrode surface.

Both multiwalled carbon nanotubes (MWCNTs) and single-walled carbon nanotubes (SWCNTs) have attracted enormous attention since their first discovery. Their unique structural, mechanical and electrical properties have made them very attractive candidates for many obvious, important applications, such as serving as active elements in field emission devices [11], as hydrogen storage materials [12], as scanning-probe microscopy tips [13,14], as well as several other uses. More specifically, the high accessible surface area, low electrical resistance, and high chemi-

* Corresponding author. Fax: +86 25 83594862.
E-mail address: hychen@nju.edu.cn (H.-Y. Chen).

0039-9140/$ – see front matter © 2008 Elsevier B.V. All rights reserved.
doi:10.1016/j.talanta.2008.03.028

cal stability suggest that SWCNTs would be suitable materials for electrodes and supports in biosensor applications. The majority of this effort is devoted to the immobilization of some enzymes on the surface of SWCNTs [15,16]. The SWCNT-modified electrodes have shown excellent catalytic properties as compared to the other materials.

To fabricate the SWCNT-modified electrodes, SWCNTs must be temporarily dispersed in some solvents such as dimethylformamide and acetone and then cast on the electrode, as SWCNTs are insoluble in essentially all the common solvents. This procedure for electrode preparation is complicated, and its application in biosensors is quite limited because of the use of organic solvents. To surmount the inherent insolubility of SWCNTs, nanotubes can be dispersed into solutions through either covalent [17] or noncovalent [18] interactions to improve solubility and, as well, to unbundled the aggregate ropes that are formed from intertube van der Waals interactions. However, chemisorption, which results in covalently bonded SWCNTs, although potentially enhancing solubility, generally alters the nanotube's electronic properties. To maintain electronic properties of the tubes, physisorption of polymer or surfactant is often used, resulting in formation of individual or very small bundle (ca. 2–5 tubes) of wrapped nanotubes.

The biopolymer chitosan (CHI) is a kind of matrix for enzyme immobilization with attractive properties that include high permeability toward water, good adhesion and biocompatibility [19]. As a good film formation material, CHI has been extensively utilized to fabricate the biosensors [20–22]. Recently, with the help of CHI, an aqueous dispersion and diameter-selective separation of SWCNTs has been accomplished with small-diameter SWCNTs existing in the solution [23]. Due to the high reactivity of small-diameter SWCNTs [24], such SWCNT–CHI system could exhibit unique film properties to fabricate glucose biosensor with a high activity. Generally, SWCNTs existed as bundles are insoluble in essentially all the common solvents, which limits their use in biosensors due to the fact that the amount of enzymes that can be immobilized is limited, providing matrixes with sensitivities and stability properties that are not fully optimized. However, the utilization of CHI wrapped individual SWCNTs in this paper could maximize the contact between SWCNTs and enzyme molecules; thus may be beneficial to an increase in sensor sensitivity and stability.

The research focus in this work is to construct a bioelectrochemical platform for the DET of GOD and for the detection of glucose based on SWCNTs and biocompatible polymer CHI. Within the film, the small-diameter SWCNTs are preferential wrapped by CHI verified by Raman spectroscopy. The direct electrochemistry and bioelectrocatalysis of GOD on the modified electrode were studied. The immobilization of GOD molecules into chitosan wrapped SWCNT film is shown to be an efficient method for the development of a new class of very sensitive, stable, and reproducible electrochemical biosensors.

2. Experimental

2.1. Reagents

Purified HiPco SWCNTs were purchased from Carbon Nanotechnologies, Inc. (Houston, TX, USA). Chitosan (85% deacetylation, average molecular weight = 1×10^6 g/mol) and glucose oxidase (from *Aspergillus niger*, E.C. 1.1.3.4) were obtained from Sigma–Aldrich Corp. All the other chemicals were of reagent grade and used as received. The buffer solution used was 0.1 M Na-phosphate buffer solution (PBS) with a pH value of 7.4. Glucose stock solutions were allowed to mutarotate overnight at room temperature before used. All solutions were prepared with pure water obtained using a Millipore Q water purification apparatus with the resistivity over 18 MΩ/cm.

2.2. Preparation of SWCNT–CHI solution

A 0.5 wt.% CHI solution was prepared by dissolving an appropriate amount of CHI powder in 0.05 M HCl aqueous solution at a temperature of ca. 80–90 °C. Then the solution was immediately filtered and cooled, the pH of the CHI solution was adjusted to 5.0 with NaOH. This stock CHI solution was stored in a refrigerator before use. 2.5 mg of HiPco SWCNTs and 5.0 mL of 0.5 wt.% CHI solution were then added to a vial and mixed ultrasonically in an ice bath for more than 5 h to accomplish dispersion. The resultant black solution with a calculated concentration of 0.5 mg/mL SWCNTs was separated after overnight standing. The resultant SWCNT–CHI solution appears homogenous and stable.

2.3. Fabrication of the SWCNTs–CHI/GC and GOD-modified SWCNT–CHI/GC electrodes

A measured volume (5 μL) of 0.5 mg/mL SWCNTs–CHI solution was transferred via a syringe onto a freshly polished glassy carbon (GC) disk (3 mm in diameter). After solvent was evaporated at room temperature, the resultant electrode was denoted as the SWCNT–CHI/GC electrode. The obtained SWCNT–CHI/GC electrode was immersed into 5 mg/mL GOD solution at 4 °C for 10 h. After that, the GOD immobilized SWCNT–CHI/GC electrode was transferred to 0.1 M PBS for 15 min before use.

All the GOD immobilized electrodes were stored at 4 °C when not in use.

2.4. Apparatus

Raman spectra were obtained using an HR800 Jobin Horiba Raman Microscope. Samples were placed in quartz cuvettes and excited with 514.5 nm laser radiation. All spectra were acquired in 30 s and the incident laser power (at the laser head) was ca. 10 mW. The image of scanning electron microscopy (SEM) was obtained with an S-4700 scanning electron microscope (Hitachi, Japan) at an acceleration voltage of 10 kV.

Electrochemical measurements were performed using a CHI 730B Potentiostat (Shanghai Chenhua Corp., China) and a conventional three-electrode cell. The bare GC or the modified electrode was used as the working electrode. The counter electrode was a Pt wire, and a saturated calomel electrode (SCE) was used as the reference electrode. All potentials were reported with respect to SCE. Amperometric detection of glucose was carried out in PBS by applying a potential of −400 mV. High-purity nitrogen or oxygen was used for deaeration of the solutions. During the measurements, a gentle gas flow was kept above the electrolyte surface.

All electrochemical experiments were performed at a temperature of ca. 20 °C.

3. Results and discussion

3.1. Dispersion of SWCNTs by CHI

In this study, the mixture of SWCNTs and CHI was sonicated for more than 5 h. It is to be noted that only small quantity of black powder spontaneously (overnight) precipitated from dispersion, with the resultant supernatant being homogeneous, stable and of dark color. The precipitate could not be re-dispersed using CHI solution in combination with centrifugation and heating, suggesting a robust method of forming stable SWCNTs in solution.

3.2. Raman spectroscopy characterization

Raman spectroscopy is a useful tool to characterize the properties of SWCNTs. Fig. 1 shows Raman spectra of the raw SWCNT sample, the dispersion of 0.5 mg/mL SWCNTs in CHI solution and the film by casting 0.5 mg/mL SWCNT solution onto GC disk. As can be seen, Raman shifts in curves (b) and (c) are essentially consistent, confirming that the SWCNT–CHI film keeps the same SWCNT properties as those in the solution. From the Raman spectra in the region above 1250 cm^{-1} (i.e., part A), hereinafter also referred to as the high-frequency region, the G band (graphite tangential mode at ca. 1593 cm^{-1}) is associated with the E_{2g} optical mode of graphite, and is characteristic of sp^2 hybridized carbon materials, as are the weak shoulder peaks near the 1551 cm^{-1}. The Raman G-band mode uniquely indicates the presence of SWCNTs. The relative intensity of the disorder-induced peak at ca. 1325 cm^{-1} (the so-called D-band) provides an indication of the relative amount of disordered carbon present; the relatively low intensity of the D-band indicates that the amount of amorphous carbon within these samples is quite low. In part B of Fig. 1, referred to hereinafter as the low-frequency region, bands attributable to radical breathing mode (RBM) vibrations of SWCNTs are clearly seen, which could provide more detailed information about the diameter and structure of SWCNTs. For raw HiPco SWCNTs (curve (a)), there are four distinct peaks at ca. 185, 208, 248 and 264 cm^{-1} (labeled as i, ii, iii and iv, respectively), corresponding to the calculated nanotube diameters of 1.30, 1.14, 0.94 and 0.89 nm, respectively, using the equation d (nm) = 223.5/ν_{RBM} (cm^{-1}) − 12.5 as the correlation between diameter d (nm) and RBM frequency [25]. However, only two RBM bands higher than ca. 240 cm^{-1} in curves (b) and (c) are observed, corresponding to the small-diameter SWCNTs [24,26]. The above observations clearly indicate that smaller-diameter SWCNTs are preferentially wrapped by CHI within the SWCNT–CHI film on the surface of GC electrode.

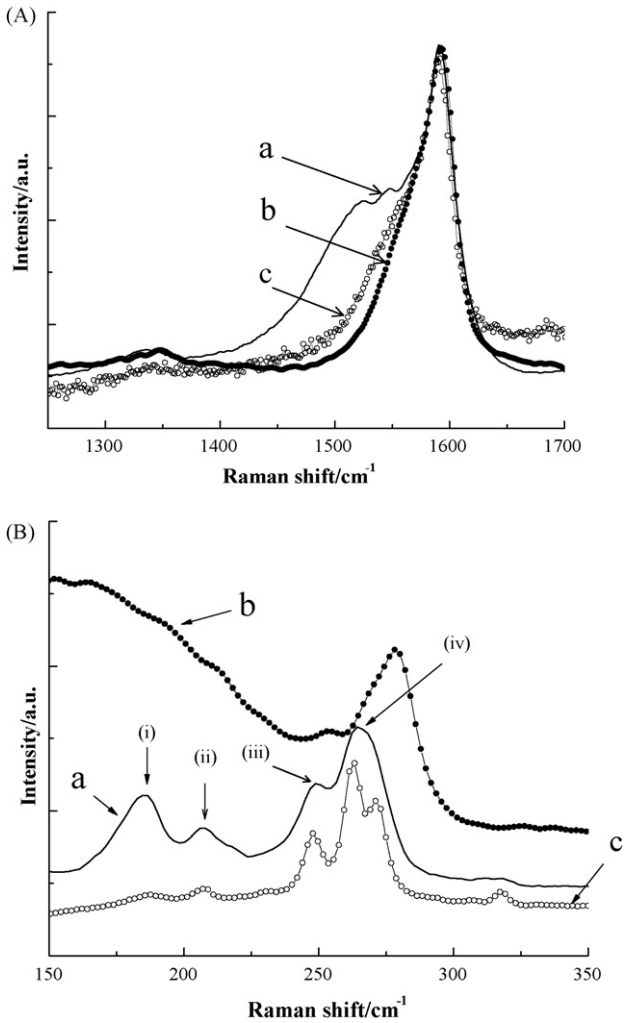

Fig. 1. Part (A) shows Raman spectra using a 514.5 nm excitation in the G-band region: (a) raw HiPco SWCNTs, (b) dispersion of 0.5 mg/mL SWCNTs in chitosan solution, and (c) film of 0.5 mg/mL SWCNTs in chitosan solution by casting onto a GC disk. Part (B) shows Raman spectra in the RBM region for the same samples (a), (b) and (c) as above.

3.3. Immobilization of GOD onto the SWCNT–CHI-modified electrode

Fig. 2 shows SEM images of the SWCNT–CHI and GOD/SWCNT–CHI films. For the SWCNT–CHI film, small bundled SWCNTs with a diameter range from ca. 5 to 15 nm are clearly seen, probably due to rebundling of SWCNTs upon drying, since the SWCNTs exist in the CHI solution as individuals. For the GOD/SWCNT–CHI film, however, one observes that there are some island-like spots attached onto the hair-like SWCNTs, indicating that GOD molecules exist as small islands within the SWCNT–CHI film.

There are two main reasons for the strong interactions between GOD molecule and SWCNTs–CHI composite. Firstly, it is well known

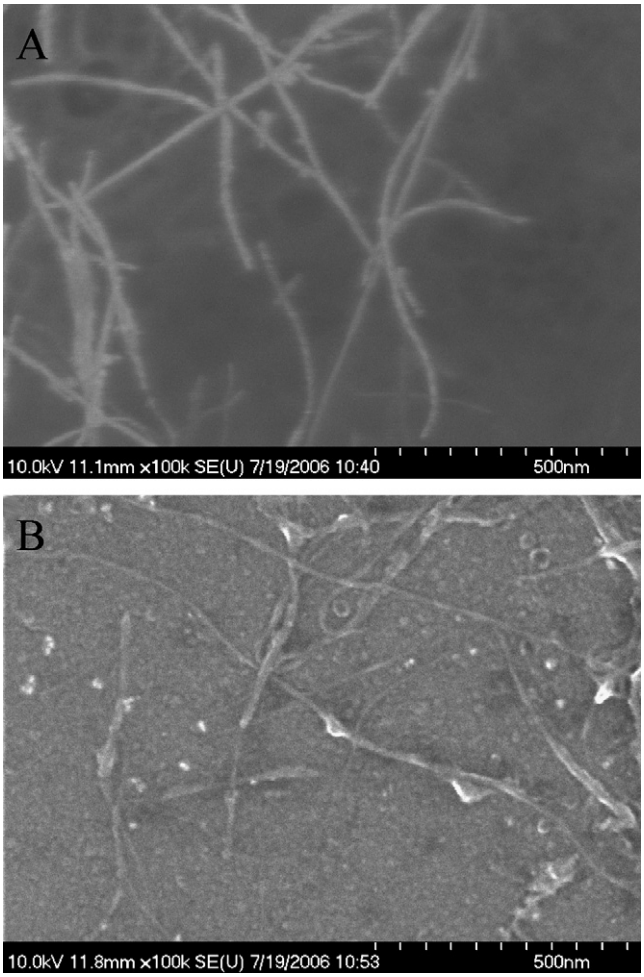

Fig. 2. SEM images of (A) CHI wrapped SWCNT film on GC surface and (B) GOD adsorbed on CHI wrapped SWCNT film on GC surface.

that hydrophobic interactions existed between SWCNTs and GOD lead to a strong adsorption of GOD on the sidewalls of SWCNTs [27]. Secondly, GOD is negatively charged in pH 7.4 PBS solution, whereas the chitosan wrapped SWCNTs composite is positively charged because of $-NH_3^+$ groups existed within the chitosan; therefore, resulting in a strong electrostatic interaction between GOD and SWCNTs–CHI films [28]. It is believed that the strong interactions between GOD and SWCNTs–CHI composite, coming from the synergetic effects of both SWCNTs and chitosan, lead to an enhanced stability of the biosensor.

3.4. Direct electron transfer of glucose oxidase on the modified electrode

Fig. 3 shows the cyclic voltammograms (CVs) of the GOD/SWCNT–CHI/GC (curve a) and GOD/CHI/GC (curve b) electrodes in an N_2-saturated PBS at a scan rate of 100 mV s^{-1}. In comparison with the GOD/CHI/GC electrode, a significantly increased current is clearly observed for the GOD/SWCNT–CHI/GC electrode. The enhancement of the double layer charging/discharging capacitance with SWCNTs could be due to the high surface area, unique structural and electrical properties of small-diameter SWCNTs. As seen in Fig. 3(a), a pair of well-defined redox peaks with a peak potential separation (ΔE_p) of 37 mV at scan rate of 100 mV/s indicates that GOD adsorbed onto the SWCNT–CHI film undergoes a quasi-reversible electron transfer process. In curve b, however, an unobvious direct electrochemical redox peak of GOD is also observed with a ΔE_p of 91 mV also at a scan rate of 100 mV/s, which is much larger than that shown in curve a, showing that GOD adsorbed on the CHI film undergoes an irreversible electron transfer process. Thus, it can be concluded that SWCNTs play an important role in promoting the DET of GOD. By integrating the redox wave area in curve a, the surface coverage of GOD is calculated to be 1.3×10^{-10} mol/cm^2, suggesting that the GOD immobilized on the SWCNT–CHI film might be a monolayer adsorption. Such a surface coverage is about five times higher than that GOD immobilized on the SWCNT–PDDA film with a value of 2.35×10^{-11} mol/cm^2 [29], suggesting that the SWCNT–CHI film provides a high active area and favorable microenvironment for enzyme immobilization. However,

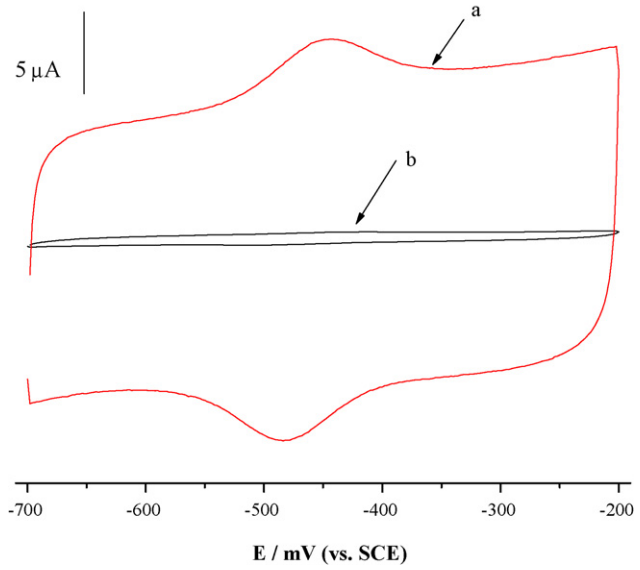

Fig. 3. CVs of (a) the GOD/SWCNT–CHI/GC and (b) GOD/CHI/GC electrodes in an N_2-saturated PBS at a scan rate of 100 mV s^{-1}. The inserts are the magnifying CVs of curve b.

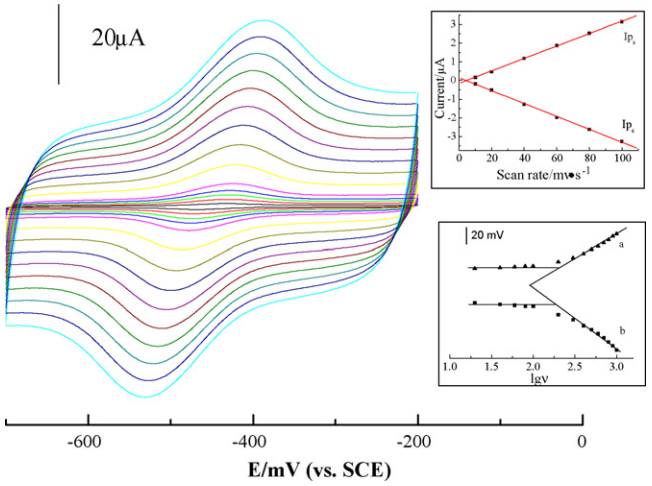

Fig. 4. CVs of the GOD/SWCNT–CHI/GC electrode in an N_2-saturated PBS at various scan rates. The upper insets are the plots of peak current vs. scan rate. The lower insets are the plots of peak potential vs. logarithm of scan rate.

in curve b, the surface GOD coverage is only 2.7×10^{-12} mol/cm^2, which is much lower than that on the SWCNT–CHI/GC film. Such a result demonstrates that SWCNTs significantly enhance the adsorptive capability of GOD molecules on the film.

Fig. 4 shows the CVs of the GOD/SWCNT–CHI/GC electrode in an N_2-saturated PBS at various scan rates. The formal potential is calculated as ca. −460 mV. The peak current increases with scan rate in the range from 20 to 1000 mV/s. The linearly dependent relationship of peak current on low scan rates from 20 to 100 mV/s (see upper insert of Fig. 4) indicates that the electrochemical behavior of GOD has the typical property of a surface electrochemical process. However, the peak potential separation remains almost constant with a value of ca. 37 mV ranged from 20 to 100 mV/s and starts to increase with scan rate from 200 to 1000 mV/s (see lower insert of Fig. 4). By using the model of Laviron [30], with ΔE_p of 100 mV at 600 mV/s, α of 0.58 calculated by the slot of line a and b (see lower insert of Fig. 4), according to the equation of $\lg k_s = \alpha \lg(1-\alpha) + (1-\alpha)\lg\alpha - \lg(RT/nF\upsilon) - \alpha(1-\alpha)nF\Delta E_p/2.3RT$, the heterogeneous surface electron transfer rate constant (k_s) on SWCNTs–CHI is ca. 3.0 s^{-1}, which is higher than that on MWCNTs–PDDA (2.76 s^{-1}) [31], on MWCNT paper (1.7 s^{-1}) [32], on MWCNTs/Nafion (1.53 s^{-1}) [33] and on gold nanoparticles (1.3 s^{-1}) [34], suggesting that SWCNTs are more effective in facilitating the DET of GOD than other nanomaterials Due to SWCNTs which benefits of their electrocatalytic properties and their small size may bring themselves close to the redox centers of GOD [35].

3.5. Performance of the SWCNT–CHI/GOD film-based biosensor

It is known that the use of low detection potential of a biosensor would be effective for the development of practical glucose amperometric biosensor because it is possible to avoid the interference of uric acid (UA) and ascorbic acid (AA) etc., which coexist with glucose in in vivo detection. The amperometric responses at the each successive addition of 1 mM glucose are presented in Fig. 5 at a detection potential of −400 mV. Inset is the calibration curve. The biosensor displayed a linear response to glucose in the concentration range from 1 to 10 mM with a correlation coefficient of 0.998. The reaction occurring at the biosensor is very fast in reaching a stable value within 10–15 s. The limit of detection, based on the signal-to-noise ratio of 3, was 0.01 mM. It is knowing that the interfering species may influence the response of glucose biosensor. However, we use the detection potential of

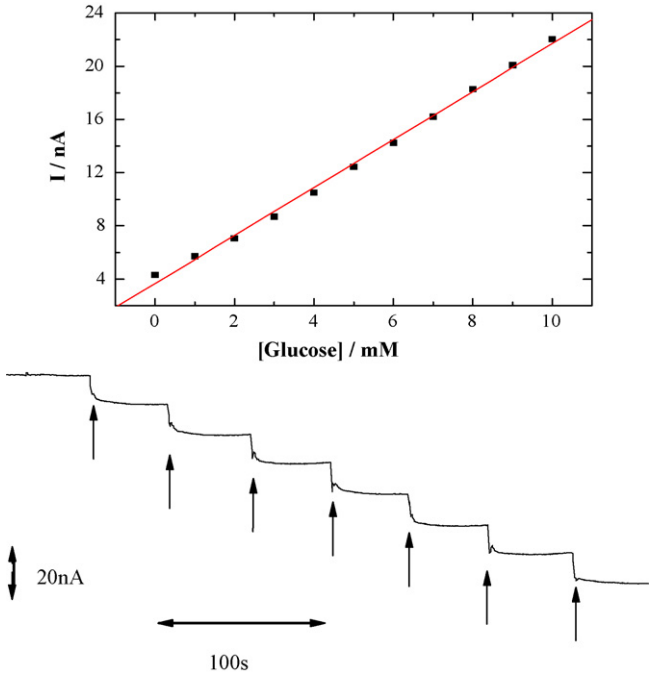

Fig. 5. Amperometric response with an increase in glucose concentration by 1 mM obtained at the GOD/SWCNT–CHI/GC electrode in 0.1 M PBS at a given potential of −400 mV. The inset shows the calibration curve.

−400 mV in this work. So no interference species was observed indicating a high selectivity of such a biosensor toward the glucose detection.

3.6. *Reproducibility and stability*

Importantly, such a biosensor displayed very good reproducibility. The relative standard deviation of nine repetitive measurements is less than 3.0% for 10.0 mM glucose solution. A single sensor could be used consecutively over a week with only ca. 10% diminution in the sensitivity. Meanwhile, there is nearly no any decrease in catalytic current after keeping the biosensor for 15 days at 4 °C. The good stability of such a biosensor should be due to the fact that the formation of network-like nanocomposite film restricts the loss of GOD.

4. Conclusions

The immobilization of enzyme molecules onto chitosan wrapped SWCNT film is shown to be a highly efficient method for the development of a new type of very sensitive, stable, and reproducible electrochemical biosensors. The use of SWCNTs in such a biosensor is based on the fact that SWCNTs can play dual roles, i.e. as immobilization matrixes for GOD molecules and as electrocatalytic material for glucose oxidation. SWCNTs significantly promote the direct electron transfer of GOD. Moreover, the adsorbed GOD is found to retain its catalytic activity toward the oxidation of glucose. Such a GOD/SWCNT–CHI film-based biosensor exhibits a rapid response time of 10–15 s, a high sensitivity, and a good linear range from 1 to 15 mM with a detection limit of 0.01 mM for the glucose detection. Both the unique electrical properties of SWCNTs and the biocompatibility of chitosan enable us to construct an excellent biosensing platform for glucose detection.

Acknowledgements

This work was supported by the National Natural Science Foundation of China (Nos. 20775033, 20521503, 20673136*), the National "863" High-Technology Research Program of China (2006AA05Z136*), and the 100 People Plan Program of the Chinese Academy of Sciences* (*for Hui Yang).

References

[1] H.J. Hecht, H.M. Kalisz, J. Hendle, R.D. Schmid, D. Schomburg, J. Mol. Biol. 229 (1993) 153.
[2] J. Wang, Electroanalysis 13 (2001) 983.
[3] L.G. Rodrigues, A.G. Wedd, A.M. Bond, J. Electroanal. Chem. 312 (1991) 131.
[4] I. Willner, V. Heleg-shabtai, R. Blonder, E. Katz, G. Tao, J. Am. Chem. Soc. 118 (1996) 10321.
[5] X. Wei, J. Cruz, W. Gorski, Anal. Chem. 74 (2002) 5039.
[6] G. Wang, S.T. Yau, Appl. Phys. Lett. 87 (2005) 253901.
[7] F.H. Zhang, S.S. Cho, S.H. Yang, S.S. Seo, G.S. Cha, H. Nam, Electroanalysis 18 (2006) 217.
[8] X.L. Luo, A.J. Killard, M.R. Smyth, Electroanalysis 11 (2006) 1131.
[9] L. Clark Jr., C. Lyons, Ann. NY Acad. Sci. 102 (1962) 29.
[10] J.J. Gooding, Electrochim. Acta 50 (2005) 3049.
[11] J.A. Misewich, R. Martel, P. Avouris, J.C. Tsang, S. Heinze, J. Tersoff, Science 300 (2003) 783.
[12] G. Gundiah, A. Govindaraj, N. Rajalakshmi, K.S. Dhathathreyan, C.N.R. Rao, J. Mater. Chem. 13 (2003) 209.
[13] H.J. Dai, J.H. Hafner, A.G. Rinzler, D.T. Colbert, R.E. Smalley, Nature 384 (1996) 147.
[14] S.S. Wong, E. Joselevich, A.T. Woolley, C.L. Cheung, C.M. Lieber, Nature 394 (1998) 52.
[15] B.R. Azamian, J.J. Davis, K.S. Coleman, C.B. Bagshaw, M.L.H. Green, J. Am. Chem. Soc. 124 (2002) 12664.
[16] S. Hrapovic, Y.L. Liu, K.B. Male, J.H.T. Luong, Anal. Chem. 76 (2004) 1083.
[17] J.L. Hudson, M.J. Casavant, J.M. Tour, J. Am. Chem. Soc. 126 (2004) 11158.
[18] V.C. Moore, M.S. Strano, E.H. Haroz, R.H. Hauge, R.E. Smalley, J. Schmidt, Y. Talmon, Nano Lett. 3 (2003) 1379.
[19] P. Sorlier, A. Denuziere, C. Viton, A. Domard, Biomacromolecules 2 (2001) 765.
[20] M. Zhang, A. Smith, W. Gorski, Anal. Chem. 76 (2004) 5045.
[21] Y. Liu, M.K. Wang, F. Zhao, Z.A. Xu, S.J. Dong, Biosens. Bioelectron. 21 (2005) 984.
[22] X.L. Luo, J.J. Xu, J.L. Wang, H.Y. Chen, Chem. Commun. 16 (2005) 2169.
[23] H. Yang, S.C. Wang, P. Mercier, D.L. Akins, Chem. Commun. 13 (2006) 1425.
[24] S. Banerjee, S.S. Wong, Nano Lett. 4 (2004) 1445.
[25] S.M. Bachilo, M.S. Strano, C. Kittrell, R.H. Hauge, R.E. Smalley, R.B. Weisman, Science 298 (2002) 2361.
[26] R. Krupke, F. Hennrich, H.V. Löhneysen, M.M. Kappes, Science 301 (2003) 344.
[27] M. Shim, N.W. Shi Kam, et al., Nano Lett. 2 (2002) 285.
[28] B. Krajewska, Enzyme Microb. Technol. 35 (2004) 126.
[29] J. Zhang, M. Feng, H. Tachikawa, Biosens. Bioelectron. 22 (2007) 3036.
[30] E. Laviron, J. Electroanal. Chem. 101 (1979) 19.
[31] D. Wen, Y. Liu, G. Yang, S. Dong, Electrochim. Acta 52 (2007) 5312.
[32] A. Guiseppi-Elie, C. Lei, R. Baughman, Nanotechnology 13 (2002) 559.
[33] C. Cai, J. Chen, Anal. Biochem. 332 (2004) 75.
[34] S. Zhao, K. Zhang, et al., Bioelectrochemistry 69 (2006) 158–163.
[35] J.J. Gooding, R. Wibowo, et al., J. Am. Chem. Soc. 125 (2003) 9006.